An Investigation of Noise Generation on a Hovering Rotor

PREPARED BY

BOEING
VERTOL DIVISION

FOR

U.S.ARMY RESEARCH OFFICE - DURHAM

CONTRACT DAHC04-69-C-0087

DISCLAIMER NOTICE

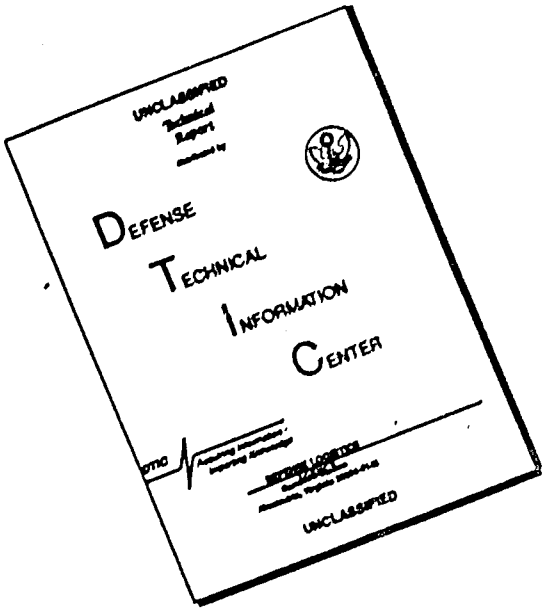

THIS DOCUMENT IS BEST QUALITY AVAILABLE. THE COPY FURNISHED TO DTIC CONTAINED A SIGNIFICANT NUMBER OF PAGES WHICH DO NOT REPRODUCE LEGIBLY.

January 1971
D210-10229-1

AN INVESTIGATION OF NOISE GENERATION ON A HOVERING ROTOR

by

H. Sternfeld
R. H. Spencer
J. O. Schairer

Prepared by

THE BOEING COMPANY, Vertol Division
Boeing Center, P.O. Box 16858
Philadelphia, Pennsylvania 19142

for

U.S. ARMY RESEARCH OFFICE - DURHAM
Durham, North Carolina

under

Contract DAHC04-69-C-0087

Unclassified

Security Classification

DOCUMENT CONTROL DATA - R & D

(Security classification of title, body of abstract and indexing annotation must be entered when the overall report is classified)

1. ORIGINATING ACTIVITY (Corporate author) The Boeing Company, Vertol Division	2a. REPORT SECURITY CLASSIFICATION Unclassified 2b. GROUP NA

3. REPORT TITLE

An Investigation of Noise Generation on a Hovering Rotor

4. DESCRIPTIVE NOTES (Type of report and inclusive dates)

Final Report: 30 June 69 - 30 January 71

5. AUTHOR(S) (First name, middle initial, last name)

H. Sternfeld
R. H. Spencer
J. O. Schairer

6. REPORT DATE	7a. TOTAL NO. OF PAGES	7b. NO. OF REFS
January 1971	353	

8a. CONTRACT OR GRANT NO. DAHC04 69 C 0087	9a. ORIGINATOR'S REPORT NUMBER(S) NA
b. PROJECT NO.	
c.	9b. OTHER REPORT NO(S) (Any other numbers that may be assigned this report) 8704.2-E
d.	

10. DISTRIBUTION STATEMENT

Approved for public release; distribution unlimited.

11. SUPPLEMENTARY NOTES	12. SPONSORING MILITARY ACTIVITY
	U. S. Army Research Office-Durham Box CM, Duke Station Durham, North Carolina 27706

13. ABSTRACT

This report presents the results of a program of helicopter rotor noise measurement. The program was carried out using a 60-foot diameter CH-47B 3-bladed rotor on the Boeing-Vertol engineering rotor whirl tower. The primary objectives were: (1) To obtain acoustical data over a frequency range wide enough to define all elements of rotor noise under well-documented ambient conditions, (2) To measure the tip vortex position with respect to a trailing blade using high-speed cameras and smoke to visualize the tip vortex and to relate blade-vortex separation distance to noise level, (3) To determine the propagation characteristics of rotor noise. (4) To evaluate two current analytical procedures for predicting rotor noise against the measured data. Tipspeeds ranged from 600 to 900 fps and thrusts ranged from 6300 to 32,000 pounds (disk load 2.2 to 11.3 pounds per square foot).

14. KEY WORDS

Vortices
Rotors
Rotary wings
Aircraft noise
Helicopters

Summary

This report presents the results of a program of helicopter rotor noise measurement. The program was carried out using a 60-foot-diameter CH-47B rotor on the Boeing-Vertol engineering rotor whirl tower shown below. The photograph displays smoke being trailed from the tip of a 2-bladed rotor and is shown to illustrate the technique of vortex visualization for measurement of tip vortex position with respect to the following blade. The data presented in this report were obtained on a 3-bladed rotor.

The primary objectives of the program were:

- To obtain acoustical data over a frequency range wide enough to define all elements of rotor noise under well-documented ambient conditions.
- To measure the tip vortex position with respect to a trailing blade using high-speed cameras and smoke to visualize the tip vortex and to relate blade-vortex separation distance to noise level.
- To determine the propagation characteristics of rotor noise.
- To evaluate two current analytical procedures for predicting rotor noise (References 1 and 2) against the measured data.

The testing on the 60-foot-diameter rotor encompassed a range of tipspeeds from 600 to 900 feet per second (fps) and thrusts from 6,300 pounds to 32,000 pounds (disk load 2.2 to 11.3 pounds per square foot, psf). The general arrangement of microphones and cameras for the test program is depicted below.

SCHEMATIC DRAWING
OF WHIRL TOWER TEST STAND

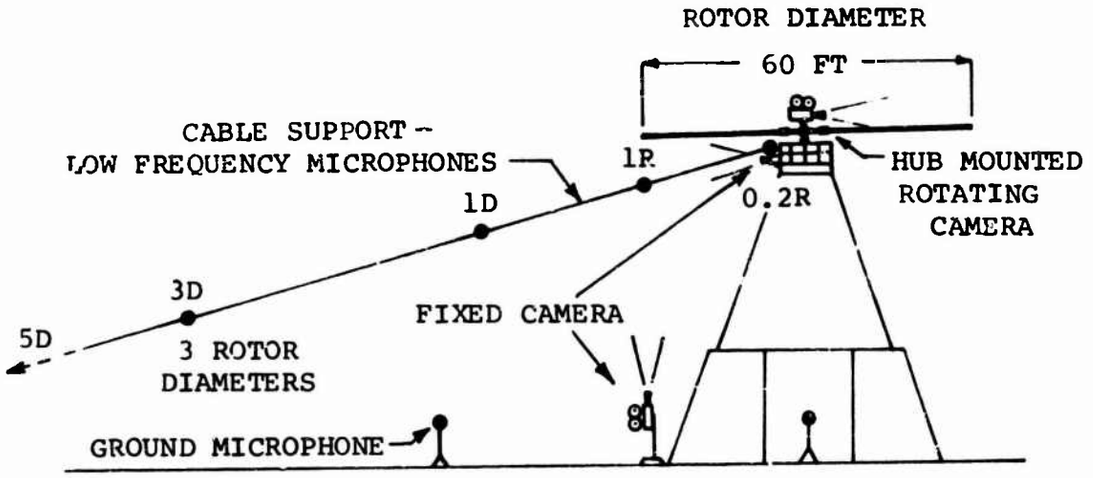

In addition to the successful acquisition and analysis of the required data, which is presented for use in future research, the following significant results were obtained:

1. Rotational noise predictions by the method of Ollerhead and Lowson[1] show good agreement with test data at low harmonics. To achieve agreement at the higher harmonics will require better definition of the higher harmonic airloads. An overall comparison between test measurements and predictions using Ollerhead and Lowson methods is displayed in the figure below which shows envelopes of test and predicted noise levels for a range of thrust and tip-speed conditions.

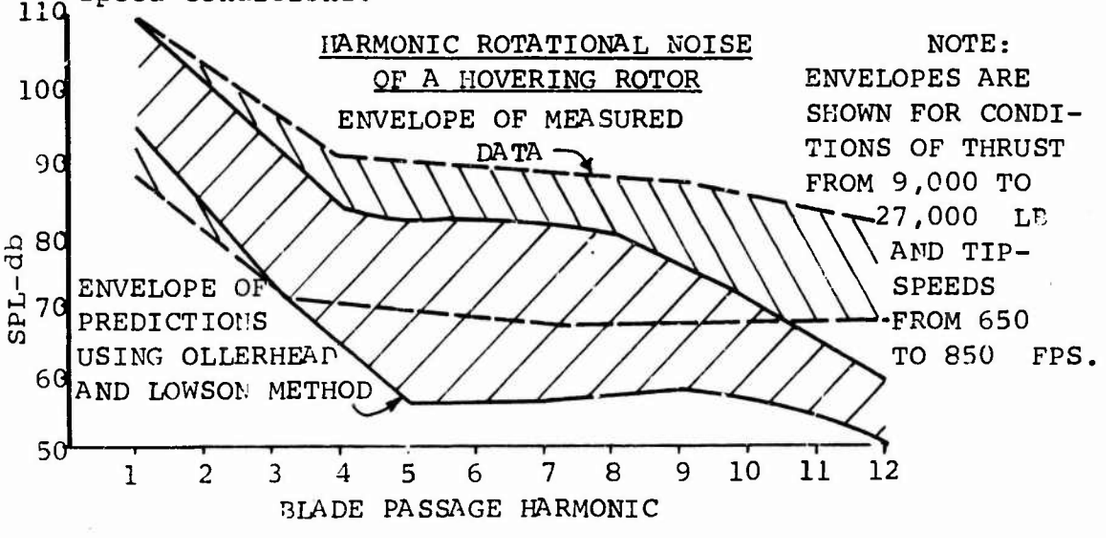

2. Broadband noise prediction by the method of Schlegel, King, and Mull[2] shows good agreement with the trends displayed by the measured data but predicted noise levels are significantly lower than those measured. An overall comparison between test measurements and predictions using the Schlegel method is displayed in the figure below.

BROADBAND NOISE

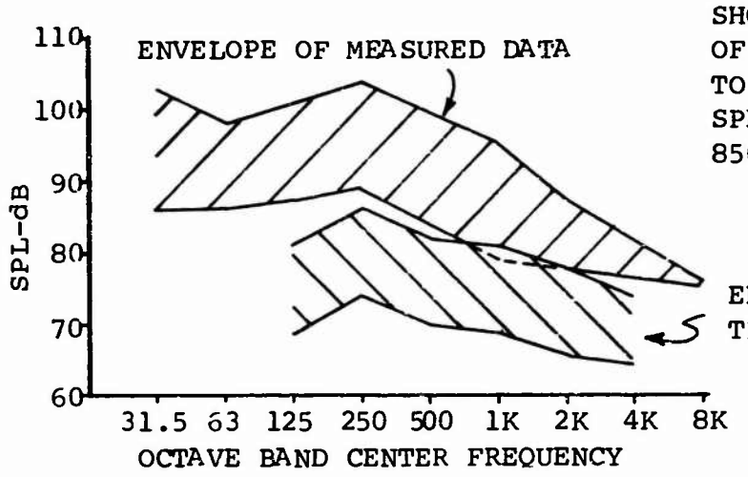

NOTE: ENVELOPES ARE SHOWN FOR CONDITIONS OF THRUST FROM 9,000 TO 27,000 LB AND TIP-SPEEDS FROM 650 TO 850 FPS.

ENVELOPE OF PREDICTION USING SCHLEGEL

3. Measurements using smoke to visualize the tip vortices showed that intersections between a rotor blade and the tip vortex shed from a preceding rotor blade can occur over the entire operating range tested in this program. These measurements established that the generation of impulsive noise is not solely a function of blade-vortex separation. Shown below are sound-pressure waveforms for two thrust conditions that produced blade-vortex intersections. For the high-thrust condition at which the waveform on the left was recorded, transient impulsive characteristics appeared which were not observed in waveforms recorded at low-thrust conditions.

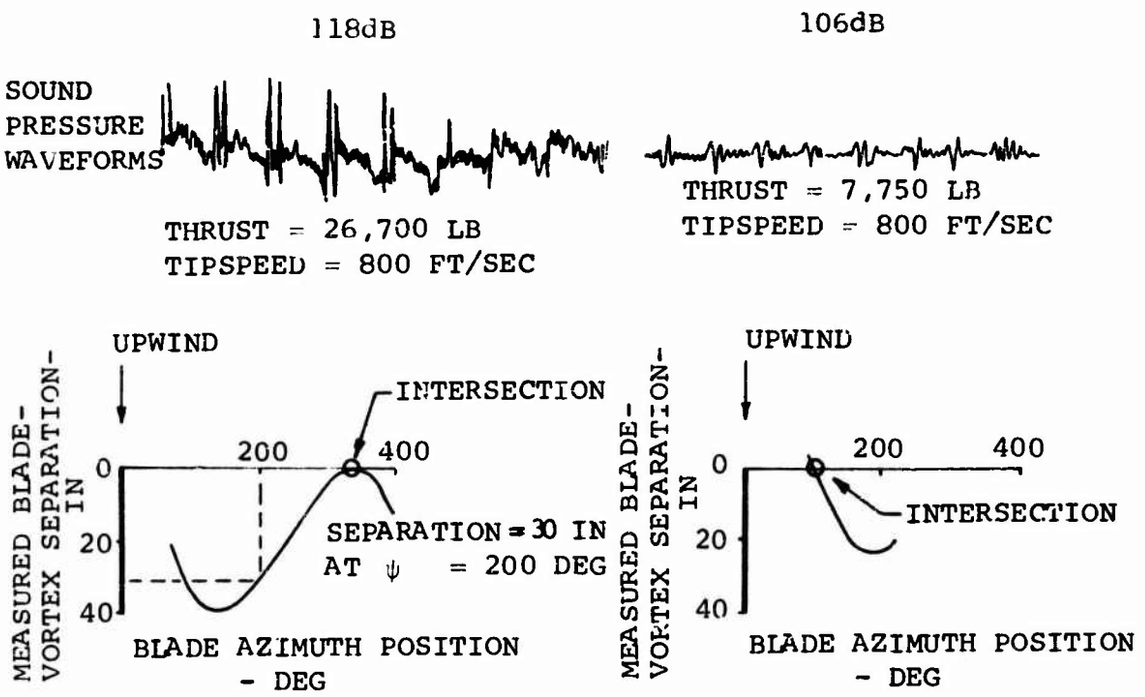

Studies of this transient noise phenomenon conducted under Boeing-funded aerodynamic research led to the examination of the aerodynamic conditions on the rotor blade at high loadings and high tipspeeds. As a result, a hypothesis was developed which states that the impulsive noise results from a combination of compressibility effects and blade-vortex interaction. At critical combinations of lift loadings and Mach number, strong shock waves exist on the blade airfoil near the tip. In recognition of this, the hypothesis states that it is the oscillation of this shock caused by a vortex intersection which generates the impulsive noise. Data from this program can contribute significantly to further research directed at testing this hypothesis.

Sound propagation of harmonics of rotor noise revealed occasionally strong interference of the wavefront reflected from the ground with the directly incident wavefronts. Corrections for this have been developed and show a significant influence on the measured data, particularly for the data which was recorded 3 diameters from the rotor center. This can be observed as a fluctuating decay of harmonic levels, at this microphone, in the data of Appendix B.

Foreword

This program was conducted in fulfillment of Contract DAHC04-69-C-0087 from the U.S. Army Research Office, Durham, North Carolina, under the technical cognizance of Dr. S. Kumar. The work was performed by the Boeing-Vertol Acoustics Staff between June 1969 and January 1971. Mr. R. F. Child, Supervisor of the Aerodynamics Research Staff, contributed the theory of impulsive rotor noise generation discussed in Section 4.4.

TABLE OF CONTENTS

LIST OF ILLUSTRATIONS

LIST OF TABLES

LIST OF SYMBOLS

A	disc area
A_b	blade area
a	attenuation coefficient
A, B	constants used in fitting curves to vortex separation data
AC	designation of data channel with standard frequency response characteristics
C_l	lift coefficient
C_t	thrust coefficient
db	decibel
j, k	point on vortex
K	plane through vortex
LF	designation of data channel with uniform low frequency response
M_t	tip Mach number
m	exponent of tipspeed
n	integer blade passage harmonic
p	pressure amplitude
q	dynamic pressure
R	radial position of vortex
r	distance from hub to microphone
rpm	rotor speed
S	blade vortex separation
SPL	sound pressure level
T	thrust
t	time

V_t	tipspeed
v	wind velocity
x,y,z	3-dimensional coordinates
z_o	tip path plane height
ε	angle (in K plane) used to obtain vortex measurements
ϕ	angle between tip located dipole axis and microphone
ψ	rotor azimuth $\psi = o$ = upwind

Section 1

Introduction

The noise of lifting rotors has come under increasing study in the past few years, particularly since rotary wing aircraft have been deployed to mobilize large portions of armed forces throughout the world. The role which rotor noise plays is vital in the areas of safety and survivability with regard to detection, and to communication and hearing damage with respect to internal noise. In addition, commercial helicopter operators have expressed a concern for improvements in rotor signatures when operations produce complaints about noise. In response to this, an increasing effort has been directed toward an understanding of the generation of rotor noise, although most investigations have frequently been directed toward the solution of a specific problem and often lacked a broad base of data for an adequate understanding. There have been several programs aimed at measurement of pressures on the surface of a rotor blade,[3, 4, 5] but they have been concerned mainly with performance of the rotor and have not gathered data with sufficient frequency response to be useful in noise research. For the most part this was due to the general unavailability of adequate instrumentation. Several programs have also been performed [6, 7] to collect noise data in the near and far field of the rotor and at several positions of rotor azimuth, although much of this data has been obtained on aircraft, and therefore also includes all the other noise sources inherent in a flight vehicle. In addition, smoke has been released at the tip of a blade to study the blade wake, in terms of the position of the tip vortex.[10] However, no published data currently exists in terms of a complete noise measurement program for adequate study of the generation and propagation of the noise of lifting rotors.

The concern with rotor noise, on the part of the military was strongly reflected by the action of the Army Research Office in sponsoring a conference with the National Academy of Engineers on July 30-31, 1968. The purpose of the conference was to assess the state of knowledge and understanding of the scientific and industrial community regarding this problem, and to recommend the areas of study which should be pursued in order to bring the rotor noise problem under adequate control.

Some of the major problems which were brought to light included:

- Inadequate airloads data in the rotating system.
- Lack of full frequency range sound pressure data.
- Lack of well defined conditions for which noise data in the fixed system was obtained.
- A requirement for blade wake geometry definition.

Without this information, there is no adequate input for improving rotor noise prediction, and certainly only superficial data exists for checking the validity of any prediction methods developed. In general, it appeared that in an effort to find rapid solutions to specific rotor noise problems, the important step of defining the basic problem had been bypassed.

In discussing helicopter rotor noise, various descriptions have appeared in the literature. These tend to categorize the noise either by the physical source or by the type of sound produced. Either terminology may be useful, depending on the context of the discussion.

Dealing with the sound descriptions first, the grouping simply divides those sounds which are not particularly impulsive in nature from those which are. This gives rise to terms such as "impulse", "bang" and "slap".

Classification of the noise by source leads, perhaps, to even more ambiguity. The non-impulsive sounds are generally termed rotational noise for those arising primarily from lifting (or thrusting) forces and vortex noise for those arising from drag and/or thickness.

Some researchers prefer to refer to the latter as drag, or wake noise in order to avoid confusion with some of the impulsive noises which are associated with tip vortices.

In the area of impulsive noise, the basic distinction is generally made between Mach number effects, otherwise called "high tip speed" or "compressibility" noise, and the noise which appears to occur when a rotor blade comes through, or near, a previously shed tip vortex. Here, no conveniently short terms are applied and one must settle for such descriptions as "blade vortex interaction"(or intersection) noise.

In view of the confusion in language, it is not too surprising that similar confusion exists with respect to correlation of analytical predictions with test results, especially if the analysis deals with one particular aspect of the problem while the data may arise from a combination of sources which may prove difficult, if not impossible, to separate.

The concept of the program described in this report was to attempt to clarify the situation (at least in part) by dealing with the simplest situation, namely a single hovering rotor, providing instrumentation adequate to the task of defining the complete acoustical signature, devising a test technique which would, insofar as possible, permit separate identification of the noise sources, and then to compare these results with current "state-of-the-art" analytical predictions in order to more accurately assess current capabilities and to identify the more serious shortcomings.

Section 2

Description of Test Procedure

2.1 ROTOR

The rotor system, tested in this program, is that designed for, and used on the U.S. Army CH-47B "Chinook" helicopter. Specifically, it is a three-bladed, fully articulated rotor of 30 feet radius and a 25.25 inch chord.

The individual rotor blades are fabricated of a steel leading edge "D" spar with fiberglass laminate covered trailing edge boxes. The airfoil is a cambered 23010-1.58 section as shown in Figure 1 and the blade is untapered in either planform or thickness. The tip of the blade terminates in a simple plate closing the end of the outboard box and therefore is termed a "square tip".

For the purpose of this investigation, the blade was modified by the addition of smoke generators at the tip.

The smoke generators had been developed previously and evolved in preparation for a flight test program on a CH-46A helicopter [10]. In the development program, requirements included a reliable system which could be ignited safely by a convenient means in a 600g environment, had a long-life, refillable casing, a burning rate which approached an explosion, and which produced sufficient smoke to be visible in two coils of the filament. The burned solids could not exceed 0.5 lb to prevent rotor imbalance. The generator which resulted, shown being installed in a blade tip in Figure 1, contained approximately 7 ounces of a granular material. The chemicals used in the burning process are proprietary to Steve Snyder Enterprises. A dual ignition system consisting of glass vial explosive squibs was selected for reliability, and the smoke color, which varied from white used against a blue sky to dark gray used for overcast conditions, was determined by the proportion of the two materials used and did not contain any dye which would have slowed the burning process. The total smoke produced was approximately 15 to 20 cubic feet. The generators required handling with reasonable precaution and were safe and generally reliable in operation.

2.2 WHIRL TOWER

Testing was conducted on the Boeing-Vertol Engineering Rotor Test Facility (Figure 2). The rotor hub on this tower is 50 ft. above the ground. It is powered by a 10,000 hp electric motor which drives through a water-cooled clutch. The electric drive, along with suitable gear reduction system, are housed in the massive concrete base of the structure. This base serves to minimize the drive system noise radiated outside to a level

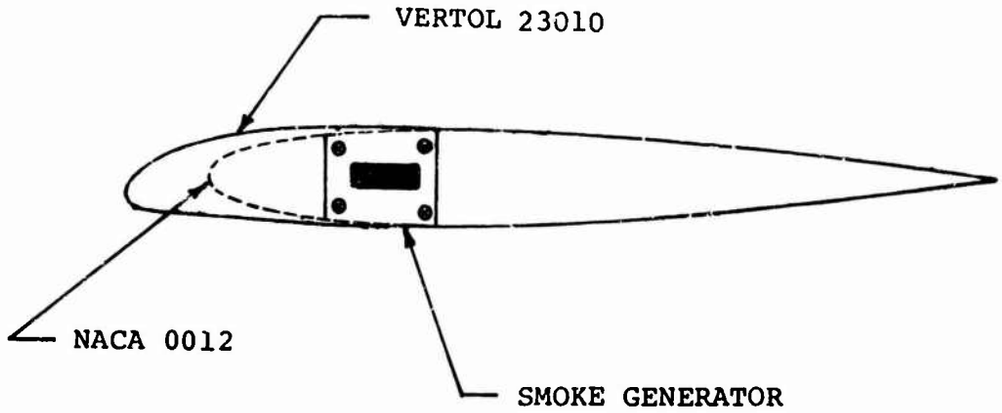

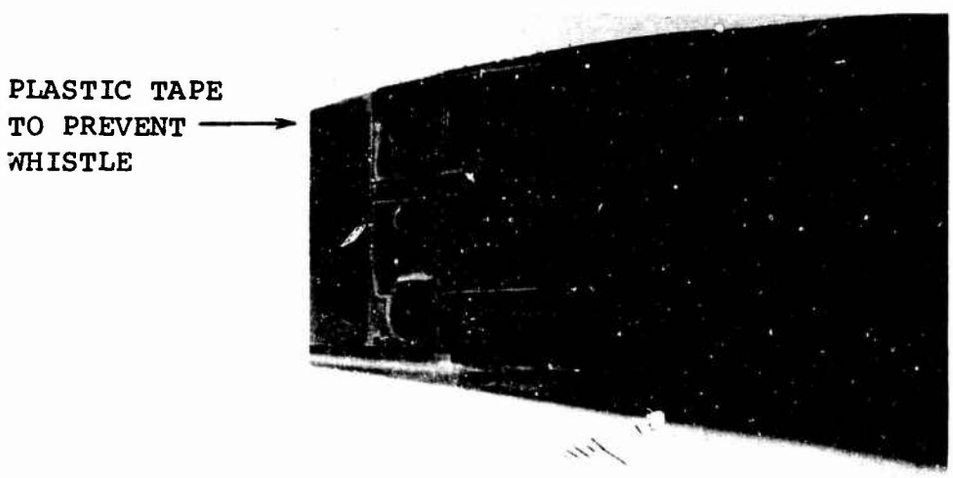

Figure 1. Test Airfoil Section and Smoke Generator Installation.

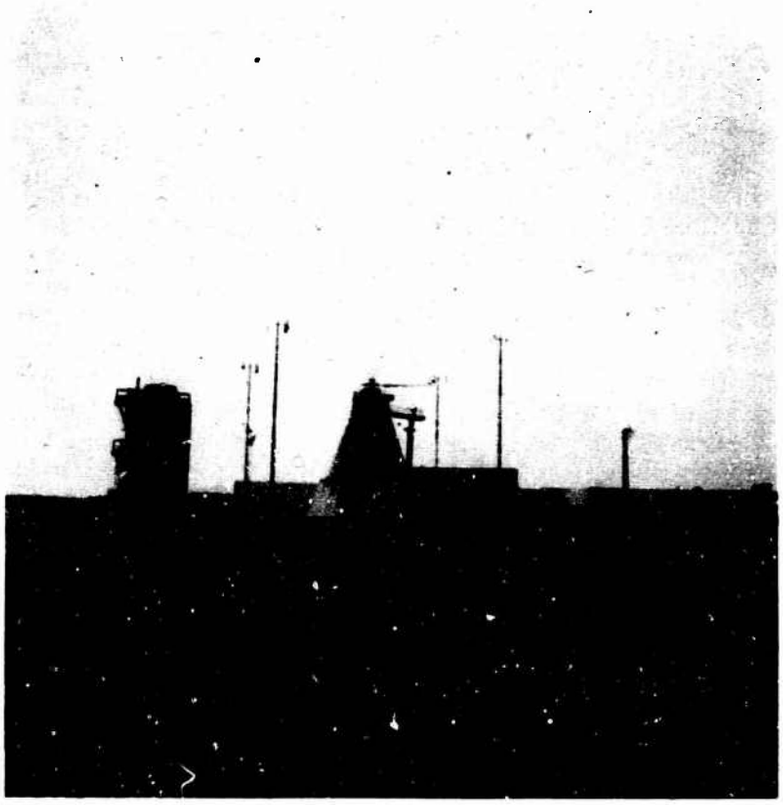

Figure 2. Engineering Whirl Tower.

which is negligible when making rotor noise measurements. The fundamental control modes available are simply rotor speed and thrust, through collective pitch. No cyclic pitch, or shaft angle variation, is available. Rotor rpm indication is directly available to the operator and can be maintained to an accuracy limited by variations in ambient wind, and generally within 1 rpm.

Rotor thrust is measured by two separate systems. The first is a set of four calibrated load cells at the rotor head. Since these are recorded independtnly on an oscillograph and require calculation to obtain thrust, the program is controlled by direct reading a motor torque. Through the use of a thrust-torque calibration which had been performed on a similar set of blades on the U.S. Air Force tower at the Aeronautical Systems Division, Air Force Systems Command, Wright Patterson AFB, Ohio, and by correcting for ambient temperature and pressure, torque values corresponding to the desired thrust values were calculated prior to each test run, and these torques were used to set up the test condition. The load cell data was obtained during the test run for more precise values in the final data. Pitch link loads, on each blade, were also recorded, and monitored, to ensure against excessive loads, instabilities, or operating too deeply into the blade stall regime.

2.3 ACOUSTICAL INSTRUMENTATION

The microphones used were all of the condenser type and were located as illustrated in Figure 3. The microphones designated 0.2R, 1R, 1D, 3D, 5D were used to acquire the primary data. As shown, they were supported by cables and arranged along a single ray line from just below the blade tip, to the ground. The direction chosen permitted a combination of a large distance without proximity to other buildings or structures and was generally upwind.

These microphones were especially selected for this program due to their unusually high sensitivity at low frequencies and flat frequency response characteristics. This is especially important for the study of rotational noise, whose fundamental frequency falls at blade passage period and may be below 10 Hz.

The specific equipment employed were Photocon 747 transducers with Dynagage DG-605D type signal conditioning.

Ideally, it would have been desirable to have several radial arrays of these low frequency microphones, each along a different azimuth direction. Since program limitations and equipment availability precluded such an extensive system, it was decided to provide four monitor systems located around the tower base as noted in Figure 3. These were Bruel and Kjaer Type 4131 condenser microphone systems of more conventional

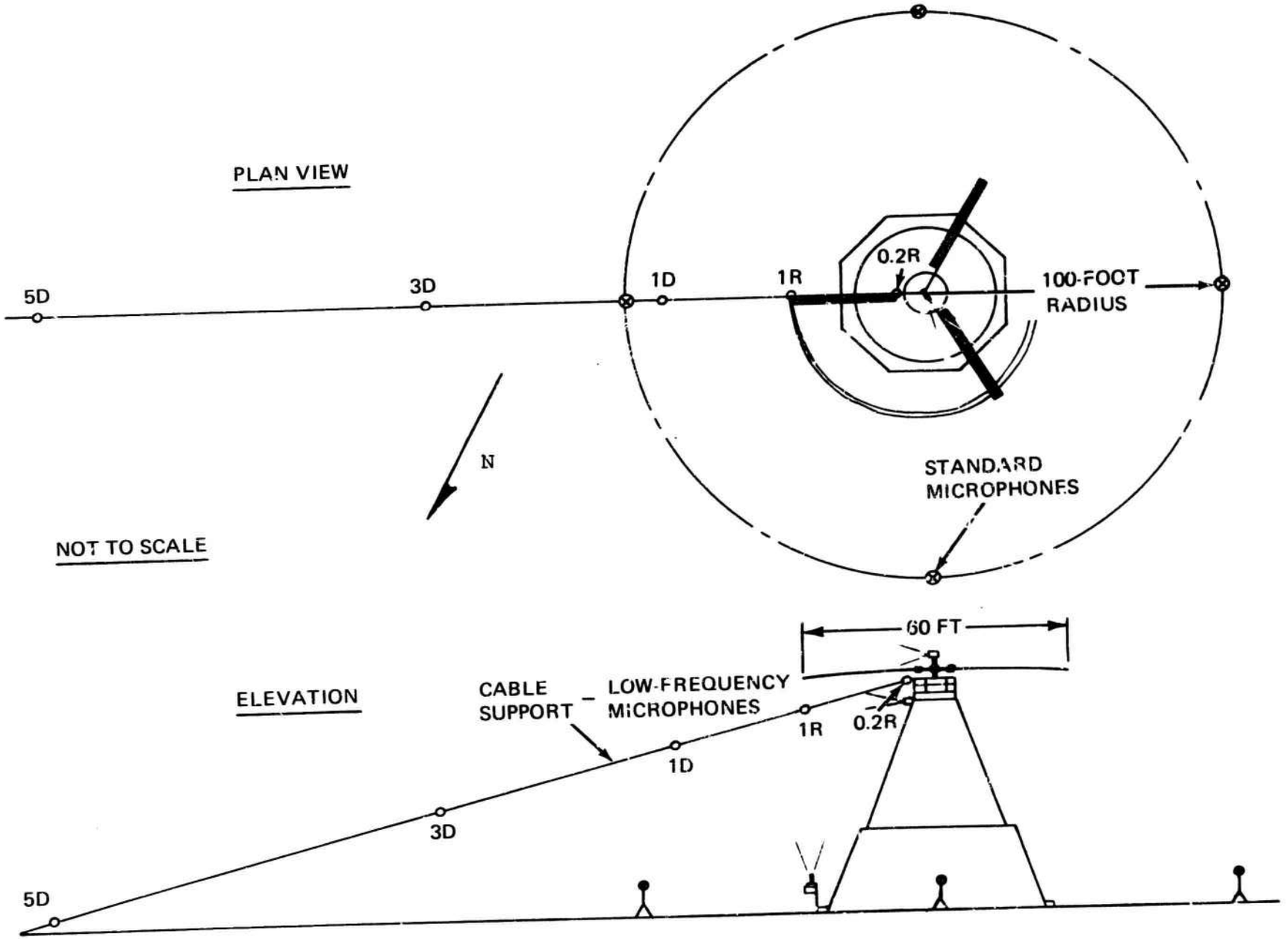

Figure 3. Microphone Array.

frequency range. In this program it was not intended that these microphones be used for primary data, but rather that this information be available so that in the event that any of the primary data should appear inconsistent, it would be possible to determine if a change in directivity of the radiated sound might be responsible.

2.3.1 Recording

The acoustical and atmospheric information was recorded on an Ampex FR-1300 wide band FM system operating at a tape speed of 30 ips. The acoustical inputs were continuously monitored on individual oscilloscopes to determine the required attenuation, or amplification in order to ensure optimum quality data with a high signal to noise ratio. The use of monitoring oscilloscopes also permits the engineer to observe noteworthy changes in noise characteristics as the test progresses. The Boeing-Vertol Mobile Acoustical Laboratory was used as a test control center for data acquisition. Figure 4 shows several views of the instrumentation employed.

2.3.2 Calibration

Prior to the test program each complete data system was calibrated. A system is defined as a combination of microphone transducer, cathode follower, all cables, signal conditioner, and tape recorder recording track. Once calibrated, the elements remained as a non-interchangeable system for the remainder of the program.

The pre-test calibration was a pistonphone and electrostatic actuator calibration in which a known pressure level is applied directly to the sensing element at all frequencies over the range of interest. The pretest calibration consisted of a frequency response of the complete microphone systems including transducer and signal conditioning. Instrumentation, traceable to the National Bureau of Standards through Boeing standards, included a Bruel and Kjaer calibration system consisting of a Type 1024 signal generator, a Type 4142 microphone calibration apparatus, a Type UA-0023 electrostatic actuator and graphic level recorder Type 2305. The signal generator and electrostatic actuator were swept over a frequency range of 20 Hz to 20 KHz. To avoid acoustical interference during the calibration, the electrostatic actuator signal was maintained more than 20 db above the ambient noise in the calibration room. Since the electrostatic actuator had a lower limiting frequency of 20 Hz, the low frequency calibration was obtained by taking the manufacturers calibration curve for the low frequency transducers (this was valid down to 0 Hz) and superimposing it on the calibration in the range where both were valid in order to extrapolate to the low frequency range. This assumes a low frequency linearity in the remainder of the system which, for the equipment used, should be valid. These calibration curves are shown

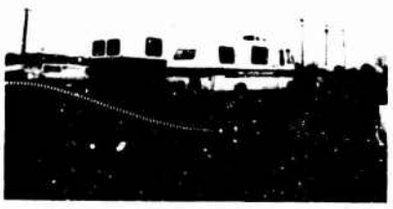

MOBILE LABORATORY
AND TAPE VAN

WEATHER INSTRUMENTS
IN MOBILE LAB

SMOKE INSTRUMENTATION

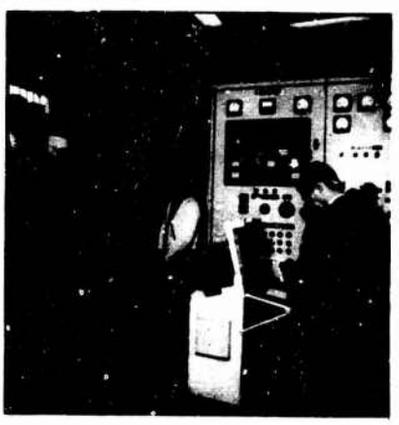

WHIRL TOWER
INSTRUMENTATION

Figure 4. Test Instrumentation.

in Figure 5.

A calibration of each system was performed in the field for a minimum of once each day. This procedure employed a B&K Type 4220 Pistonphone which applies a 124 db rms, 250 Hz signal at the microphone cartridge. By recording this signal on the same tape as the data, a constant check is kept on system sensitivity.

2.3.3 Atmospheric Conditions Monitoring

Since this was essentially a hover program, small changes in ambient wind conditions could become important. To monitor these, an anemometer and wind vane were erected on a 50 foot high mast approximately 150 ft. from the rotor tower. This located the instrumentation at the same height above the ground as the rotor, but kept it far enough away to be relatively unaffected by the rotor downwash. The output of the velocity indicator was recorded directly on the magnetic tape along with the sound pressure level data.

Ambient temperature and barometric pressure were measured at ground level but not recorded on tape. This data was used both to correlate with the acoustical information and for the tower torque/thrust calibration.

2.4 REVERBERATION EVALUATION

Prior to the test program, an evaluation was made to determine the effect, if any, of the tower structure, nearby buildings, and the terrain itself on the acoustical signals sensed by the microphones.

The evaluation was performed by firing blank cartridges from several points at the top of the tower and recording the signal on all microphones. Acoustical reflections would then be indicated by multiple signals at the sensors, by distorted waveforms, or by failure to follow an orderly decrease in signal strength with distance from the source.

2.5 PHOTOGRAPHIC INSTRUMENTATION

Smoke generators were ignited in the blade tips to mark the vortex. High speed motion pictures were taken of the smoke. Two cameras (see Figure 6) were placed on the tower, one looking out from just under the rotor (Camera H) and one looking up from the ground (Camera V). These two cameras provided vortex position measurements at one azimuth. Two additional cameras were mounted in the rotating system to measure the separation between the vortex and the blade which follows the vortex generating blade. Table I describes these cameras.

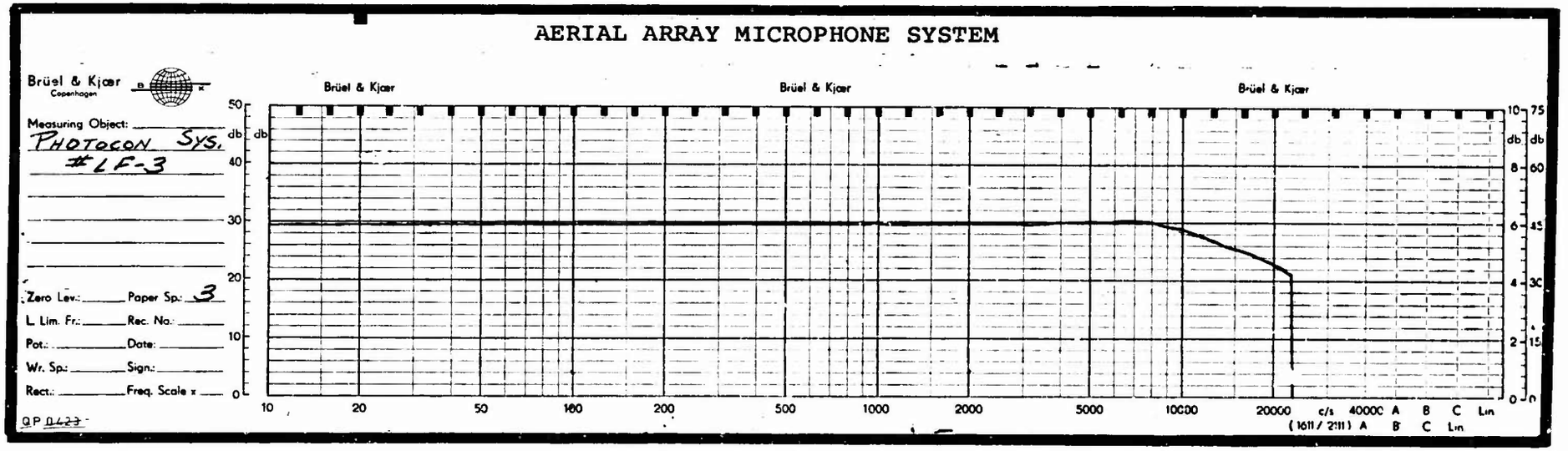

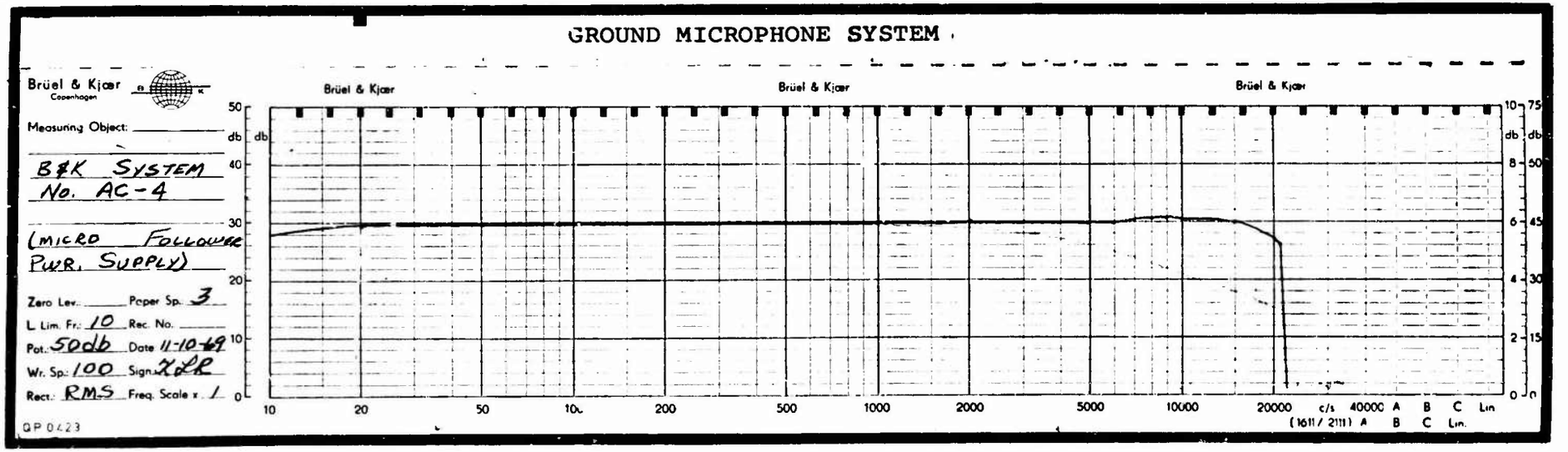

Figure 5. Acoustical System Calibrations.

CAMERA H

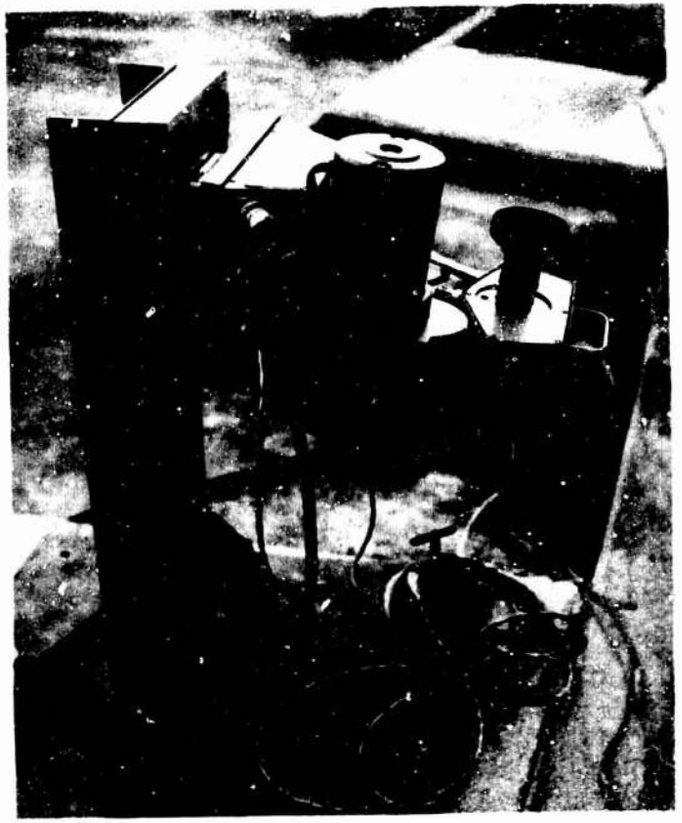

CAMERA V

Figure 6. Camera Installation.

TABLE I

DESCRIPTION OF CAMERAS

Camera	Make	Model	Size	Speed Units	Focal Length
H (Horizontal)	Red Lake Lab.	HI CAM	16 mm	1600 fps	10 mm
V (Vertical)	Red Lake Lab.	HI CAM	16 mm	400	10 mm
Rotating 1	Milliken	DBM	16 mm	400	10 mm
Rotating 2	Milliken	DBM	16 mm	400	10 mm

In order to measure the films for vortex position, camera positions and orientations were needed. Two cable grids with ping-pong balls securely attached for the targets were used as shown in Figure 7. This grid, visible from Camera H and the rotating cameras, was positioned on the four flood light standards surrounding the tower. The other grid was composed of two cables strung from the top of the tower to the ground so that the targets were visible from Camera V. Measuring the images of the targets and combining those measurements with knowledge of the camera positions and the target positions, produced the desired camera orientations. Data was read using a Benson Lehner Oscar N data reader. Camera positions were measured, and camera orientations were then established by photographing a grid of targets placed at known locations in the field. A detailed description of this procedure is presented in Appendix A.

2.6 TEST PROCEDURE

The control of the rotor tower was such that the most expedient method of testing was to perform thrust variations at fixed rotor speeds, and most data was taken in this manner. A stabilized operating condition was established prior to the start of each data point and a minimum of 30 seconds of acoustical data was obtained at each point.

For those runs where smoke visualization instrumentation was employed, the start of the acoustical record preceded ignition of the smoke generator and continued until all visible smoke had dissipated. Separate signals on the acoustical data tape were initiated by the start of the camera motors and by the firing of the smoke generators. Figure 8 illustrates a typical data sequence. Figure 9 and Table IV show the thrust, tip speed matrix of all data points obtained. The matrix was limited only by tower capability, blade strength, and/or entry into blade stall.

ELEVATION VIEW

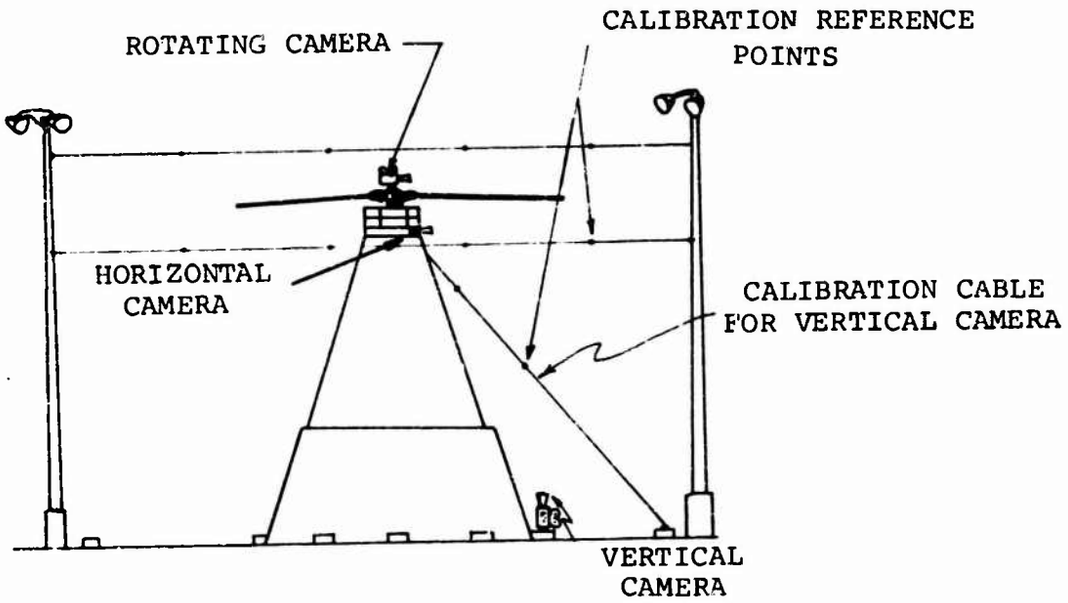

VIEW FROM HORIZONTAL CAMERA

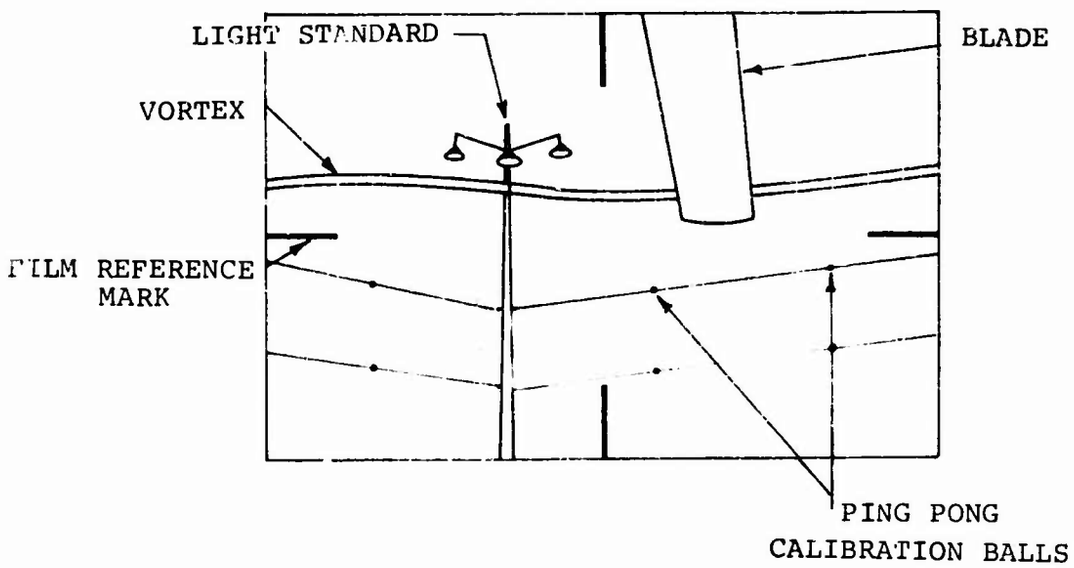

Figure 7. Camera and Calibration Grid Locations.

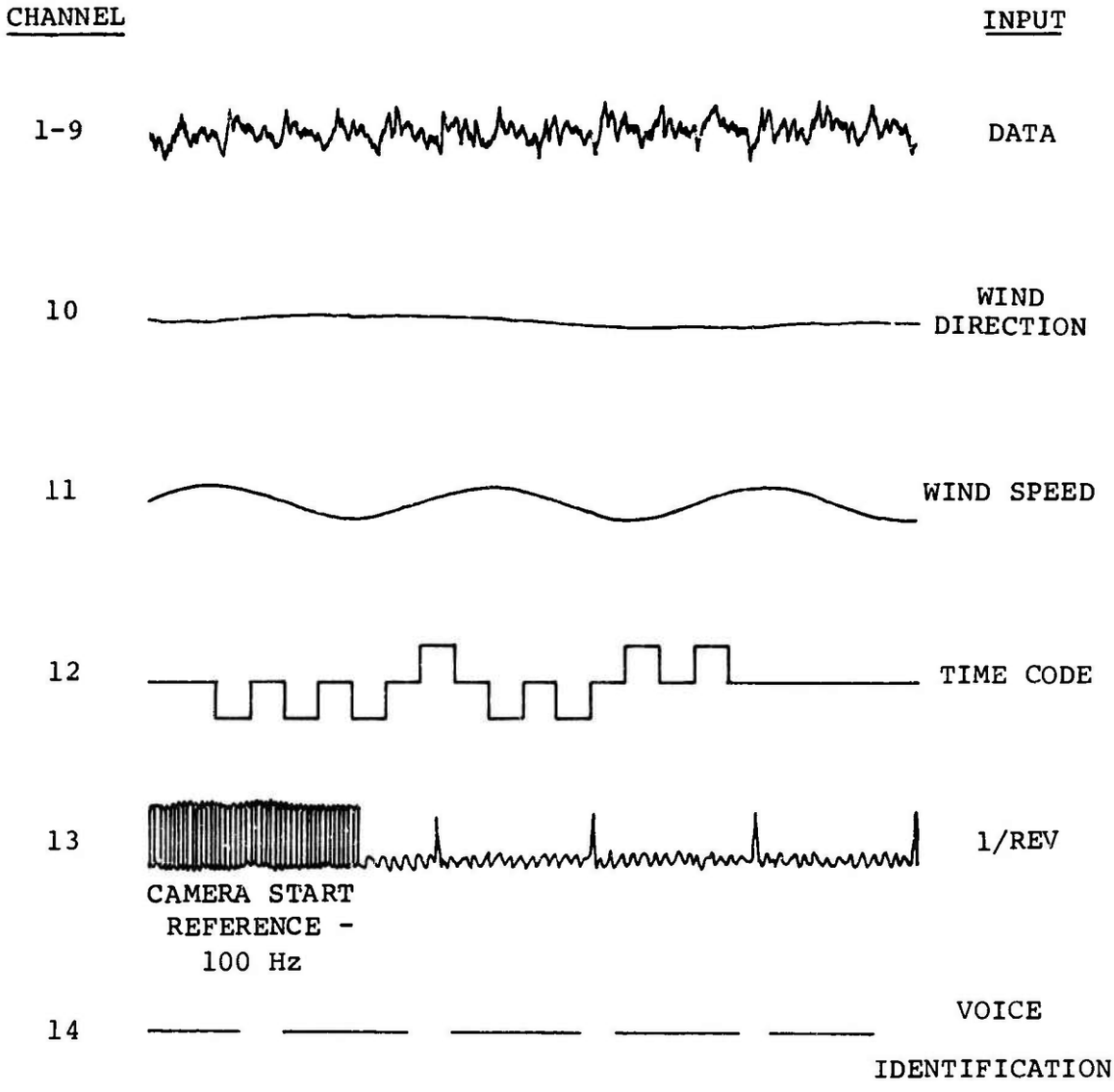

Figure 8. Data Sequence Time History.

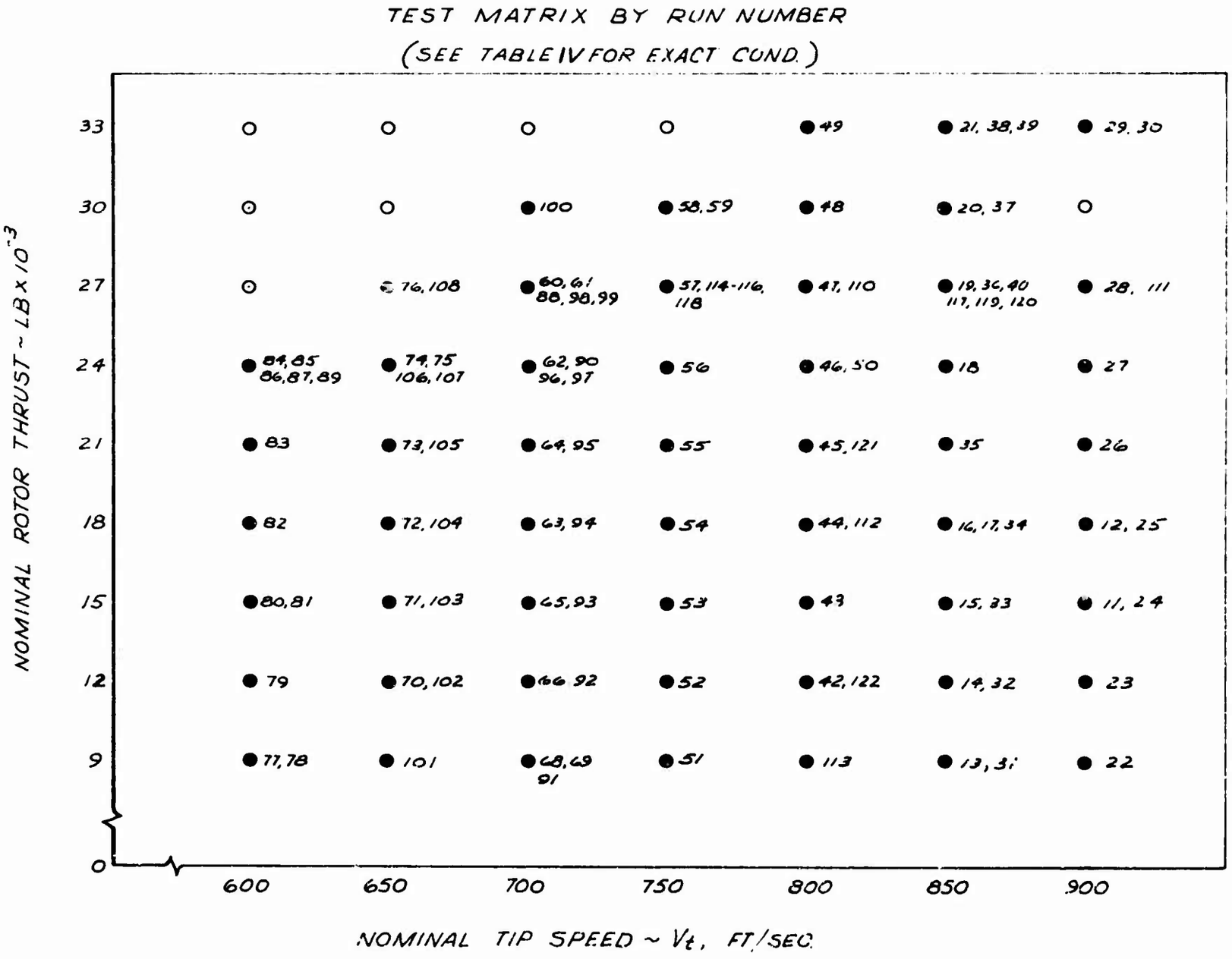

Figure 9. Test Matrix.

Section 3

Data Reduction

3.1 ACOUSTICAL DATA

The primary analysis used for the reduction of the acoustical data employed techniques and equipment referred to as Real Time Digital Analysis. Application of this relatively new technique to the study of rotor noise is believed to be one of the major innovations of this program.

In order to interpret correctly the results, it is important to understand the fundamental concepts of the analysis and its application and limitations with respect to rotor noise data. Fundamentally, the recorded analog signal is continuously digitized at a high rate and is processed in the digital mode. Since it is in a digital form, it may be stored in a memory, for detailed study, and/or operated on by various computational techniques. As with most acoustical information, the data may be studied in two primary manners. The first is the time domain, or pressure-time history of the waveform and the second is the frequency domain, often referred to as amplitude-frequency spectrum.

Before discussing the detailed application of the processing to rotor noise data, it will be helpful to characterize some aspects of rotor noise and to agree on convenient terminology. First of all, it is important to recognize that any real data, even low wind hover, will display many transient changes due to uncontrollable variables. These may be minor in nature, or as will be described in the Discussion of Results, may be so large that they completely dominate the acoustical signature. For many purposes, especially when comparing data with analytical predictions, it is important to know if the data under discussion is invarient with time or contains the aforementioned transients. In this report, all data will be defined either as "steady state", implying that it is valid at any time, or as "transient", implying that it is only valid at a particular instant in time.

A second set of definitions which apply to the frequency (rather than the time) domain are the terms discrete and broadband which describe the amplitude frequency distribution. There is no rigorous definition of discrete but it can be easily understood that it implies a concentration of acoustical energy in a rather narrow range such that the levels at adjacent higher and lower frequencies are significantly less. It should be kept in mind that these discrete frequencies may be harmonically related to the rotor passage, (and to each other) or may be independent if produced by a non-harmonic source.

The term broadband noise implies an absence of discrete frequencies and, therefore, an amplitude-frequency spectrum envelope which is free from sharp peaks. The envelope of broadband noise may, however, be gradually and continuously shaped such that one frequency range is higher than another.

3.1.1 Time Domain Analysis

Time domain analysis was performed using a Federal Scientific 129H Signal Averager. In its operation, the input consists of the acoustical data and a trigger pulse at once per rotor revolution which was generated by a transducer at the rotor tower.

In its simplest mode of operation, the averager, upon initiation of a starting signal, will accept and digitize the next full rotor cycle (between trigger pulses) and retain it in memory for display or further operation. In this program the display was on an oscilloscope screen and photographed for retention.

In order to obtain a steady state waveform representative of the entire test condition, the averager may be instructed to admit a specific number of rotor cycles and to sum them, with precise phasing, in the memory prior to display. In this manner, any elements which are random in the time pattern will tend to cancel each other out, those which are highly repetitive will reinforce each other, and levels which are transient will have little effect, provided enough cycles are employed. In analyzing the rotor noise, 128 cycles were included in each summation. If transient waveforms are desired, the number of cycles selected for summation can be reduced to as low as one. Here it becomes important to carefully time edit the data in order to ensure capturing the moment of interest.

3.1.2 Frequency Domain Analysis

Frequency Analysis was performed using a Federal Scientific UA-6 "Ubiquitious" Analyzer. When working in the frequency domain, similar principles apply except that the sweep rate and resolution are functions of the frequency range selected. The data analysis procedure employed in this program provided a resolution of 1 Hz and produced approximately one spectrum per second. Steady state spectra consisted of summing thirty-two sweeps.

In studying transient spectra, the maximum harmonic amplitudes are generally of greatest interest. A simple method of capturing this information is to open the lens of the oscilloscope camera and take a time exposure which then superimposes all the individual spectra analyzed during the run. Figure 10 illustrates averaged and non-averaged waveforms and spectra for

AVERAGED

UNAVERAGED

SPECTRA

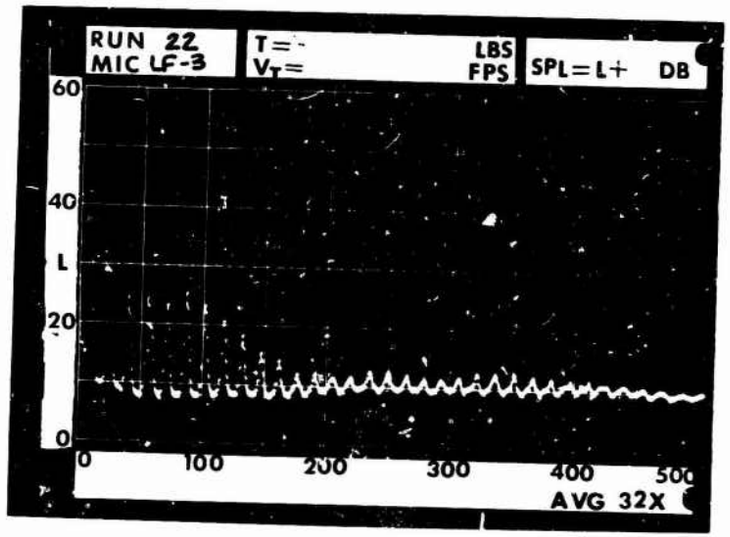

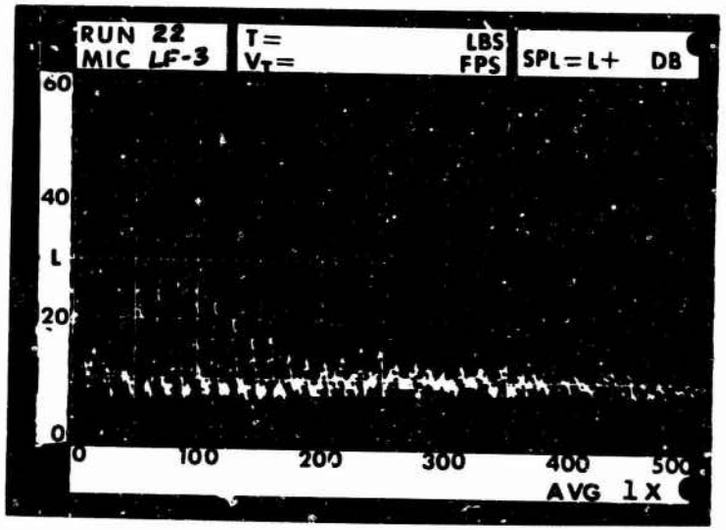

WAVEFORM

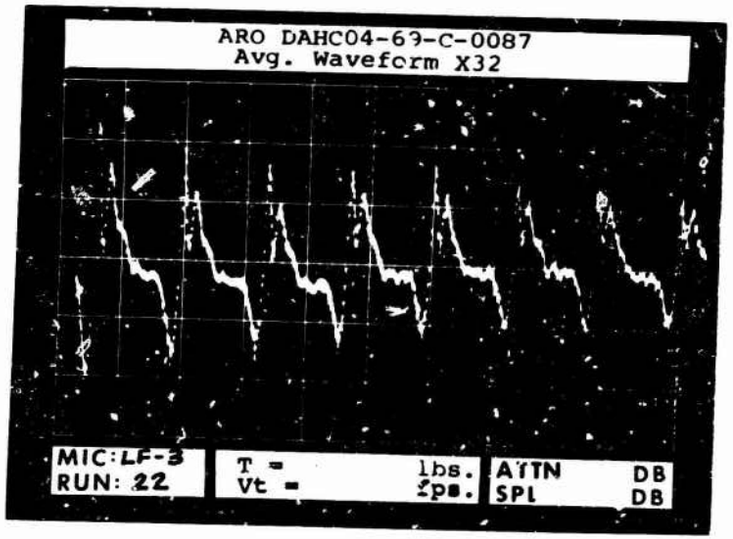

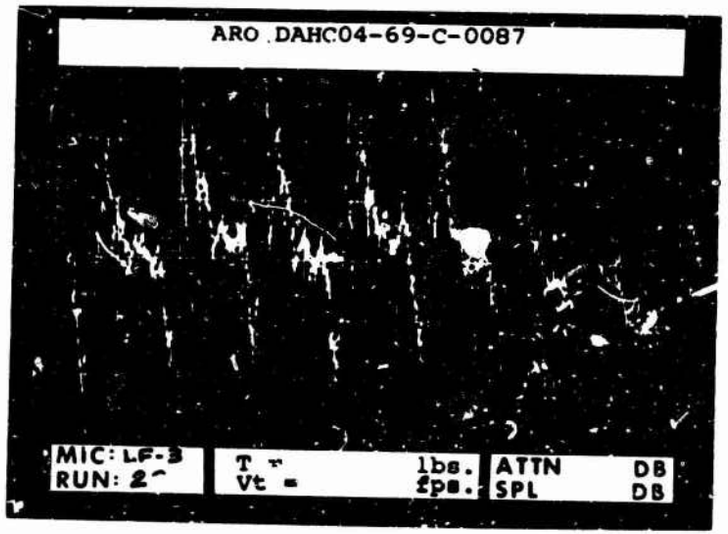

Figure 10. Comparison of Averaged and Unaveraged Spectra Waveforms.

steady-state and transient conditions.

In this program, steady state harmonic analyses were used for comparison with analytical predictions while transient analysis was used to study tip vortex induced noise phenomena. In order to compare the broadband vortex noise with analytical prediction, conventional octave band analyses were performed using analog equipment (B&K 2112 Spectrum Analyzer and B&K 2305 Level Recorder). This method was used because the prediction method is essentially a statistical matching of data, analyzed in this manner, with blade operating parameters. Introduction of an analyzer with substantilly different frequency response characteristics, therefore, requires a further correction.

3.2 PHOTOGRAPHIC DATA

The detailed methodology for measuring blade-vortex separations from motion picture film is given in Appendix A. The following is a general description of the procedure.

3.2.1 Stationary Cameras

In order to find the position of a point in space using two cameras, the method of triangulation could be used. However, this method cannot be used on a curve such as the vortex. Figure 11 illustrates the arrangement.

The difficulty arises because any point chosen on the vortex, j, as viewed by Camera H is not readily found in the picture from from Camera V. In fact, a point chosen from Camera V, for instance, k, could be anywhere along the vortex.

In order to surmount this problem, the plane K, defined by the y_y axis and $\overline{Vk}$, is constructed. I, the point of intersection between $\overline{HIj}$ and plane K, is found. Thus the angle εjk between $\overline{VI}$ and $\overline{Vk}$ can be found. Now εjk is a measure of how far k is from j; when $\varepsilon jk = 0$, j and k are the same point.

Thus in order to find the coordinates of j, any point on the vortex seen from Camera H, it is only necessary to move k along the vortex until $\varepsilon jk = 0$. j and k will then be the same point and its coordinates can be found by triangulation.

In order to do this using the high speed movie film on this program, two prerequisites must be met:

(1) frame pairs must be chosen consisting of one frame from each camera taken simultaneously.

(2) in order to find the lines $\overline{Vk}$ and $\overline{Hj}$, camera positions and orientations must be known.

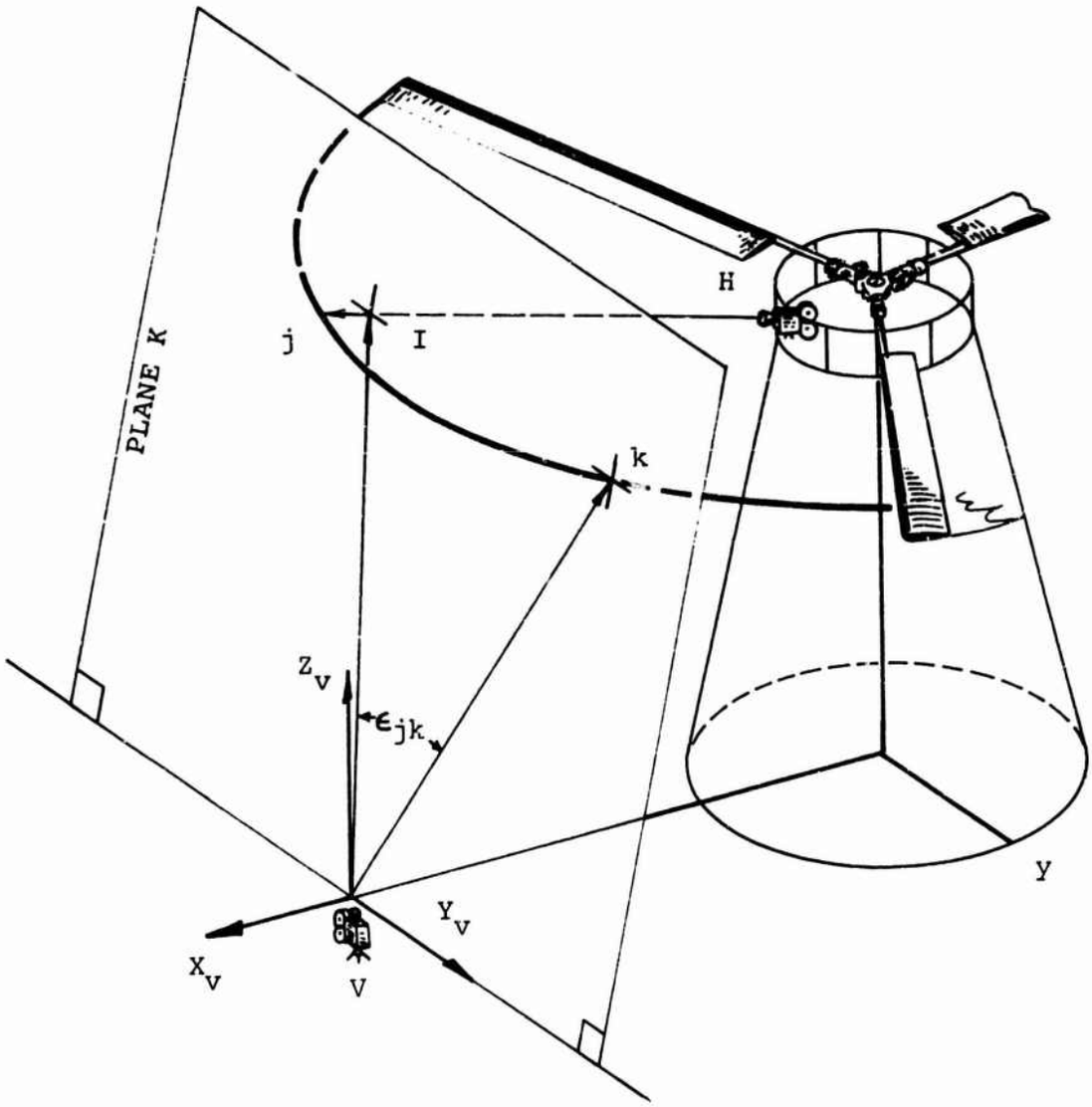

Figure 11. Schematic for Analyzing Stationary Camera Data.

In order to obtain frame pairs whose exposures were taken simultaneously, first, frames were chosen from Camera V. Then blade tip positions were measured on the photographs. Using these measurements along with the camera orientations and positions, the blade azimuth could be calculated for frames from each camera. Thus, azimuth was determined as a function of frame number. The frame from Camera H, which came closest in azimuth to each frame from Camera V, was found. Since Camera V was photographing 1600 frames/second, the longest time that could have elapsed between the two exposures, one from Camera V and one from Camera H, is half the time between frames on Camera H or 1/3200th seconds. This is a short enough time that the two frames can be considered to have been taken simultaneously.

Camera orientations were obtained from the film taken of the calibration grid. Camera positions were known from a previous survey and camera orientations were determined by measuring the target positions on the film.

Using the above method measurements were made of the vortex position from frame pairs chosen at intervals commencing with a pair showing the vortex generating blade and ending when the smoke was no longer visible from one of the cameras. Figures 12 through 18 show the results of these measurements.

The separation between the blade and the vortex generated by the preceding blade was found by subtracting the measured blade vertical position from the measured vortex vertical position when the blade was in the field of view of the stationary cameras. Thus the measurements from the stationary cameras provided accurate vortex trajectory measurements and separations at only a limited range of azimuths, $\sim 25^{o}$, because of the limited field of view of the horizontal camera.

3.2.2 Rotating Camera Measurements

In order to surmount the problem of limited field of view, two cameras were mounted on the hub. The cameras were positioned as shown in Figure 19. From these cameras, the vortex positions could be found around the entire azimuth for a constant vortex age.

The rotating cameras were calibrated by photographing the calibration targets when the rotor was stationary. Combining the measured positions of the balls on the film with the known ball positions in the field produced the orientation of the camera. Thus, measuring the image positions from the film, the directions to the vortex and the blade were determined. In order to find the vertical position of the vortex, however, the distance from the camera to the vortex must be known.

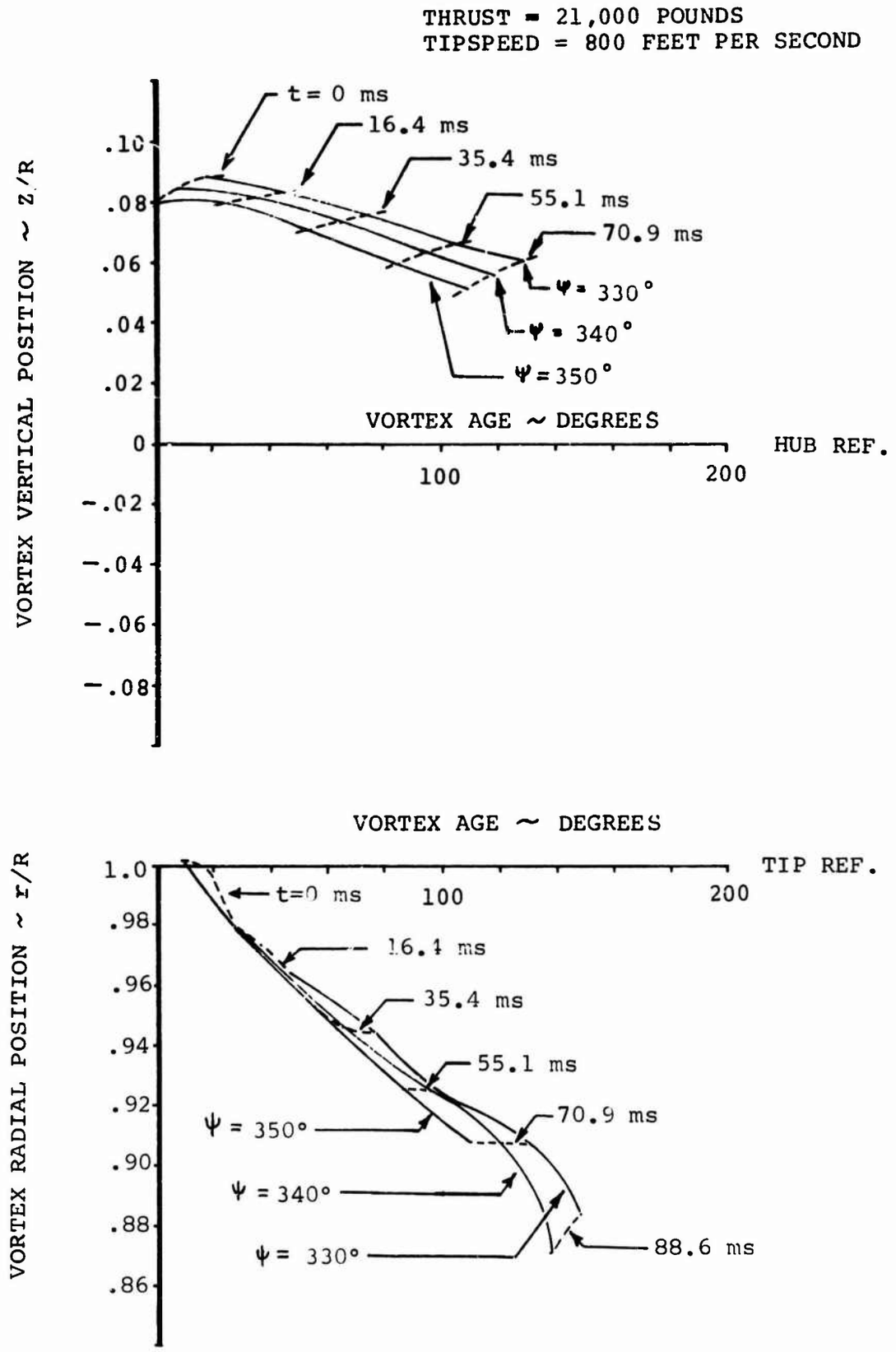

Figure 12. Vortex Position Measurements, Run 121.

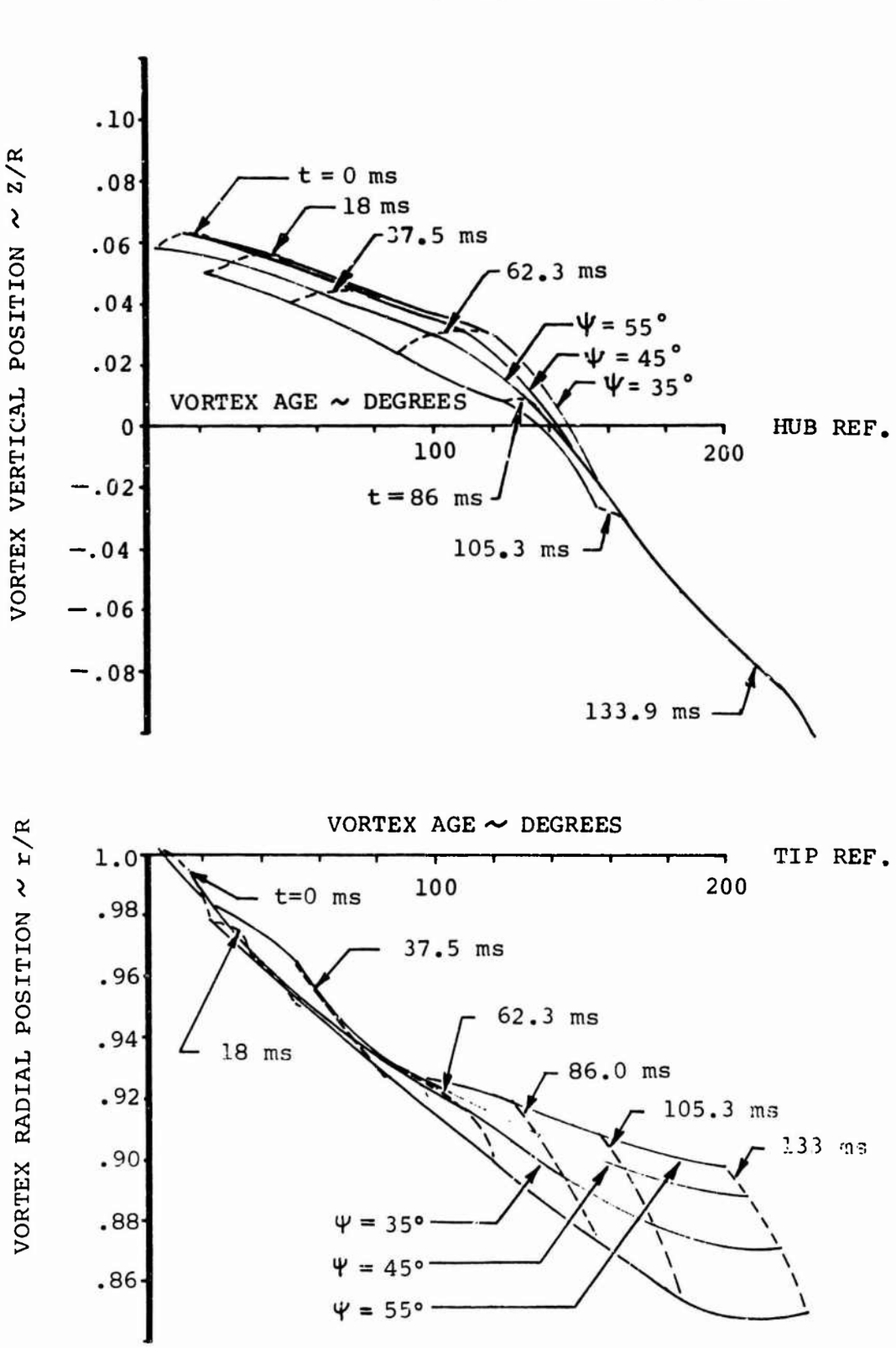

Figure 13. Vortex Position Measurements, Run 112.

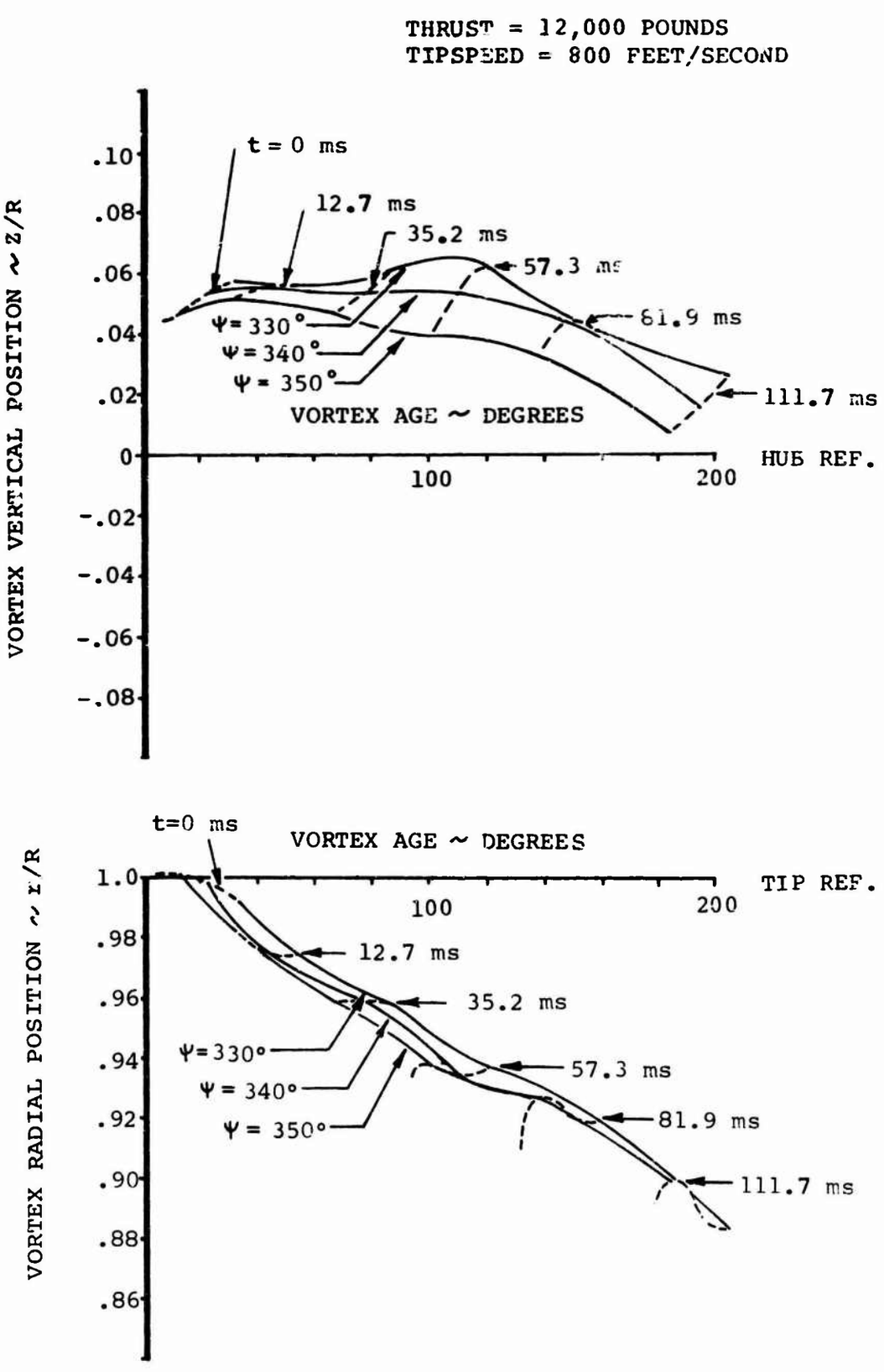

Figure 14. Vortex Position Measurements, Run 122.

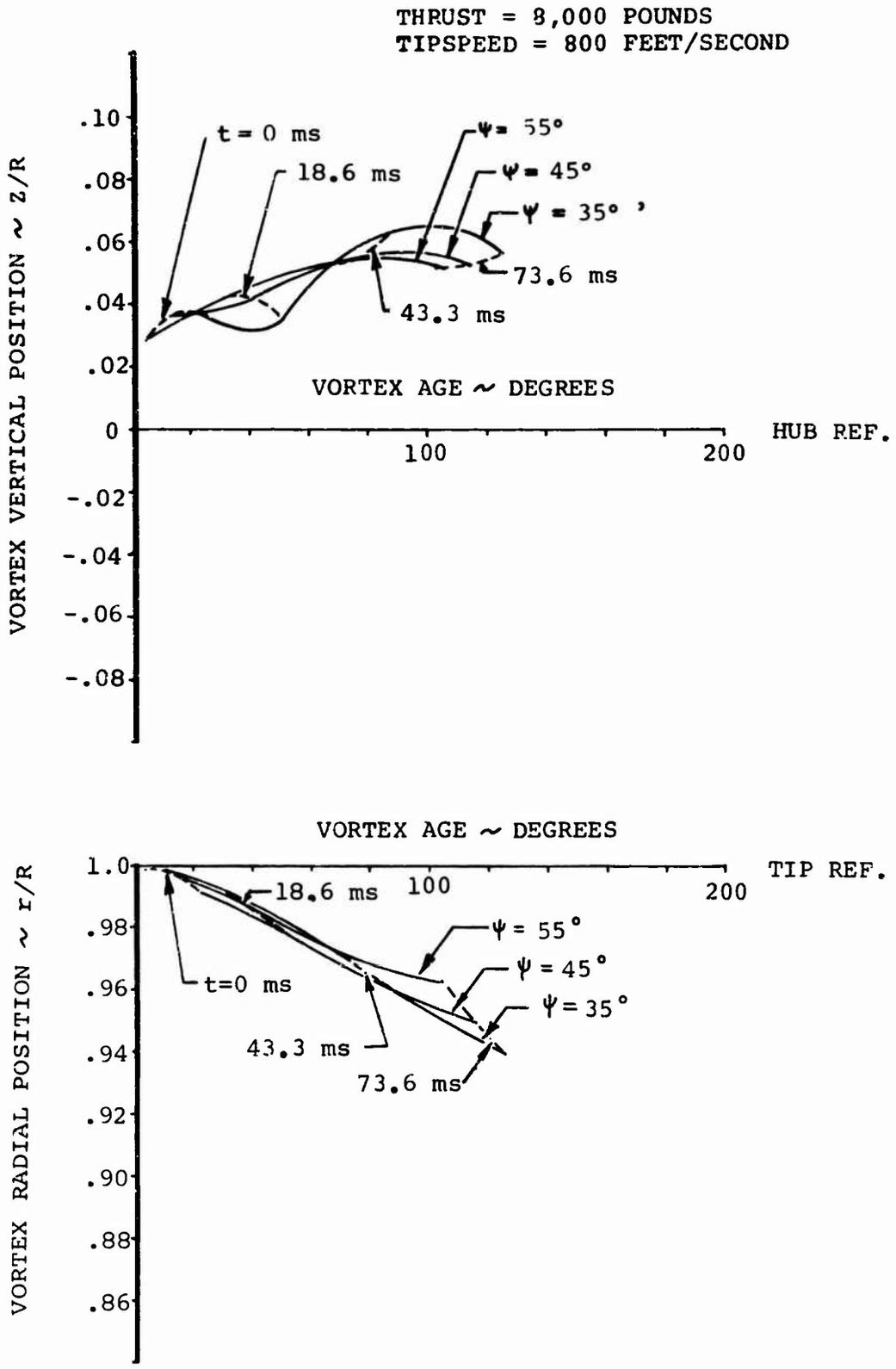

Figure 15. Vortex Position Measurements, Run 113.

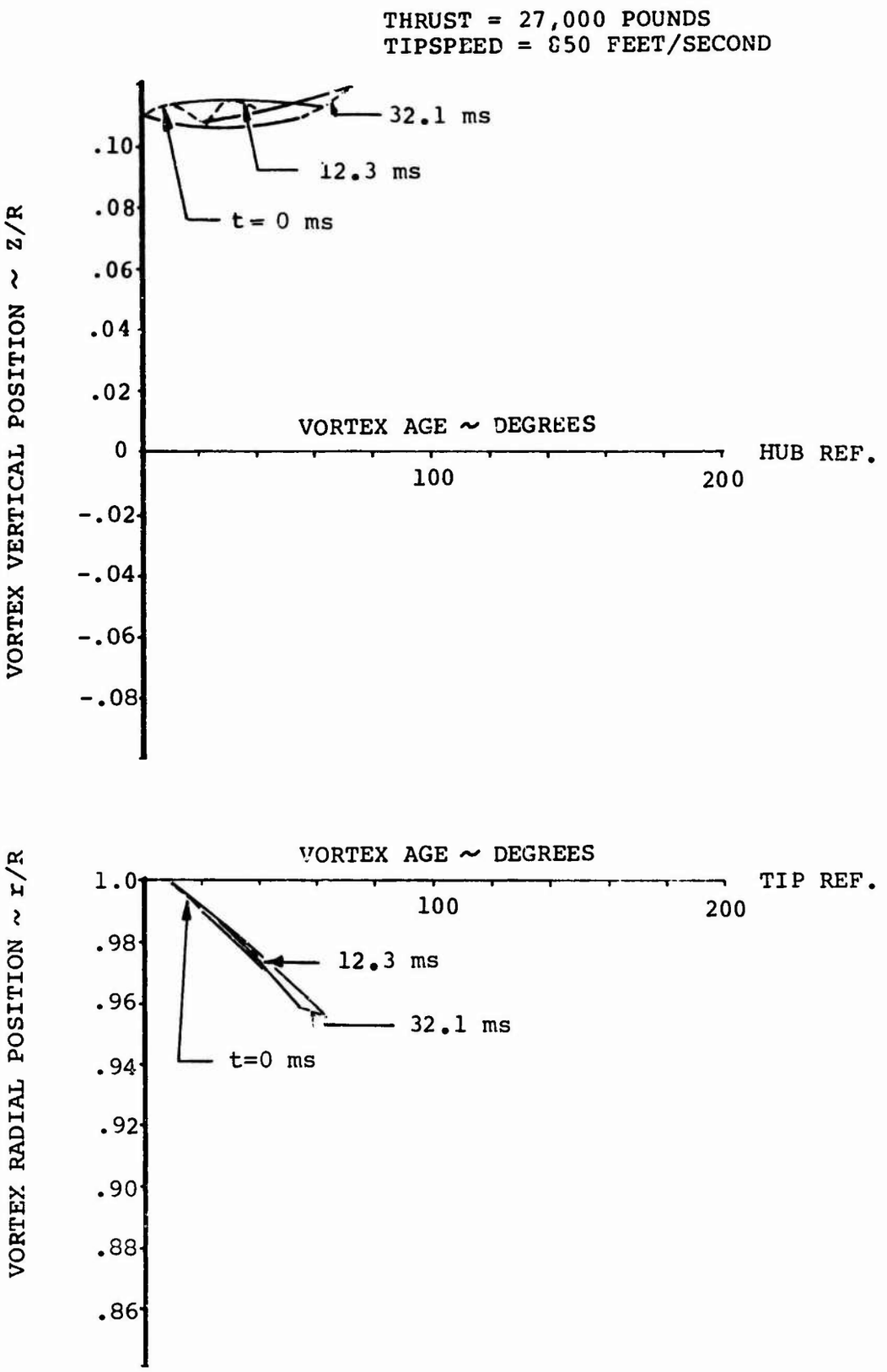

Figure 16. Vortex Position Measurements, Run 120.

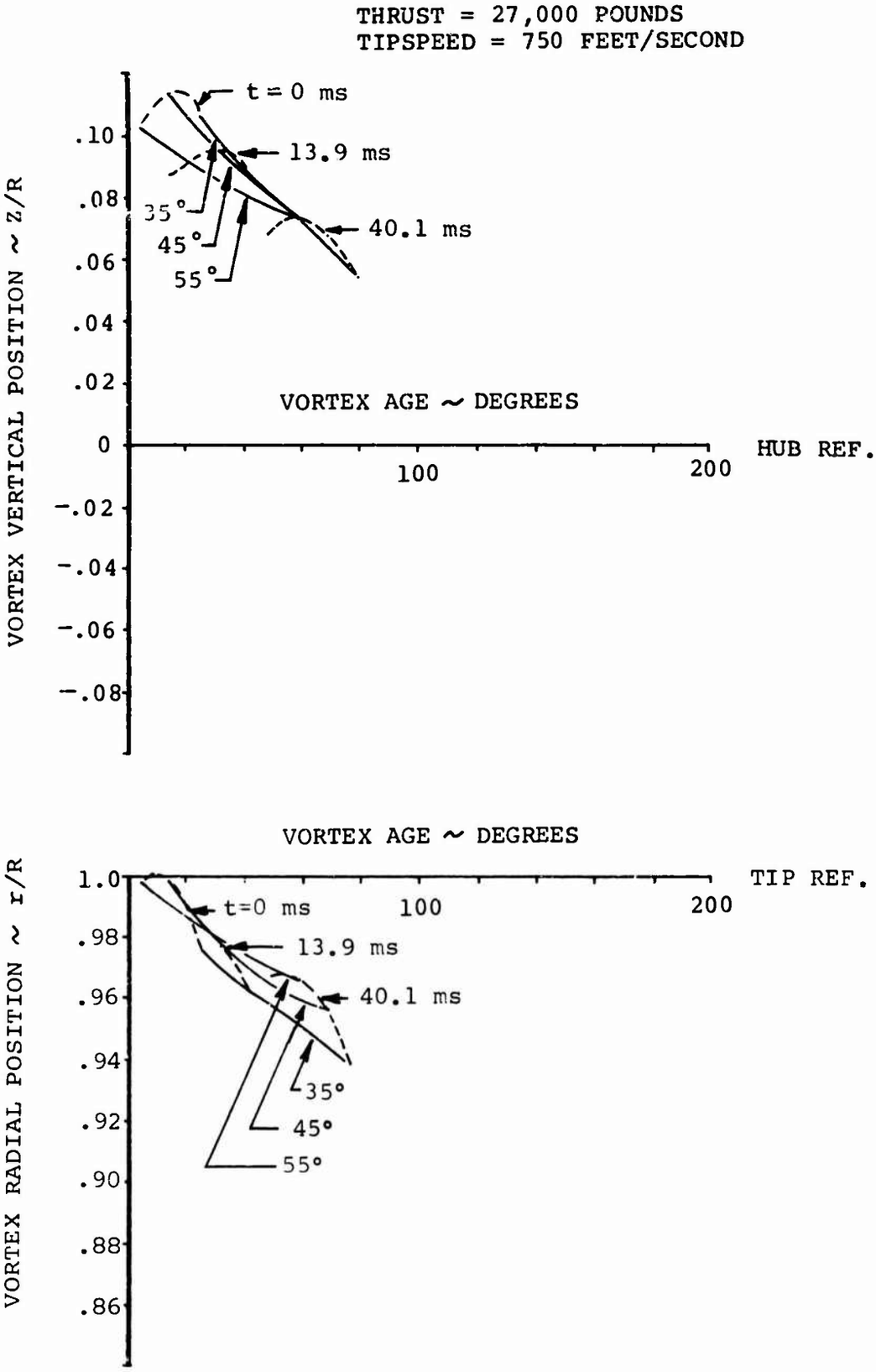

Figure 17. Vortex Position Measurements, Run 116.

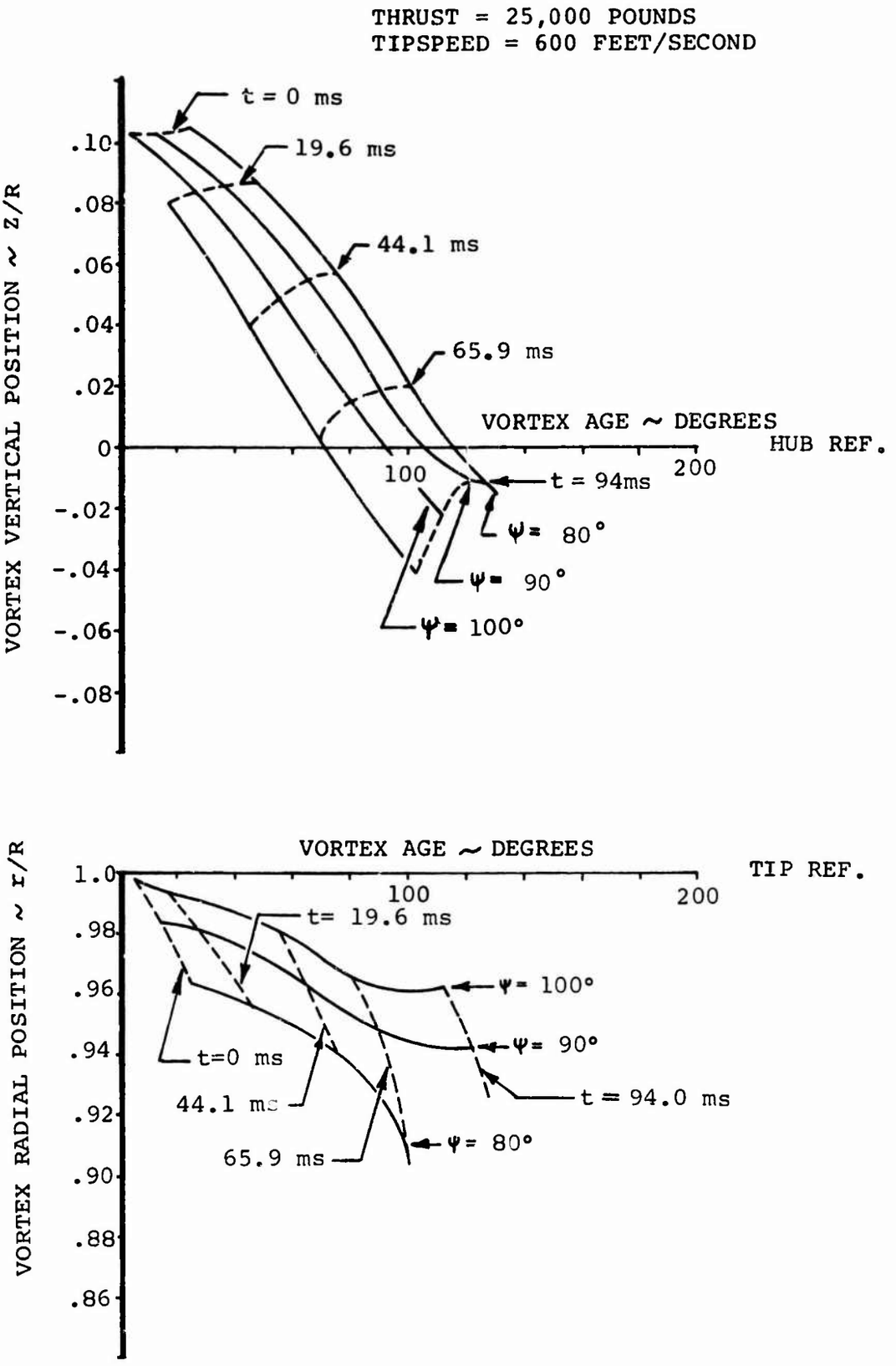

Figure 18. Vortex Position Measurements, Run 89.

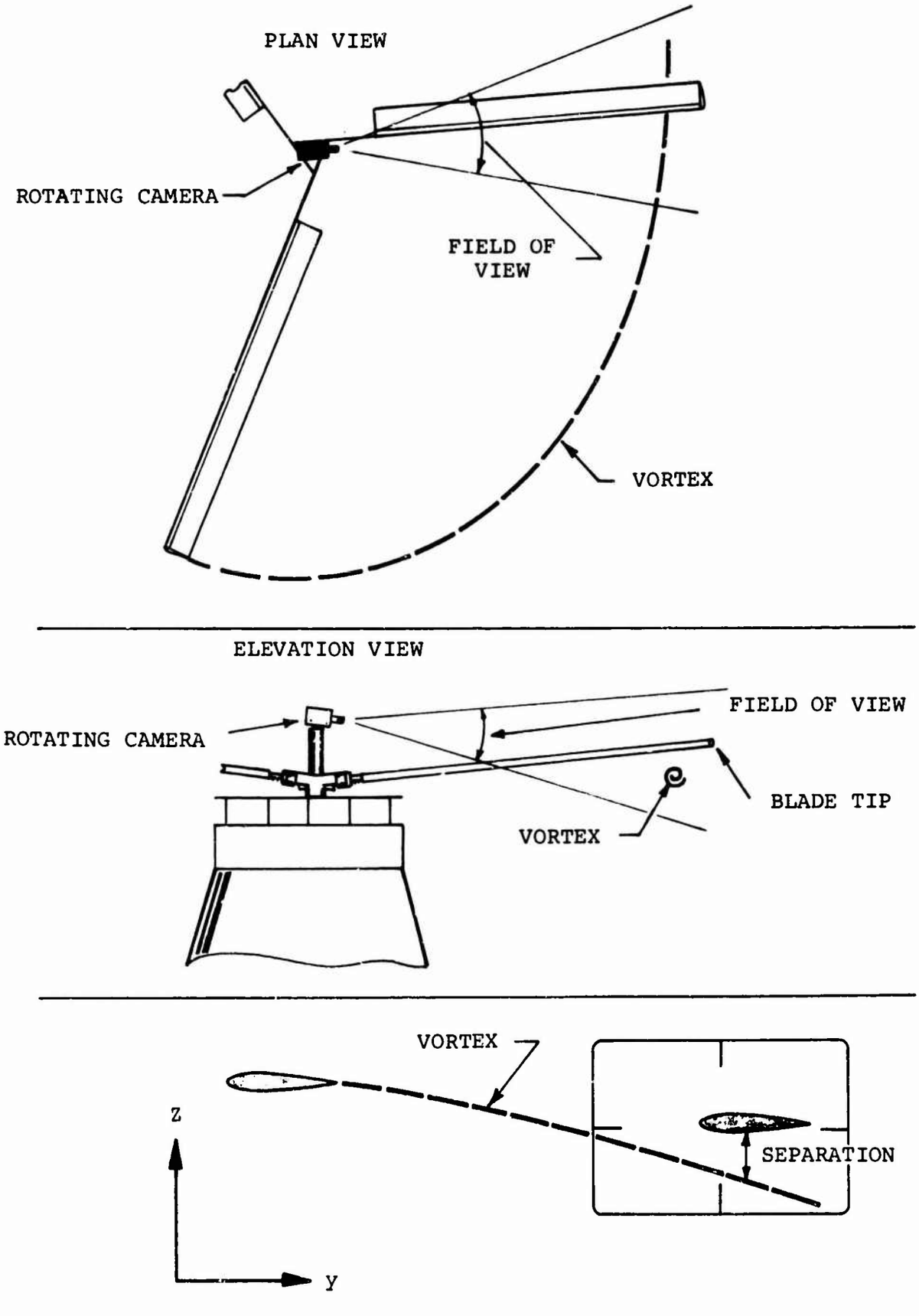

Figure 19. Rotating Camera Position.

An appropriate measure of the radial position of the vortex at the vortex age desired was derived from the stationary system measurements. By assuming that the horizontal position of the vortex is defined by the superposition of contraction and wind:

$$R = R_{contraction} - v \cdot t \cdot \cos \psi$$

where:

R = radius of the vortex at any azimuth, ψ

$R_{contraction}$ = radius of the vortex when there is no wind

v = wind velocity

t = time corresponding to vortex age

ψ = azimuth of vortex, $\psi = 0$ = upwind

The wind velocity and direction were recorded in the field. The only unknown factor was $R_{contraction}$. It was found from the stationary camera measurements by:

$$R_{contraction} = R_{measured} + v \cdot t \cdot \cos (\psi \text{ stationary cameras})$$

For runs where stationary camera measurements were available, trend curves were plotted and $R_{contraction}$ was interpolated from them. Fortunately, the desired accuracy was not prohibitive. In order to have 5% accuracy in the vertical position, the radius of the vortex must only be known to within $.05R_o$ or 18". Discussion of the application of these procedures is found in Section 4.4.3.

Section 4

Discussion of Results

4.1 NOISE GENERATION - TERMINOLOGY

Section 3.1 defined a set of general terminology which can be used to describe acoustical data. In order to apply these definitions to a helicopter rotor, they may be more specifically defined as:

- Harmonic - The component of the noise which arises from harmonic blade loadings.
- Broadband - The component arising from the non-periodic pressures on the blade.
- Transient - Those components of noise, including the impulsive components, which occur over only a small segment of the rotor azimuth or which arise from such aperiodic effects as wind variations.

4.2 RECORDED DATA

A fundamental purpose of the program was to document the noise of a rotor over a broad range of test variables and under conditions which were closely monitored. This was accomplished with a recording system which, as previously described, had a frequency response which had no variation over a frequency range of 2 - 5000 Hz and was within 2 db of the nominal value over the range 5000-10,000 Hz.

All the acoustical data, as analyzed, is presented in Appendix B and has been ordered by run number. As noted in Section 2.6, Figure 9 displays the test program nominal thrust and tip speed matrix by run. The actual run conditions, including atmospheric conditions are presented in Appendix B.

The basic data was analyzed for the range 0-500 Hz and averaged over 32 rotor cycles to preserve definition of individual harmonics of blade passage for a broad frequency range. A representative matrix of data was also analyzed over the frequency range 0-10,000 Hz and this has also been included, as well as selected data recorded at the ground microphone positions (100 ft radius).

To obtain the sound pressure level for a given test point and microphone location, the level of the ordinate, L, is read and added to the calibration factor presented in the upper right corner of the graph. Thus, the first harmonic level for Run 1, Microphone LF-2 (1 Dia.) is (re 0.0002 dyne/cm^2)

$$SPL = 50 + 56 = 106 \text{ db}$$

The averaged waveforms accompanying the frequency spectra have been normalized to the same approximate amplitude and period for waveform evaluation. Data analysis procedures are described more fully in Section 3.1.

When cut along the centerline, the photographic gradicules used for analysis of all the acoustical data can be used to conveniently scale the ordinate levels, L. A page of blank gradicules has been included. Due to occasional power cable interference, the 60 Hz level may appear higher than that of adjacent harmonics. When this occurs, the level at this frequency should not be interpreted as rotor noise. The signal at this frequency can be estimated, however, by interpolating between adjacent harmonics.

4.3 REVERBERATION

The influence of reflective surfaces, including the ground plane, was investigated as noted in Section 2.4. The microphone positions at 0.2R, 1R and 1D were not generally degraded from acoustical reflection. Data observed at the 3D and 5D locations were not totally free field, however. A summary of the times between incident and reflected wavefronts, and the attentation (relative amplitudes) between them was measured on Figure 20 and Table II. Agreement between the prediction and measurement is evidence that only the ground reflected wave is the major source of interference. Other structures do not present surfaces of any significance. Destructive interference of the ground reflected ray with the unreflected incident wave occurs in the range of signal frequencies which correspond to one-half the wavelength of the time delay between incident and reflected wavefronts. For the 3 diameter position, whose ray path is illustrated in Figure 21, this frequency is $\frac{1}{2 \cdot \Delta t}$ = $\frac{1}{2(.0096)}$ = 52 Hz. The pressure amplitude at this microphone resulting from the incident and time delayed reflected wave is,

$$P_{3D} = P_o \sin t + aP_o \sin \left\{ \omega (t + \Delta t) \right\}$$

P_o = Pressure amplitude of original wave

a = attenuation coefficient

Δt = time delay of reflected wave (sec)

ω = sound frequency (rad/sec)

expanding,

$$P_{3D} = P_o \sin \omega t + aP_o \{\sin \omega \cdot t \cos \omega \cdot \Delta t + \cos \omega \cdot t \sin \omega \cdot \Delta t\}$$

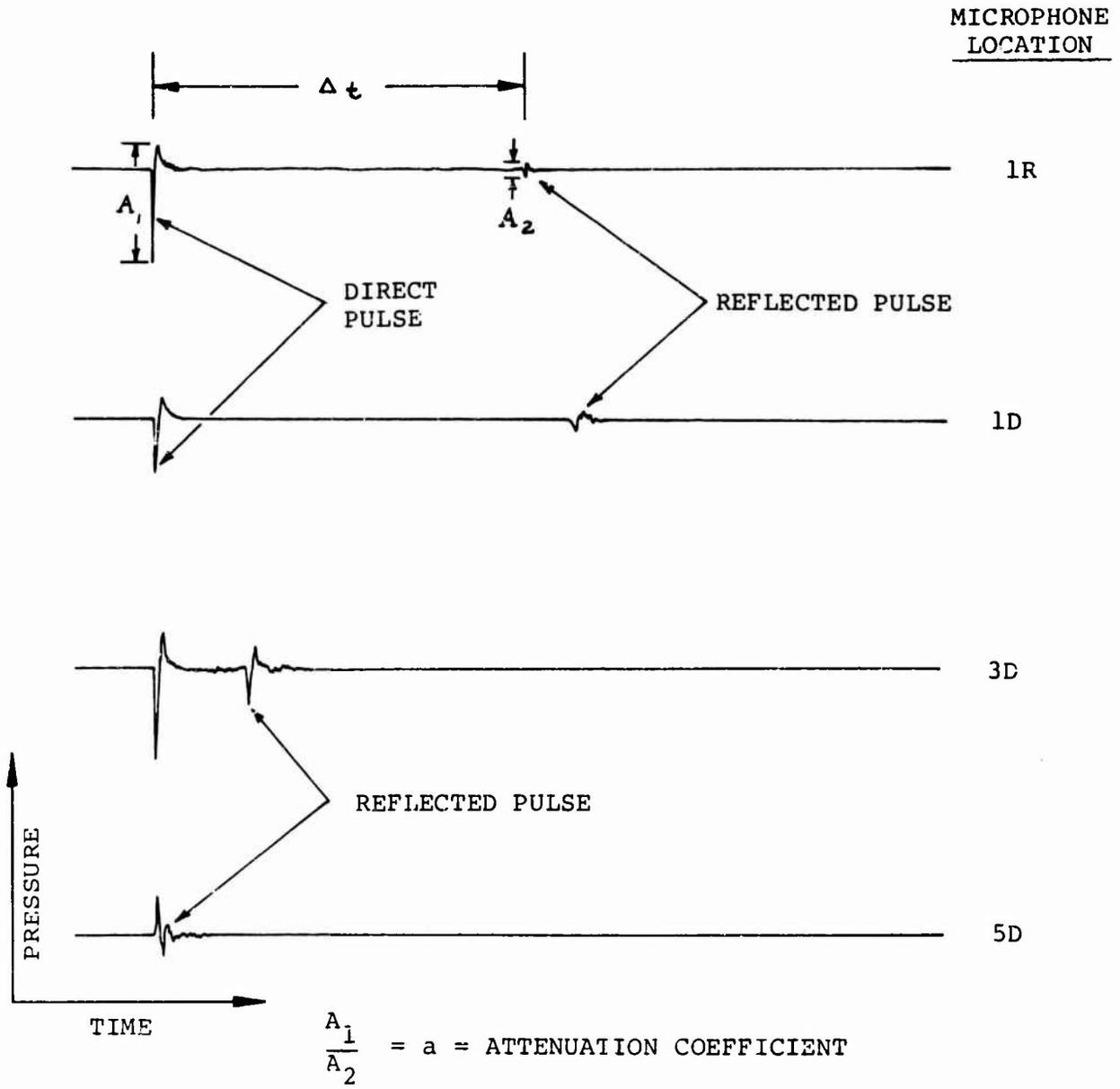

Figure 20. Reverberation Test Time History.

TABLE II

REVERBERATION TEST DATA

MICROPHONE LOCATION	Δt CALCULATED (sec.)	Δt MEASURED (sec.)	20 log a_o MEASURED (db)
1R	.040	.039	-20.
1D	.0445	.044	-14.
3D	.0096	.0096	- 6.
5D	.0009	.001	- 6.

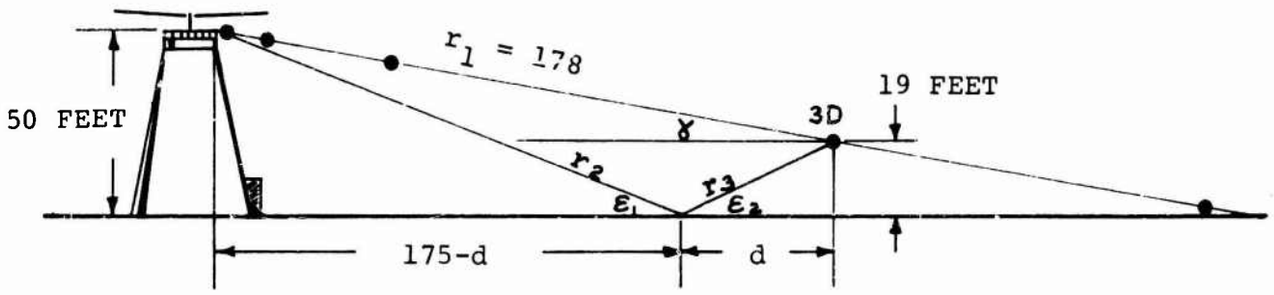

Figure 21. Raypath Diagram, 3-Diameter Microphone.

$$= P_o \sin \omega t \,(1 + a \cos \omega \cdot \Delta t) + (aP_o \sin \omega \Delta t)\,(\cos \omega t)$$

$$= P_o\, a' \sin (\omega t + \psi)$$

where $a' = \{(1 + a \cos \omega \cdot \Delta t)^2 + a^2 \sin^2 (\omega \cdot \Delta t)\}^{\frac{1}{2}}$

and $\psi = \tan^{-1} \left\{ \dfrac{a \sin (\omega \cdot \Delta t)}{1 + a \cos \omega \cdot \Delta t} \right\}$

In the form of the identify,

$$a' = \{1 + 2a \cos \omega \cdot \Delta t + a^2 \cos^2 \omega \cdot \Delta t + a^2 \sin^2 \omega \cdot \Delta t\}^{\frac{1}{2}}$$

or $$a' = \{1 + 2a \cos \omega \cdot \Delta t + a^2\}^{\frac{1}{2}}$$

The measured sound level at 3 diameters is

$$SPL_{3D} = SPL_o + 20 \log a'$$

where SPL_o is the level from the incident wave only.

Evaluation of the attenuation coefficient, a', then permits a correction to be made to obtain free field data. 20 log a' is plotted as a function of frequency in Figure 22. The range of corrections is not negligible and varies from +3.7 to -6.6 db. A similar correction has been developed for the 1D and 5D microphones that is also presented in Figure 22.

4.4 NOISE GENERATION

Comparison of the data from this program has been with a relatively limited number of published prediction methods due to the scope of the program, although additional comparisons will certainly be more revealing. The evaluation of data was also made with a representative 3 x 3 matrix of test conditions in thrust and tip speed (or C_t and M_t) and was selected based on the lowest tip speed in which a thrust of 27,000 lb. could be achieved. At the lowest test rpm (V_t = 600 ft/sec) the maximum value of thrust obtained was 25,000 lb., and this was judged to be too low to be representative of the high rotor thrust achieved during the program since the maximum value obtained was 33,000 lb. Thus the lowest tip speed where a thrust of 27,000 lb. was achieved was selected for an end point of the matrix. This matrix is listed below.

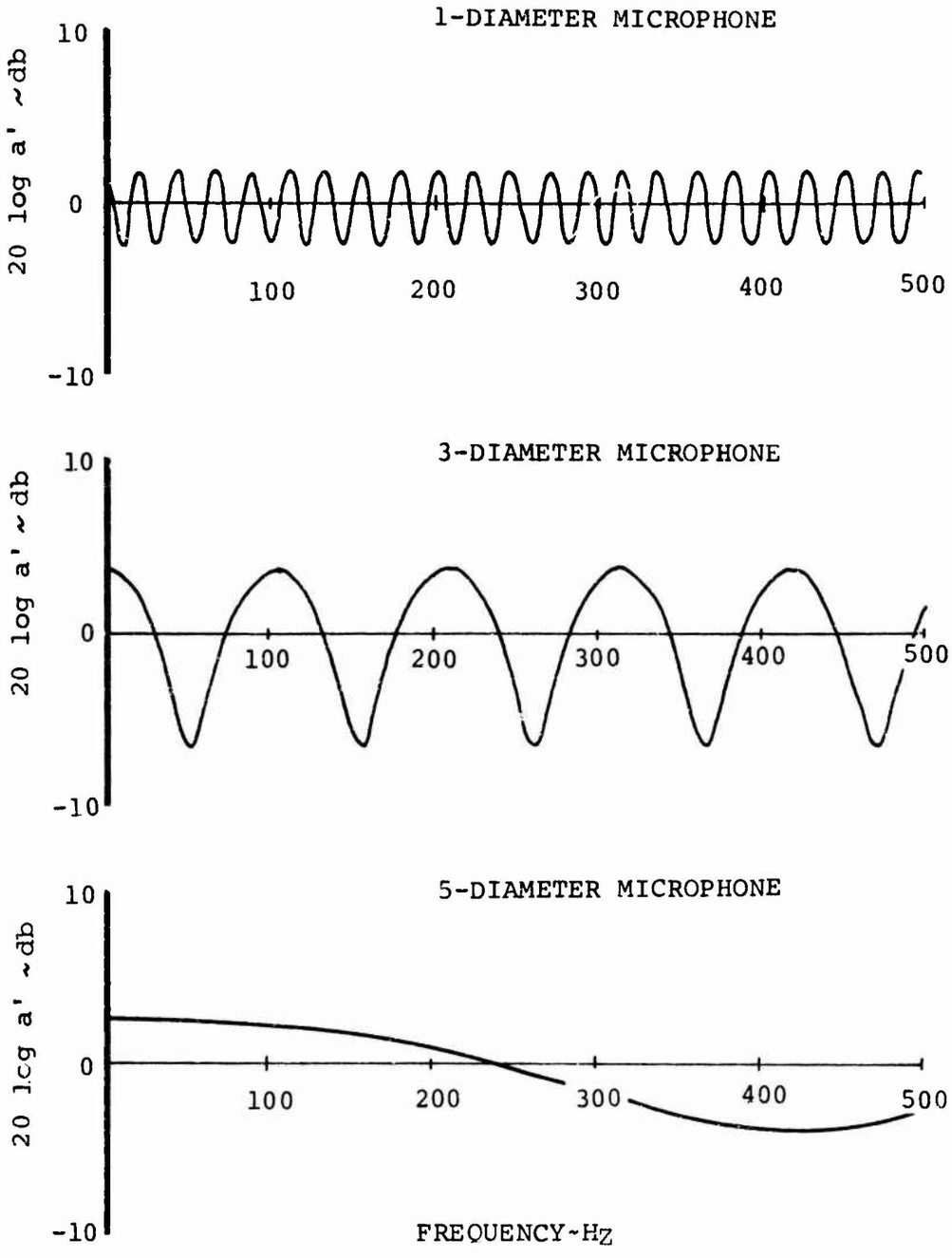

Figure 22. Signal Amplification Due to Reflection.

Data Matrix Evaluated
(By Run Number)

Thrust ~ lb.	650	750	850
27,000	108	57	36
18,000	104	54	34
9,000	101	51	31

Tip Speed ~ ft/sec

For the trend studies, data from the microphone located at three diameters from the rotor centerline has been used since it is the closest one which is in the acoustic far field. Predictions of the theory of Lowson and Ollerhead.[1] For the specific cases of this program were performed using the design charts included in that report.

4.4.1 Harmonic

Predicted levels for the test rotor have been compared with measurements in Figure 23 through 25 for those frequencies which are identifiable as harmonics of blade passage. The theory of Reference 1 has been corrected for the specific test site conditions for reflection by the method developed in Section 4.3 and the reflected wave amplitude has been corrected for source directivity. The underprediction, as noted by Lowson, is thought to result from the lack of adequate high harmonic sensitivity of the instrumentation which measured airloads utilized by Lowson and Ollerhead in developing the theory. This difference between predicted and measured levels is also illustrated in Figure 26, the zero reference being the data value.

A comparison of the data with predictions in terms of tip Mach number and thrust coefficient is made and shown in Figures 27 and 28. Good agreement is also displayed at harmonic numbers of blade passage below five. Because of this agreement, the fundamental blade passage frequency was used in investigating data trends with tip speed, illustrated in Figure 29. The data shown for the lowest thrust, displays a 5.3 power law trend decreasing with thrust to ^{m} = 3.4. Straight lines were fit to the data by the methods of least squares. Power law trends at the low thrust values are in conformance with other published data.

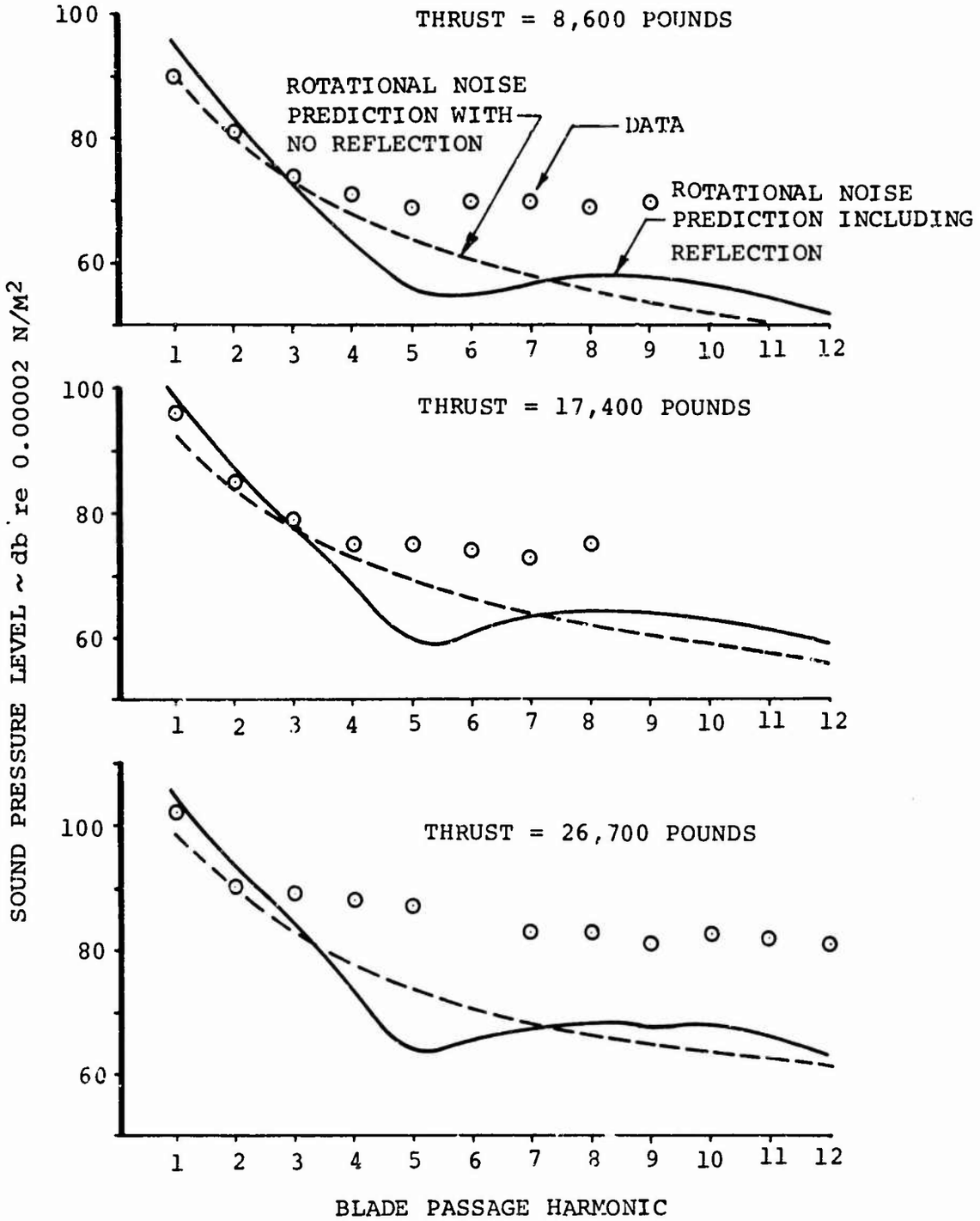

Figure 23. Comparison of Harmonic Data With Theory of Reference 1, Tipspeed = 650 Feet per Second.

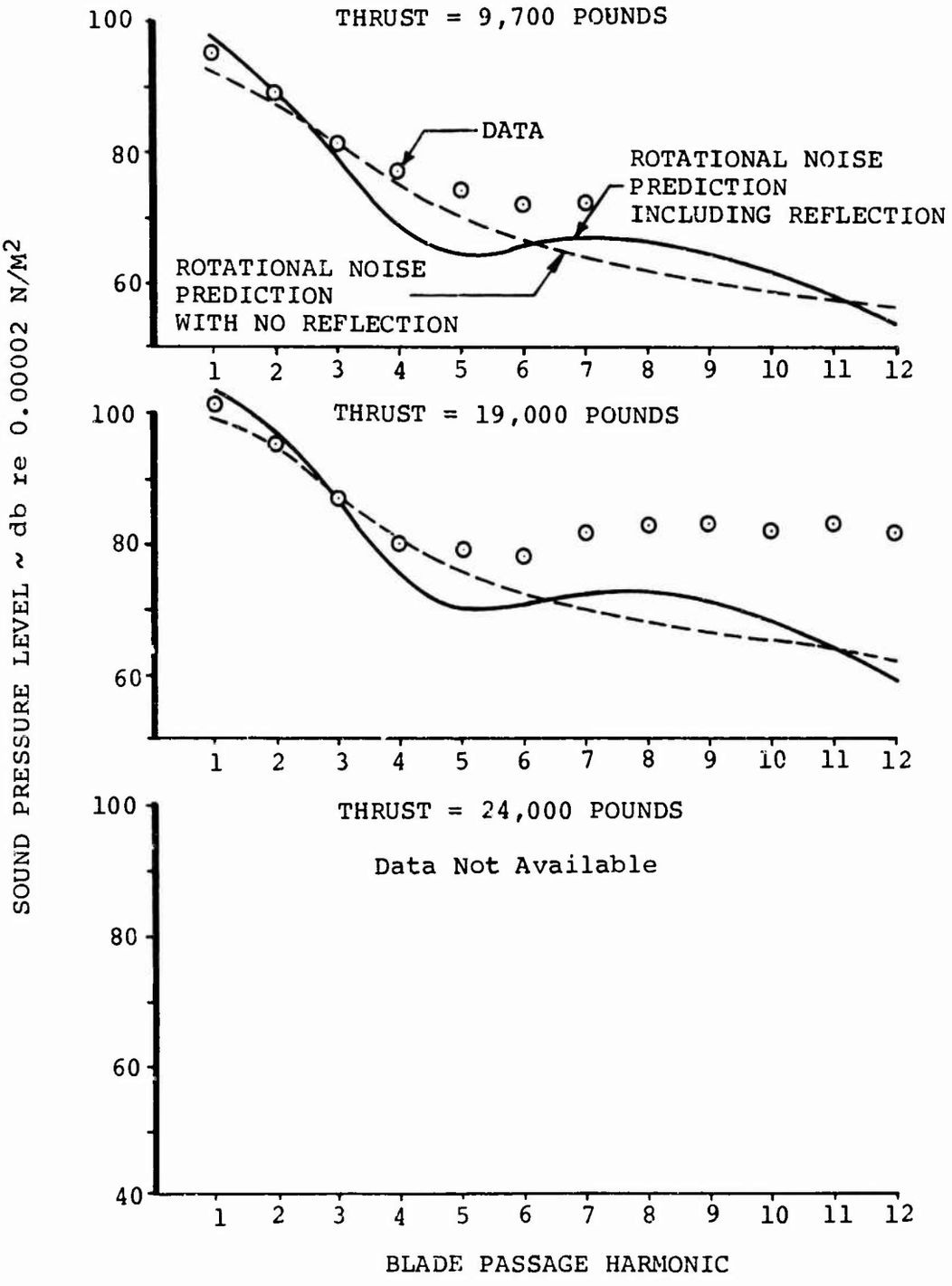

Figure 24. Comparison of Harmonic Data With Theory of Reference 1, Tipspeed = 750 Feet per Second.

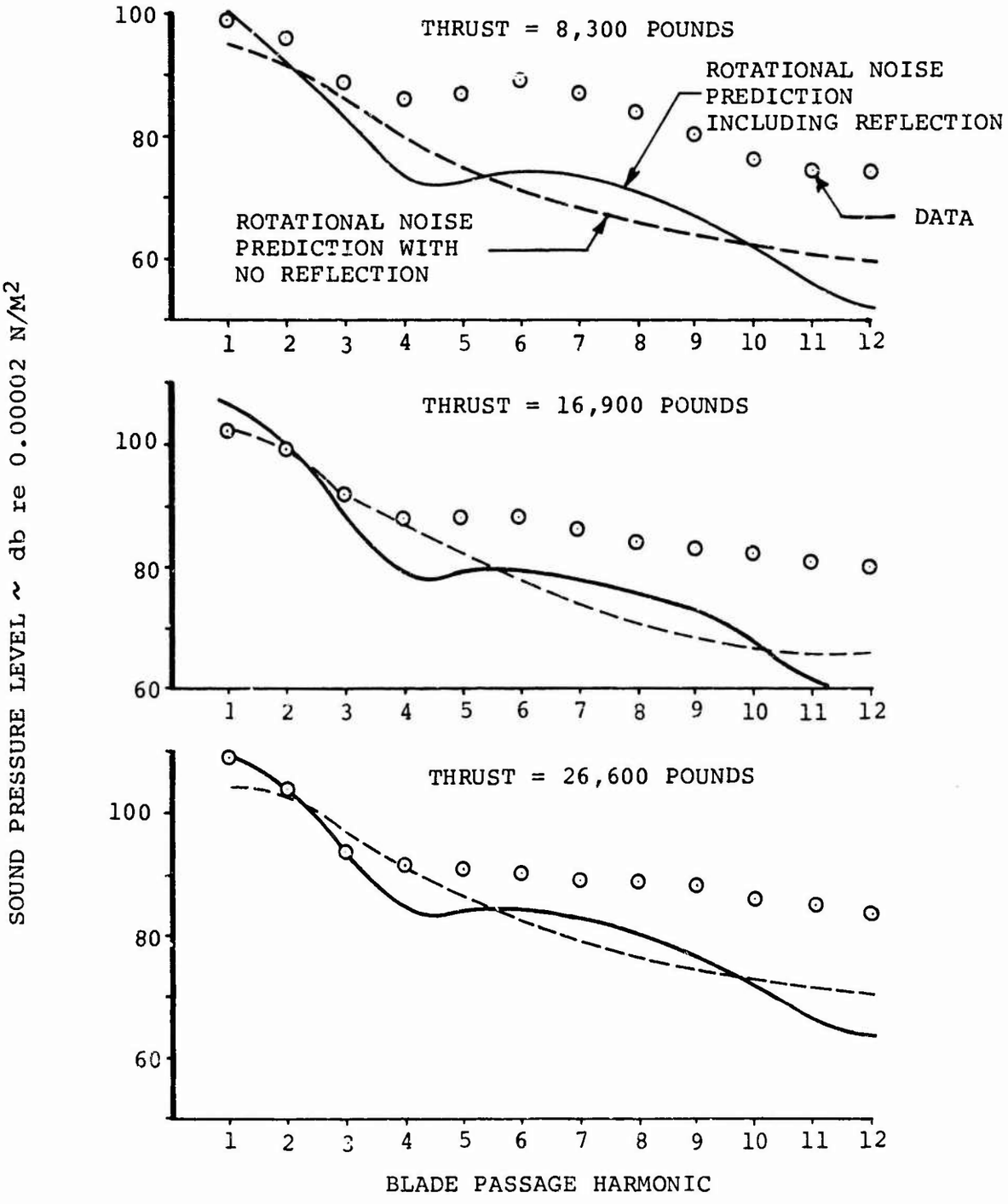

Figure 25. Comparison of Harmonic Data With Theory of Reference 1, Tipspeed = 850 Feet per Second.

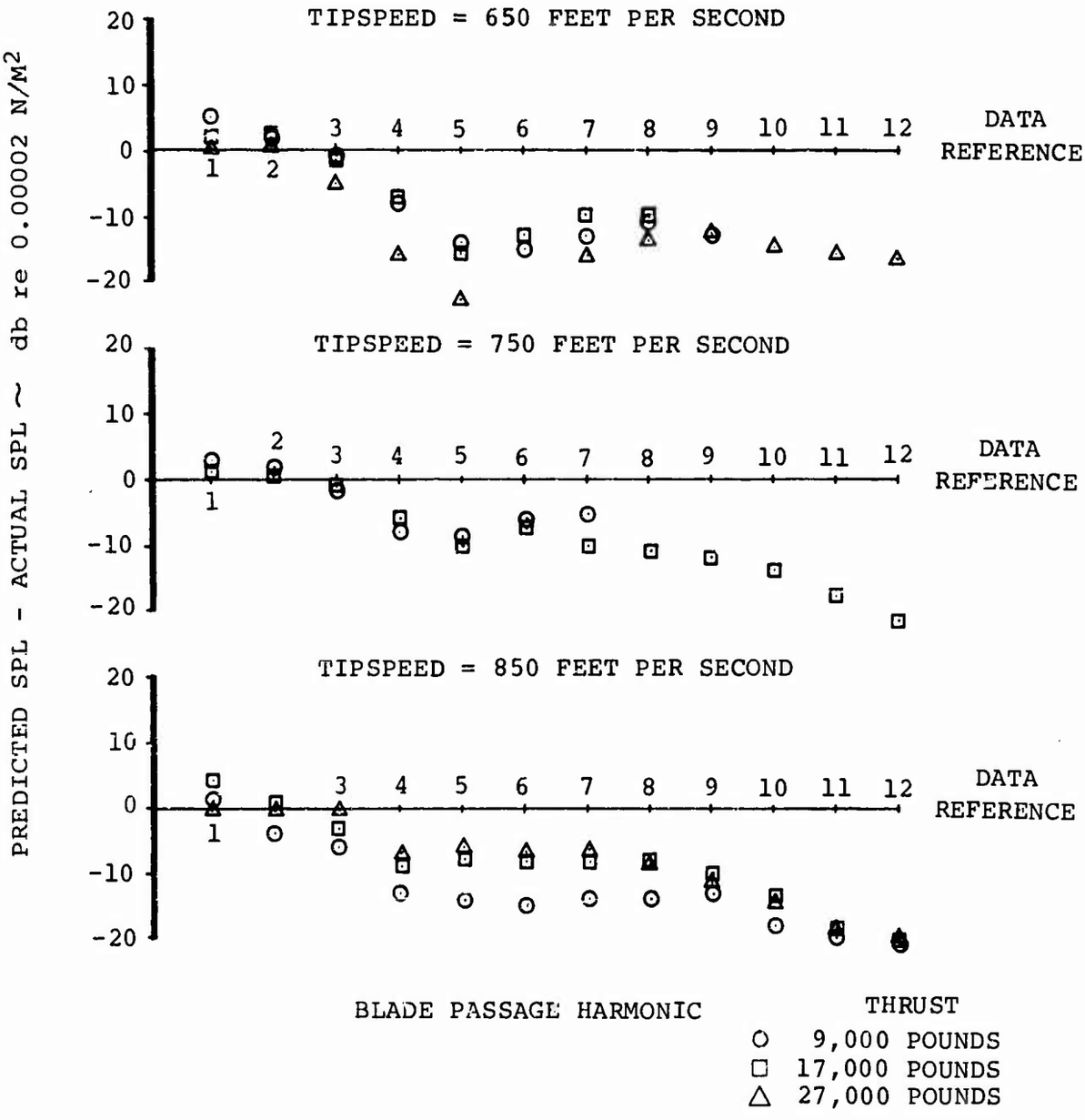

Figure 26. Normalized Comparison of Harmonic Data With Theory.

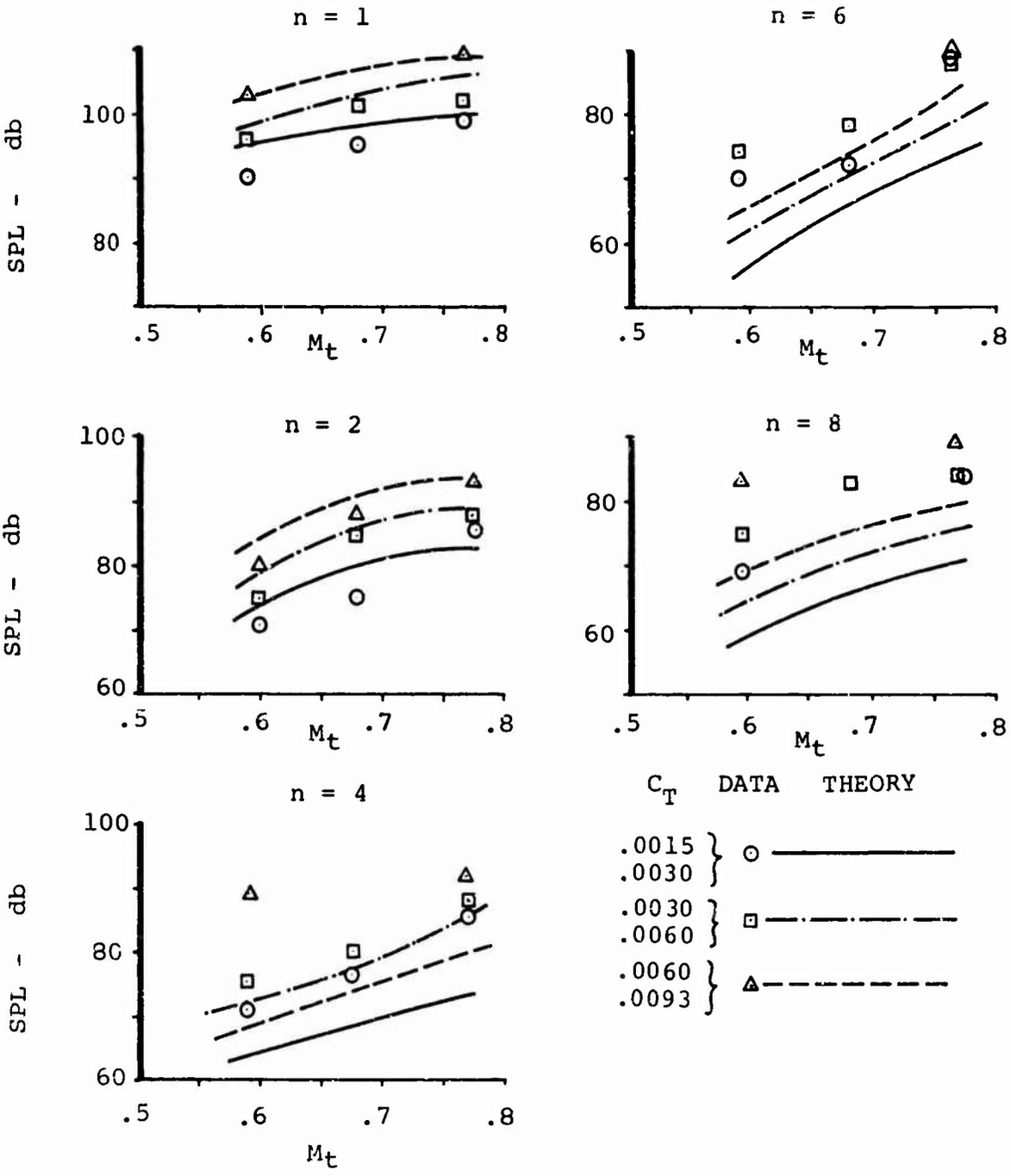

Figure 27. Effect of Tip Mach Number on Rotor Noise Measured at 3 Diameters

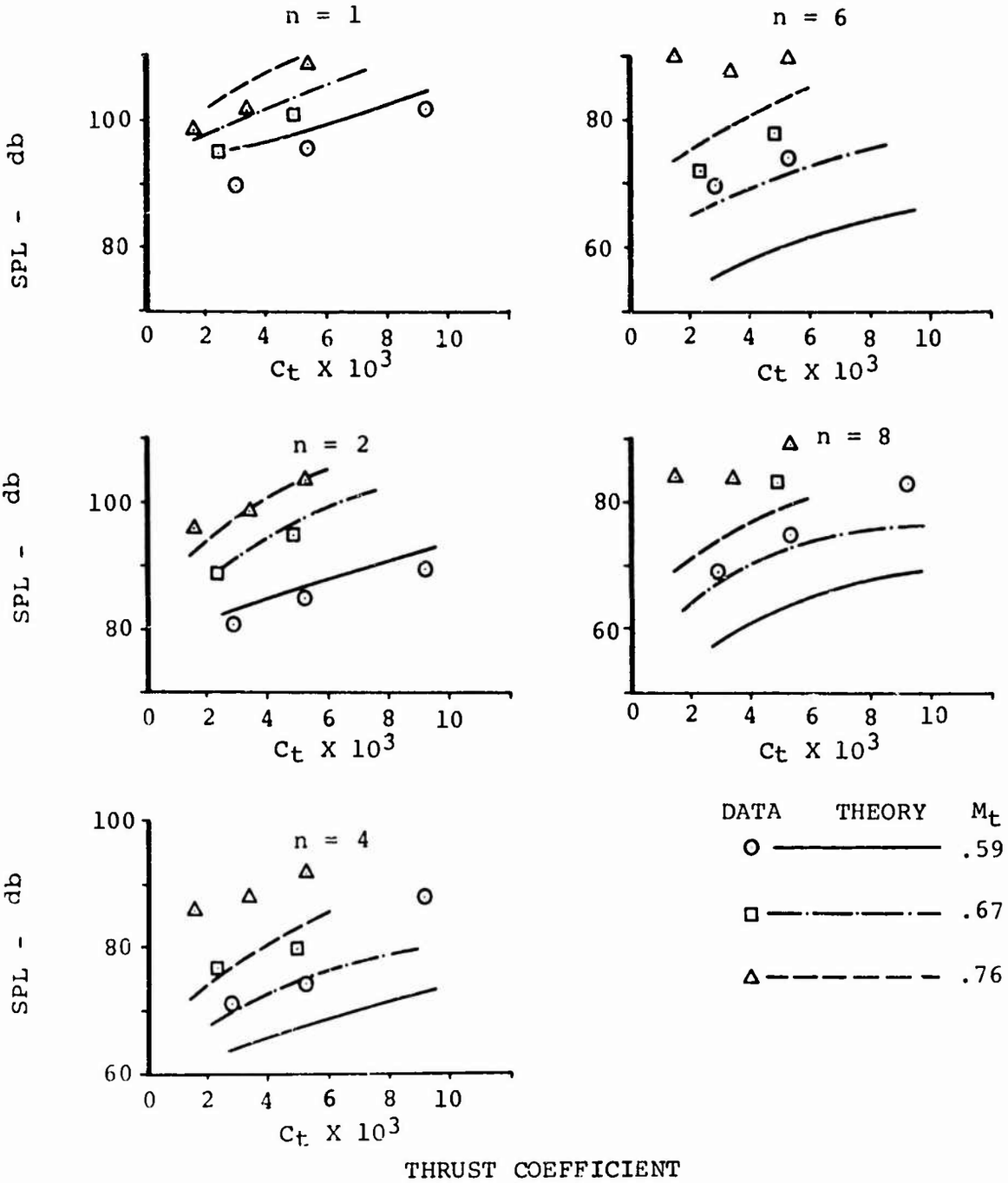

Figure 28. Effect of Thrust on Rotor Noise Measured at 3 Diameters

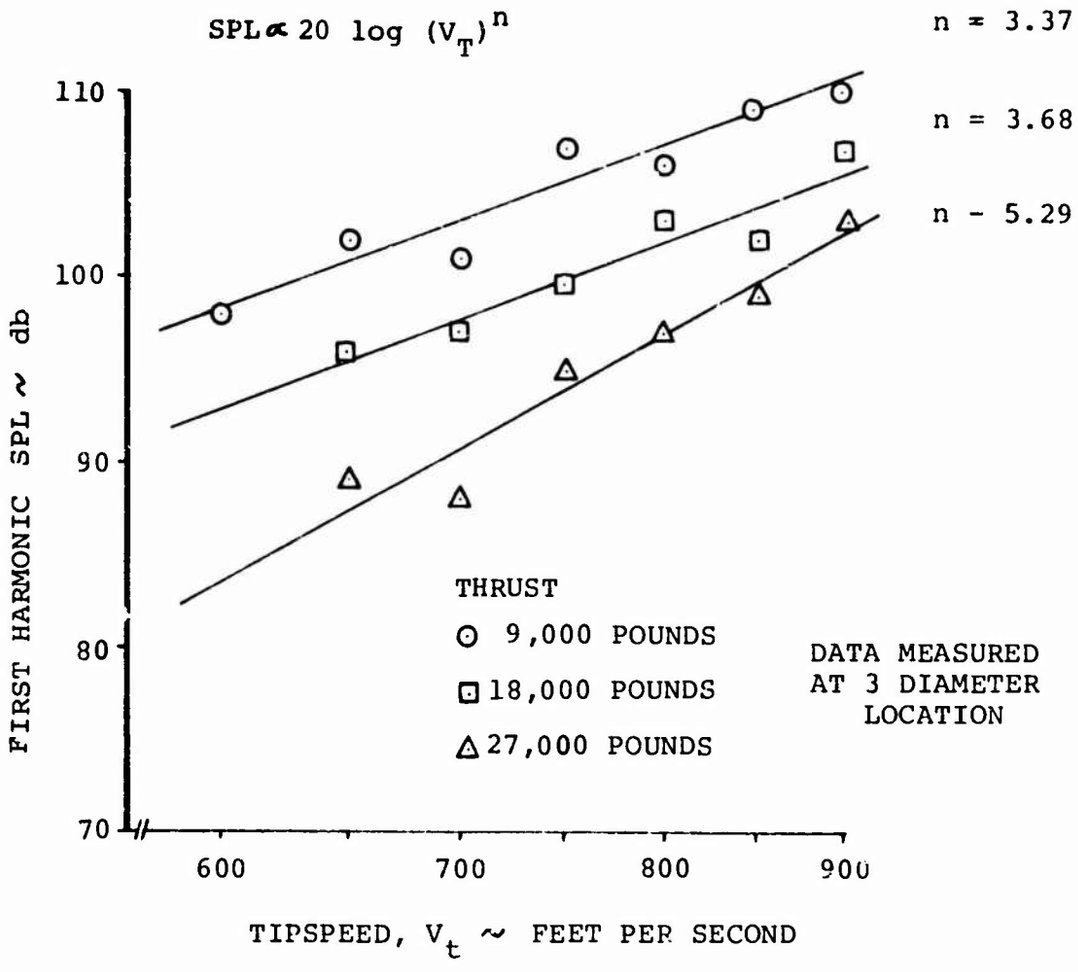

Figure 29. Tipspeed Trends.

It can be generally concluded that the low harmonics of blade passage are predictable in that they can be estimated to within 5 db of the measurement value, at least over the range of operating conditions investigated in this program. Further, it is not surprising that the best agreement between theory and data is in the same range of tip speeds and thrusts as the airload data which Scheiman reported and which Lowson utilized for development of Reference 1 theory. Airloading data with improved high harmonic content appears to be the solution to increased accuracy of noise prediction of lifting rotors.

4.4.2 Broadband Noise

In scanning the many illustrations of frequency spectra, it is evident that many conditions evaluated on the test rotor impart a non-harmonic quality to the data. A method for estimating this contribution to the rotor spectra was developed by Schlegel.[2] This method, based on the theory of Reference 8 for propellers, is in a useful form for rotors in that it provides a method for estimating the broad spectra of noise normally associated with helicopter lifting rotors. Broadband noise calculated by the method of Reference 2 is shown in the comparison of data with theory in Figures 30 through 32. The octave band measurements of the data from this report are 5 to 10 db higher than the Reference 2 theory predicts for this rotor. However, Schlegel reports good agreement with two large rotors not the same as that used in the subject test, and this may point up a requirement for additional terms in the expression for broadband noise to account for specific airfoil profile, planform, tip shape or other characteristics which may influence the broadband noise radiated by a rotor system.

Table III presents a comparison of methods for broadband noise prediction developed by other researchers working in helicopter noise. The constants in the expressions presented account for the field point where comparison data was obtained. Predictions have been made for only one data point. The constants obtained for several of the methods would provide a closer approximation to the measured data from this program.

4.4.3 Transient Impulsive Noise

In previous investigations of the noise generated from a hovering rotor as reported in Reference 9, a transient, impulsive noise was observed above the relatively constant rotational noise. This noise dominates the signature and becomes greater in magnitude with increasing tip speed and thrust. Figure 33, taken from Reference 10, gives a rough delineation of the previously observed region where this transient impulsive noise becomes dominant. It had been previously hypothesized that this impulsive signature was due to blade-vortex intersections and, therefore, smoke visualization of the vortex was

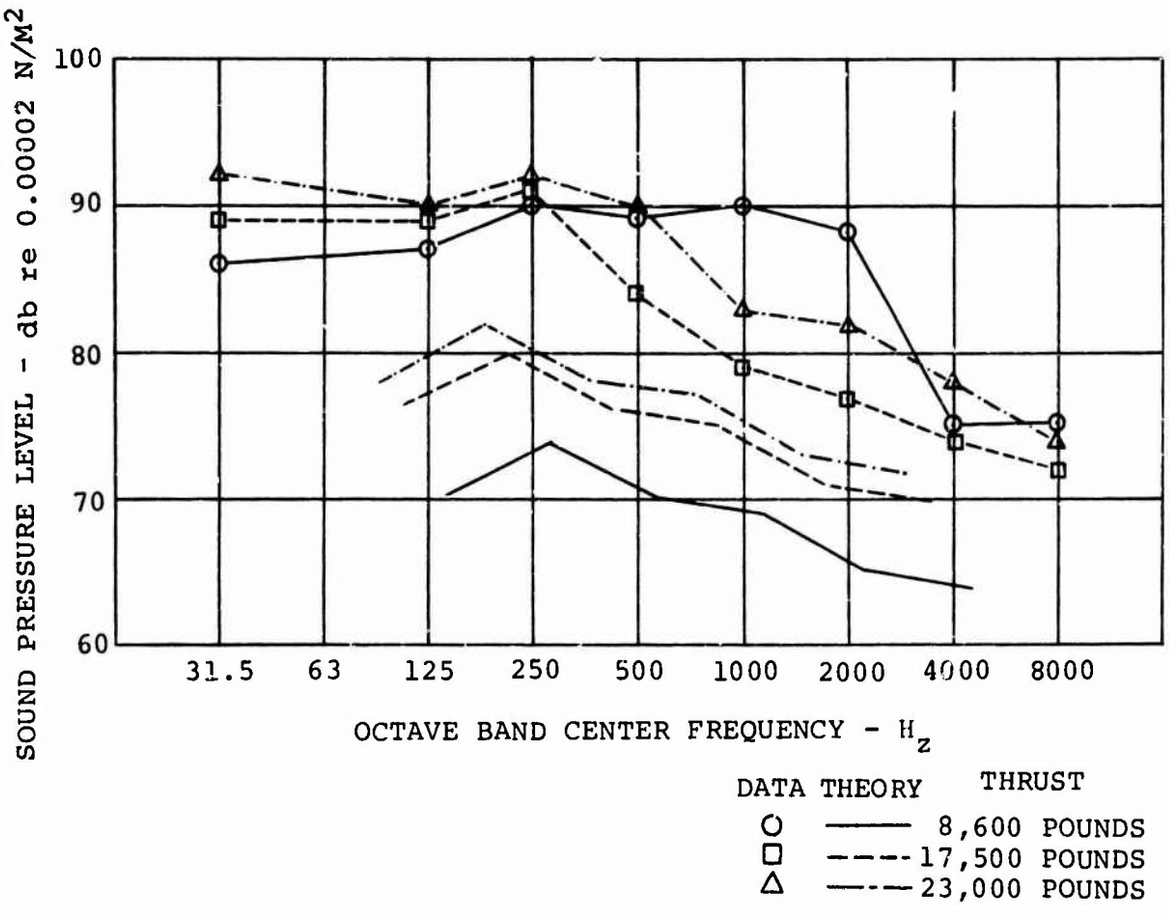

Figure 30. Comparison of Broadband Noise With Theory of Reference 2, Tipspeed = 650 Feet per Second.

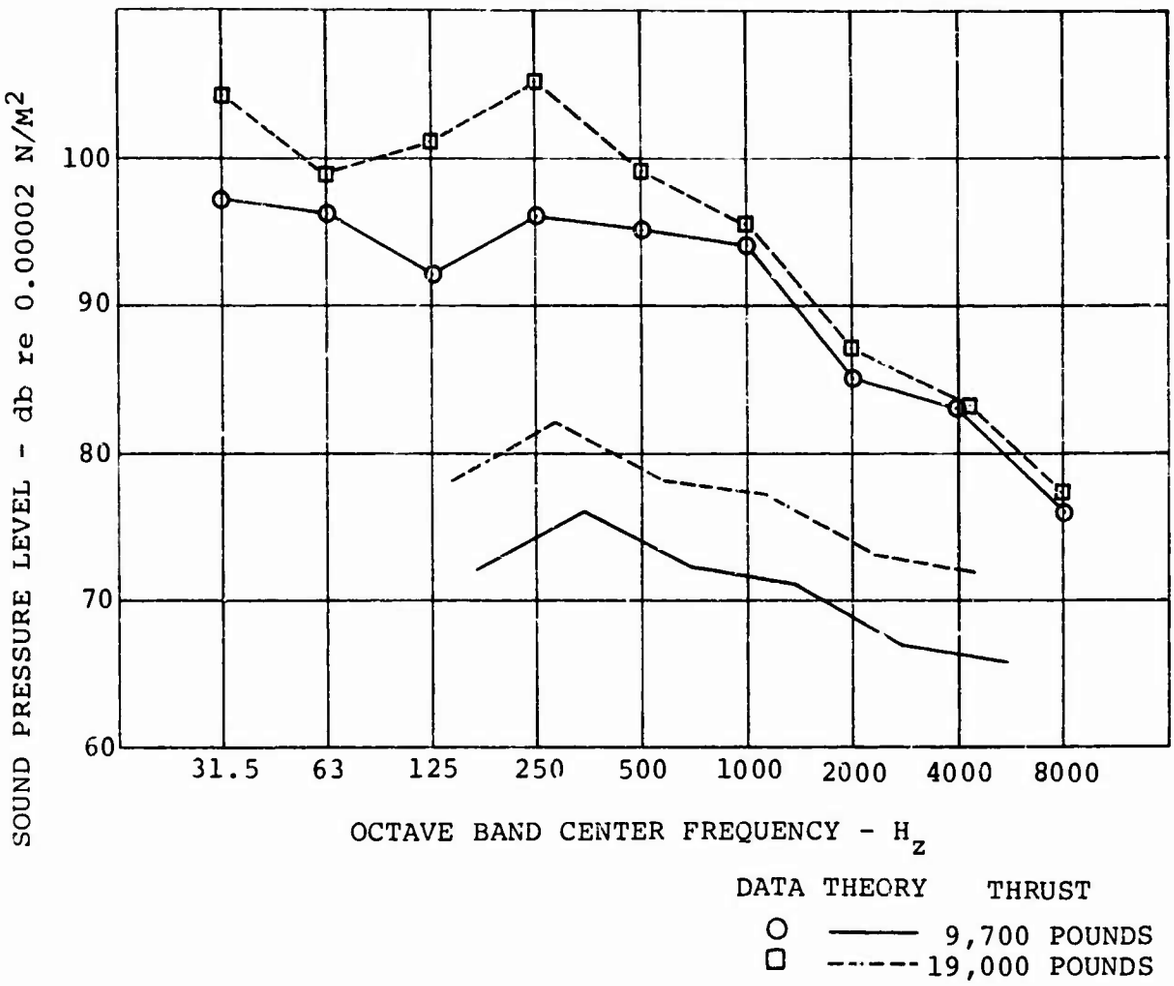

Figure 31. Comparison of Broadband Noise With Theory of Reference 2, Tipspeed = 750 Feet per Second.

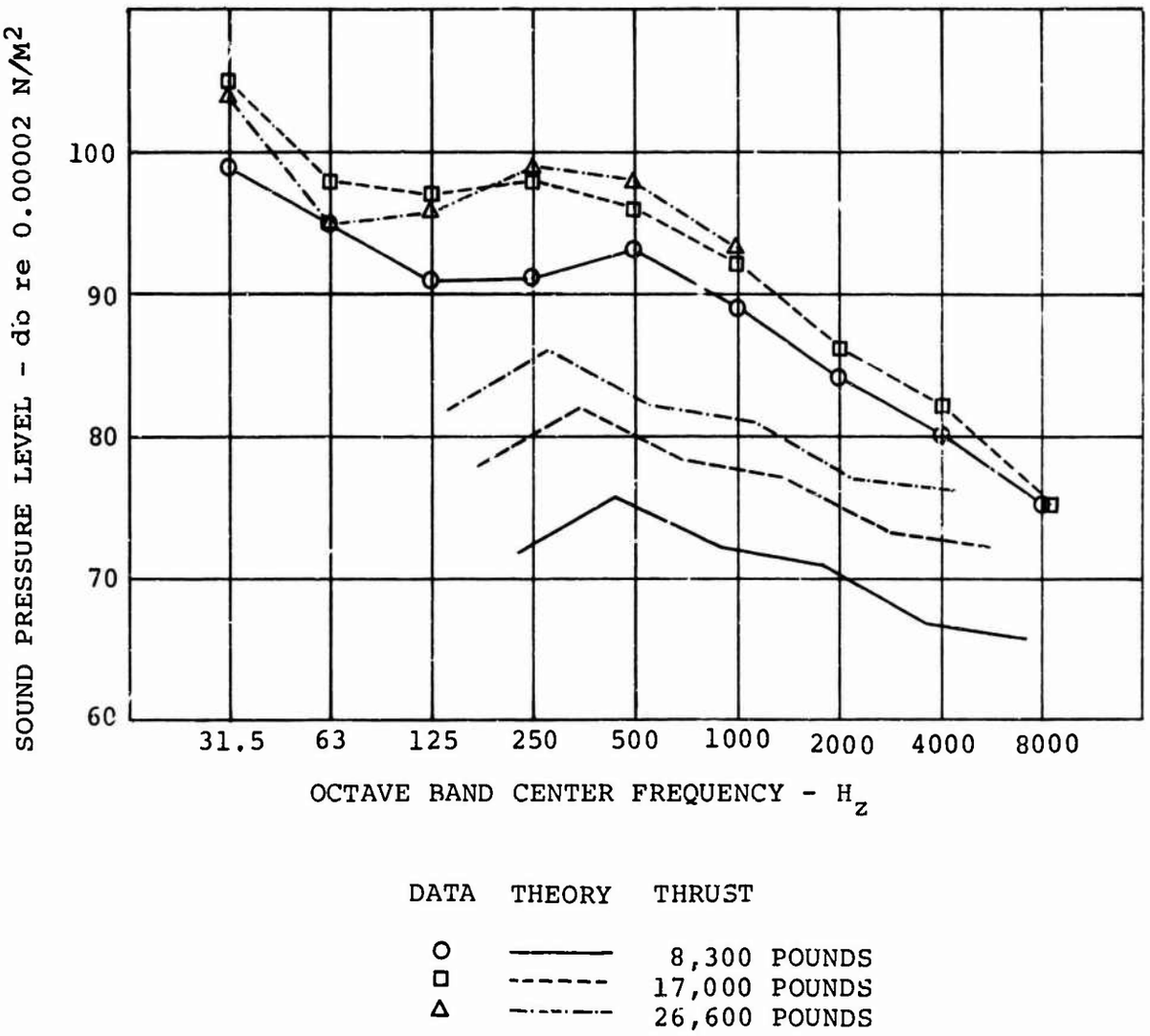

Figure 32. Comparison of Broadband Noise With Theory of Reference 2, Tipspeed = 850 Feet per Second.

TABLE III

COMPARISON OF VORTEX NOISE PREDICTION METHODS WITH MEASURED DATA

AUTHOR	FORM	f MAX	PREDICTION db	DATA db
HUBBARD	$SPL_{180} = 10 \log \left(\frac{KSV_{0.7}^{6}}{10^{16}} \right) + 4.6$			EQUIVALENT TO OVERALL VORTEX NOISE LEVEL
SCHLEGEL KING & MULL	$SPL_{180} = 20 \log V_{0.7} + 20 \log T - 10 \log A_6 - 31.3$	$\frac{0.28\ V_{0.7}}{h}$	86.1	102
DAVIDSON & HARGEST	$SPL_{180} = 20 \log V_t + 20 \log T - 10 \log S - 16.5$		104.0	102
STUCKEY & GODDARD	$SPL_{180} = 26.8 \log V_t + 16.6 \log T - 20 \log SEC\ \phi - 49.2$	$\frac{0.18\ V}{0.4C}$	98.6	102
LEVERTON	$SPL_{180} = 60 \log V_t + 10 \log S - 91$		104.1	102

V = BLADE VELOCITY 750 FT/SEC

T = ROTOR THRUST 19,000 LB.

S = A_b = BLADE AREA 182.5 FT^2

r = DISTANCE TO MICROPHONE 180 FT

ϕ = ANGLE BETWEEN TIP LOCATED DIPOLE AXIS AND MICROPHONE

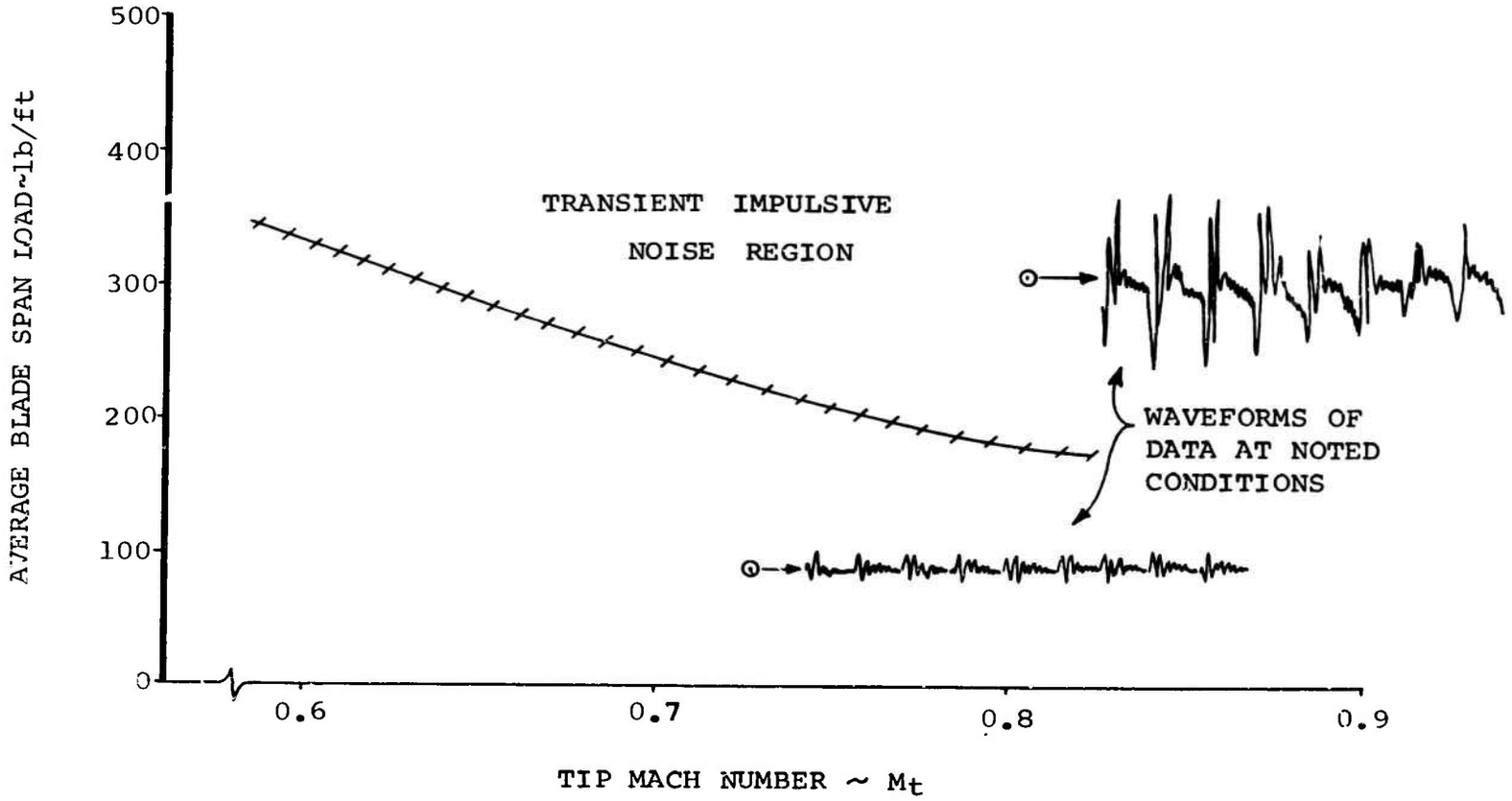

Figure 33. Regions of Transient Impulsive Noise.

used to measure vortex position in order to correlate blade-vortex separation with recorded noise level. The results of the program to measure blade vortex separations obtained as discussed in Section 3.2.2 are shown in Figures 34 through 38. It can be noted in these figures that no measurements exist for large portions of the rotor azimuth. This resulted from the vortex rising above the horizon as viewed by the rotating camera. The smoke did not have sufficient intensity in most cases to be observed against the sky. In one run (Figure 34), however, the smoke could be observed for all azimuth locations. It was noted that this shape described an extremely close approximation to a sine curve with its peak approximately in the upwind directions as would be anticipated.

In order to estimate the location of the vortex at all azimuth locations, sine curves were fitted to the data for the remaining runs. In order to do this, it was assumed that:

$$S = A \sin (\psi - \psi_o) + B$$

where: S = blade-vortex separation

A and B are constants

ψ = azimuth, $\psi = 0$ = upwind

ψ_o = phase angle

ψ_o was determined by finding the minimum in the data and adding 90^o. Then S was plotted against $\sin (\psi - \psi_o)$ to describe a line. The slope of that line was A, and its intercept, B. Stationary camera separation measurements were used to substantiate these and are plotted on Figures 35 and 36 for cases where both measurements were available. The close agreement between the two measurement systems strongly supports the accuracy of the system.

These measurements and extrapolations indicate that intersections occur for all the conditions observed. Of special interest is the fact that intersections were observed for a low thrust condition (Figure 36) for which no transient impulsive noise was observed, and for a higher thrust condition, Figure 34, which did display a transient impulsive noise in its signature. Intersections were extrapolated for all other cases. Thus any correlation between separation and the occurrence of this impulsive noise is not meaningful.

Since the existence or absence of transient impulses in an acoustical signature cannot be determined by the existence or absence of blade-vortex intersections alone, one of the following conclusions can be drawn: (a) the vortex does not enter into the requirement for impulsive noise generation,

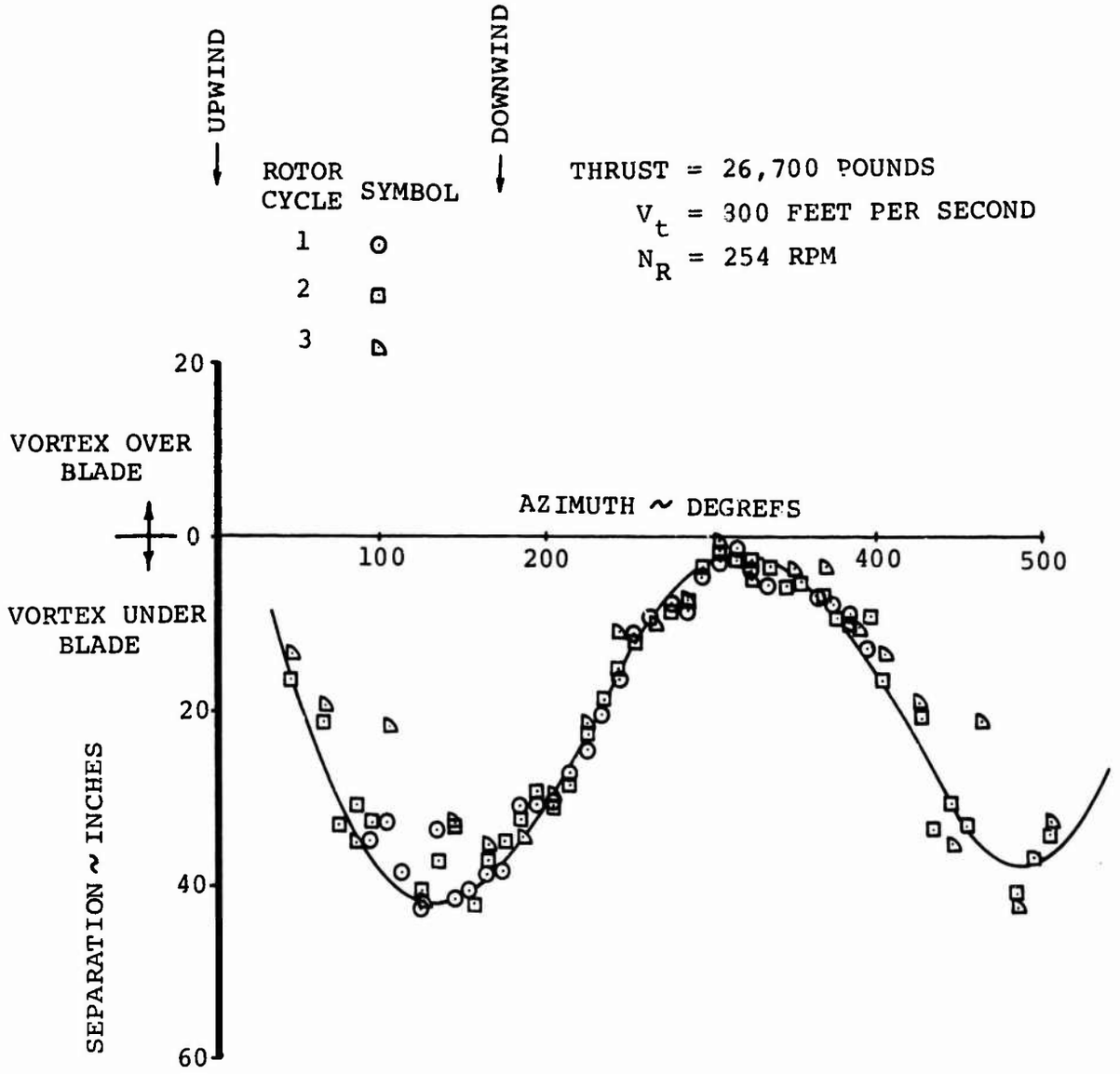

Figure 34. Blade Vortex Separation Measurements With Rotating Camera, Run 110.

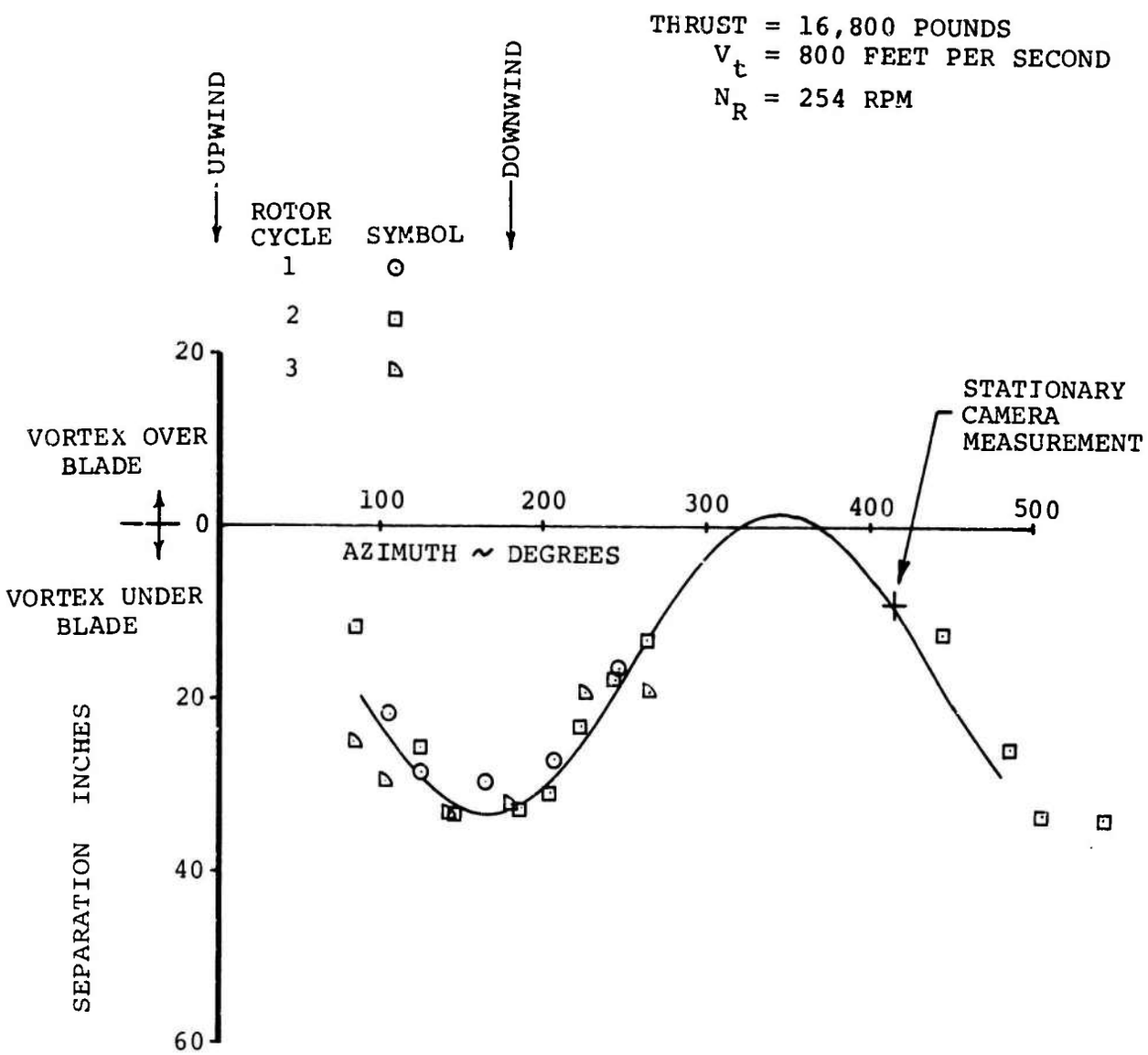

Figure 35. Blade Vortex Separation Measurements With Rotating Camera, Run 112.

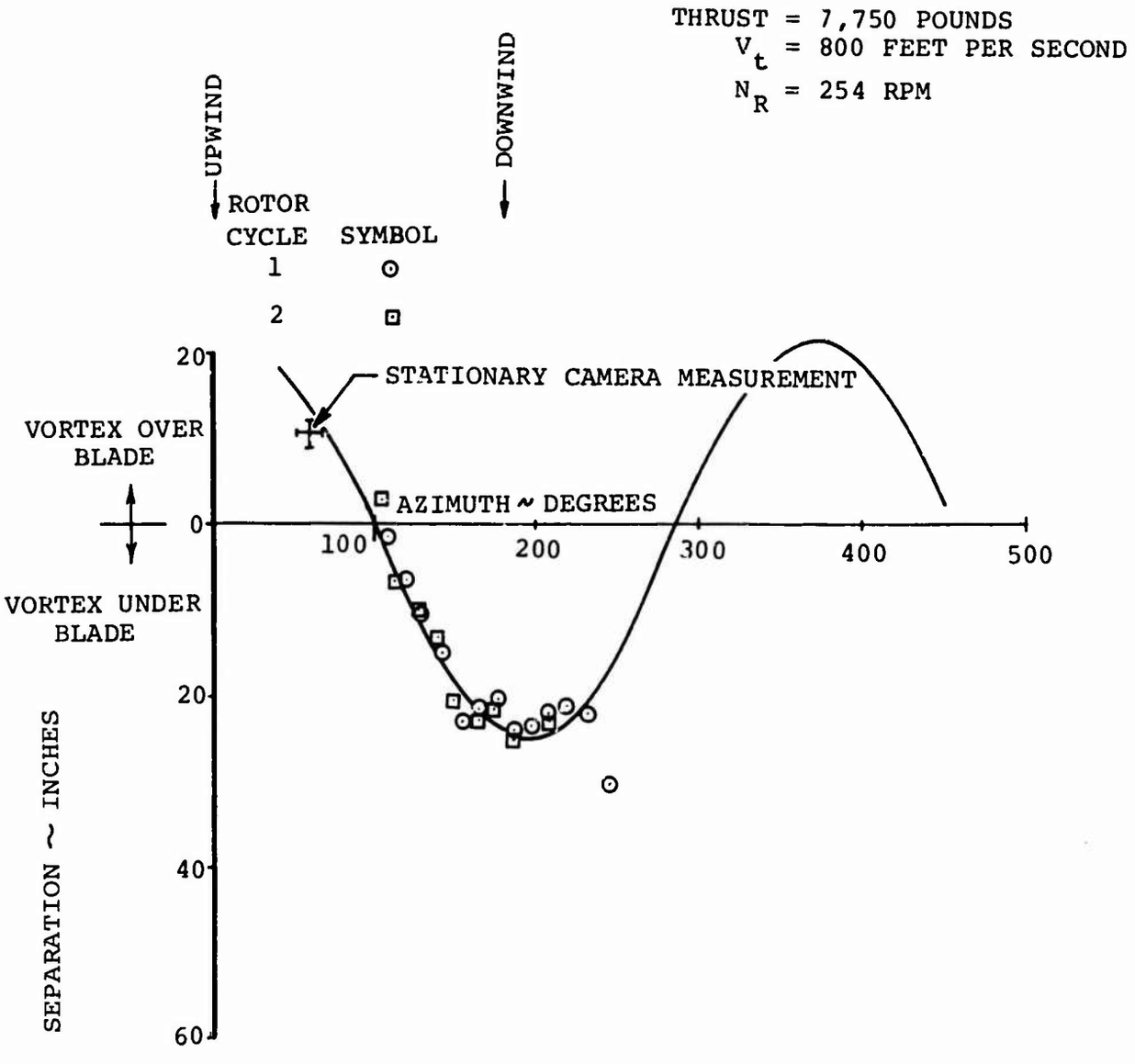

Figure 36. Blade Vortex Separation Measurements With Rotating Camera, Run 113.

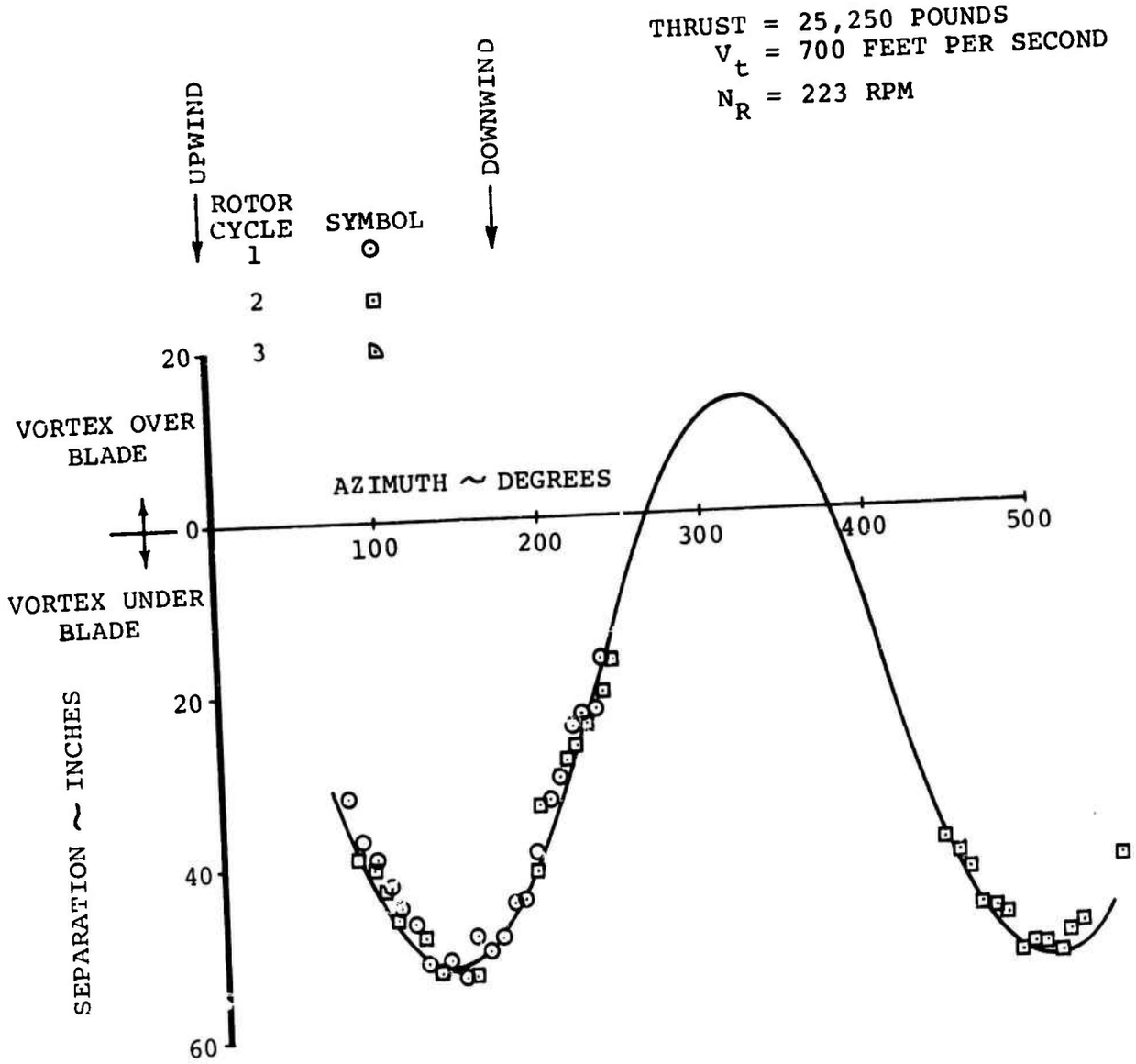

Figure 37. Blade Vortex Separation Measurements With Rotating Camera, Run 90.

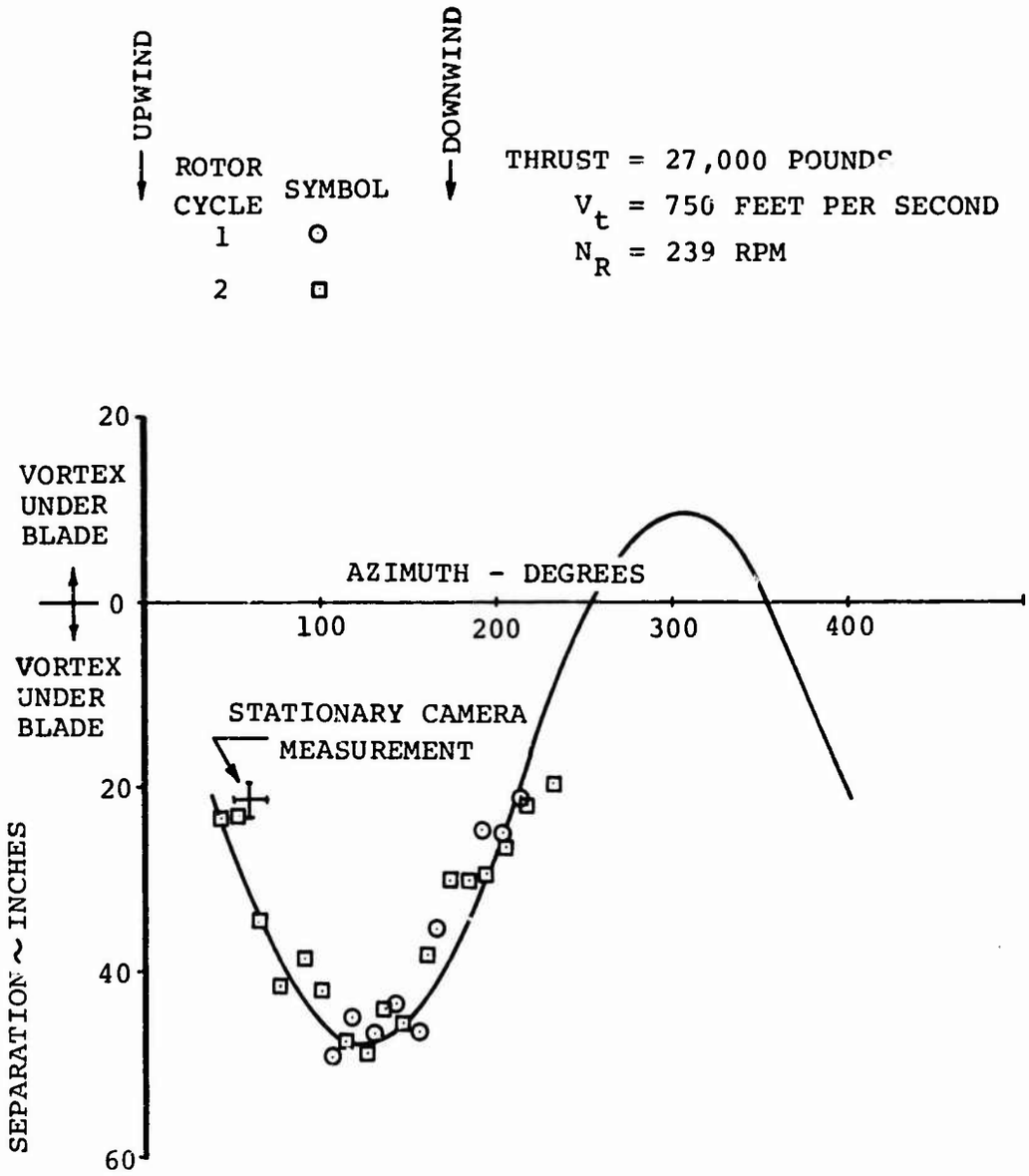

Figure 38. Blade Vortex Separation Measurements With Rotating Camera, Run 116.

or (b) the presence of the vortex is not the total determinant of impulsive noise generation. The Aerodyramics Research Staff at Vertol has suggested that the most probable source of the noise is the fluctuation of an attached shock, during conditions of critical flow, caused by blade-vortex intersection. Thus single rotor impulsive noise during hovering conditions cannot occur if the rotor is operated at tip speeds less than the critical Mach number for the airfoil section on the blade. Figure 39 gives support to this possibility. It shows a method of delineating the regions of transonic and subsonic flow on the airfoil. The locus where $\left(\frac{\partial C_L}{\partial M}\right) = 0$ for a constant angle of attack, α, roughly indicates when the Prandtl-Glauert law fails. The shaded area is reproduced from Figure 33. Further investigation in this area appears to be warranted.

4.5 NOISE PROPAGATION

Harmonic levels of data recorded at 1 rotor diameter and 5 rotor diameters generally attenuate in an orderly manner. However, the 3 diameter data displays a 'fluctuating decay' to the higher harmonics of discrete noise.

The data illustrates the wave interference noted in Section 4.3 resulting from the reflected wave and is not a real characteristic of the signal. A comparison of the difference in sound level between the 1D and 3D positions and 3D and 5D positions as a function of sound harmonic is illustrated in Figure 40 for both measured data and the theory predicted by the method of a previous section. The agreement noted lends credence to the interference effect hypothesis. Correction for data from the 1R and 5D positions, while not negligible, is not so dramatic as the 3D position, and does in fact also describe a similar 'fluctuating decay' characteristic. The propagation of rotor noise generally follows the spherical law in the acoustic far field. Sound pressure attenuation in the near field (1R to 1D) displays the more rapid decay generally associated with this region, and is approximately 20 db per doubling of distance. See Figure 41. Attenuation between the 3 diameter and 5 diameter position includes not only spherical spreading but the increased pressure due to the incident wave reflected from the ground plane. The range of levels expected at the 5D position can be predicted from spherical spreading and pressure doubling of the reflected wave. Evaluated, this is $20 \log \frac{290}{180} = 4.1$ db. If the reflected wave is in phase with the incident wave, then pressure doubling will result and the measured level will be 6 db above that predicted for incident wave alone. Phase reversal of the signal at 5D relative to the 3D signal may

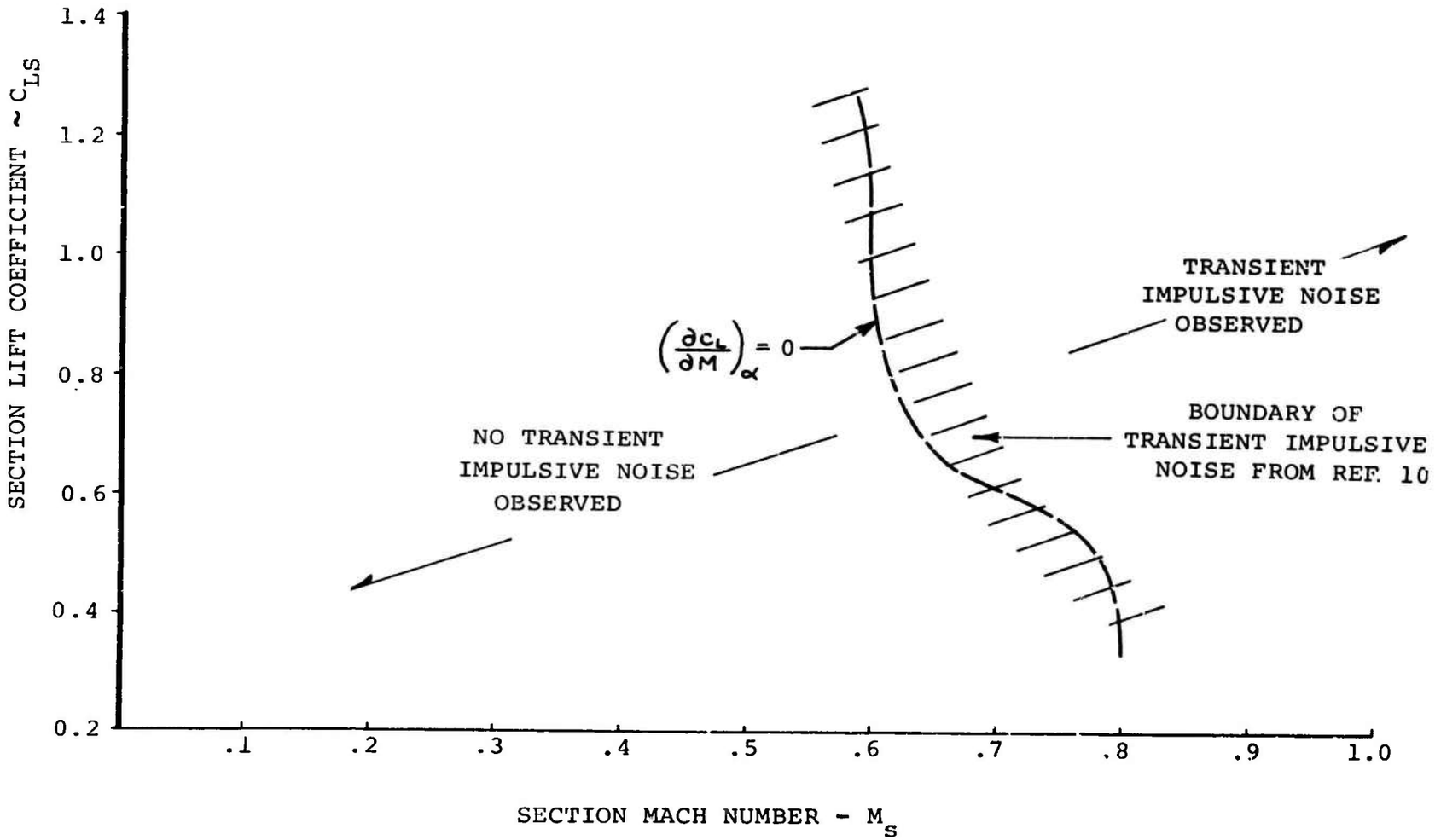

Figure 39. Transient Impulse Noise Region.

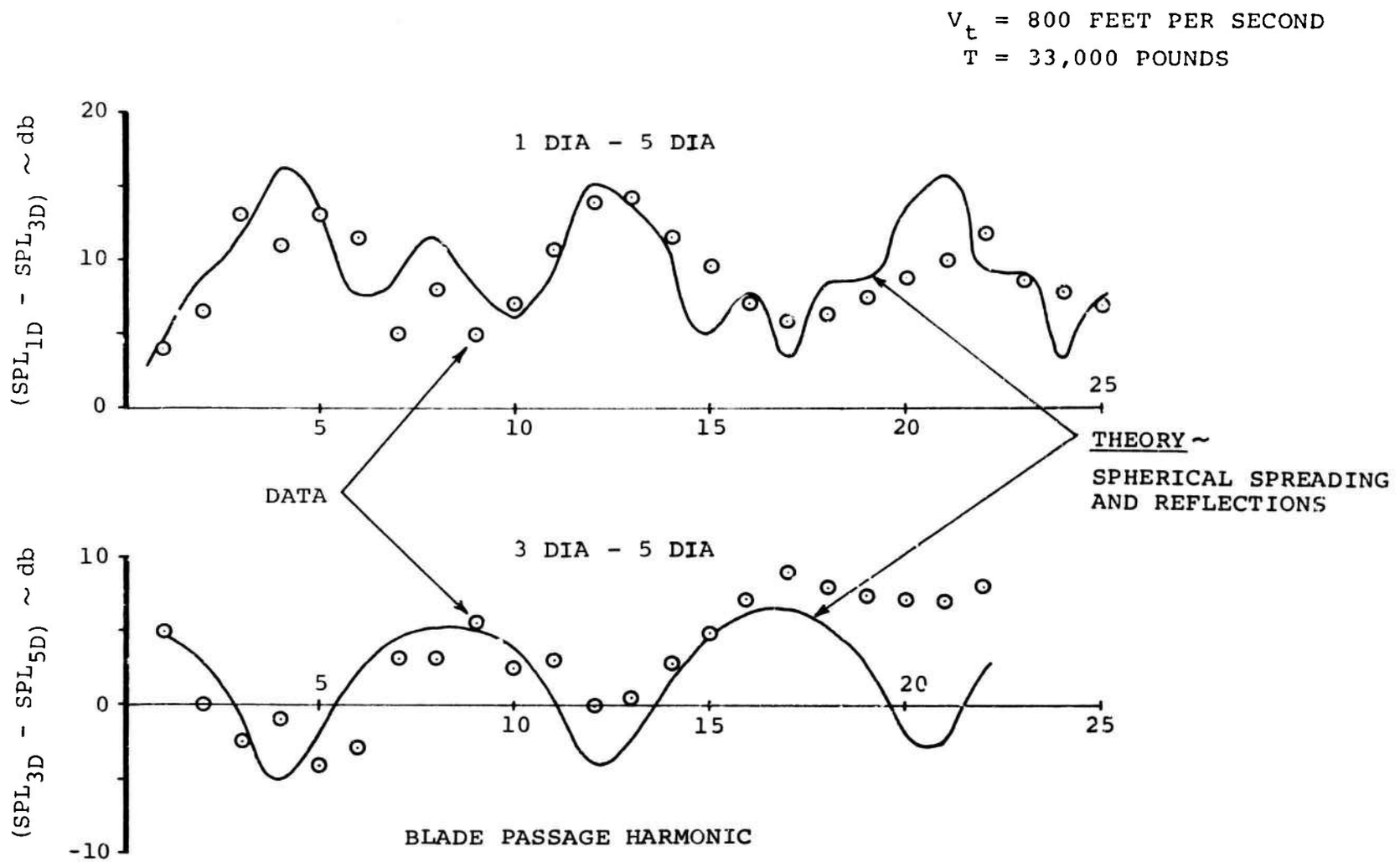

Figure 40. Effect of Reflections on Sound Propagation.

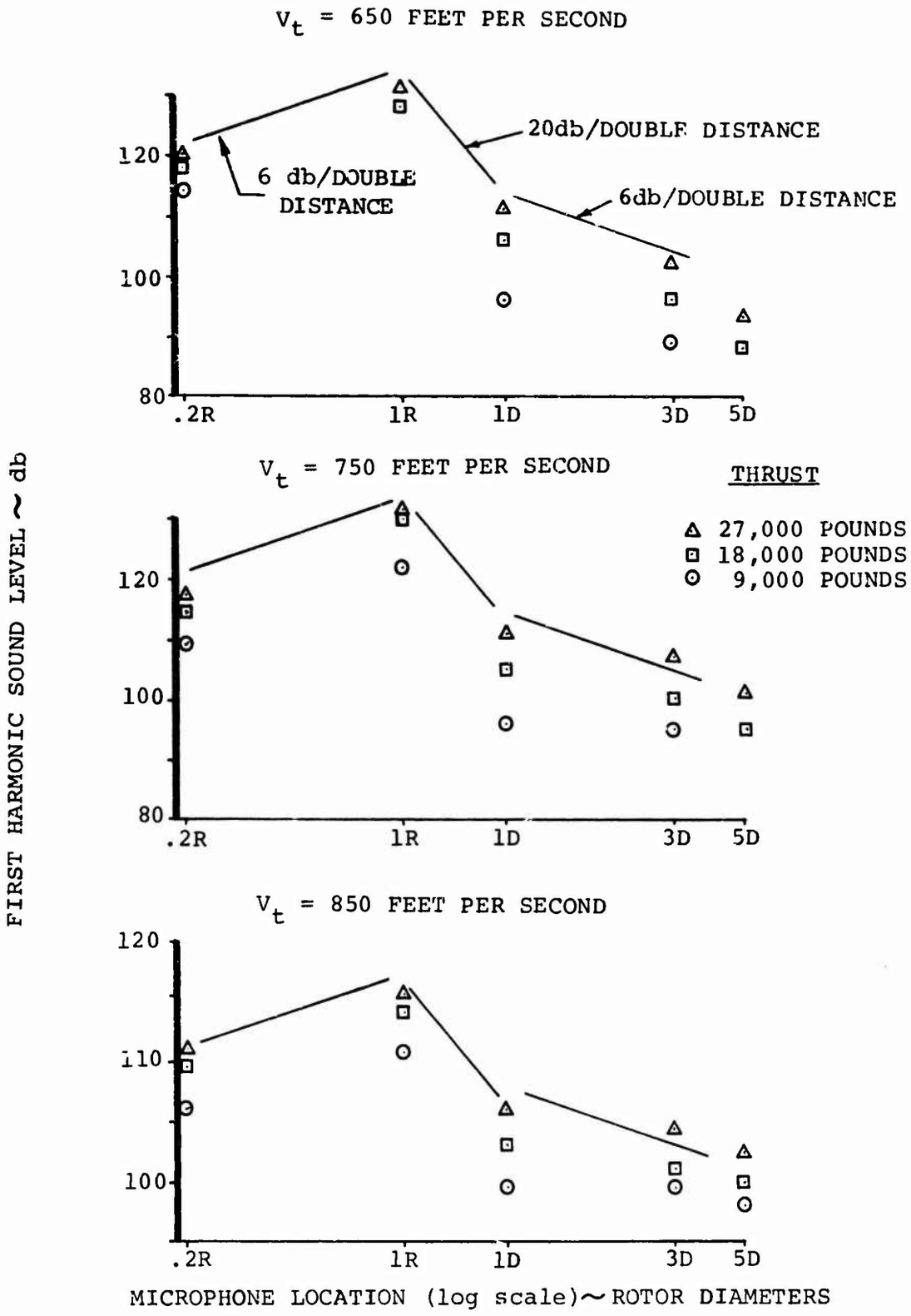

Figure 41. Propagation of First Harmonic Sound Levels.

occur as a result of a strong reflected ray signal shown on the ray path diagram illustrated in Figure 21. The pressures at the 5D location range from,

$$(SPL_{300} - SPL_{500}) = -4.1 \text{ db relative to the 3D position}$$

to

$$(SPL_{300} - SPL_{500}) + \quad SPL \text{ (Reflected Wave)}$$

$$= -4.1 + 6 = 1.9 \text{ db}$$

higher than the 3 diameter levels. Because of variation in phase relationships, a range of levels can be expected.

As previously noted, these data display wave interference effects near the 3rd, 4th and 5th harmonics of blade passage. For destructive interference to occur, the signal wave length must be twice the wave length of that associated with the time delay between incident and reflective wave. At the 3 diameter location, the time delay from incident to reflected pulse is 0.0096 seconds. The frequency associated with twice this period is, $f' = \frac{1}{2\Delta t} = \frac{1}{2(.0096)} = 52\text{Hz}.$

The blade passage frequencies and harmonics where wave interference would be expected for the tip speeds of the evaluation matrix are,

RPM	V_t	SHAFT ROTATION, (f_1) (Hz)	BLADE PASSAGE ($3f_1$) (Hz)	INTERFERENCE HARMONIC $\left(\frac{52}{3f_1}\right)$
271	850	4.5	13.5	3.8
239	750	4.0	12.0	4.3
207	650	3.45	10.35	5.0

The frequency of the rotor noise signal coincides with the frequency of the time delay between incident and reflected pulse at approximately the 4th harmonic number at a tip speed of 850 ft/sec, 4th harmonic at 750 ft/sec and 5th harmonic at 650 ft/sec. This interference is shown in the noted illustra-

tions and in the data recorded at the 3 diameter microphone locations. While the spectra recorded at 1D and 5D decays in a more regular manner with frequency, data at the 3D position displays a constructive/destructive interference pattern at the odd integer harmonics of 52 Hz, i.e., 52, 156, 260, 364 Hz, etc.

Data contained in Appendix B can be used in studying noise propagation of broadband noise of rotors and should be helpf l for evaluating this area of the rotor noise spectra.

Literature Cited

1. Lowson, M. V., and Ollerhead, J. B., Studies of Helicopter Noise, U.S. Army Aviation Materiel Laboratories Technical Report TR 68-60, January 1969.

2. Schlegel, R. G.; King, R. J.; and Mull, H. R., Helicopter Rotor Noise Generation and Propagation, U.S. Army Materiel Laboratories Technical Report TR 66-4, October 1966.

3. Pruyn, R. R., In-Flight Measurement of Rotor Blade Airloads, Bending Moments, and Motions, Together With Rotor Shaft Loads and Fuselage Vibration on a Tandem Rotor Helicopter, U. S. Army Aviation Materiel Laboratories Technical Report TR 67-9, May 1967.

4. Scheiman, J., A Tabulation of Helicopter Rotor-Blade Differential Pressures, Stresses, and Motions, as Measured in Flight, National Aeronautics and Space Administration, NASA TM-X-952, Washington, D.C., March 1964.

5. Burpo, F. B., and Lynn, R. R., Measurement of Dynamic Airloads on a Full Scale Semi-Rigid Rotor, U.S. Army Transportation Research Command Technical Report TR 62-42, December 1962.

6. Spencer, R. H., and Sternfeld, H., Measurement of Rotor Noise Levels and Evaluation of Porous Blade Tips on a CH-47A Helicopter, U.S. Army Aviation Materiel Laboratories Technical Report TR 69-18, September 1969.

7. Stuckey, T. J., and Goddard, J. O., Investigation and Prediction of Helicopter Rotor Noise: 1 - Wessex Whirl Tower Results, Journal of Sound and Vibration, Volume 5, Number 1, pp. 50-80, January 1967.

8. Hubbard, H. H., and Regier, A. A., Propeller Loudness Charts for Light Airplanes, NASA TN 1358, Washington, D.C., July 1947.

9. Sternfeld, H., and Spencer, R. H., Recent Research in Rotor Noise Reduction, Paper Presented at National Aeronautic and Space Engineering and Manufacturing Meeting, Los Angeles, California; October 6-10, 1969.

10. Spencer, R. H., Application of Vortex Visualization Test Techniques to Rotor Noise Research, Paper Presented at the 26th Annual National Forum of the American Helicopter Society, Washington, D.C., June 1970.

Appendix A

This Appendix gives the details of the method used to calculate vortex positions from measurements made from the films. It is divided into three sections. Section I describes the method used to calibrate the camera orientations and convert measurements on the film into unit vectors pointing toward objects in real space. Section II takes the unit vectors pointed toward the blade tip and develops the equations required for finding the blade azimuths required for frame correlation. Section III develops the equations which relate the film measurements of the vortex with the vortex position in space.

SECTION I - METHOD USED TO TRANSFORM FILM MEASUREMENTS TO UNIT VECTORS

In a coordinate system centered at the optical center of the camera lens with its x-axis directed along the optical axis (Figure 42), any point on the film plane is represented by $(-f, y_c, z_c)$ where y_c and z_c are measured from the film. In this coordinate system, the unit vector e_1 directed toward the object has components,

$$(+f/r, -y_c/r, -z_c/r) \text{ where } r = (f^2 + y_c^2 + z_c^2)^{\frac{1}{2}} \quad 1.$$

In order to convert e_1 from the camera oriented coordinate system to e_1', the same vector expressed in a coordinate system with the same origin but oriented with the tower (see Figure 43), the following rotation, A, is used:

$$e_1' = A \cdot e_1$$

In order to determine A, it is necessary to know only three unit vectors in each system:

$$e_1' = A \cdot e_1$$

$$e_2' = A \cdot e_2$$

$$e_3' = A \cdot e_3$$

These define the matrix E, whose columns are the unit vectors (e_1, e_2, e_3) and the matrix E', whose rows are the vecors (e_1', e_2', e_3') then

$$E' = A \cdot E$$

Thus

$$A = E' \cdot E^{-1} \quad 2.$$

This requires that E have an inverse which means that the three images on the film cannot be in a straight line.

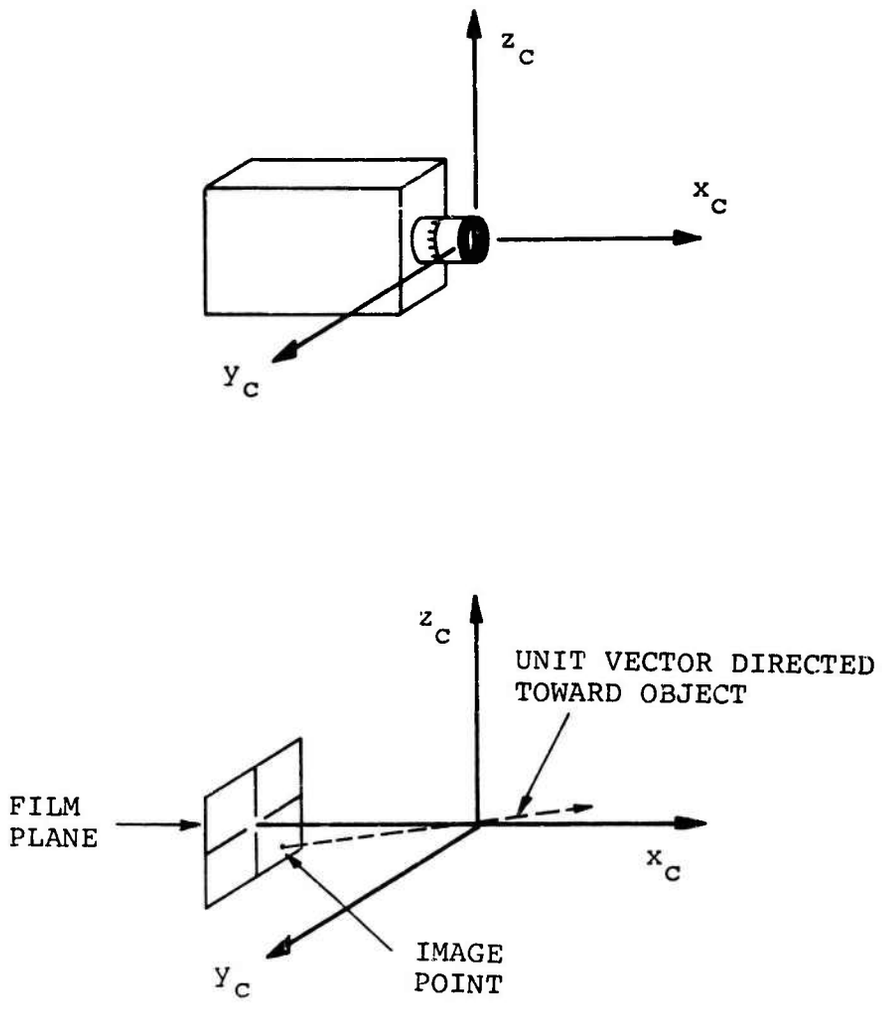

Figure 42. Camera Coordinate System.

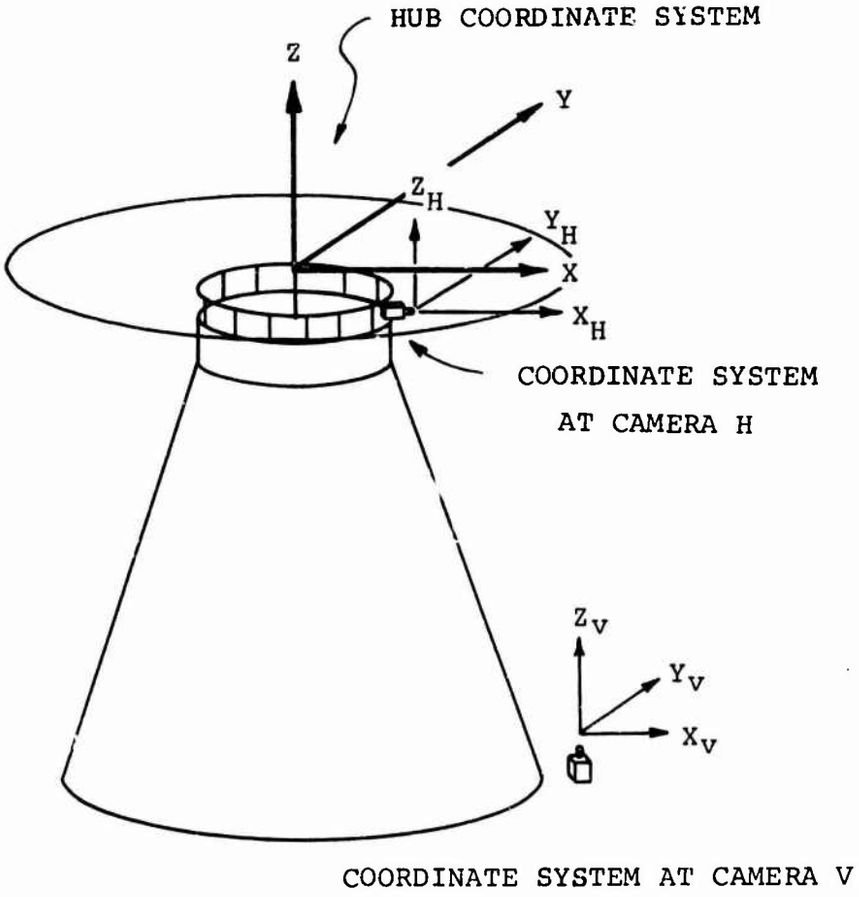

Figure 43. Coordinate Systems Used in Calculating Vortex Positions

Targets from the calibration grid photographed were chosen and from their coordinates on the film, e_1, e_2 and e_3 were calculated; e_1', e_2', and e_3' were found from the known positions of the targets in space. A was then found from Equation 2.

SECTION II - CALCULATION OF BLADE AZIMUTH FROM TIP IMAGE POSITION

In order to find the blade azimuth in each frame of the film from all cameras, the film coordinates of the blade tip were read. These measurements were then converted to unit vectors by the method of Section I. Figure 44 shows the two methods used to find the azimuth of the blade from a unit vector. Unit vectors at Camera H were extended until they intersected the sphere of possible blade positions. This method, however, would have produced inaccurate results if used for the points from Camera V. Instead, on each run, the height of the tip path plane was determined from Camera H and unit vectors from Camera V were extended until they intersected the tip path plane.

Horizontal Camera Points

The unit vector $(\bar{x}, \bar{y}, \bar{z})$ pointing to the blade tip is found from film measurements. A point along the line defined by this unit vector has the equation:

$$\begin{aligned} x &= \bar{x}\,\rho + a \\ y &= \bar{y}\,\rho + b \\ z &= \bar{z}\,\rho + c \end{aligned} \qquad 1.$$

where (x, y, z) = coordinates of a point on the line in hub coordinate system

$(\bar{x}, \bar{y}, \bar{z})$ = unit vector defining the line

ρ = distance from origin of camera coordinate system

(a, b, c) = coordinates of the origin of the horizontal camera in hub coordinate system

The sphere of possible blade tip positions is defined by:

$$x^2 + y^2 + z^2 = R_o^2$$

where R_o = blade radius

Intersecting the line and the sphere gives

$$\rho^2(\bar{x}^2 + \bar{y}^2 + \bar{z}^2) + 2\rho\,(\bar{x}a + \bar{y}b + \bar{z}\,c) + a^2 + b^2 + c^2 - R_o^2 = 0$$

Since $(\bar{x}, \bar{y}, \bar{z})$ is a unit vector, this reduces to

$$\rho^2 + 2\rho\,(\bar{x}a + \bar{y}b + \bar{z}c) + a^2 + b^2 + c^2 - R_o^2 = 0$$

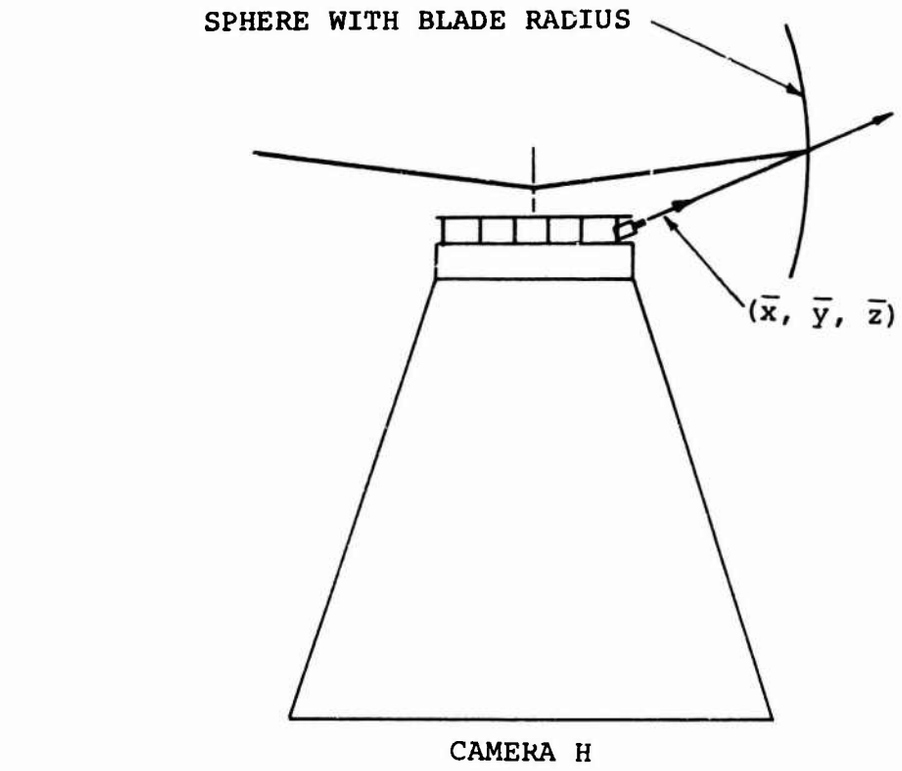

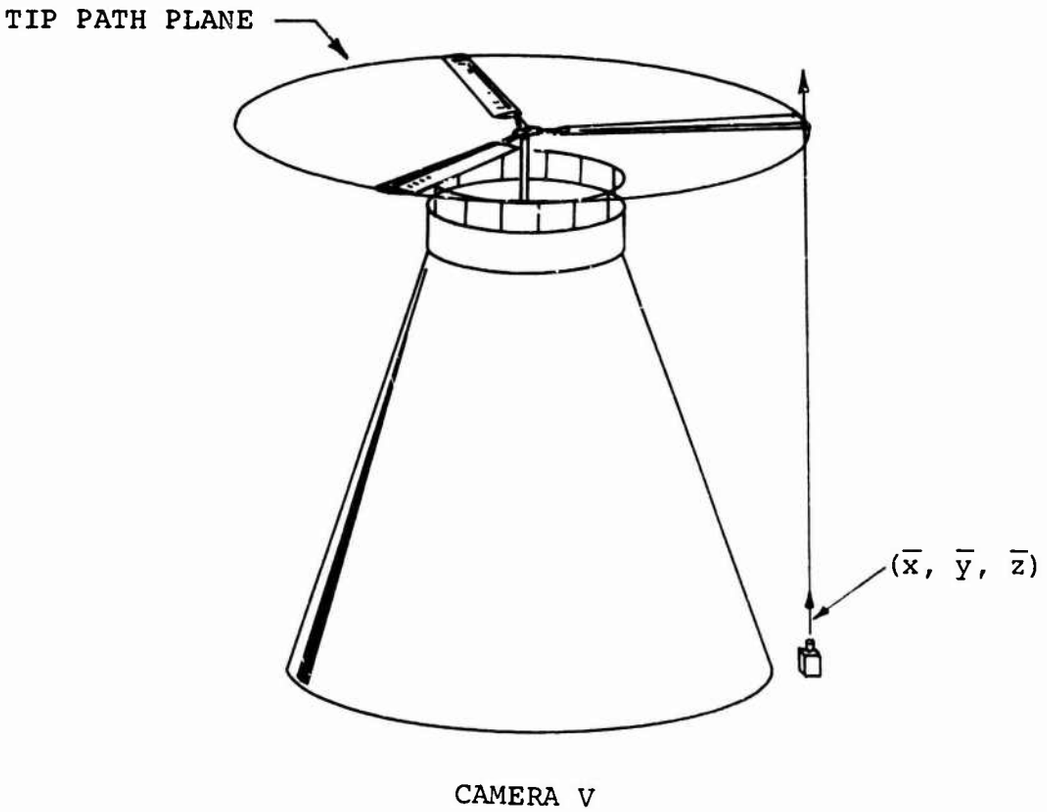

Figure 44. Schematic Used in Finding Blade Azimuth.

This can be solved for ρ using the quadratic formula

$$\rho = -(\bar{x}a + \bar{y}b + \bar{z}c) + \{ (\bar{x}a + \bar{y}b + \bar{z}c)^2 - (a^2 + b^2 + c^2 - R_o^2) \}^{\frac{1}{2}}$$

The discriminate was added because the point in front of the camera corresponding to a positive ρ was desired. From ρ, (x, y, z) can be found by Equation 1 and the azimuth of the blade by

$$\psi = -\tan^{-1}\left(\frac{y}{x}\right) \qquad 2.$$

Vertical Camera Points

Again the unit vector $(\bar{x}, \bar{y}, \bar{z})$ was derived from the film measurements and the line extending in the direction of one of these unit vectors is given by Equation 1.

The tip path plane is determined from horizontal camera measurements on the same run. The equation for this plan is:

$$z = z_o$$

where z_o = tip path plane height.

Intersecting the line with the plane gives:

$$z = z_o = \bar{z}\rho + c$$

Thus

$$\rho = \frac{z_o - c}{\bar{z}}$$

Again the coordinates of the blade tip are found from Equation 1 and the azimuth of the blade by Equation 2.

SECTION III - METHOD TO FIND VORTEX POSITION

Measurements of the vortex image were made from each frame pair. Enough points were measured in each frame to insure accuracy of a linear interpolation between them. These measurements were converted to unit vectors pointing toward the vortex as described in Appendix A, Section I. Thus for a given frame pair, n unit vectors, $(\bar{x}_{Hj}, \bar{y}_{Hj}, \bar{z}_{Hj})$, j = 1, n have been found from Camera H toward the vortex and m unit vectors, $(\bar{x}_{Vk}, \bar{y}_{Vk}, \bar{z}_{Vk})$ k = 1, m have been found from Camera H toward the vortex. The coordinate systems of these two sets of unit vectors are shown in Figure 11. All equations are referred to this figure.

The parametric equation of a line from Camera H to the j^{th} point on the vortex is:

$$X_{Vj} = \bar{X}_{Hj} \cdot r_H + a'$$

$$Y_{Vj} = \bar{Y}_{Hj} \cdot r_H + b'$$

$$Z_{Vj} = \bar{Z}_{Hj} \cdot r_H + c'$$

in the Camera V coordinate system

where: $(\bar{x}_{Hj}, \bar{y}_{Hj}, \bar{z}_{Hj})$ = unit vector toward j^{th} vortex point from Camera H

r_H = distance from Camera H to any point on the line

(a', b', c') = coordinate of Camera H in Camera V's coordinate system

choosing the k^{th} point from Camera V with unit vector $(\bar{x}_{Vk}, \bar{y}_{Vk}, \bar{z}_{Vk})$, the plane containing this point and the y_V axis can be found (Plane K in Figure 11).

The equation of this plane is

$$X_v = M_k Z_v$$

where $$M_k = \frac{\bar{X}_{Vk}}{\bar{Z}_{Vk}}$$

Finding the point of intersection of this plane and line gives

$$r_{Hjk} = \frac{M_k c' - a'}{\bar{X}_{Hj} - M_k \bar{Z}_{Hj}}$$

where $(x_{V_I}, y_{V_I}, z_{V_I})$, the coordinates of this point, I, can be found from Equation 3 above.

The angle ε_{jk} is then the same of the angle from $\overline{Vk}$ to the (x_V, z_V) plane and the angle from the (x_V, z_V) plane to $\overline{VI}$:

$$\varepsilon_{jk} = \tan^{-1}\left\{\frac{\bar{y}_{Vk}}{(\bar{x}_{Vk}^2 + \bar{z}_{Vk}^2)^{1/2}}\right\} + \tan^{-1}\left\{\frac{y_{VI}}{(x_{VI}^2 + z_{VI}^2)^{1/2}}\right\}$$

The method of solution thus commenced by choosing a point as seen from Camera H, j = 1. Then calculating ε_{jk} with k = 1, 2,

3, etc. until ϵ_{jk} changes sign. Thus using a linearly interpolated value of r_{Hj}, the coordinates of the point on the vortex could be found from Equation 3. This gives the coordinates of the point on the vortex pointed to by the first unit vector from Camera H. This process is continued until the coordinates of all the points chosen from Camera H have been found.

Appendix B

Acoustical Data

All sound levels in this appendix, as well as throughout the report, are relative to the standard acoustical pressure of 0.0002 dyne/cm^2. In keeping with the recommendations of current international organizations and the U.S. National Bureau of Standards, when this pressure is referred to in this report, it has been noted in terms of its MKS system equivalent, 0.00002 Newton/$meter^2$.

To obtain the sound pressure level for a given test point and microphone location, the level of the ordinate, L, is read and added to the calibration factor presented in the upper right corner of the graph. Thus, the first harmonic level for Run 1, Microphone LF-2 (1 Dia.), is

$$SPL = 50 + 56 = 106 \text{ db.}$$

The averaged waveforms accompanying the frequency spectra have been normalized to the same approximate amplitude and period for waveform evaluation. Discussion of this is found in Section 4.2, Recorded Data, page 32, as well as Data Analysis Procedures, Section 3.1, page 17.

Data has been omitted for a small number of test conditions and microphone positions where the instrumentation did not perform consistently and the resulting information was therefore not suitable for publication.

TABLE IV

TEST CONDITIONS

Run Number	Tip Speed ft/sec	Rotor Speed rpm	Thrust lb	Coll Pitch deg@.7R	Shaft Torque in-lb X 10^{-6}	Wind Speed mph	Wind Direction	Temperature °F	Barometric Pressure in. H_G
1	897	286	8357	4° 20'	0.310	6	N.N.W	46	30.48
2	901	287	11692	5° 20'	0.402	5	N.W.		
3	901	287	15027	6° 10'	0.505	6	N.W.		
4	894	285	17699	6° 55'	0.605	6	N.W.		
5	901	287	20274	7° 35'	0.745				
6	901	287	24700	9° 35'	0.902	6	S.W.		
7	897	286	26786	9° 50'	1.100				
8	897	286	26783	9° 50'	1.100	5	S.W.		
9	897	286	31480	11° 40'	1.350	0	W		
10	897	286	32351	12° 0'	1.410	8	S.W.	40	30.48
11	901	287	14463	6° 10'	0.500	10	S.W.	45	30.44
12	897	286	17093	6° 55'	0.610	10	W	45	30.44
13	850	271	9059.	4° 50'	0.270	9	S.W.	50.	30.24
14	850	271	11260.	5° 50'	0.343	9	S.W.		
15	847	270	14004.	6° 55'	0.420	7	S.W.		
16	845	269	17031.	7° 25'	0.541	7	S.W.		
17	847	270	17615.	8° 0'	0.660	10	S.		
18	847	270	24233.	9° 25'	0.822	7	S.W.		
19	850	271	27977.	10° 40'	1.010	9	S.W.		
20	850	271	31280.	11° 50'	1.270	9	W.		
21	847	270	32489.	12° 25'	1.420	10	W.	50.	30.24
22	901	287	7023	4° 30'	0.310	10	N.N.W	47	30.27
23	901	287	12503	5° 25'	0.408	12			
24	897	286	15630	6° 10'	0.500	14			
25	901	287	18050	7° 0'	0.598	15			
26	897	286	20527	7° 50'	0.735	13			
27	901	287	24703	9° 10'	0.882	11			
28	897	286	27491	10° 5'	1.100	13			
29	897	286	33279	12° 5'	1.360	10			
30	901	287	33211	12° 25'	1.410	13	N.N.W	47	30.27
31	850	271	8271	4° 45'	0.258	11	N.N.W	50	30.29
32	850	271	11458.	5° 50'	0.345	12	N.N.W	50	30.29

TABLE IV - Continued

Run Number	Tip Speed	Rotor Speed	Thrust	Coll Pitch	Shaft Torque	Wind Speed	Wind Direction	Temper-ature	Barometric Pressure
	ft/sec	rpm	lb	deg@.7R	in-lb X10^{-6}	mph		°F	in.HG
33	847	270	15527.	6° 40'	0.425	14	N.N.W	50	30.29
34	847	270	16863.	7° 25'	0.518	10			
35	847	270	19861.	8° 10'	0.645	10			
36	850	271	26630.	10° 10'	0.895	13			
37	847	270	28822.	11° 0'	1.050	16			
38	850	271	31849.	12° 6'	1.230	10			
39	847	270	33449.	12° 40'	1.400	11		50	30.29
40	847	270	26827.	10° 0'	0.880	10	N.N.W	51	30.27
41	797	254	6346.	5° 10'	0.233	14.	N.N.W	52.	30.24
42		254	11118.	6° 15'	0.310	7.			
43		254	14640.	7° 20'	0.397	12.			
44	797	254	17825	8° 10'	0.490	16.			
45	800	255	20628.	9° 0'	0.605	14.			
46	797	254	23543.	10° 10'	0.755	15.			
47	800	255	27443.	11° 25'	0.938	17.			
48	797	254	30620.	12° 35'	1.150	14.			
49	797	254	33039.	13° 25'	1.400	12.			
50	797	254	23912.	10° 10'	0.755	15.	N.N.W	52.	30.24
51	753	240	9701.	5° 50'	0.238	11.	N.N.W	52.	30.24
52	750	239	12167.	6° 55'	0.310	13.			
53	750	239	15802.	8° 10'	0.412	10.			
54	750	239	18985.	9° 25'	0.530	12.			
55	753	240	21511.	10° 5'	0.635	13.			
56	750	239	24154.	11° 20'	0.780	11.			
57	750	239	26963.	12° 20'	0.920	14.			
58	750	239	29210.	12° 55'	1.090	12.			
59	753	240	31363.	13° 40'	1.260	12.	N.N.W	52.	30.24
60	703	224	264-7	13° 0'	0.938	9.	N.N.W	52	30.24
61	700	223	26803	13° 30'	1.010	13.	N.N.W		
62	700	223	23649	12° 20'	0.785	11.	N.N.W		
63	703	224	11836	10° 10'	0.528	12.	N.N.W		
64	703	224	21727	11° 20'	0.655	13.	N.N.W		
65	697	222	14938	9° 10'	0.418	13.	N.N.W	52	30.24

TABLE IV - Continued

Run Number	Tip Speed	Rotor Speed	Thrust	Coll Pitch	Shaft Torque	Wind Speed	Wind Direction	Temper-ature	Barometric Pressure
	ft/sec	rpm	lb	deg@.7R	in-lb X10^{-6}	mph		°F	in. Hg
66	697	222	12986	8° 0'	0.324	13.	N.N.W	52	30.24
68	703	224	8809	6° 10'	0.220	9.	N.N.W	53.	30.28
69	713	227	8235	7° 5'	0.227	10.	N.N.W	42.	29.49
70	650	207	11632	8° 50'	0.325	12.	W.	42	29.49
71		207	14198	10° 10'	0.429	10.	W.		
72		207	18139	11° 35'	0.550	11.	W.		
73		207	20669	12° 50'	0.701	14.	W.		
74	650	207	23456	13° 50'	0.855	10.	W.		
75	653	208	25369	15° 0'	1.100	11.	W.		
76	647	206	27713	16° 0'	1.180	6.	N.W.		
77	603	192	9276	7° 40'	0.232	15-16	N	29	29.90
78	600	191	8845	7° 40'	0.234	17	N.W	29	29.90
79	600	191	12510	9° 30'	0.338	14	N.W.		
80	600	191	15405	11° 15'	0.452	14	N.W		
81	596	190	15400		0.448	8-9	N.W		
82	600	191	18411	12° 45'	0.610	11	N.		
83			21478	14° 0'	0.760	11	M.W		
84			23229	15° 30'	0.915	10	N.W		
85	600	191	24918	16° 5'	1.050	13	N.W		
86	596	190	24641	17°	1.140	13	N.	29	29.90
87	600	191	24581	16° 5'	1.050	13	W.	39	29.73
88	700	223	26594	12° 50'	0.945	11.	W.	39.	29.73
89	600	191	24668	16° 10'	1.010	12	W.	46	29.41
90	700	223	25247	12° 50'	0.925	12.	W.	46.	29.41
91		223	8996	6° 10'	0.235	13.	N.W	43	29.38
92		223	12356	7° 45'	0.329	16.	N.W.		
93	703	224	15205	8° 50'	0.425	N.W.			
94	703	224	17731	9° 50'	0.530	14.	N.W		
95	700	223	20430	11° 0'	0.645	15.			
96		223	23303	12° 0'	0.790	13.			
97		223	24341	12° 40'	0.950	10.			
98	703	224	26108	13° 15'	1.090	9.			
99	700	223	28096	14° 10'	1.310	12.			
100	697	222	29247	14° 50'	1.400	15.	N.W.	43.	29.38

TABLE IV - Continued

Run Number	Tip Speed ft/sec	Rotor Speed rpm	Thrust lb	Coll Pitch deg@.7R	Shaft Torque in-lb X10^{-6}	Wind Speed mph	Wind Direction	Temperature °F	Barometric Pressure in. H_G
87	600	191	24581	16° 5'	1.050	13	W	39	29.73
88	700	223	26594	12° 50'	0.945	11		39	29.73
89	600	191	24668	16° 10'	1.010	12		46	29.41
90	700	223	25247	12° 50'	0.925	12	W	46	29.41
110	800	255	26706	10° 35'	.920-1.100	11	N.W	45	30.23
111	898	286	27372	9° 35'	1.000	8			
112	797	254	16805	7° 40'	0.505	8			
113	800	255	7746	4° 35'	0.248	8		45	30.23
114	747	238	26757	12° 5'	0.975	9	N.W	49	29.97
115	747	238	26925						
116	747	238	27079						
117	850	271	26318	10° 10'	1.100	9	N.W	49	29.97
118	750	239	26109	11° 45'	0.928	12-15	N.N.W		
119	850	271	27642	10° 15'	1.050	9	N.N.W		
120	850	271	26932						
121	797	254	21338	9° 10'	0.690	13-15	N.N.W		
122	797	254	12119	6° 10'	0.352	13	N.N.W	49	29.97

TEST CONDITIONS - SMOKE RUNS

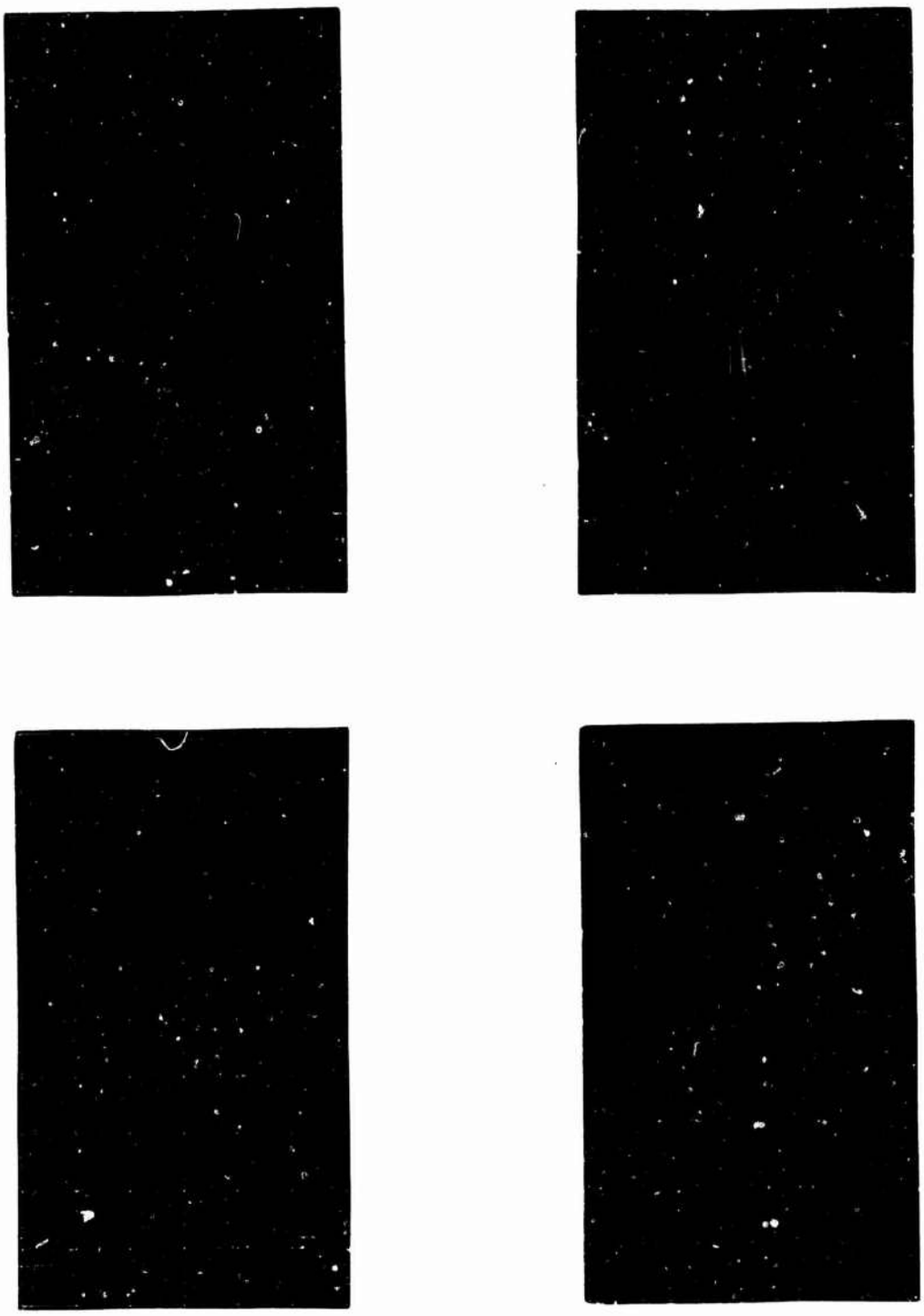

These gradicules, when cut along the centerline, may be used for scaling acoustical data.

RUN 1

TIP SPEED 900 FT/SEC

THRUST 8360 LB

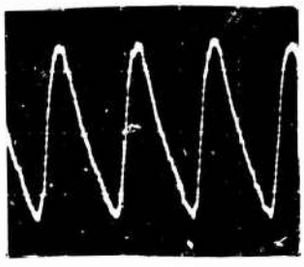

.2 RAD.

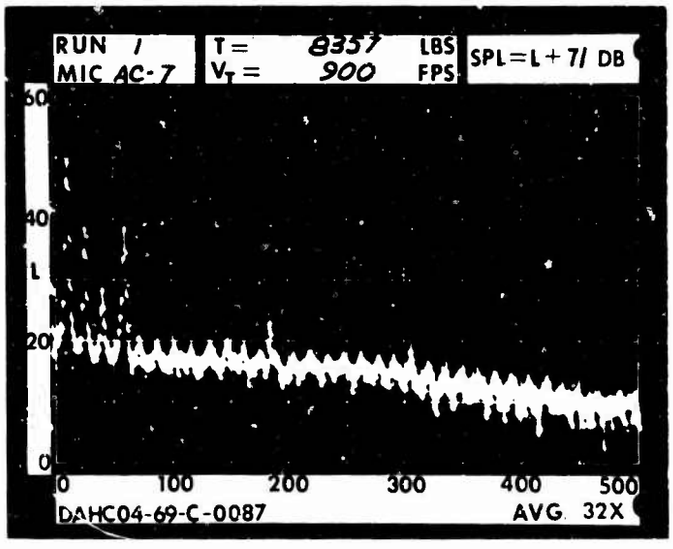

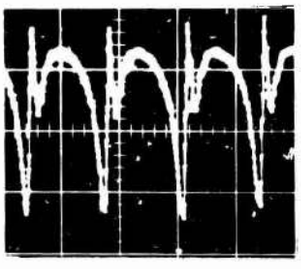

1 RAD.

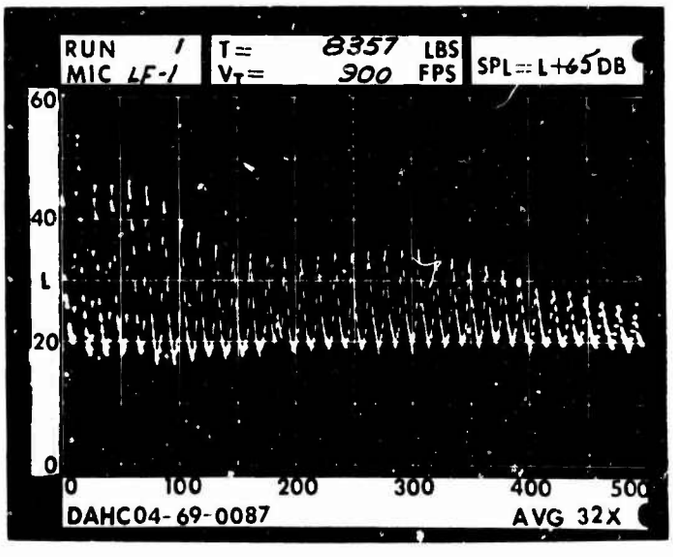

Preceding page blank

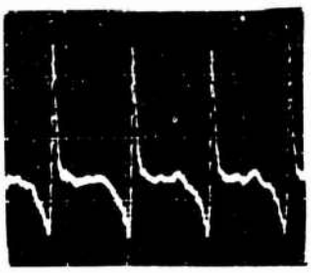

1 DIA.

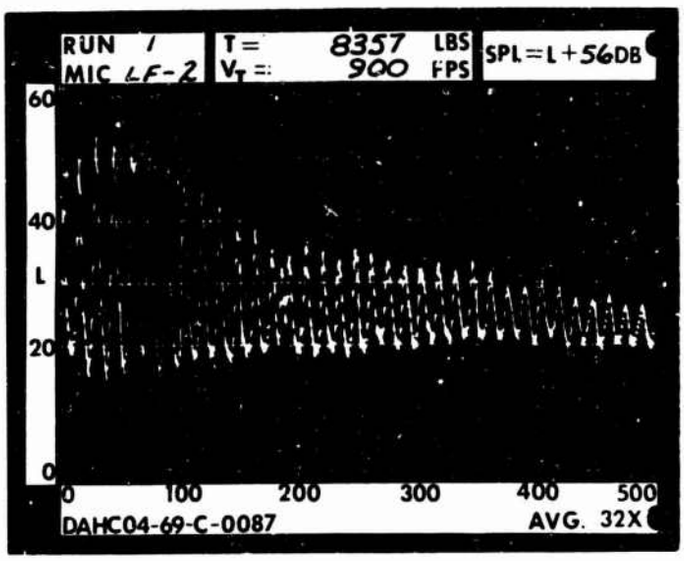

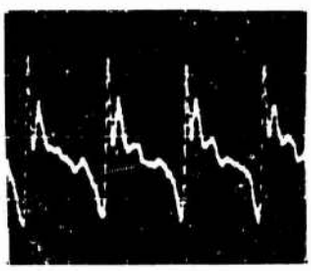

3 DIA.

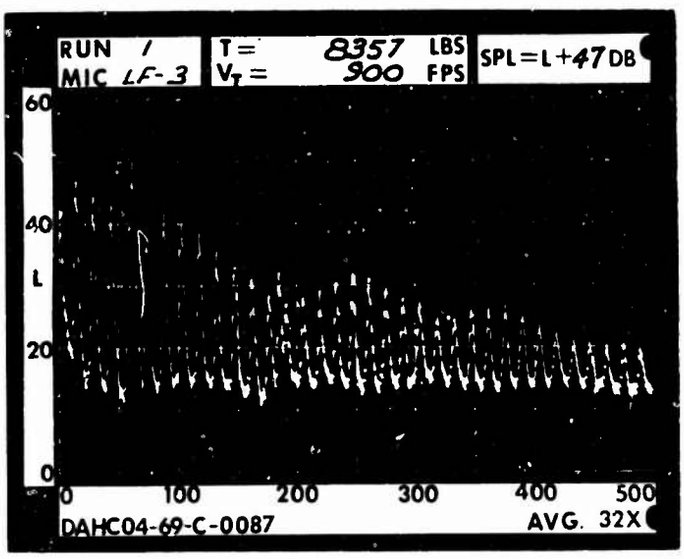

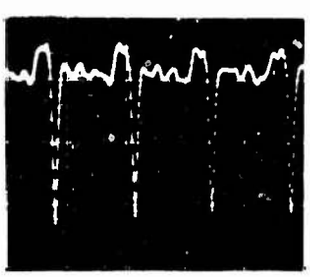

5 DIA.

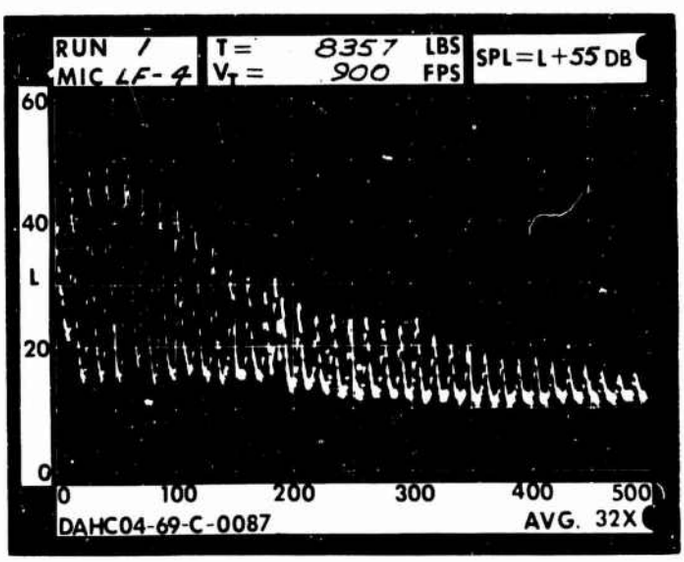

RUN 2

TIP SPEED 900 FT/SEC

THRUST 11700 LB

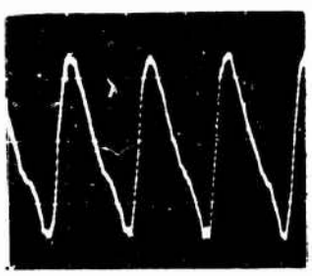

.2 RAD.

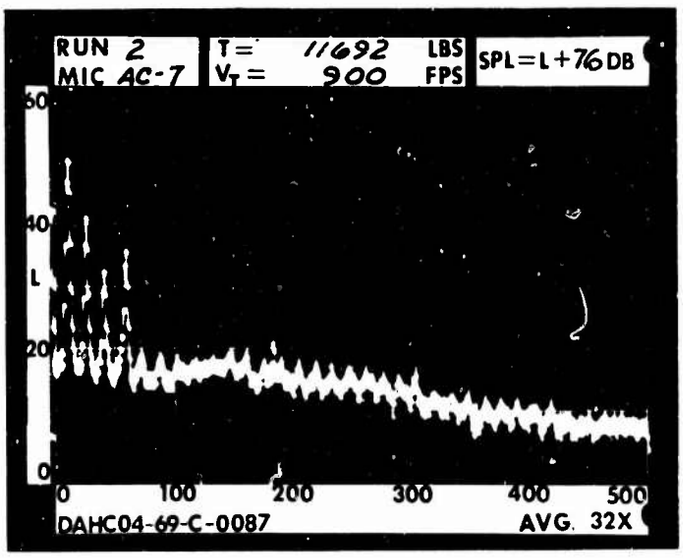

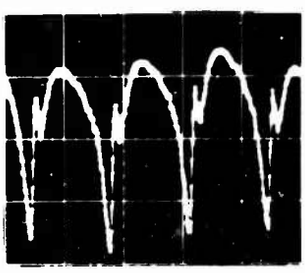

1 RAD.

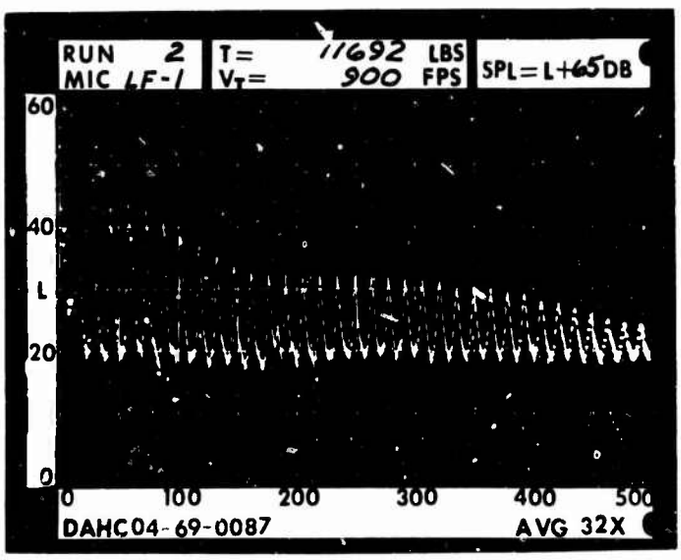

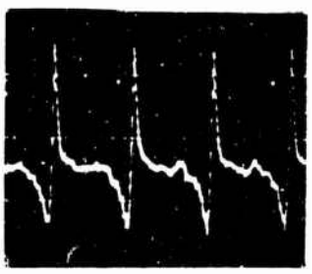

1 DIA.

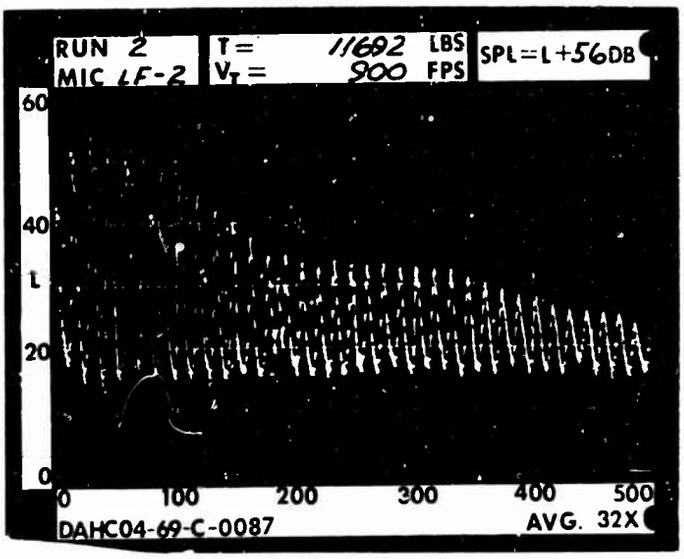

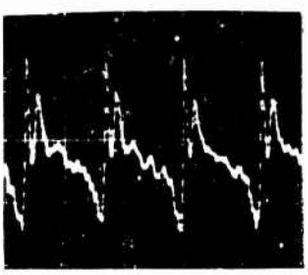

3 DIA.

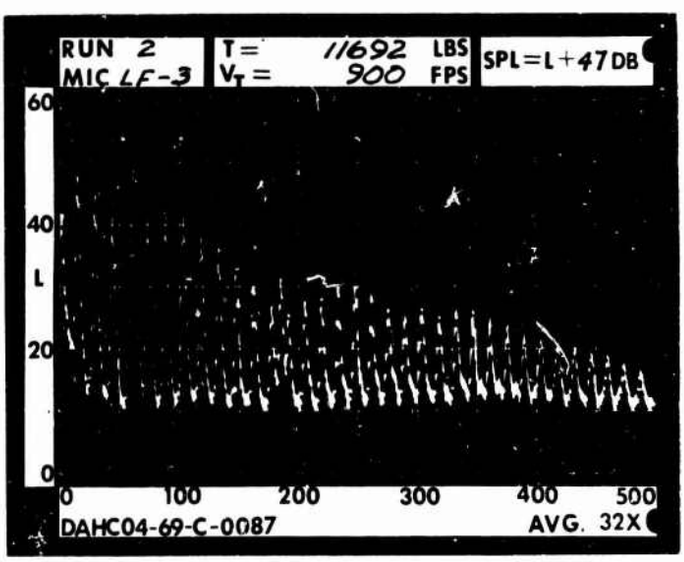

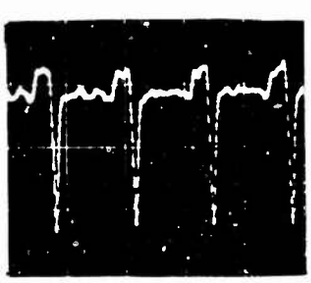

5 DIA.

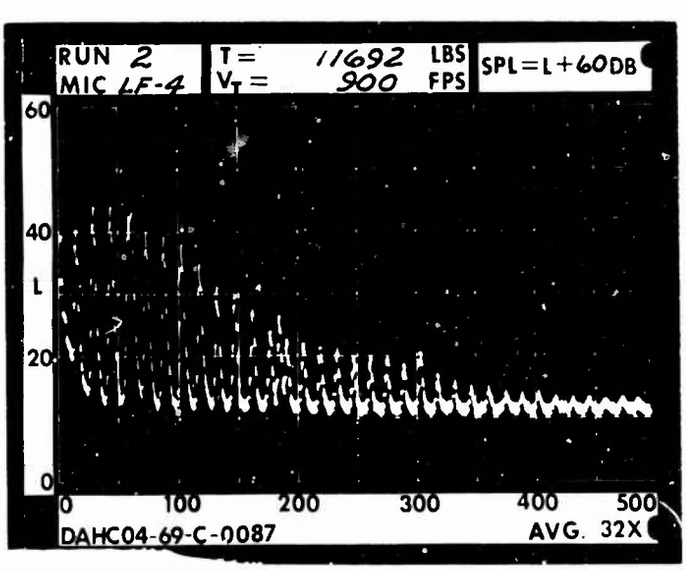

RUN 3

TIP SPEED 900 FT/SEC

THRUST 15000 LB

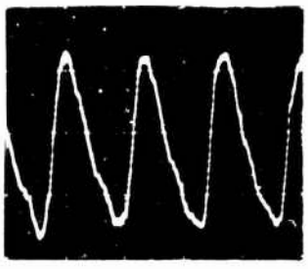

.2 RAD.

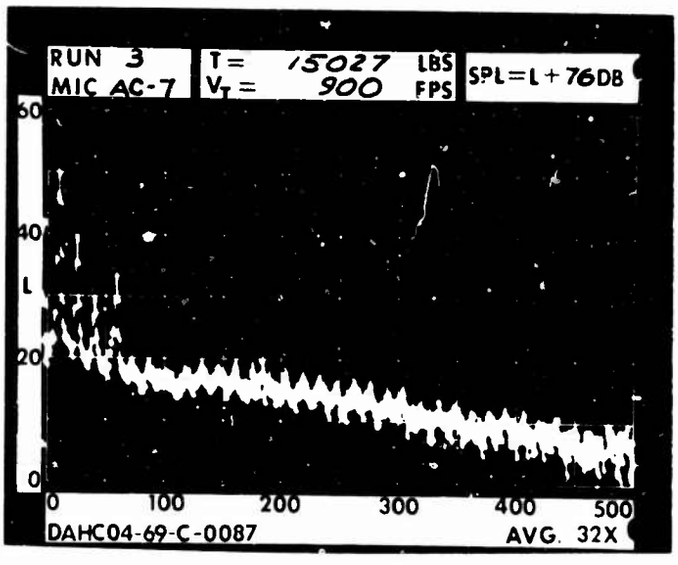

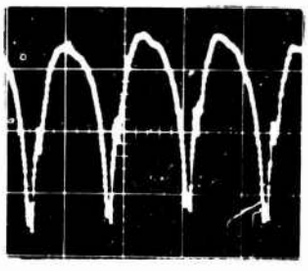

1 RAD.

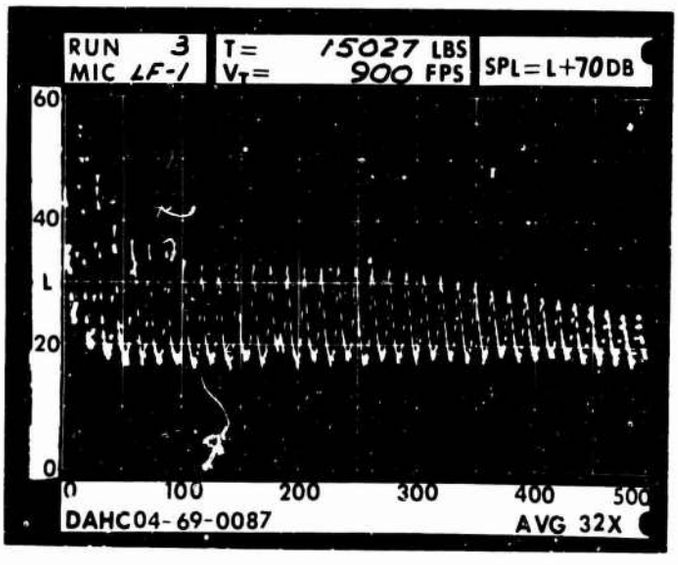

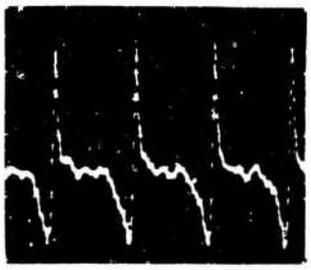

1 DIA.

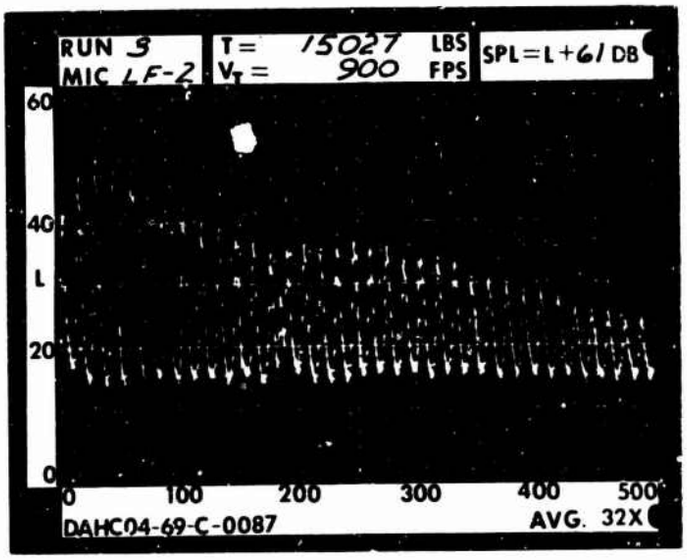

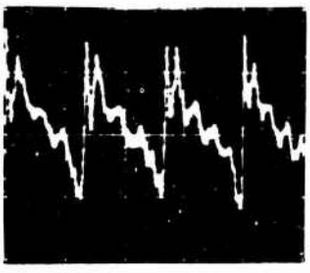

3 DIA.

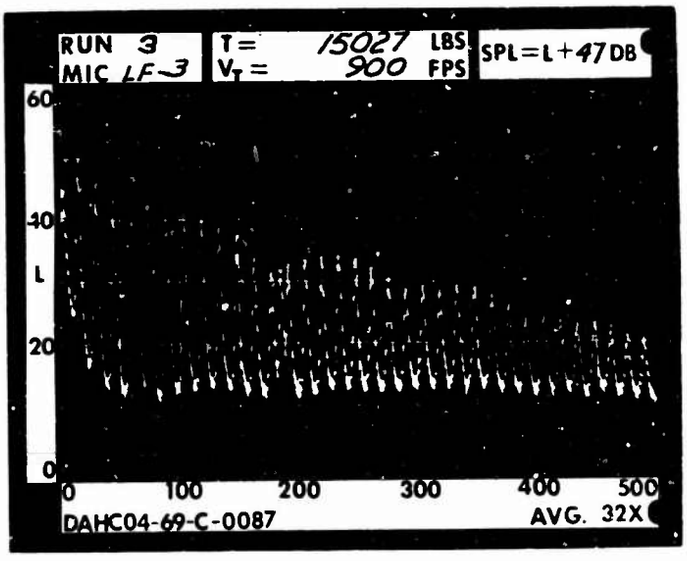

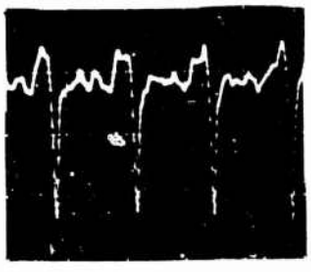

5 DIA.

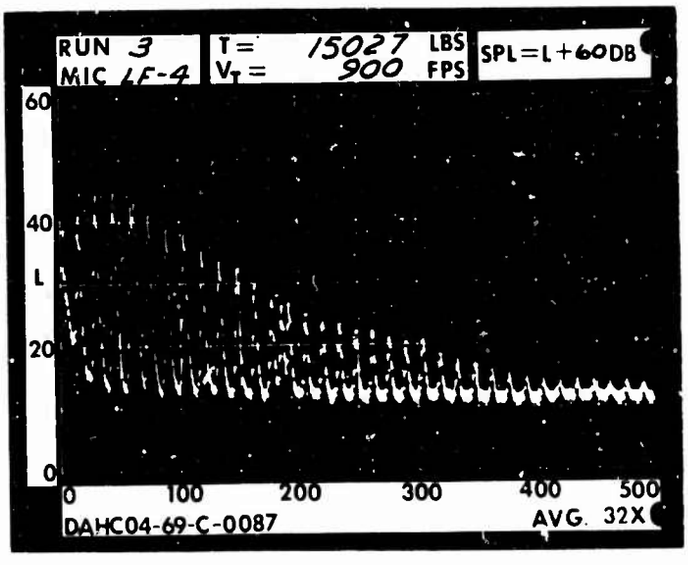

RUN 4

TIP SPEED 900 FT/SEC

THRUST 17700 LB

.2 RAD.

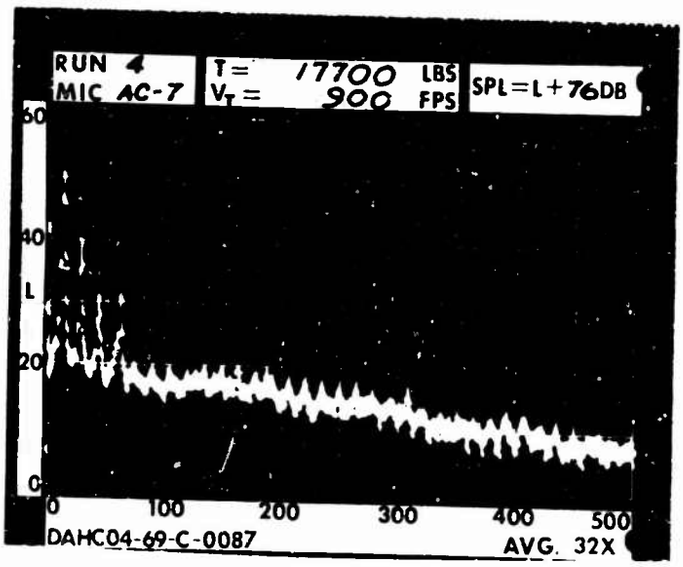

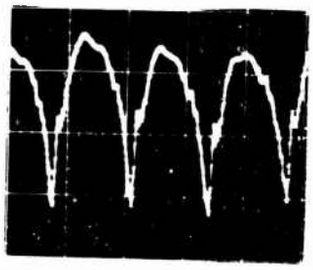

1 RAD.

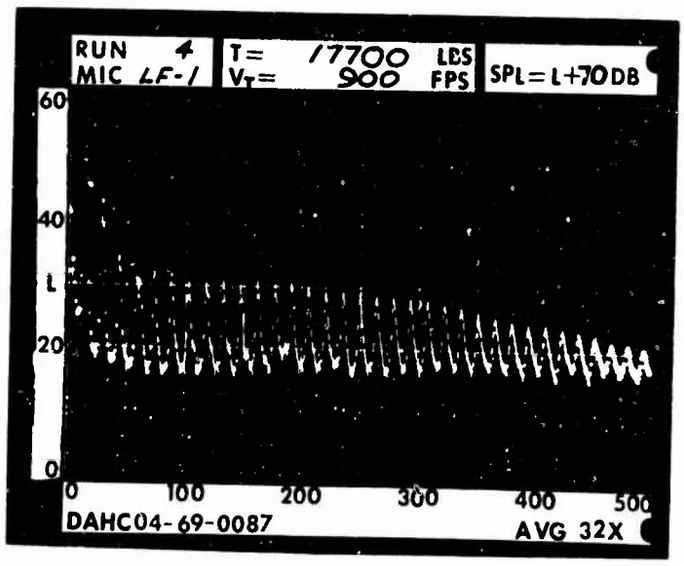

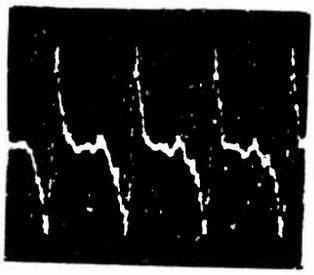

1 DIA.

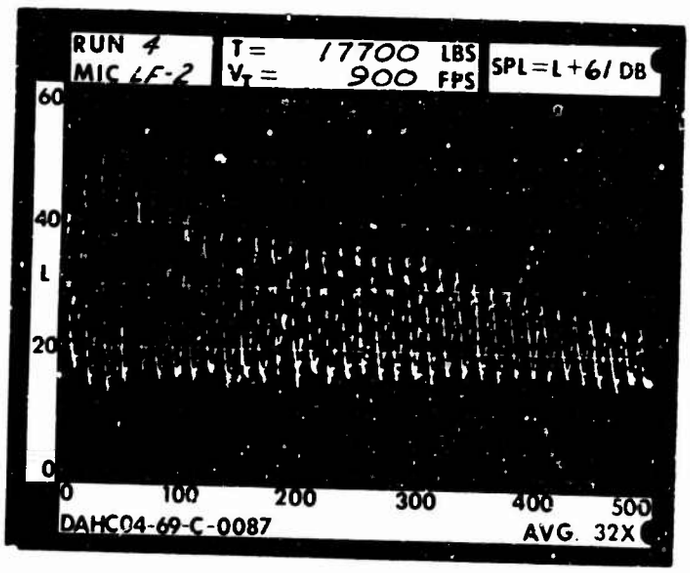

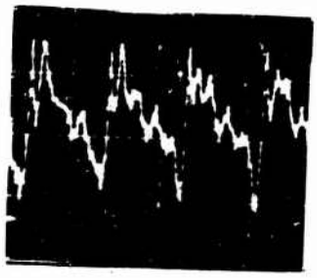

3 DIA.

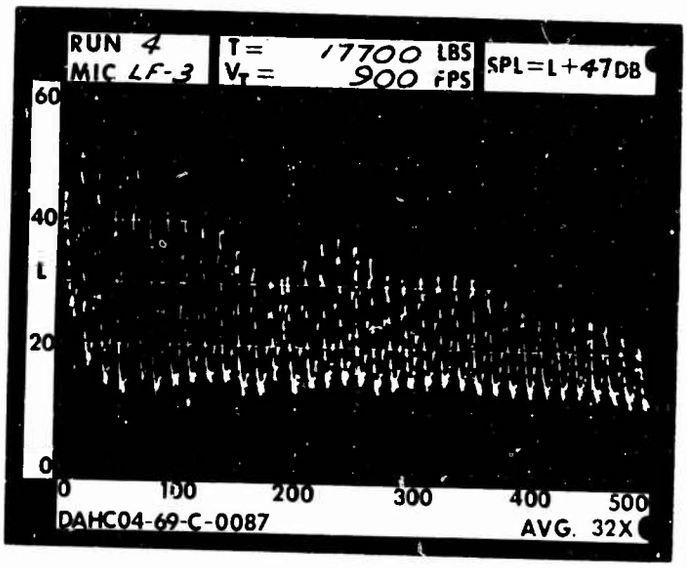

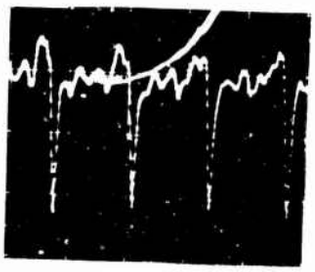

5 DIA.

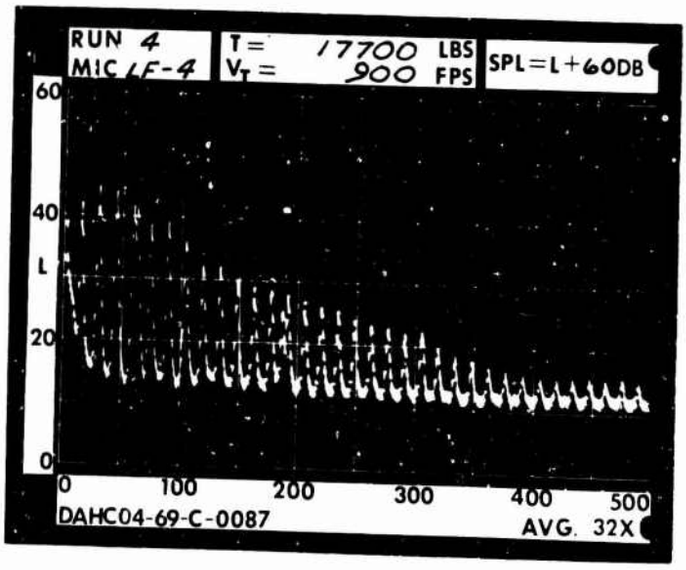

RUN 5

TIP SPEED 900 FT/SEC

THRUST 20300 LB

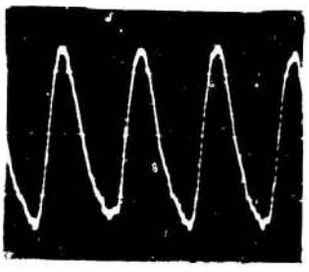

.2 RAD.

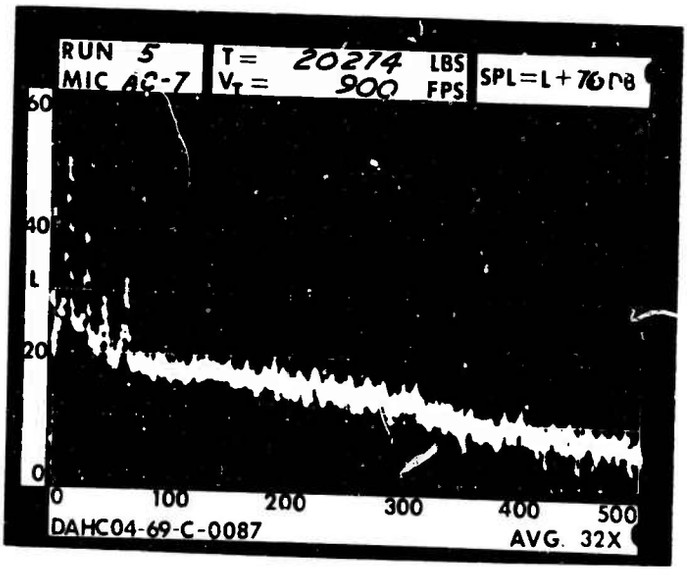

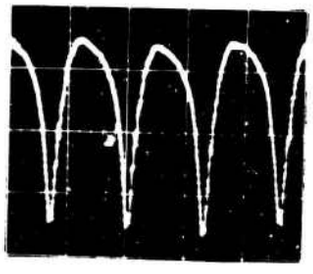

1 RAD.

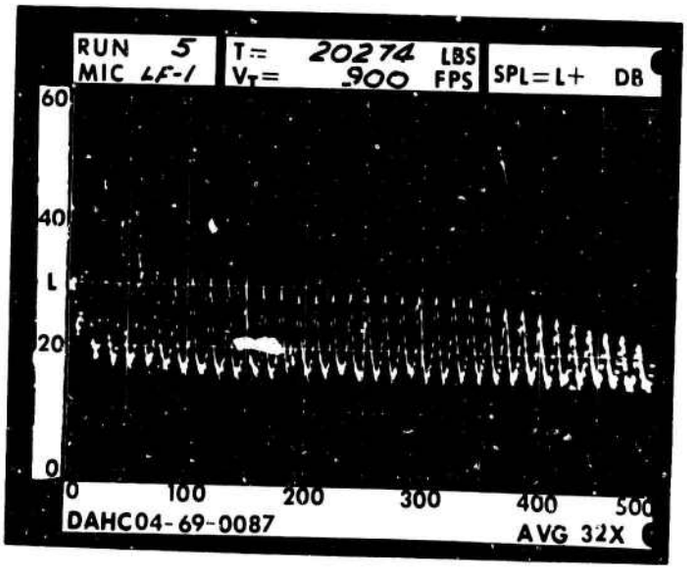

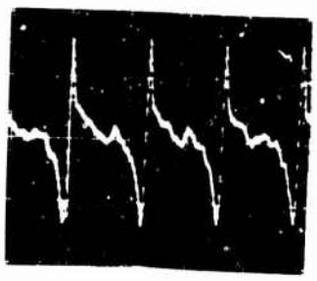

1 DIA.

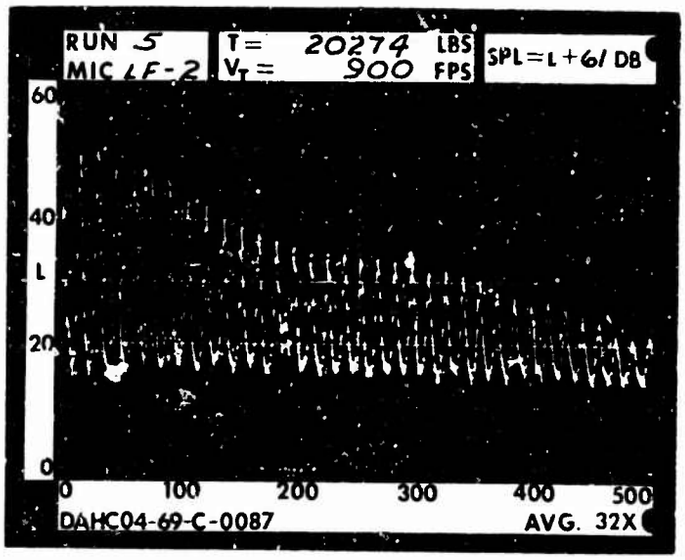

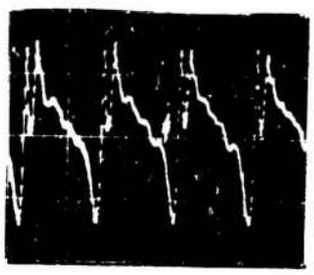

3 DIA.

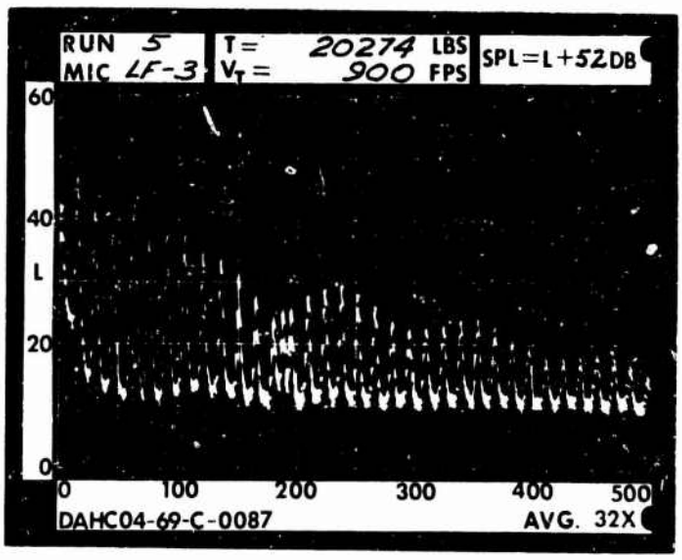

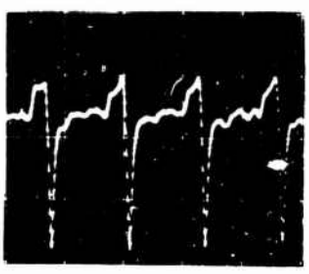

5 DIA.

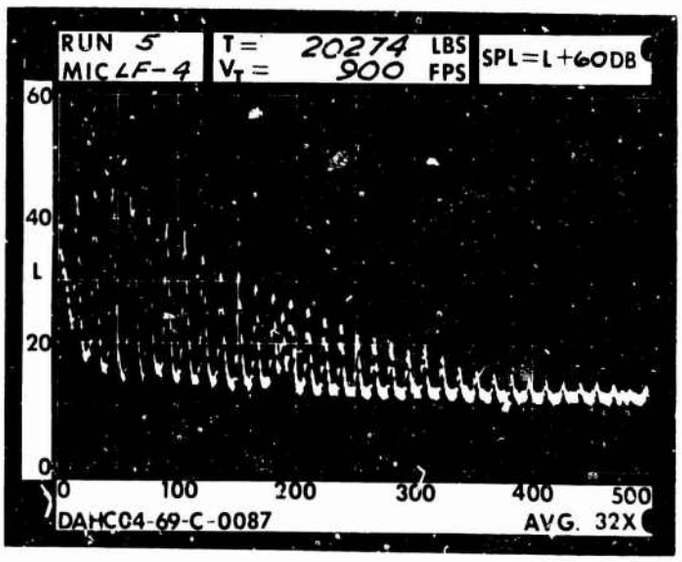

RUN 6

TIP SPEED 900 FT/SEC

THRUST 24700 LB

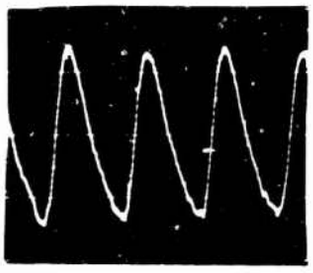

.2 RAD.

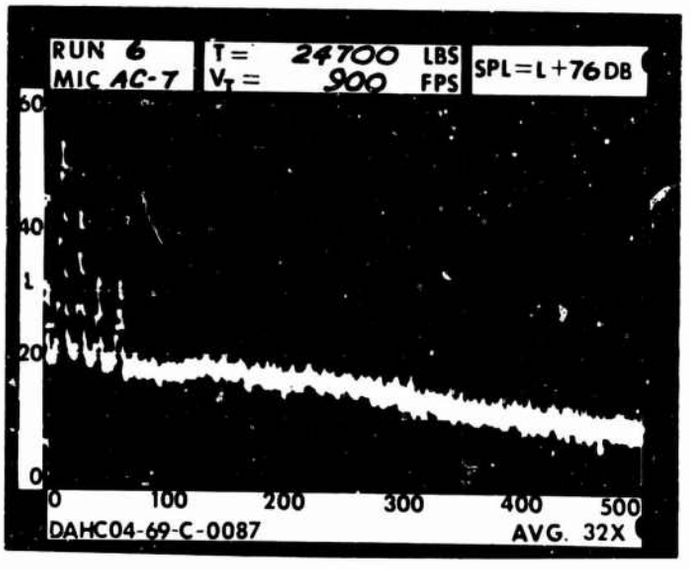

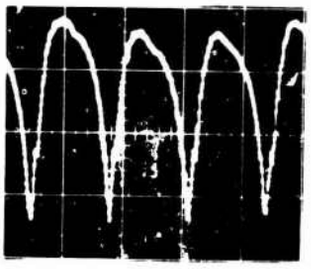

1 RAD.

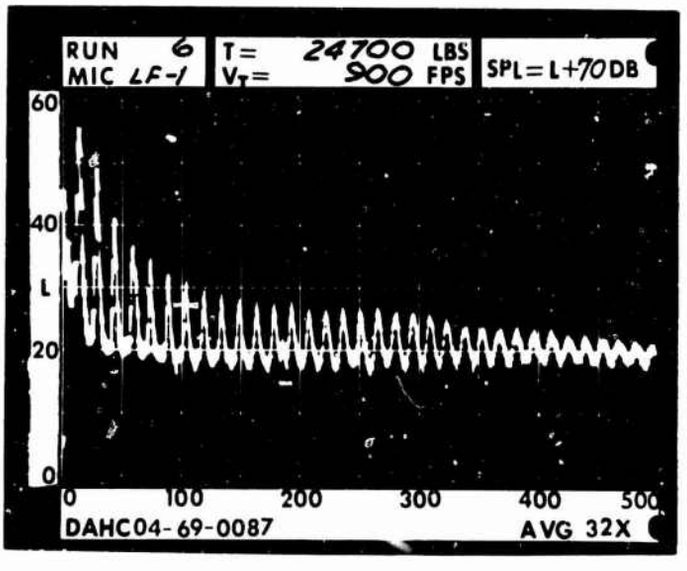

1 DIA.

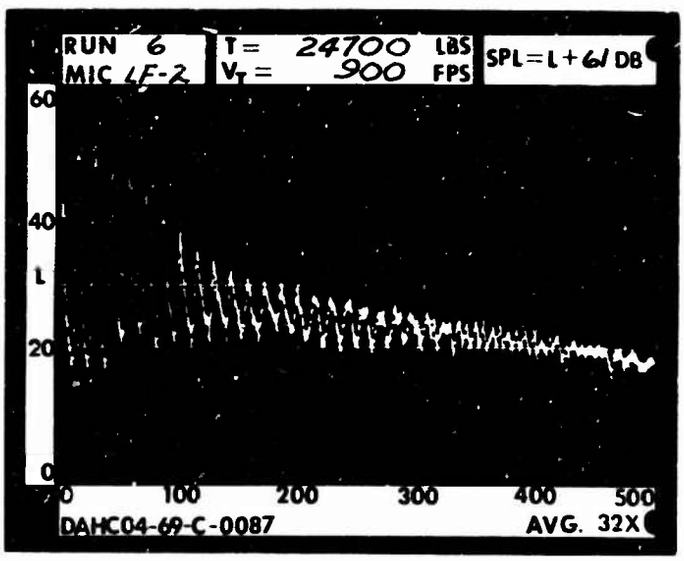

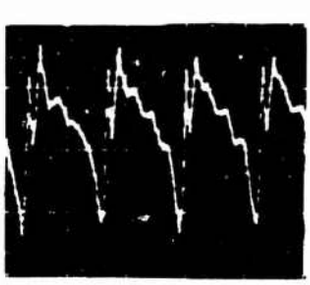

3 DIA.

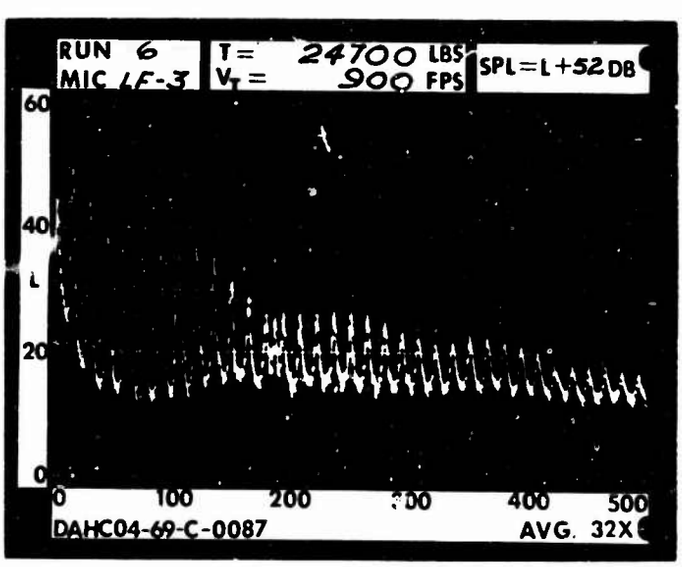

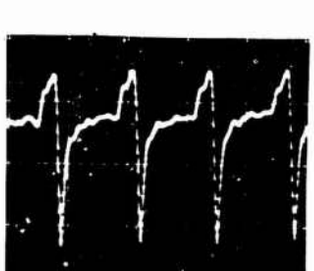

5 DIA.

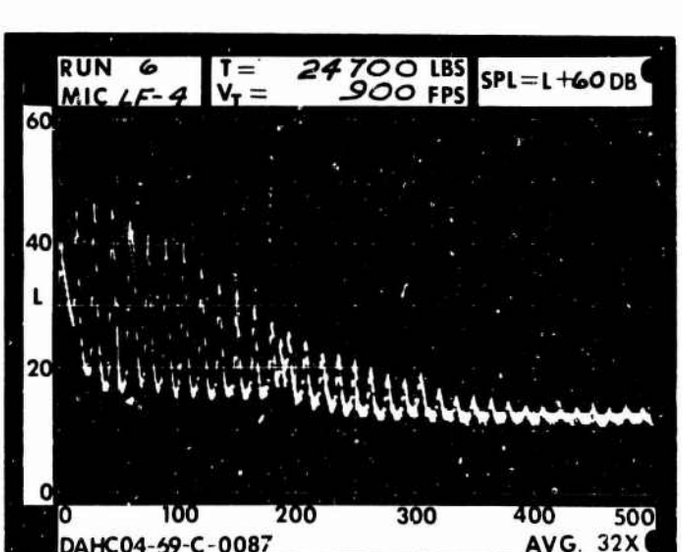

RUN 8

TIP SPEED 900 FT/SEC

THRUST 26800 LB

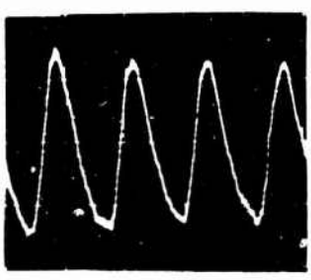

.2 RAD.

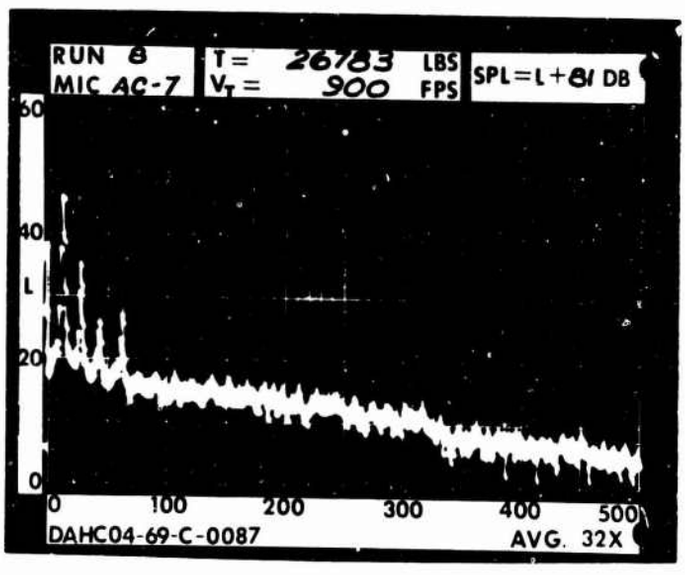

1 RAD.

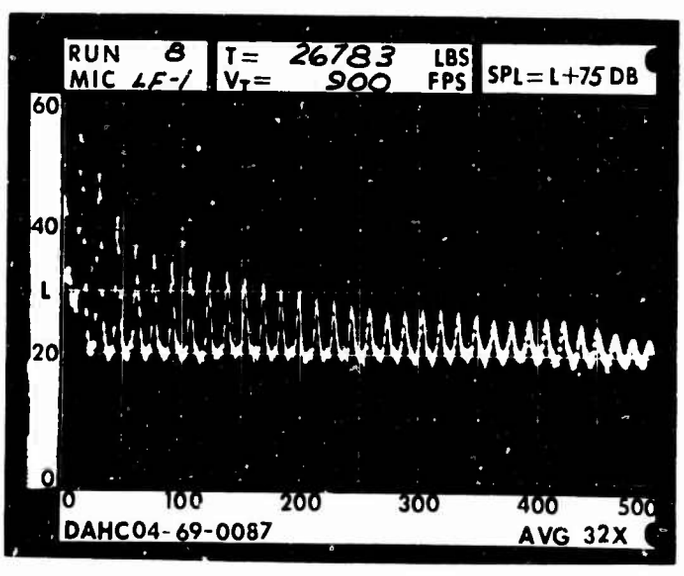

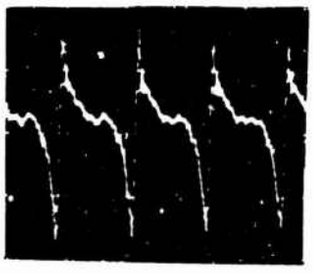

1 DIA.

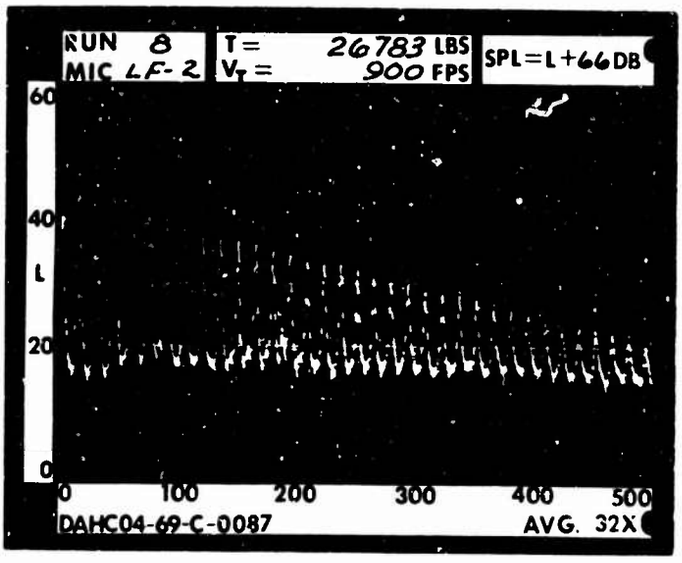

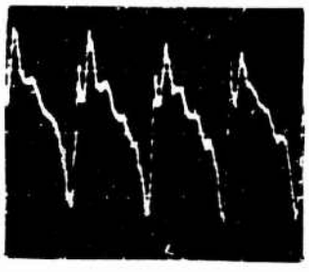

3 DIA.

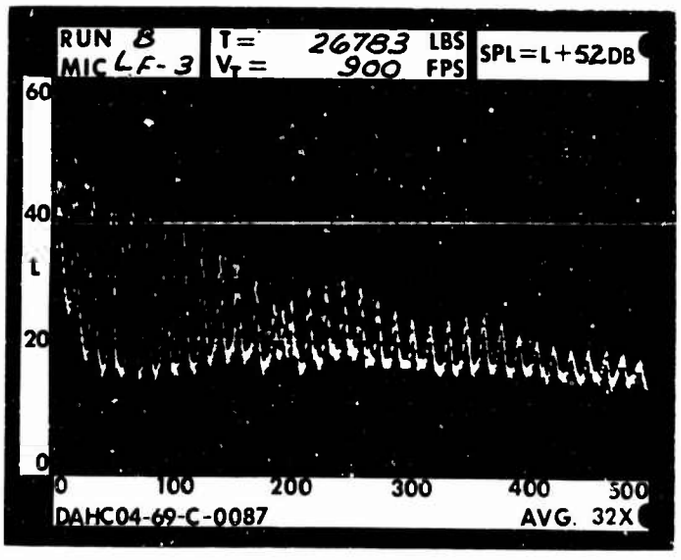

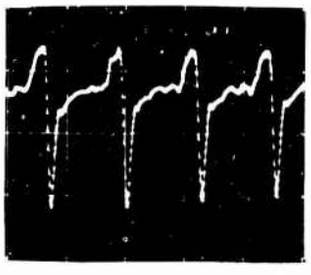

5 DIA.

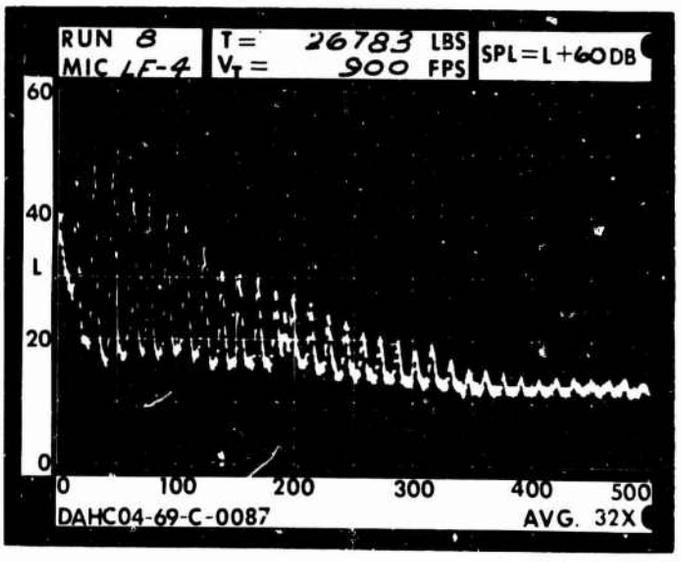

RUN 9

TIP SPEED 900 FT/SEC

THRUST 31500 LB

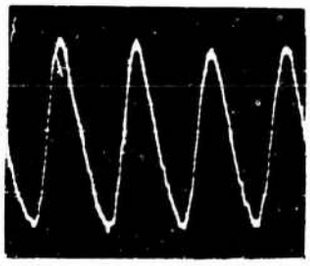

.2 RAD.

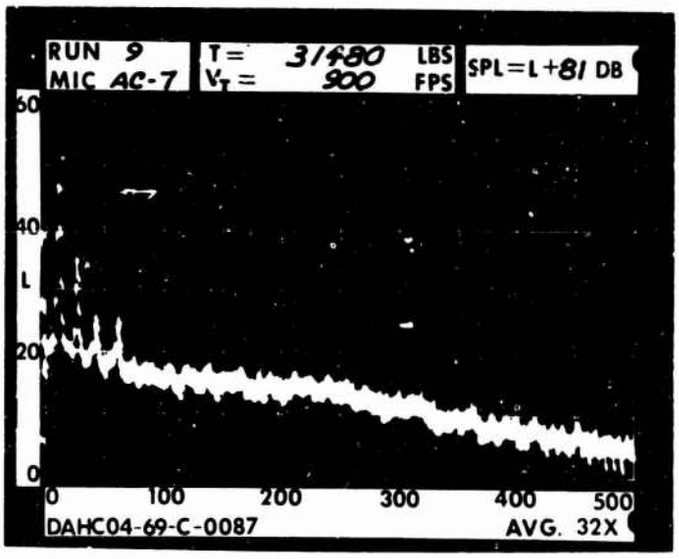

1 RAD.

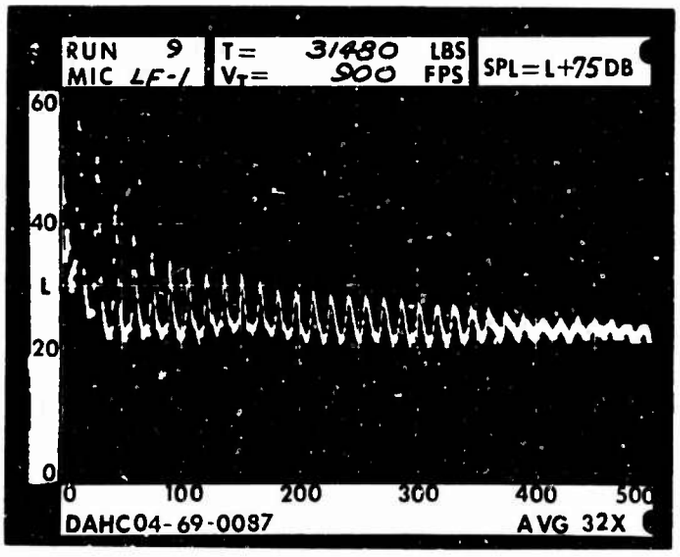

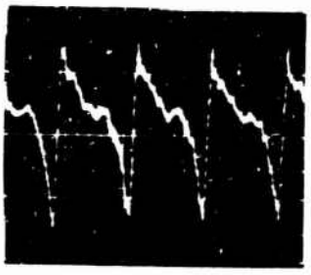

1 DIA.

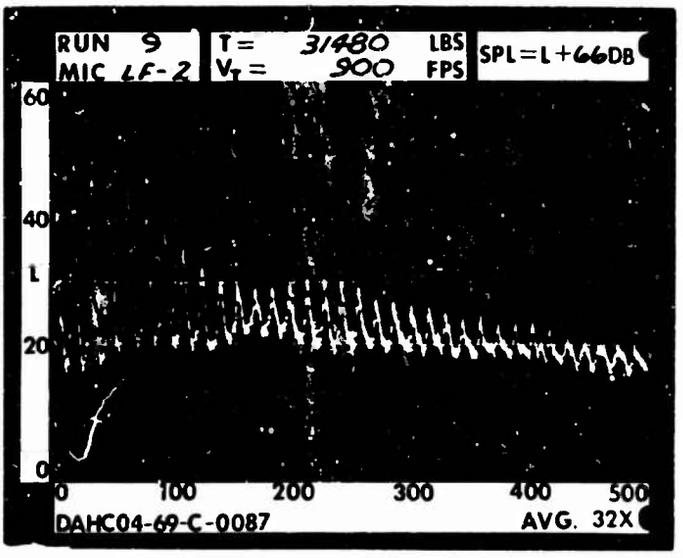

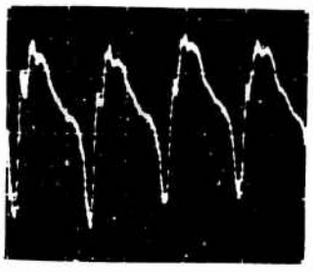

3 DIA.

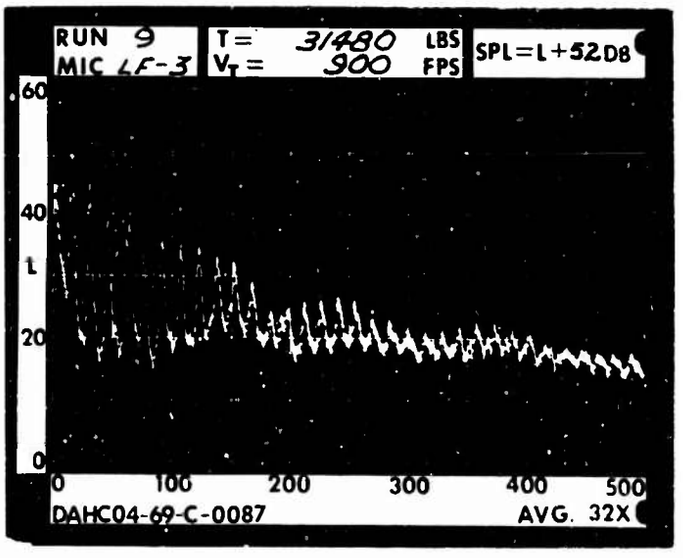

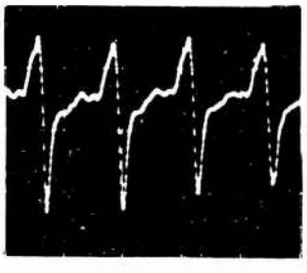

5 DIA.

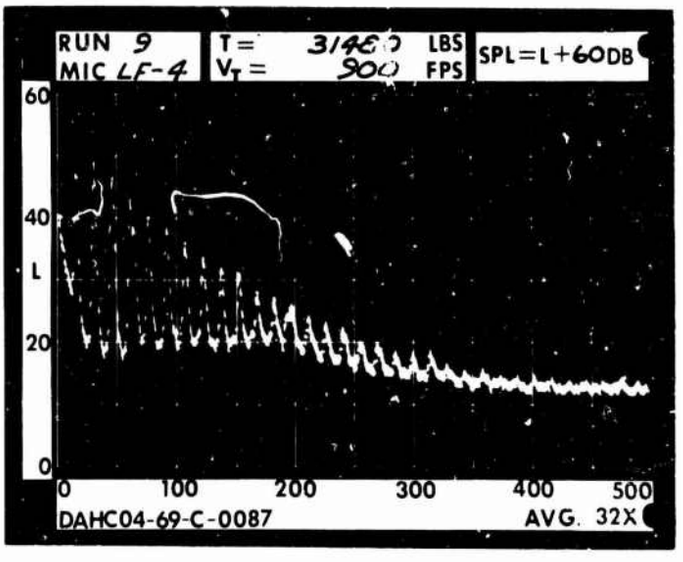

RUN 10

TIP SPEED 900 FT/SEC

THRUST 32350 LB

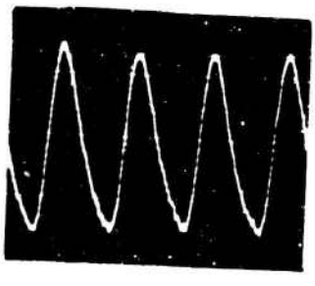

.2 RAD.

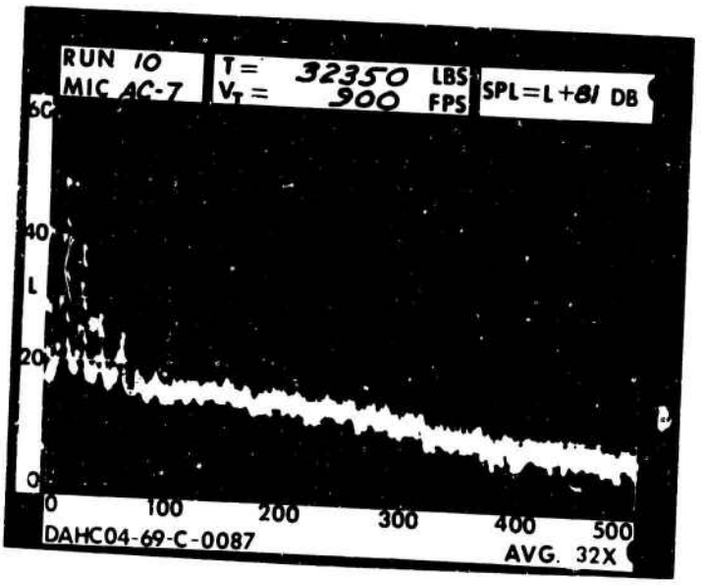

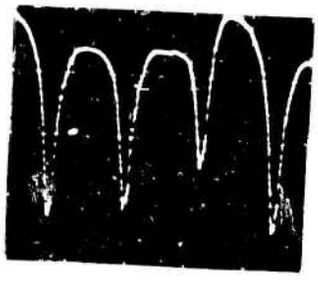

1 RAD.

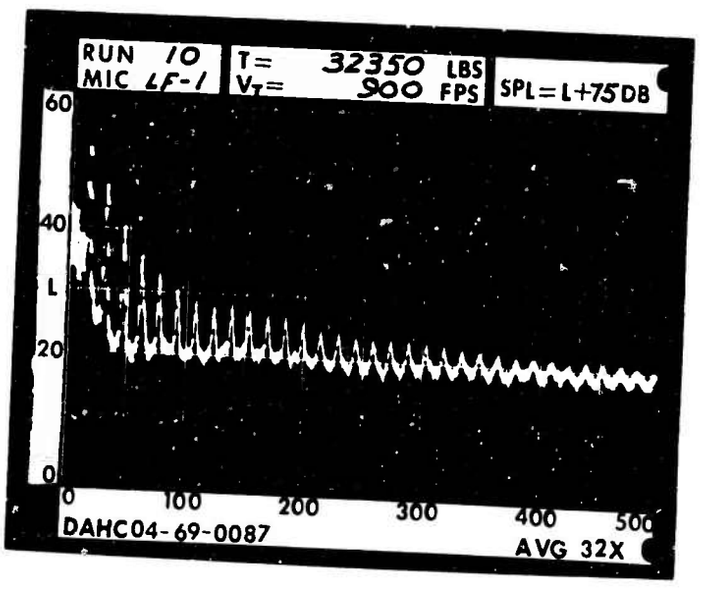

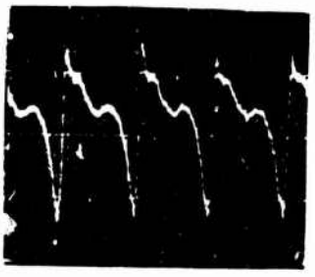

1 DIA.

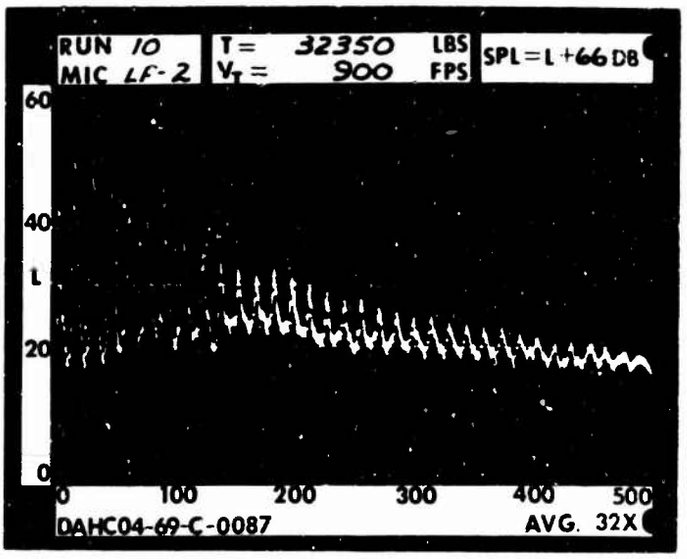

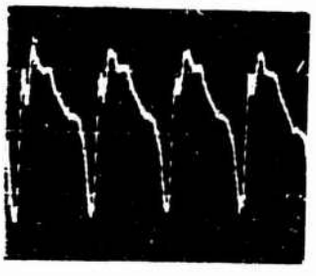

3 DIA.

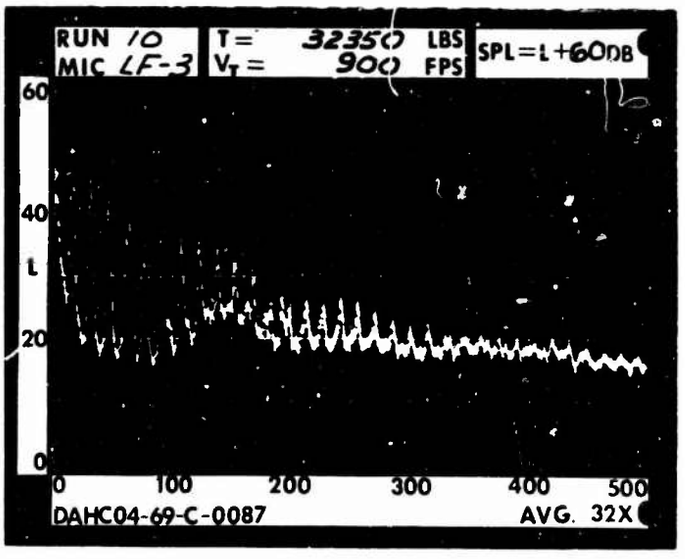

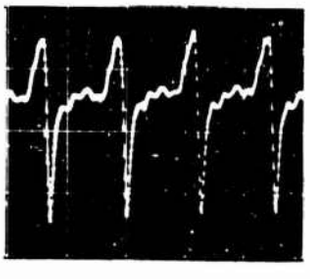

5 DIA.

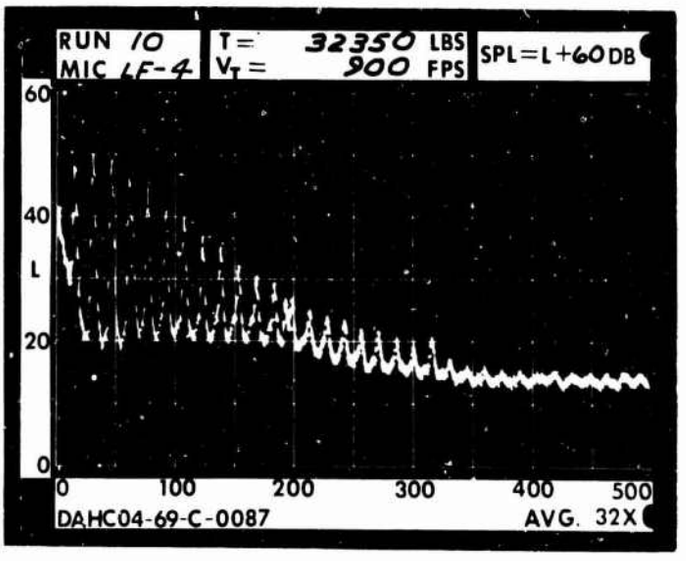

RUN 11

TIP SPEED 900 FT/SEC

THRUST 14500 LB

.2 RAD.

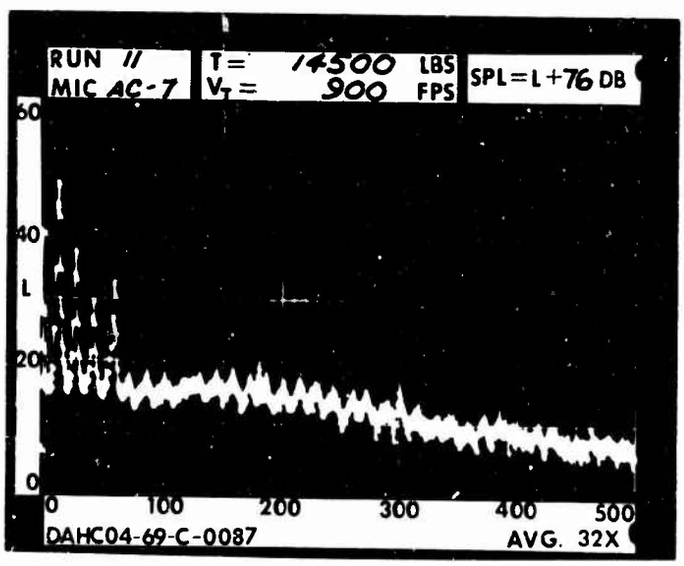

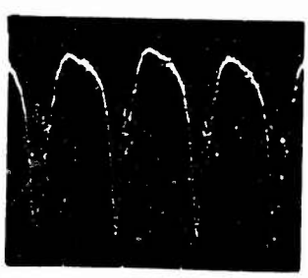

1 RAD.

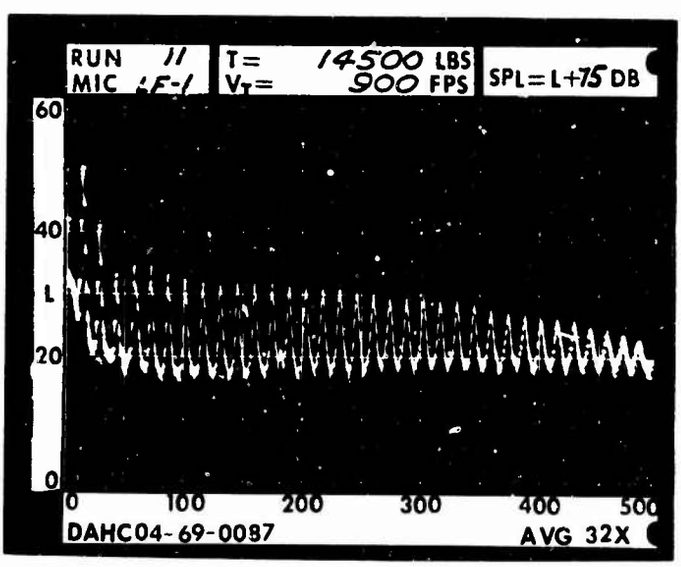

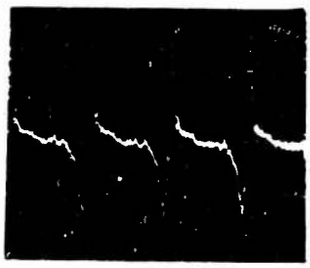

1 DIA.

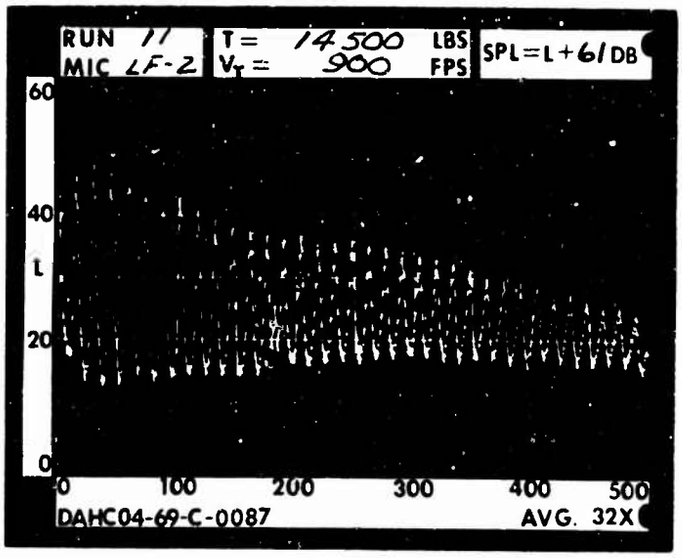

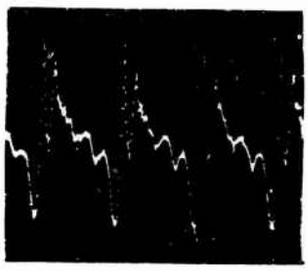

3 DIA.

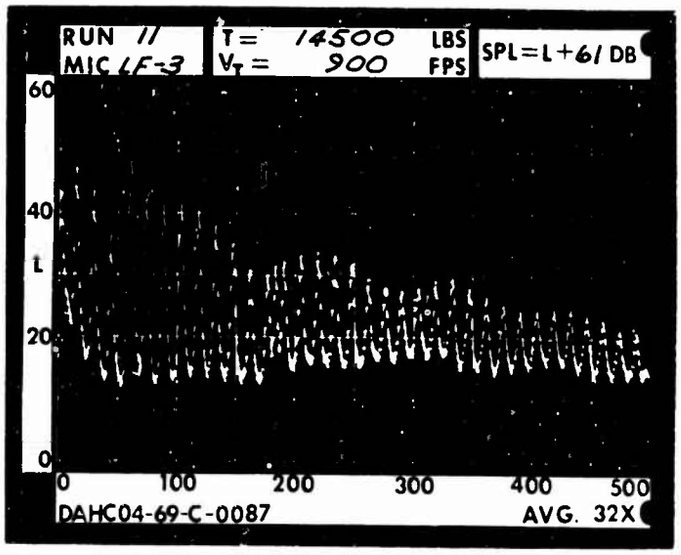

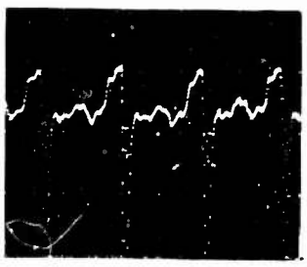

5 DIA.

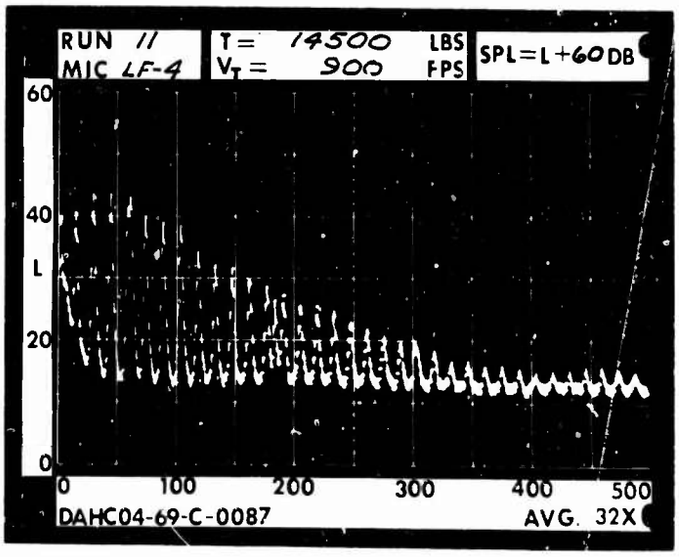

RUN 12

TIP SPEED 900 FT/SEC

THRUST 17100 LB

.2 RAD.

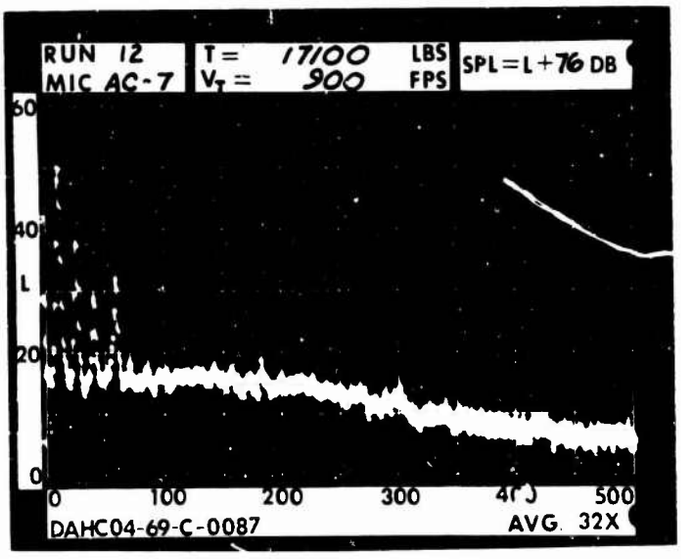

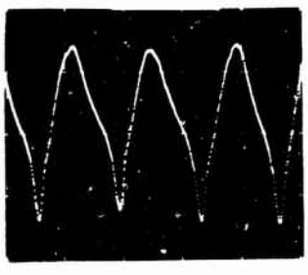

1 RAD.

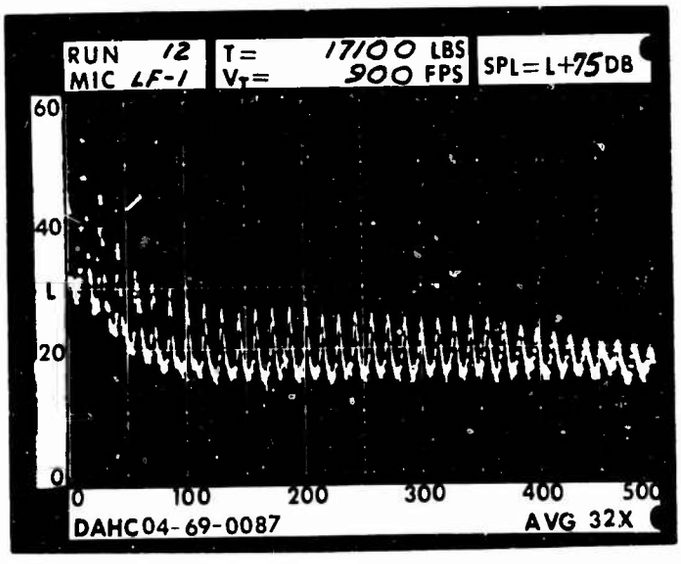

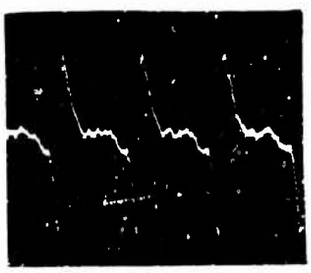

1 DIA.

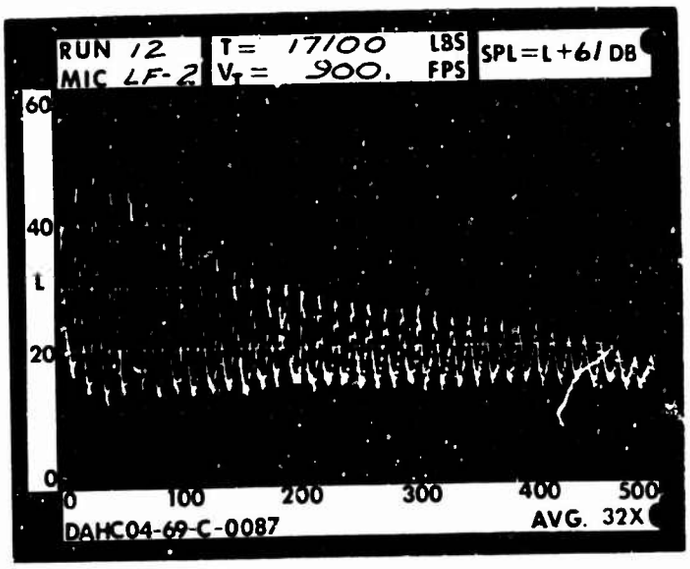

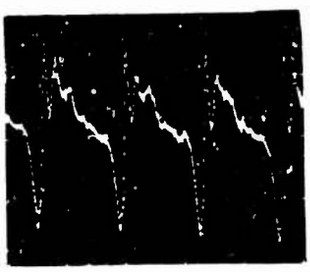

3 DIA.

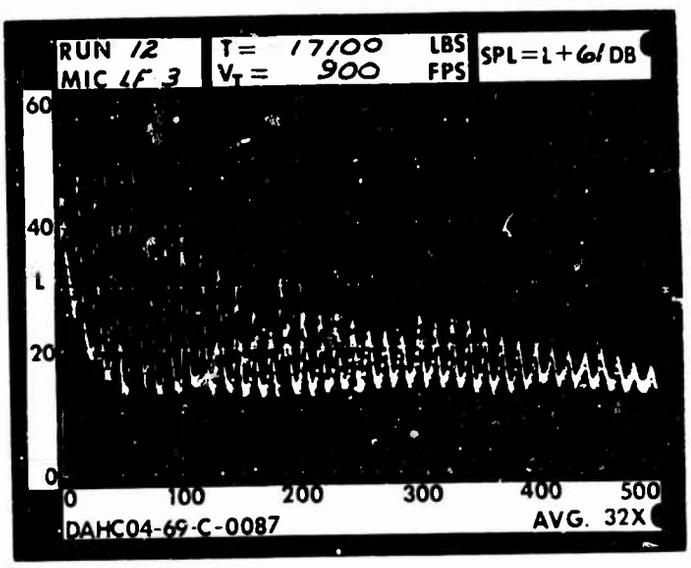

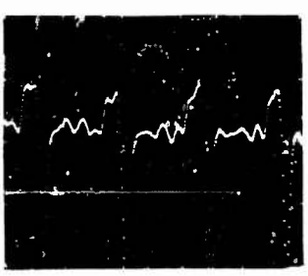

5 DIA.

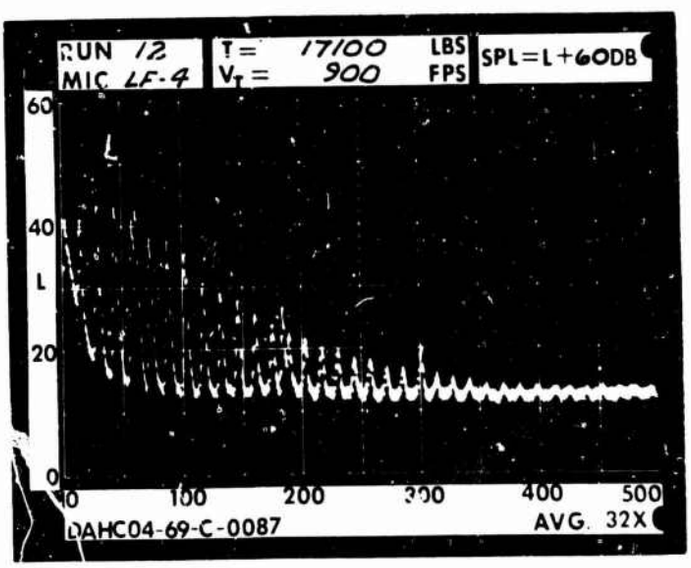

RUN 13

TIP SPEED 850 FT/SEC

THRUST 9100 LB

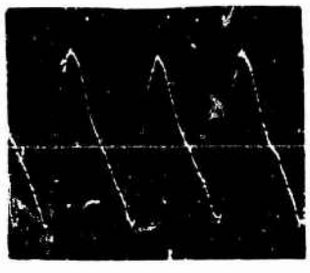

.2 RAD.

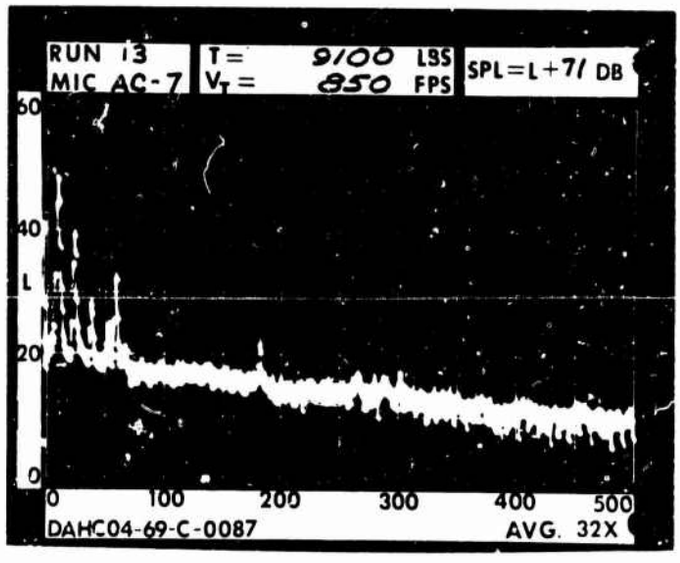

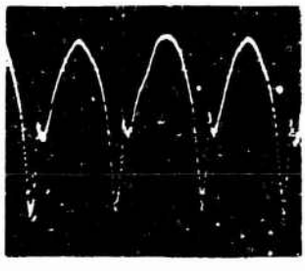

1 RAD.

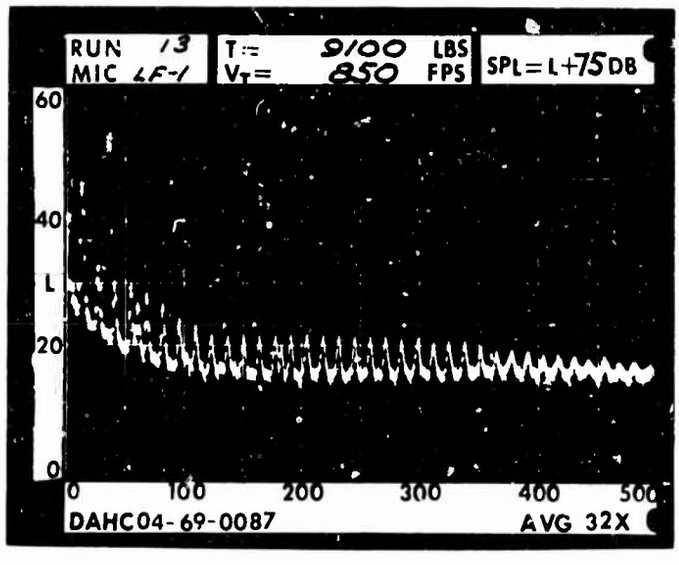

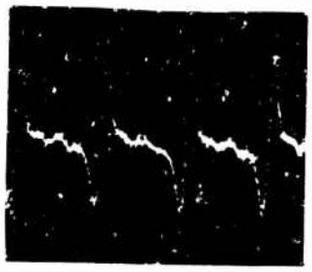

1 DIA.

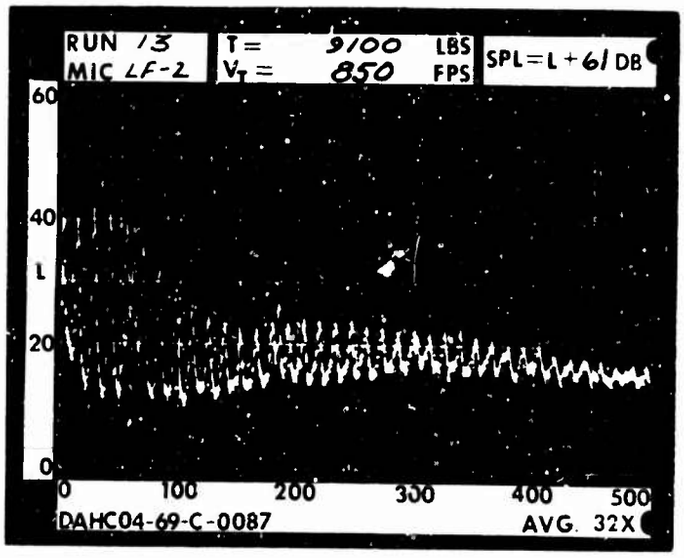

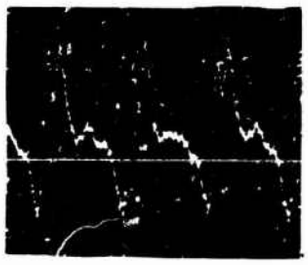

3 DIA.

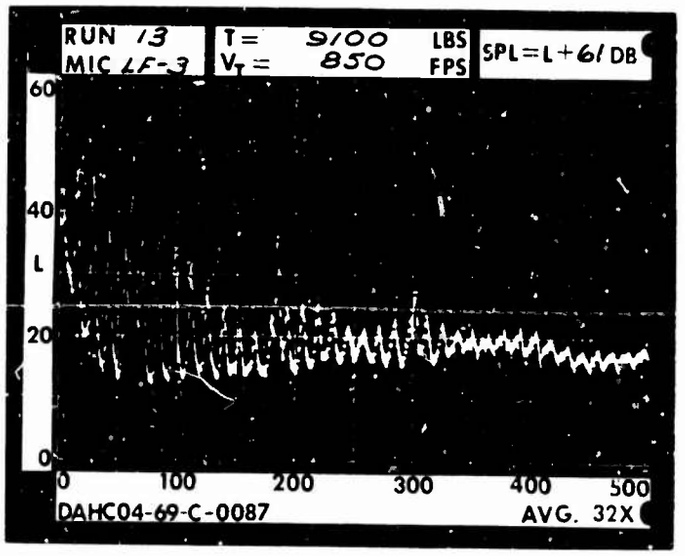

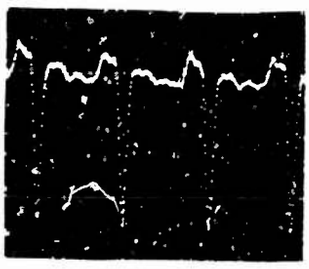

5 DIA.

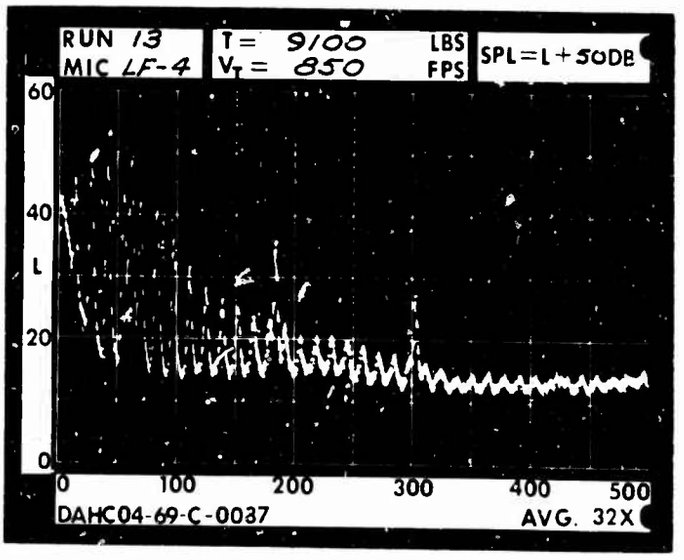

RUN 14

TIP SPEED 850 FT/SEC

THRUST 11300 LB

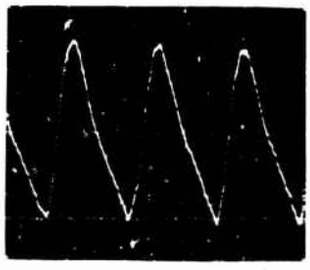

.2 RAD.

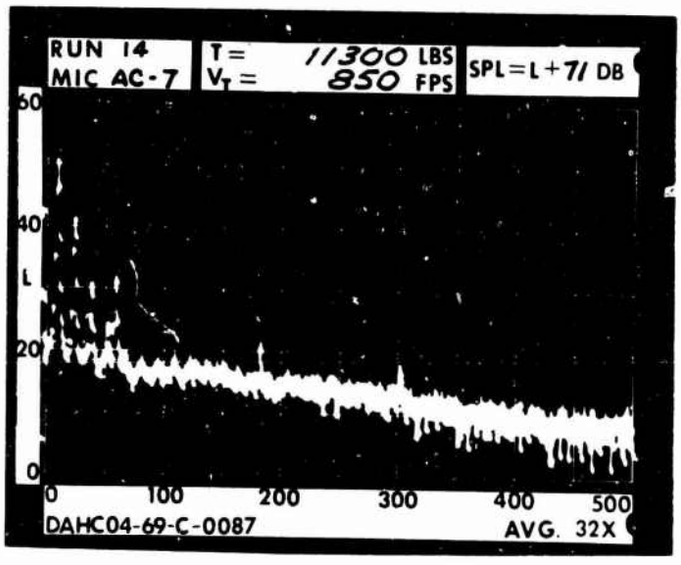

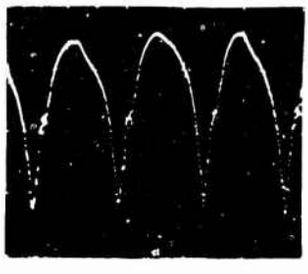

1 RAD.

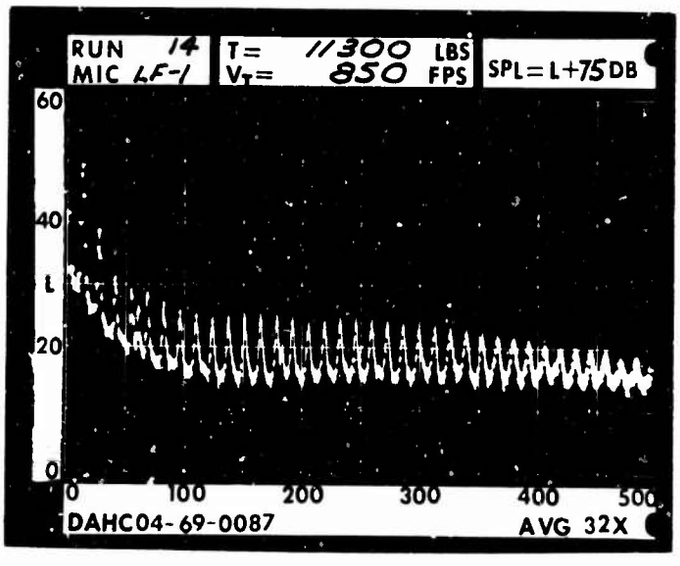

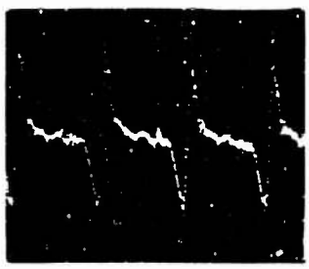

1 DIA.

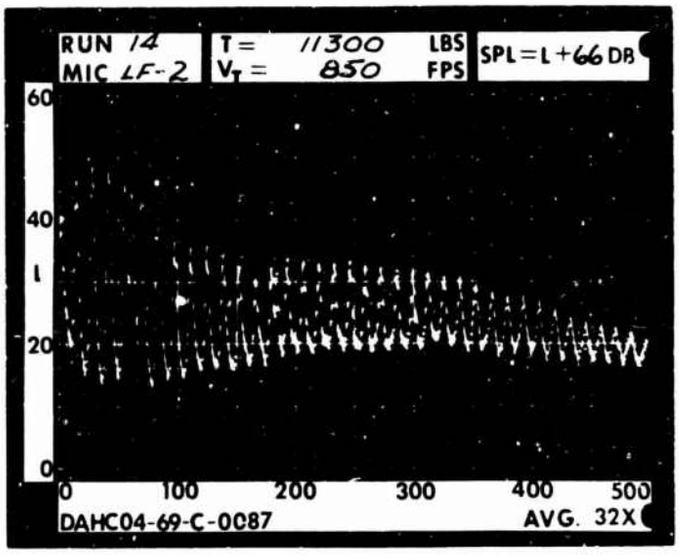

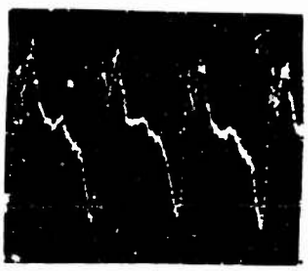

3 DIA.

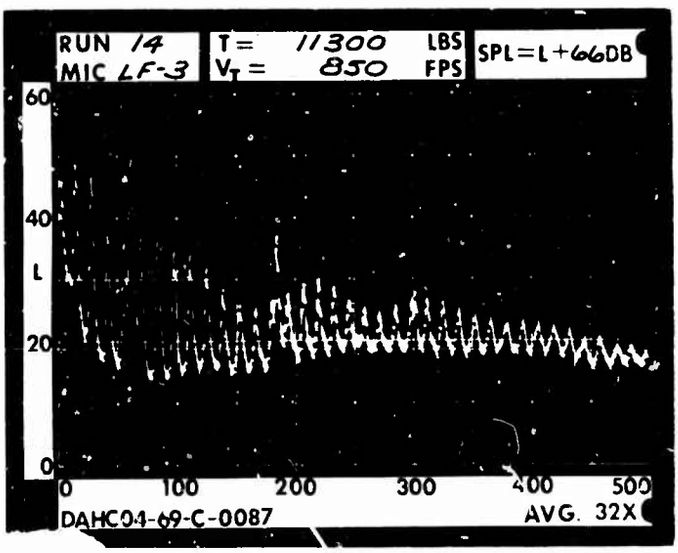

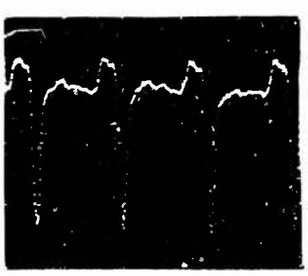

5 DIA.

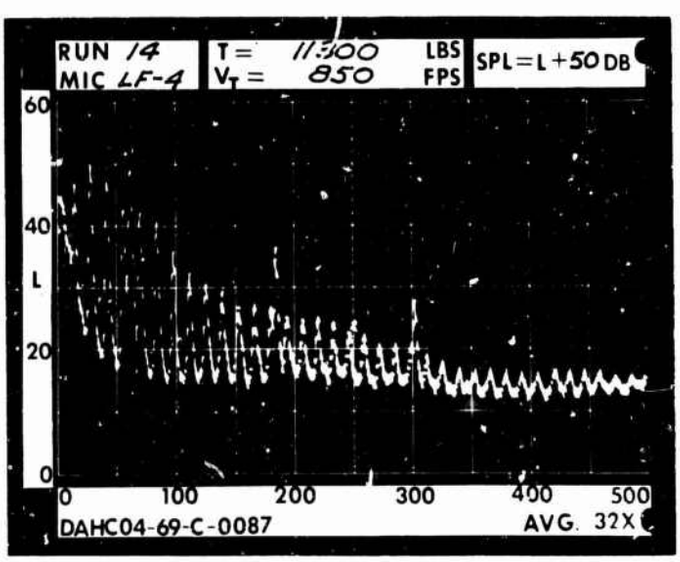

RUN 15

TIP SPEED 850 FT/SEC

THRUST 14000 LB

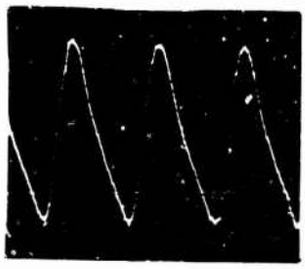

.2 RAD.

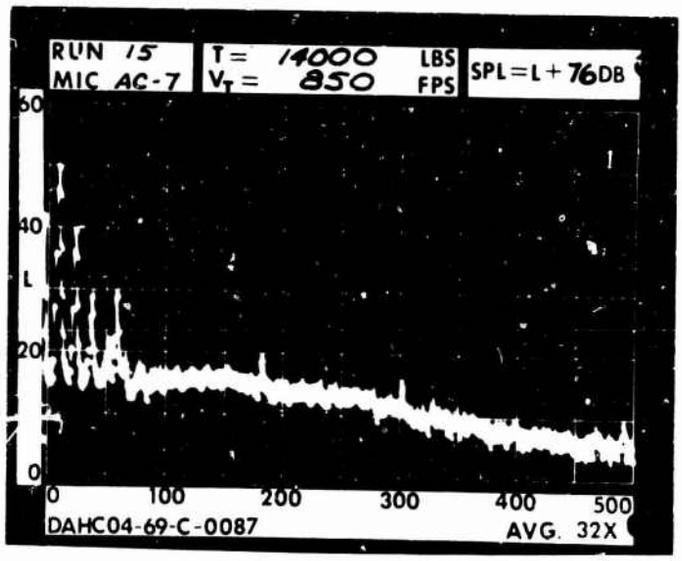

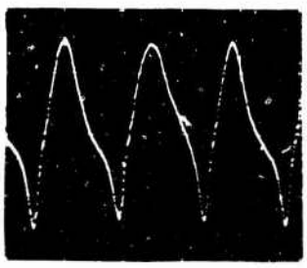

1 RAD.

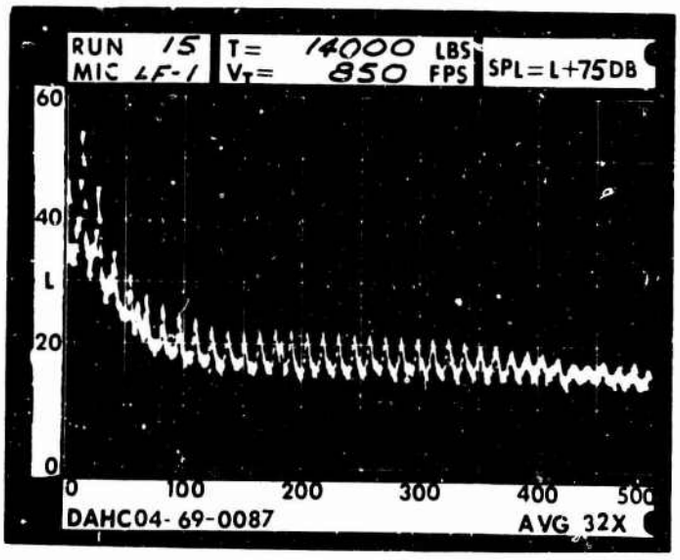

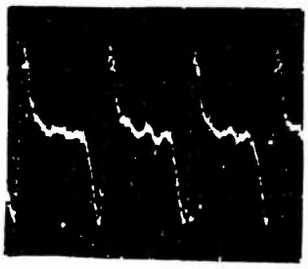

1 DIA.

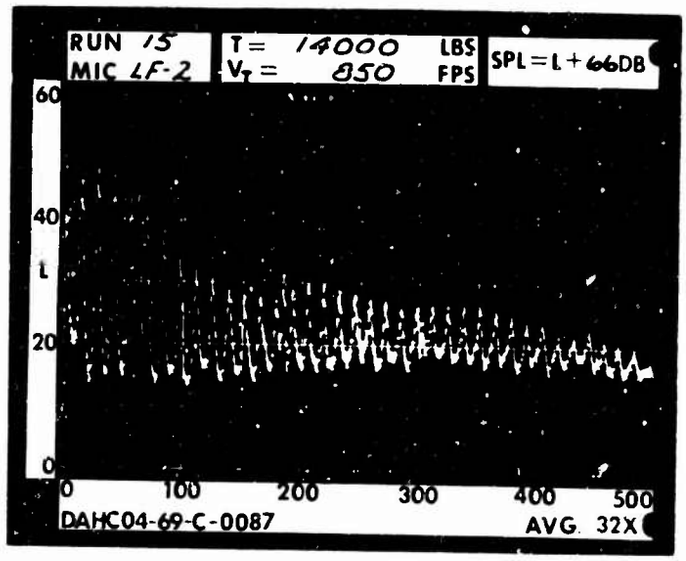

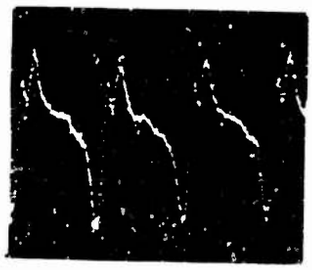

3 DIA.

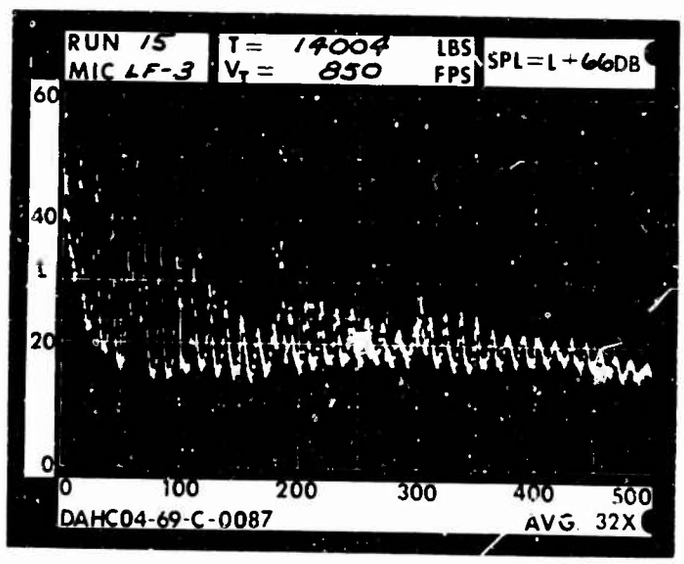

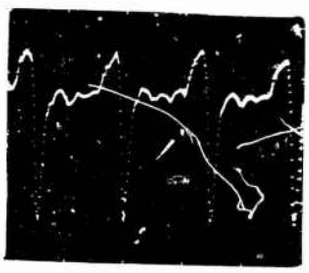

5 DIA.

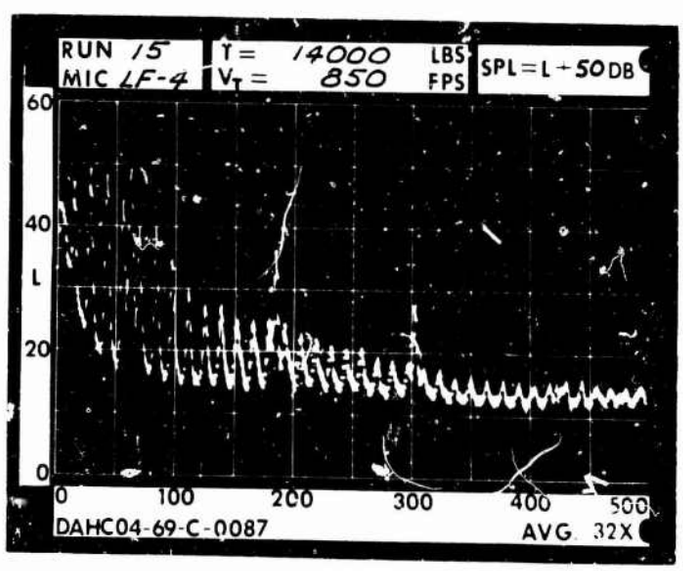

RUN 16

TIP SPEED 850 FT/SEC

THRUST 17000 LB

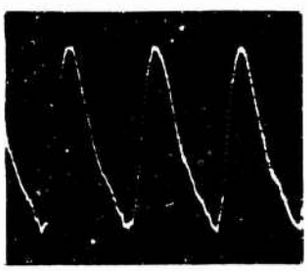

.2 RAD.

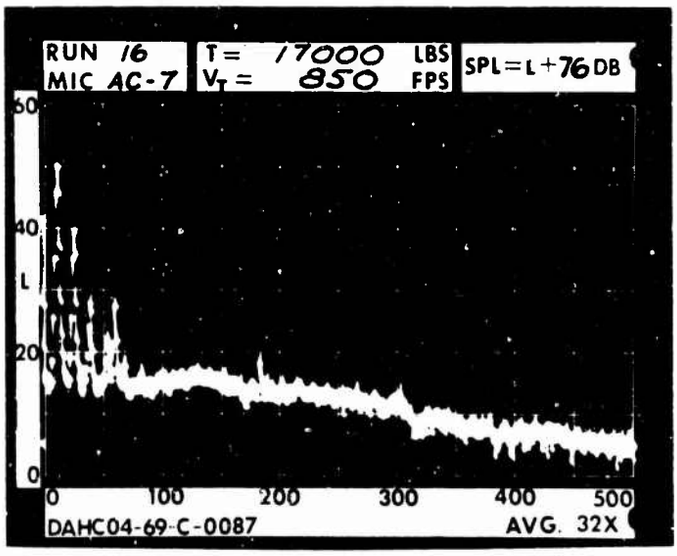

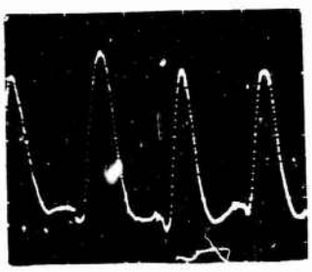

1 RAD.

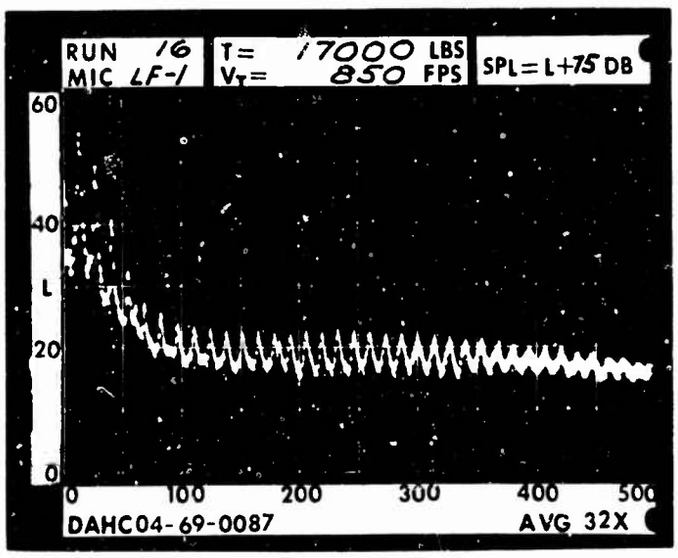

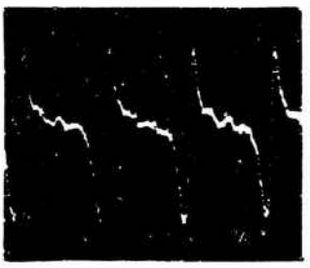

1 DIA.

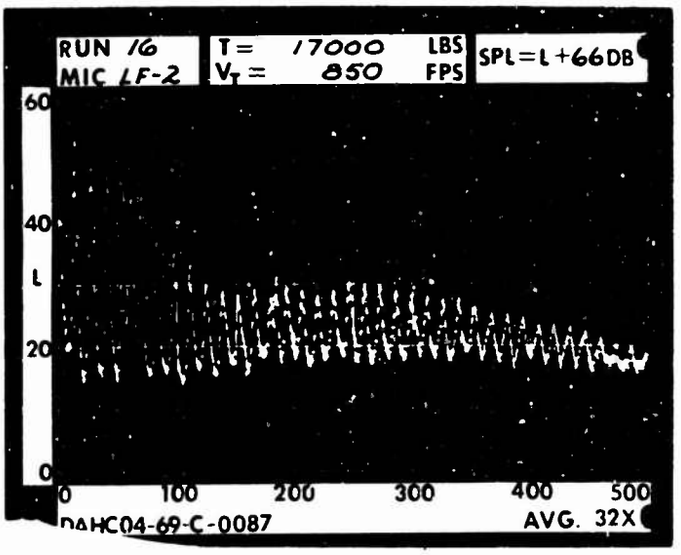

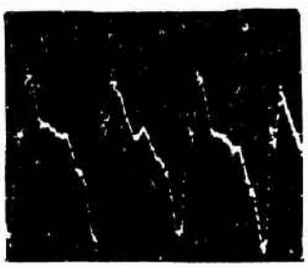

3 DIA.

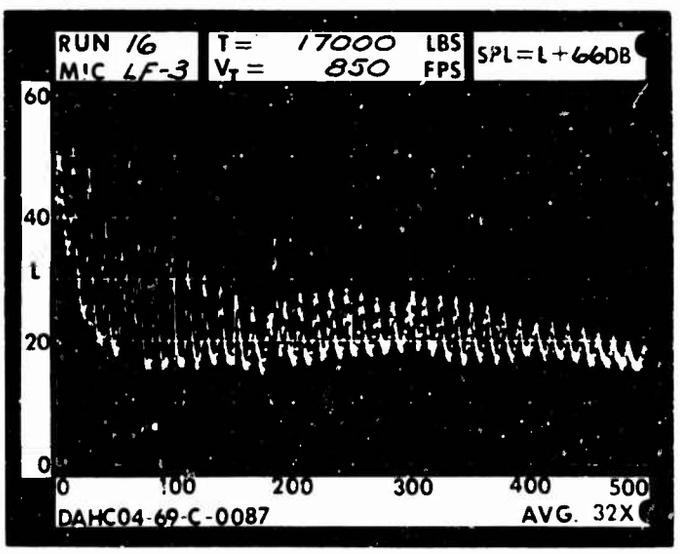

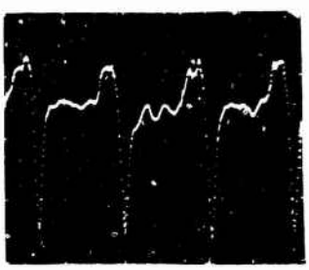

5 DIA.

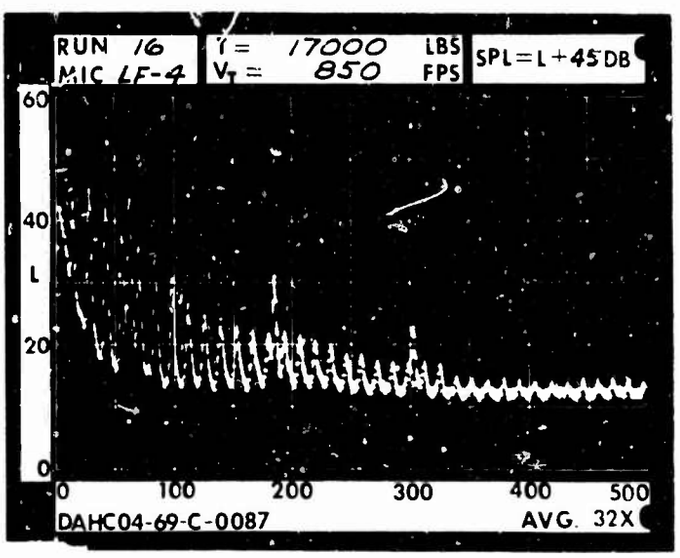

RUN 17

TIP SPEED 850 FT/SEC

THRUST 17600 LB

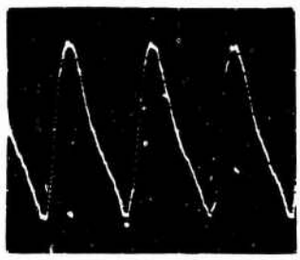

.2 RAD.

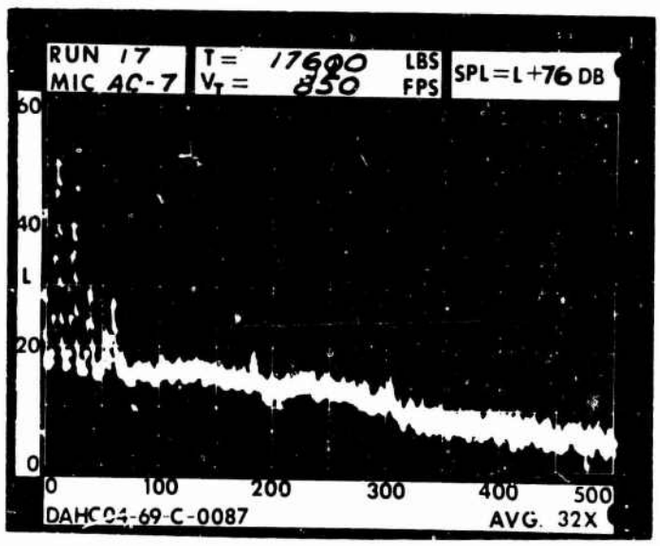

1 RAD.

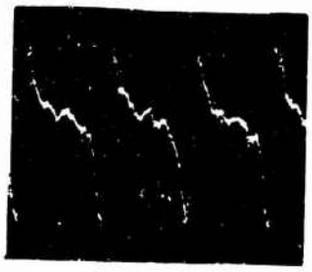

1 DIA.

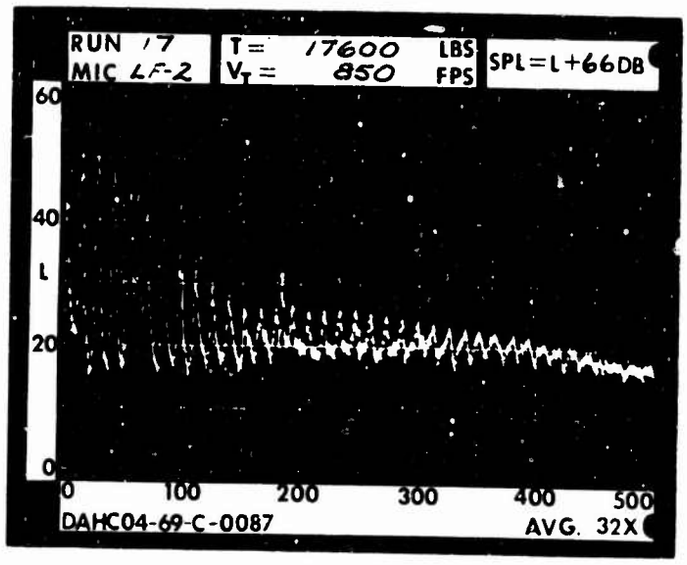

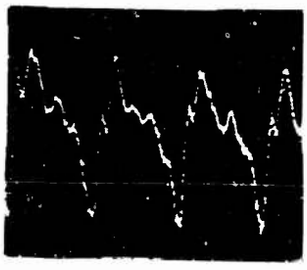

3 DIA.

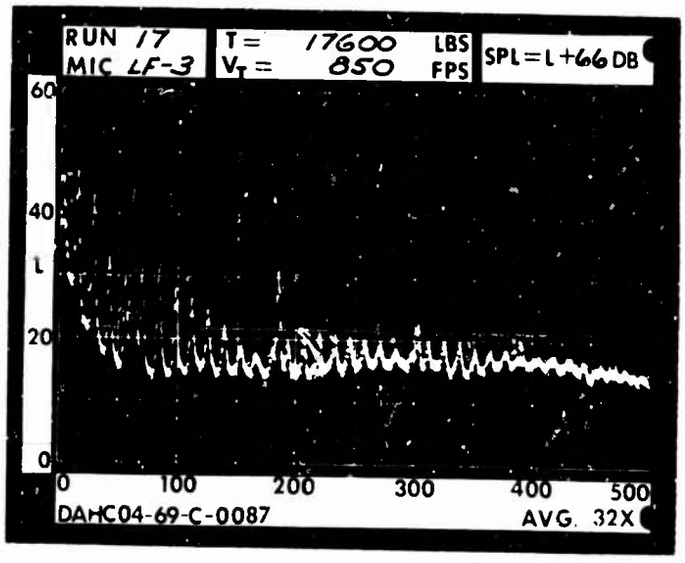

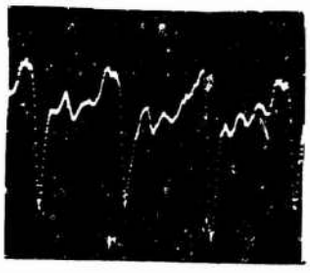

5 DIA.

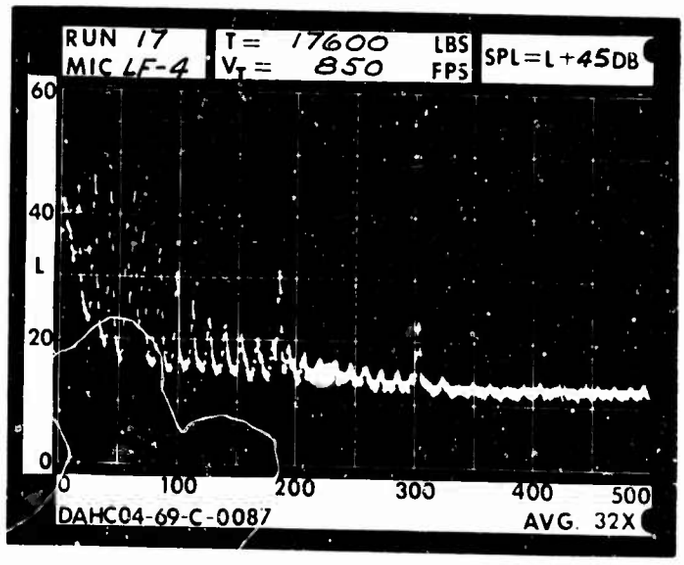

RUN 18

TIP SPEED 850 FT/SEC

THRUST 24200 LB

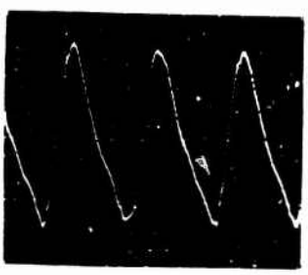

.2 RAD.

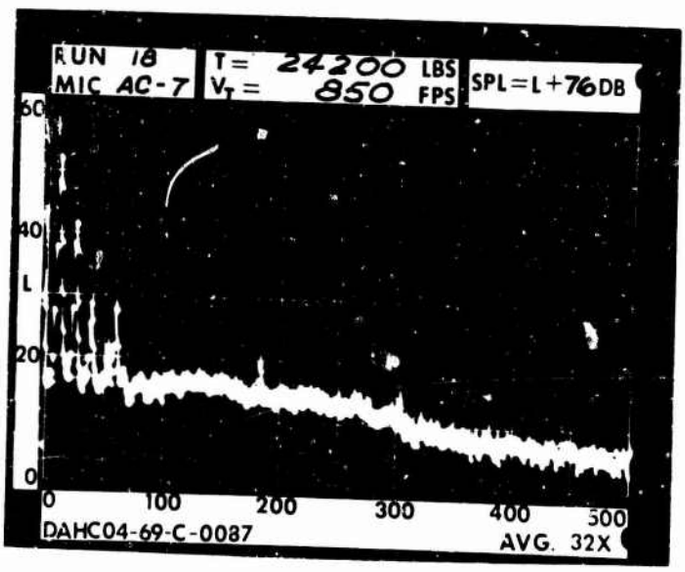

1 RAD.

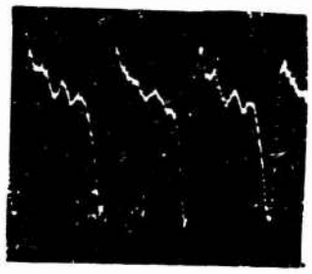

1 DIA.

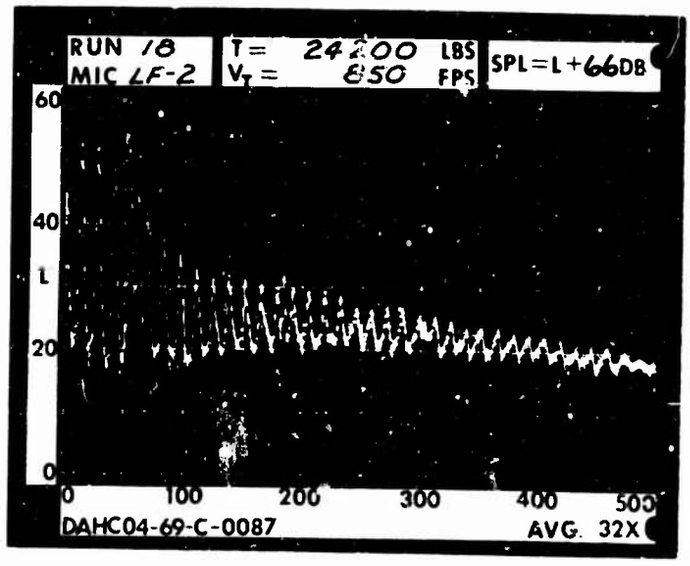

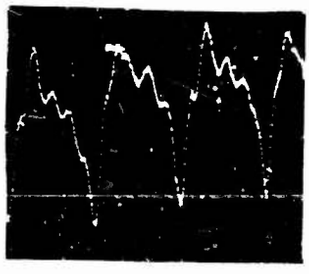

3 DIA.

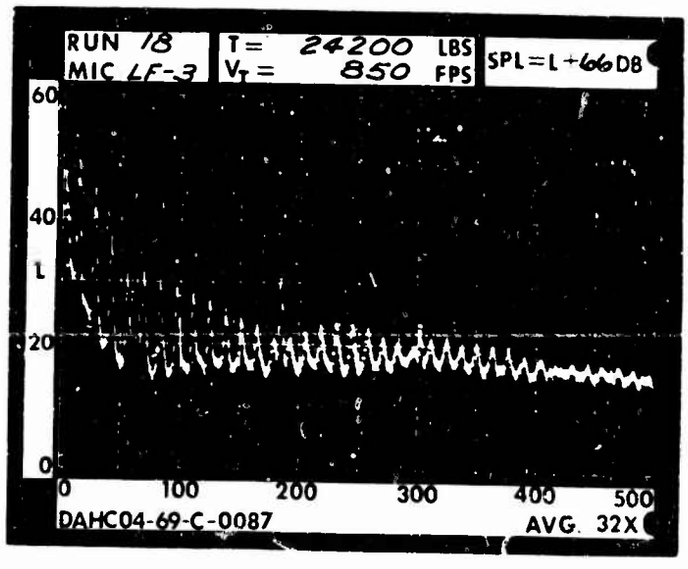

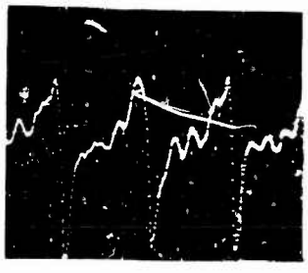

5 DIA.

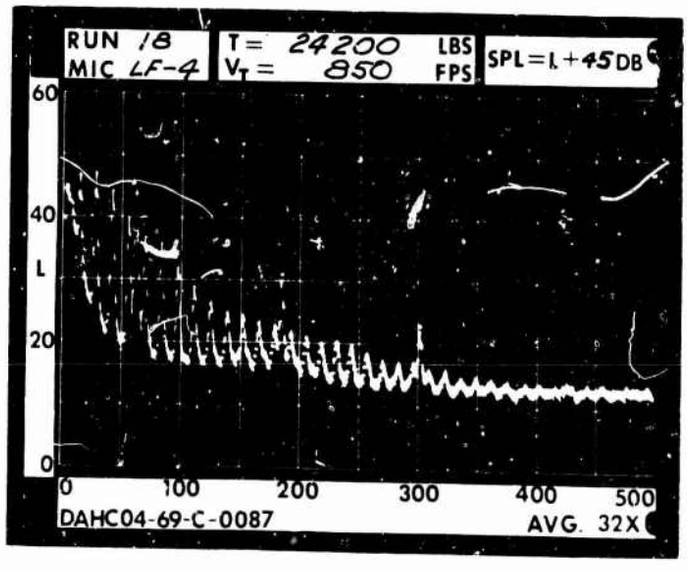

RUN 19

TIP SPEED 850 FT/SEC

THRUST 28000 LB

.2 RAD.

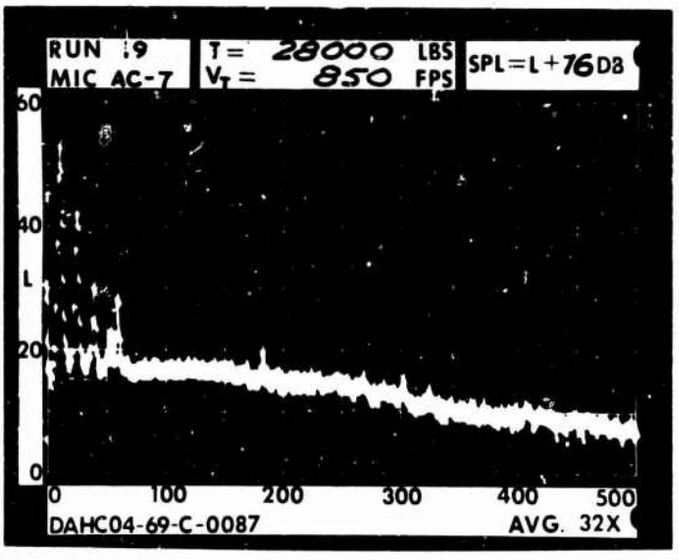

1 RAD.

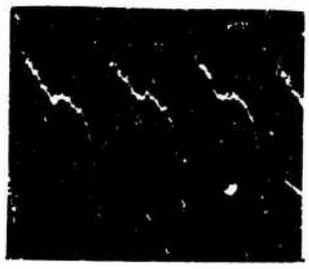

1 DIA.

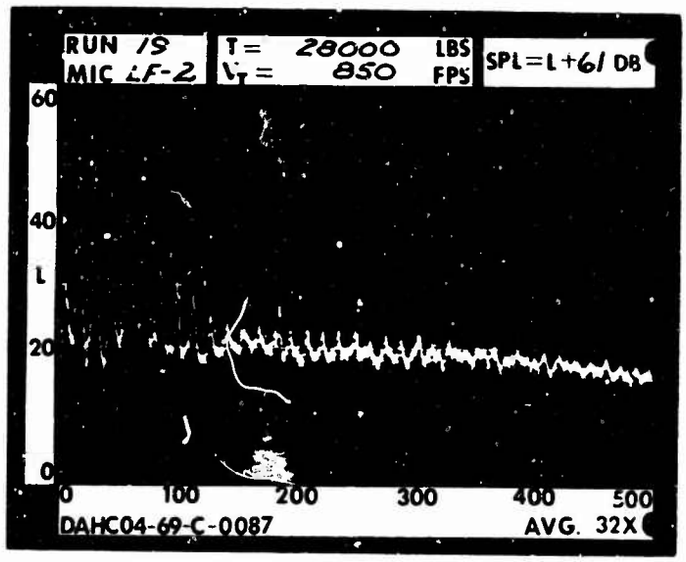

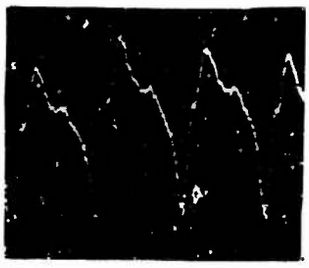

3 DIA.

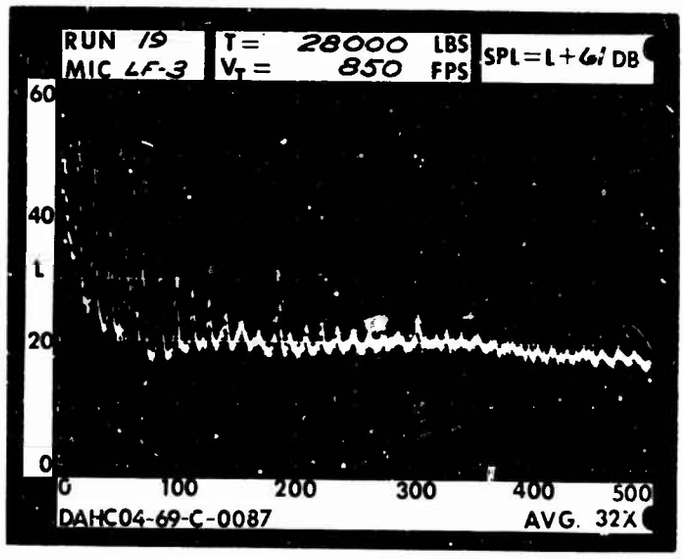

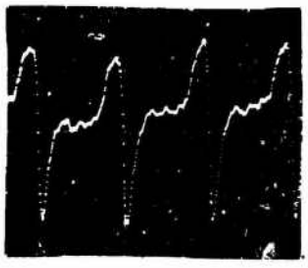

5 DIA.

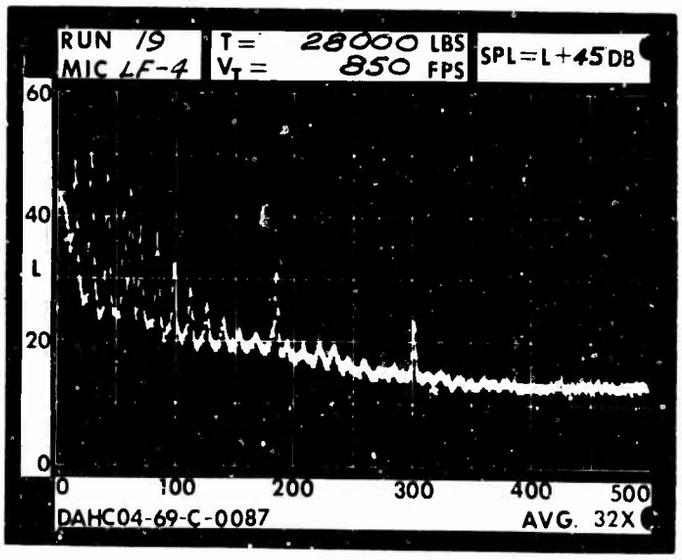

RUN 20

TIP SPEED 850 FT/SEC

THRUST 28000 LB

.2 RAD

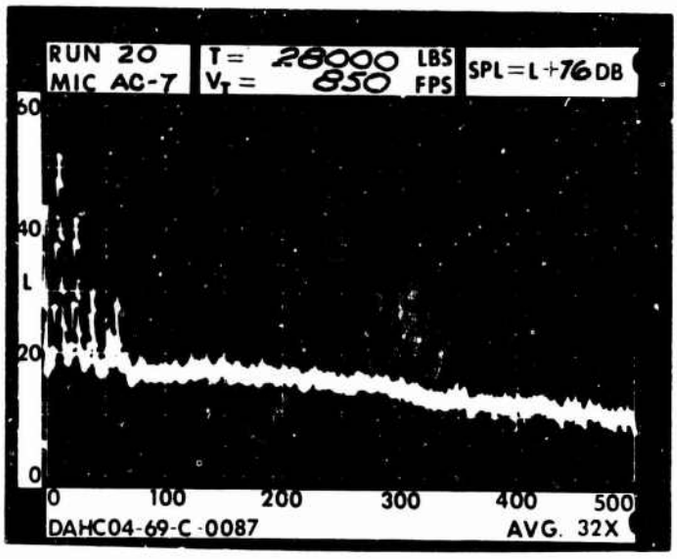

1 RAD.

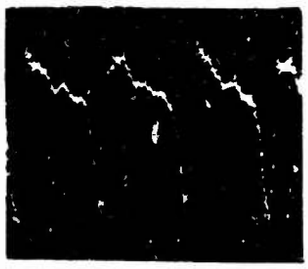

1 DIA.

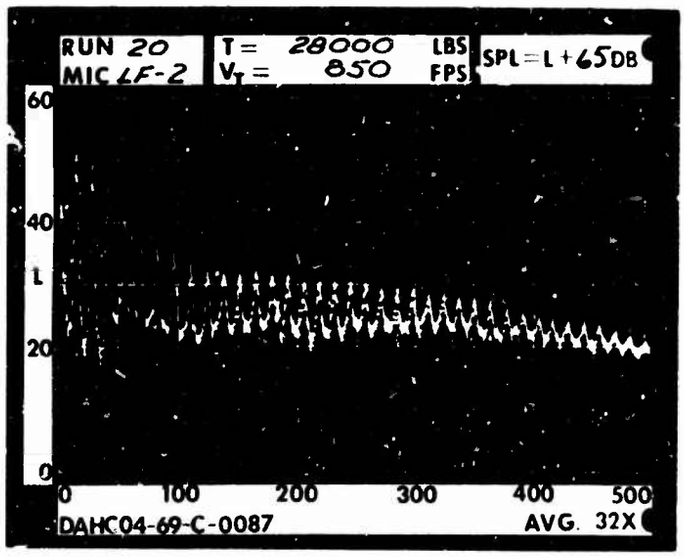

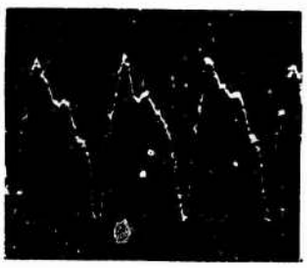

3 DIA.

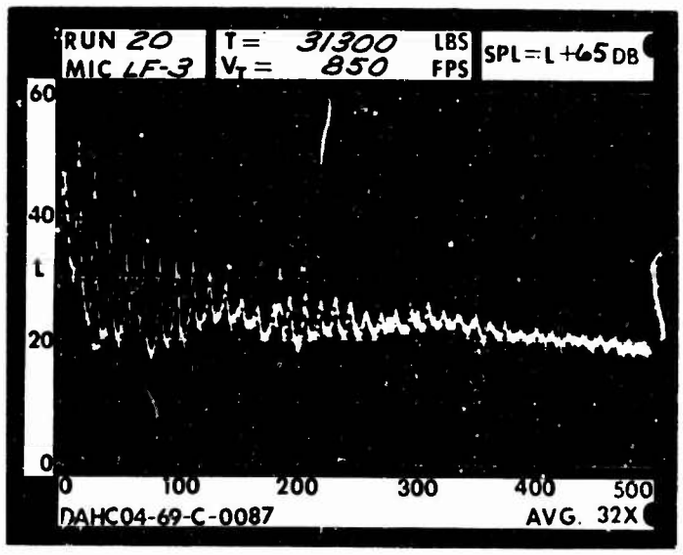

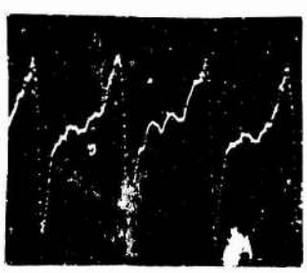

5 DIA.

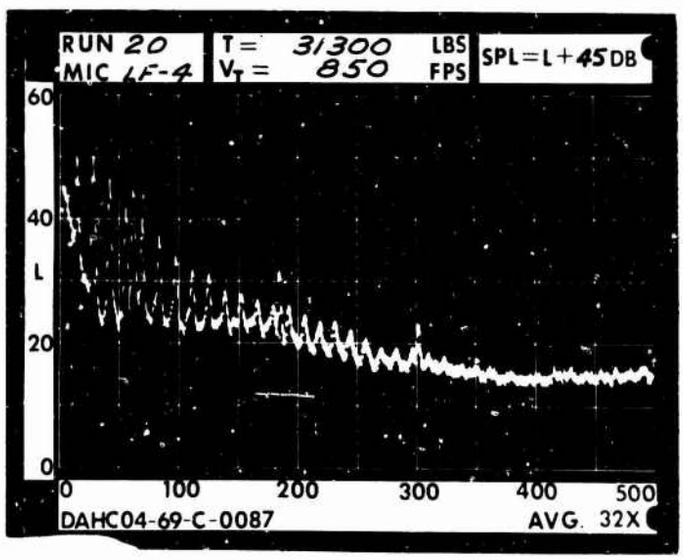

RUN 21

TIP SPEED 850 FT/SEC

THRUST 32500 LB

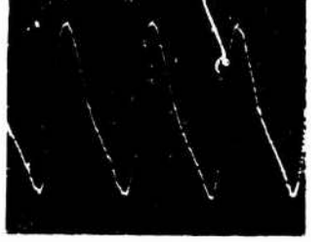

.2 RAD.

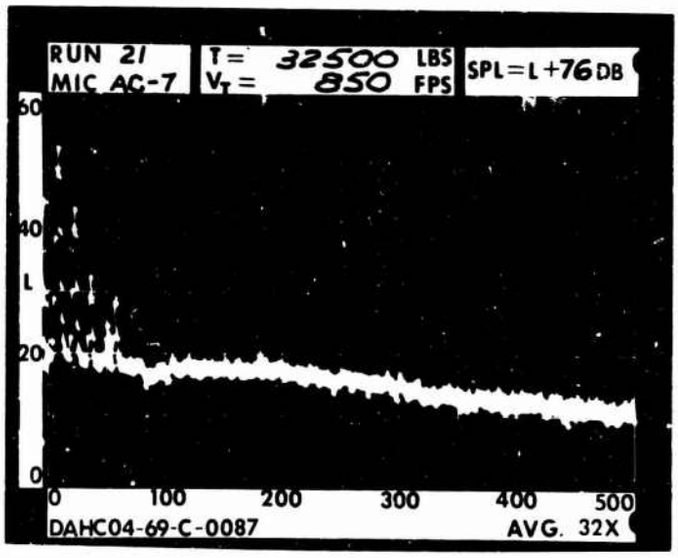

1 RAD.

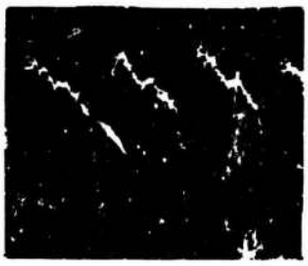

1 DIA.

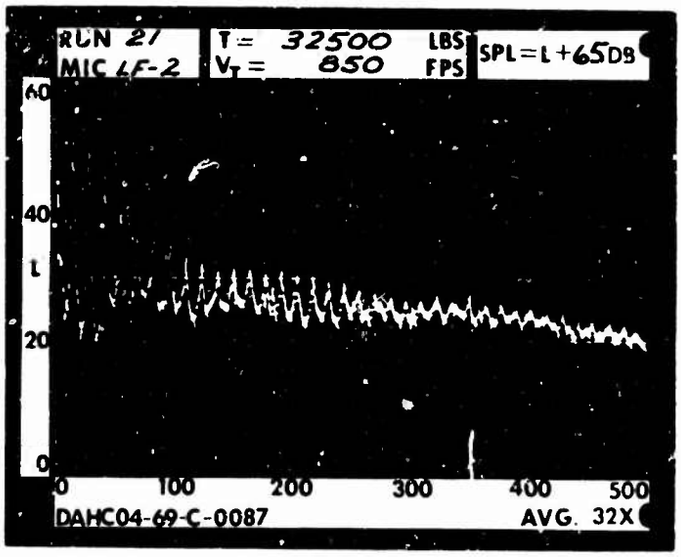

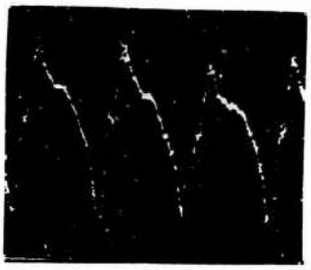

3 DIA.

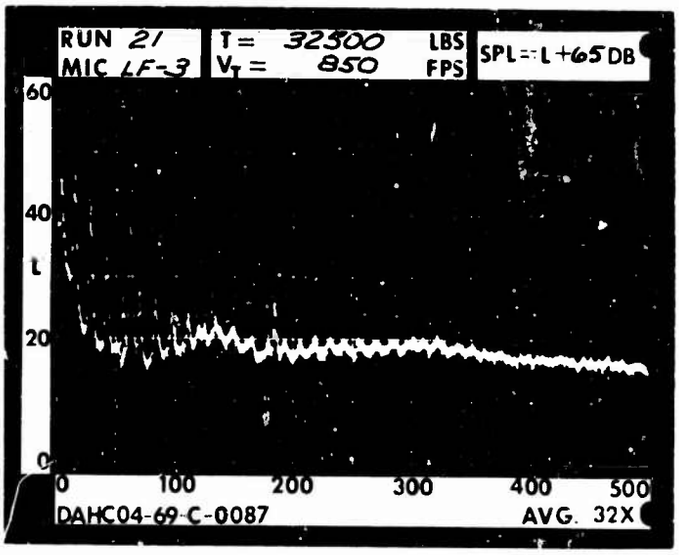

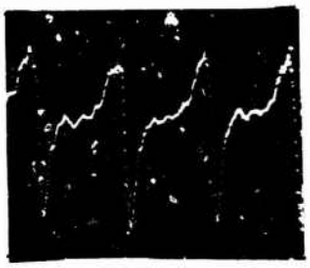

5 DIA.

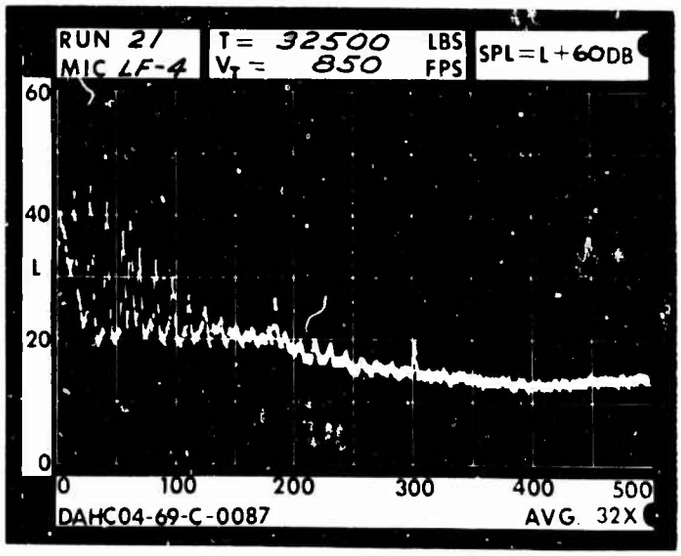

RUN 22

TIP SPEED 900 FT/SEC

THRUST 7000 LB

.2 RAD.

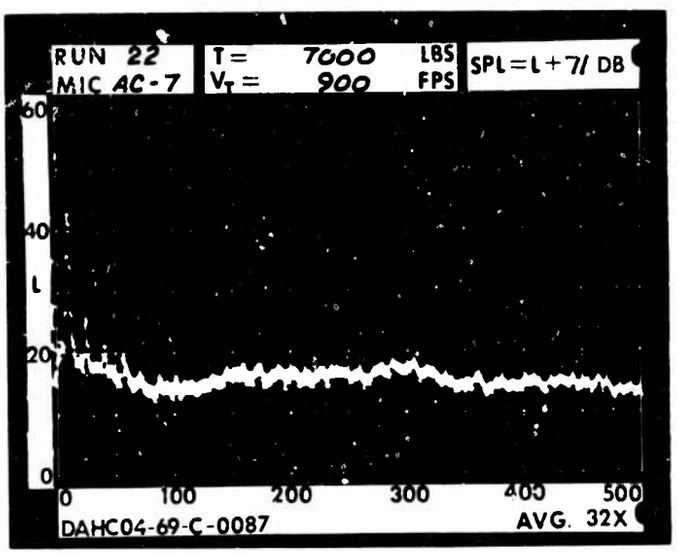

1 RAD.

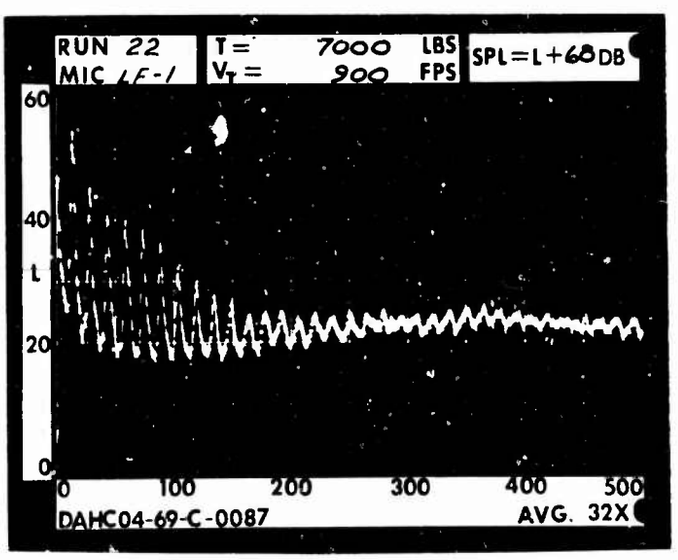

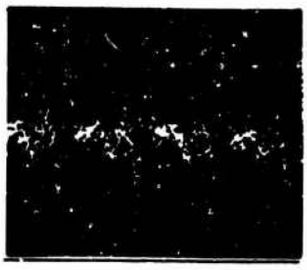

1 DIA.

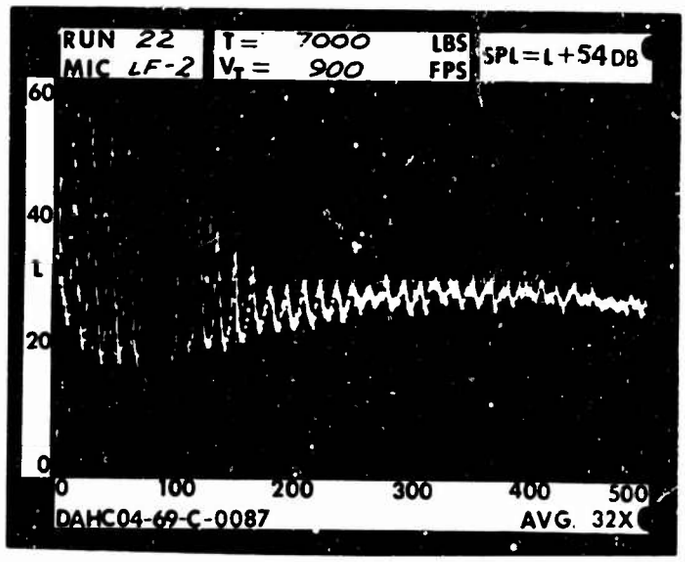

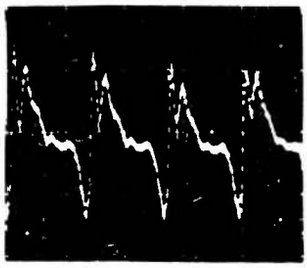

3 DIA.

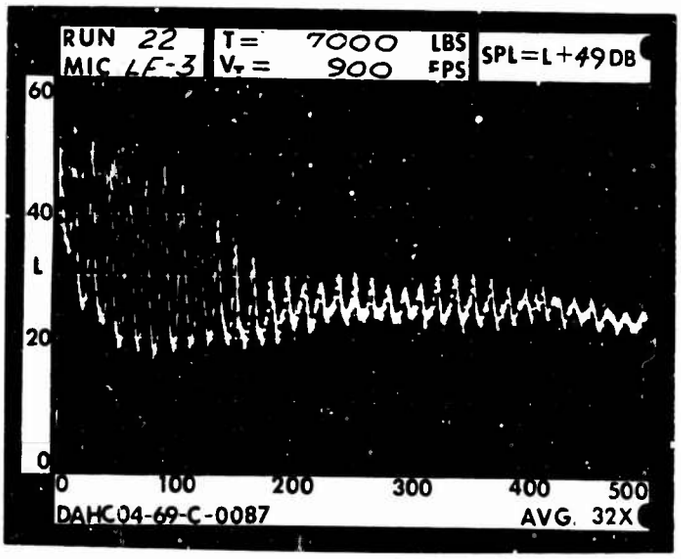

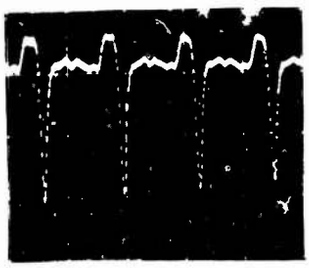

5 DIA.

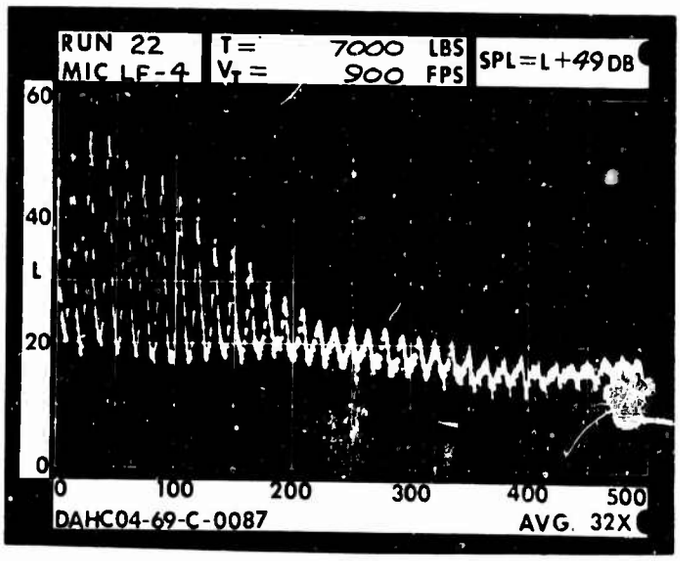

RUN 23

TIP SPEED 900 FT/SEC

THRUST 12500 LB

.2 RAD.

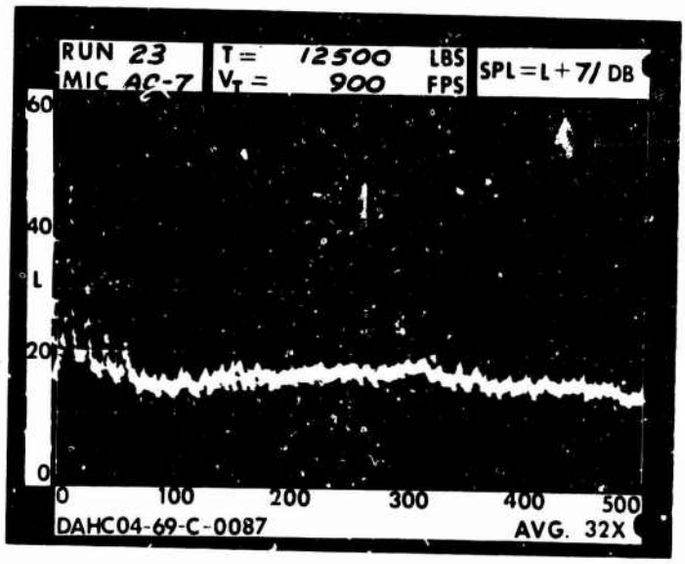

1 RAD.

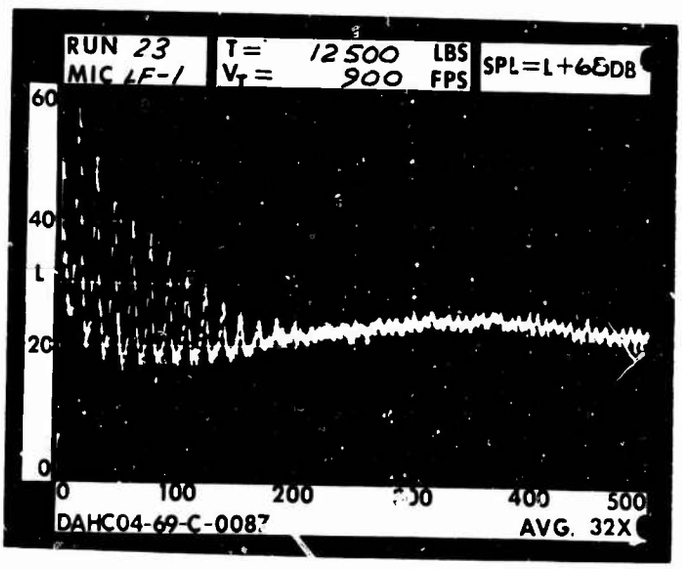

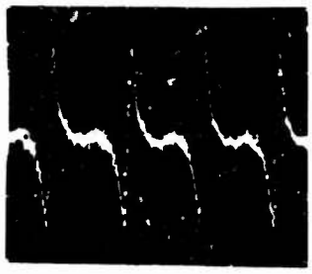

1 DIA.

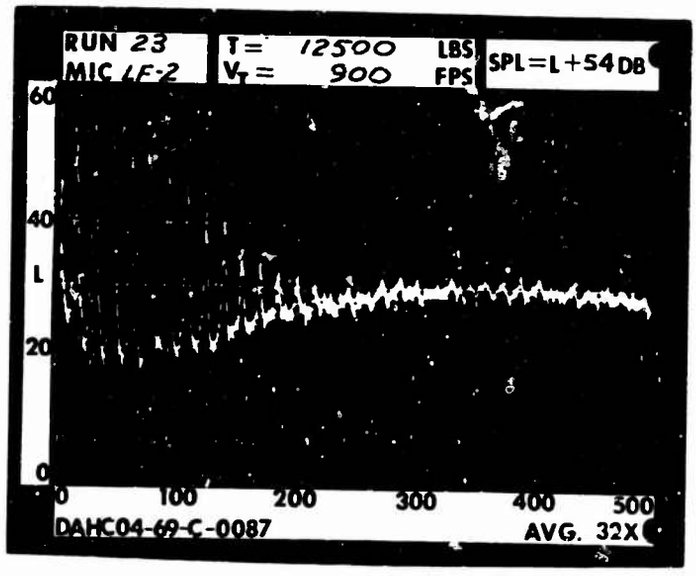

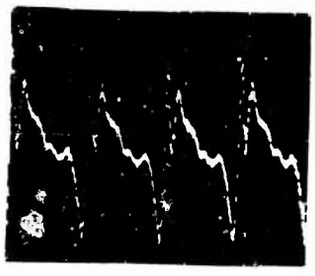

3 DIA.

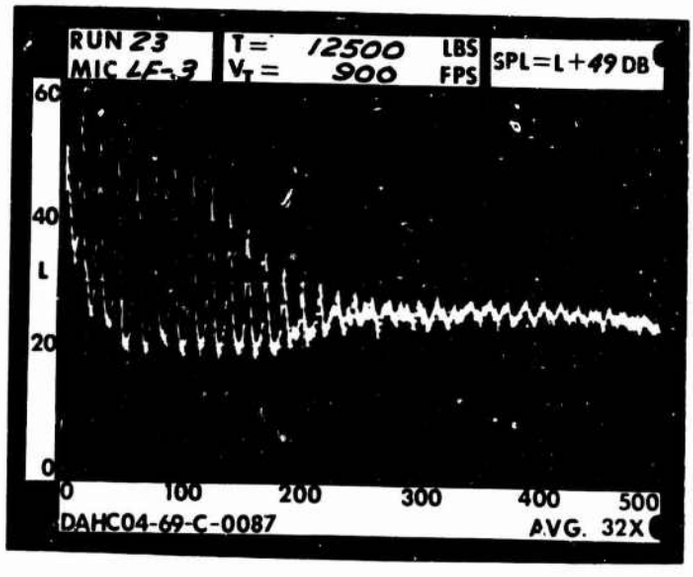

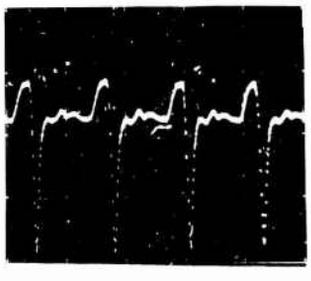

5 DIA.

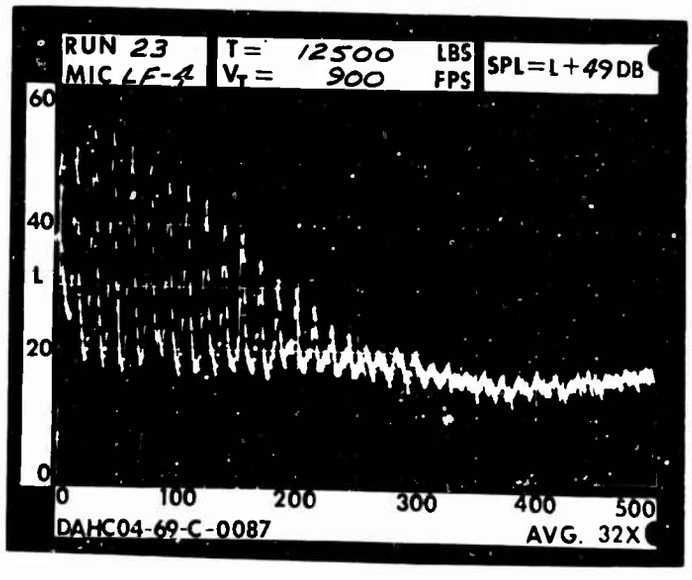

RUN 24

TIP SPEED 900 FT/SEC

THRUST 15600 LB

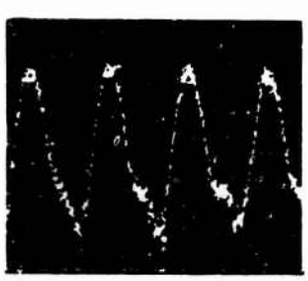

.2 RAD.

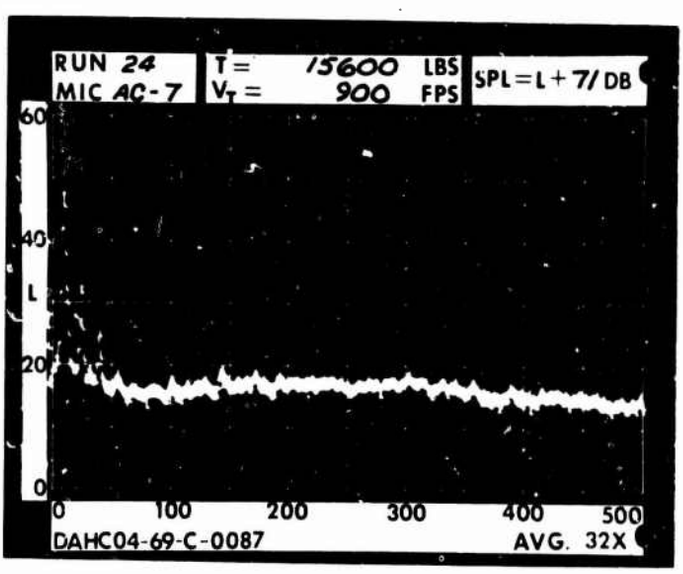

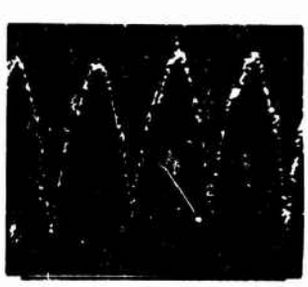

1 RAD.

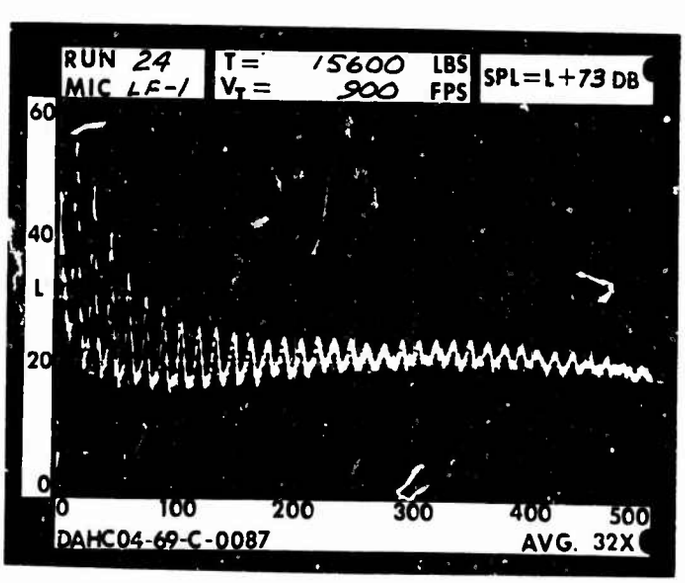

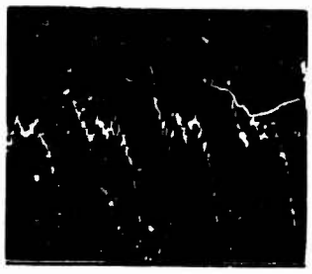

1 DIA.

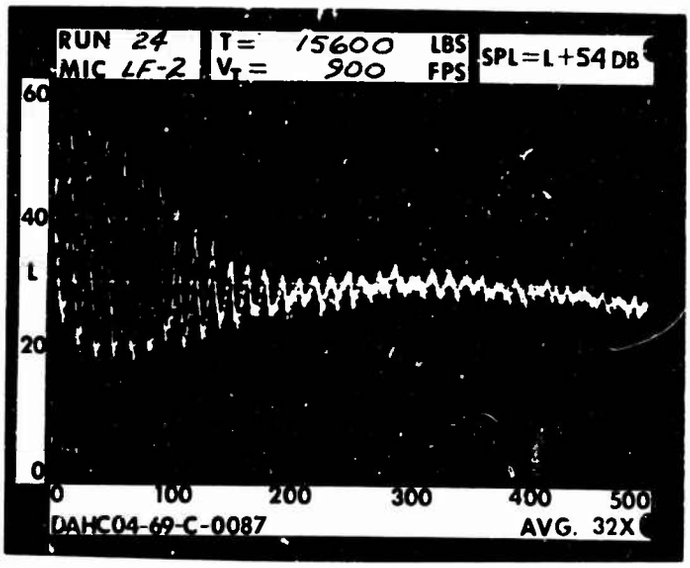

3 DIA.

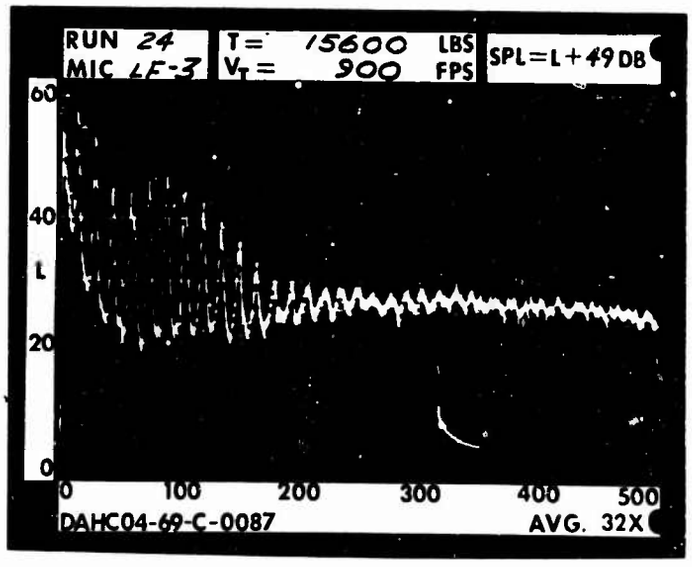

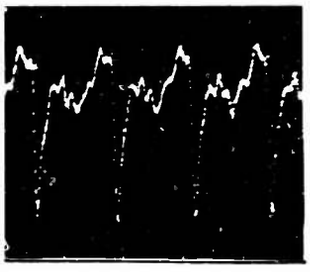

5 DIA.

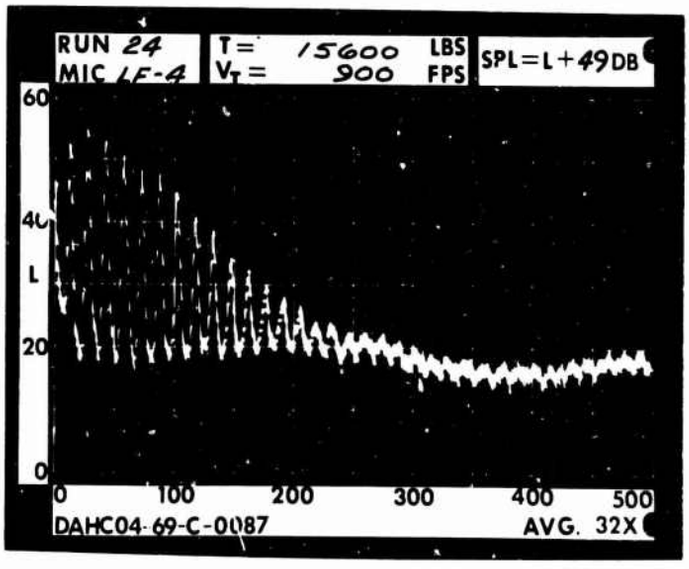

RUN 25

TIP SPEED 900 FT/SEC

THRUST 18100 LB

.2 RAD.

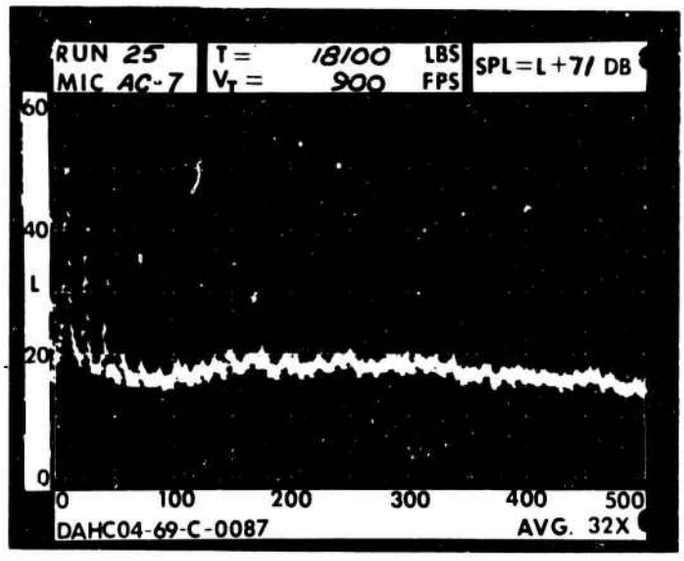

1 RAD.

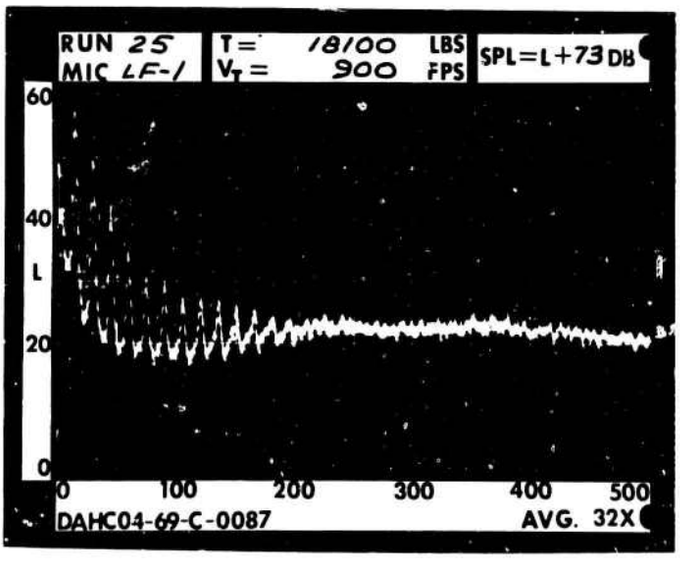

1 DIA.

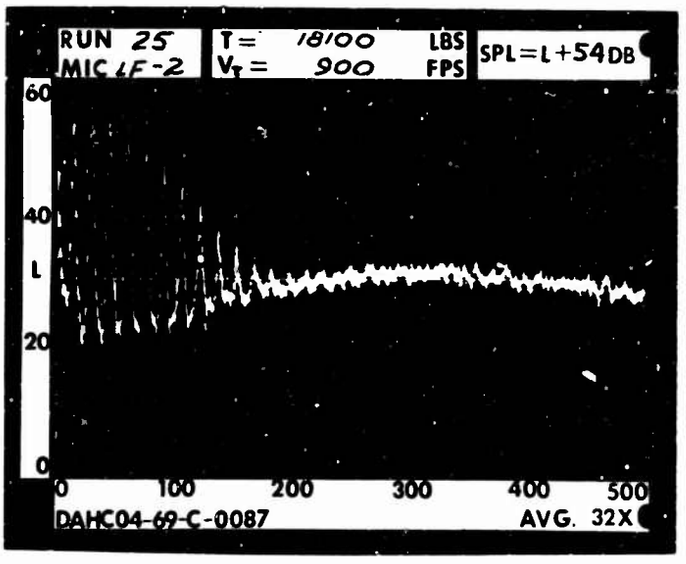

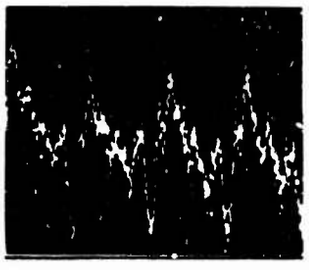

3 DIA.

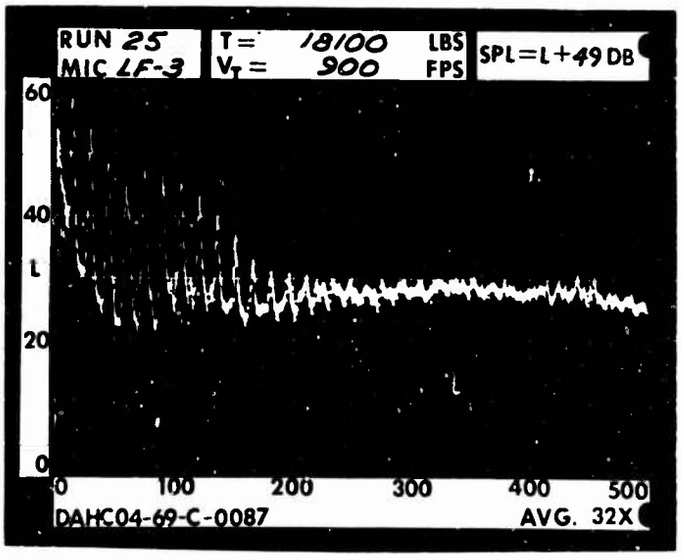

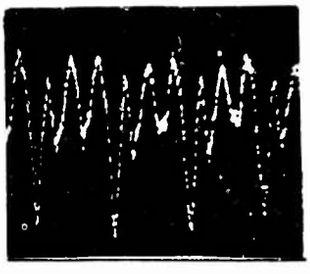

5 DIA.

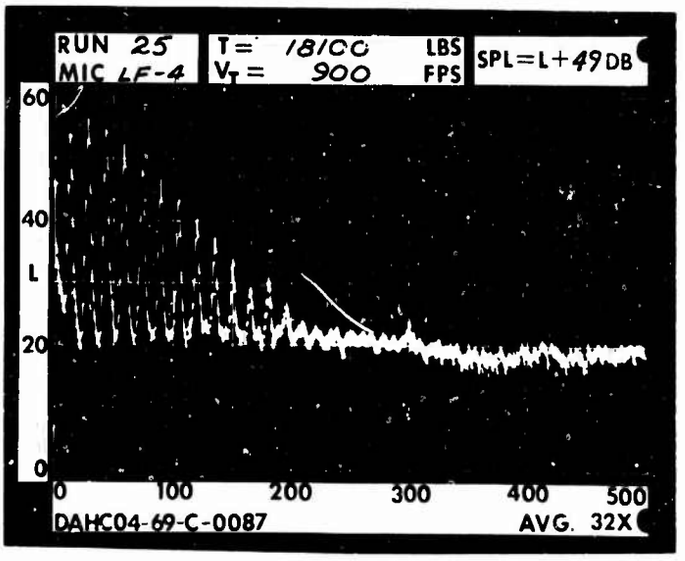

RUN 26

TIP SPEED 900 FT/SEC

THRUST 20500 LB

.2 RAD.

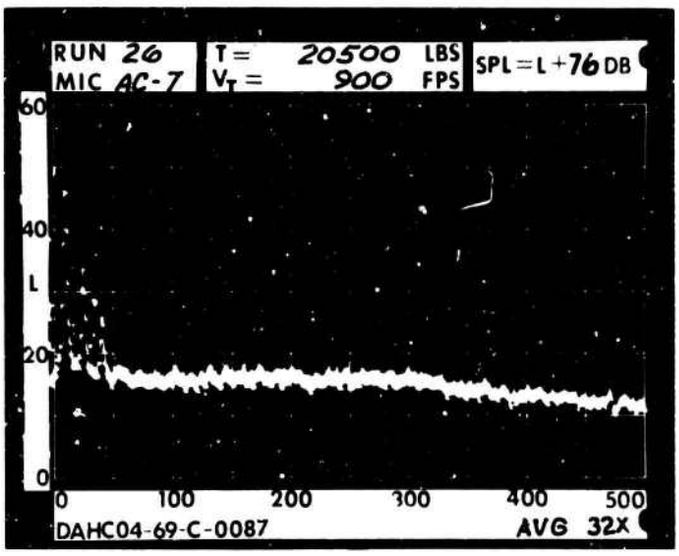

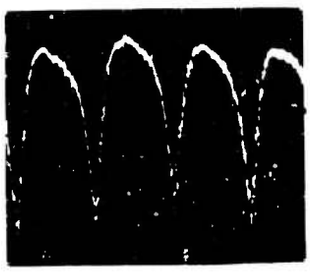

1 RAD.

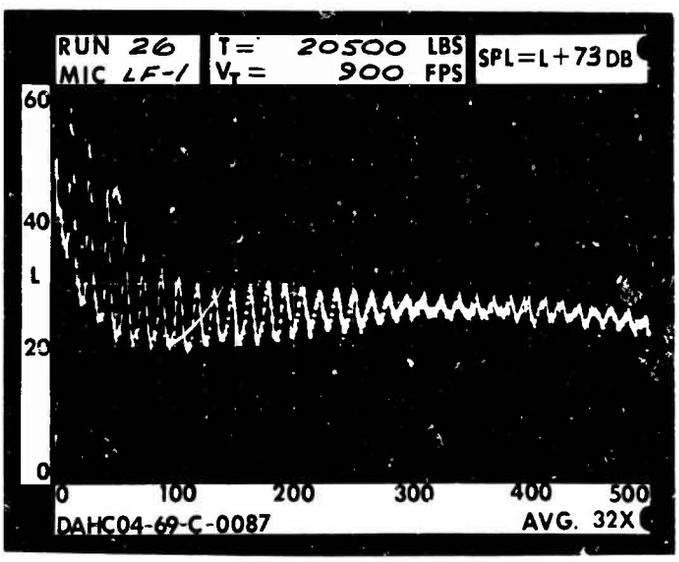

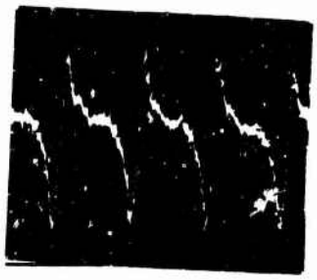

1 DIA.

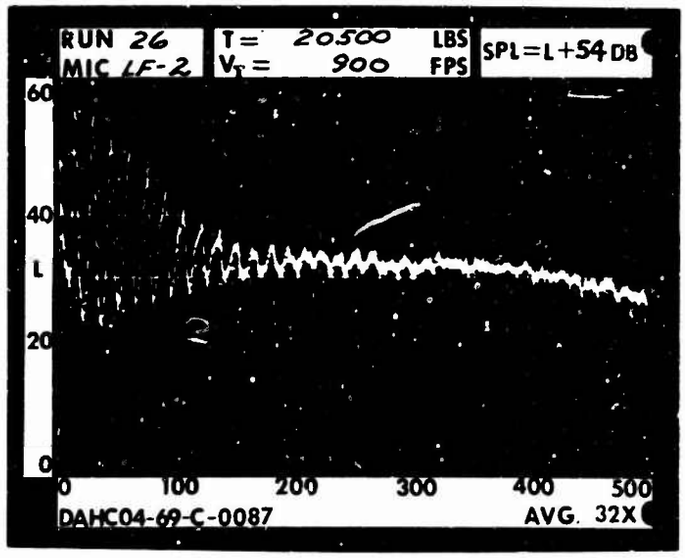

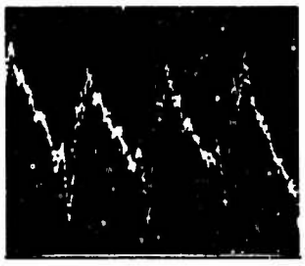

3 DIA.

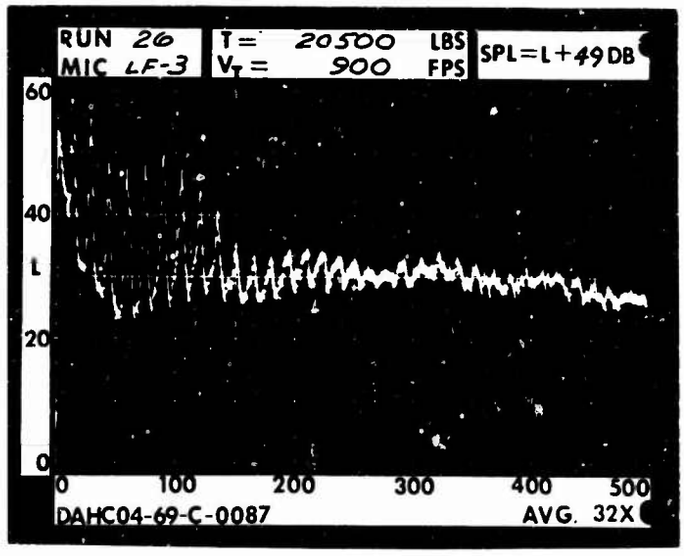

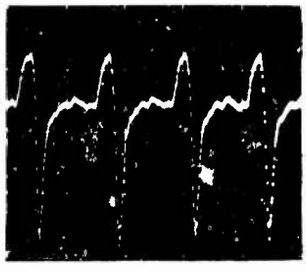

5 DIA.

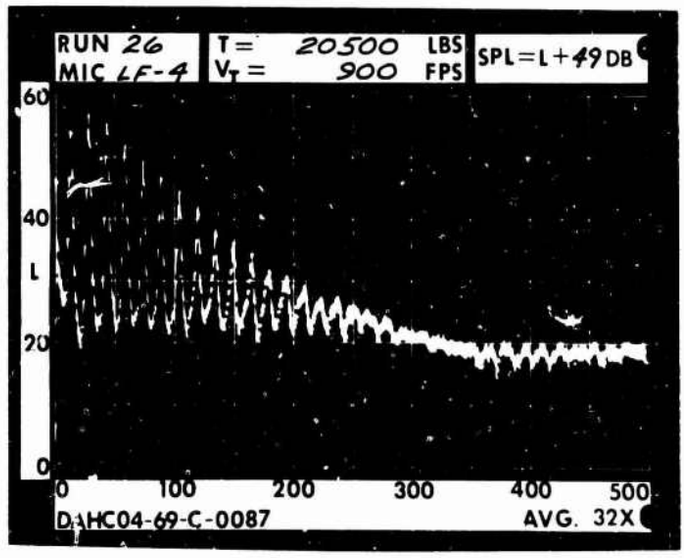

RUN 27

TIP SPEED 900 FT/SEC

THRUST 24700 LB

.2 RAD.

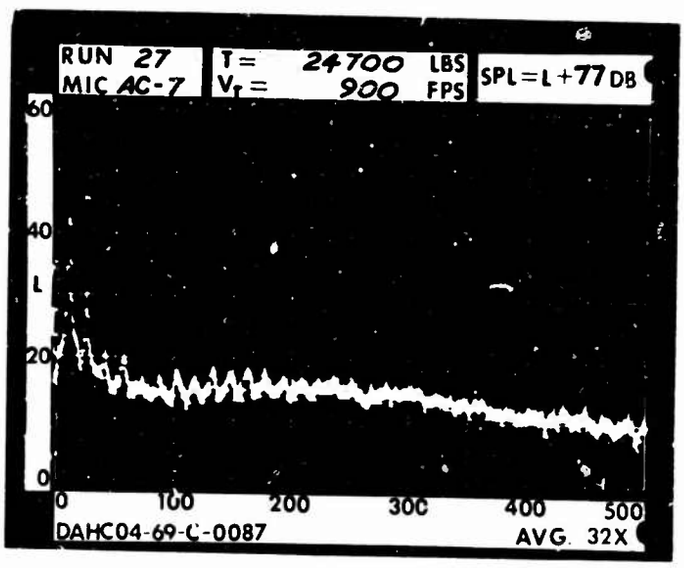

1 RAD.

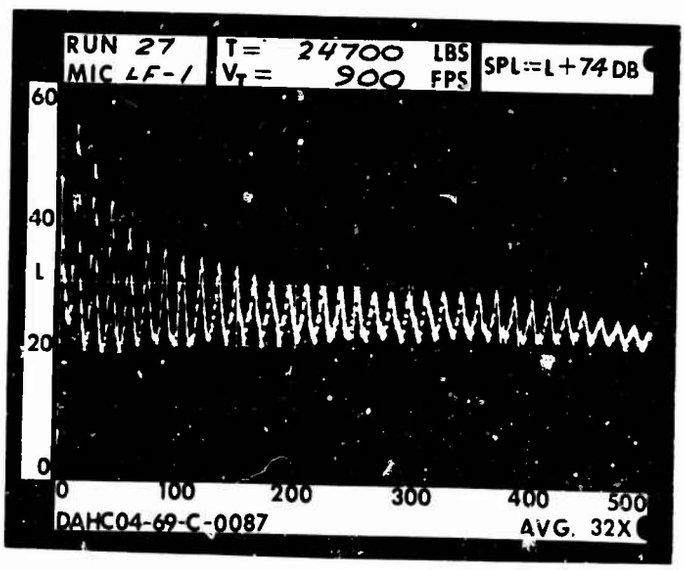

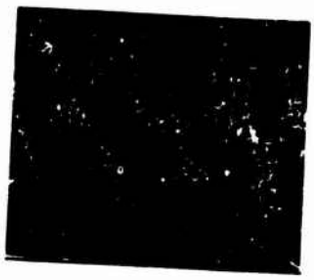

1 DIA.

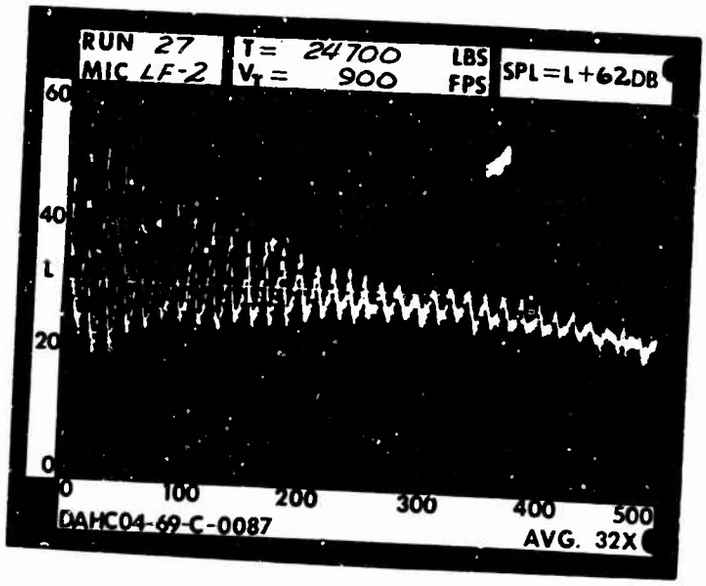

3 DIA.

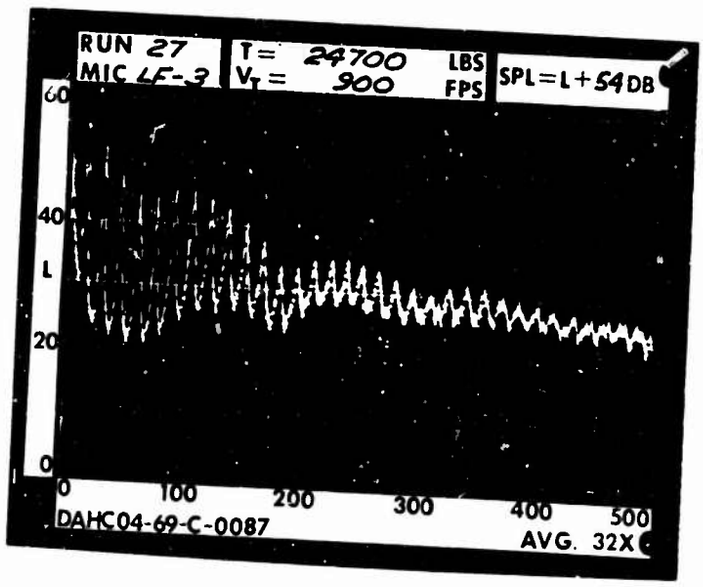

5 DIA.

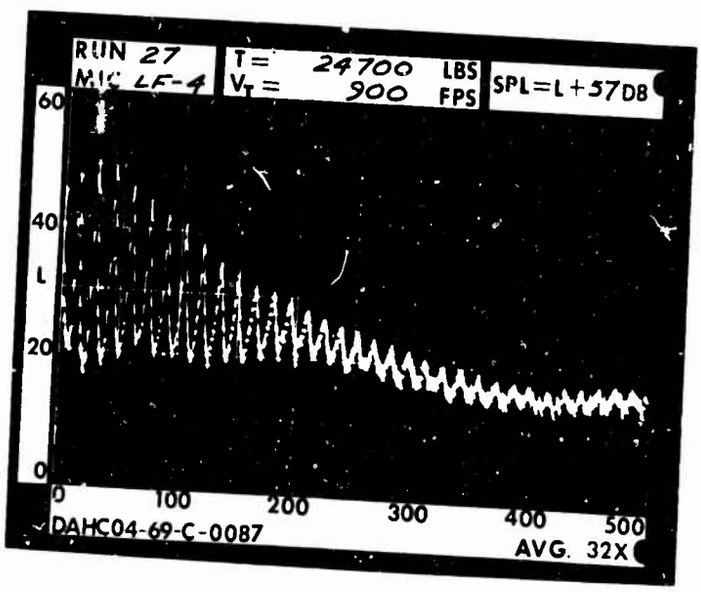

RUN 28

TIP SPEED 900 FT/SEC

THRUST 27500 LB

.2 RAD.

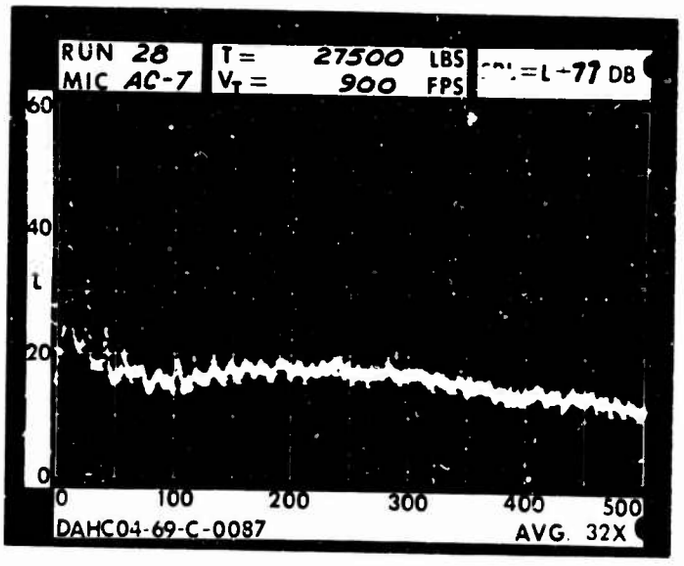

1 RAD.

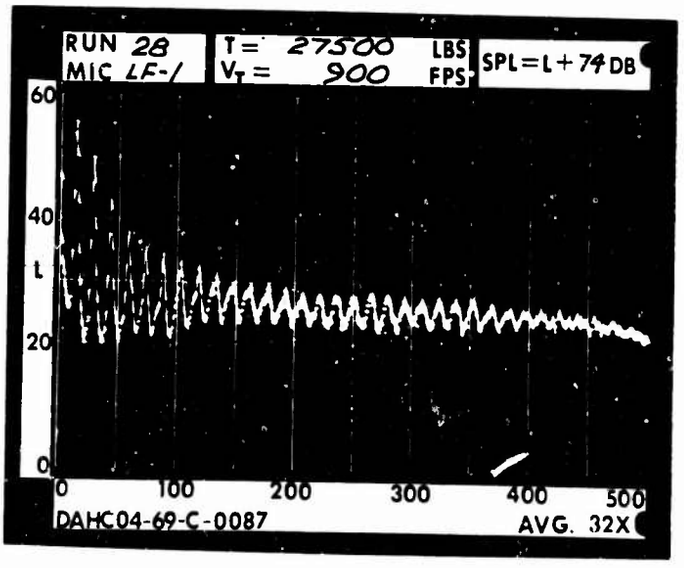

1 DIA.

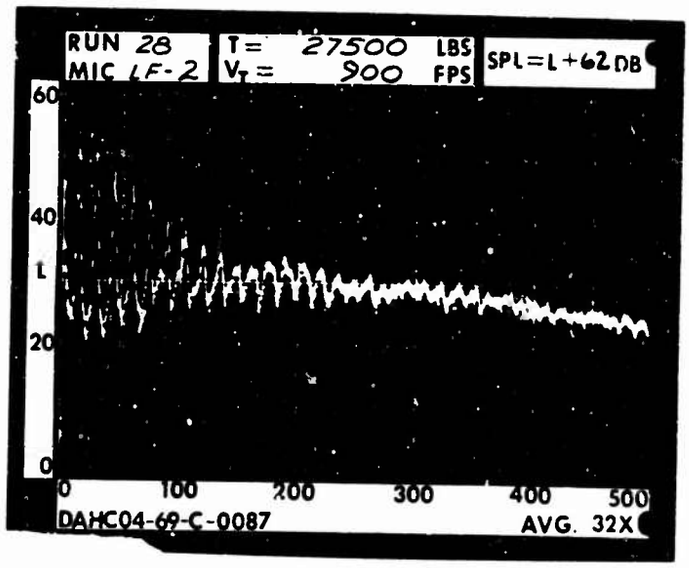

3 DIA.

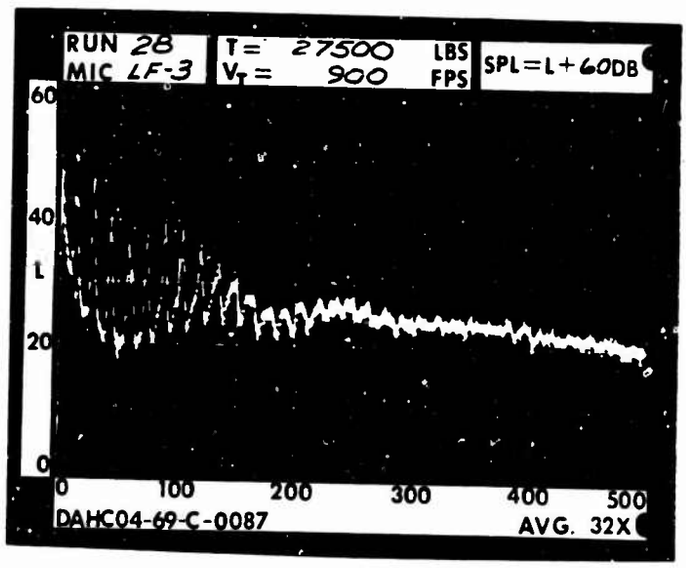

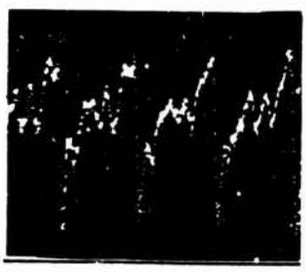

5 DIA.

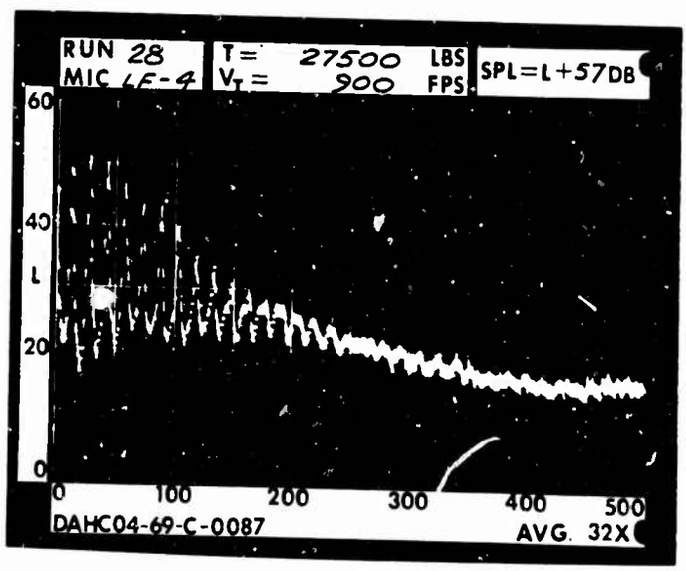

RUN 29

TIP SPEED 900 FT/SEC

THRUST 33300 LB

.2 RAD.

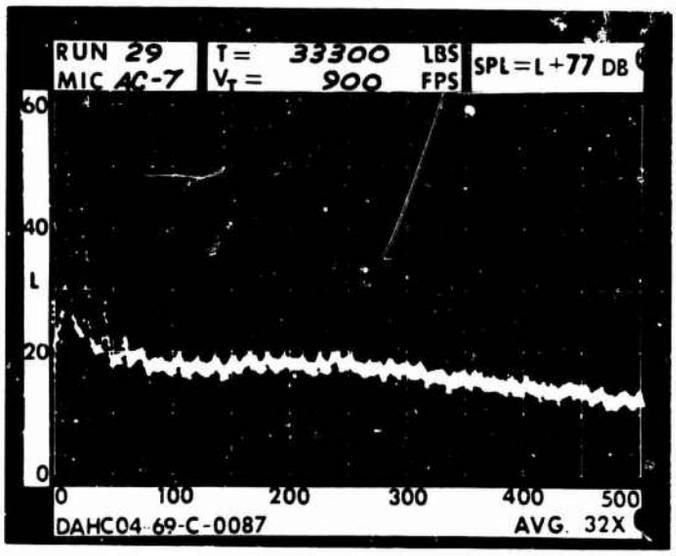

1 RAD.

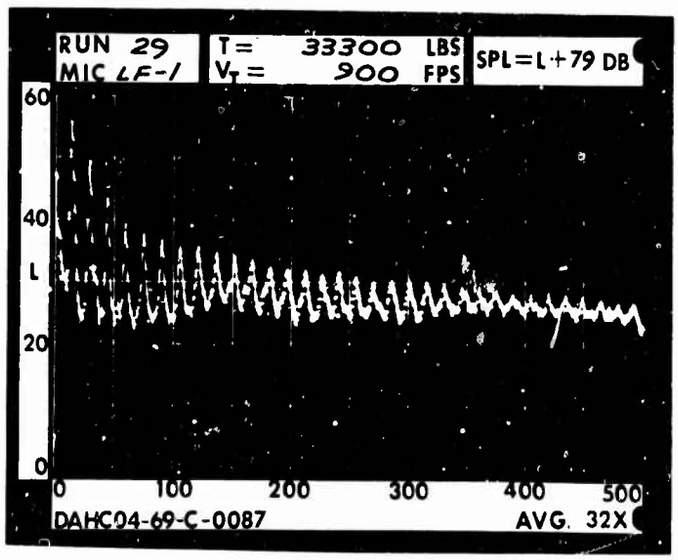

1 DIA.

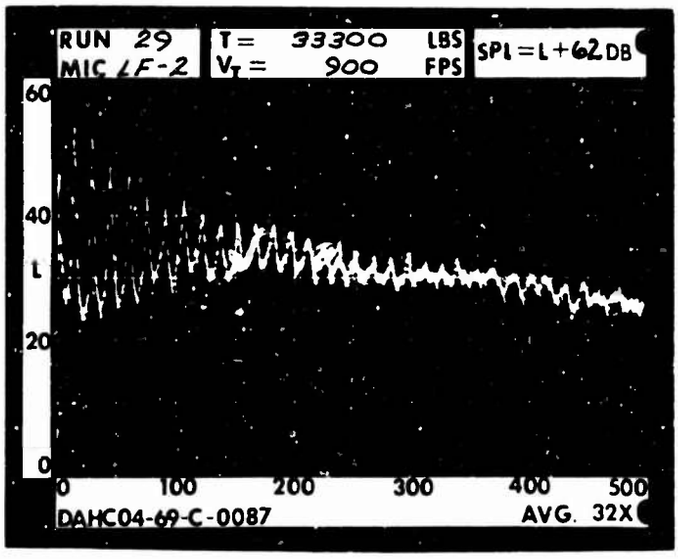

3 DIA.

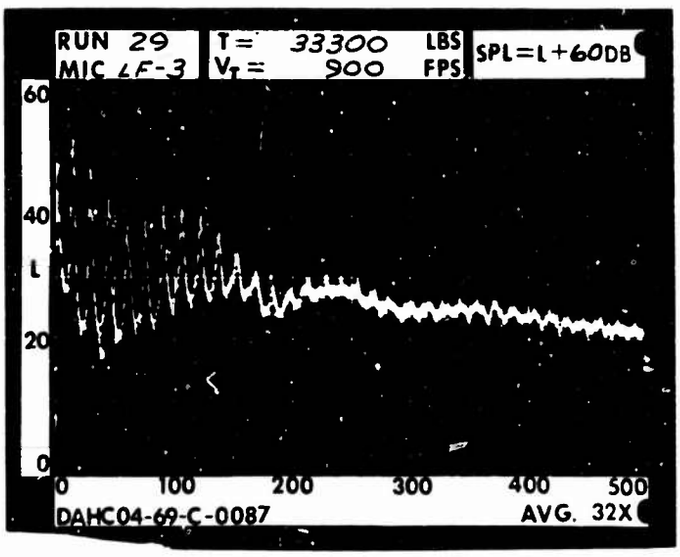

5 DIA.

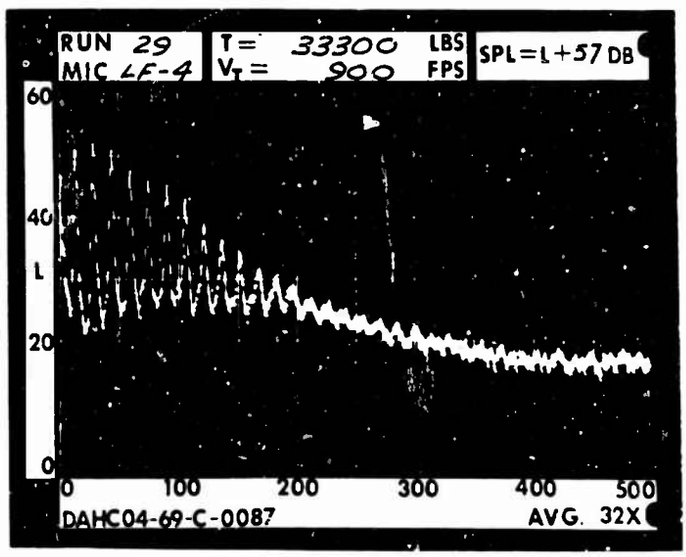

RUN 30

TIP SPEED 900 FT/SEC

THRUST 33200 LB

.2 RAD.

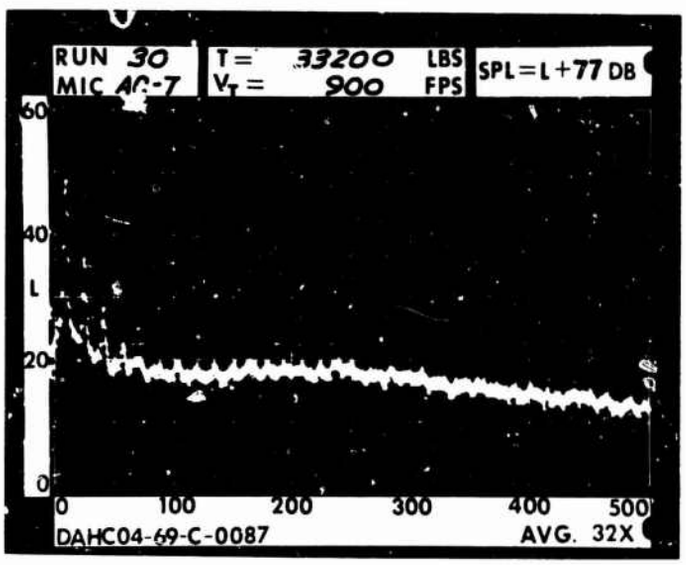

1 RAD.

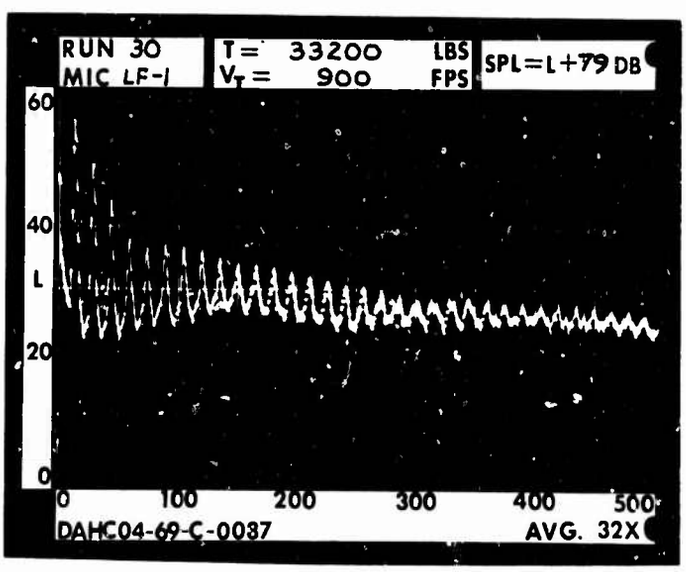

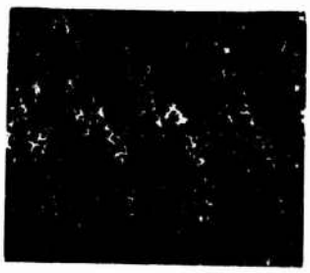

1 DIA.

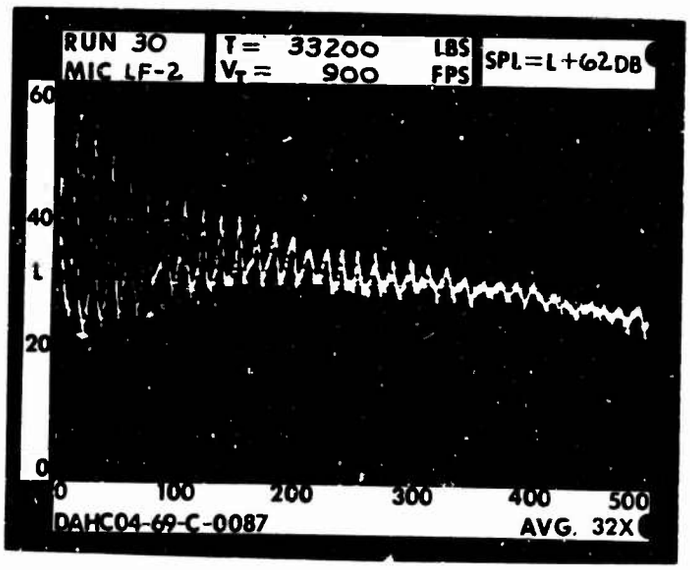

3 DIA.

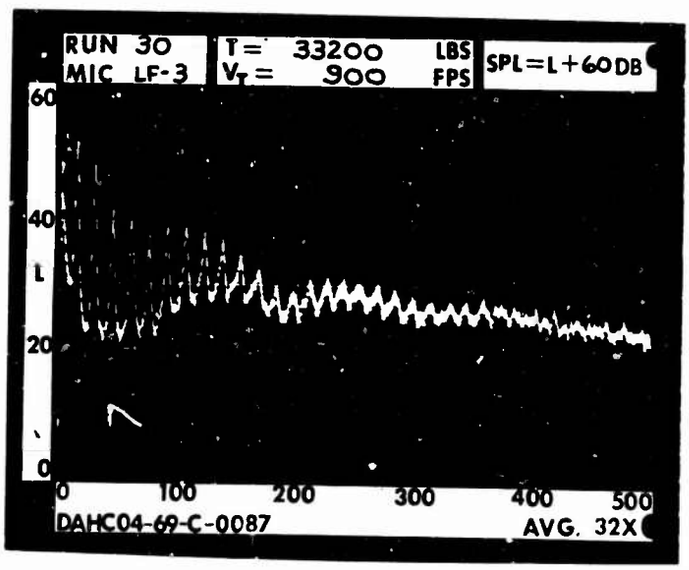

5 DIA.

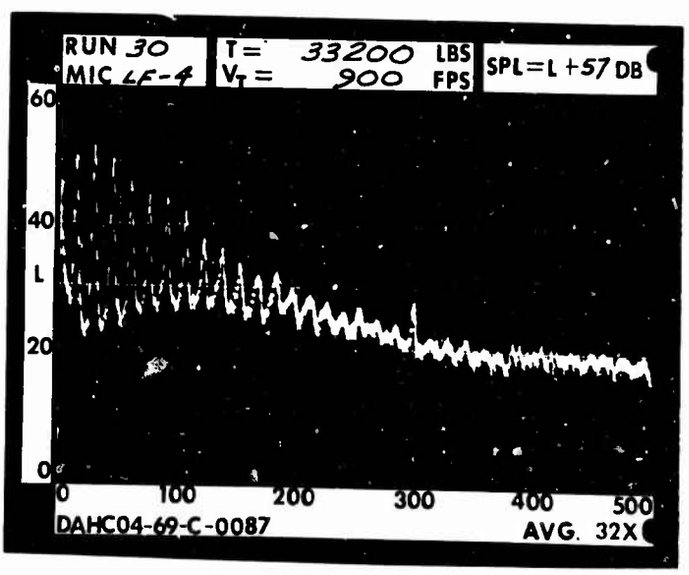

RUN 31

TIP SPEED 850 FT/SEC

THRUST 8300 LB

.2 RAD.

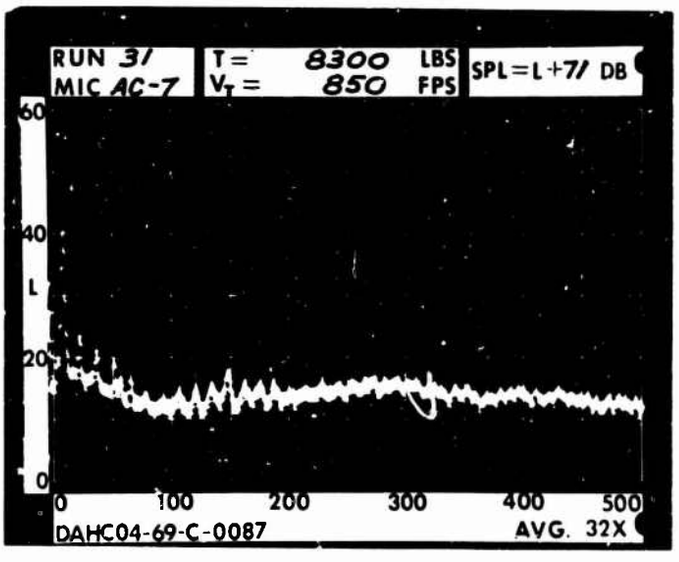

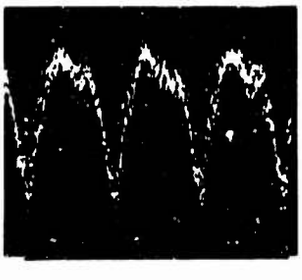

1 RAD.

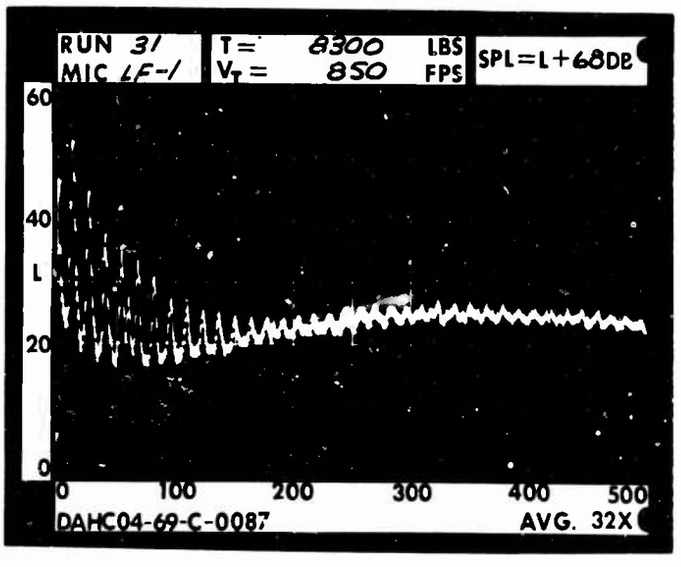

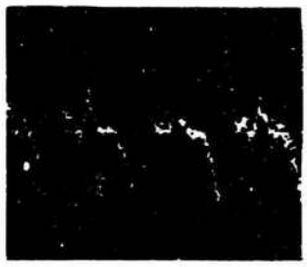

1 DIA.

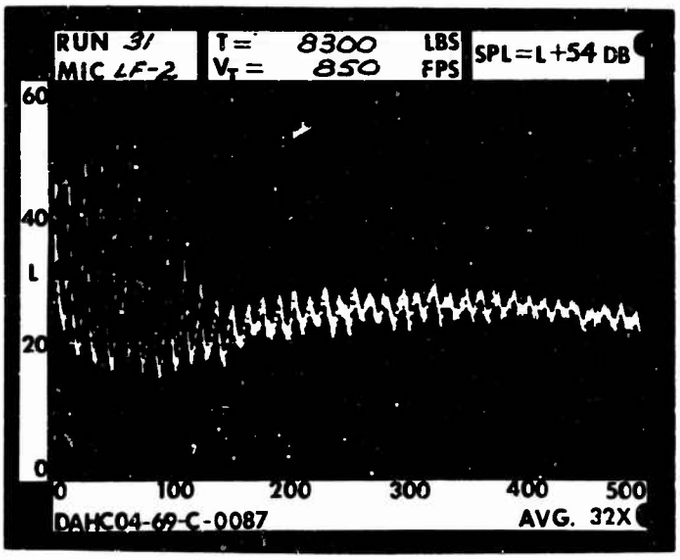

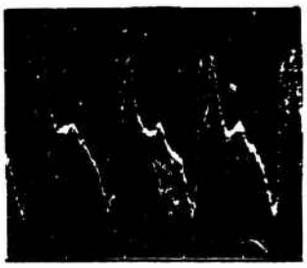

3 DIA.

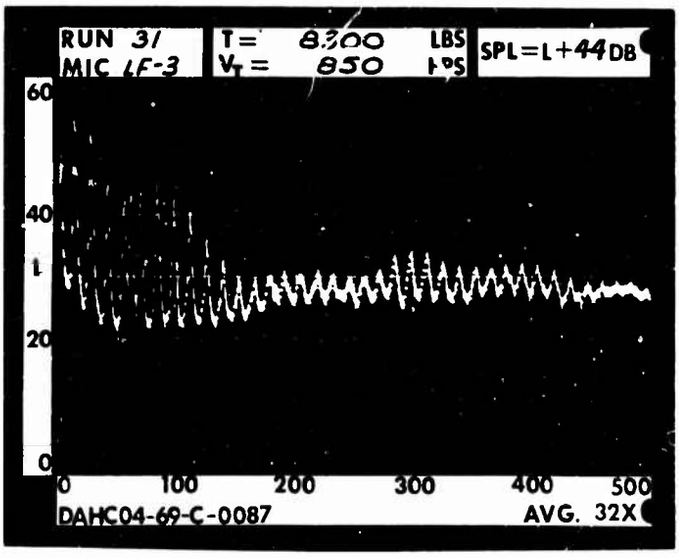

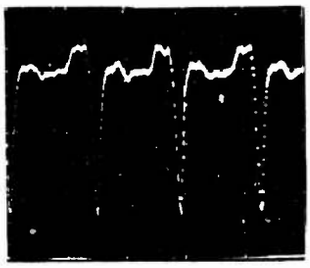

5 DIA.

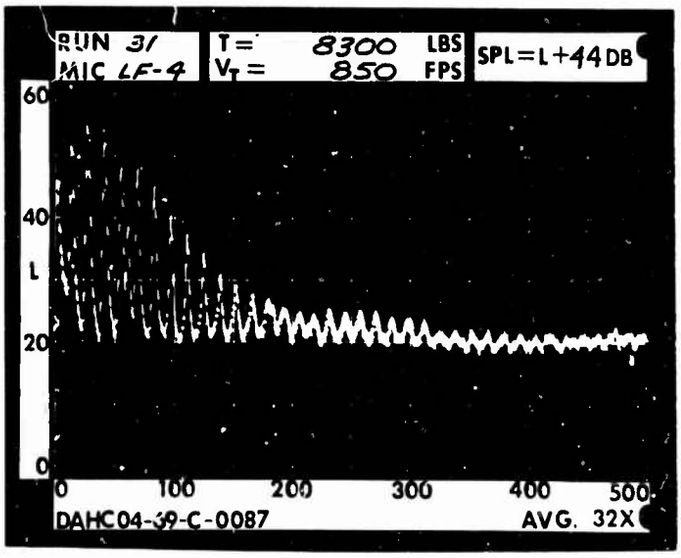

RUN 32

TIP SPEED 850 FT/SEC

THRUST 11500 LB

.2 RAD.

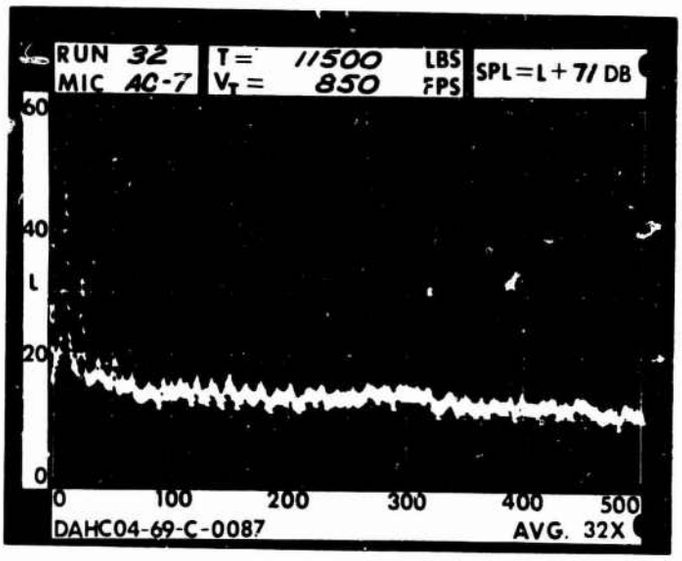

1 RAD.

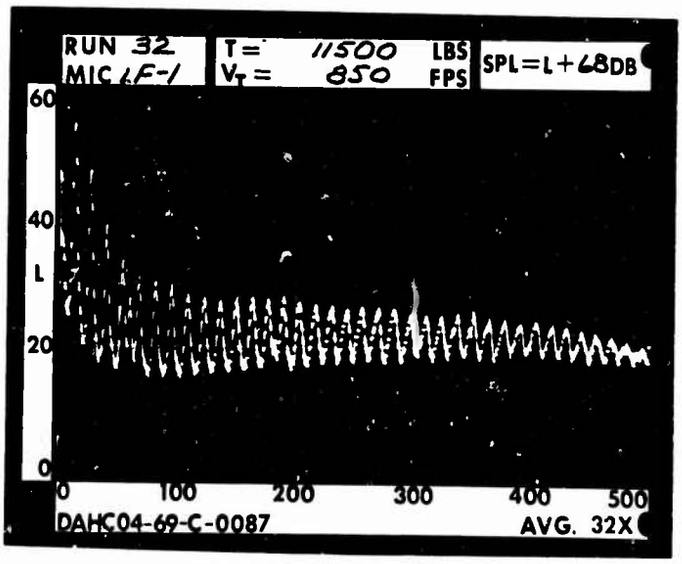

1 DIA.

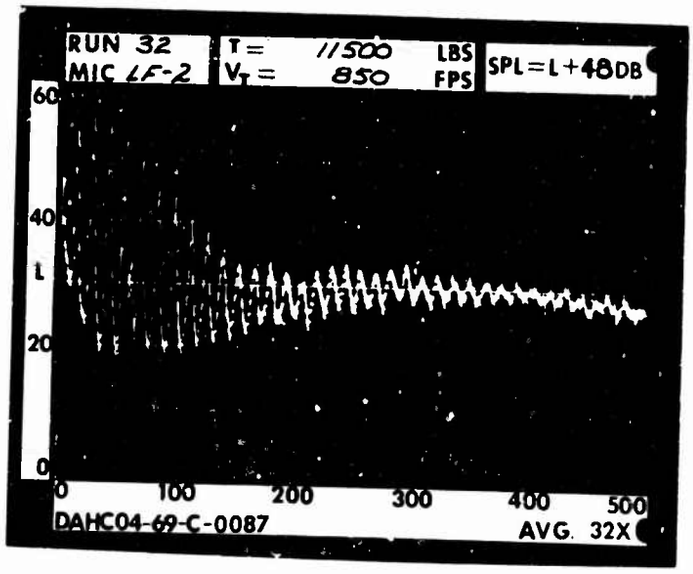

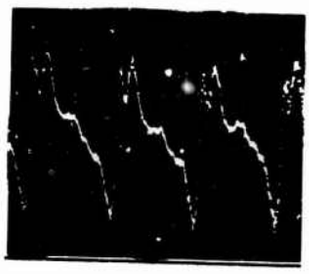

3 DIA.

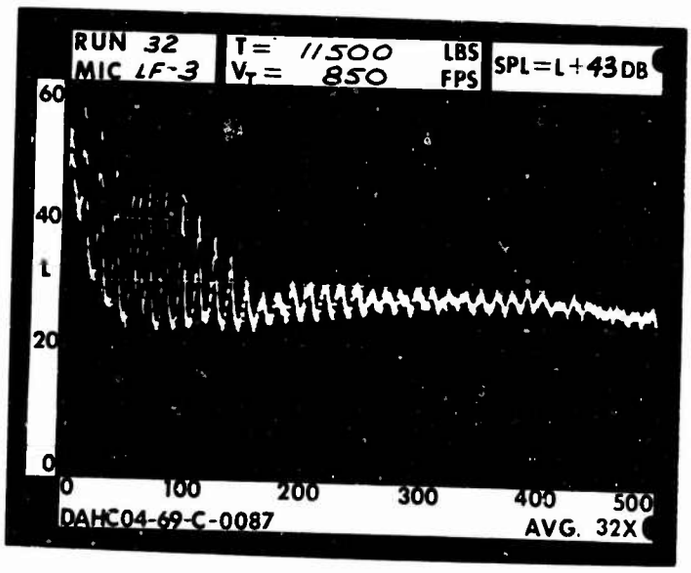

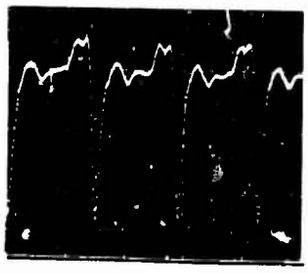

5 DIA.

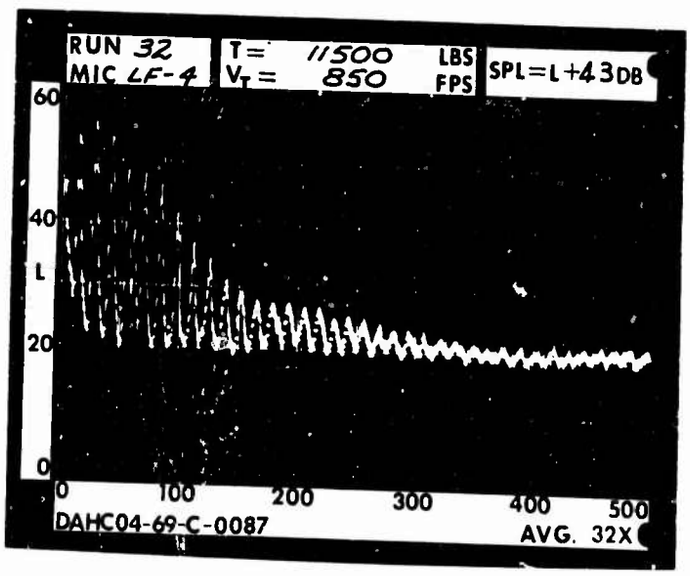

RUN 33

TIP SPEED 850 FT/SEC

THRUST 15500 LB

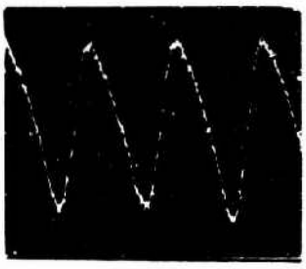

.2 RAD.

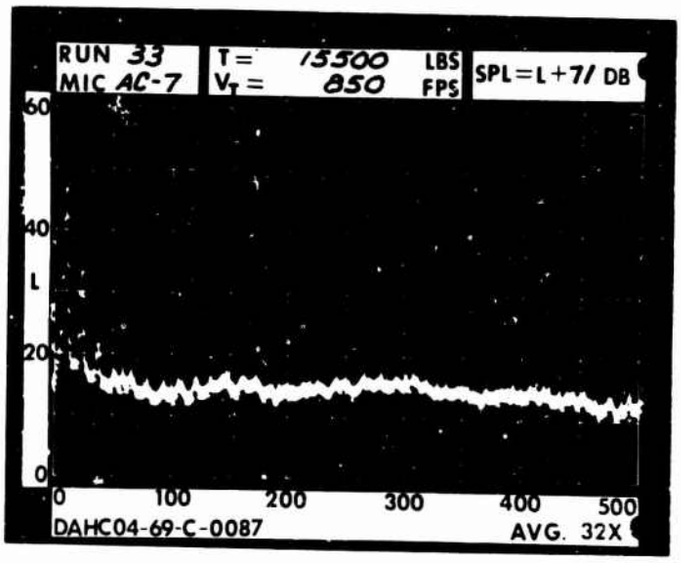

1 RAD.

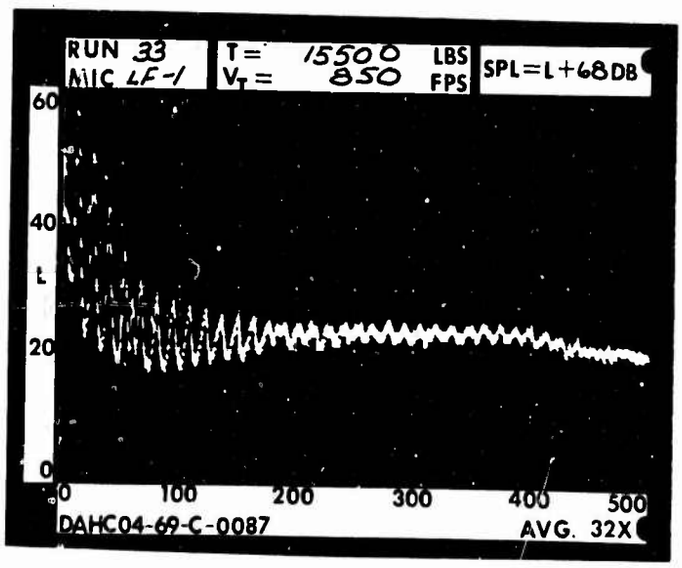

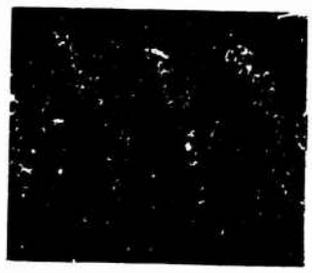

1 DIA.

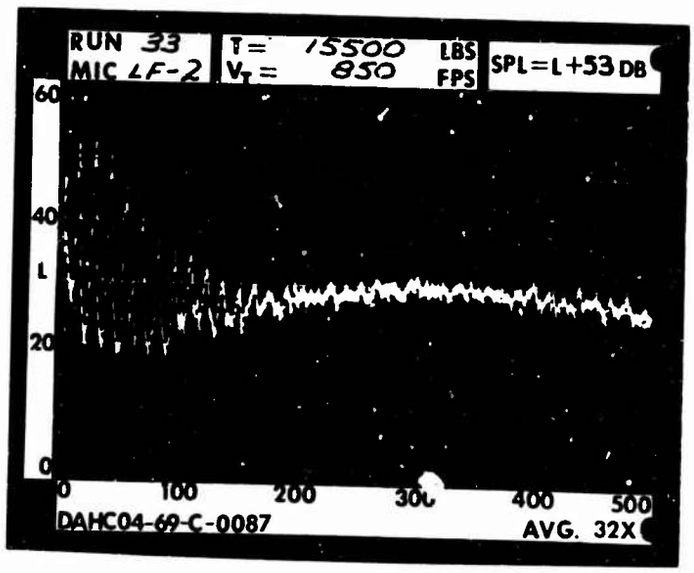

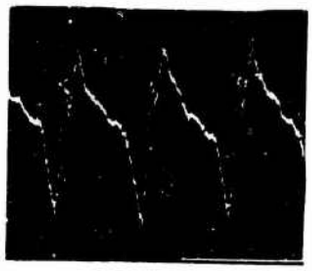

3 DIA.

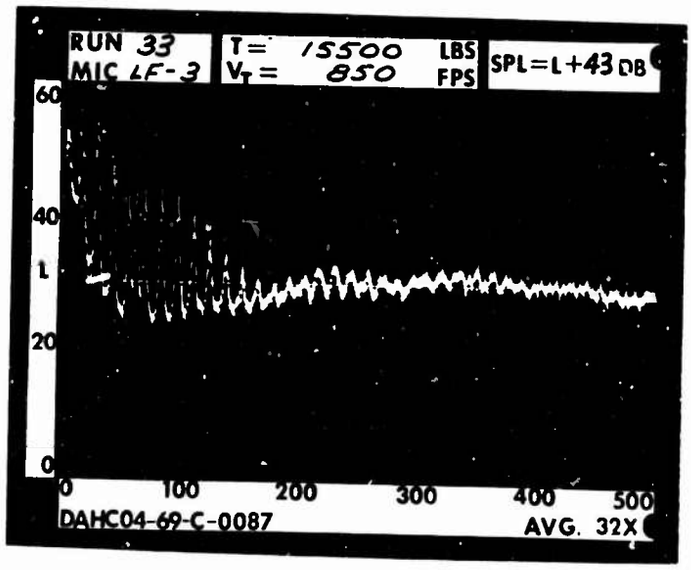

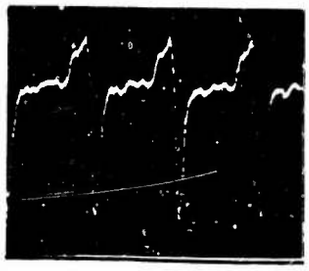

5 DIA.

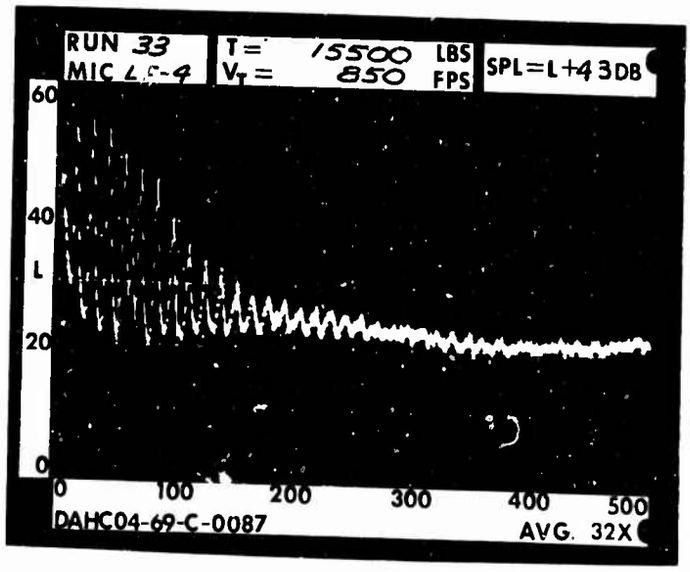

RUN 34

TIP SPEED 850 FT/SEC

THRUST 16900 LB

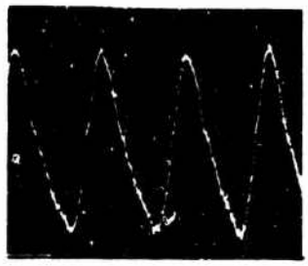

.2 RAD.

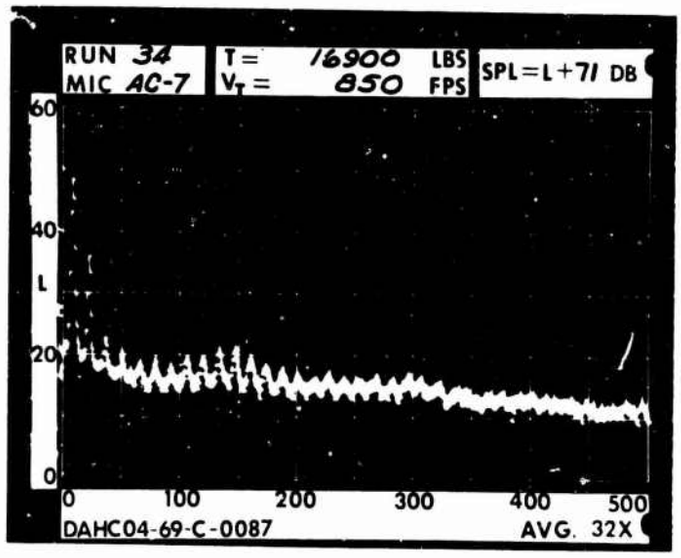

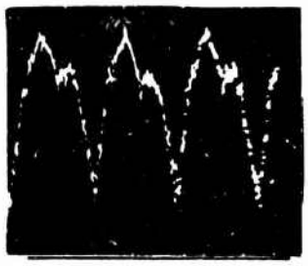

1 RAD.

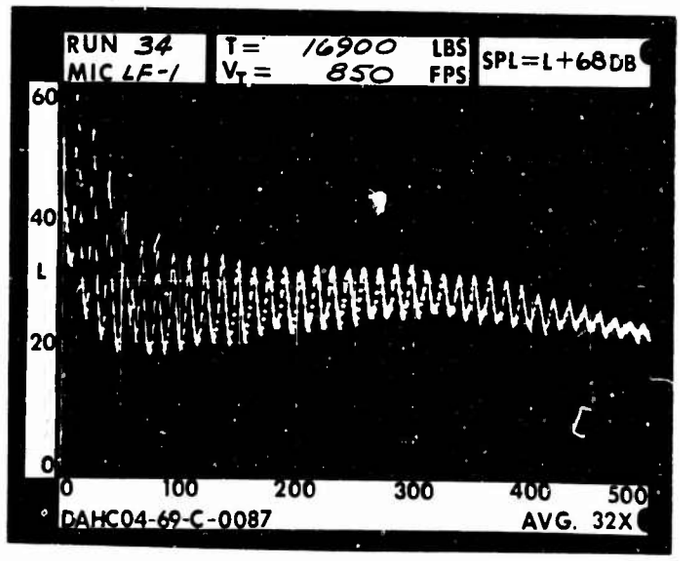

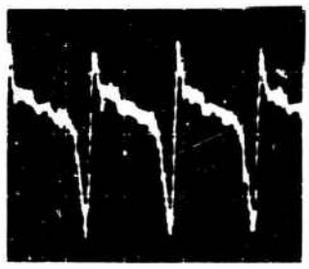

1 DIA.

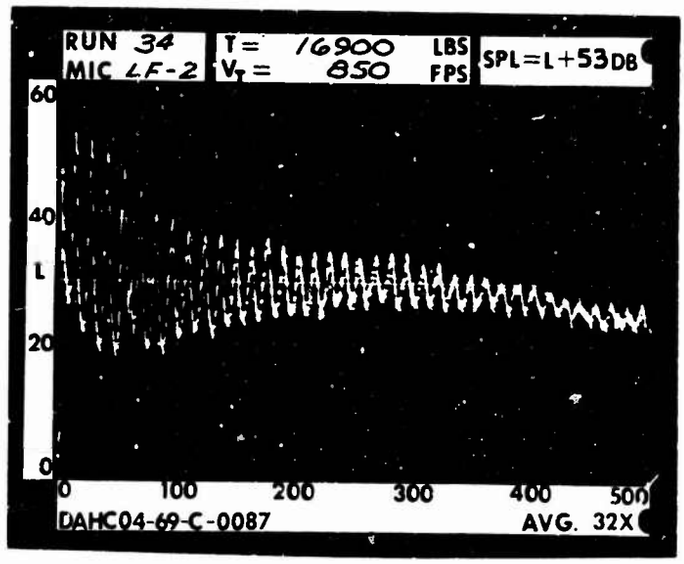

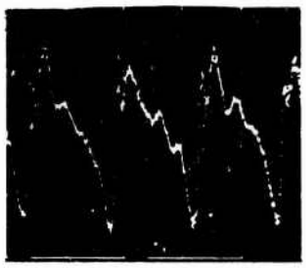

3 DIA.

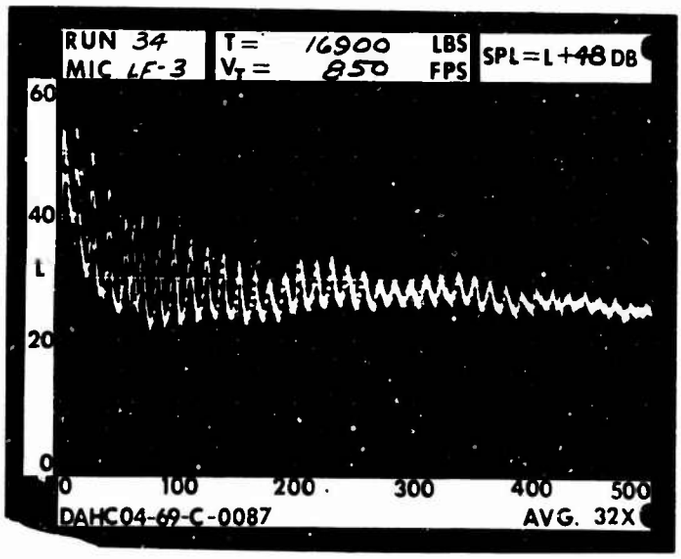

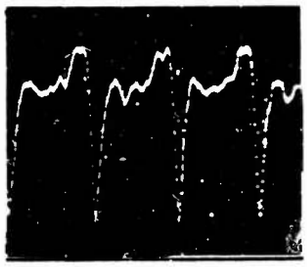

5 DIA.

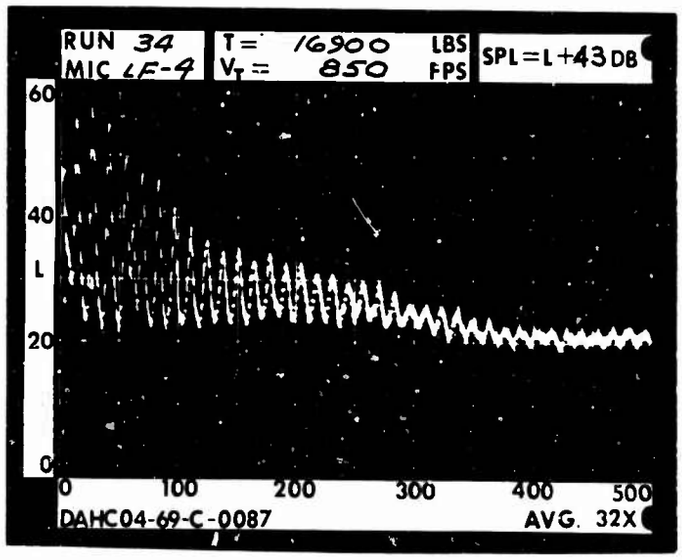

RUN 35

TIP SPEED 850 FT/SEC

THRUST 19900 LB

.2 RAD.

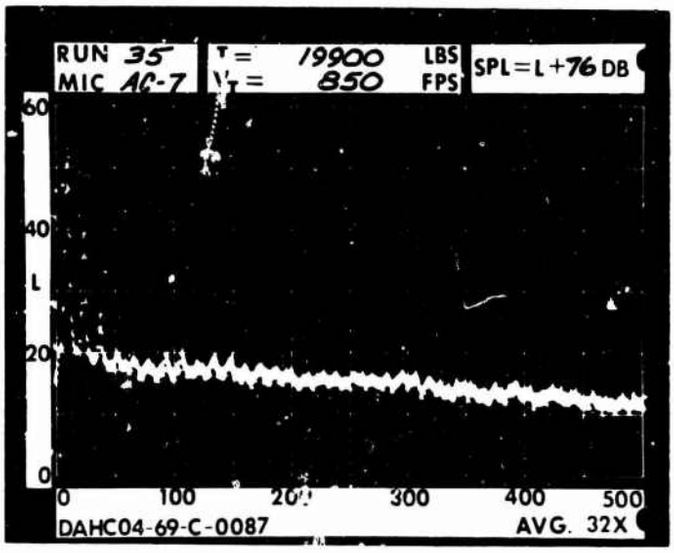

1 RAD.

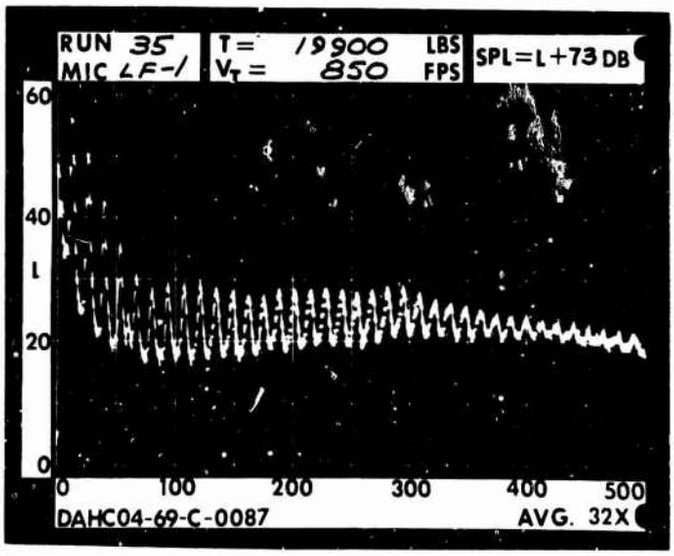

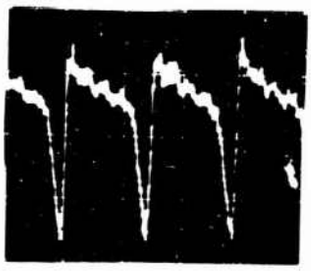

1 DIA.

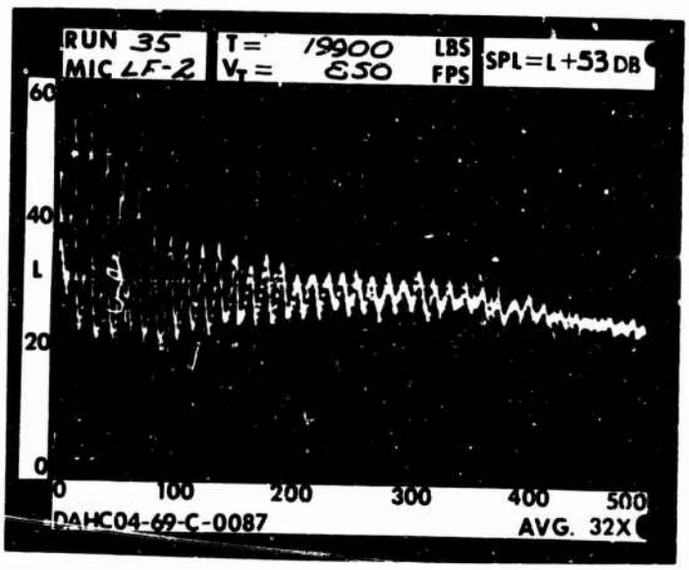

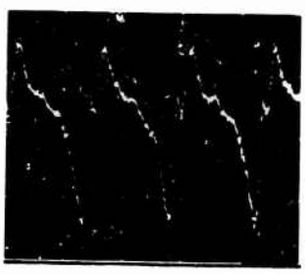

3 DIA.

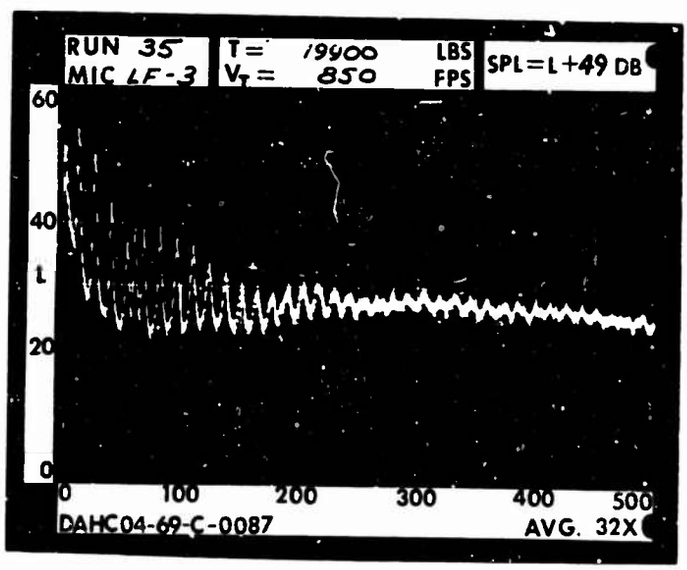

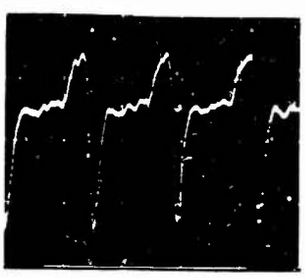

5 DIA.

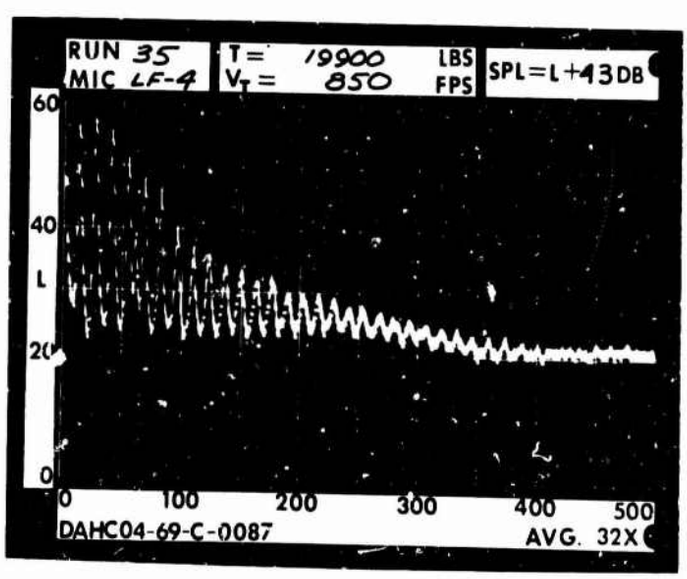

RUN 36

TIP SPEED 850 FT/SEC

THRUST 26600 LB

.2 RAD.

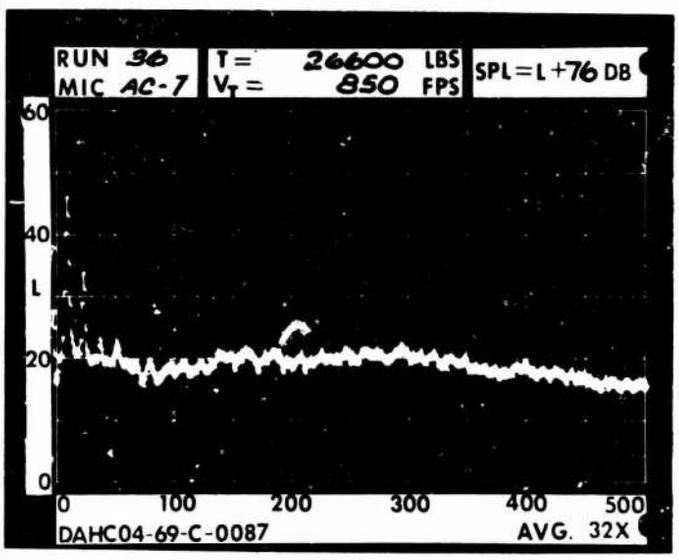

1 RAD.

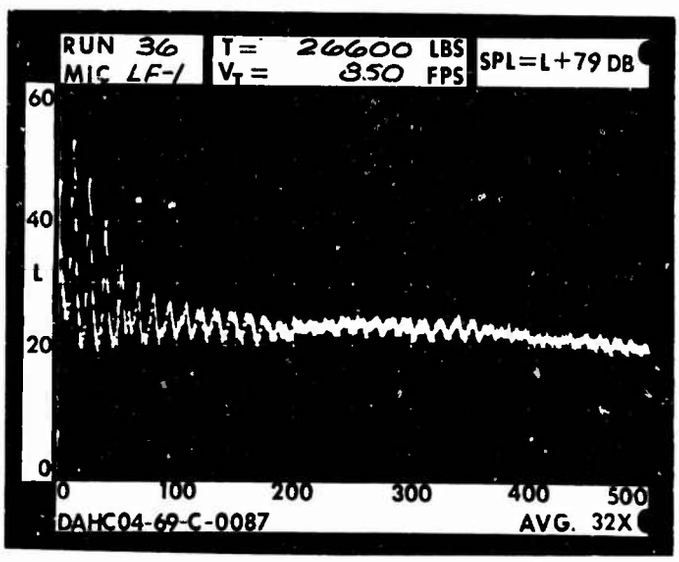

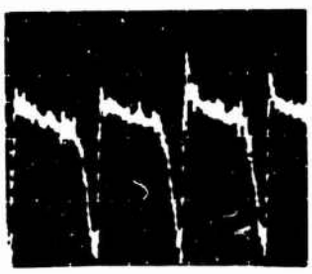

1 DIA.

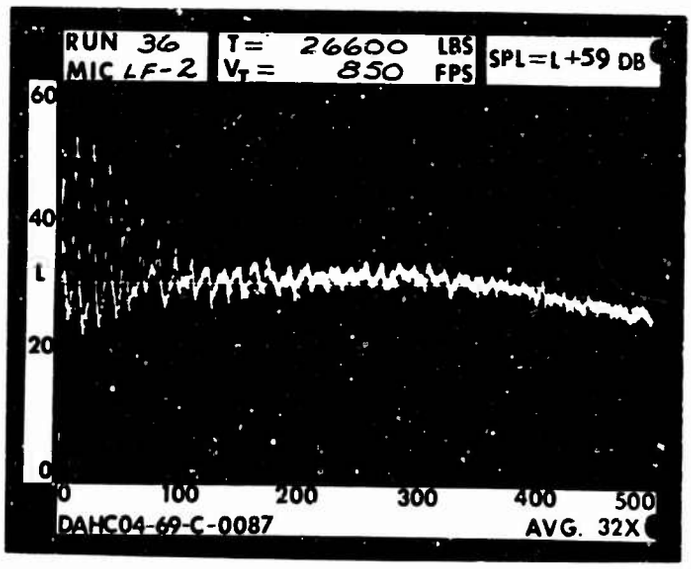

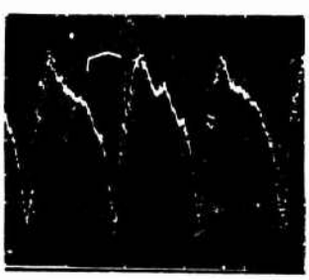

3 DIA.

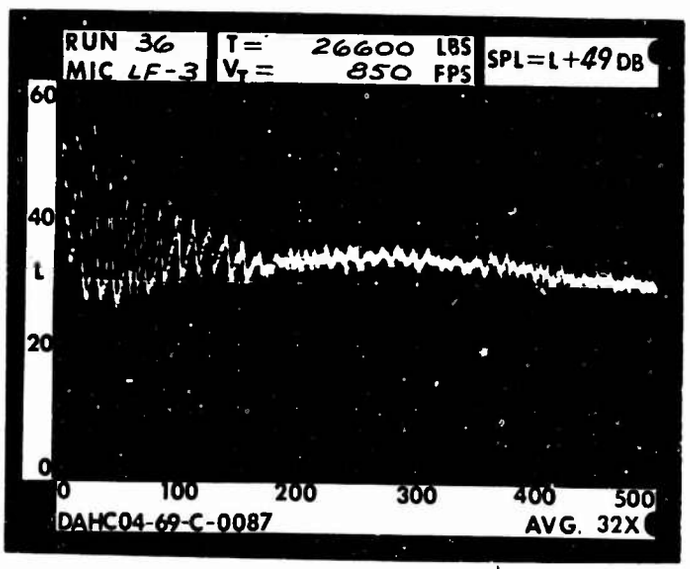

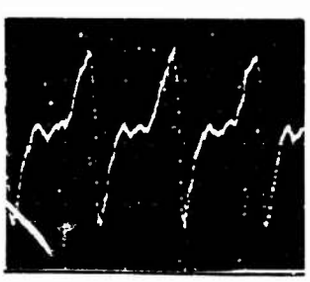

5 DIA.

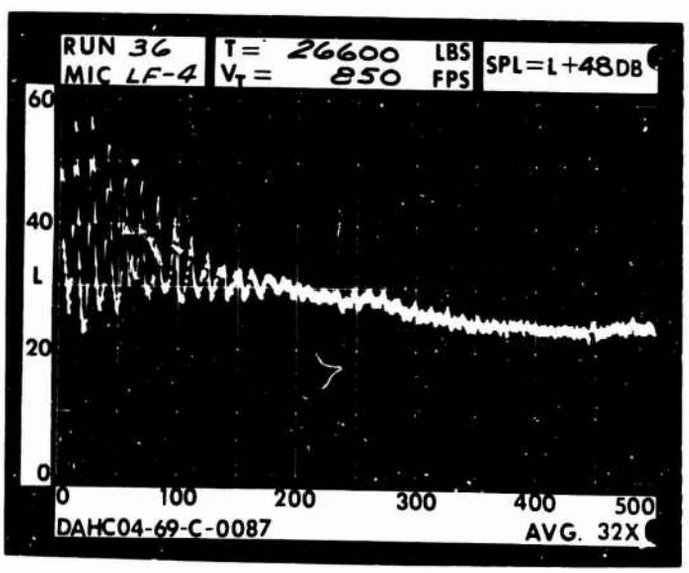

RUN 37

TIP SPEED 850 FT/SEC

THRUST 28800 LB

.2 RAD.

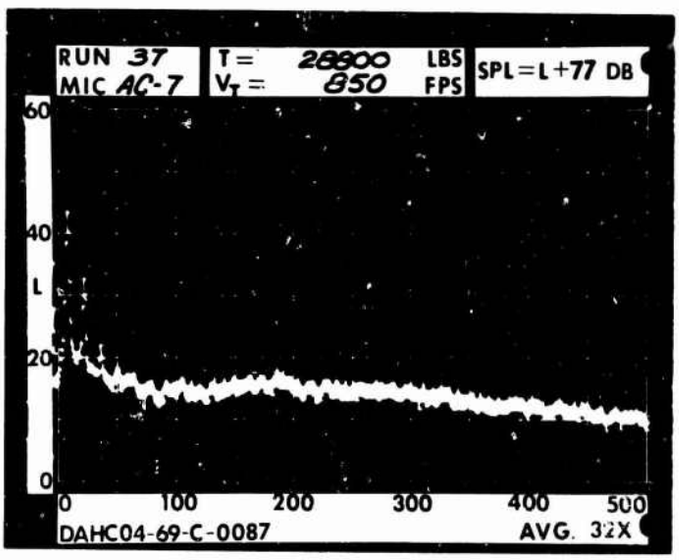

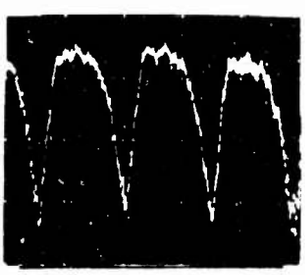

1 RAD.

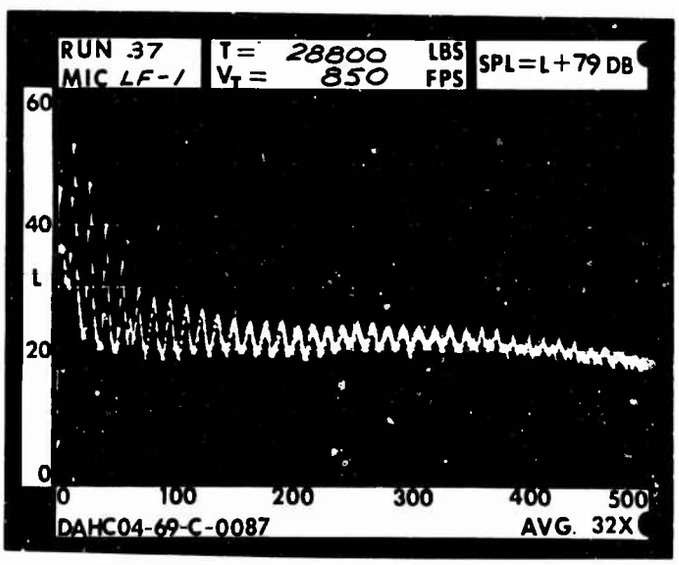

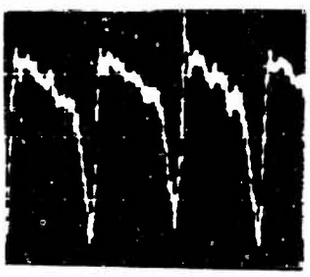

1 DIA.

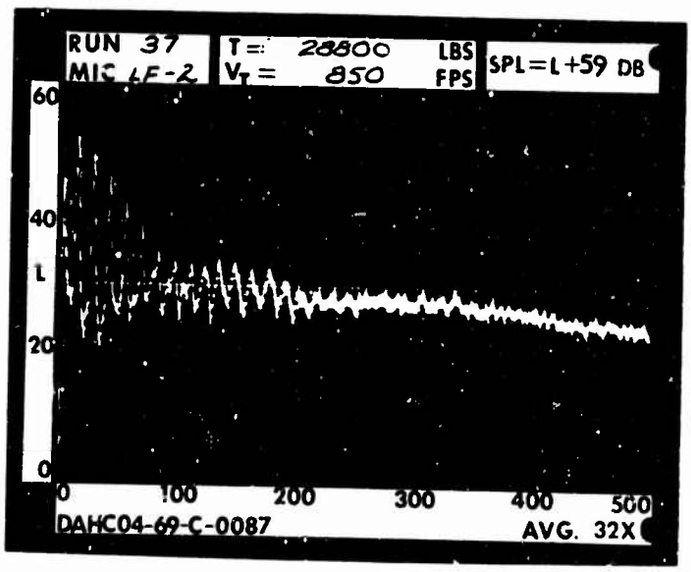

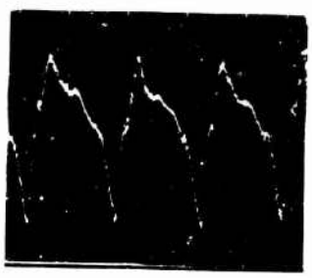

3 DIA.

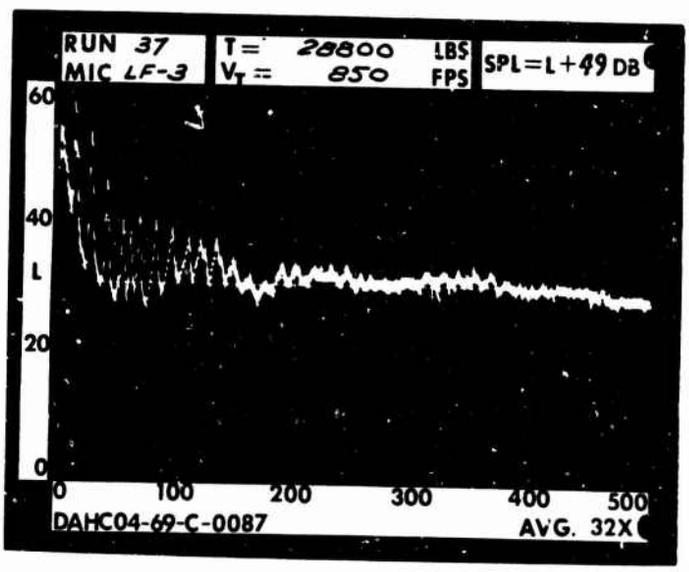

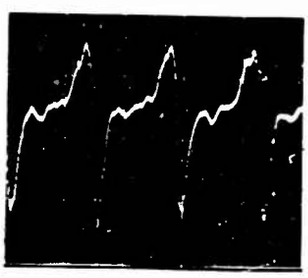

5 DIA.

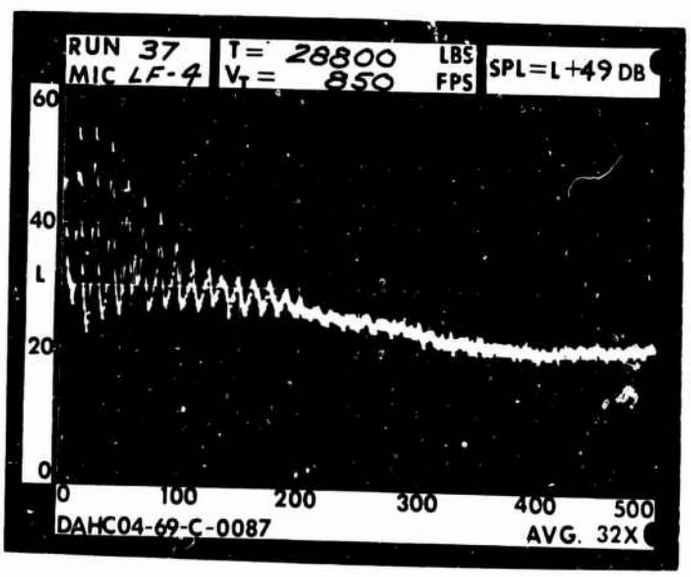

RUN 38

TIP SPEED 850 FT/SEC

THRUST 31800 LB

.2 RAD.

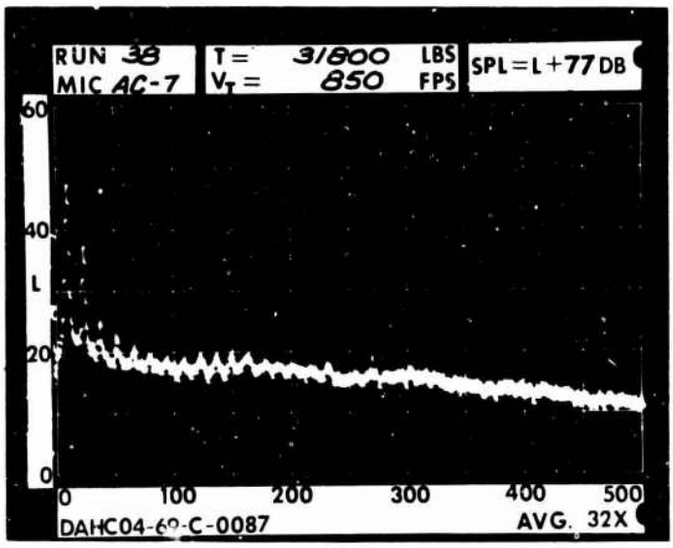

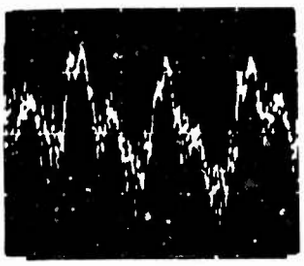

1 RAD.

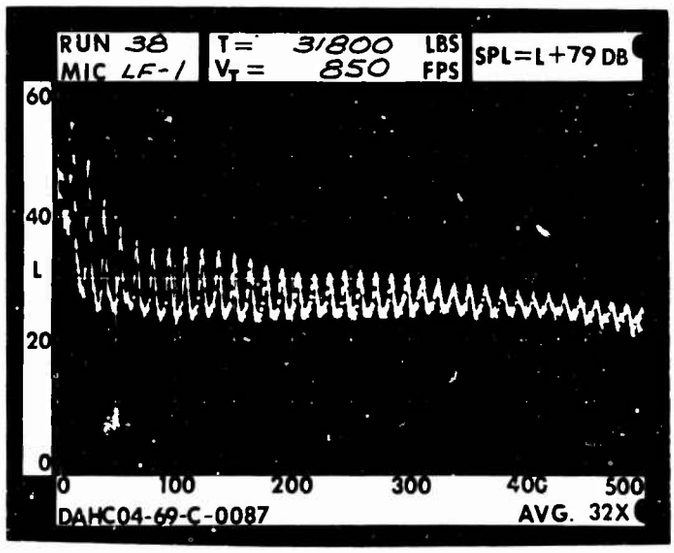

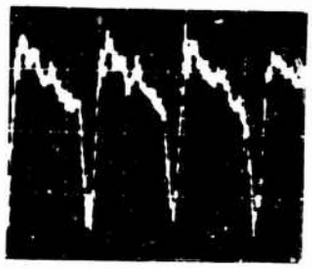

1 DIA.

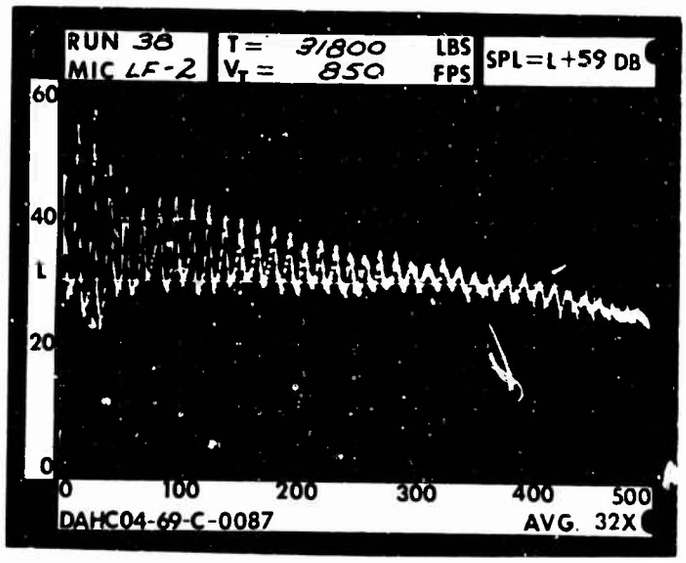

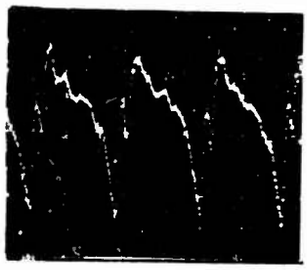

3 DIA.

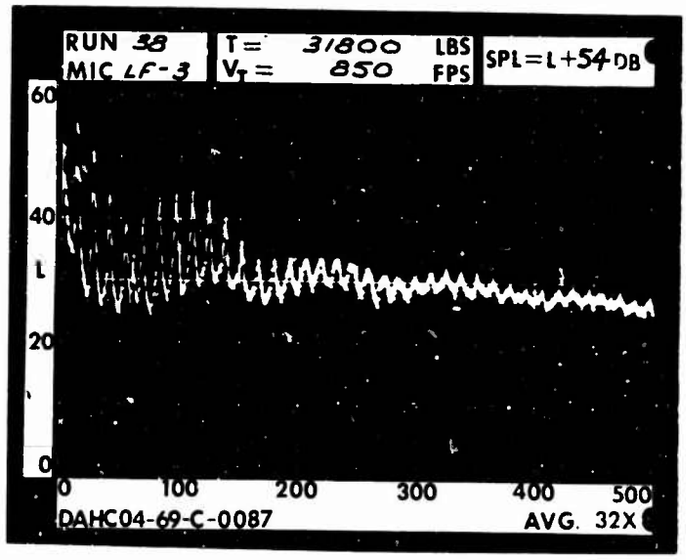

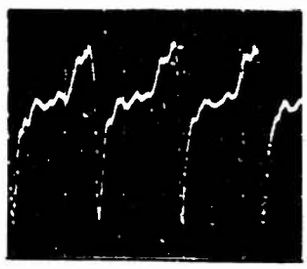

5 DIA.

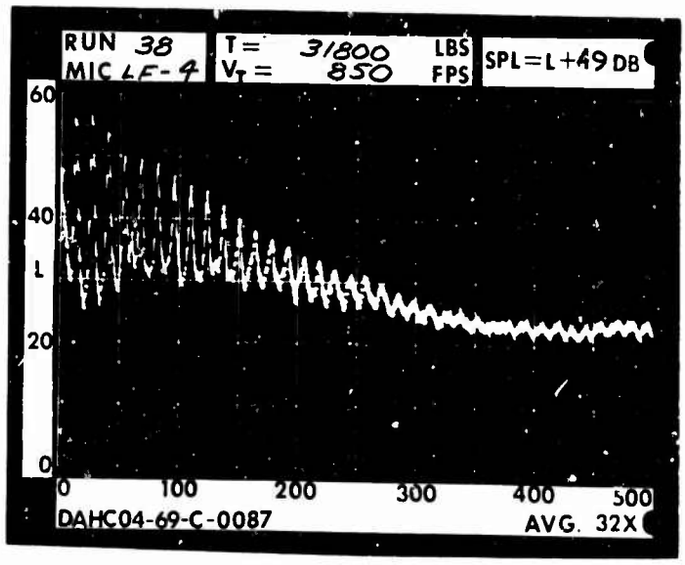

RUN 39

TIP SPEED 850 FT/SEC

THRUST 33400 LB

.2 RAD.

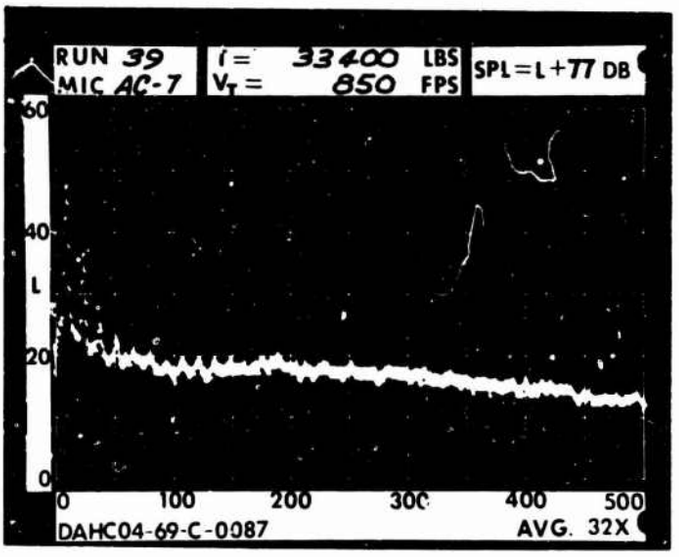

1 RAD.

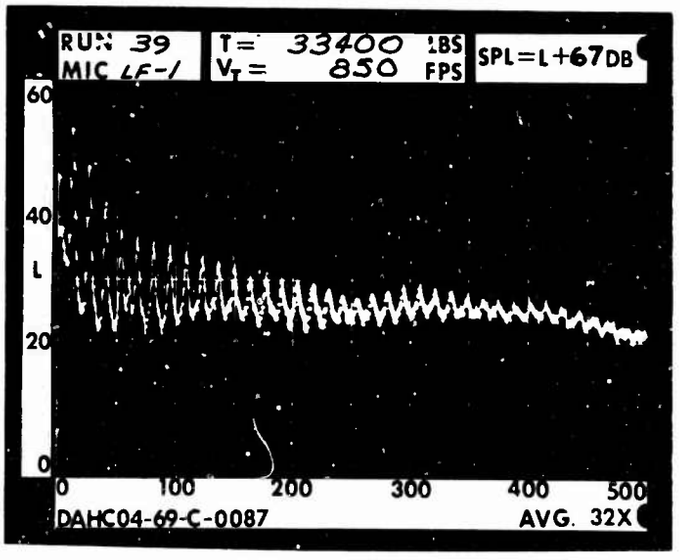

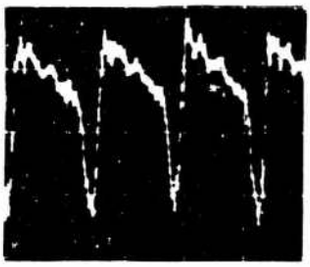

1 DIA.

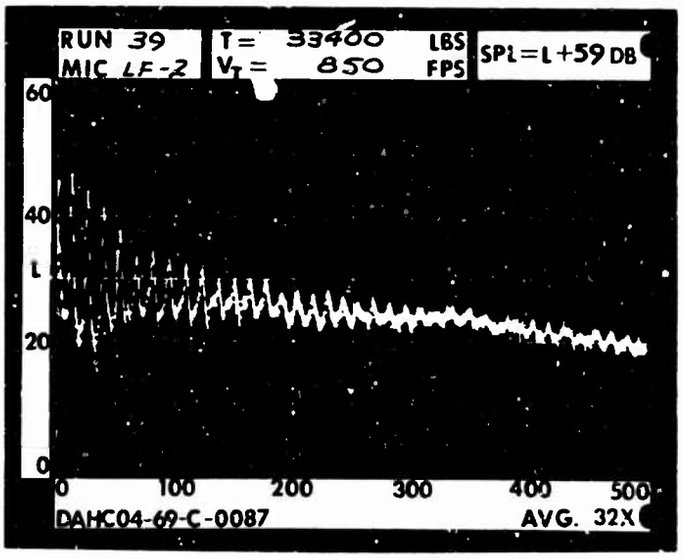

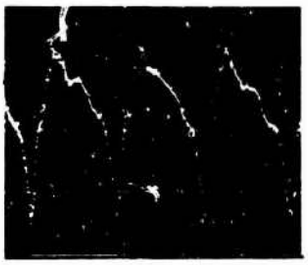

3 DIA.

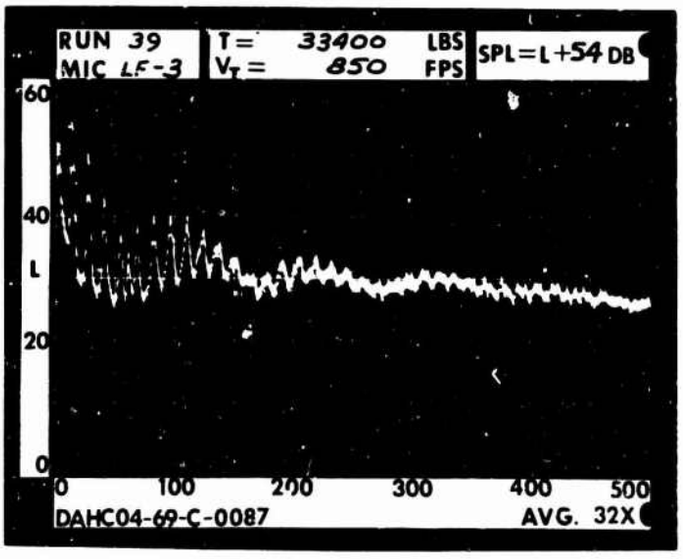

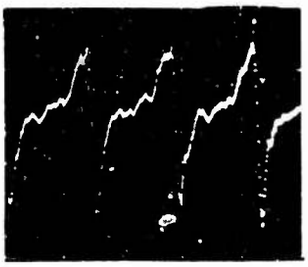

5 DIA.

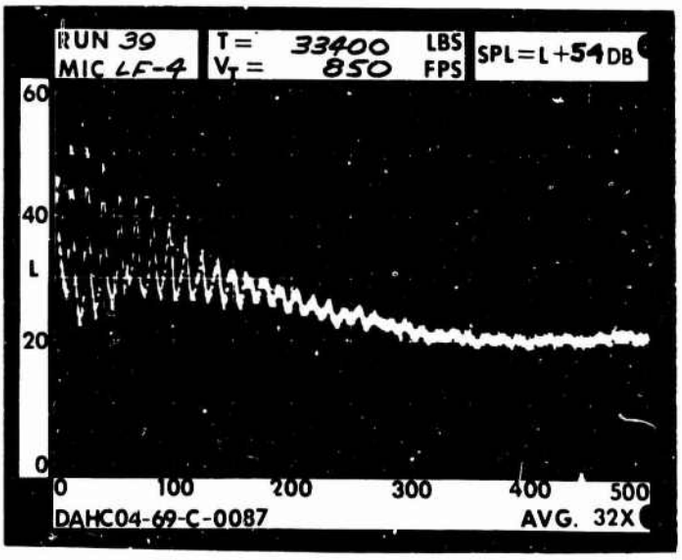

RUN 40

TIP SPEED 850 FT/SEC

THRUST 26800 LB

.2 RAD.

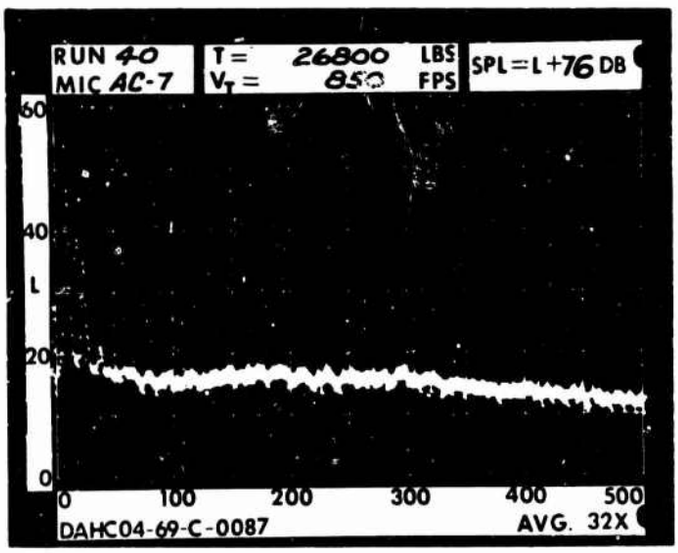

1 RAD.

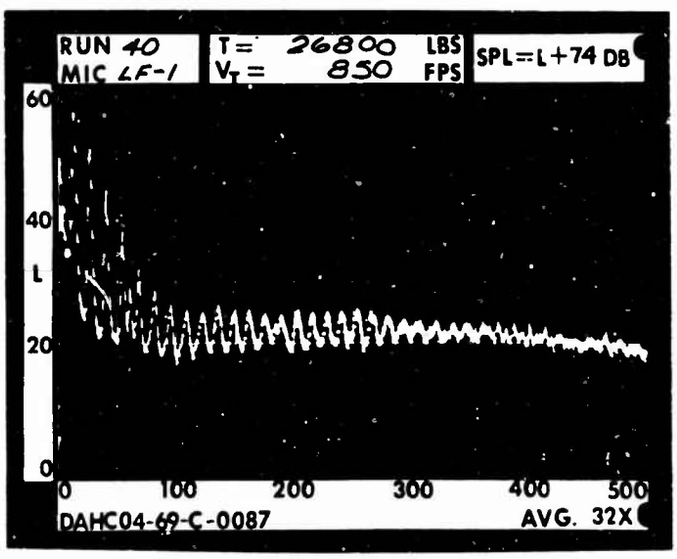

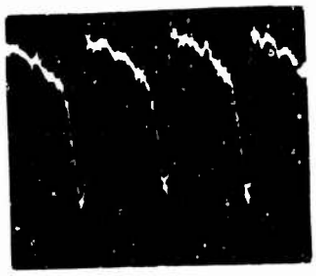

1 DIA.

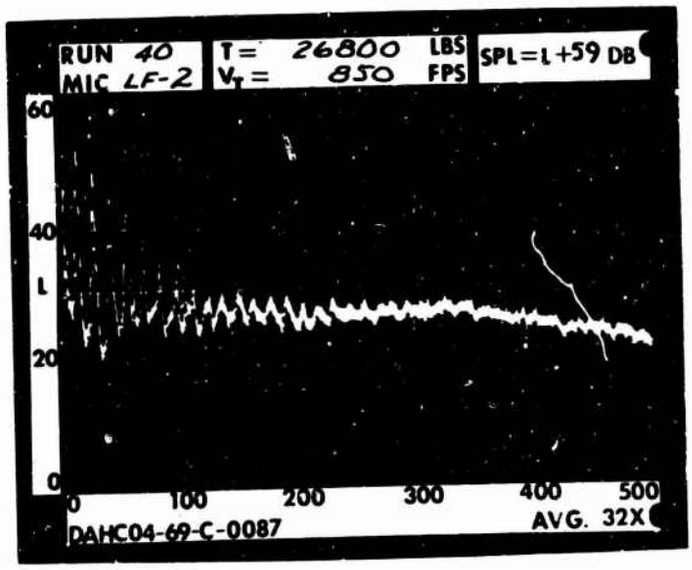

3 DIA.

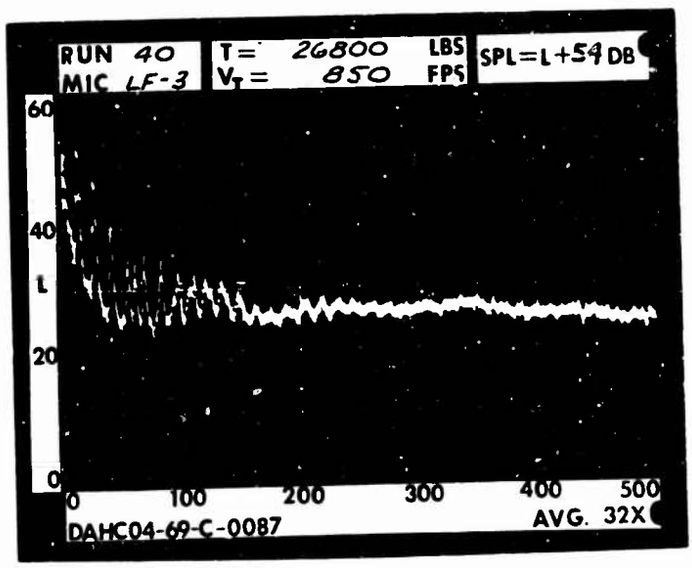

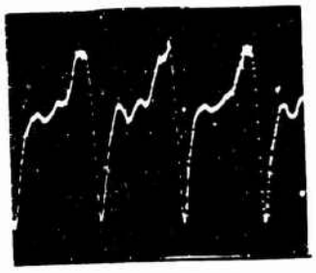

5 DIA.

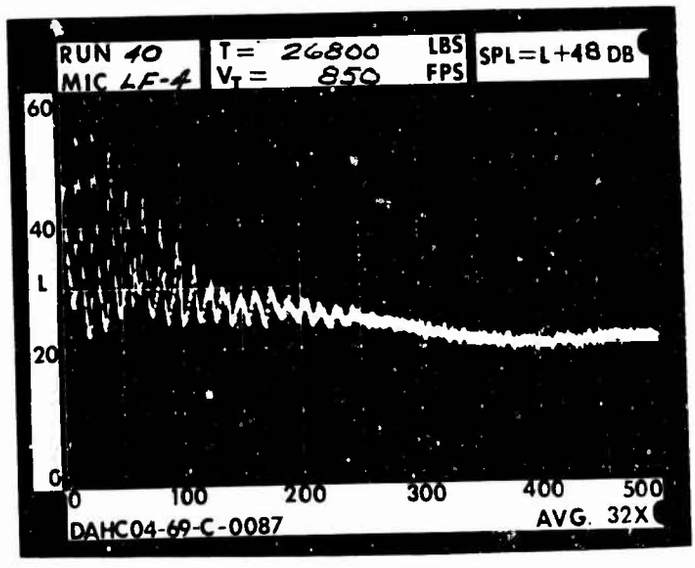

RUN 41

TIP SPEED 800 FT/SEC

THRUST 6300 LB

.2 RAD.

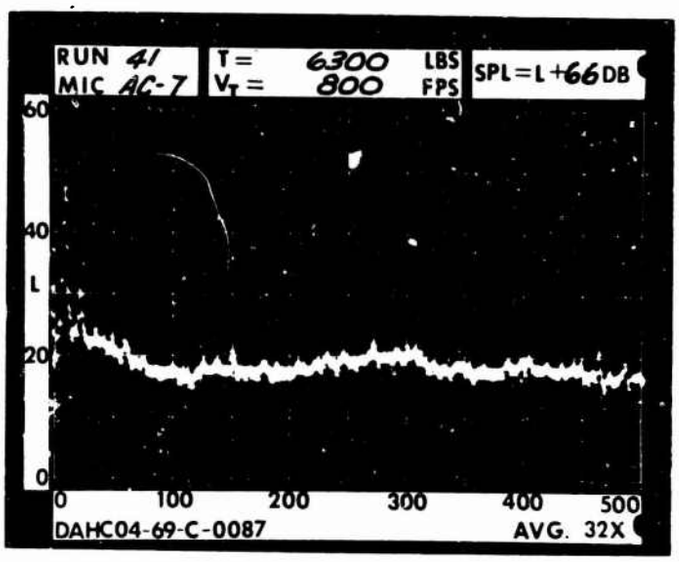

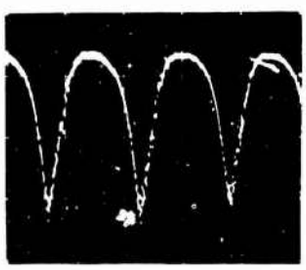

1 RAD.

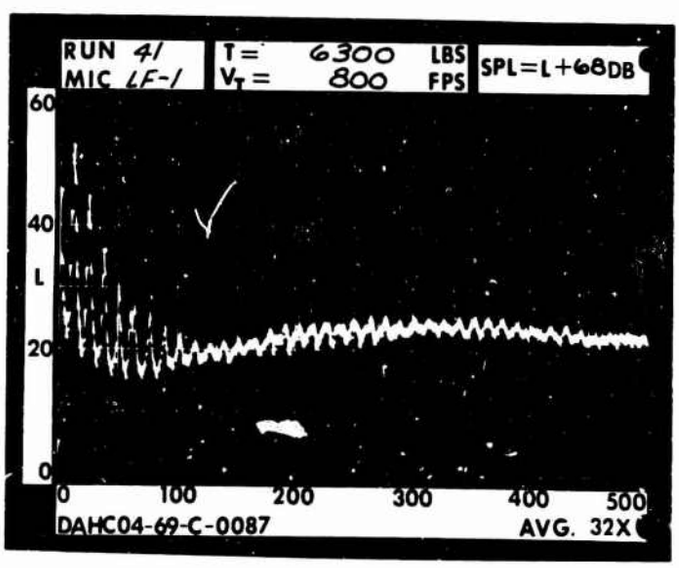

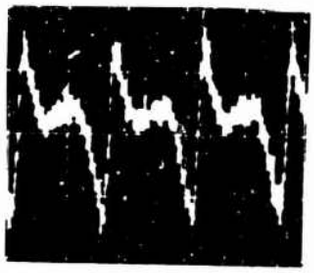

1 DIA.

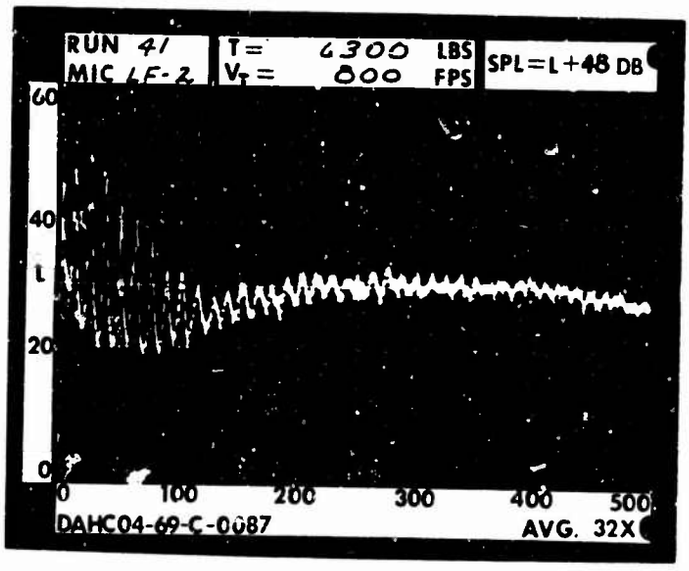

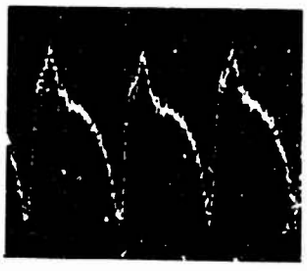

3 DIA.

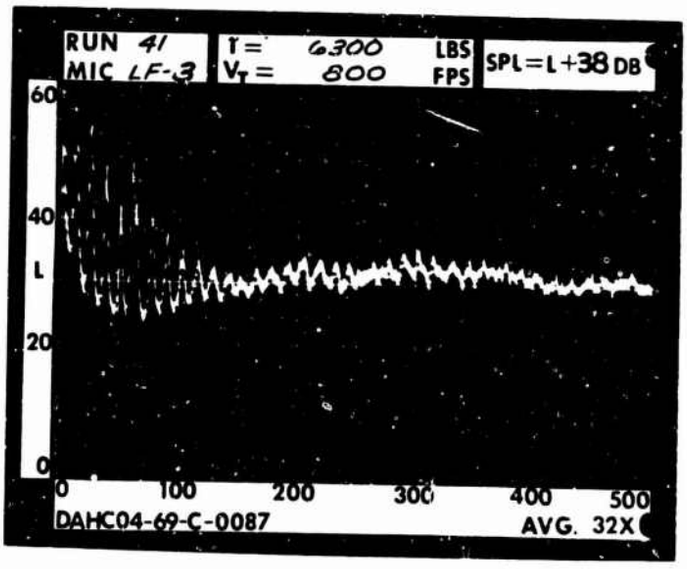

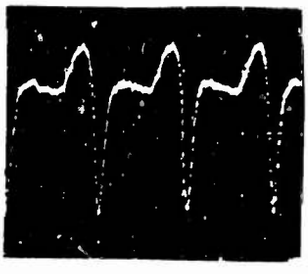

5 DIA.

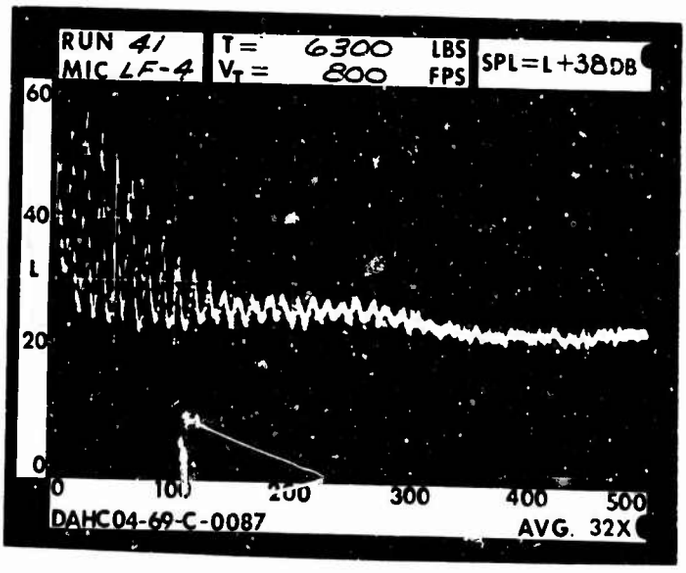

RUN 42

TIP SPEED 800 FT/SEC

THRUST 11100 LB

.2 RAD.

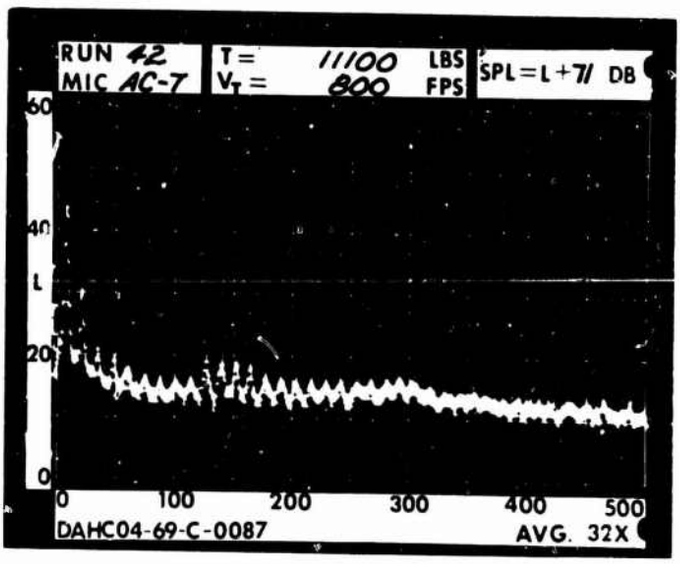

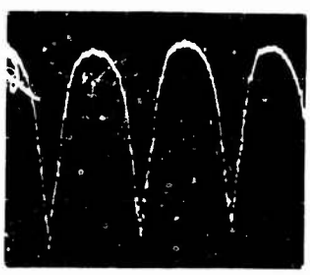

1 RAD.

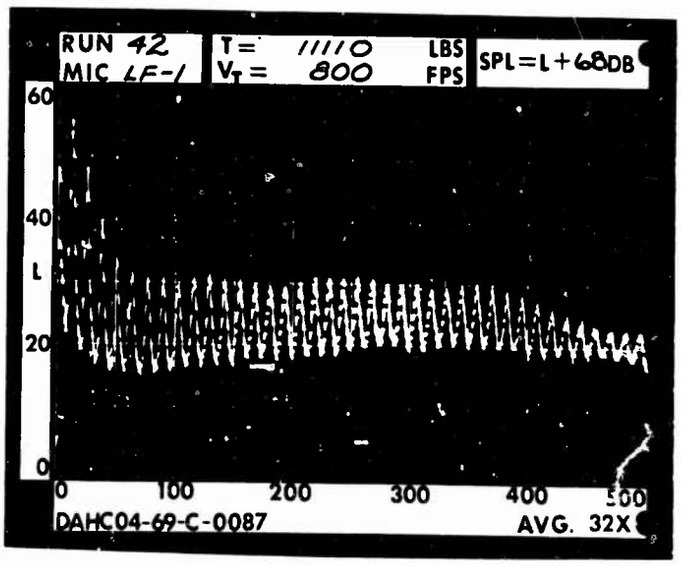

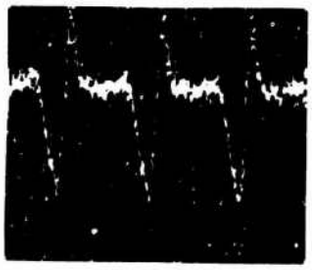

1 DIA.

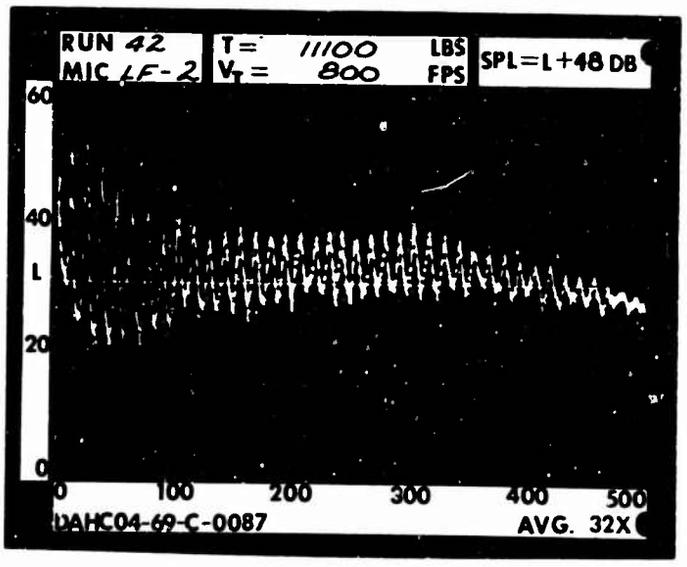

3 DIA.

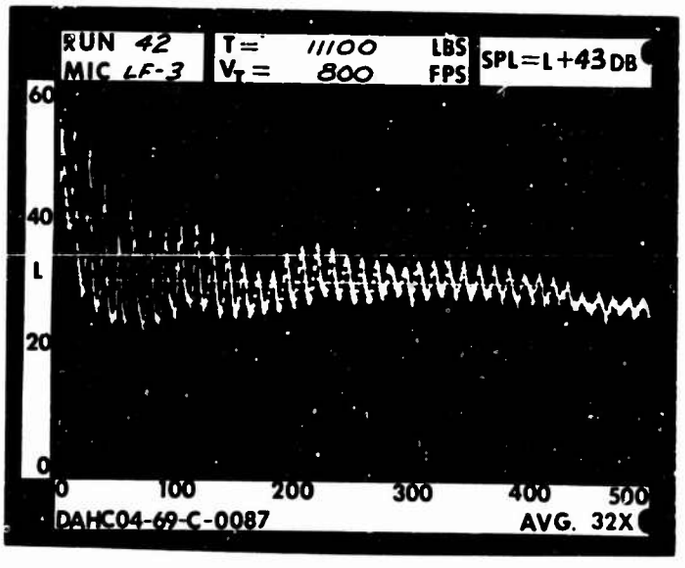

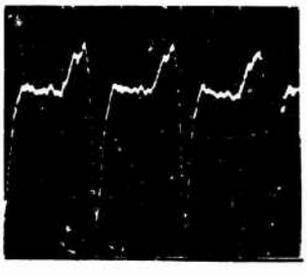

5 DIA.

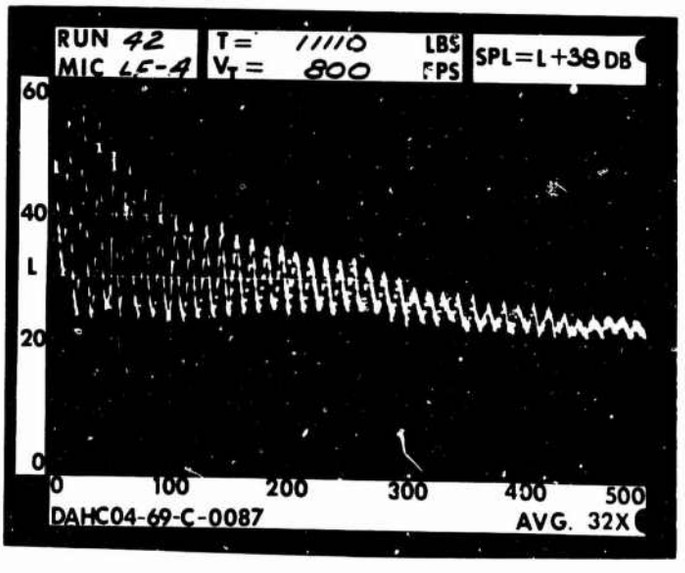

RUN 43

TIP SPEED 800 FT/SEC

THRUST 14600 LB

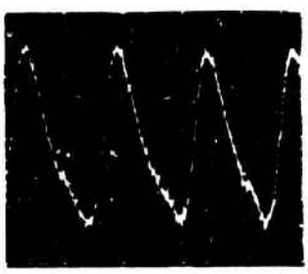

.2 RAD.

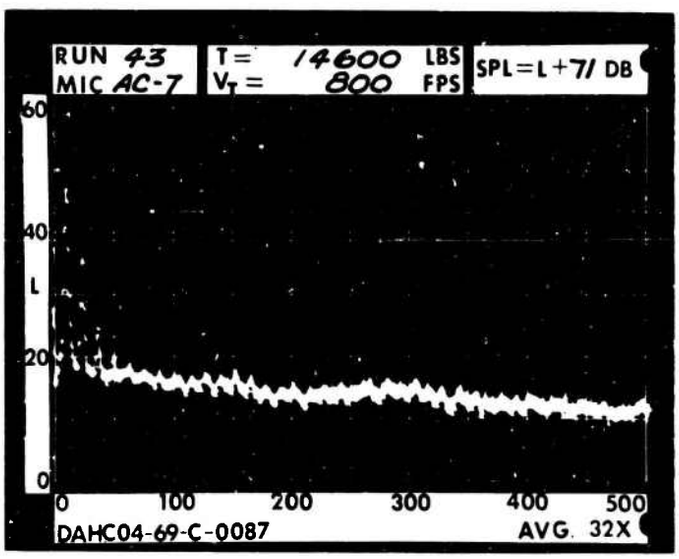

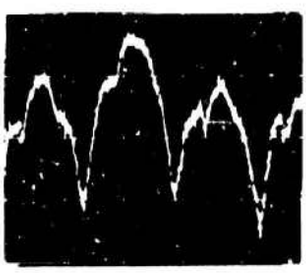

1 RAD.

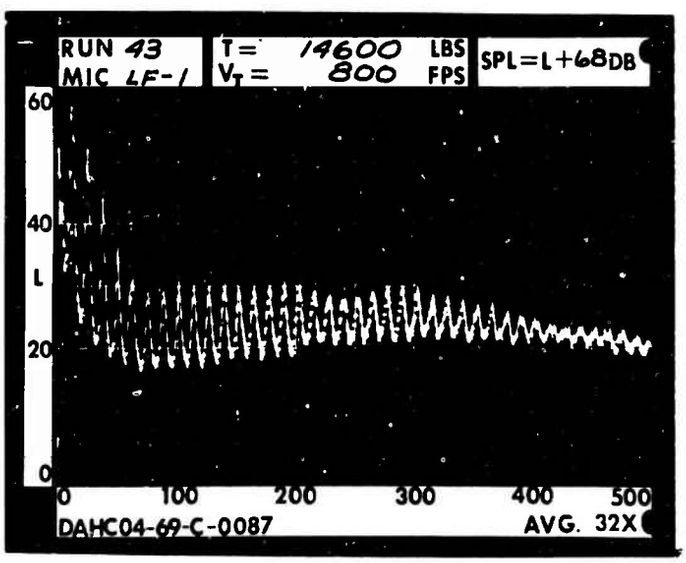

1 DIA.

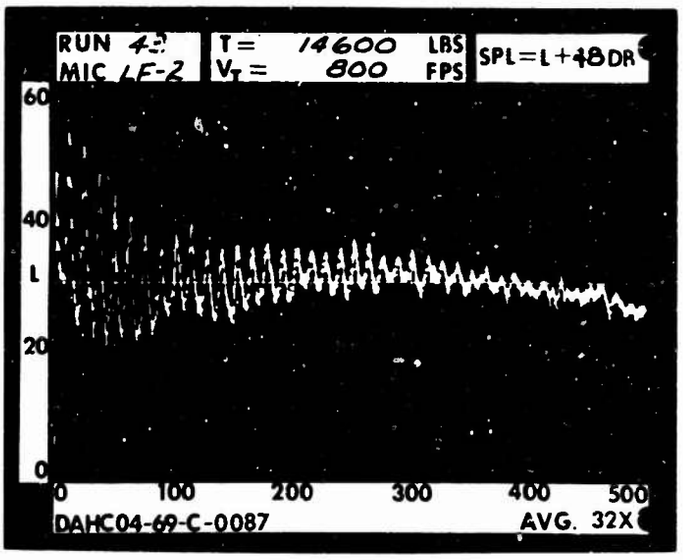

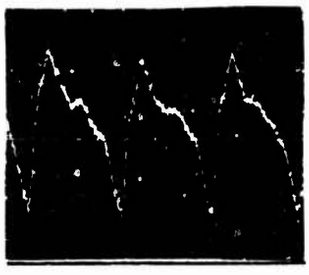

3 DIA.

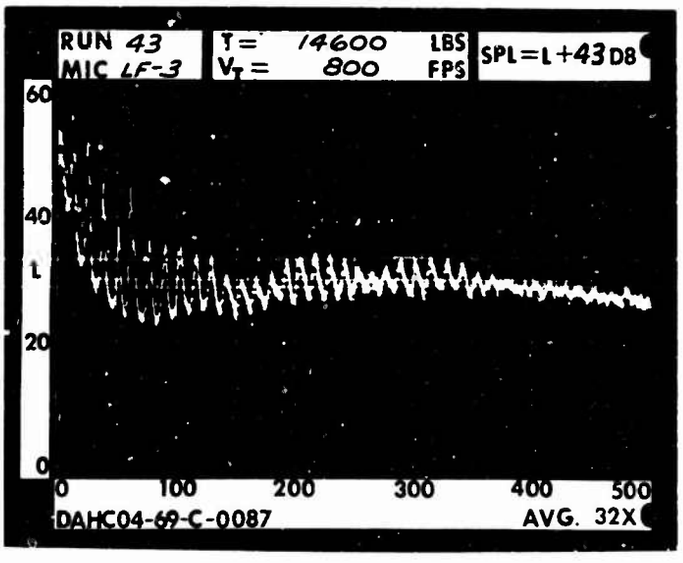

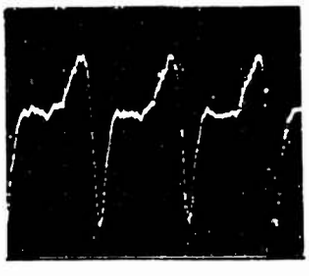

5 DIA.

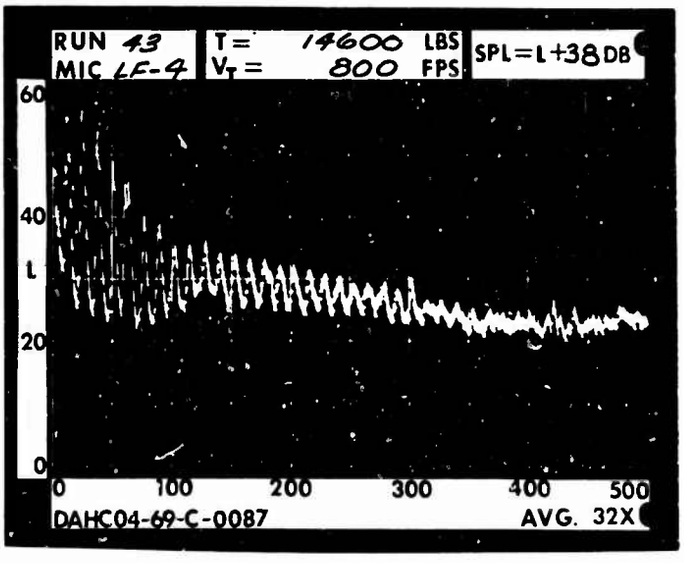

RUN 44

TIP SPEED 800 FT/SEC

THRUST 17800 LB

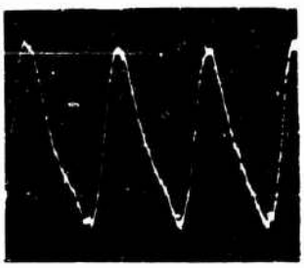

.2 RAD.

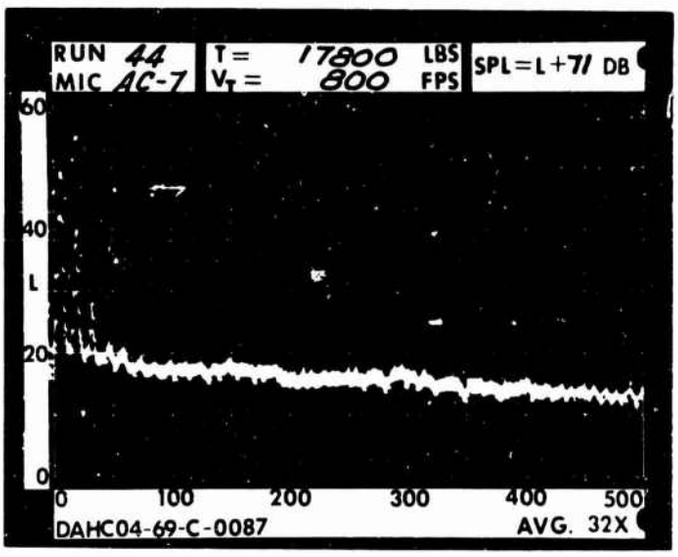

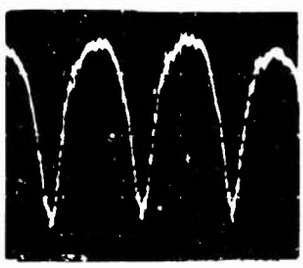

1 RAD.

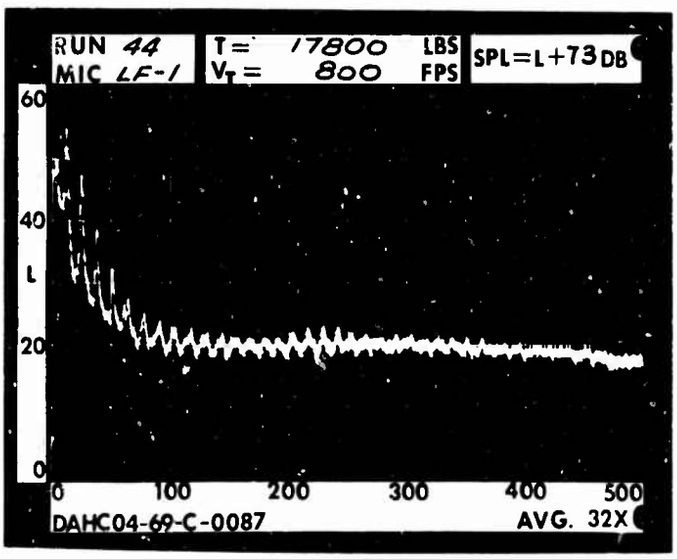

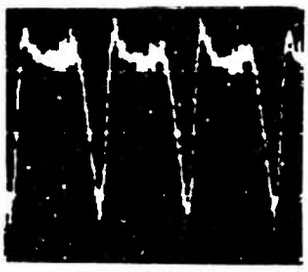

1 DIA.

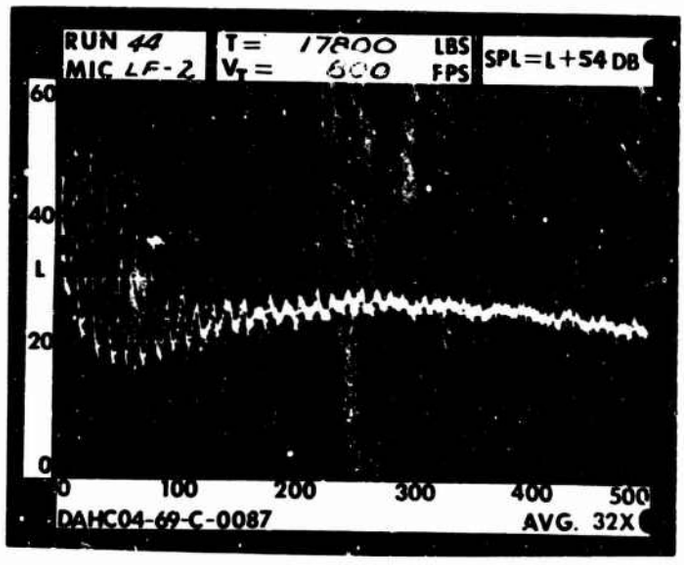

3 DIA.

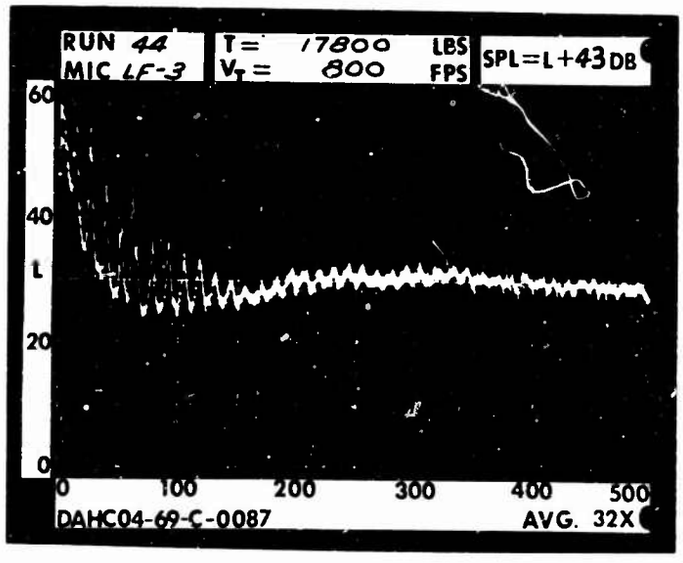

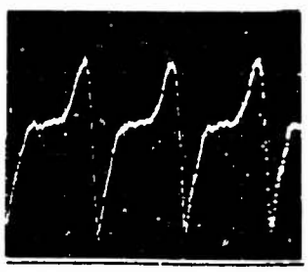

5 DIA.

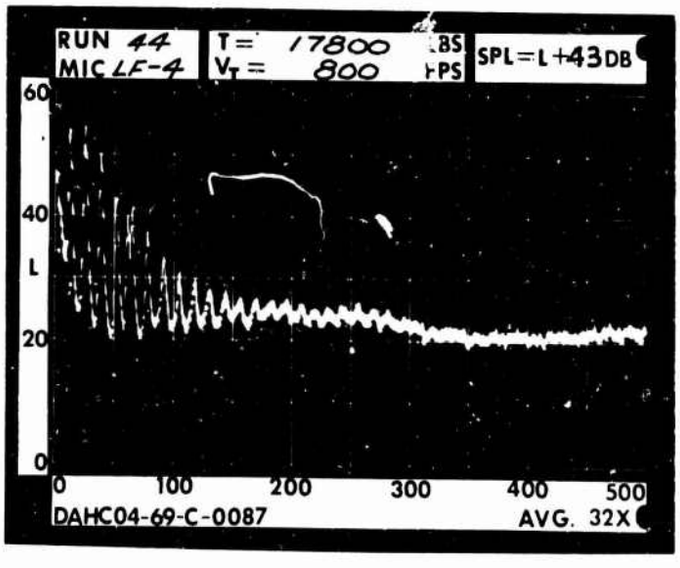

RUN 45

TIP SPEED 800 FT/SEC

THRUST 20600 LB

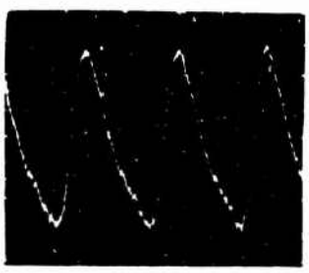

.2 RAD.

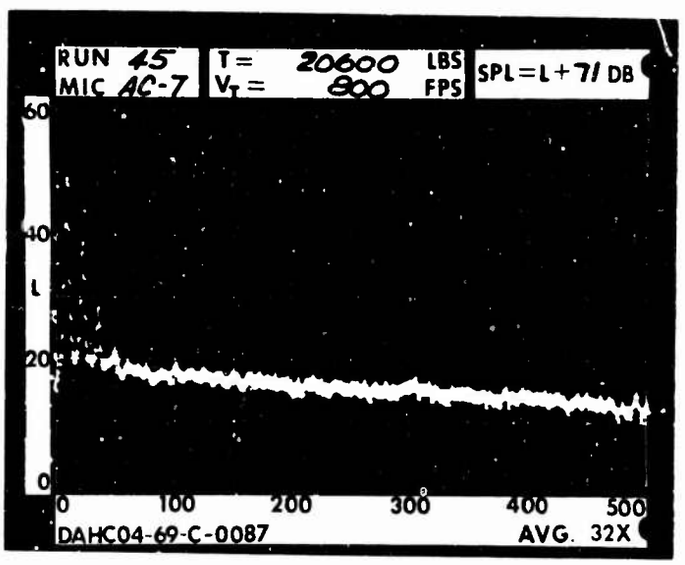

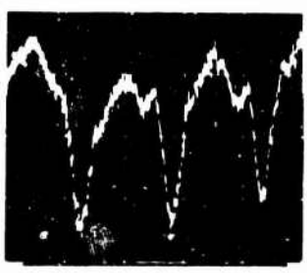

1 RAD.

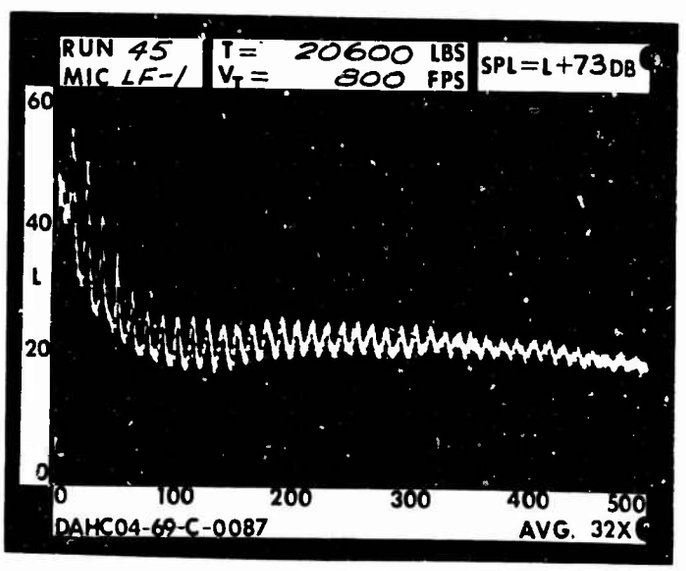

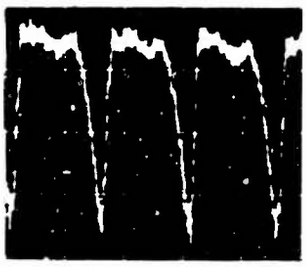

1 DIA.

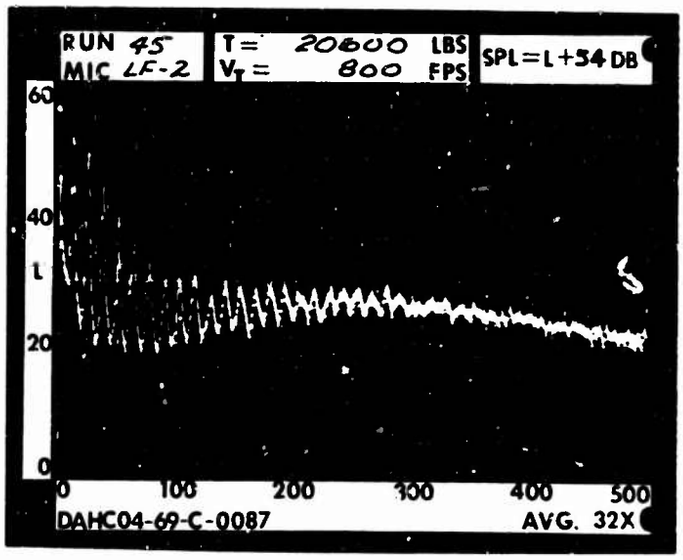

3 DIA.

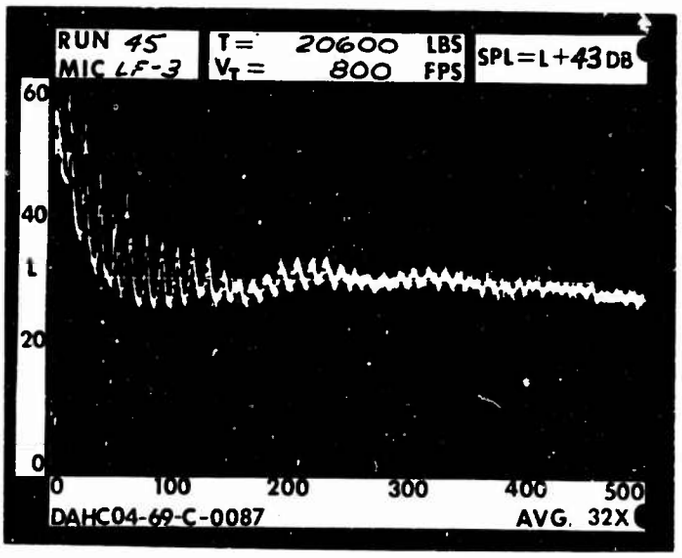

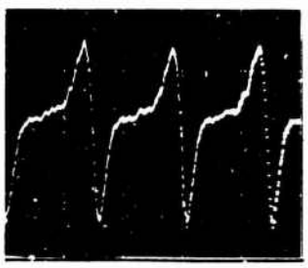

5 DIA.

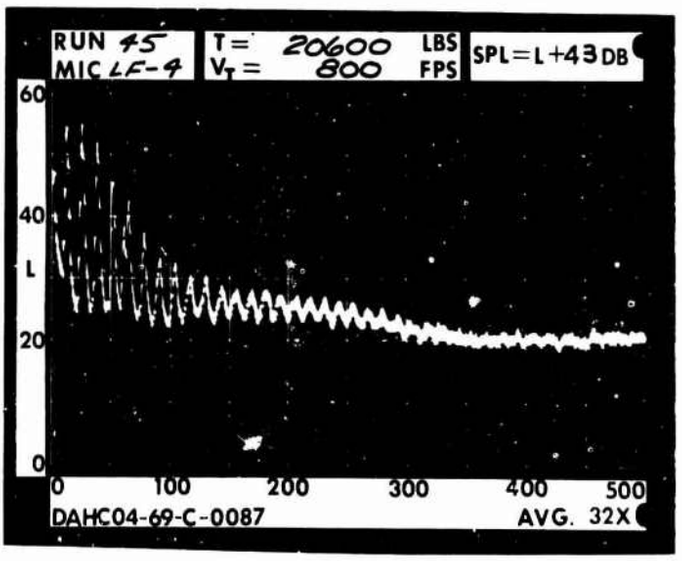

RUN 46

TIP SPEED 800 FT/SEC

THRUST 23500 LB

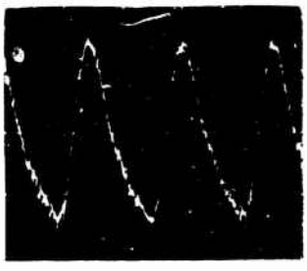

.2 RAD.

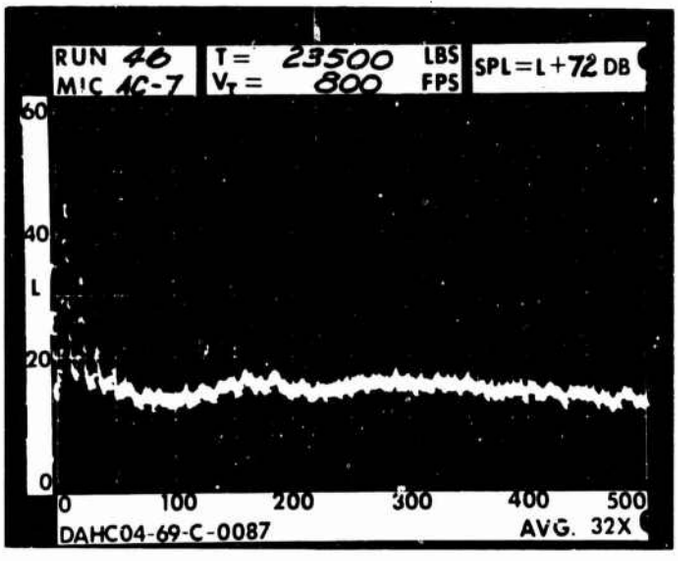

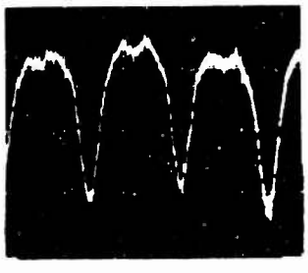

1 RAD.

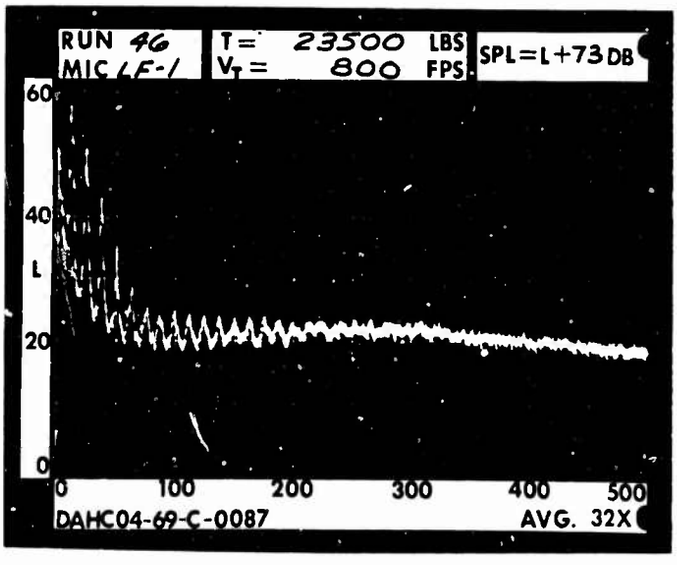

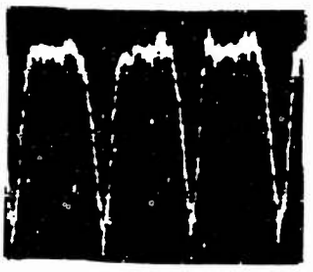

1 DIA.

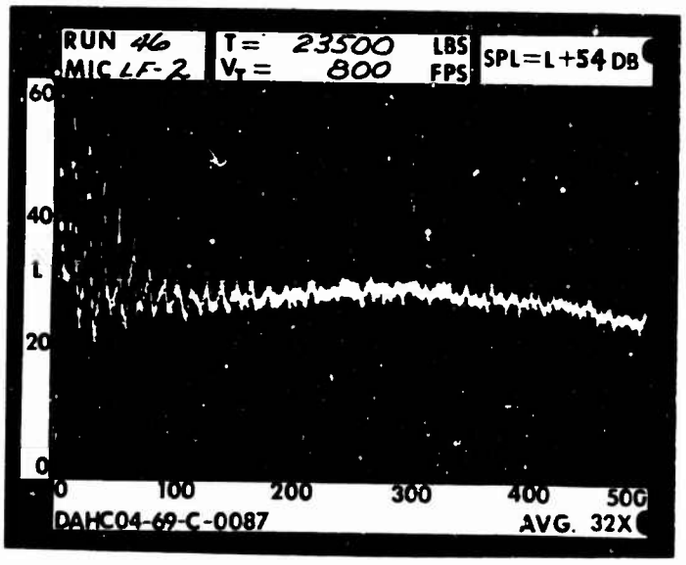

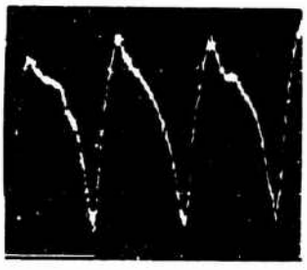

3 DIA.

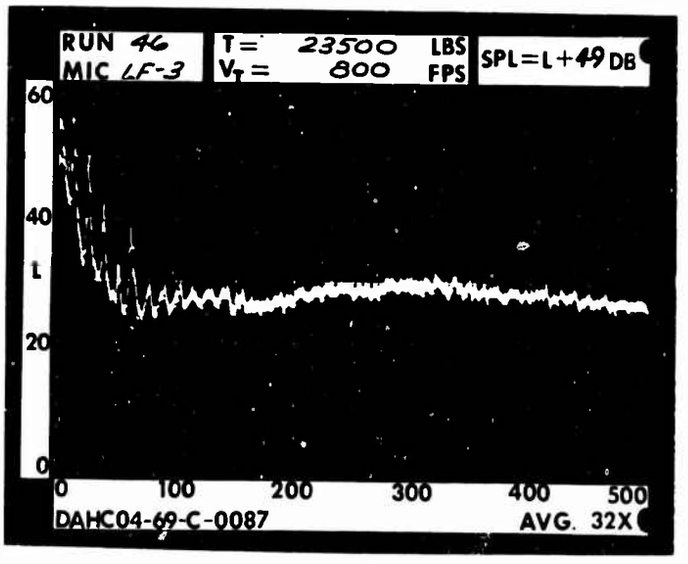

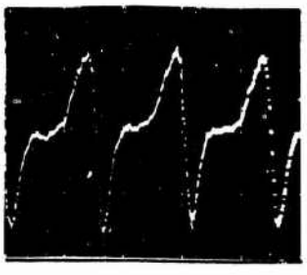

5 DIA.

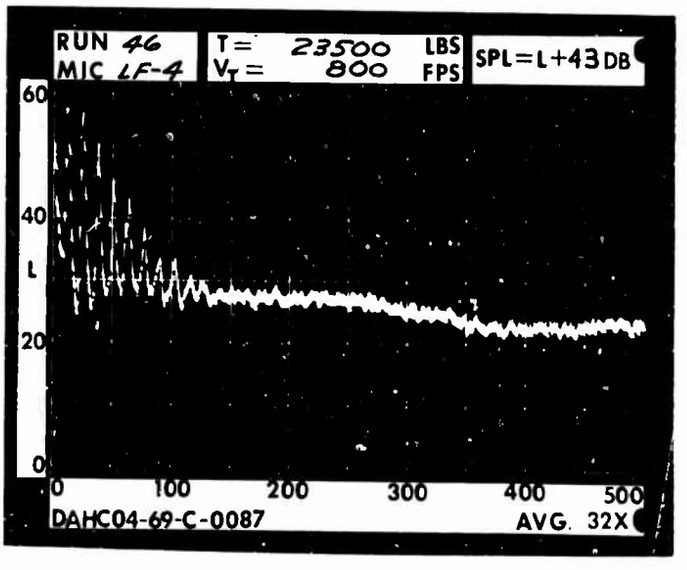

RUN 47

TIP SPEED 800 FT/SEC

THRUST 27400 LB

.2 RAD.

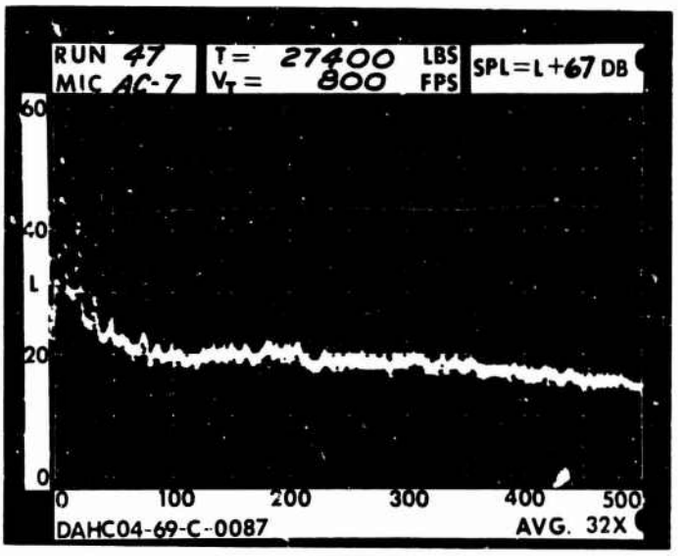

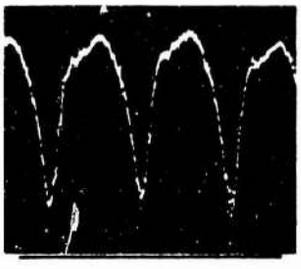

1 RAD.

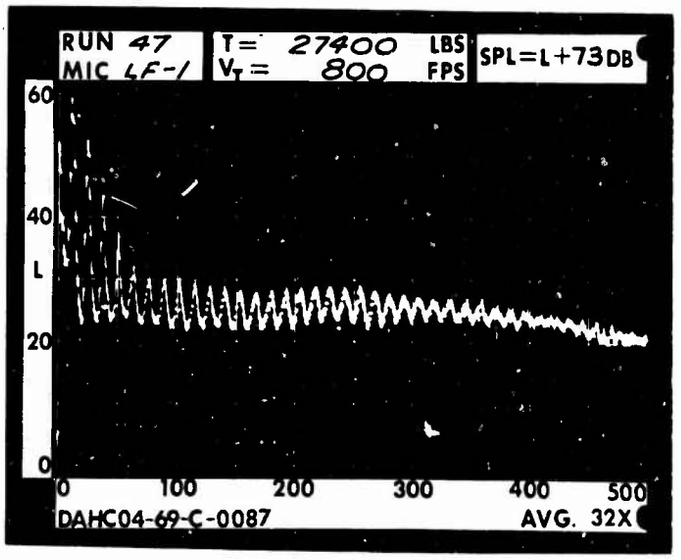

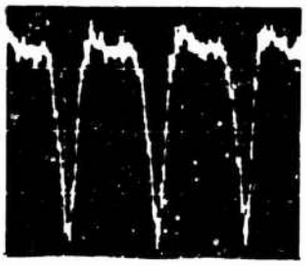

1 DIA.

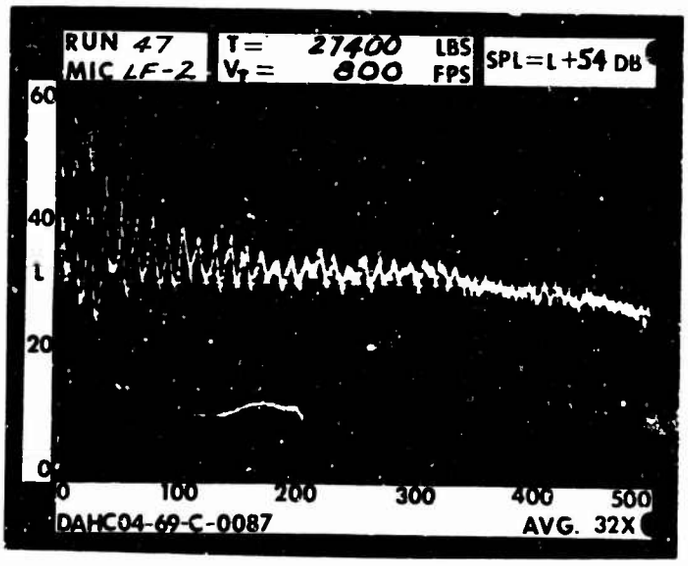

3 DIA.

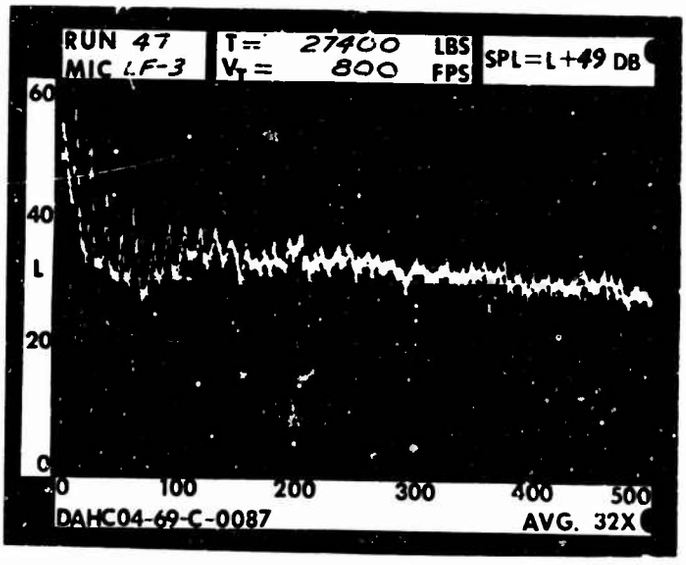

5 DIA.

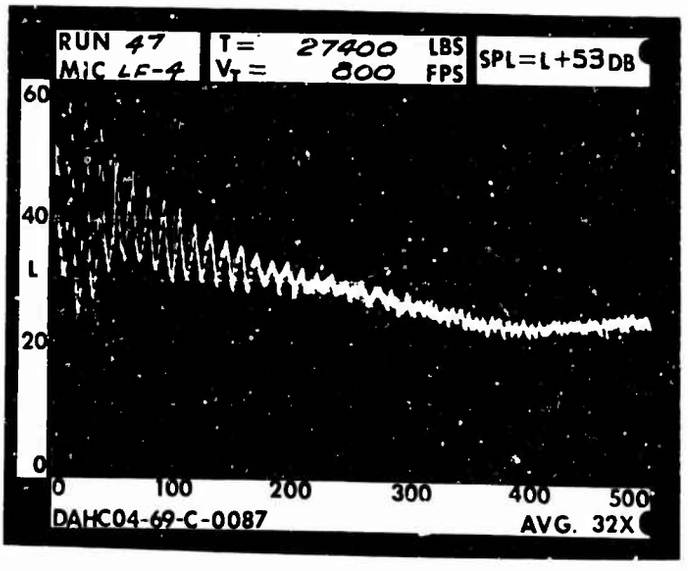

RUN 48

TIP SPEED 800 FT/SEC

THRUST 30600 LB

.2 RAD.

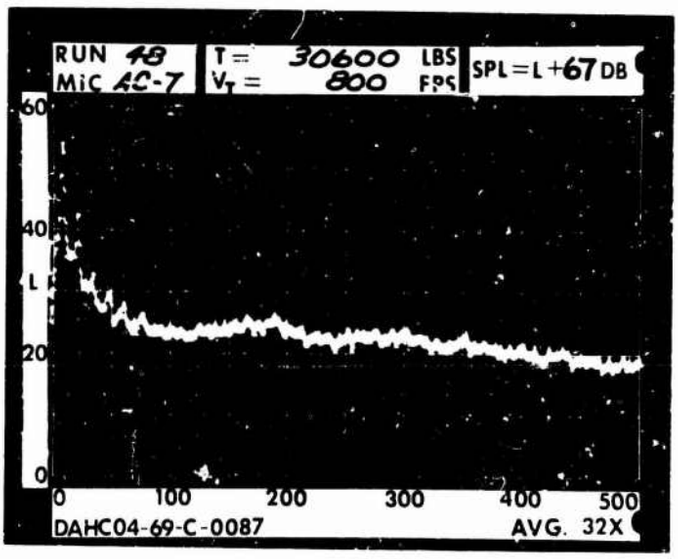

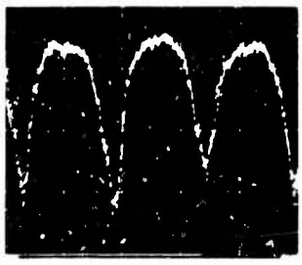

1 RAD.

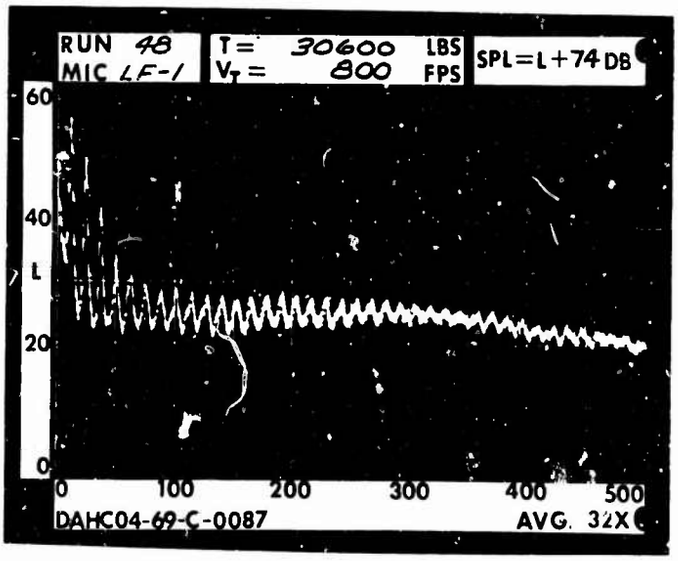

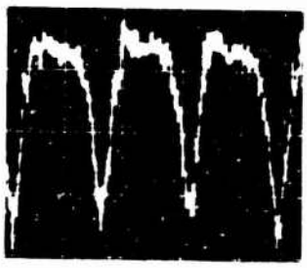

1 DIA.

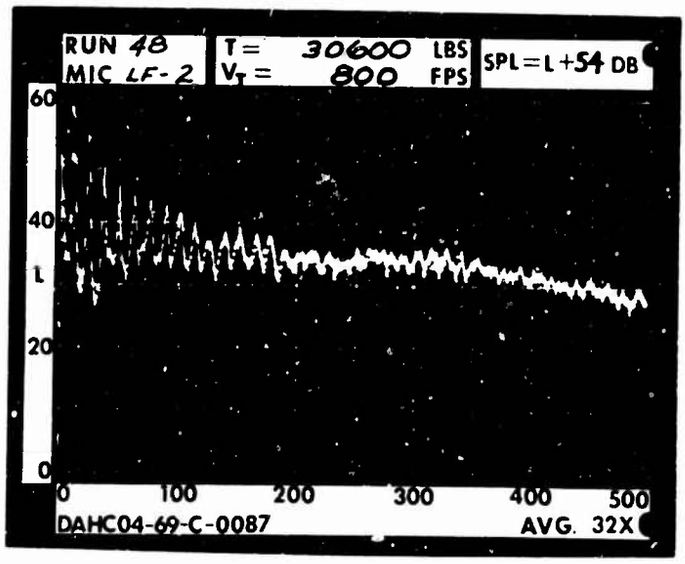

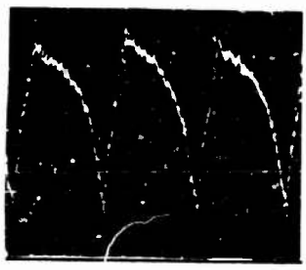

3 DIA.

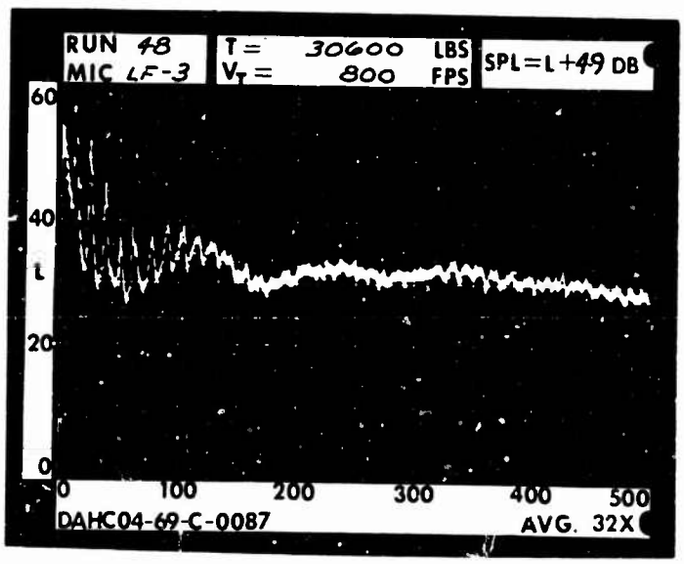

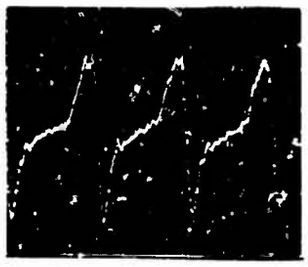

5 DIA.

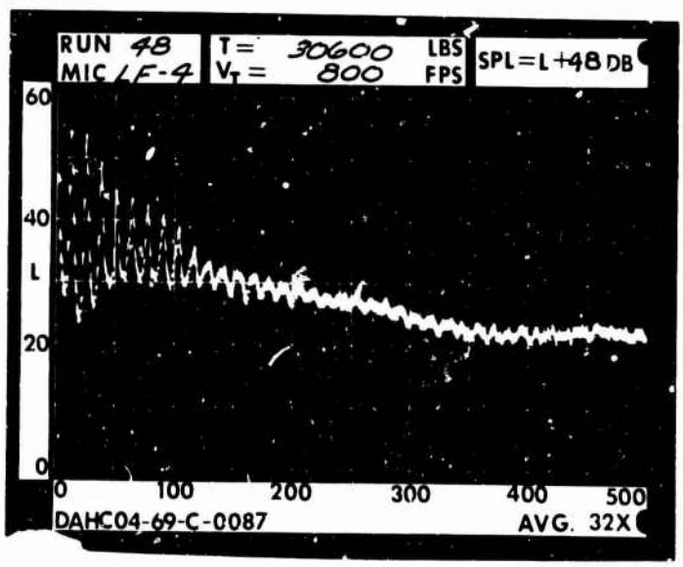

RUN 49

TIP SPEED 800 FT/SEC

THRUST 33000 LB

.2 RAD.

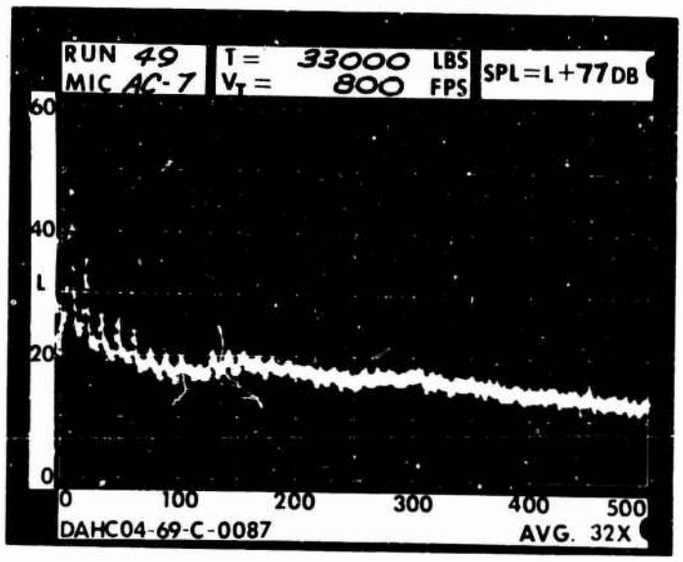

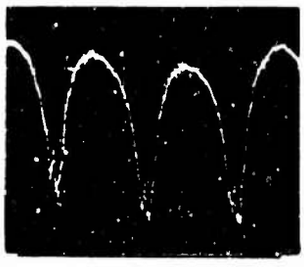

1 RAD.

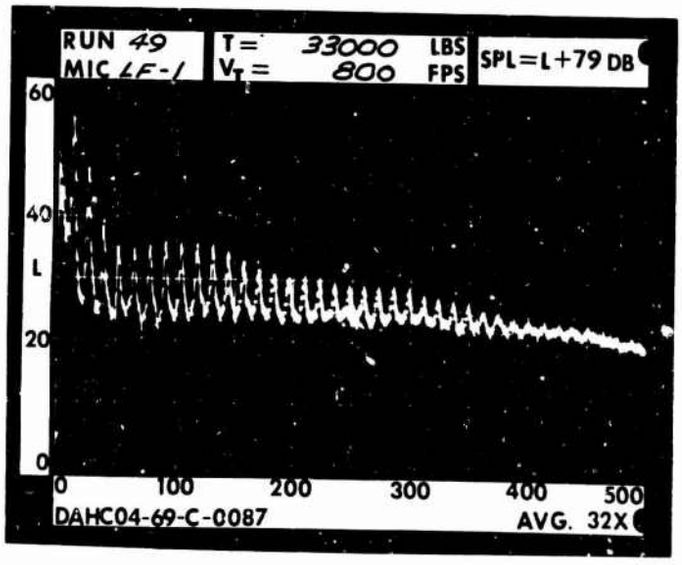

1 DIA.

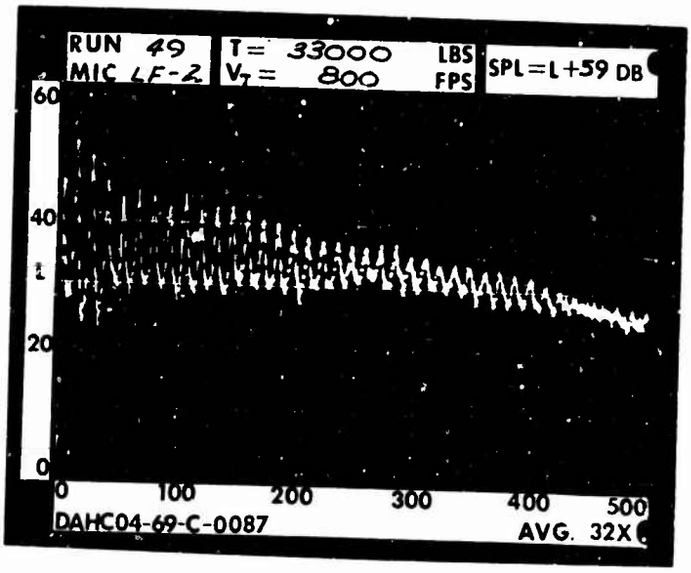

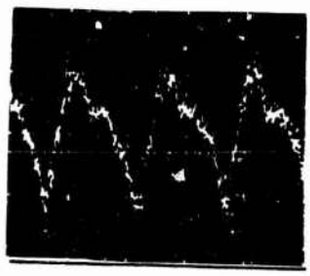

3 DIA.

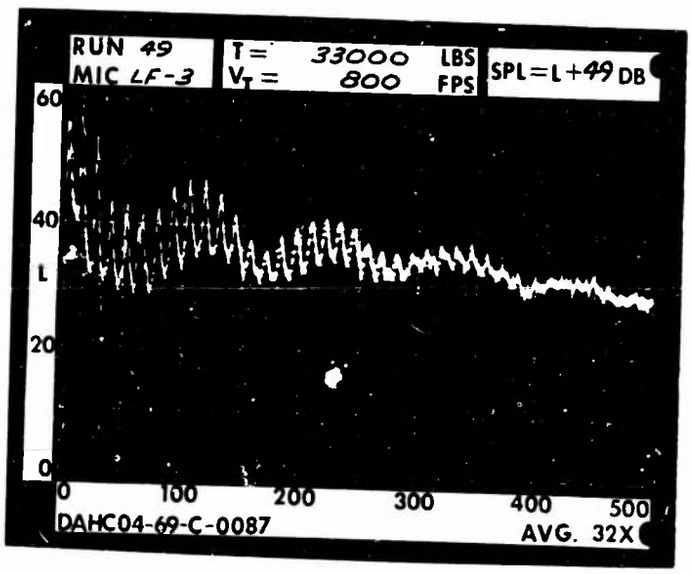

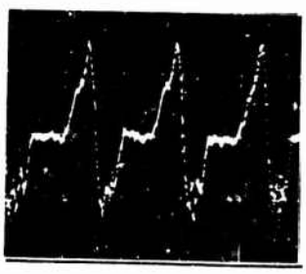

5 DIA.

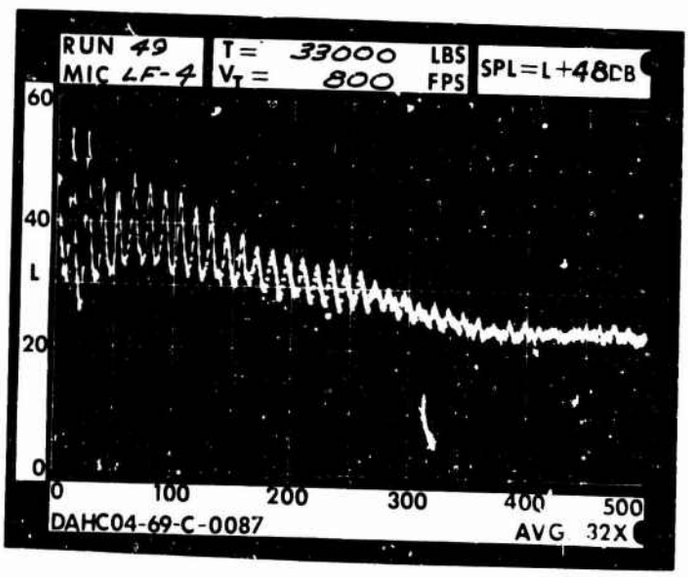

RUN 50

TIP SPEED 800 FT/SEC

THRUST 23900 LB

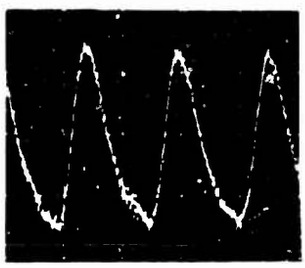

.2 RAD.

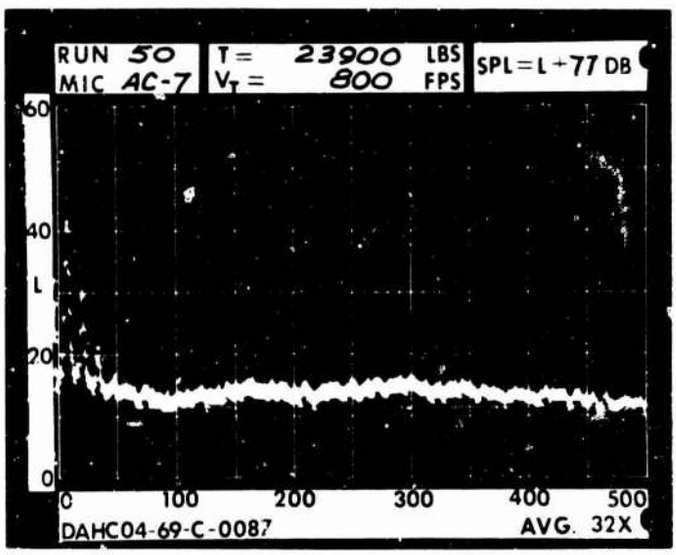

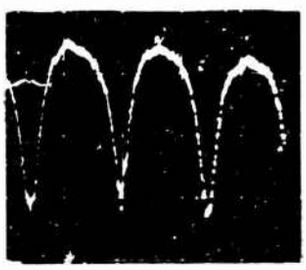

1 RAD.

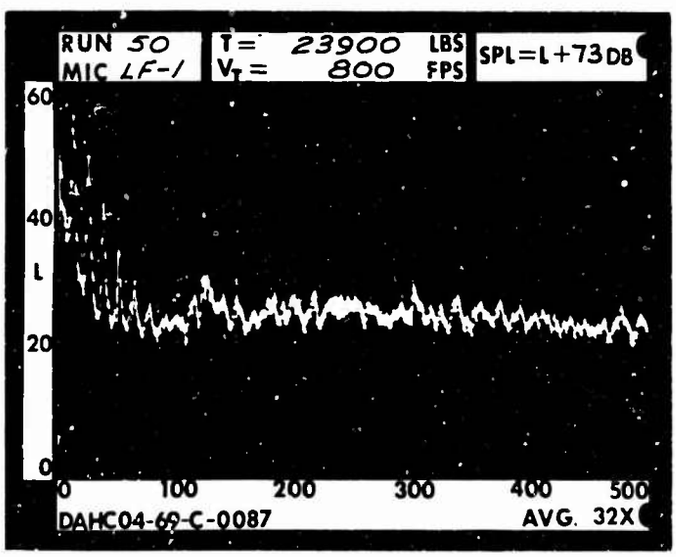

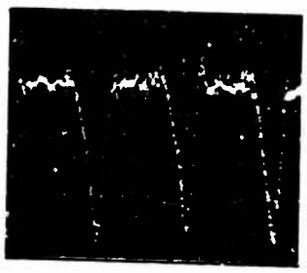

1 DIA.

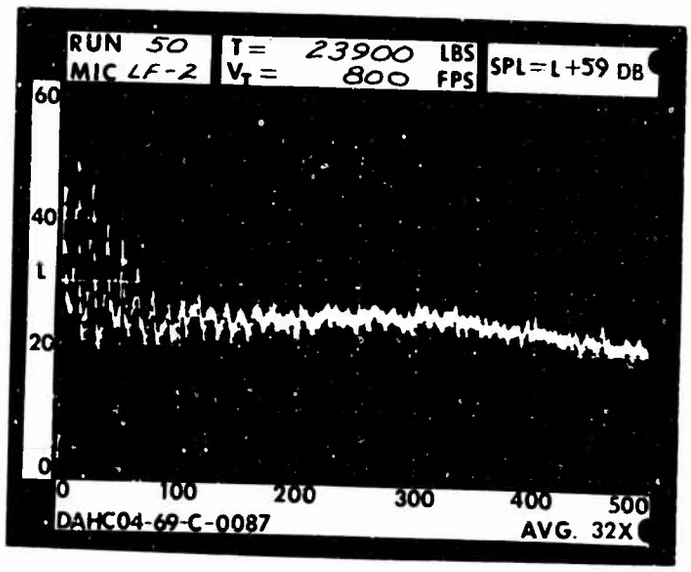

3 DIA.

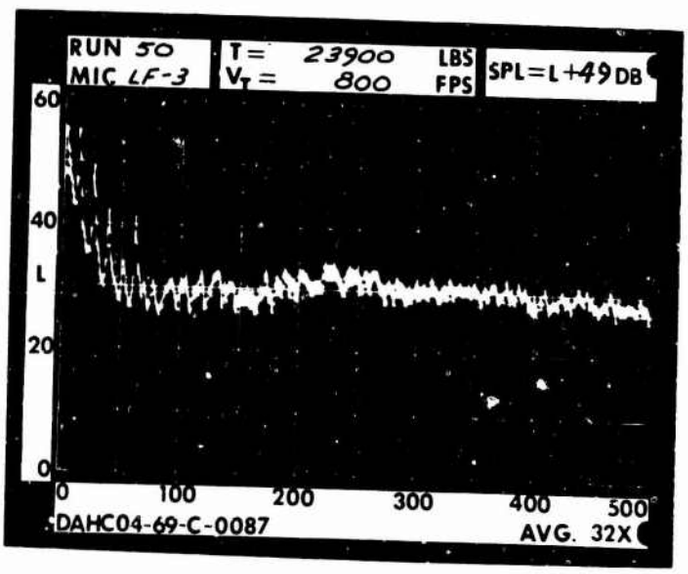

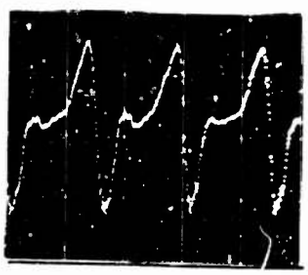

5 DIA.

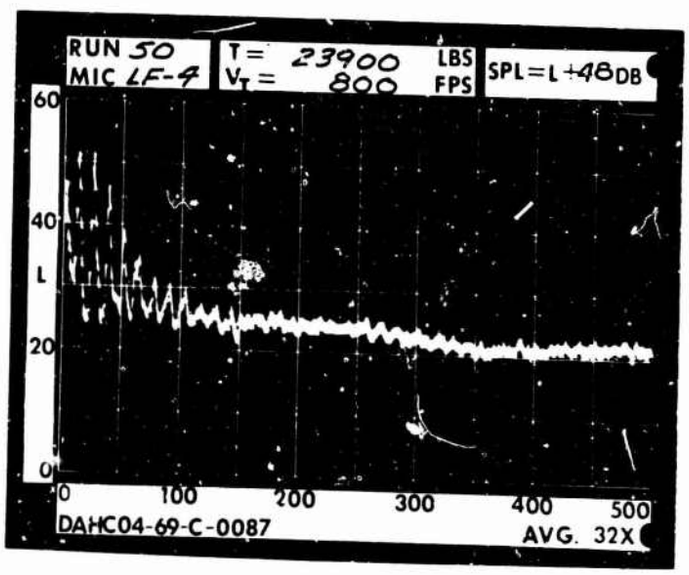

RUN 51

TIP SPEED 750 FT/SEC

THRUST 9700 LB

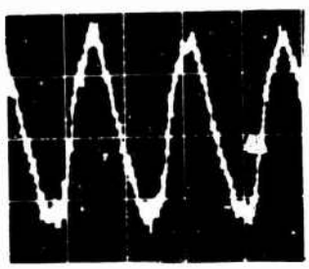

.2 RAD.

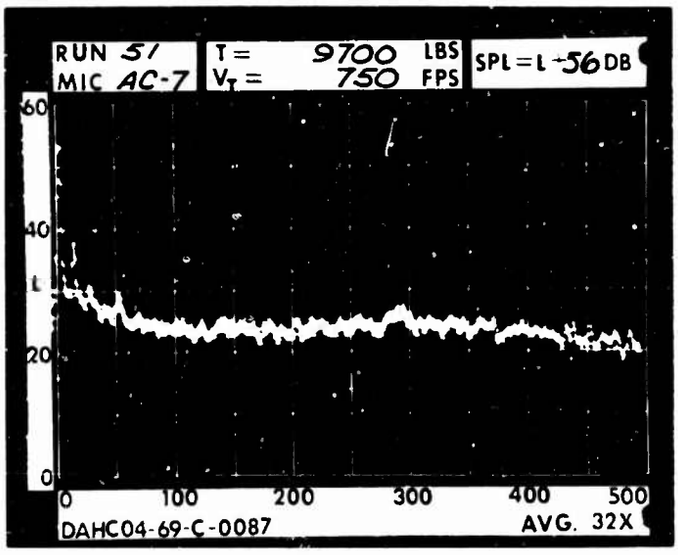

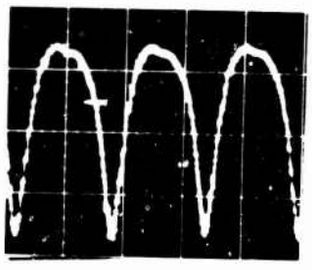

1 RAD.

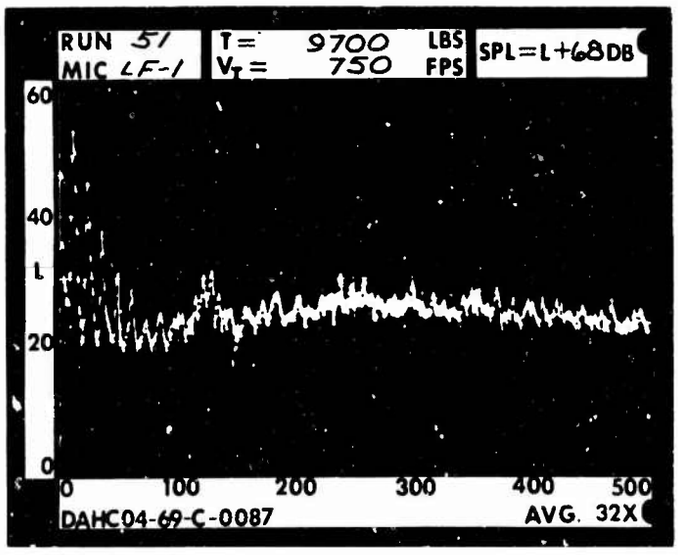

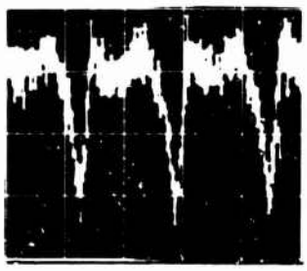

1 DIA.

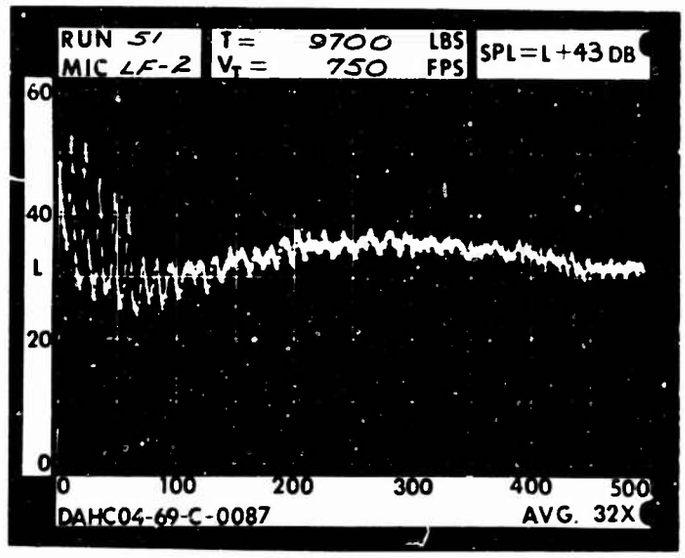

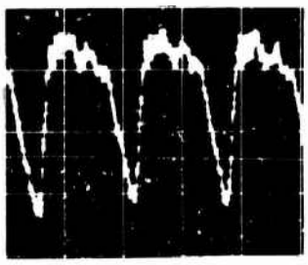

3 DIA.

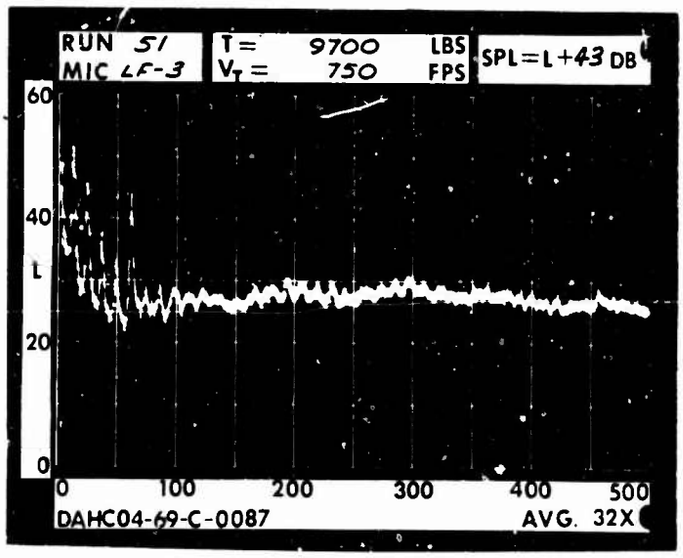

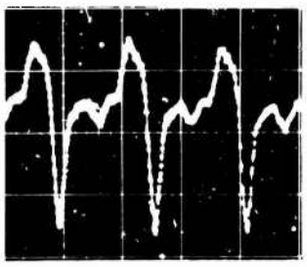

5 DIA.

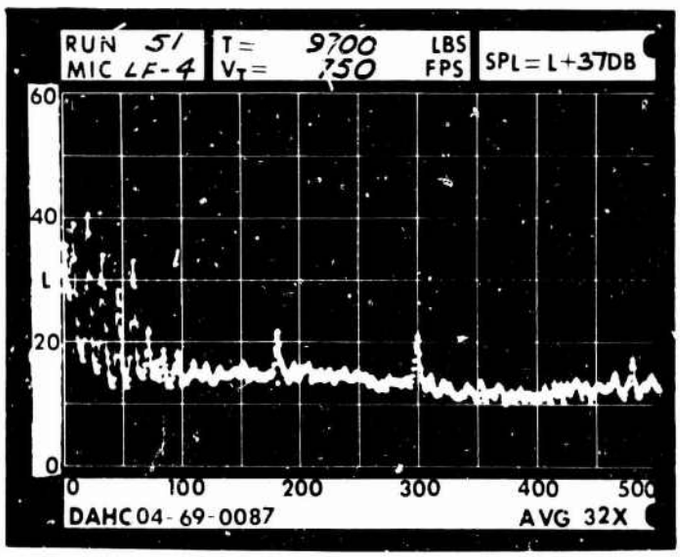

RUN 52

TIP SPEED 750 FT/SEC

THRUST 12200 LB

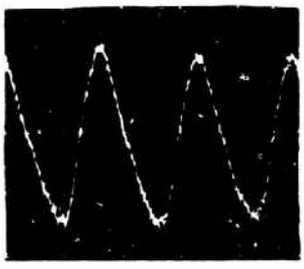

.2 RAD.

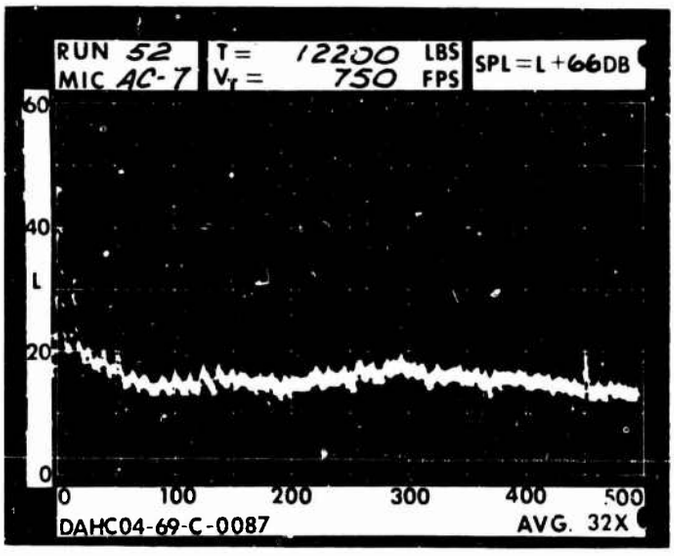

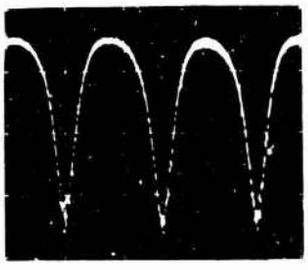

1 RAD.

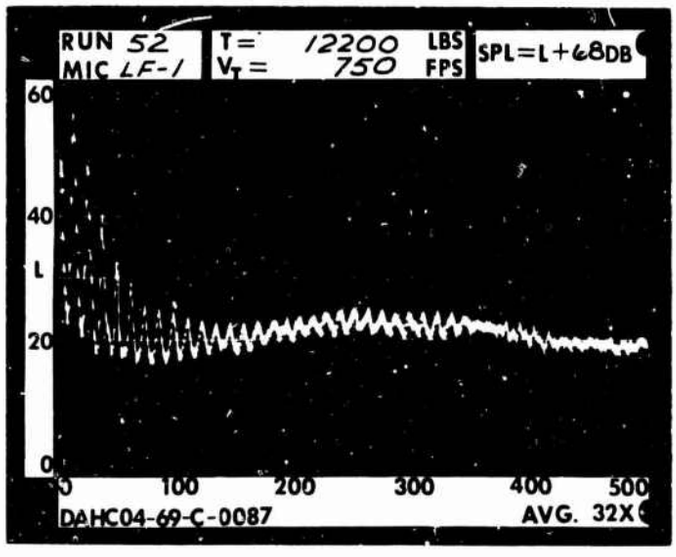

1 DIA.

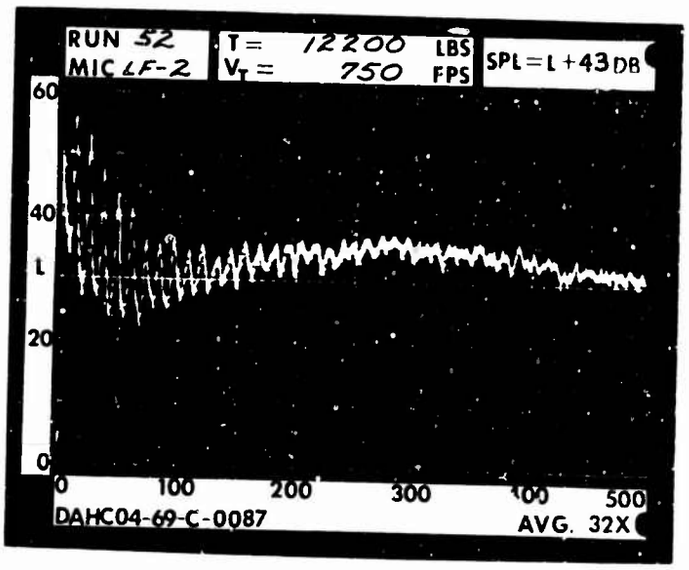

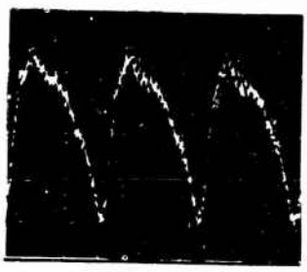

3 DIA.

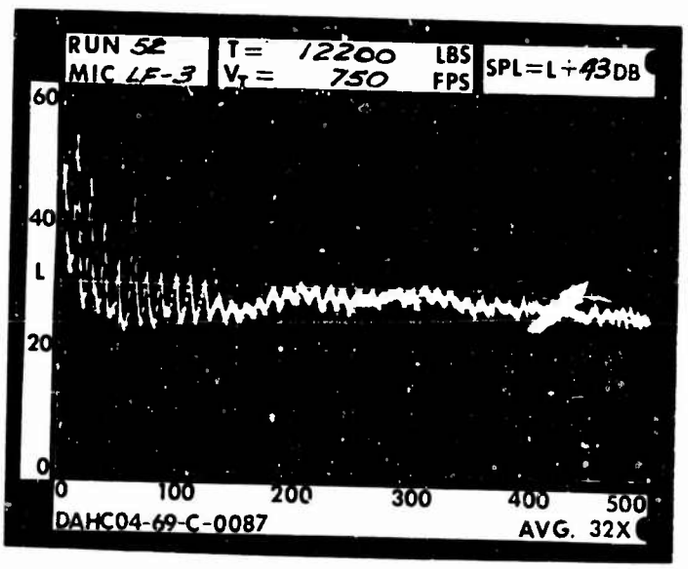

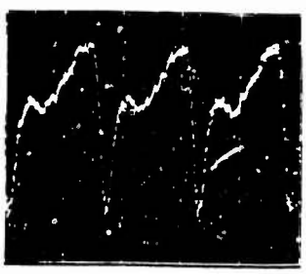

5 DIA.

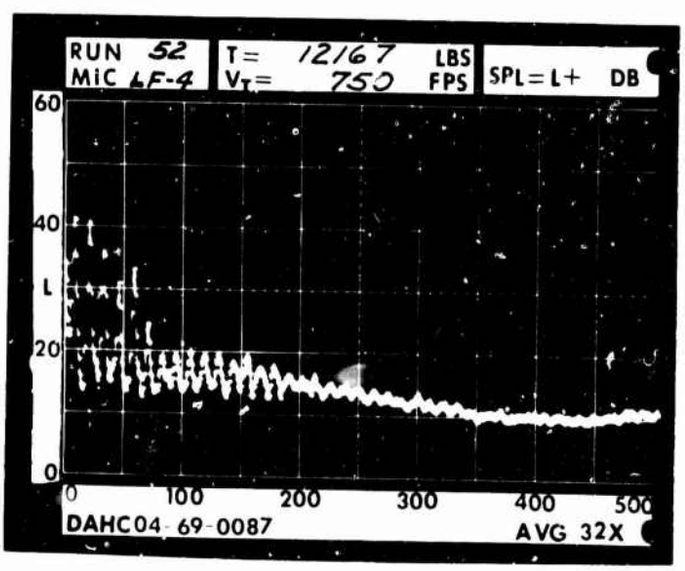

RUN 53

TIP SPEED 750 FT/SEC

THRUST 15800 LB

.2 RAD.

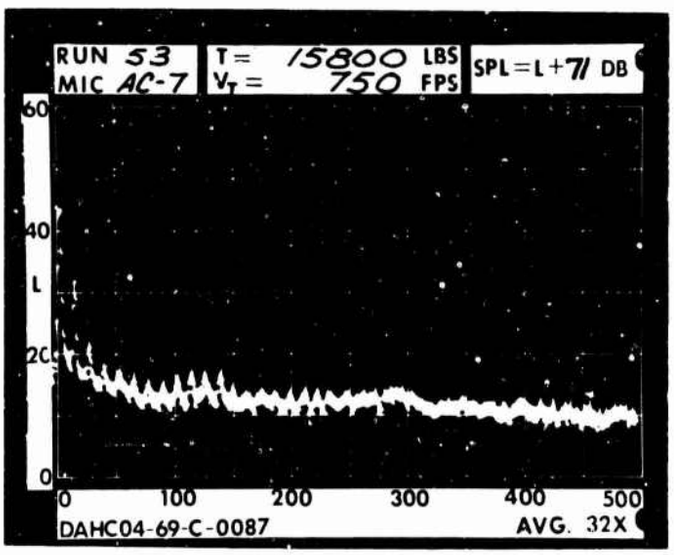

1 RAD.

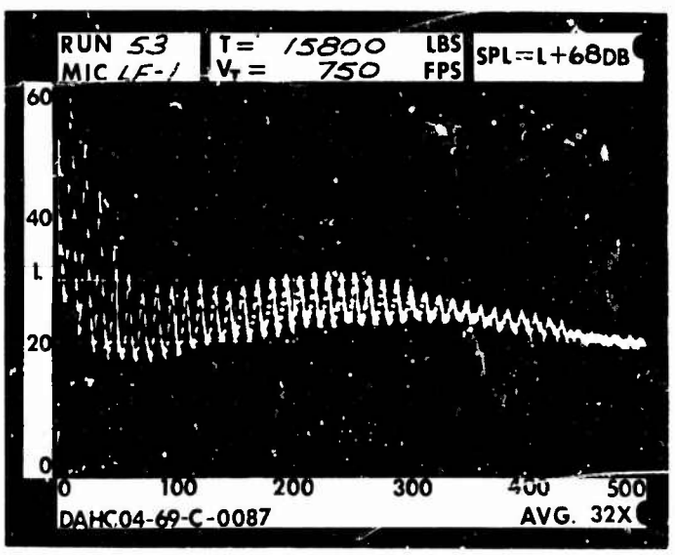

1 DIA.

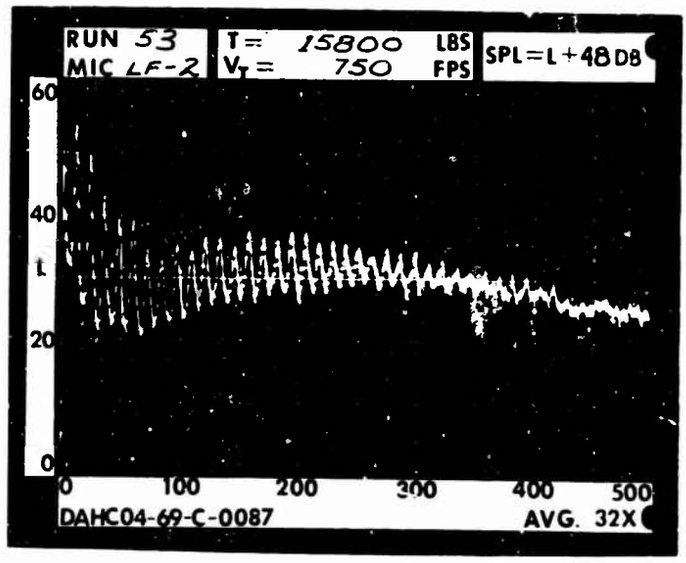

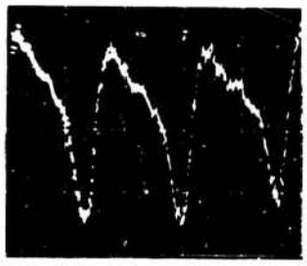

3 DIA.

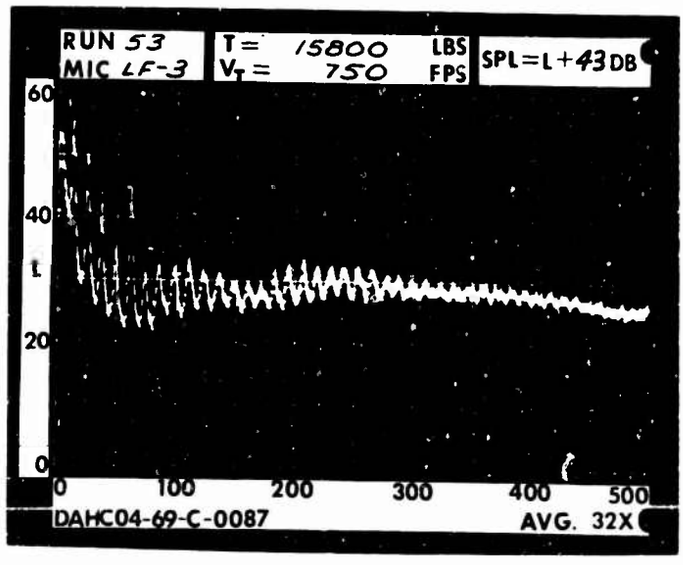

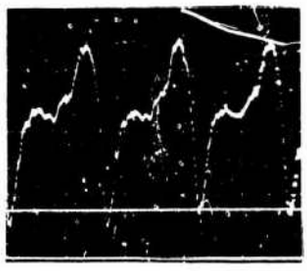

5 DIA.

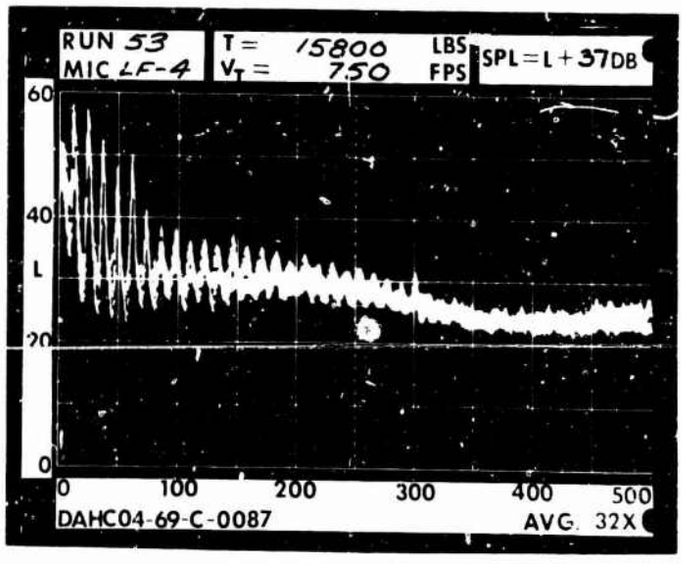

RUN 54

TIP SPEED 750 FT/SEC

THRUST 19000 LB

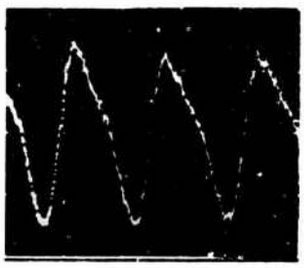

.2 RAD.

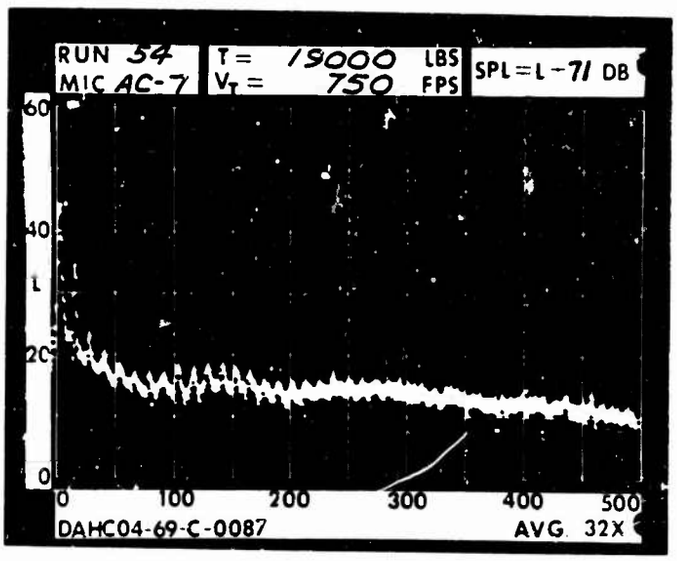

1 RAD.

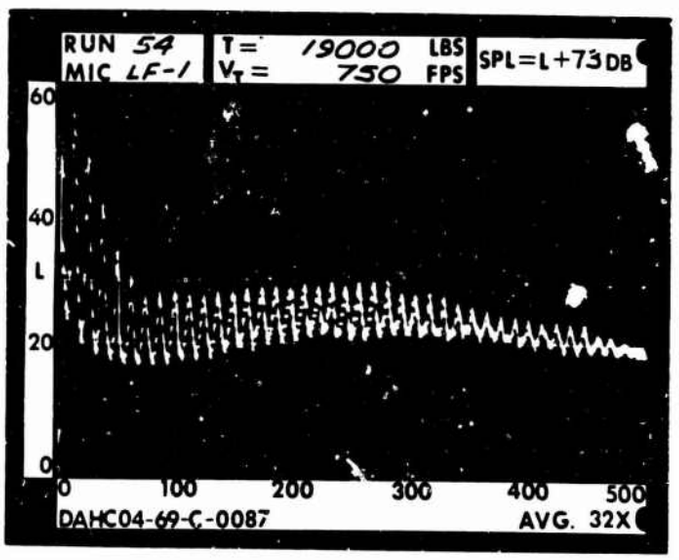

1 DIA.

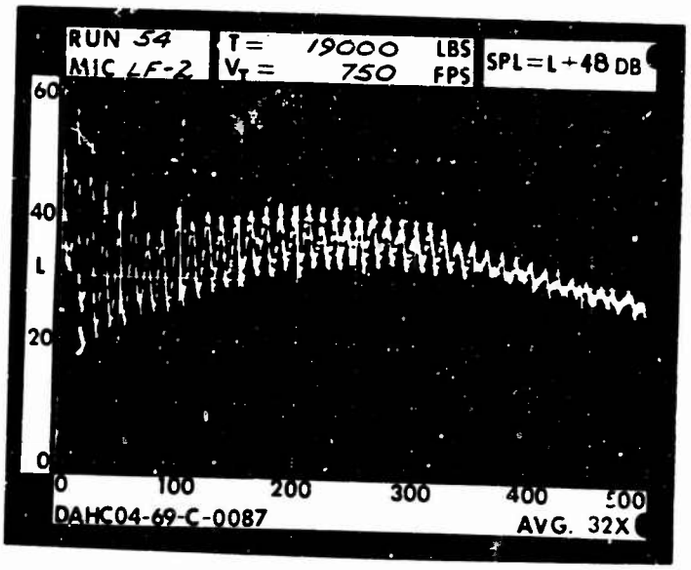

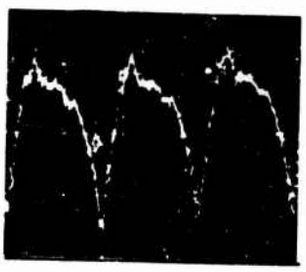

3 DIA.

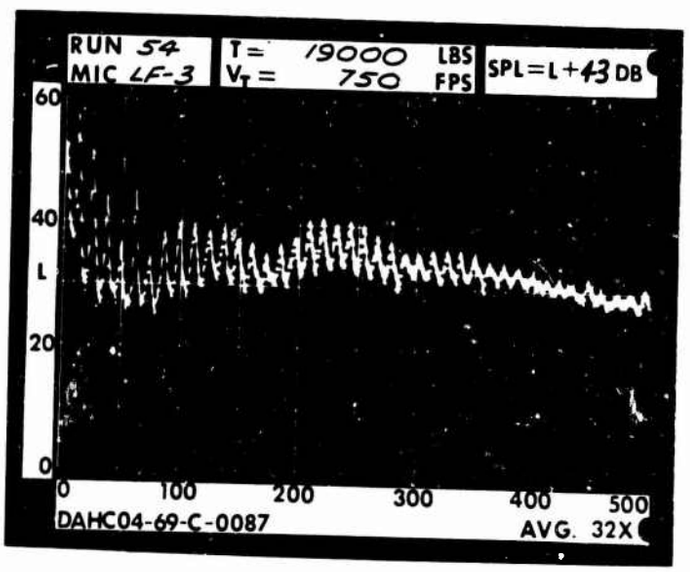

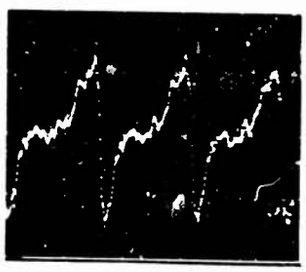

5 DIA.

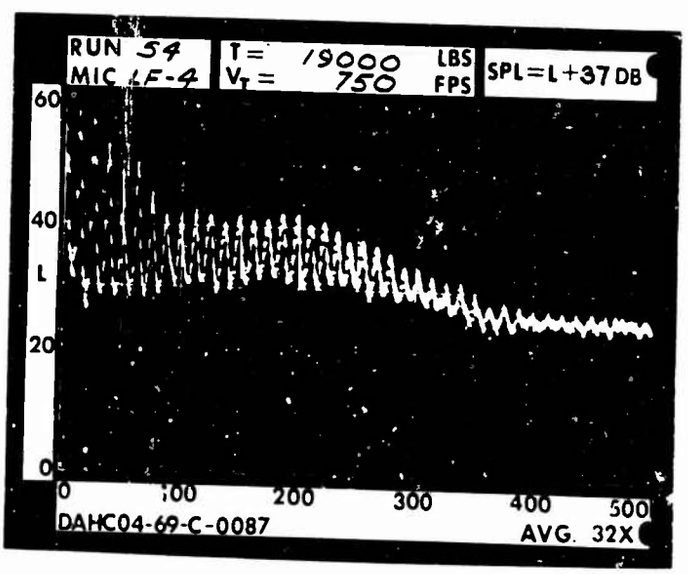

RUN 55

TIP SPEED 750 FT/SEC

THRUST 21500 LB

.2 RAD.

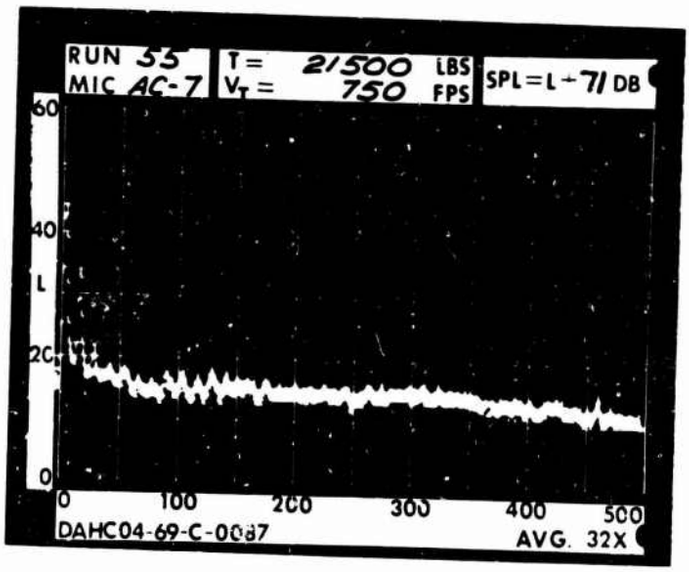

1 RAD.

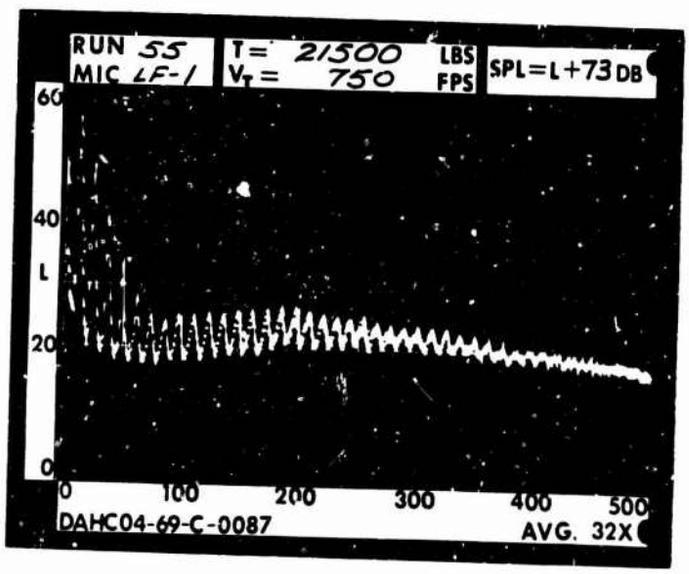

1 DIA.

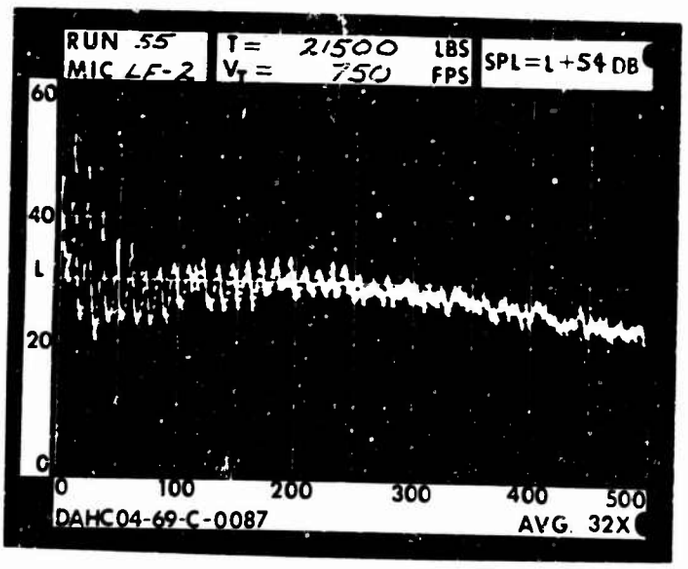

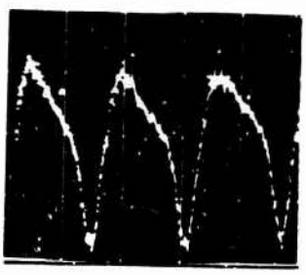

3 DIA.

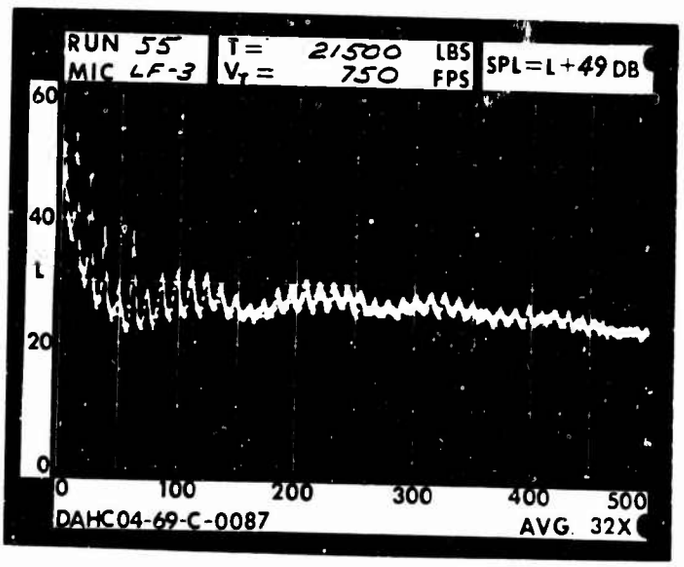

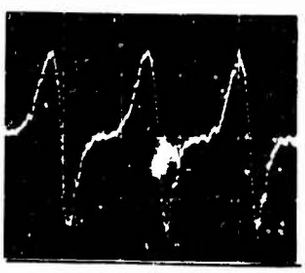

5 DIA.

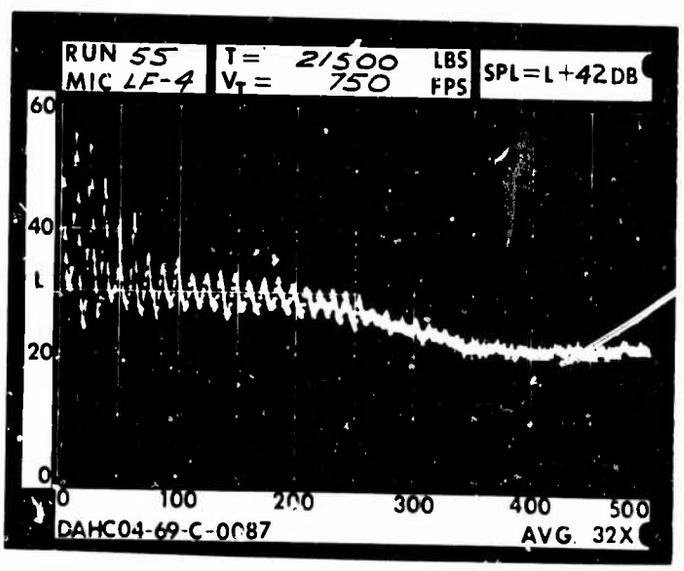

RUN 56

TIP SPEED 750 FT/SEC

THRUST 24200 LB

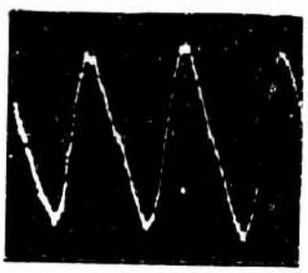

.2 RAD.

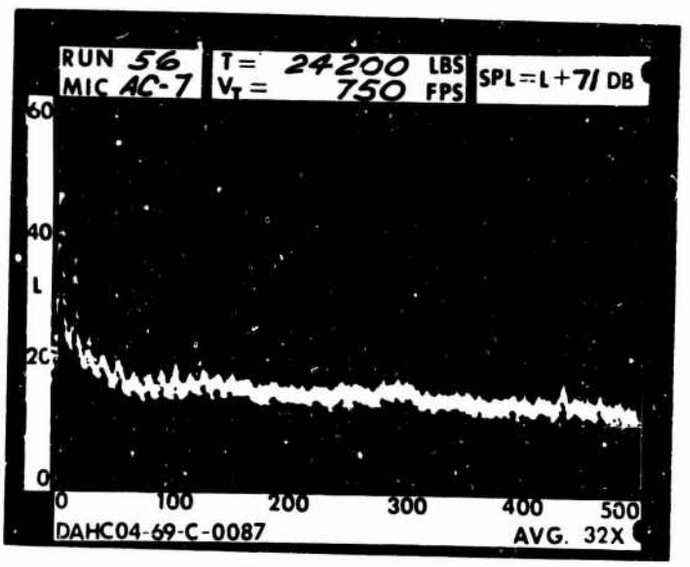

1 RAD

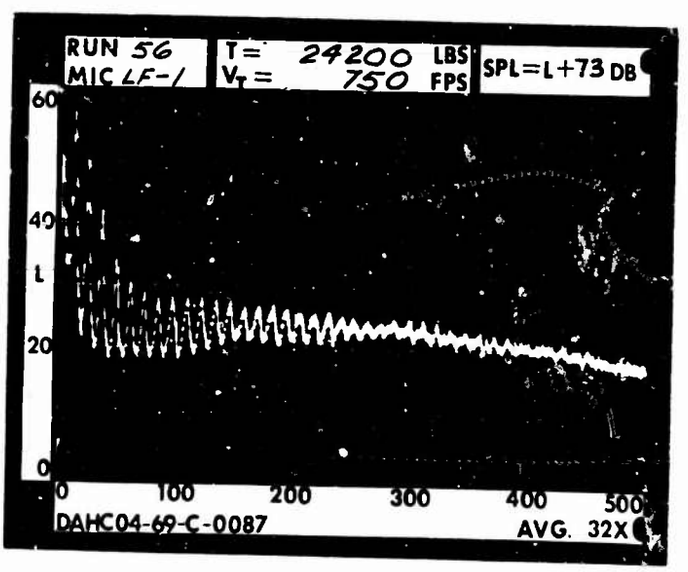

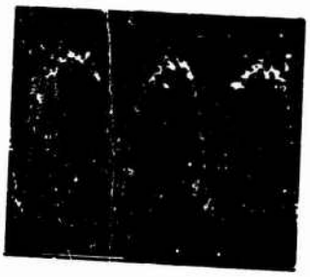

1 DIA.

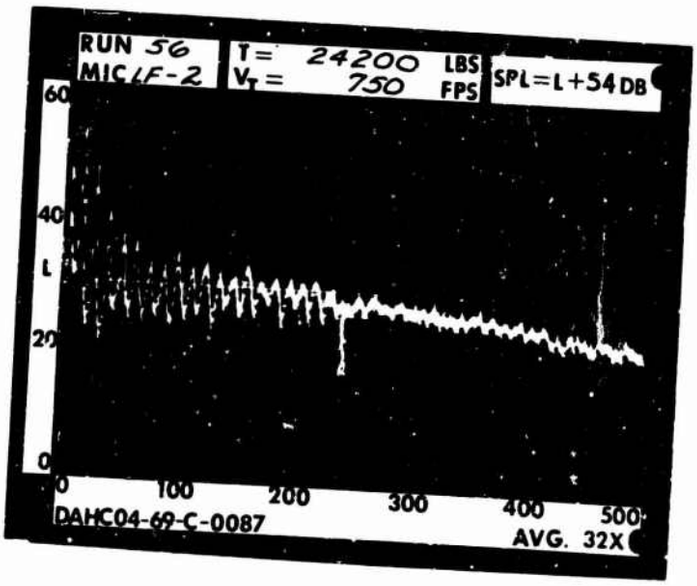

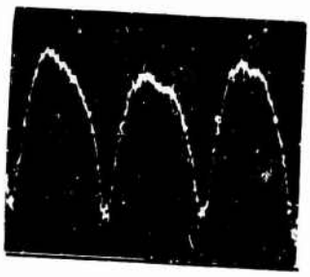

3 DIA.

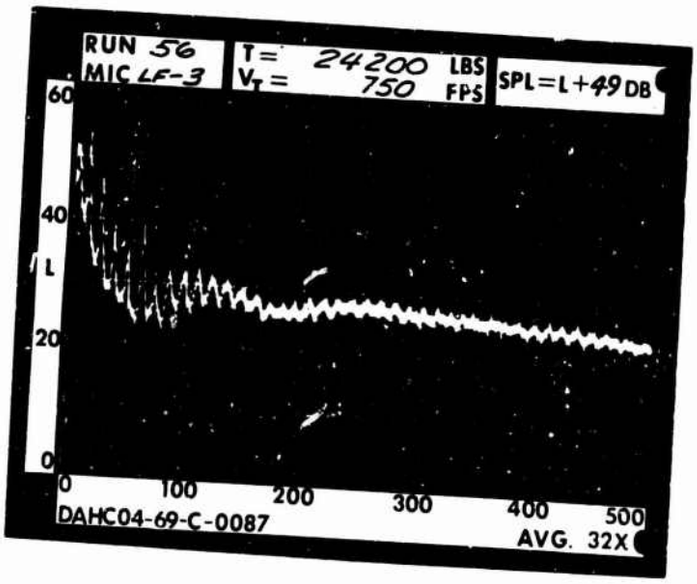

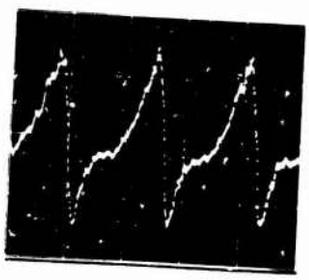

5 DIA.

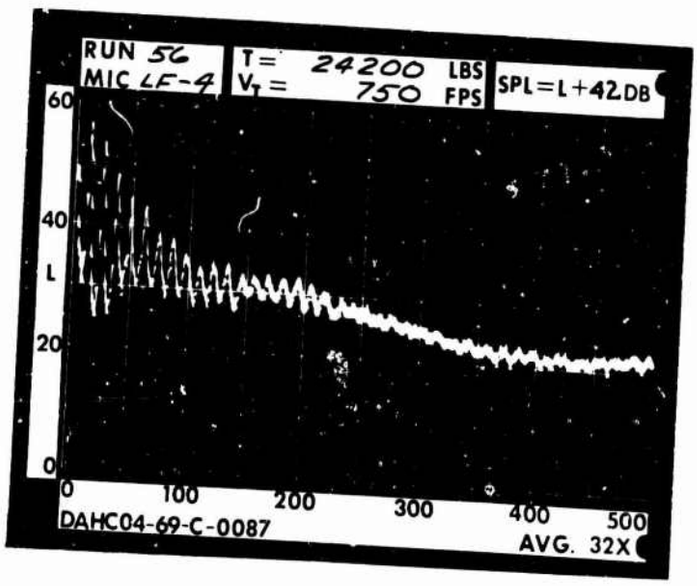

RUN 57

TIP SPEED 750 FT/SEC

THRUST 27000 LB

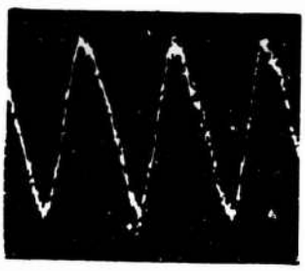

.2 RAD.

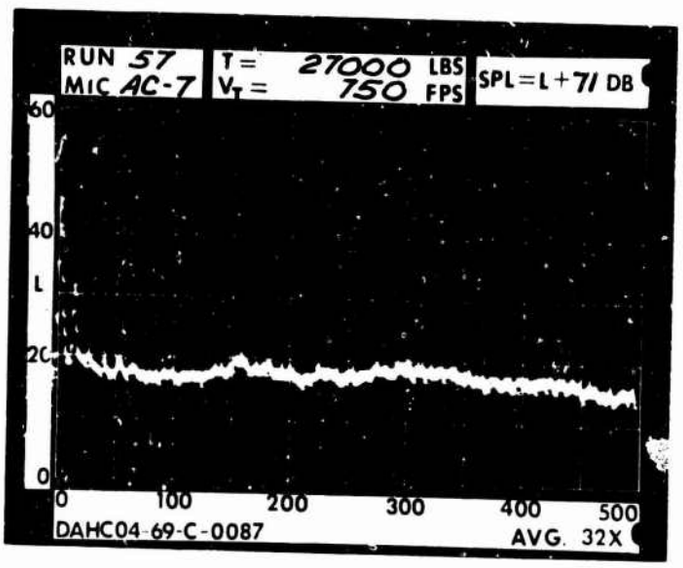

1 RAD.

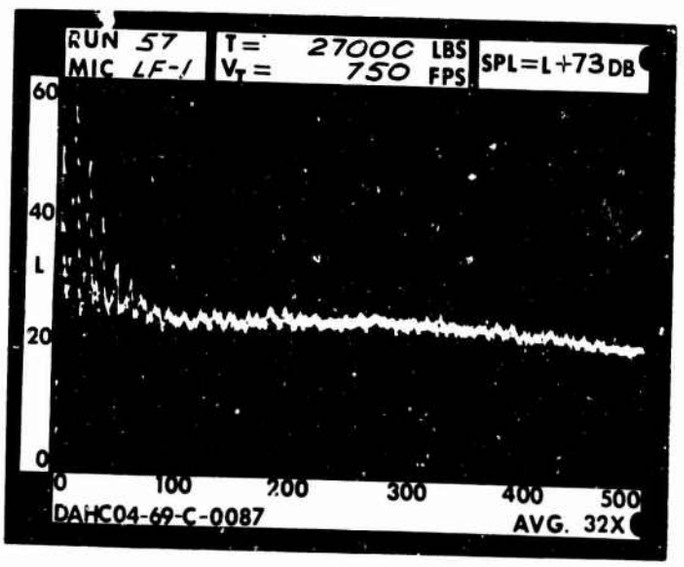

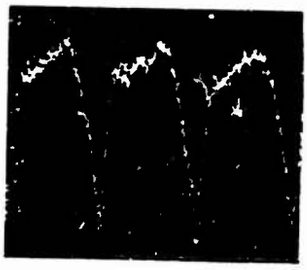

1 DIA.

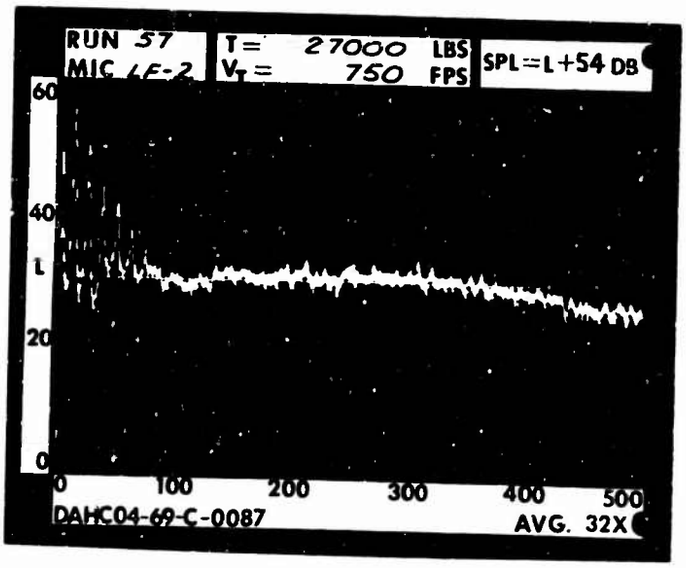

3 DIA.

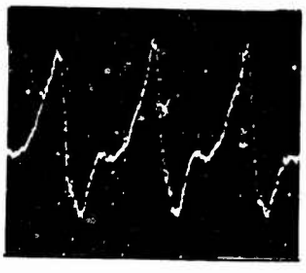

5 DIA.

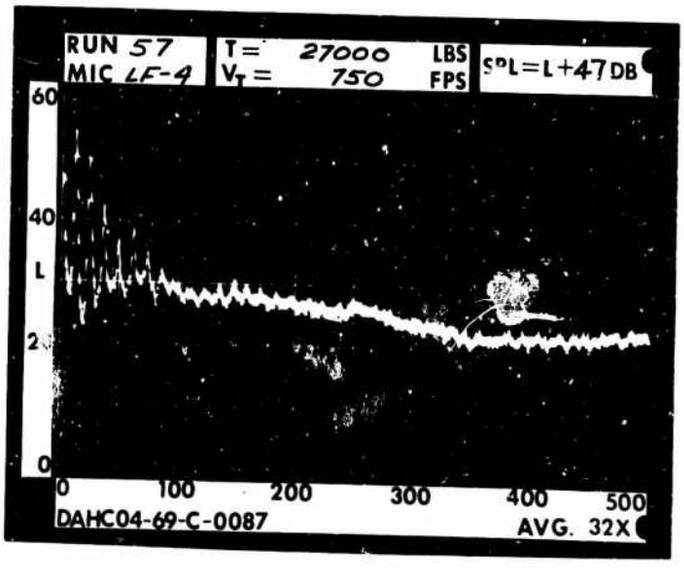

RUN 58

TIP SPEED 750 FT/SEC

THRUST 29200 LB

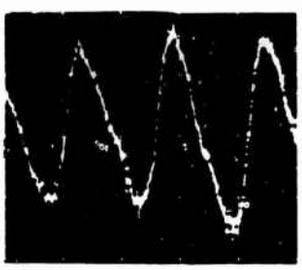

.2 RAD.

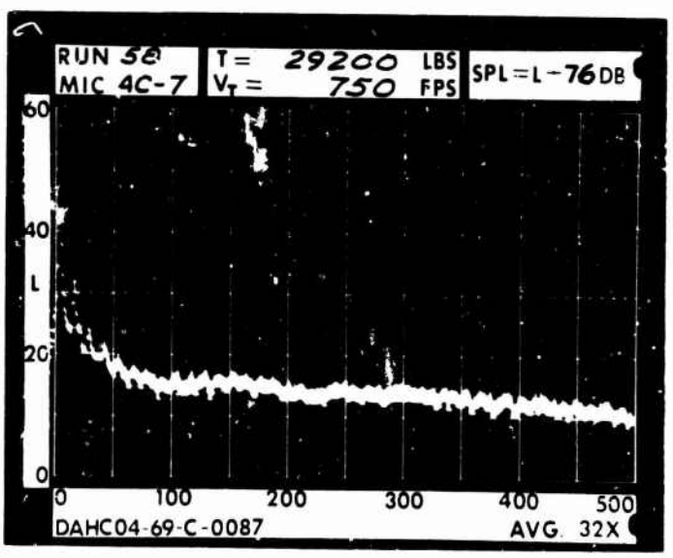

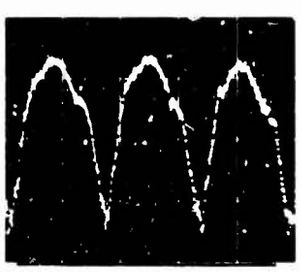

1 RAD.

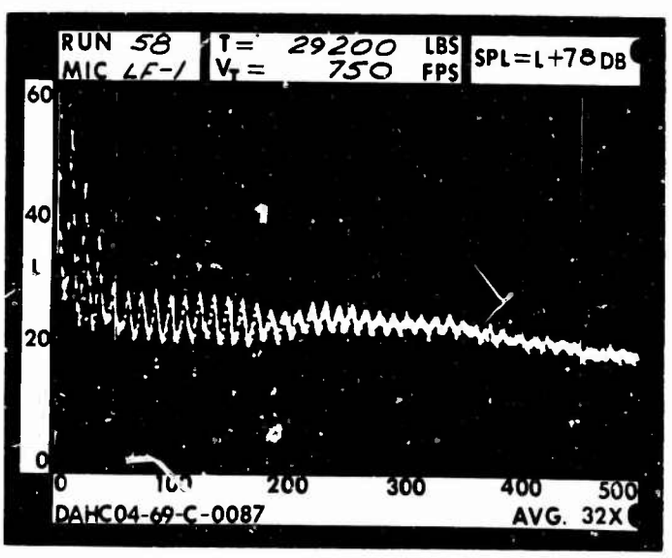

1 DIA.

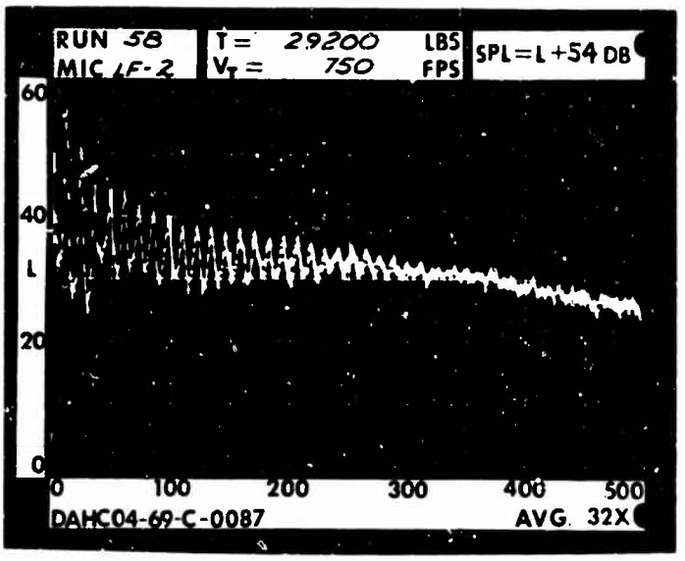

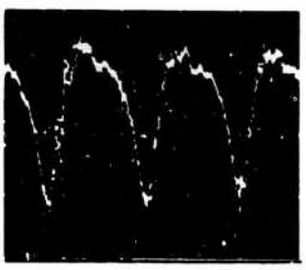

3 DIA.

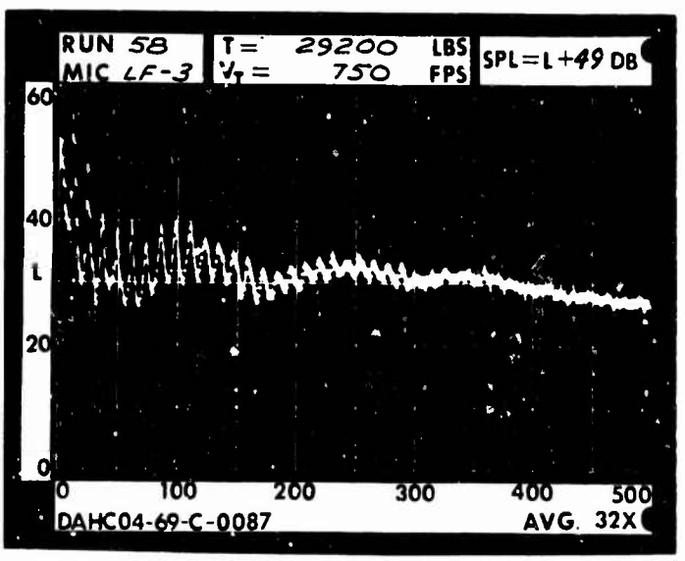

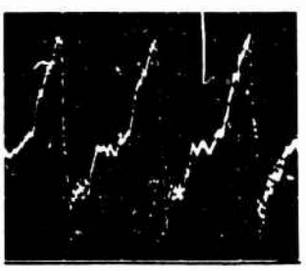

5 DIA.

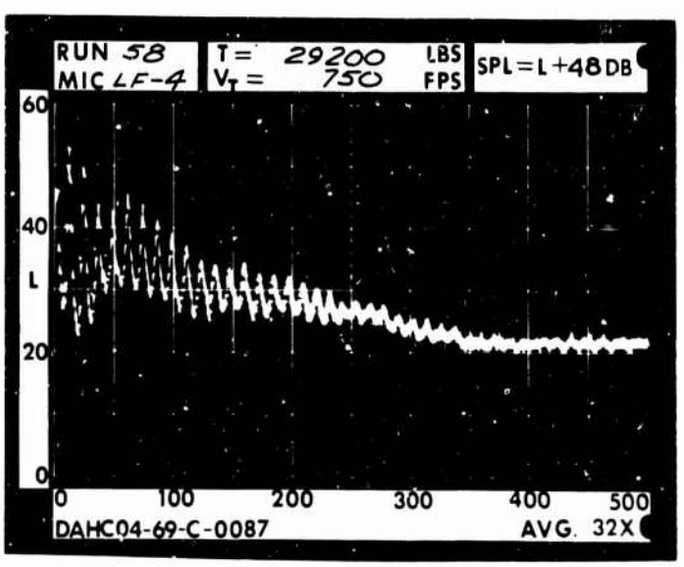

RUN 59

TIP SPEED 750 FT/SEC

THRUST 31400 LB

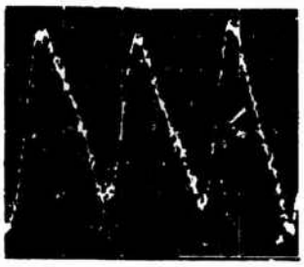

.2 RAD.

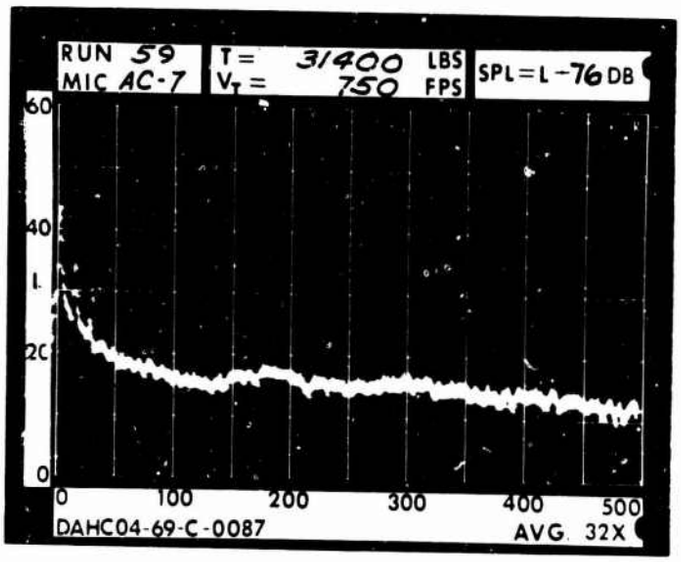

1 RAD.

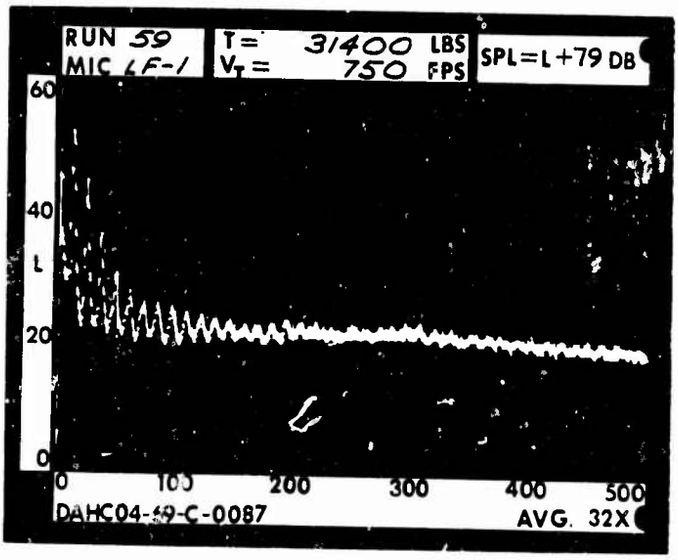

1 DIA.

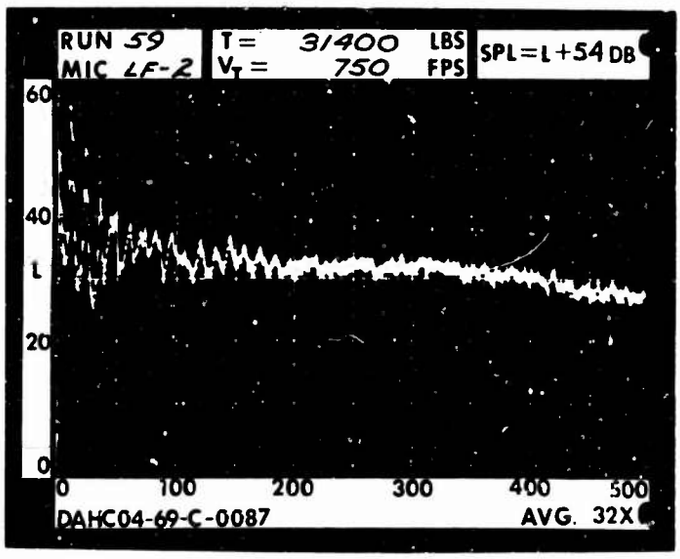

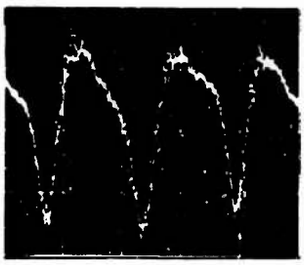

3 DIA.

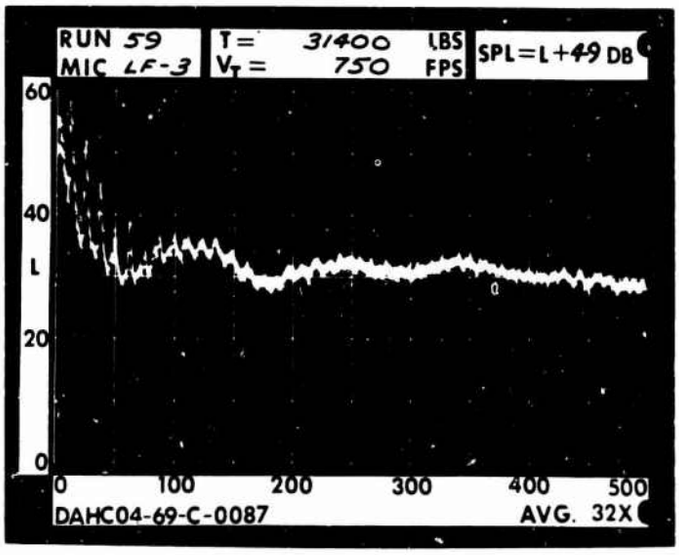

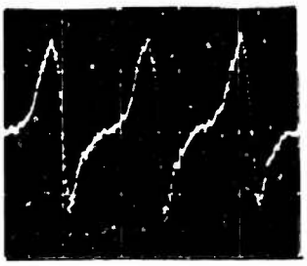

5 DIA.

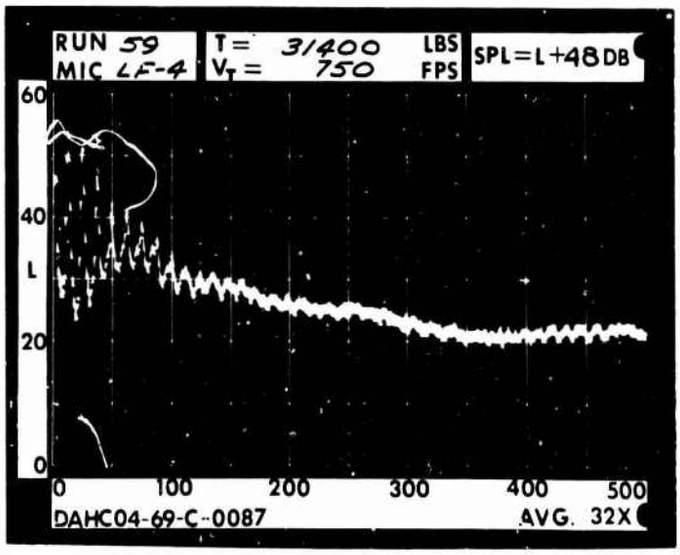

RUN 60

TIP SPEED 700 FT/SEC

THRUST 26400 LB

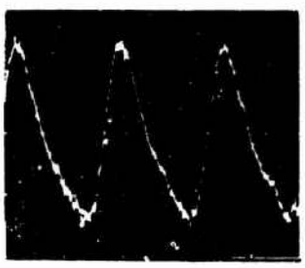

.2 RAD.

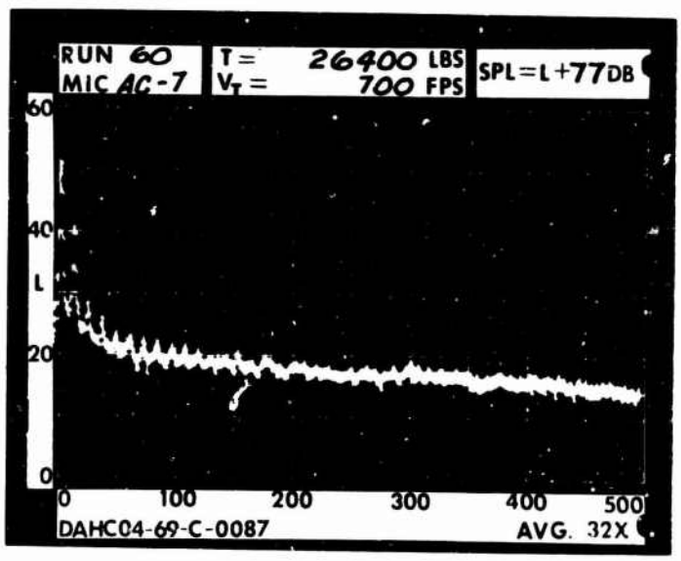

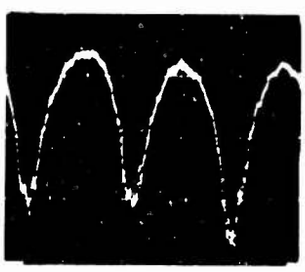

1 RAD.

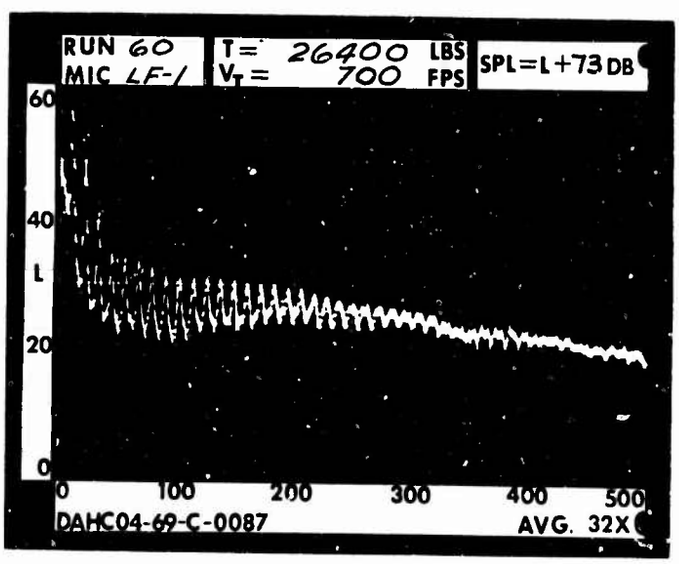

1 DIA.

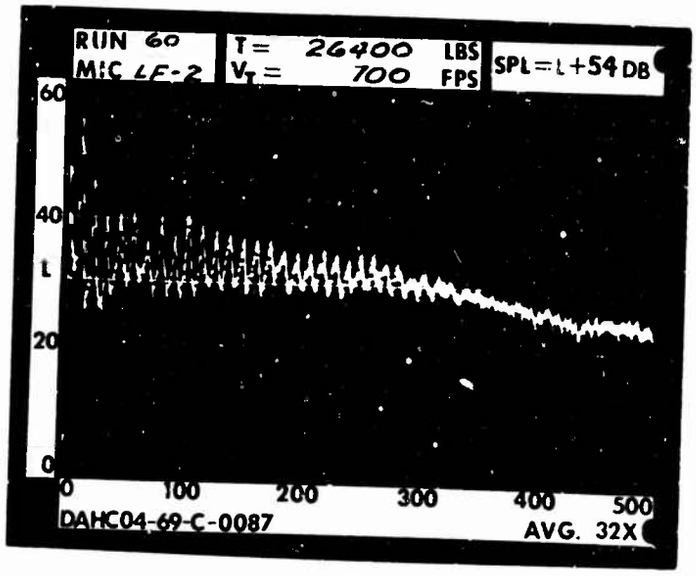

3 DIA.

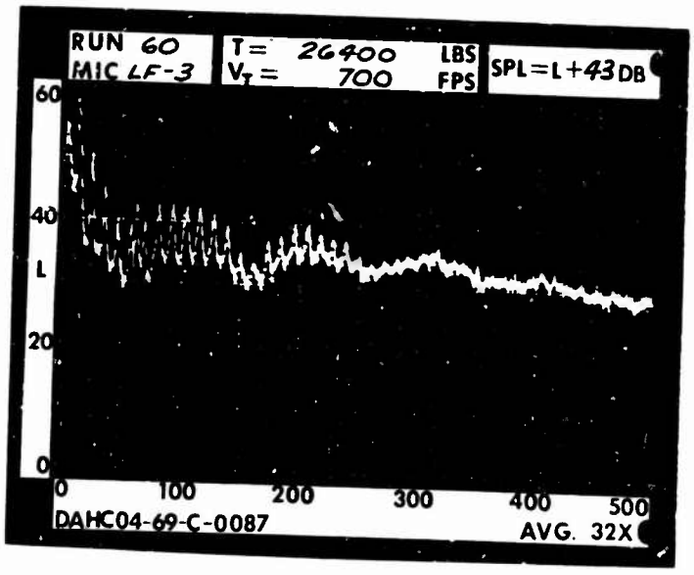

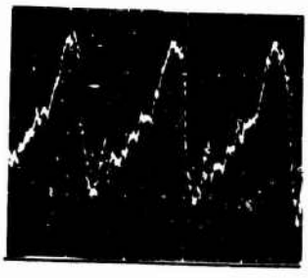

5 DIA.

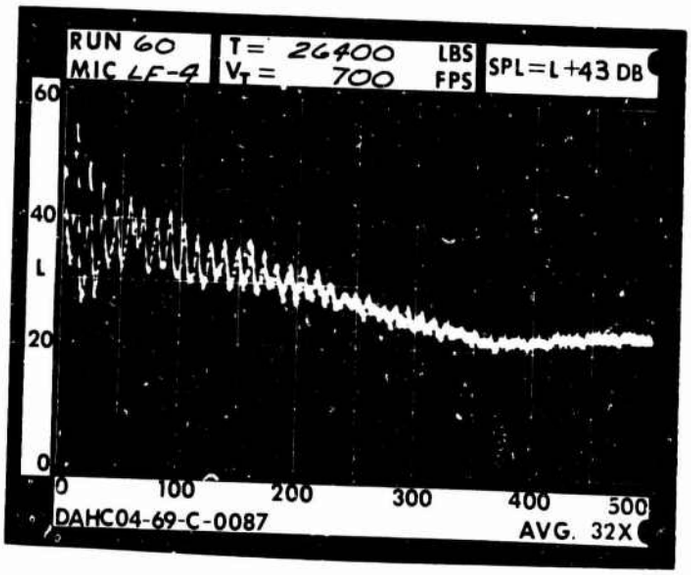

RUN 61

TIP SPEED 700 FT/SEC

THRUST 26800 LB

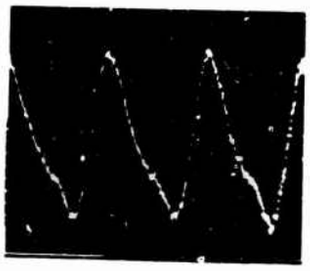

.2 RAD.

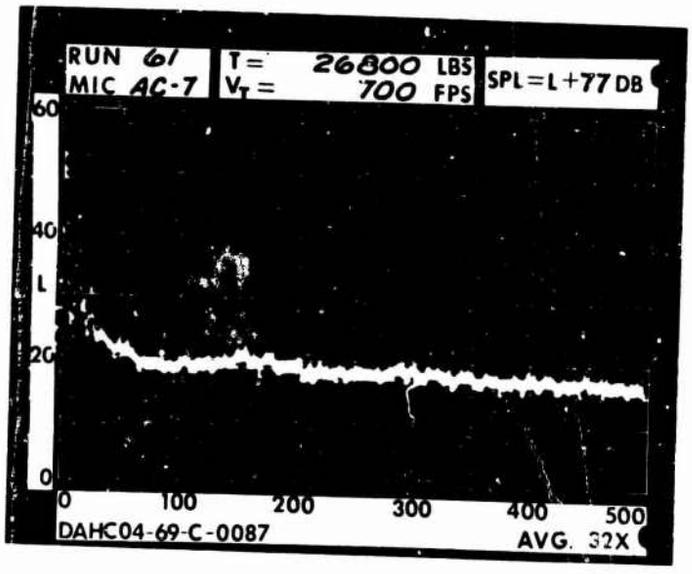

1 RAD.

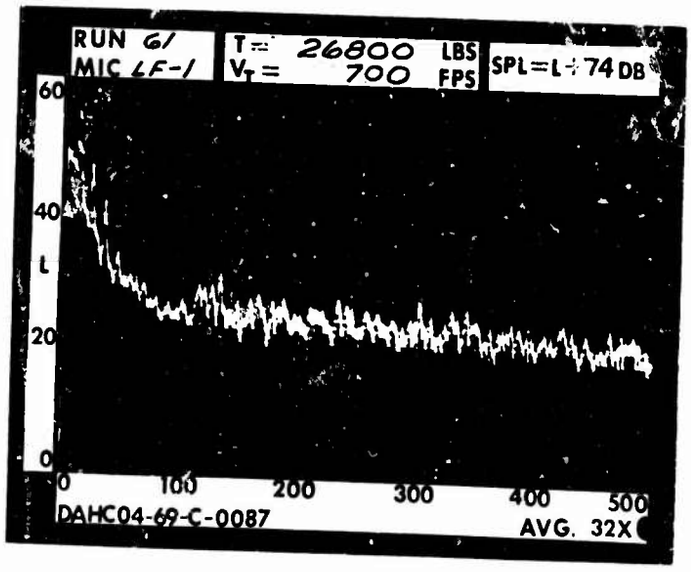

1 DIA.

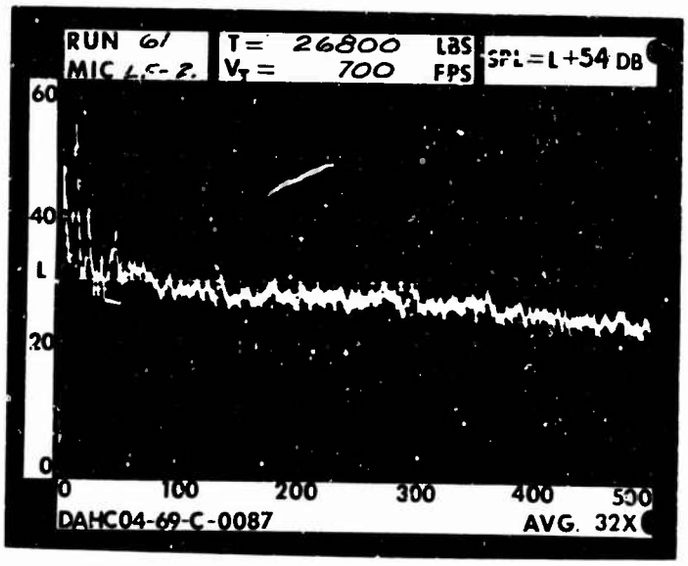

3 DIA.

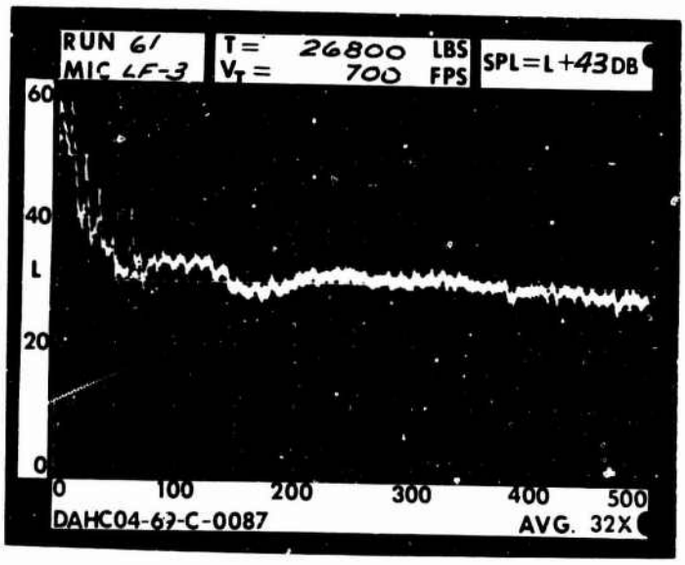

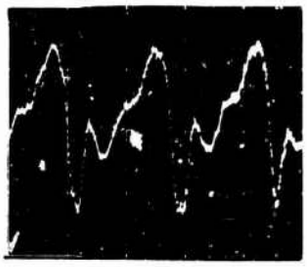

5 DIA.

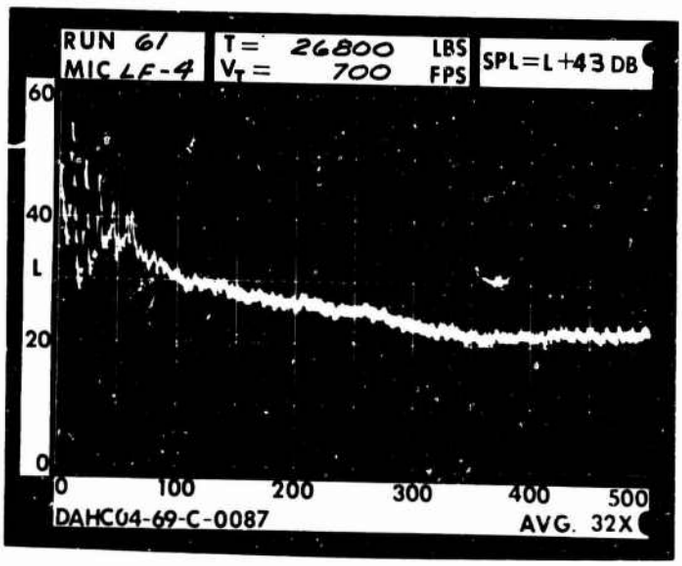

RUN 62

TIP SPEED 700 FT/SEC

THRUST 23600 LB

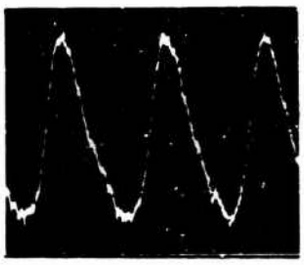

.2 RAD.

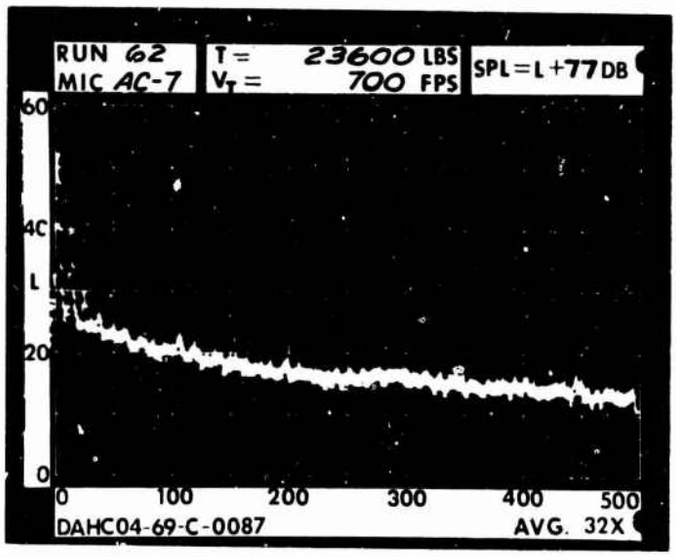

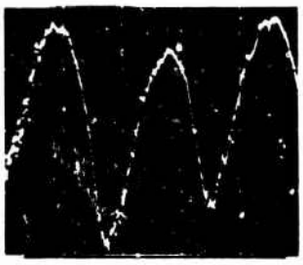

1 RAD.

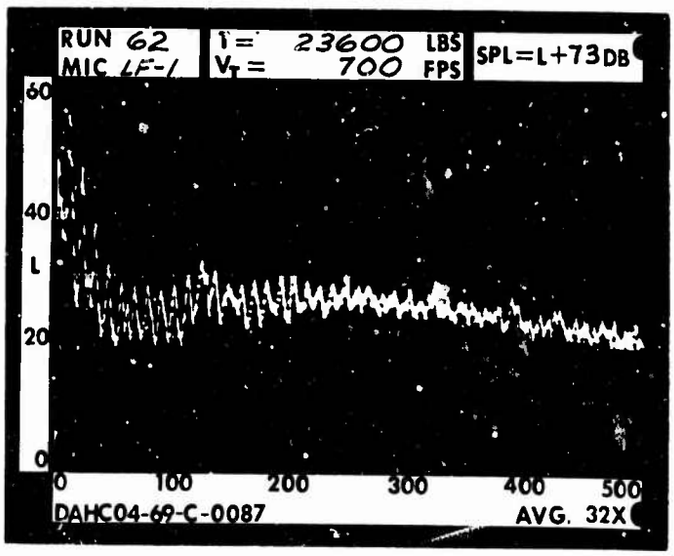

1 DIA.

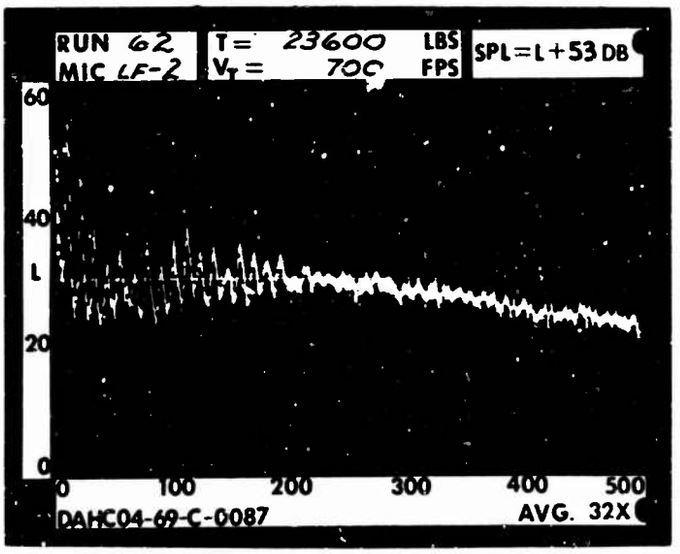

3 DIA.

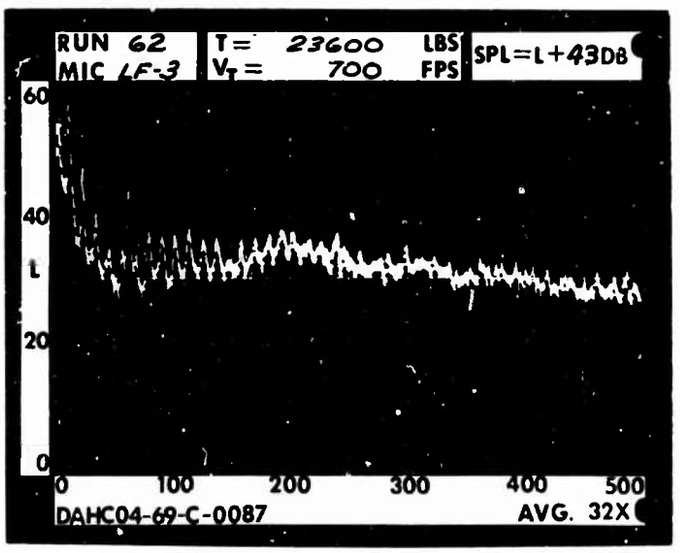

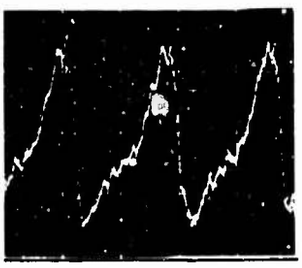

5 DIA.

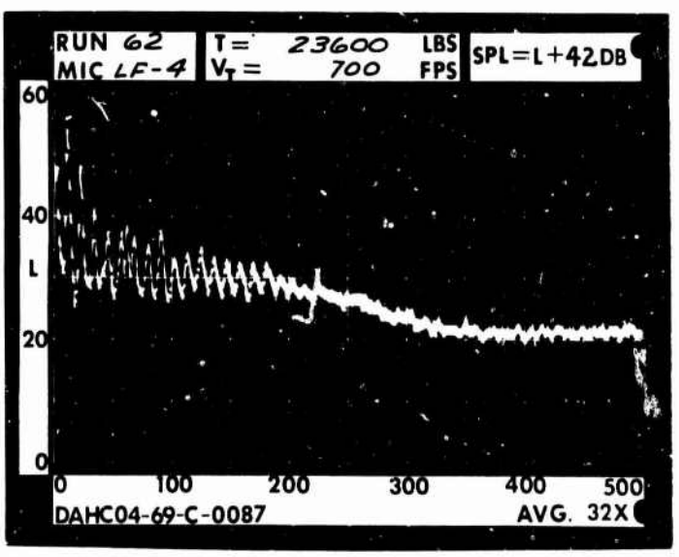

RUN 63

TIP SPEED 700 FT/SEC

THRUST 18800 LB

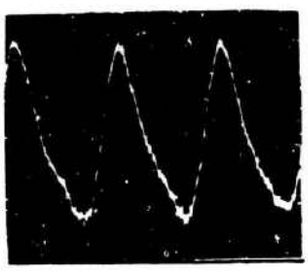

.2 RAD.

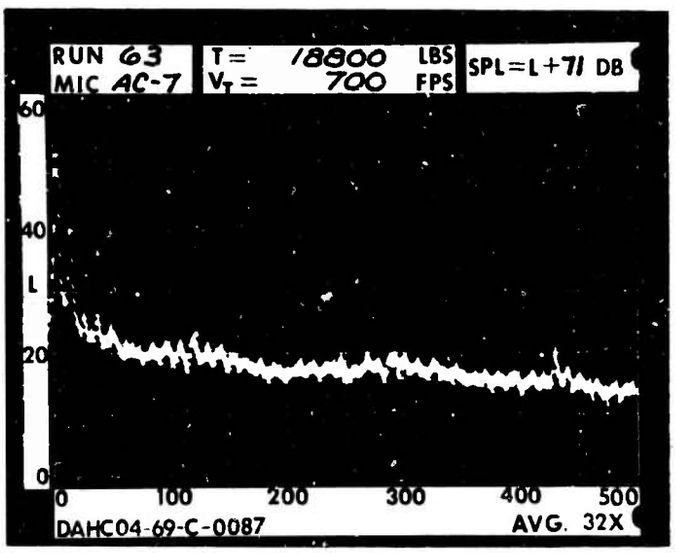

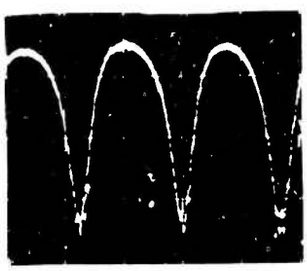

1 RAD.

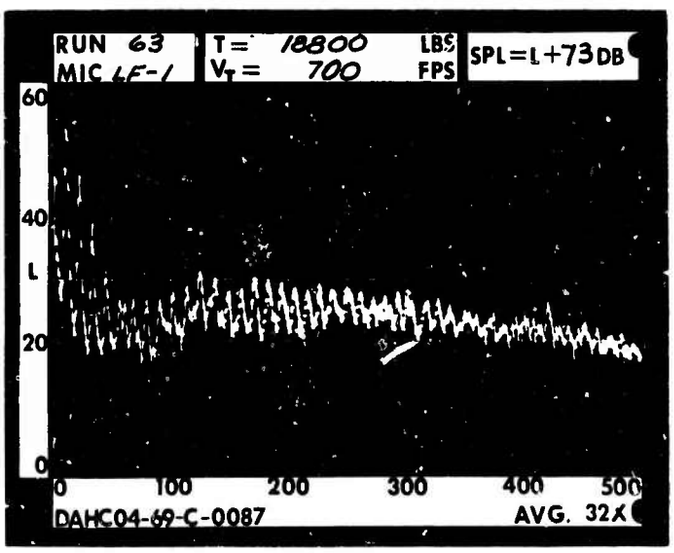

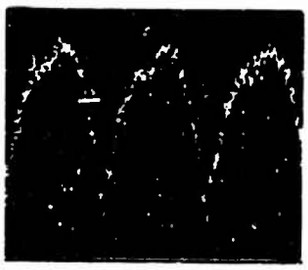

1 DIA.

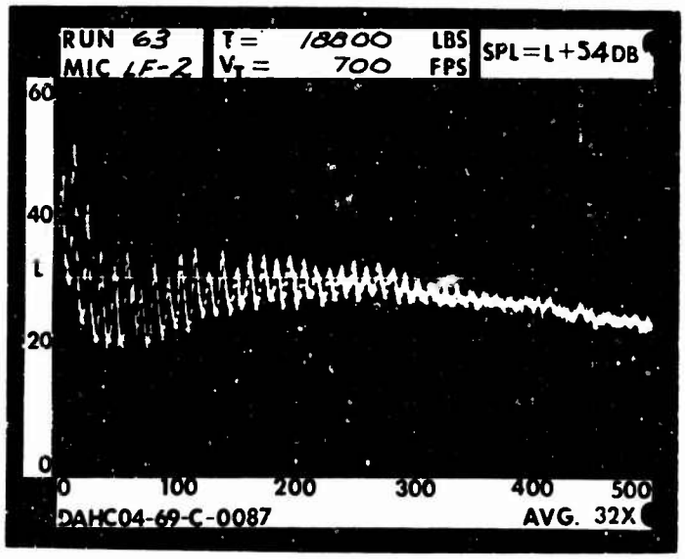

3 DIA.

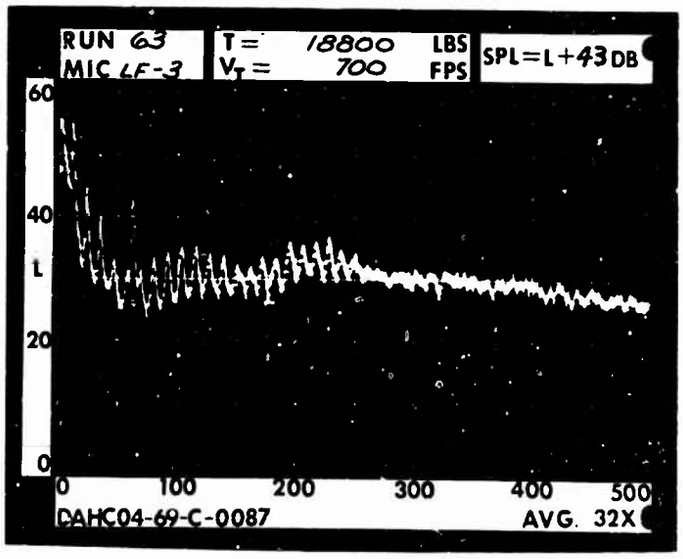

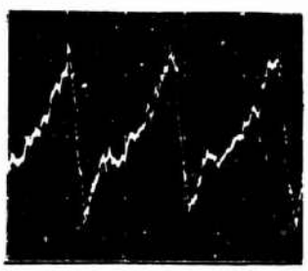

5 DIA.

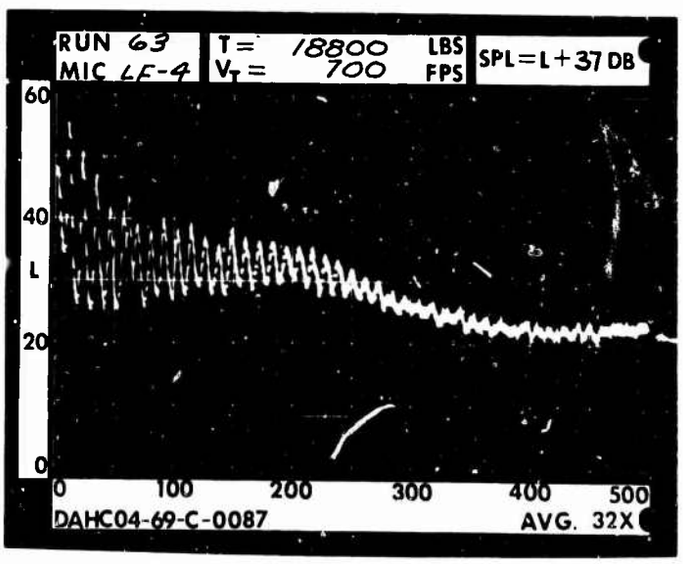

RUN 64

TIP SPEED 700 FT/SEC

THRUST 21700 LB

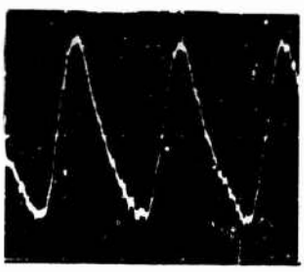

.2 RAD.

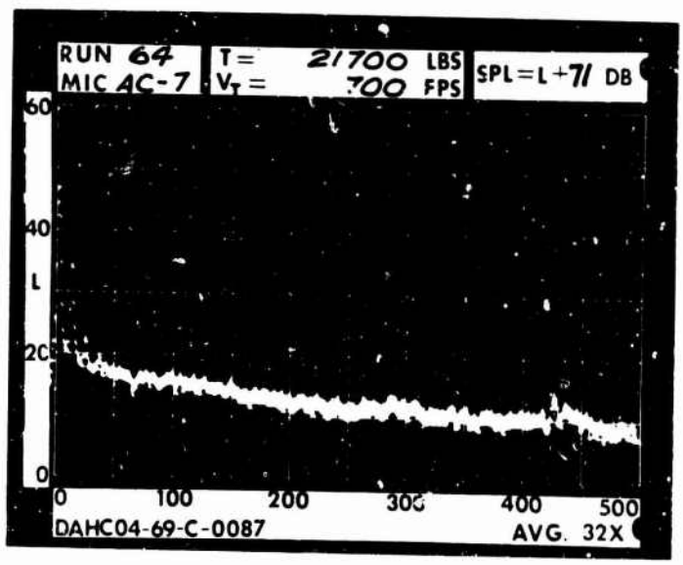

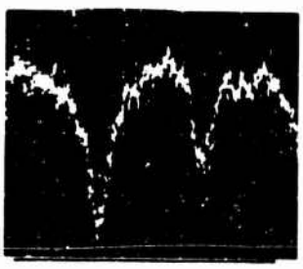

1 RAD.

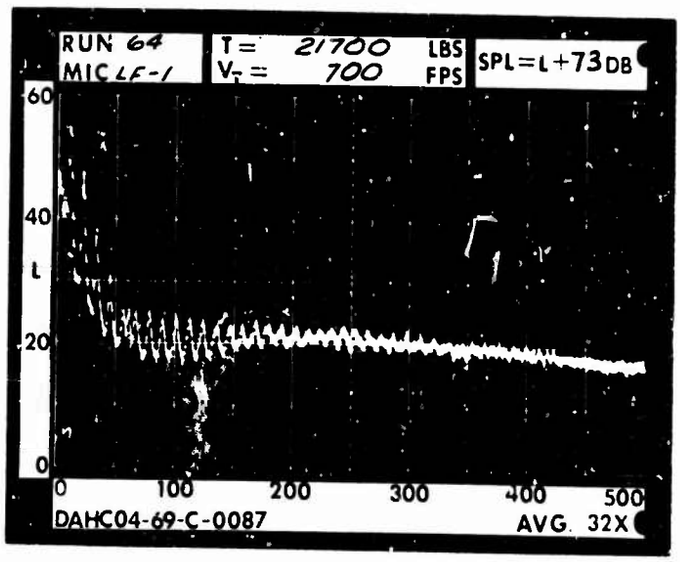

1 DIA.

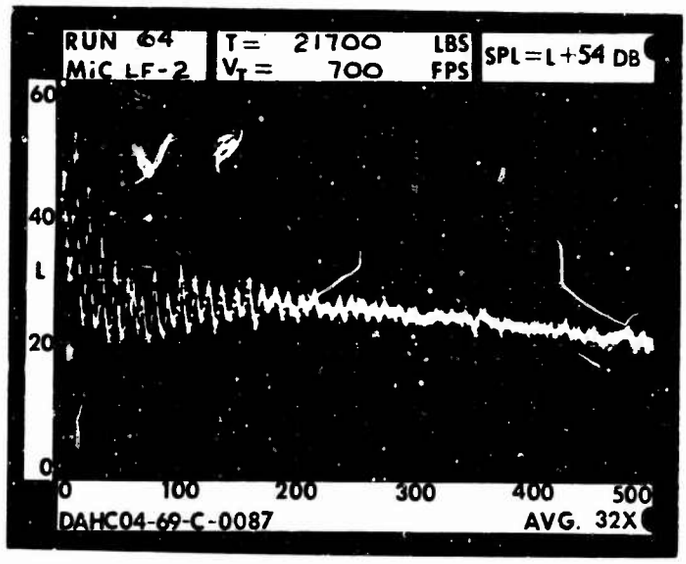

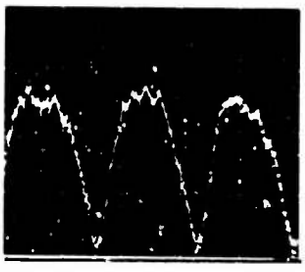

3 DIA.

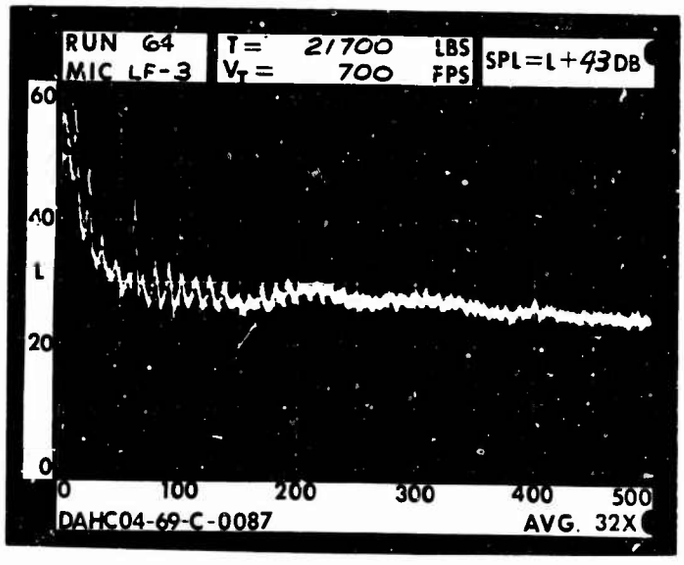

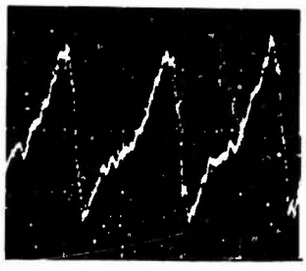

5 DIA.

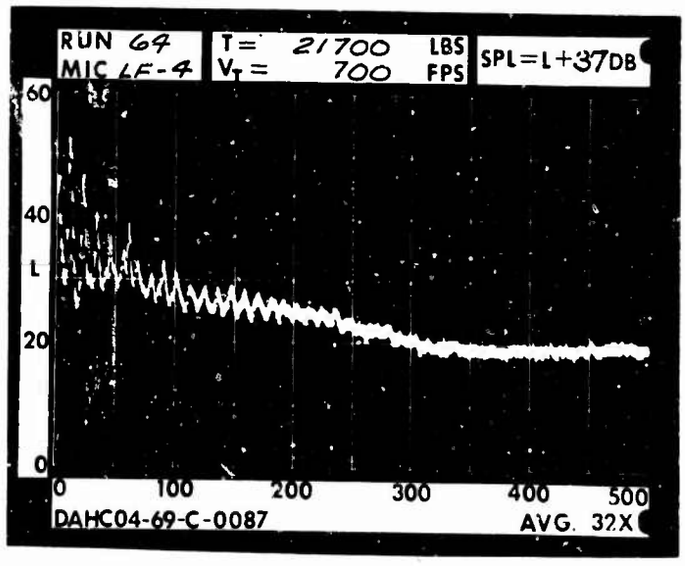

RUN 65

TIP SPEED 700 FT/SEC

THRUST 14900 LB

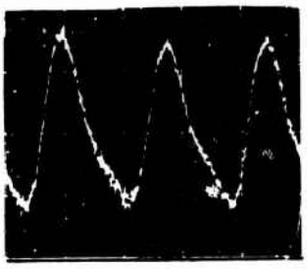

.2 RAD.

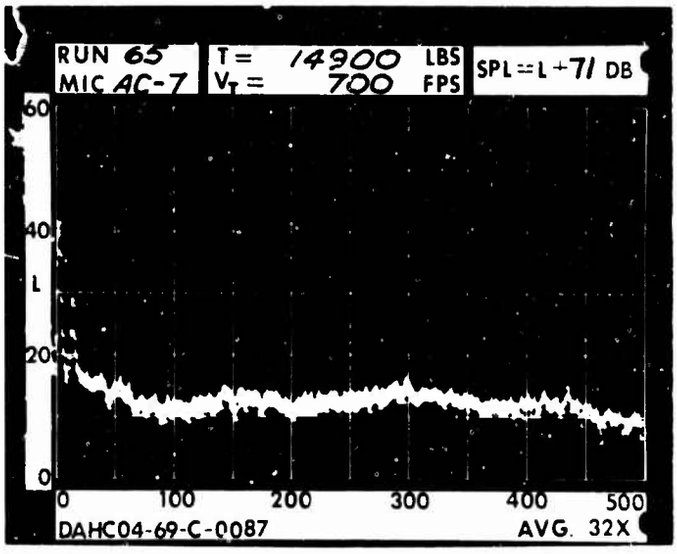

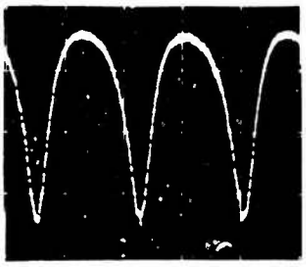

1 RAD.

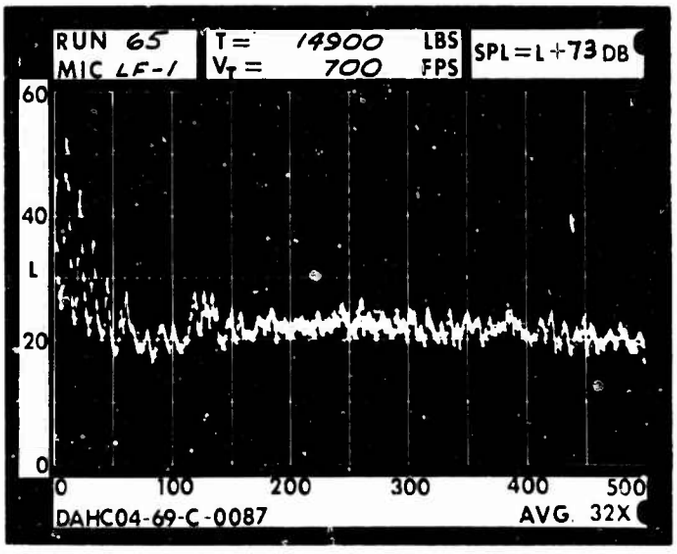

1 DIA.

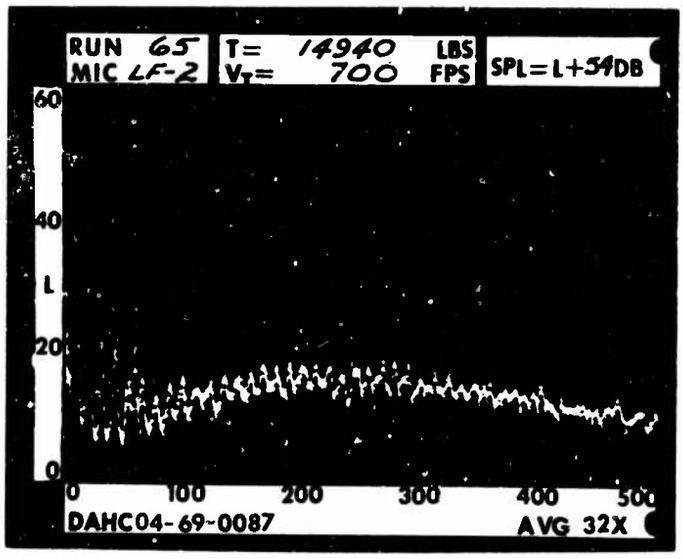

3 DIA.

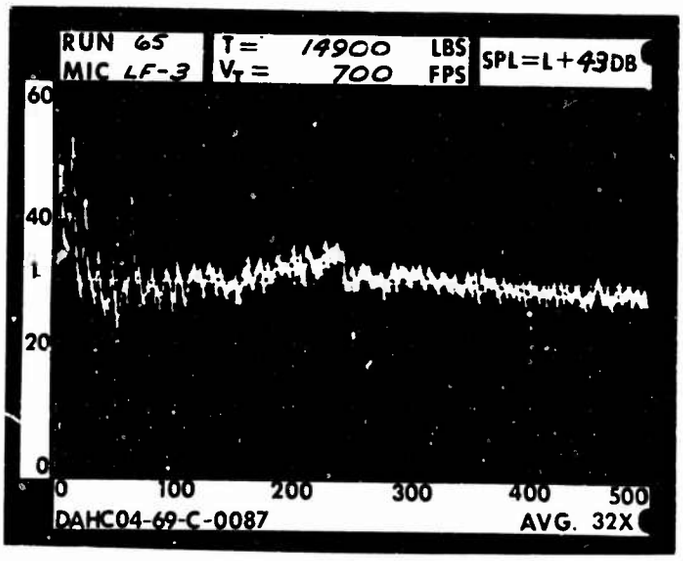

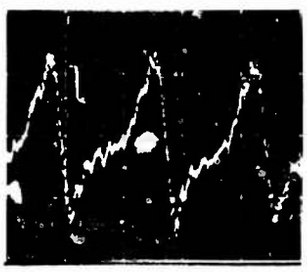

5 DIA.

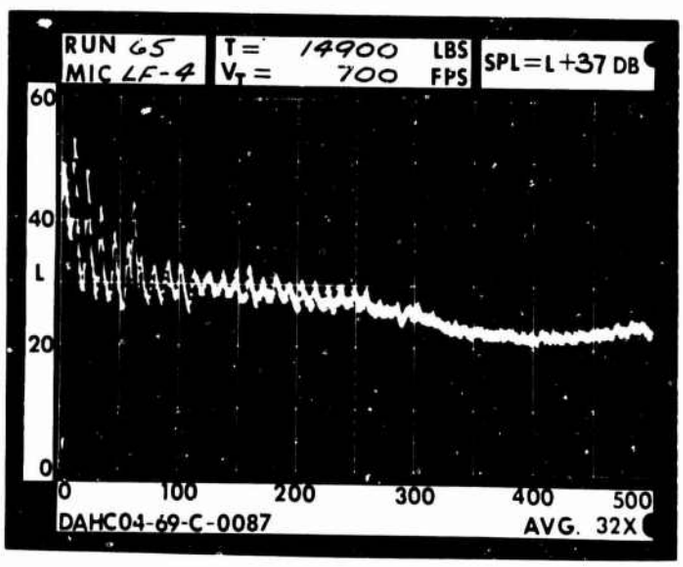

RUN 66

TIP SPEED 700 FT/SEC

THRUST 13000 LB

.2 RAD.

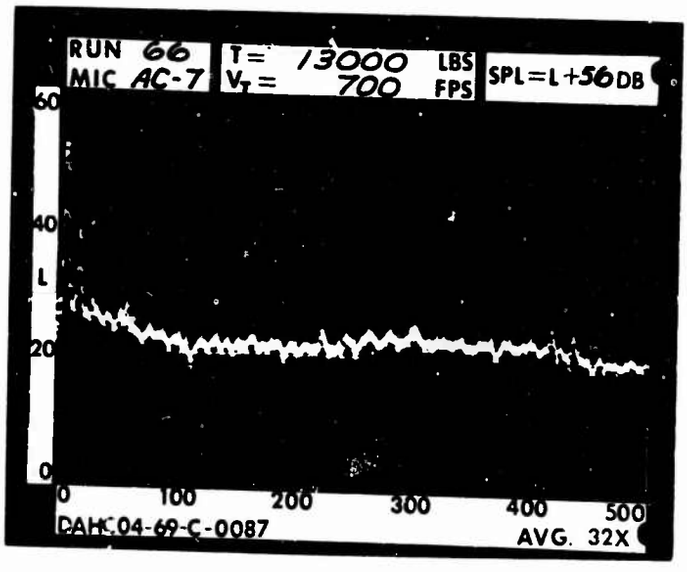

1 RAD.

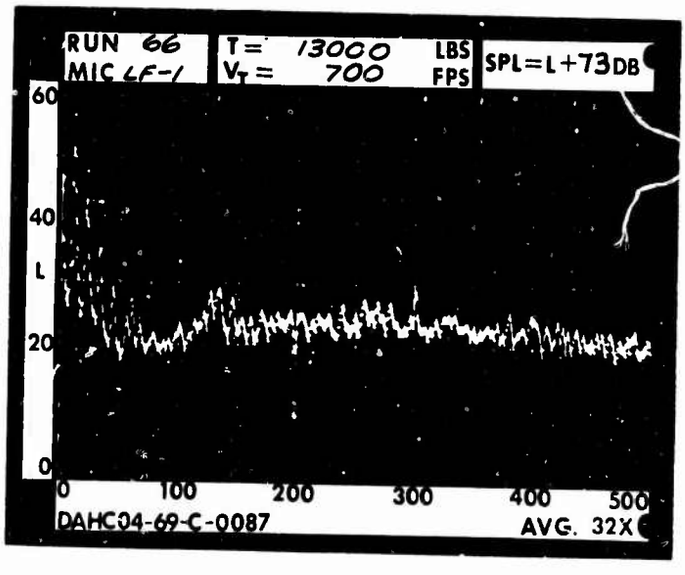

1 DIA.

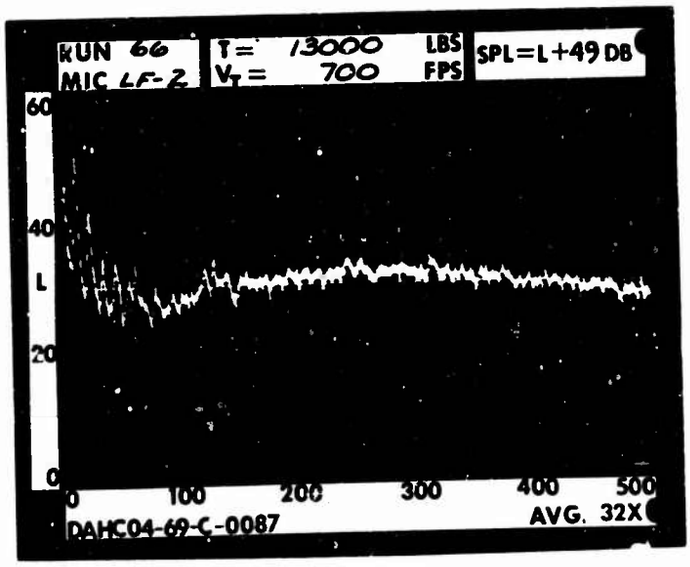

3 DIA.

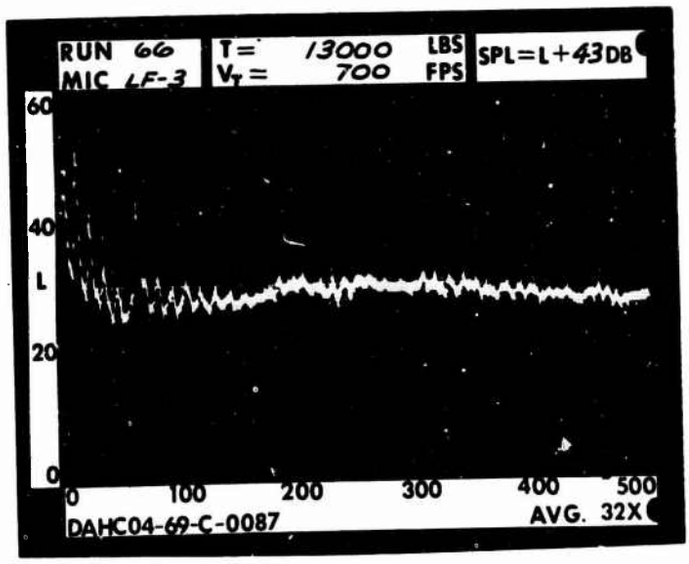

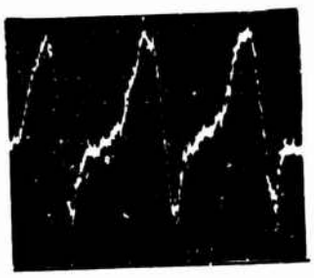

5 DIA.

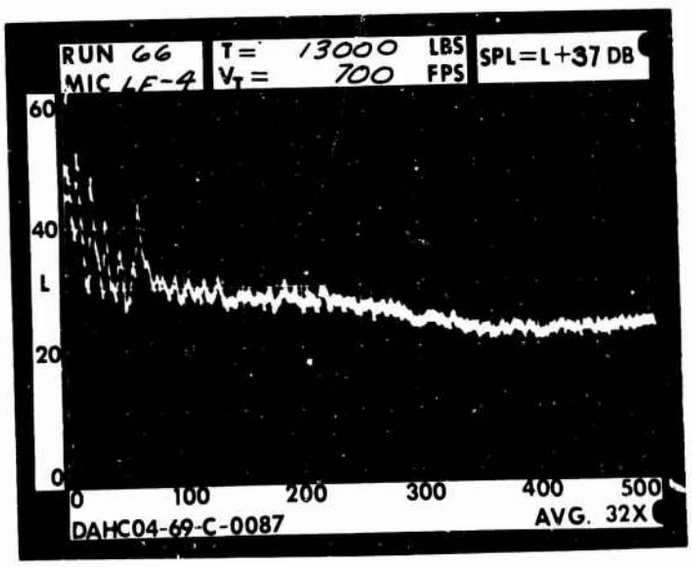

RUN 68

TIP SPEED 700 FT/SEC

THRUST 8800 LB

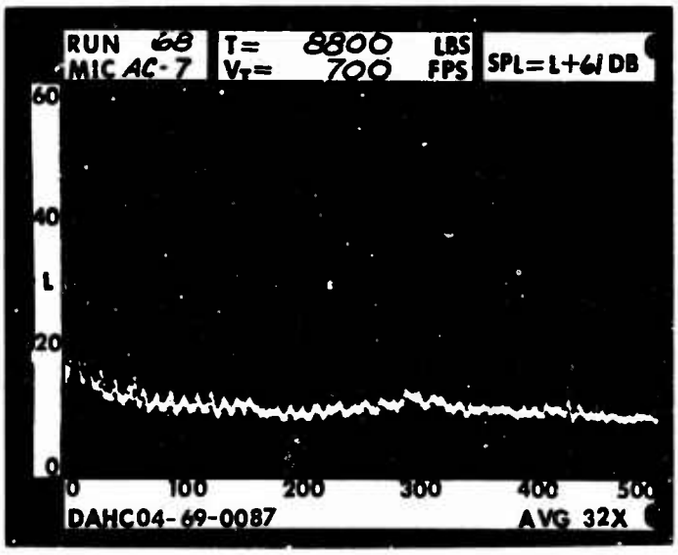

.2 RAD.

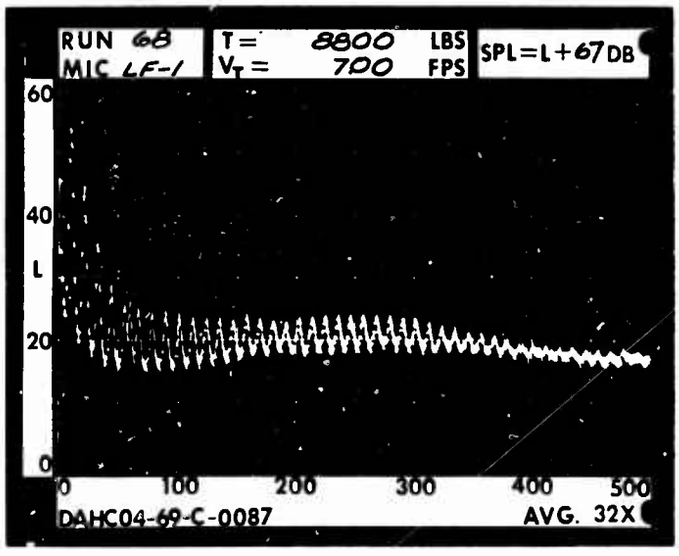

1 RAD.

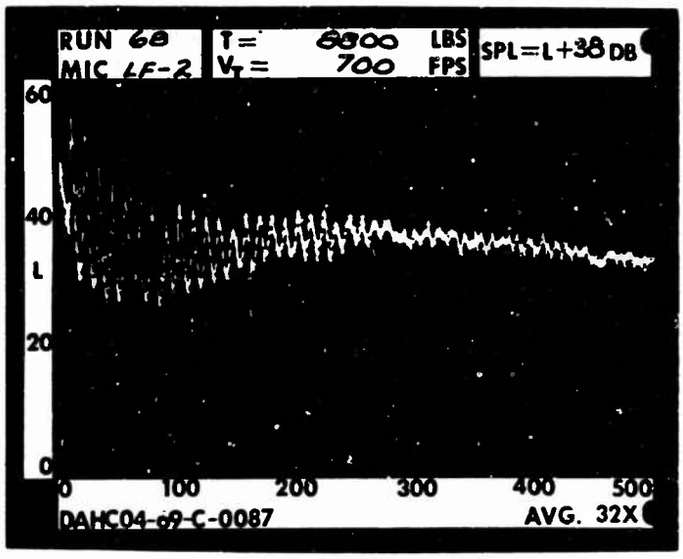

1 DIA.

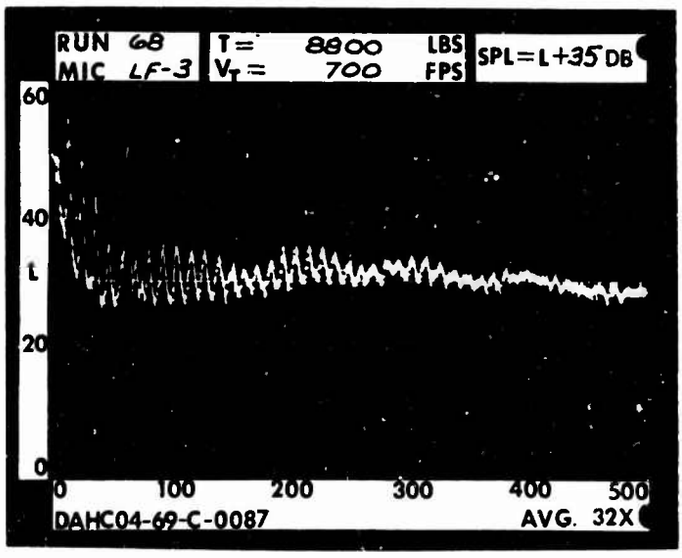

3 DIA.

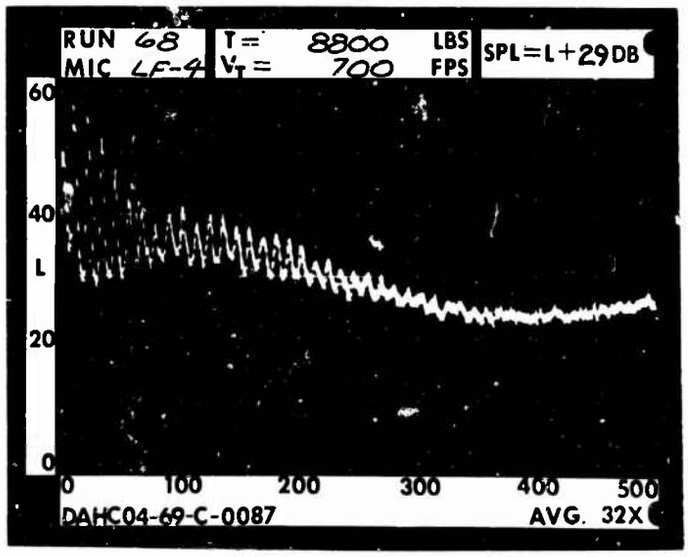

5 DIA.

RUN 69

TIP SPEED 700 FT/SEC

THRUST 8200 LB

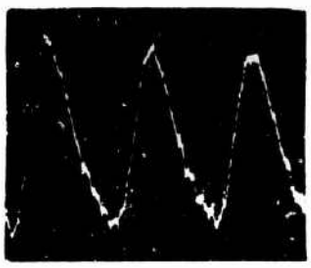

.2 RAD.

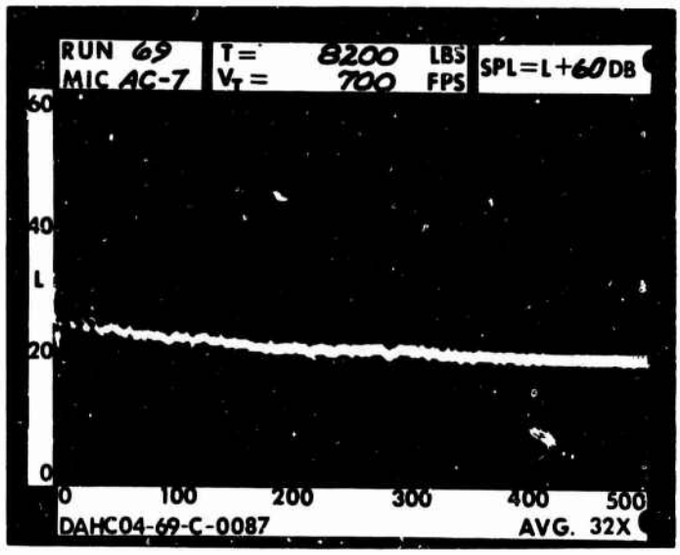

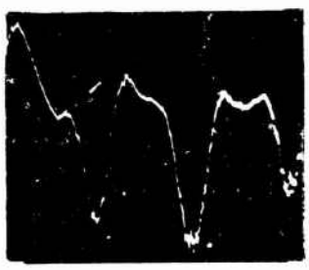

1 RAD.

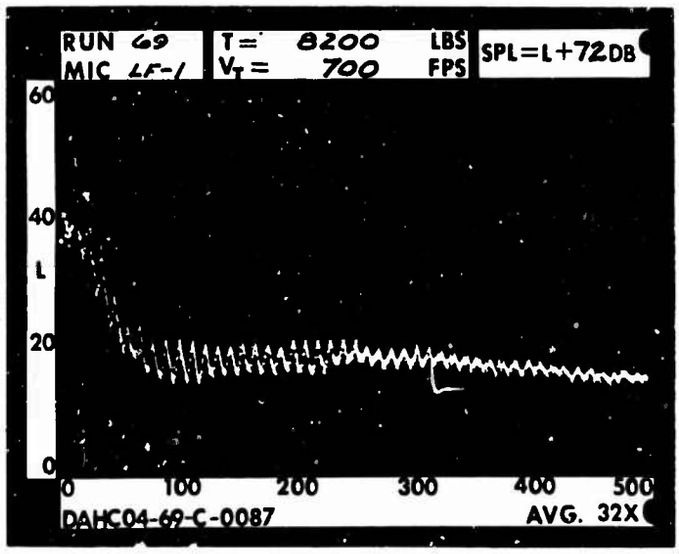

1 DIA.

3 DIA.

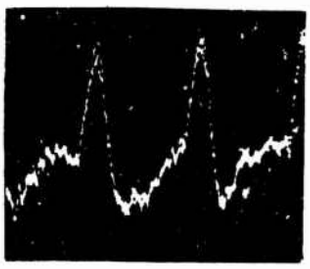

5 DIA.

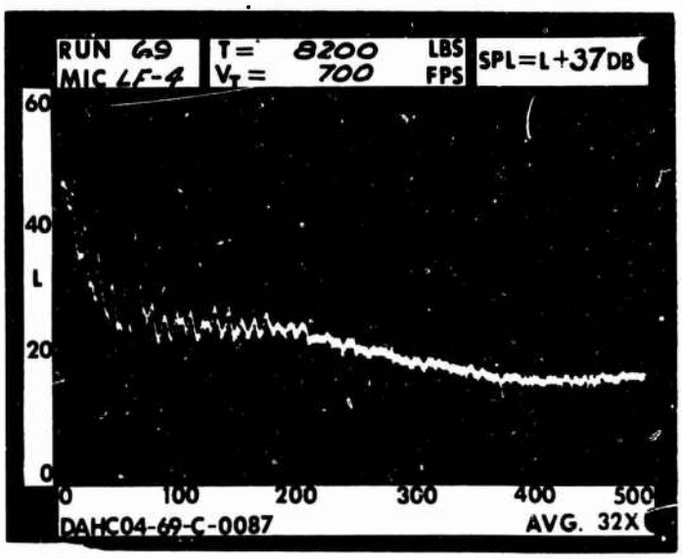

RUN 70

TIP SPEED 650 FT/SEC

THRUST 11600 LB

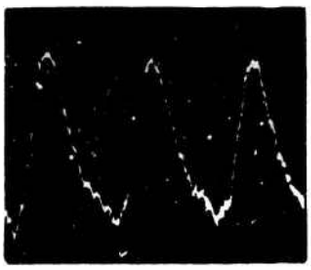

.2 RAD.

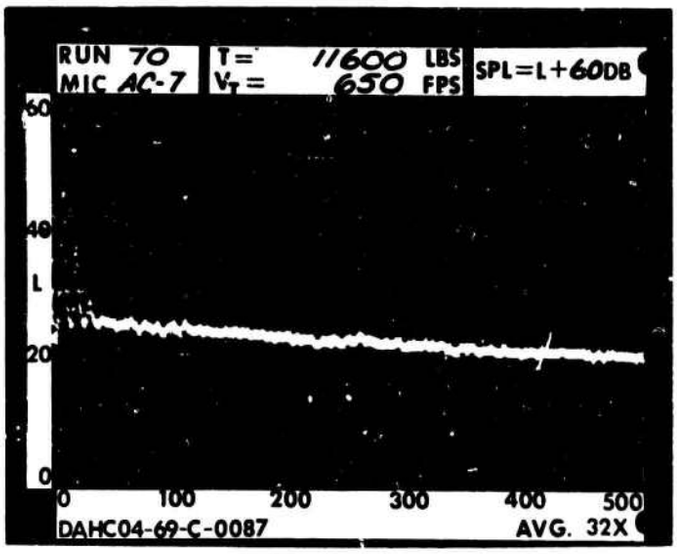

1 RAD.

1 DIA.

3 DIA.

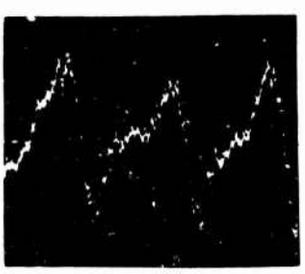

5 DIA.

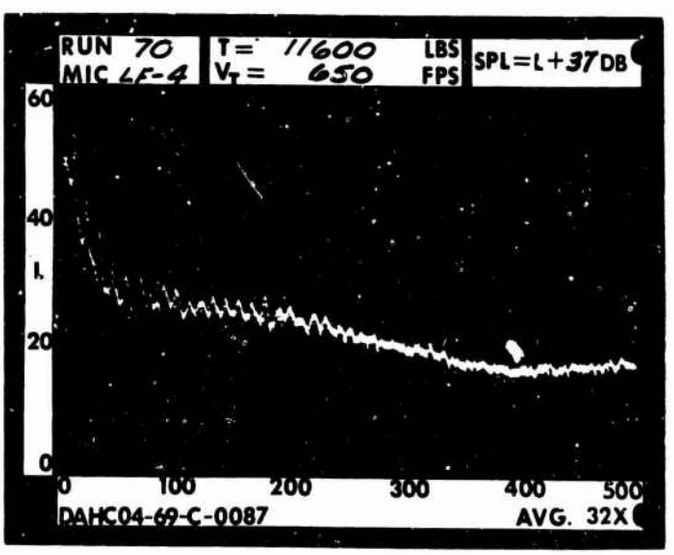

RUN 72

TIP SPEED 18100 FT/SEC

THRUST 650 LB

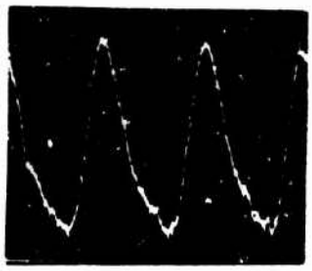

.2 RAD.

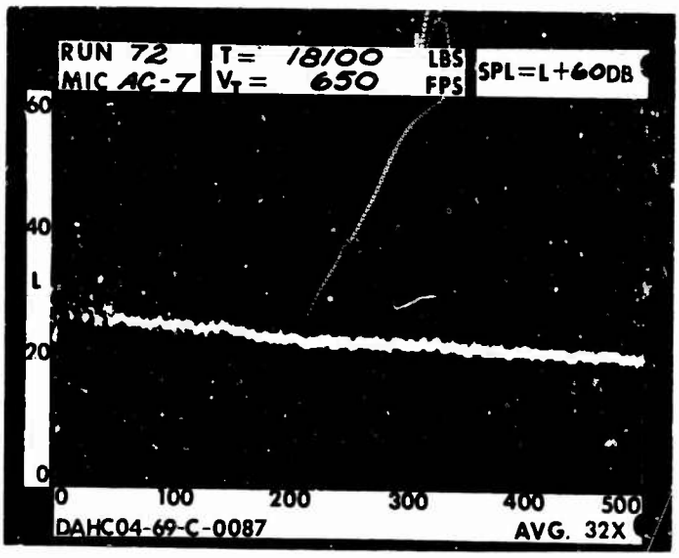

1 RAD.

1 DIA.

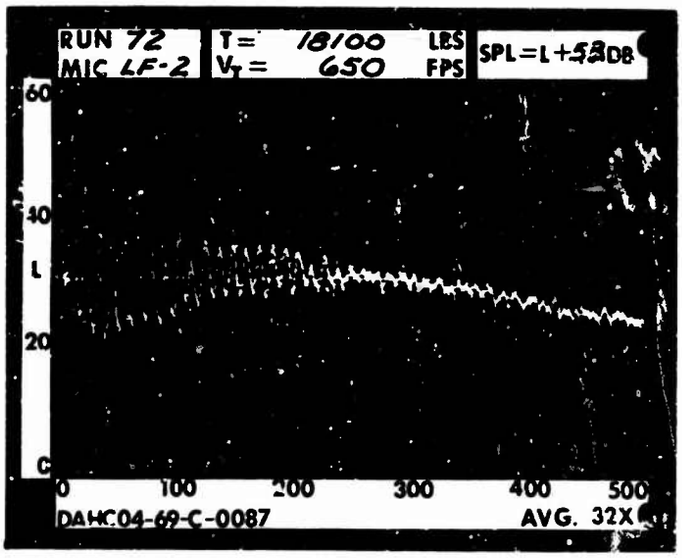

3 DIA.

5 DIA.

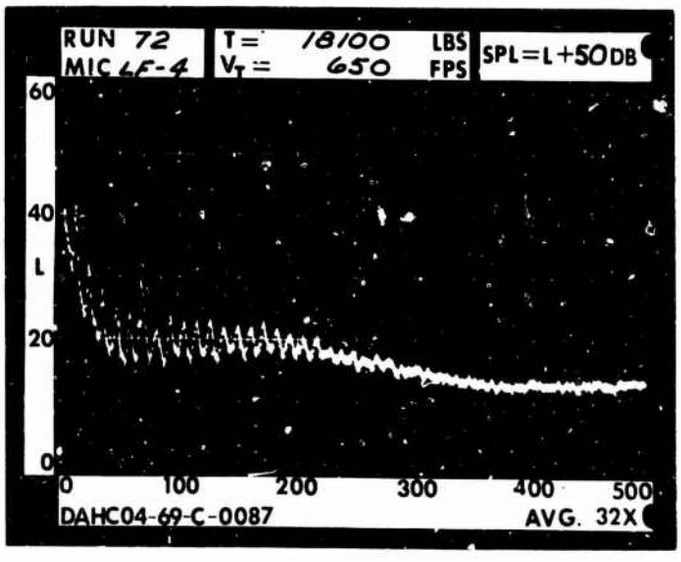

RUN 73

TIP SPEED 650 FT/SEC

THRUST 20700 LB

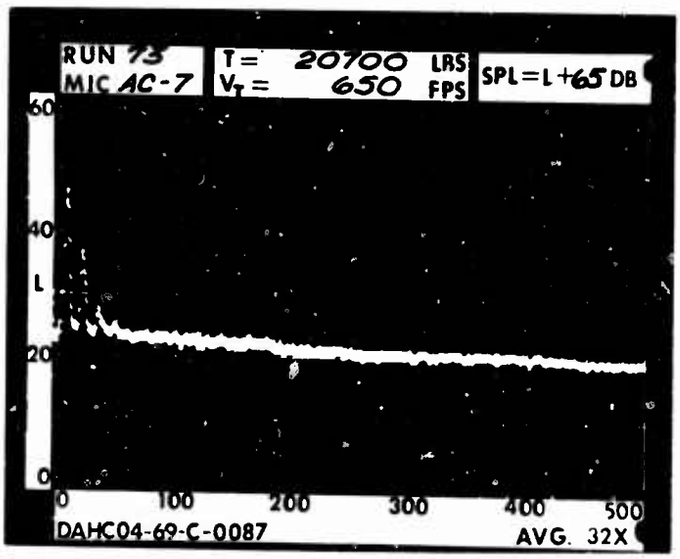

.2 RAD.

1 RAD.

1 DIA.

3 DIA.

5 DIA.

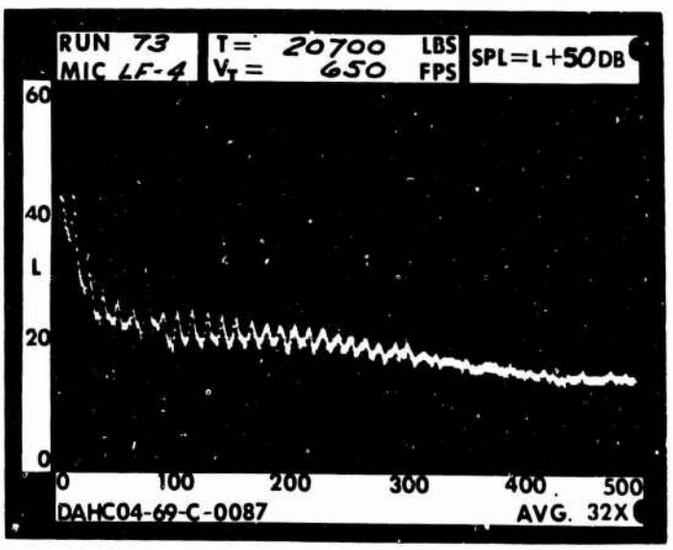

RUN 74

TIP SPEED 650 FT/SEC

THRUST 23500 LB

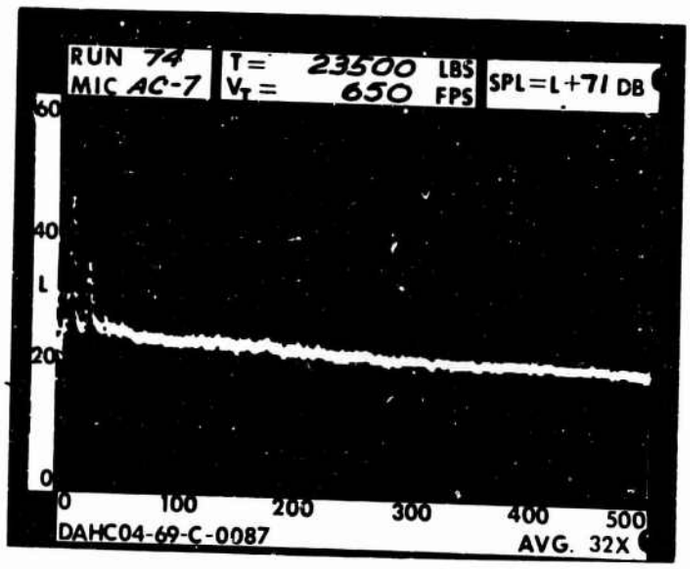

.2 RAD.

1 RAD.

1 DIA.

3 DIA.

5 DIA.

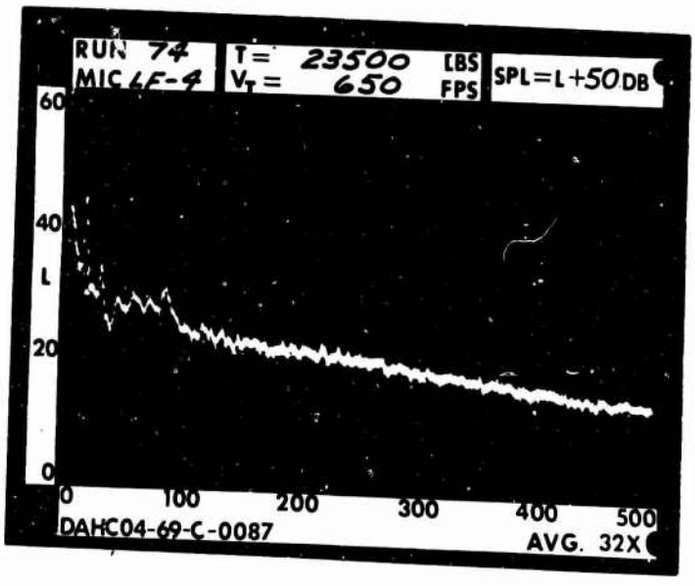

RUN 75

TIP SPEED 650 FT/SEC

THRUST 25400 LB

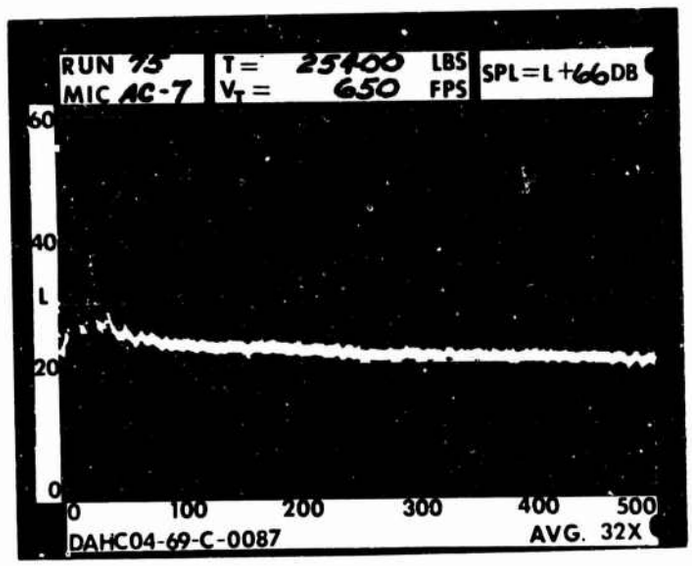

.2 RAD.

1 RAD.

1 DIA.

3 DIA.

5 DIA.

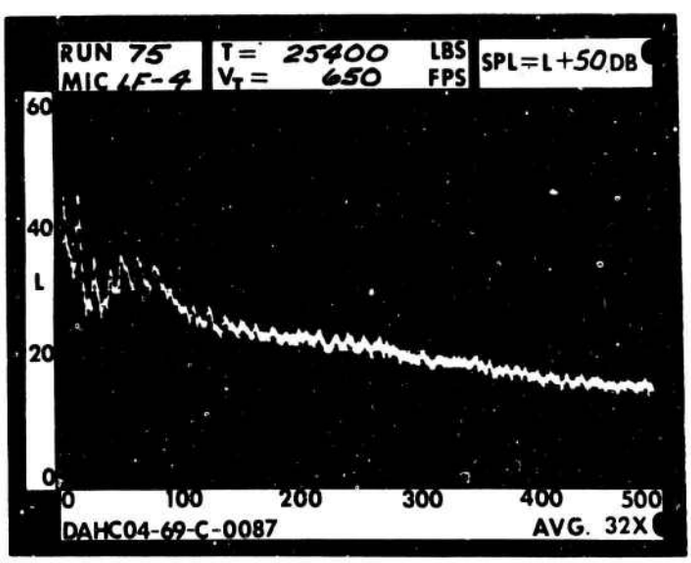

RUN 76

TIP SPEED 650 FT/SEC

THRUST 27700 LB

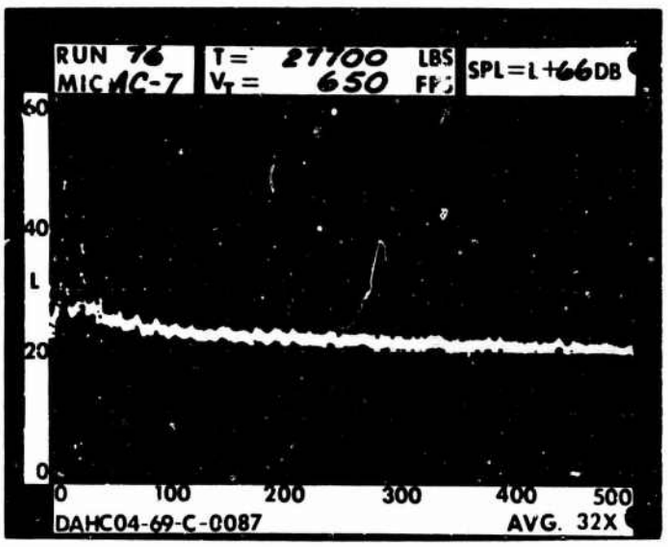

.2 RAD.

1 RAD.

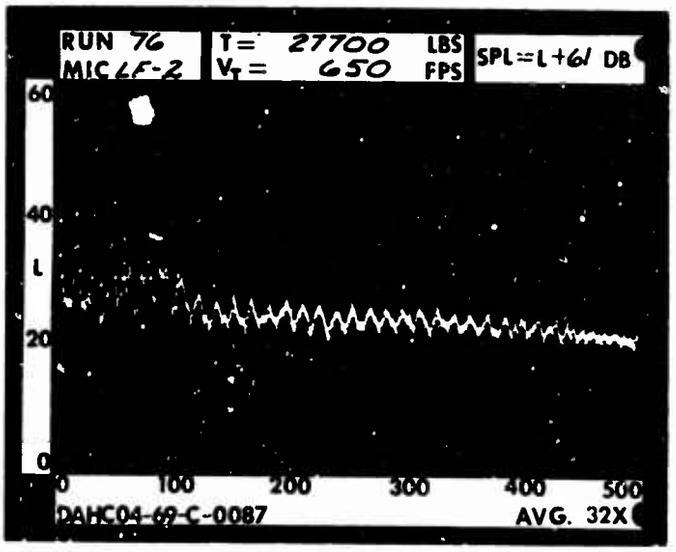

1 DIA.

3 DIA.

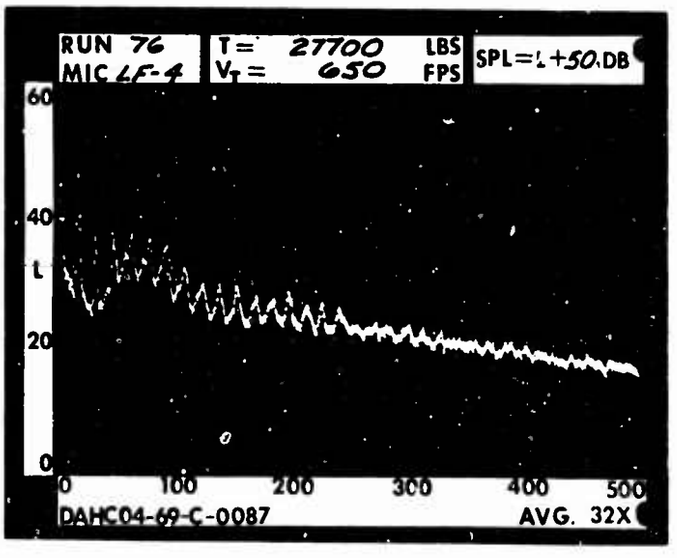

5 DIA.

RUN 77

TIP SPEED 600 FT/SEC

THRUST 9300 LB

.2 RAD.

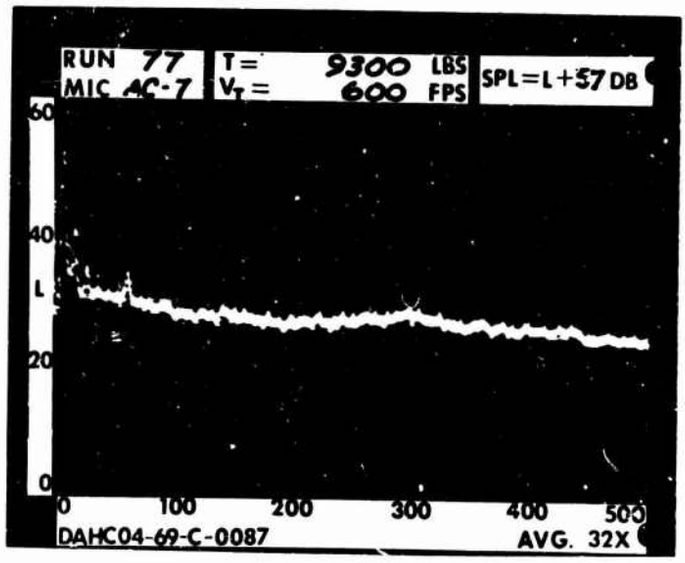

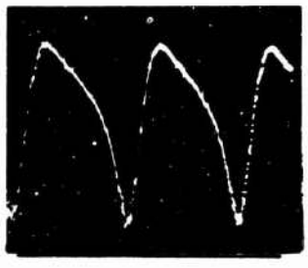

1 RAD.

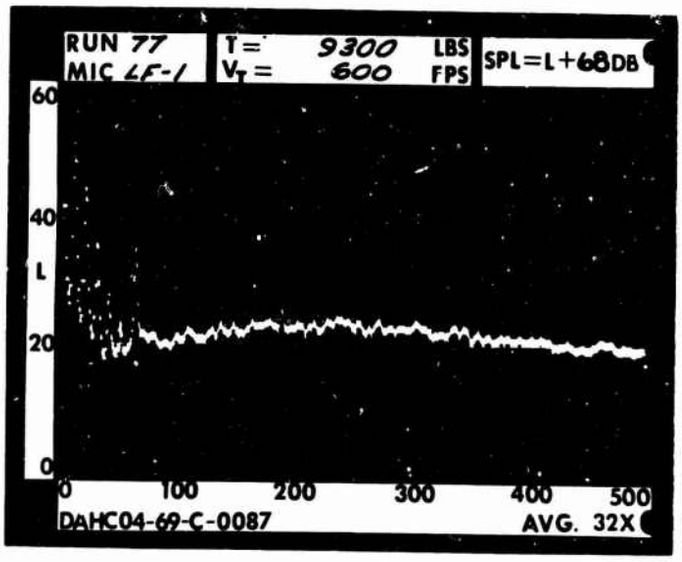

1 DIA.

3 DIA.

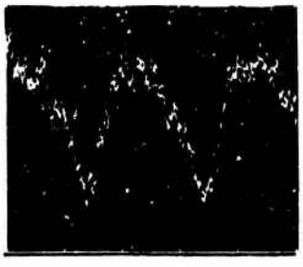

5 DIA.

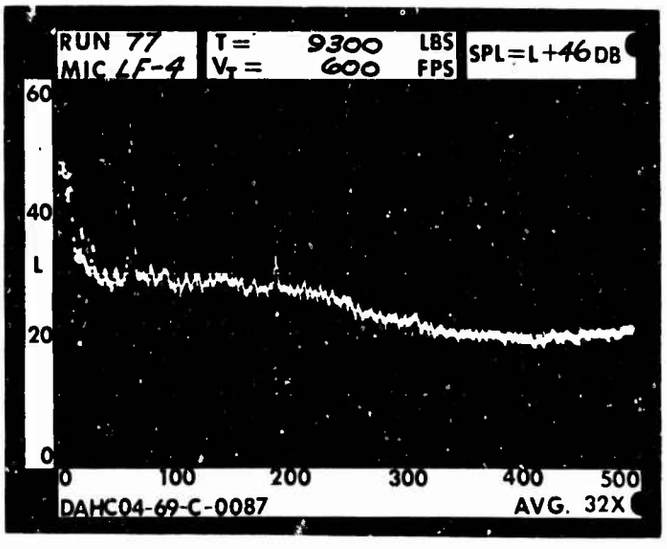

RUN 78

TIP SPEED 600 FT/SEC

THRUST 8800 LB

.2 RAD.

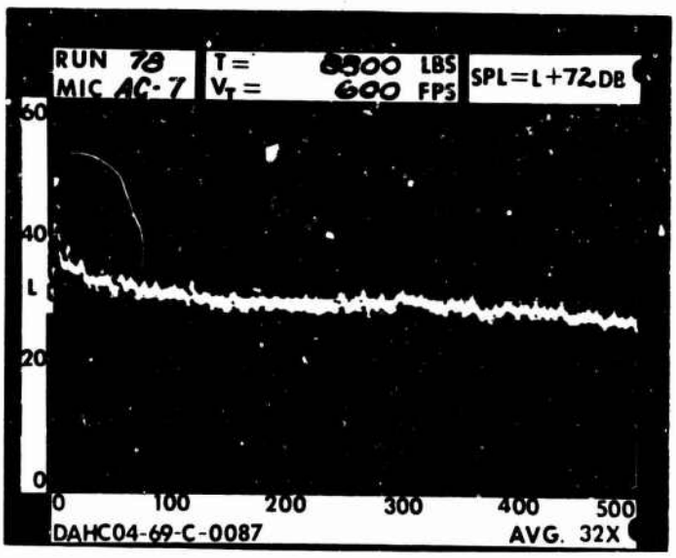

1 RAD.

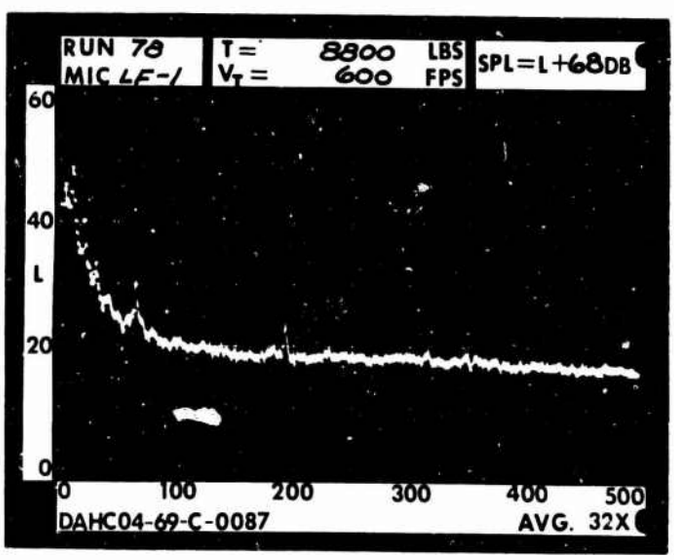

1 DIA.

3 DIA.

5 DIA.

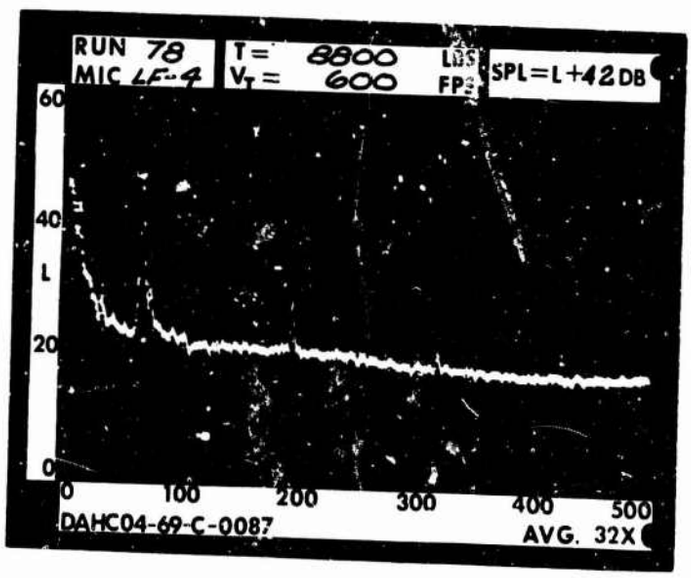

RUN 79

TIP SPEED 600 FT/SEC

THRUST 12500 LB

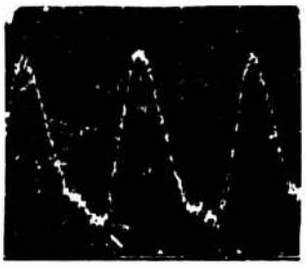

.2 RAD.

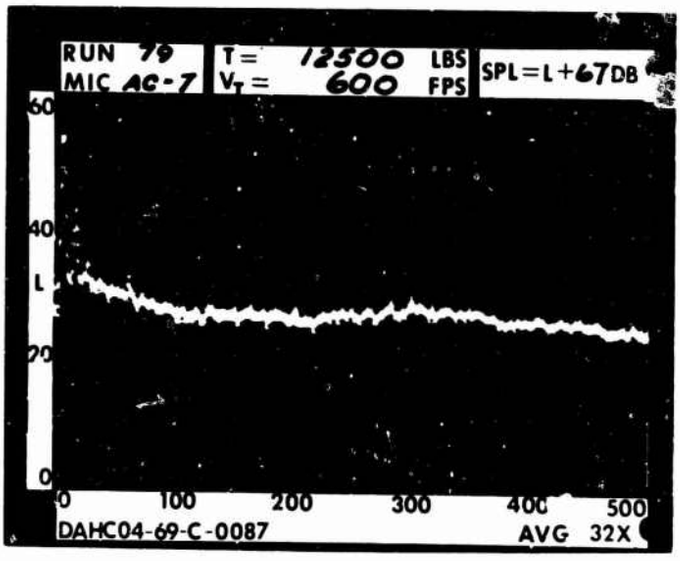

1 RAD.

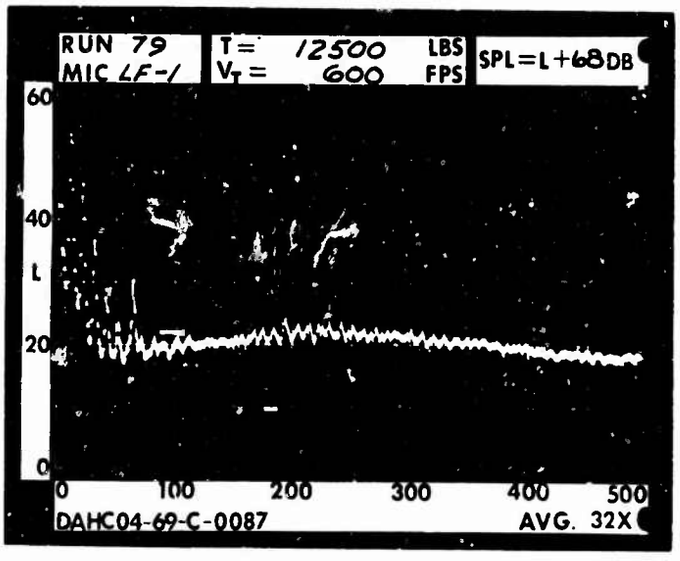

1 DIA.

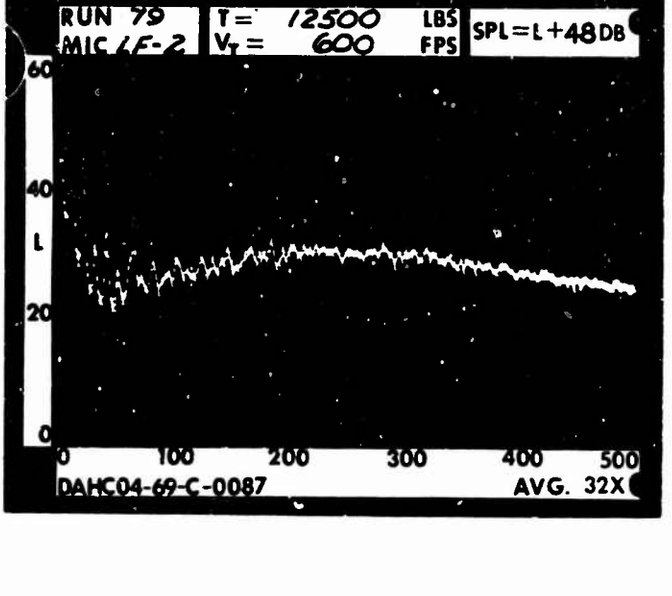

3 DIA.

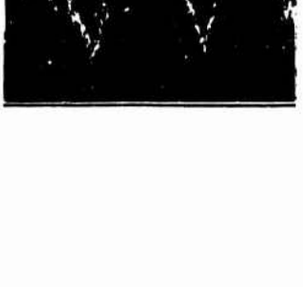

5 DIA.

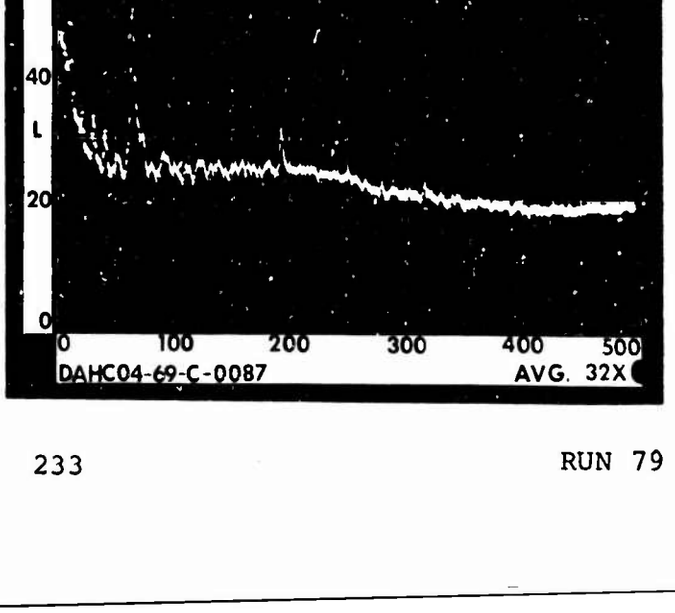

RUN 80

TIP SPEED 600 FT/SEC

THRUST 15400 LB

.2 RAD.

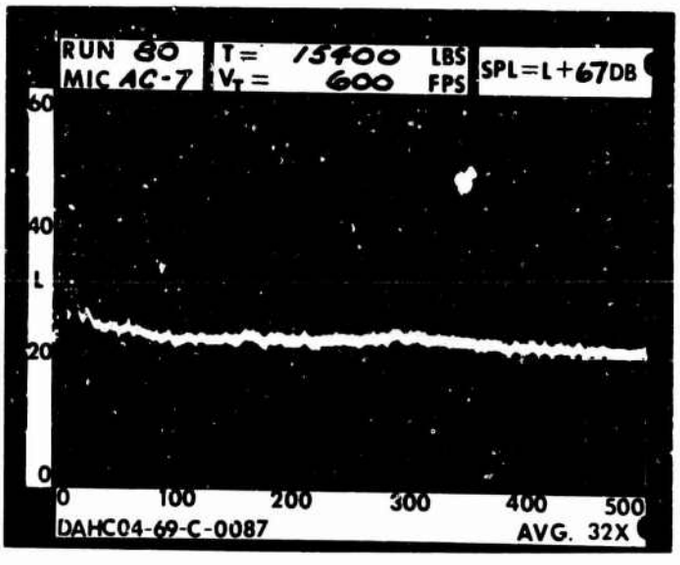

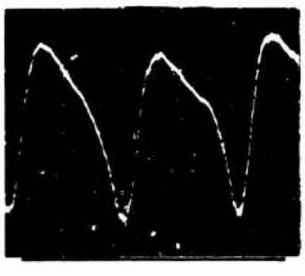

1 RAD.

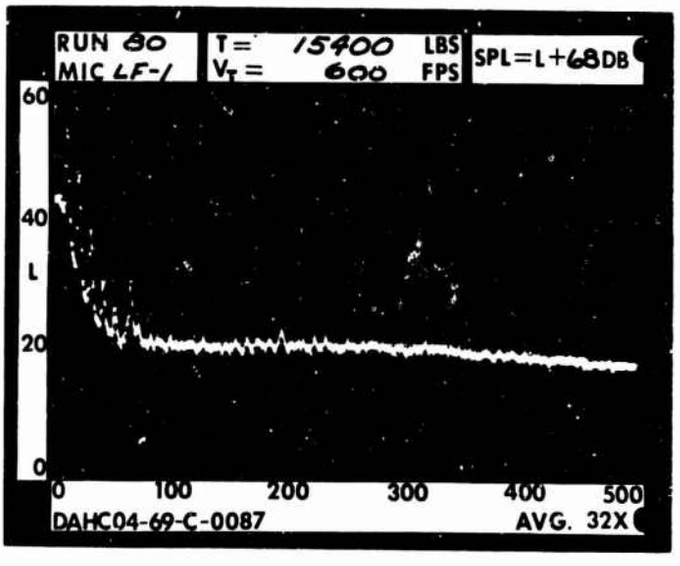

1 DIA.

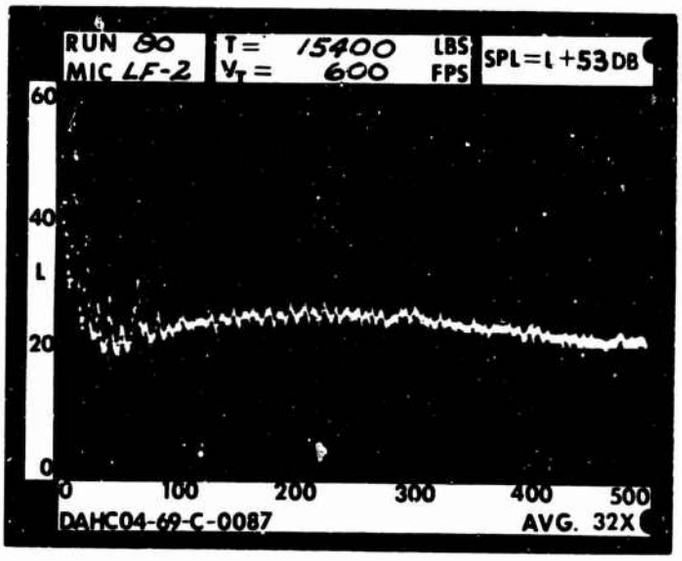

3 DIA.

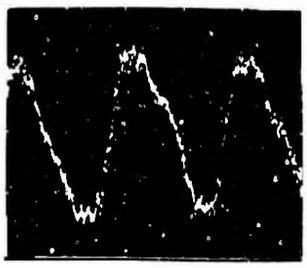

5 DIA.

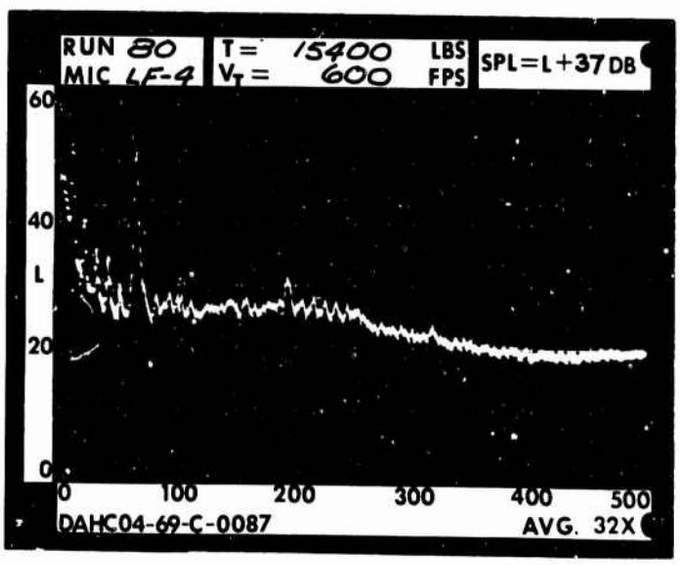

RUN 81

TIP SPEED 600 FT/SEC

THRUST 15400 LB

.2 RAD.

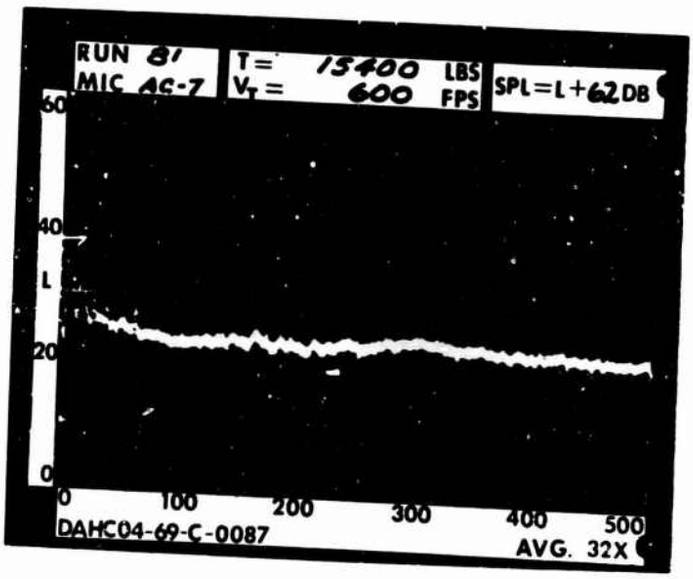

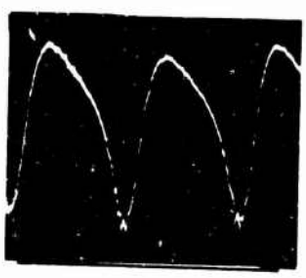

1 RAD.

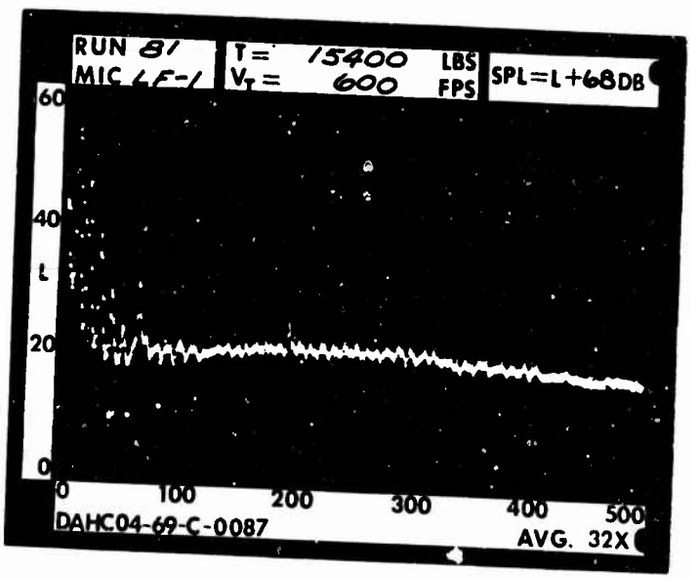

1 DIA.

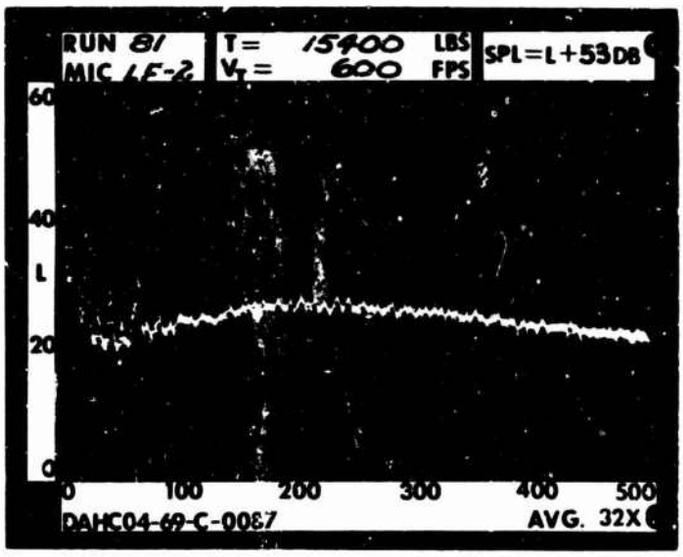

3 DIA.

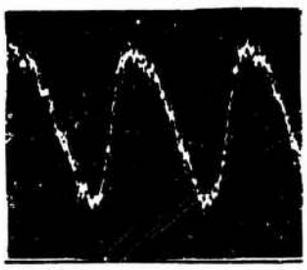

5 DIA.

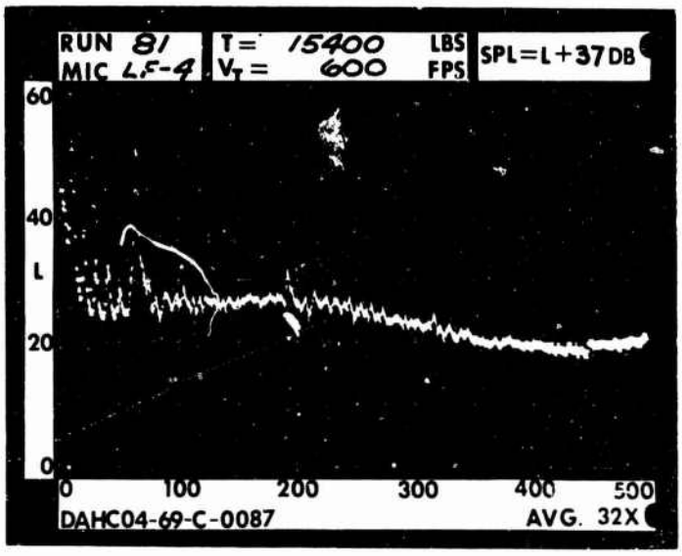

RUN 82

TIP SPEED 600 FT/SEC

THRUST 18400 LB

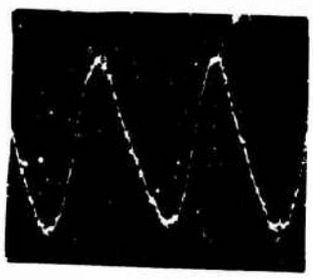

.2 RAD.

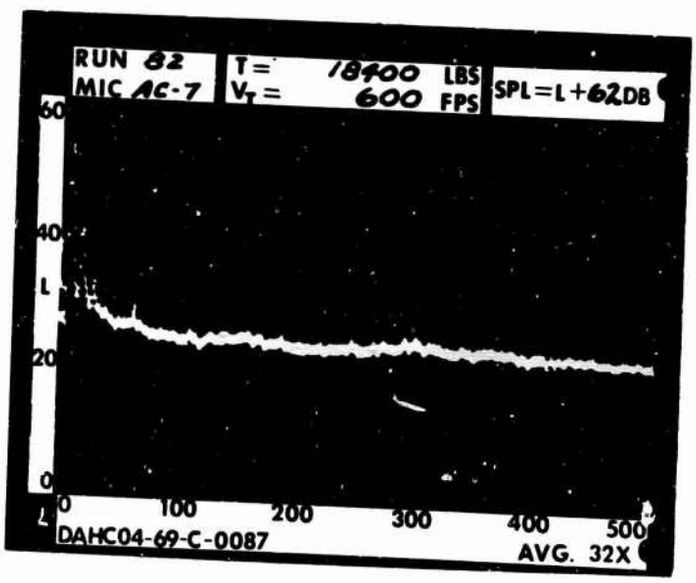

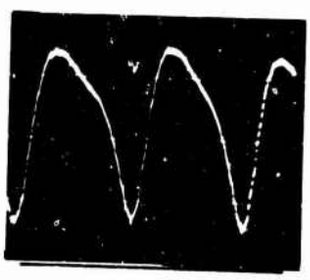

1 RAD.

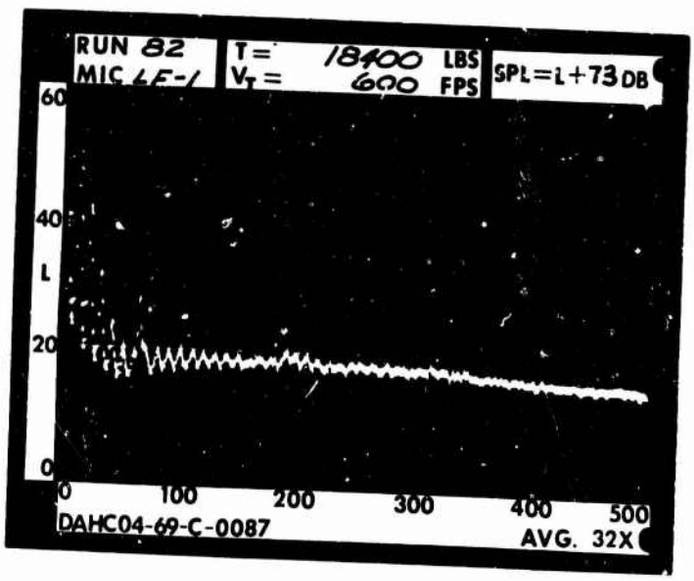

1 DIA.

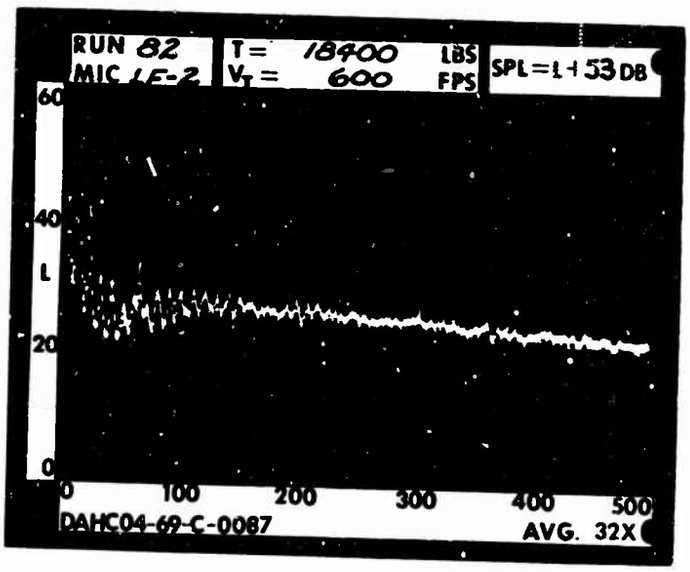

3 DIA.

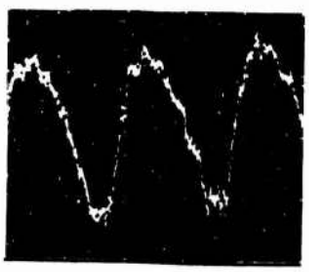

5 DIA.

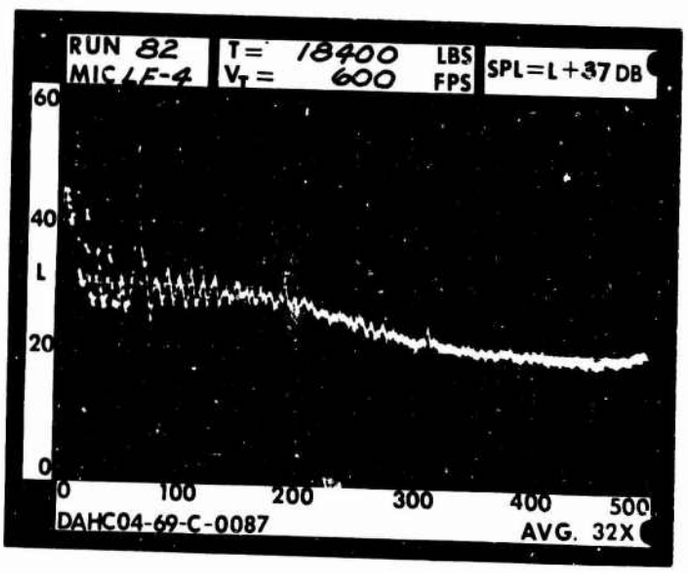

RUN 83

TIP SPEED 600 FT/SEC

THRUST 21500 LB

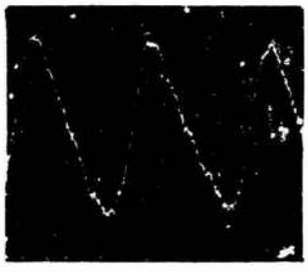

.2 RAD.

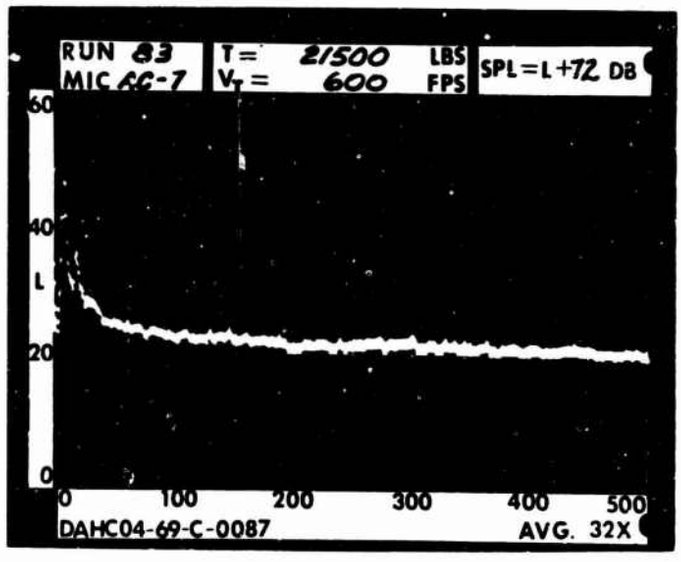

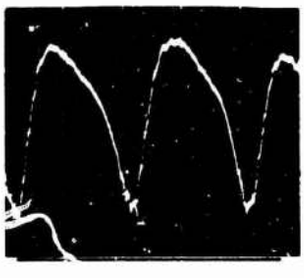

1 RAD.

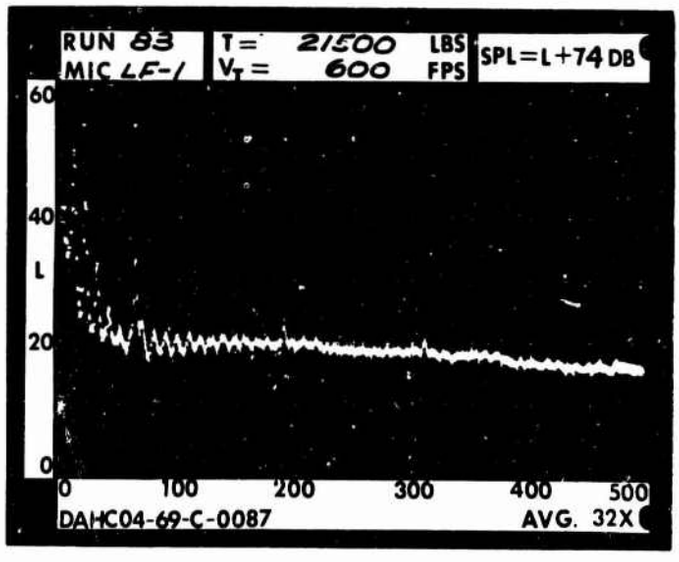

1 DIA.

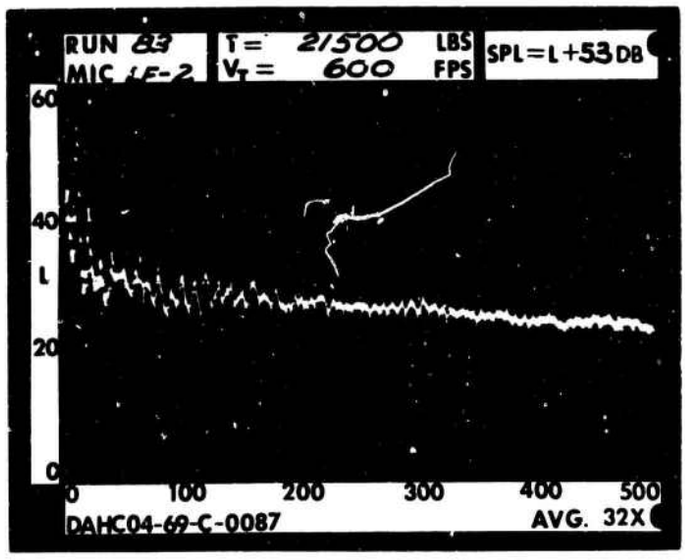

3 DIA.

5 DIA.

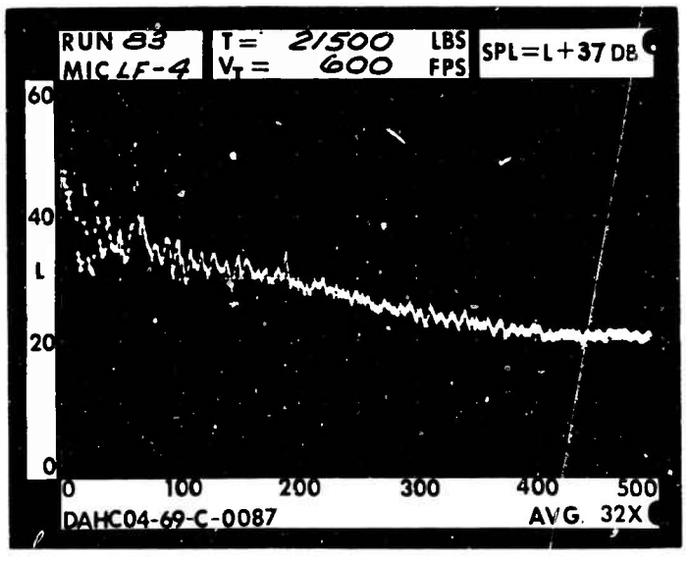

RUN 84

TIP SPEED 600 FT/SEC

THRUST 23200 LB

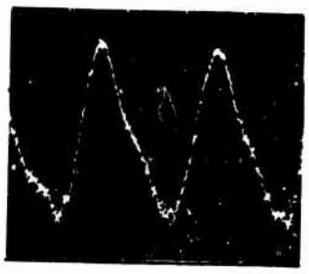

.2 RAD.

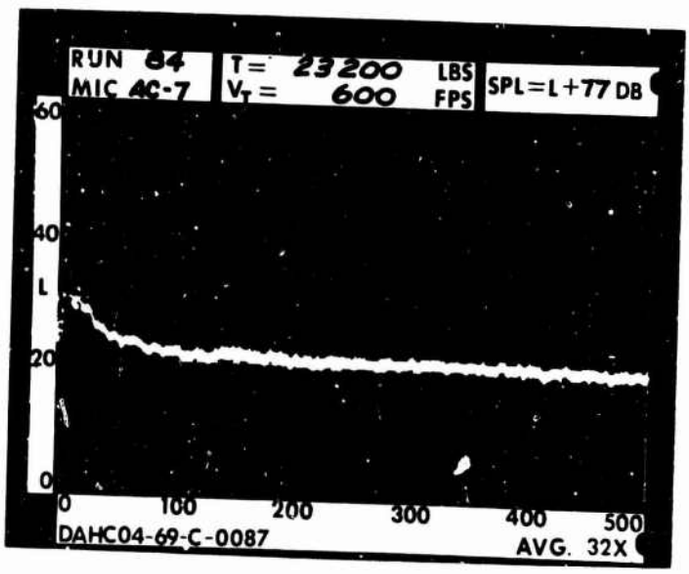

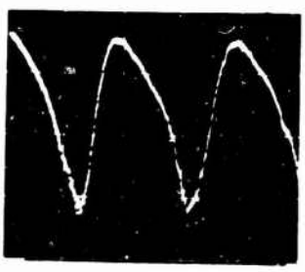

1 RAD.

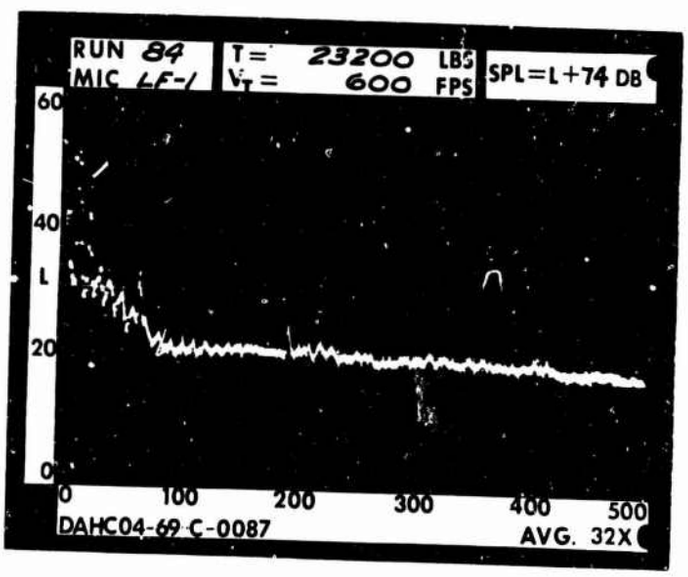

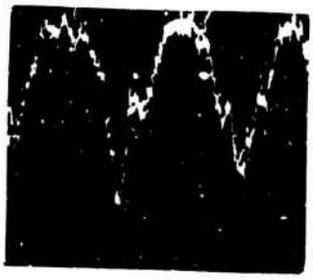

1 DIA.

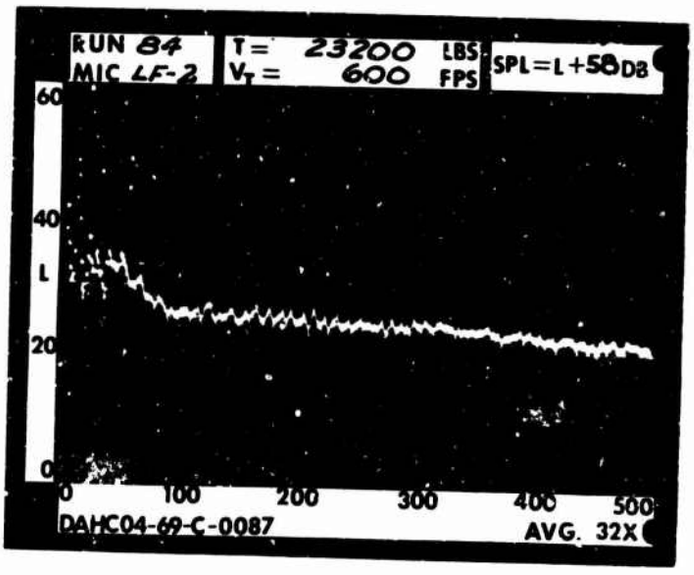

3 DIA.

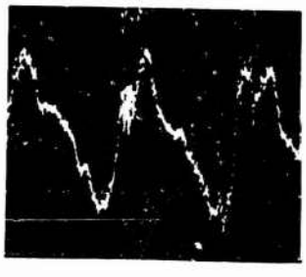

5 DIA.

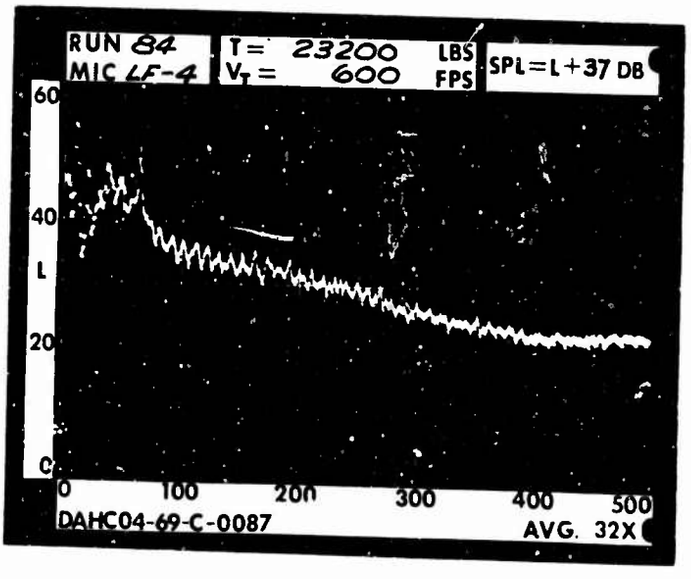

RUN 85

TIP SPEED 600 FT/SEC

THRUST 24900 LB

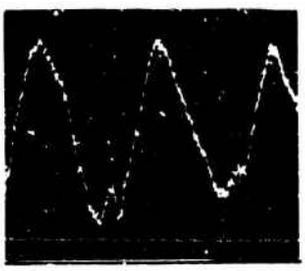

.2 RAD.

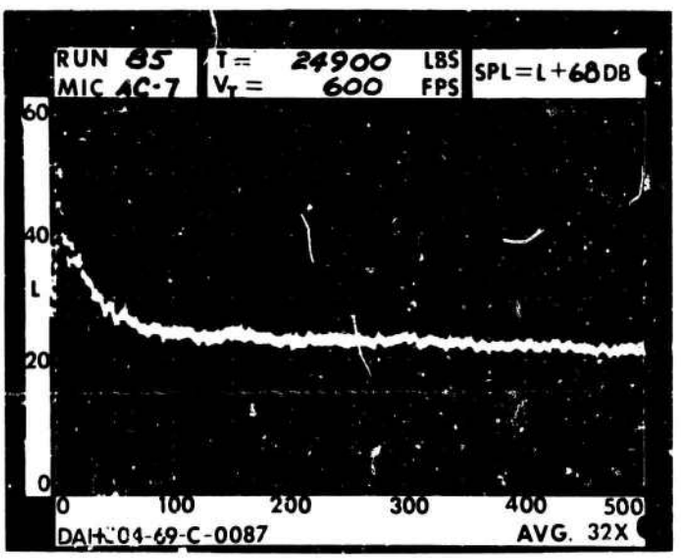

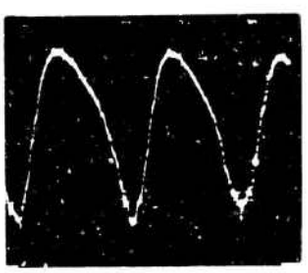

1 RAD.

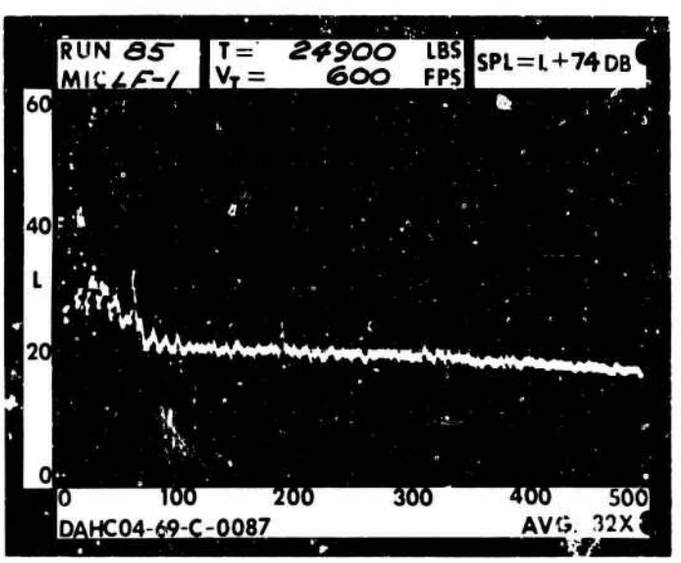

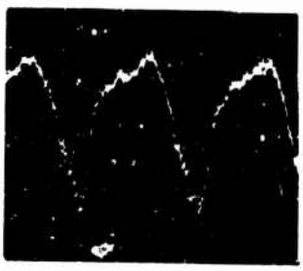

1 DIA.

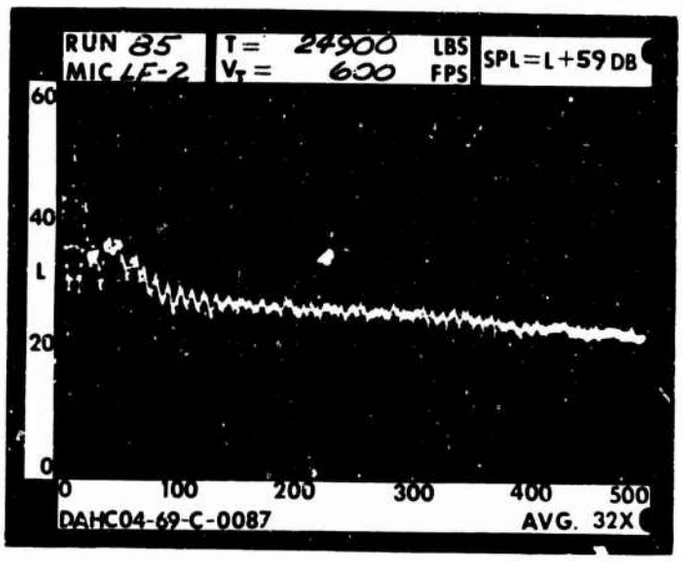

3 DIA.

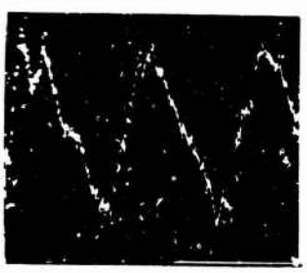

5 DIA.

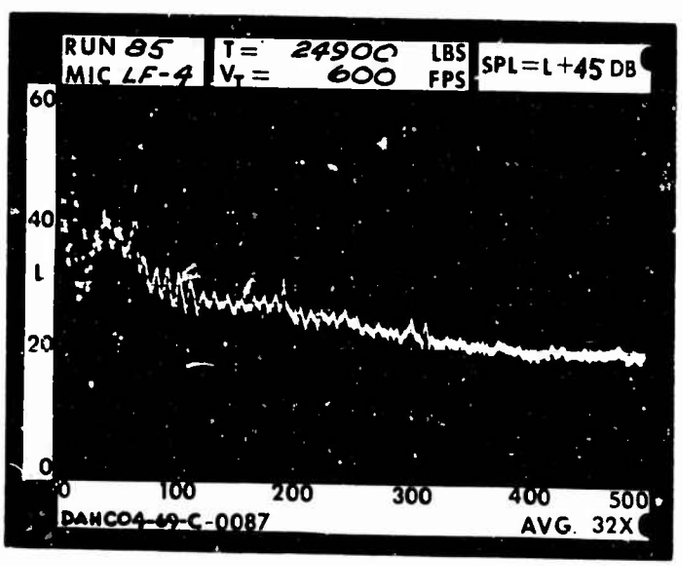

RUN 86

TIP SPEED 600 FT/SEC

THRUST 24600 LB

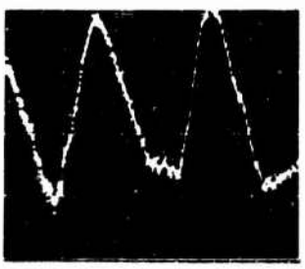

.2 RAD.

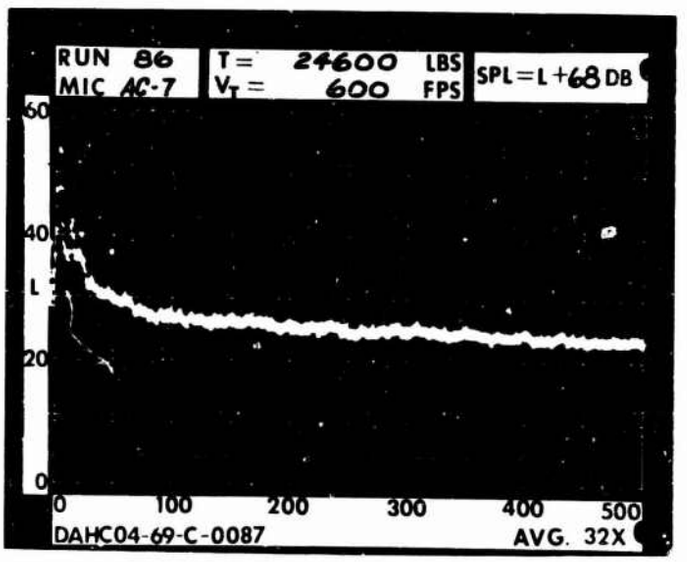

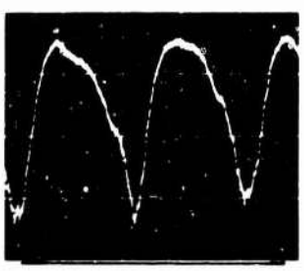

1 RAD.

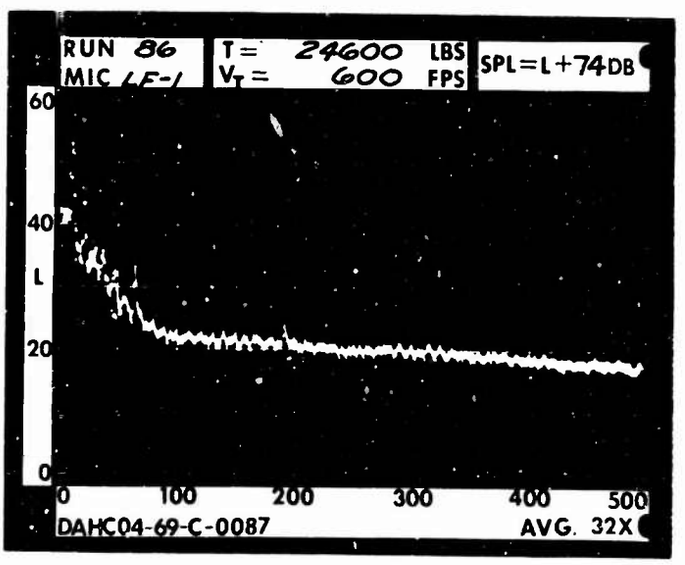

1 DIA.

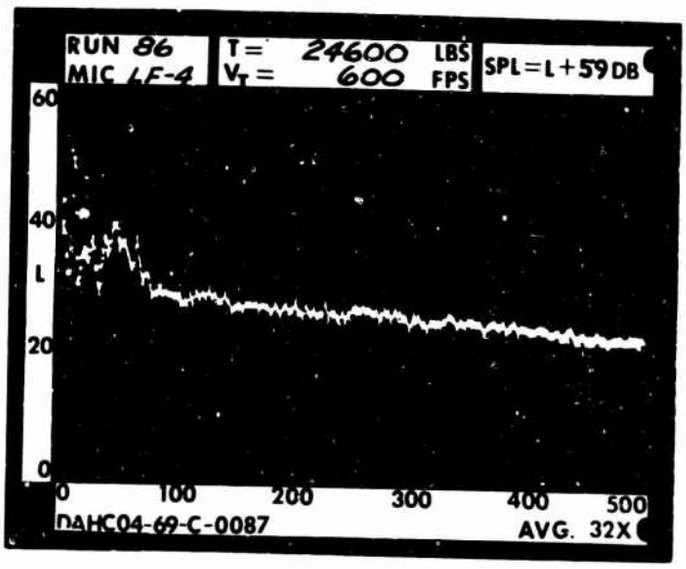

3 DIA.

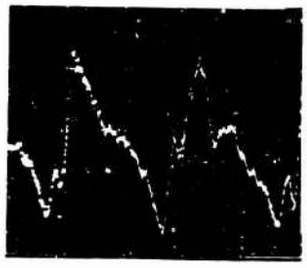

5 DIA.

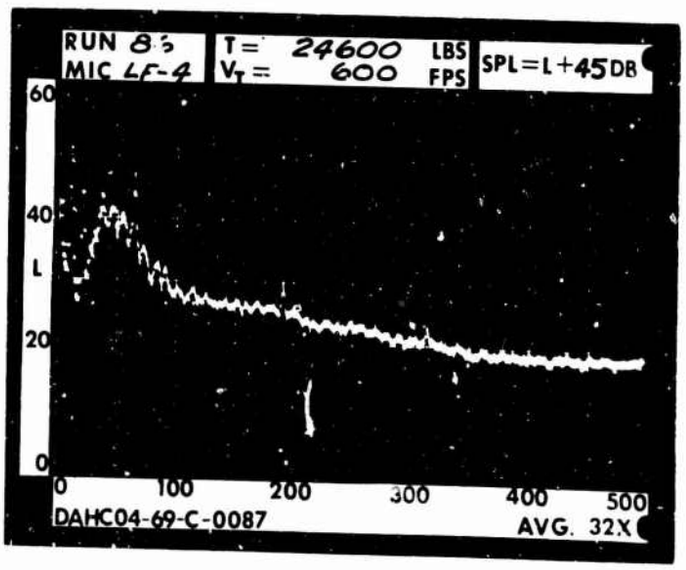

RUN 87

TIP SPEED 600 FT/SEC

THRUST 24600 LB

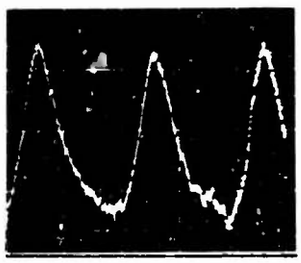

.2 RAD.

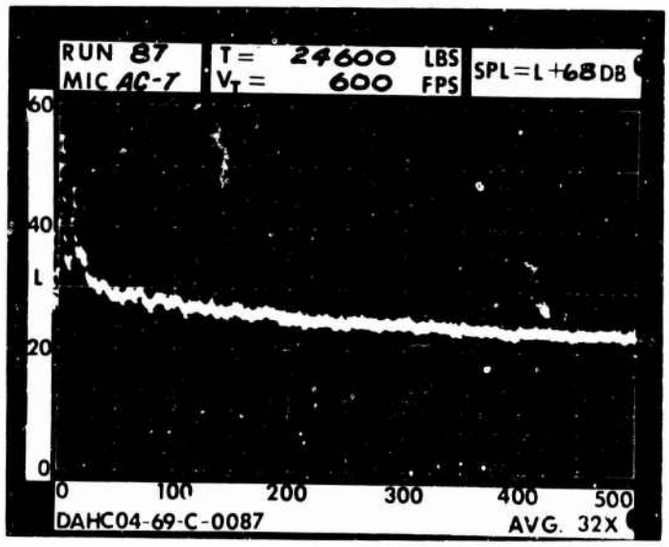

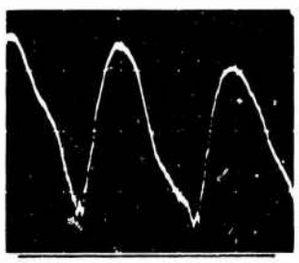

1 RAD.

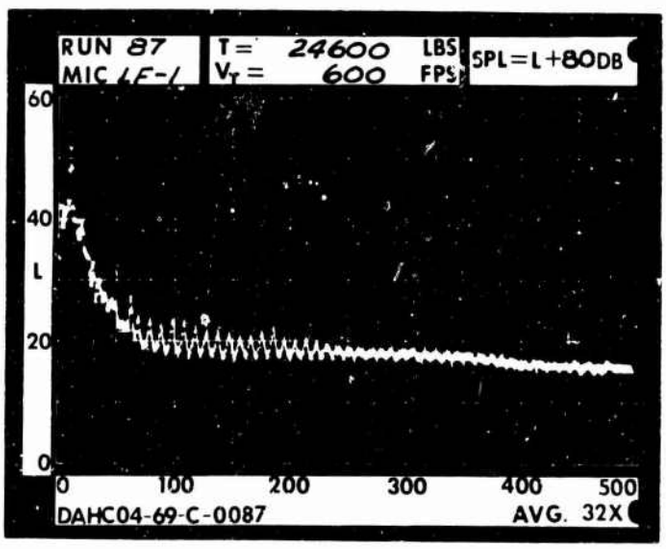

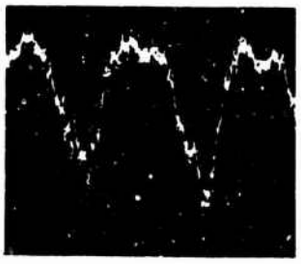

1 DIA.

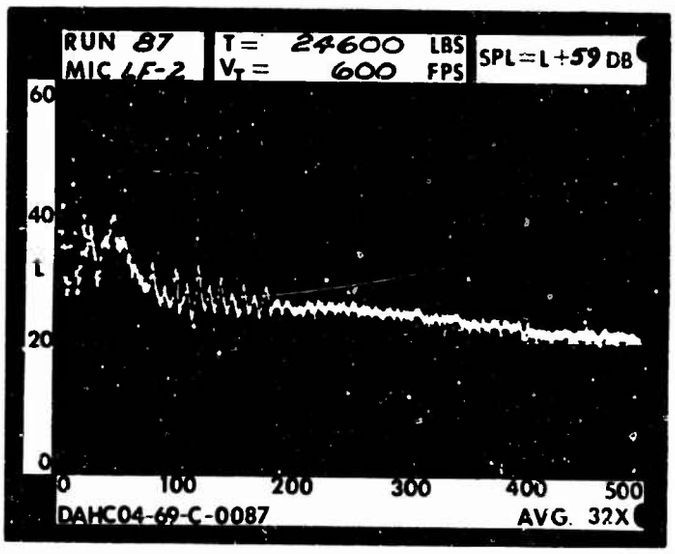

3 DIA.

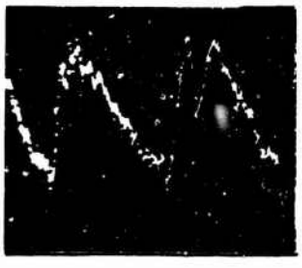

5 DIA.

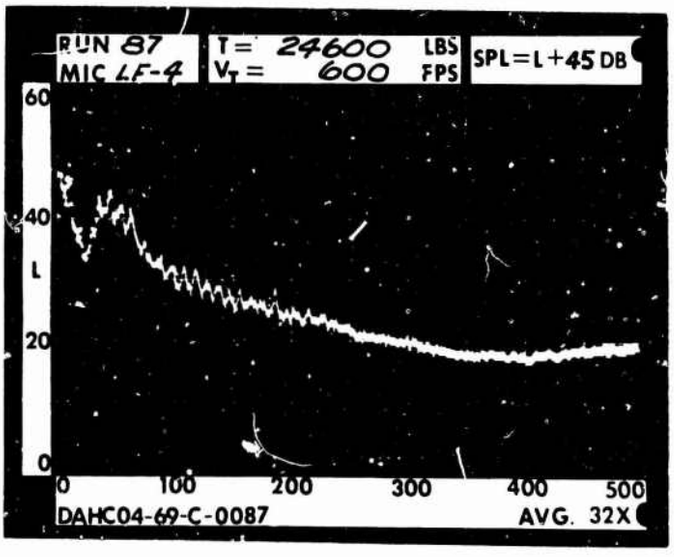

RUN 88

TIP SPEED 700 FT/SEC

THRUST 26600 LB

.2 RAD.

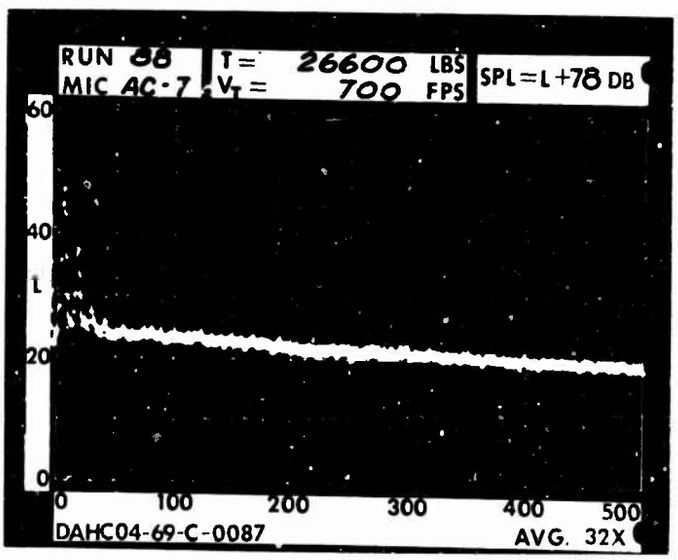

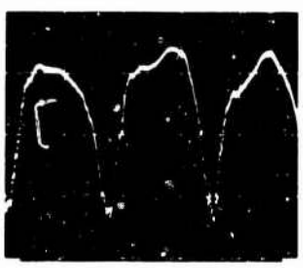

1 RAD.

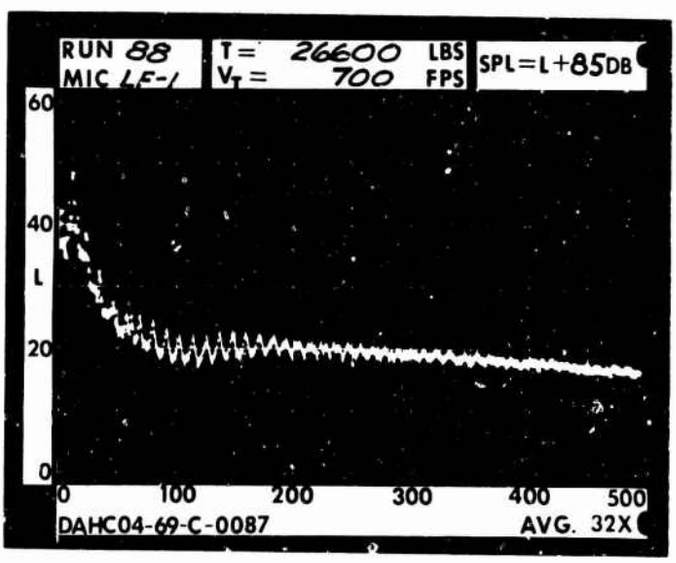

1 DIA.

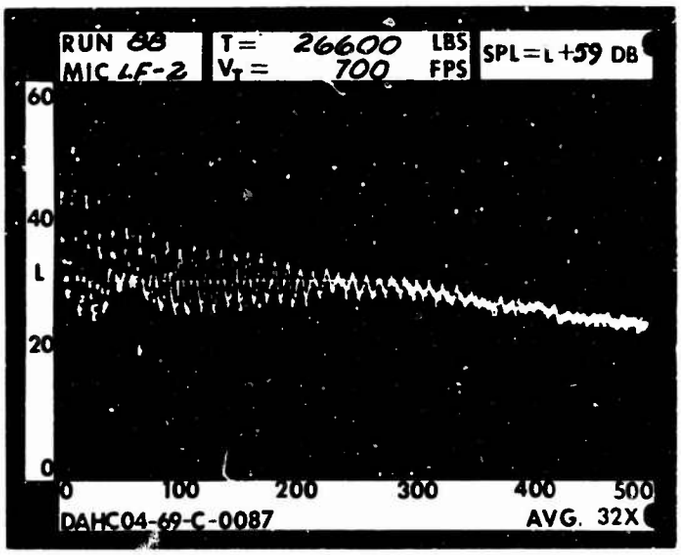

3 DIA.

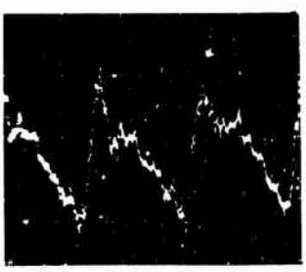

5 DIA.

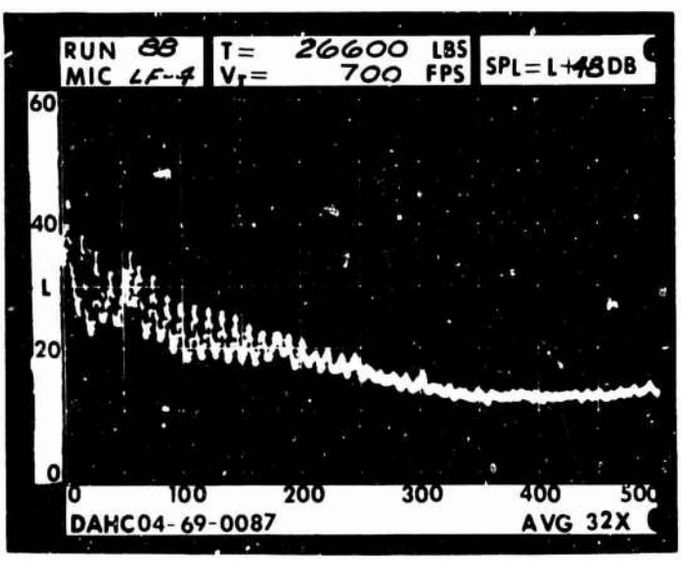

RUN 89

TIP SPEED 600 FT/SEC

THRUST 24700 LB

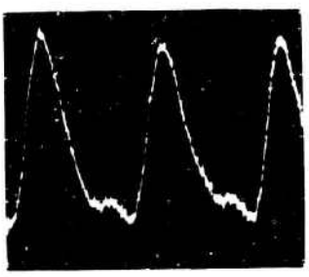

.2 RAD.

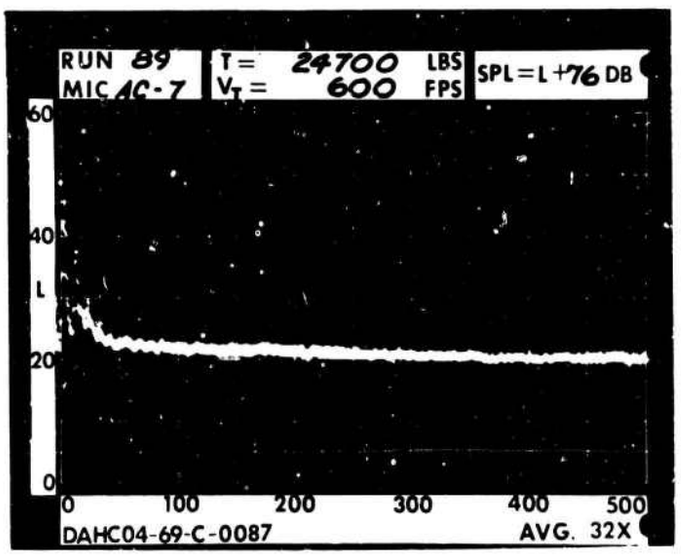

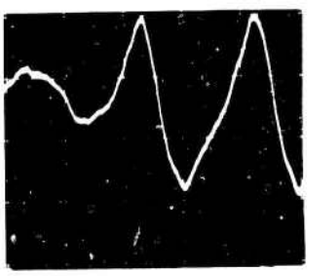

1 RAD.

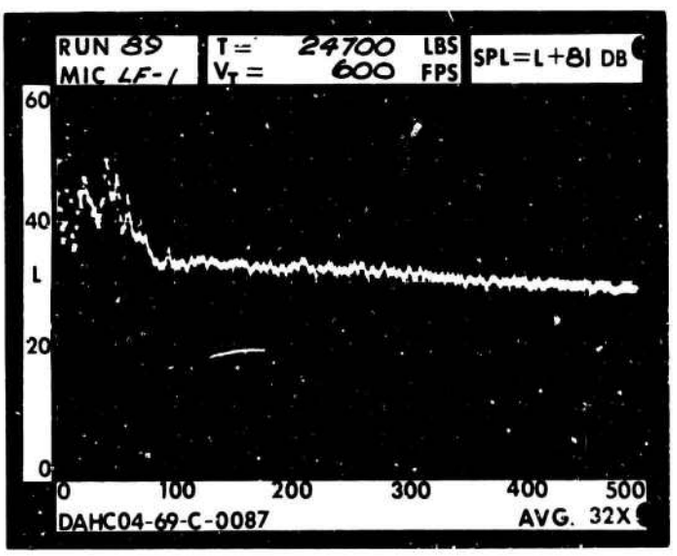

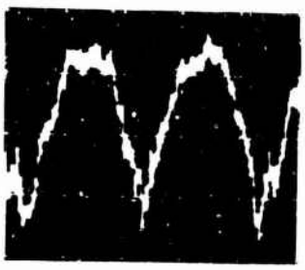

1 DIA.

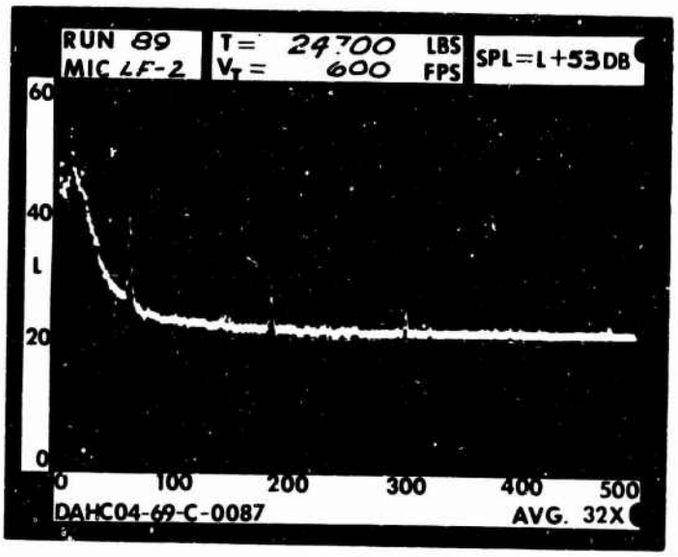

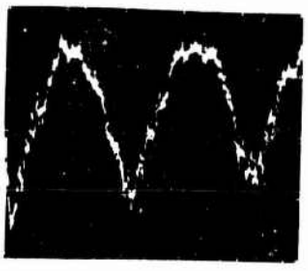

3 DIA.

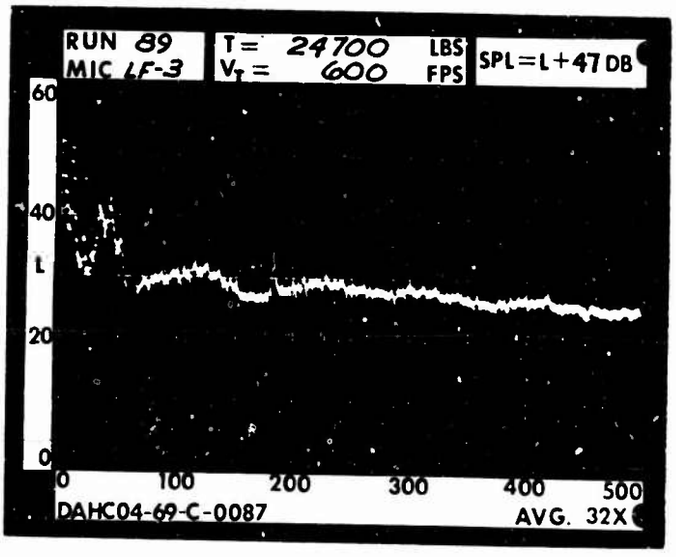

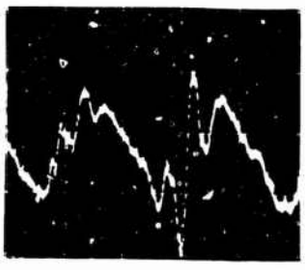

5 DIA.

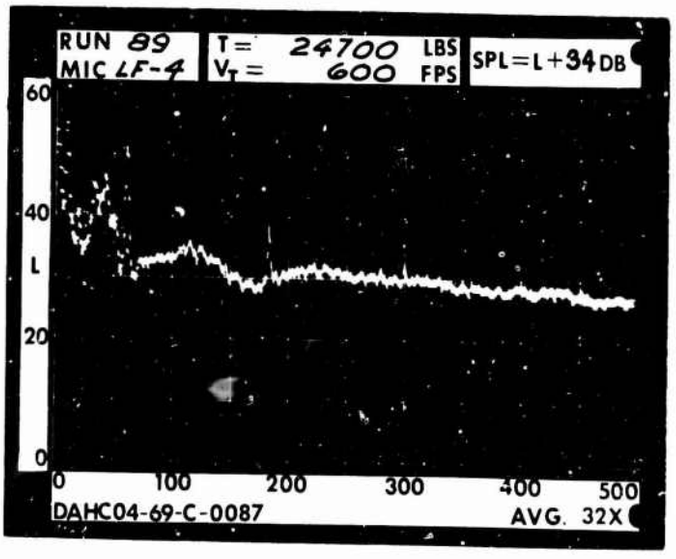

RUN 90

TIP SPEED 700 FT/SEC

THRUST 25200 LB

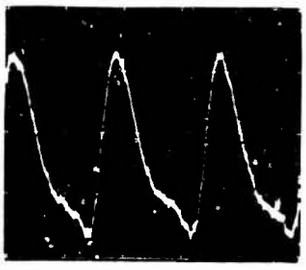

.2 RAD.

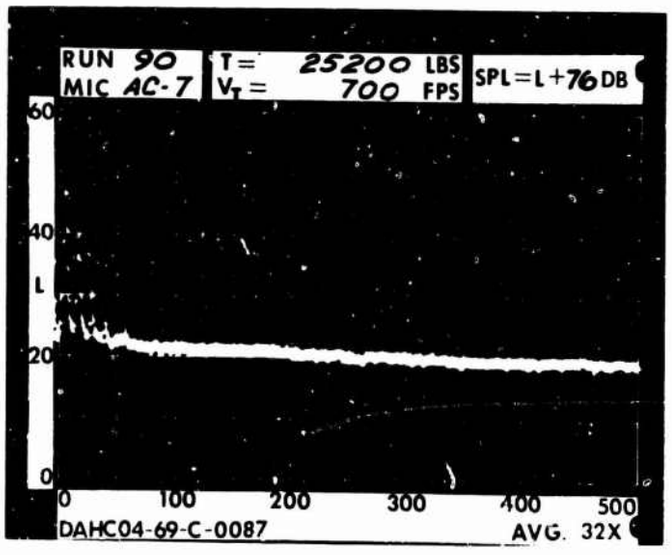

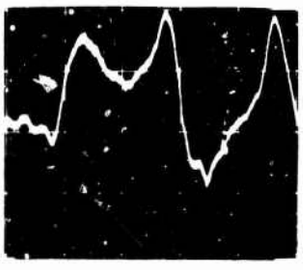

1 RAD.

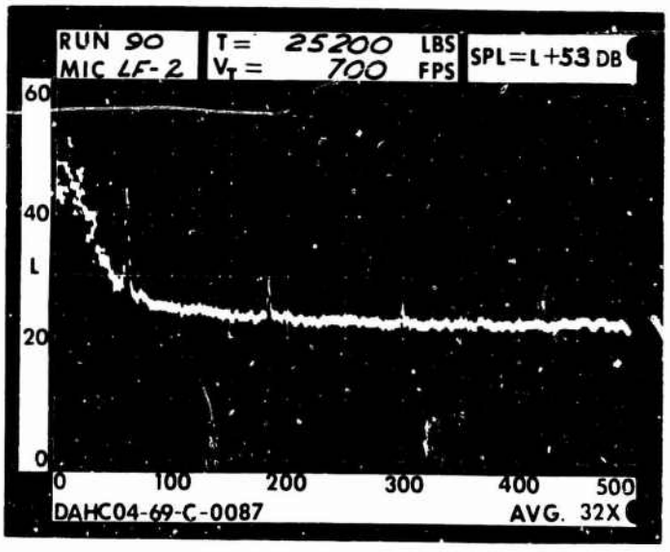

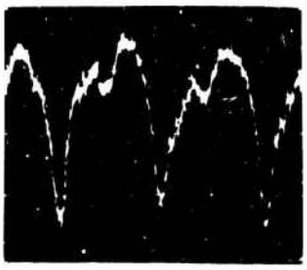

1 DIA.

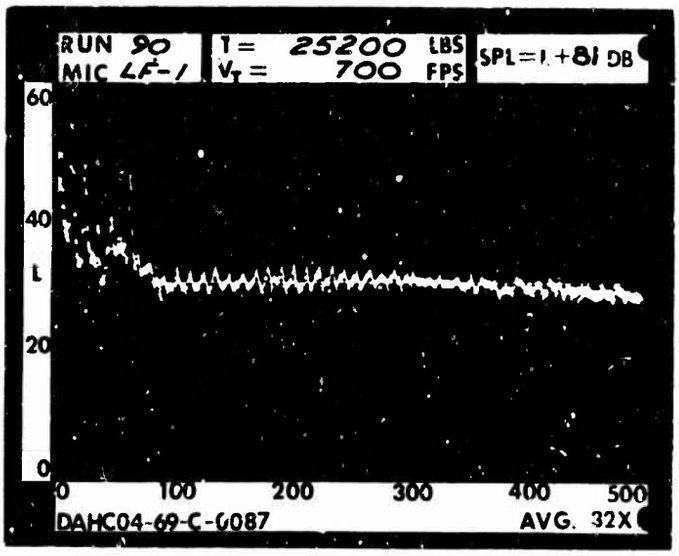

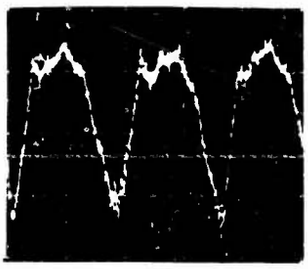

3 DIA.

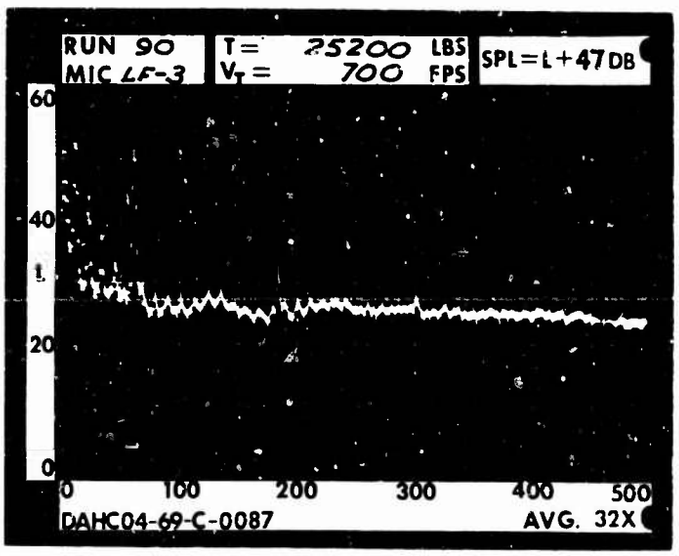

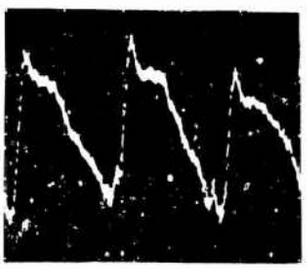

5 DIA.

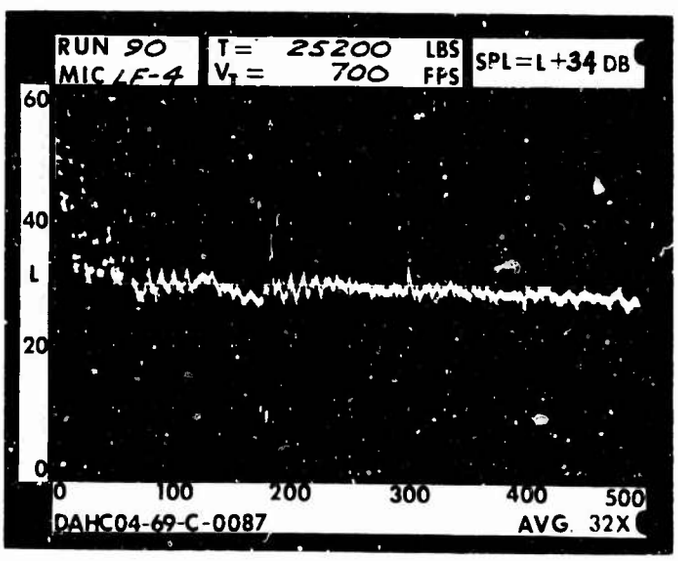

RUN 91

TIP SPEED 700 FT/SEC

THRUST 9000 LB

.2 RAD.

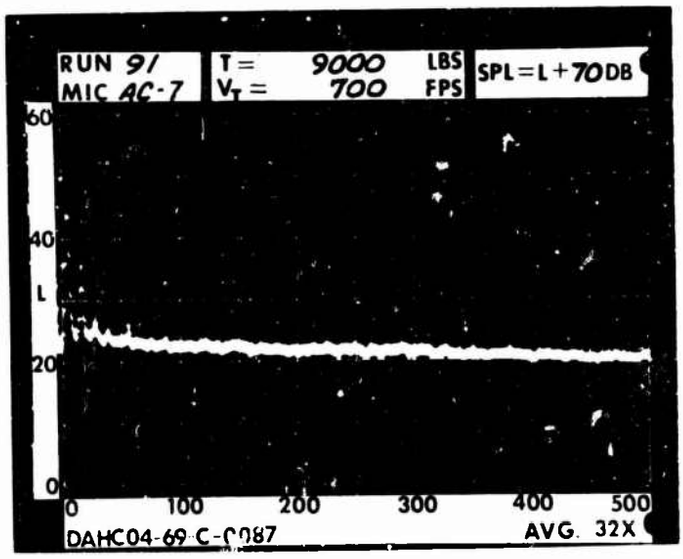

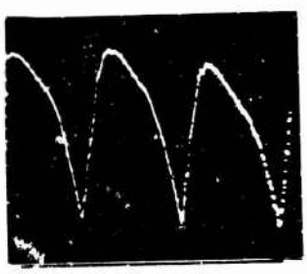

1 RAD.

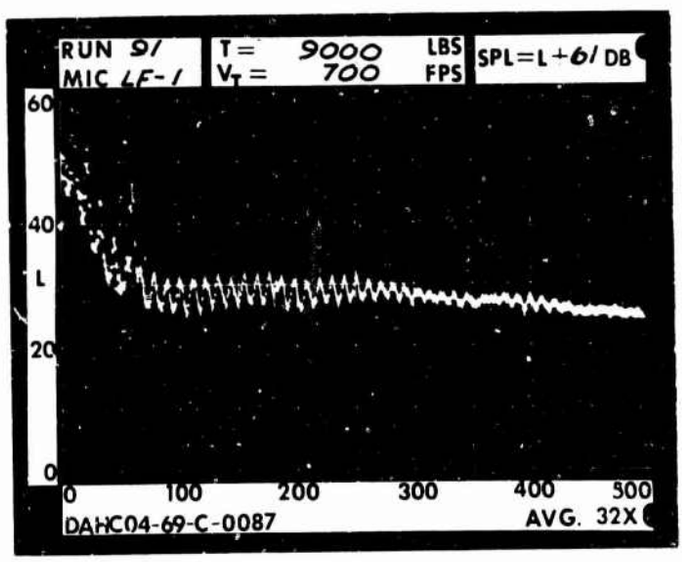

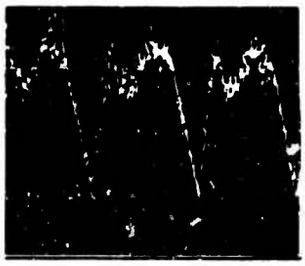

1 DIA.

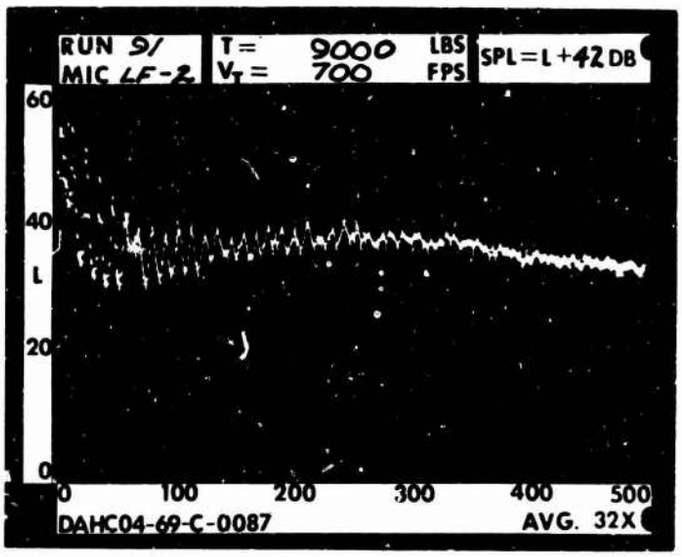

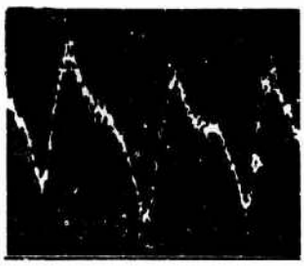

3 DIA.

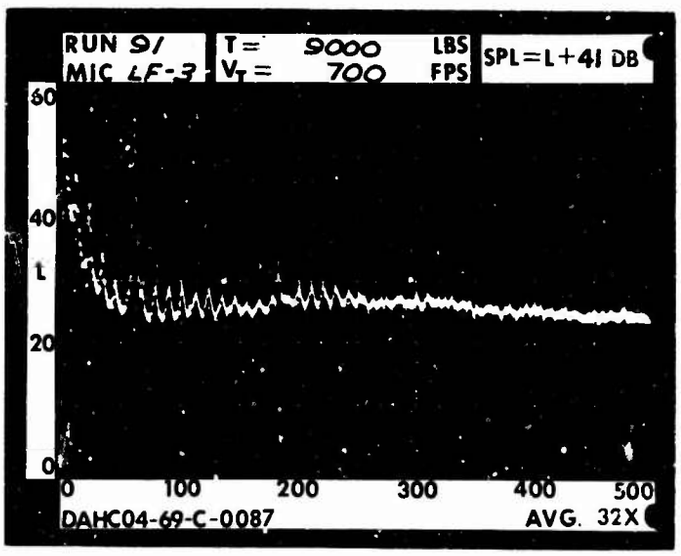

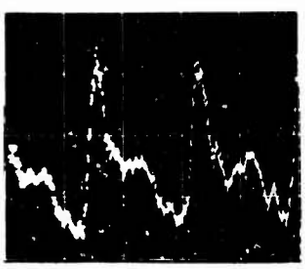

5 DIA.

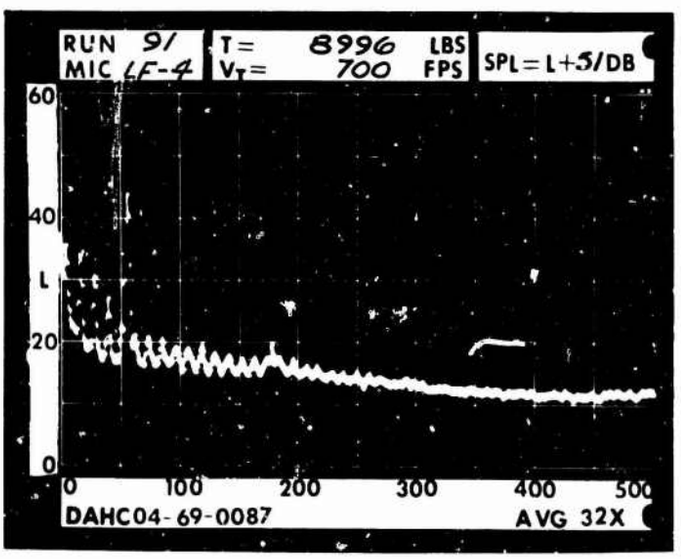

RUN 92.

TIP SPEED 700 FT/SEC

THRUST 12400 LB

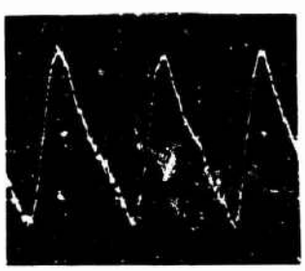

.2 RAD.

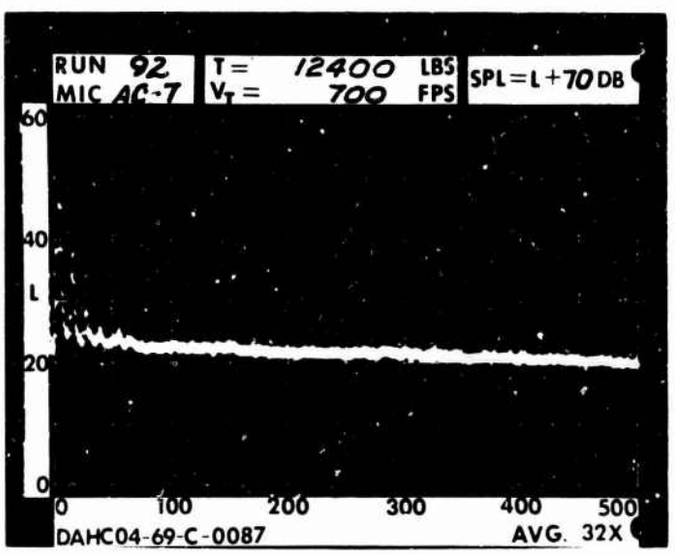

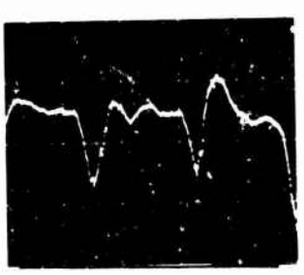

1 RAD.

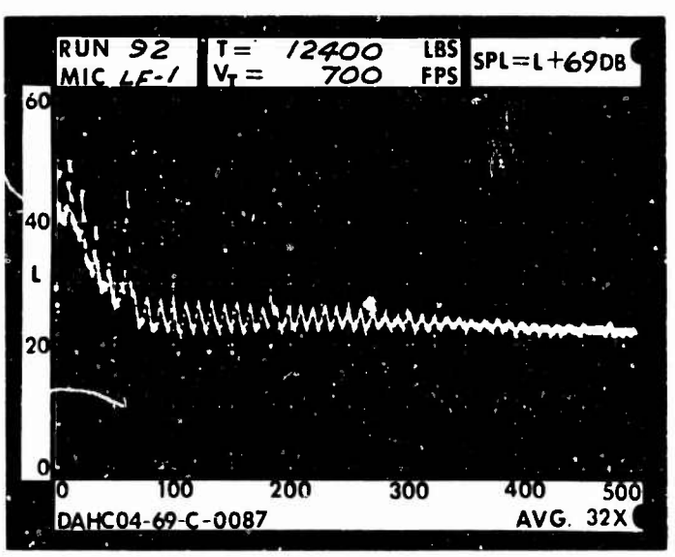

1 DIA.

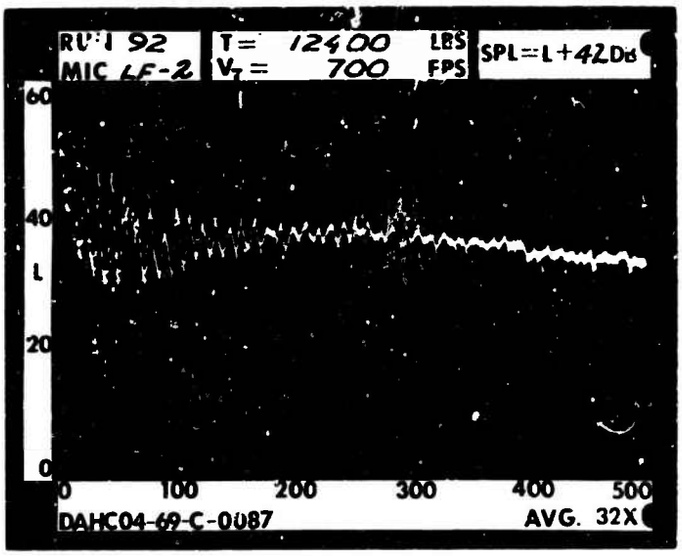

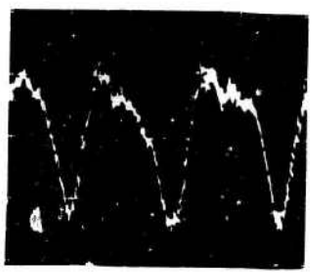

3 DIA.

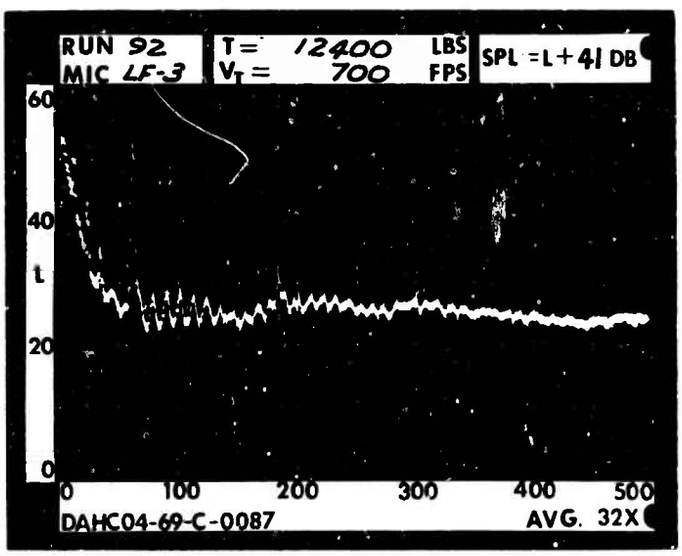

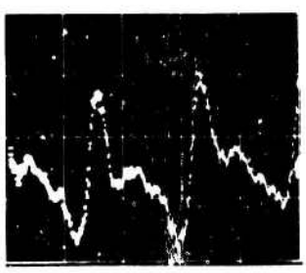

5 DIA.

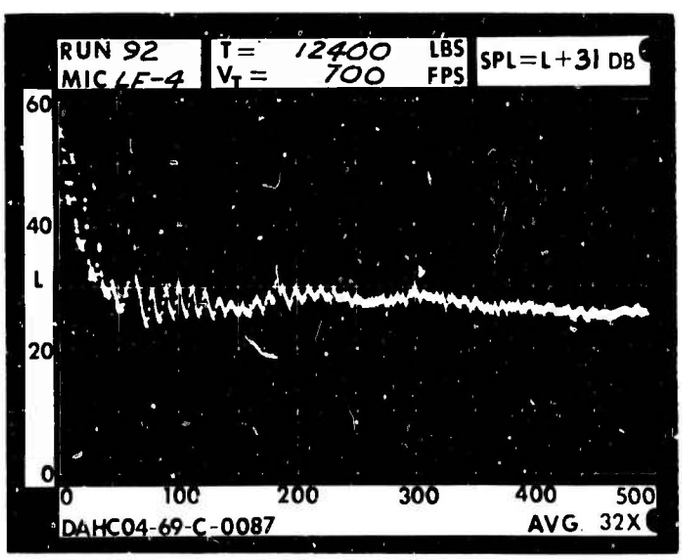

RUN 93

TIP SPEED 700 FT/SEC

THRUST 15200 LB

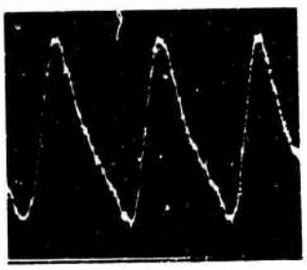

.2 RAD.

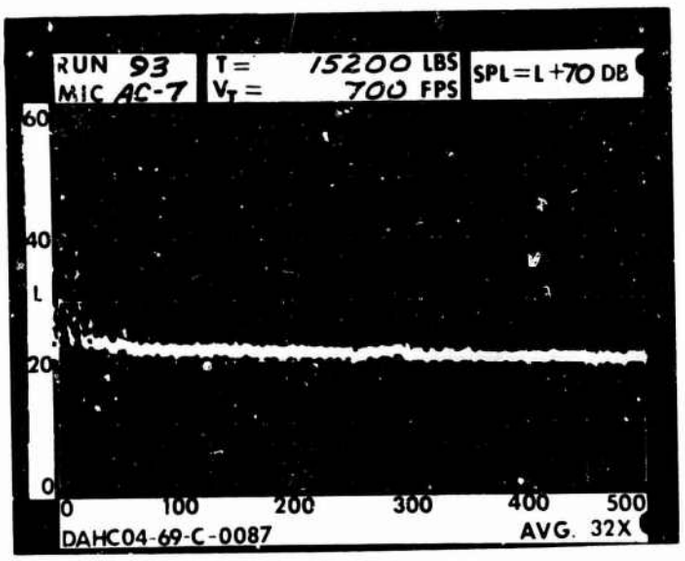

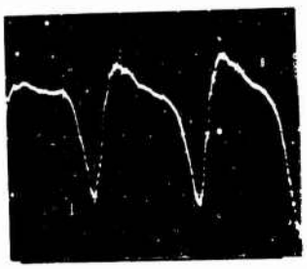

1 RAD.

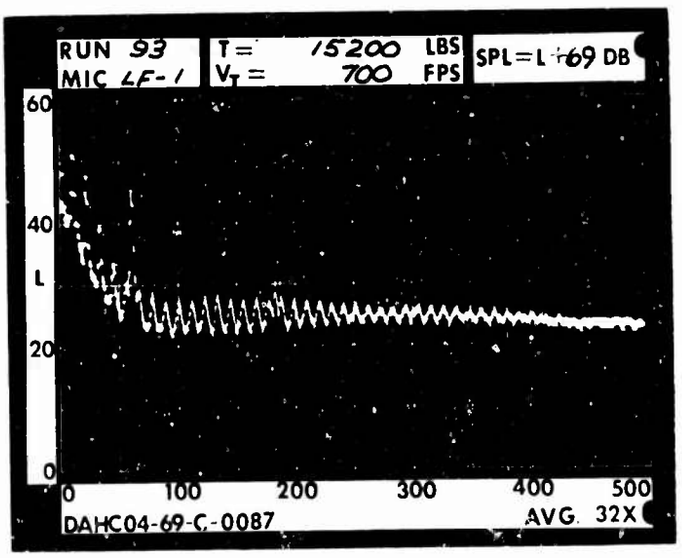

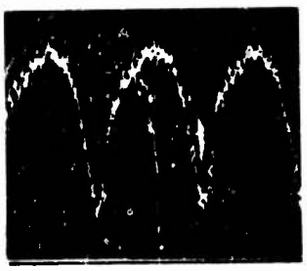

1 DIA.

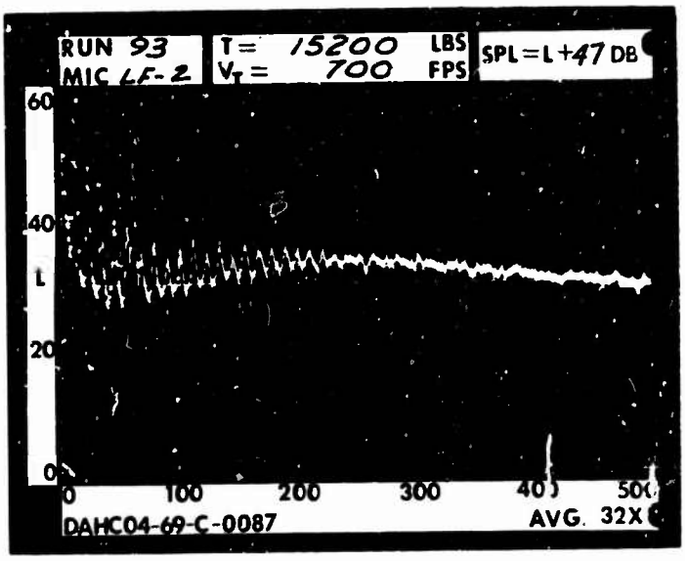

3 DIA.

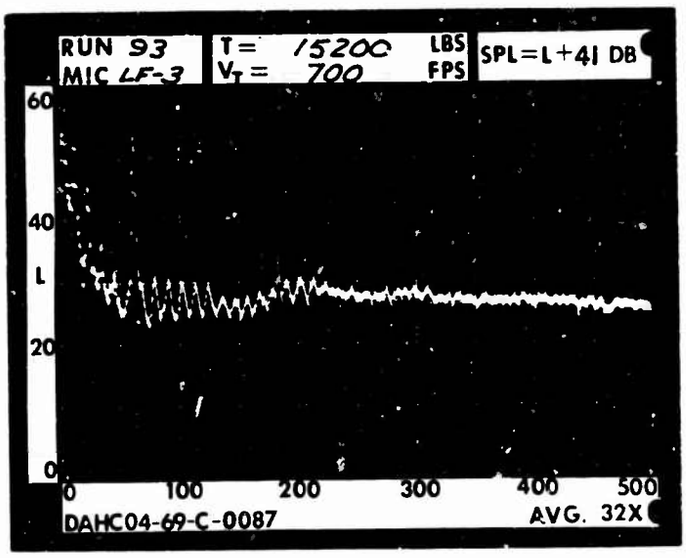

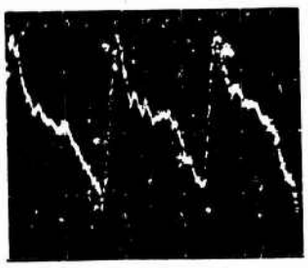

5 DIA.

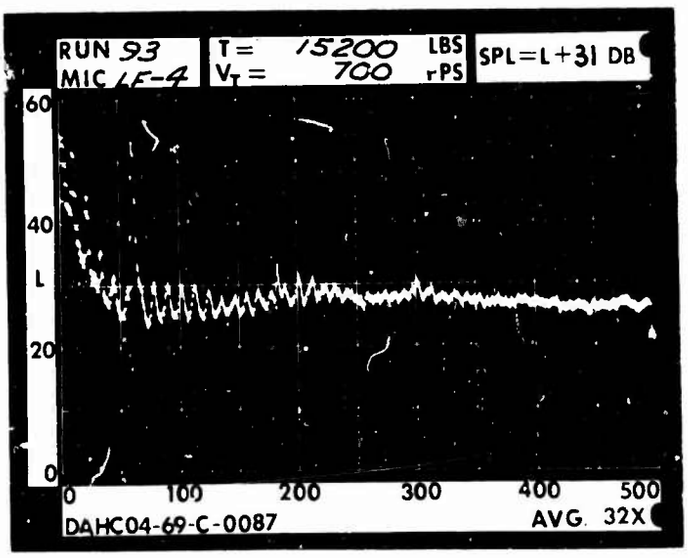

RUN 94

TIP SPEED 700 FT/SEC

THRUST 17700 LB

.2 RAD.

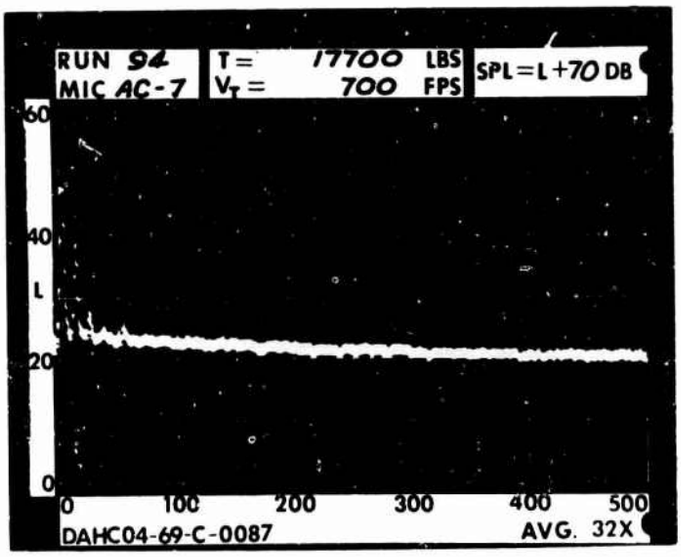

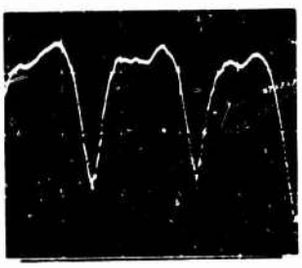

1 RAD.

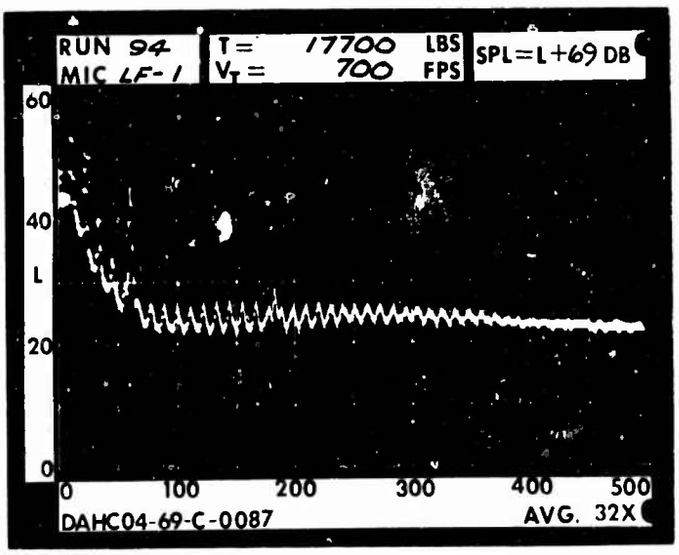

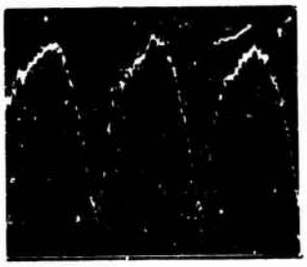

1 DIA.

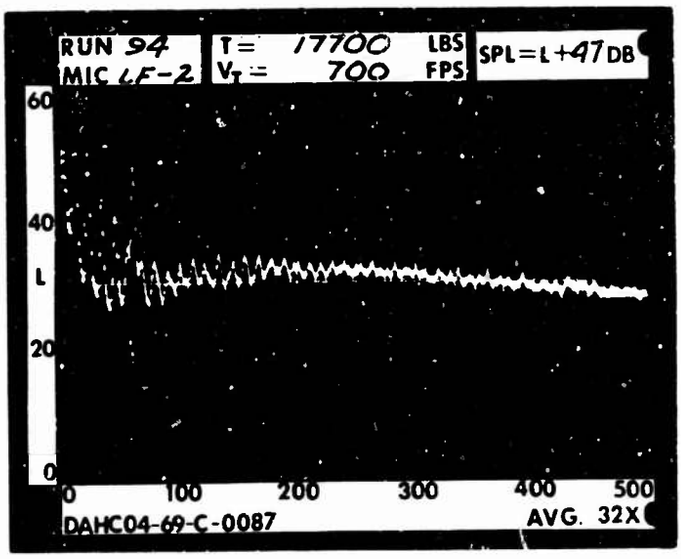

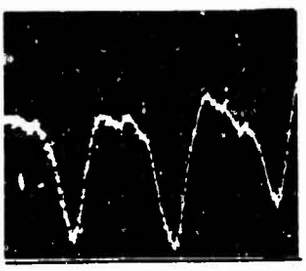

3 DIA.

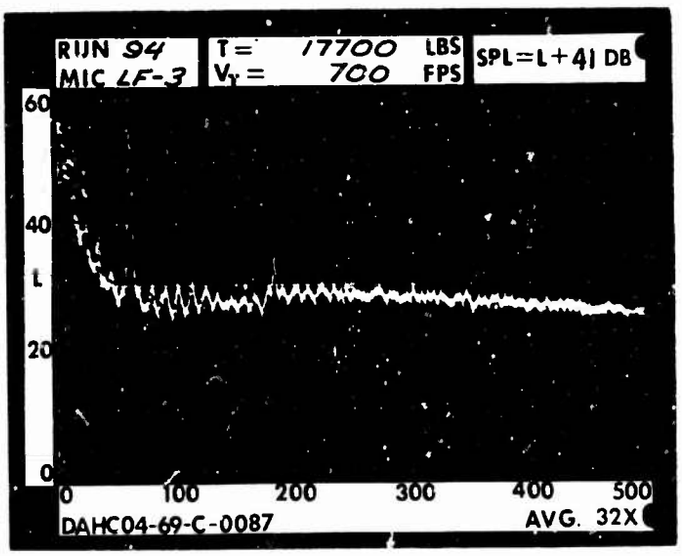

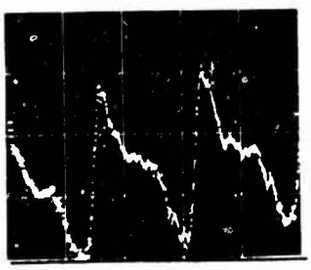

5 DIA.

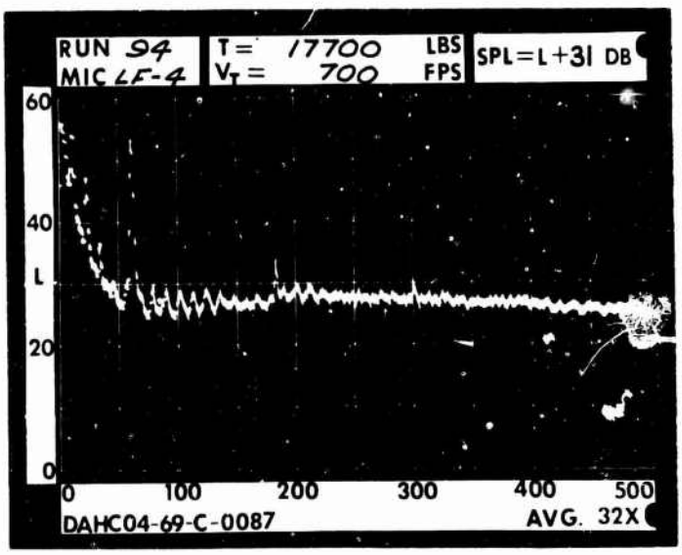

RUN 95

TIP SPEED 700 FT/SEC

THRUST 20400 LB

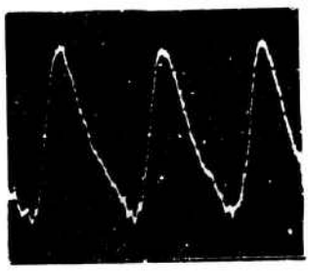

.2 RAD.

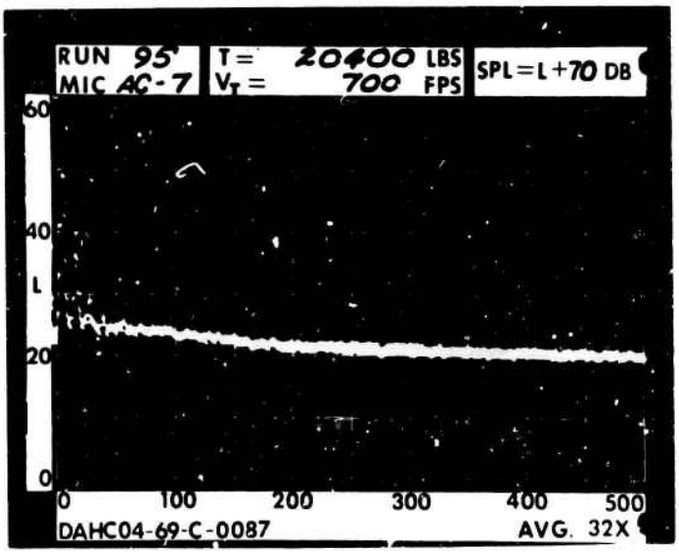

1 RAD.

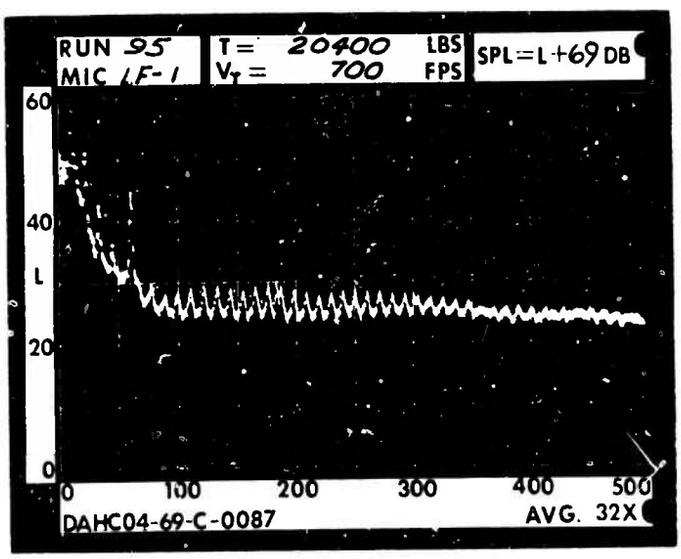

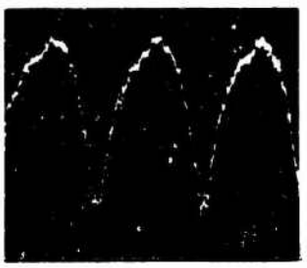

1 DIA.

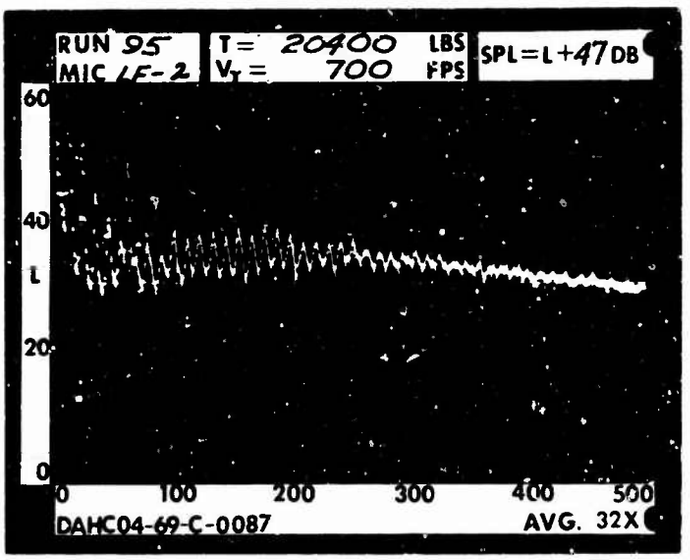

3 DIA.

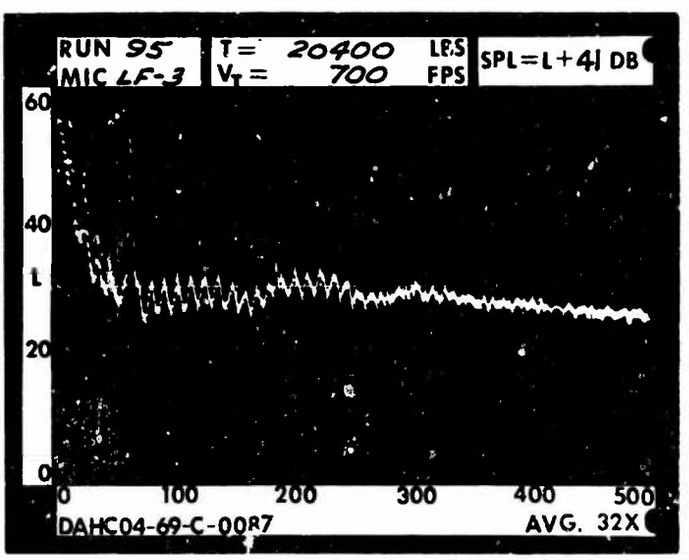

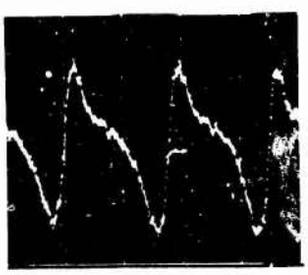

5 DIA.

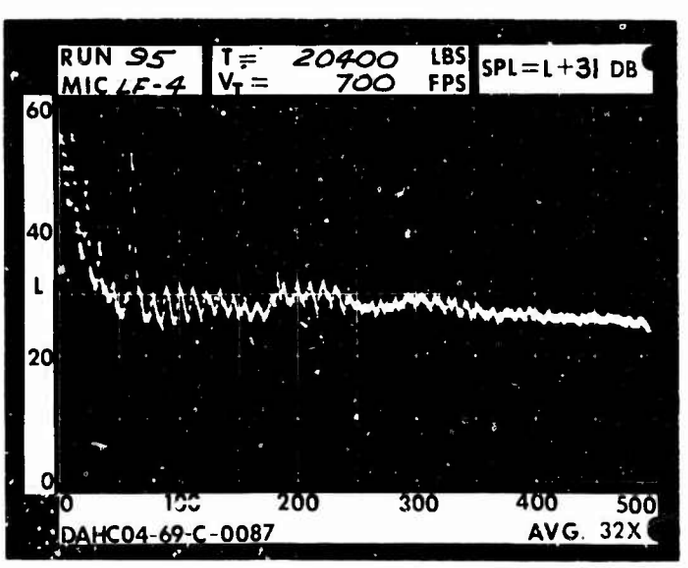

RUN 96

TIP SPEED 700 FT/SEC

THRUST 23300 LB

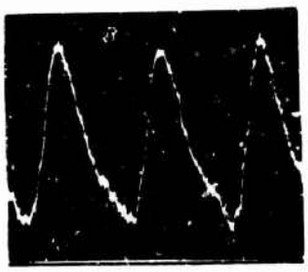

.2 RAD.

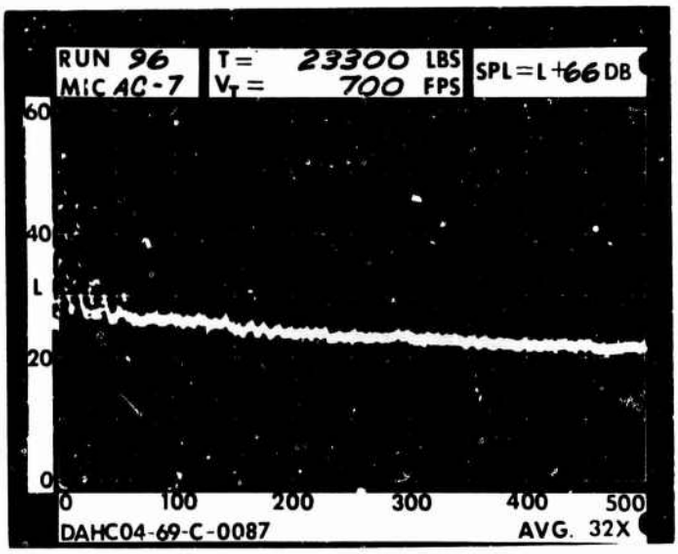

1 RAD.

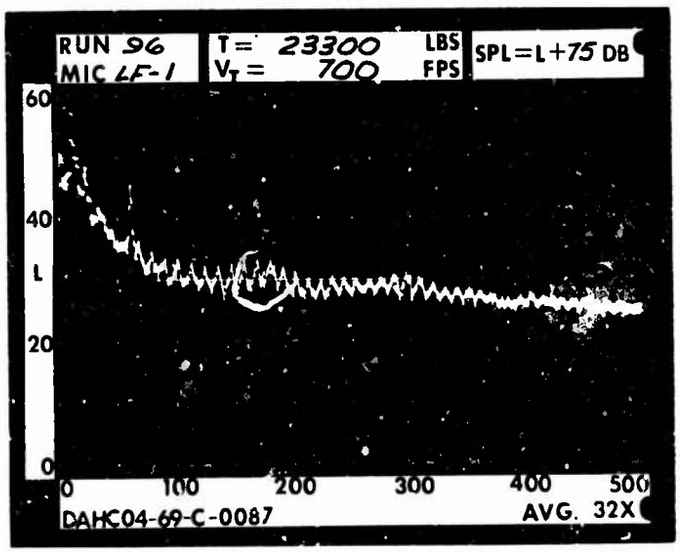

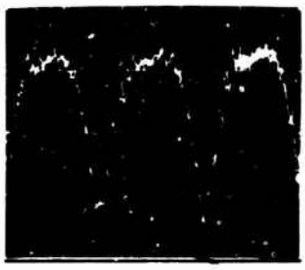

1 DIA.

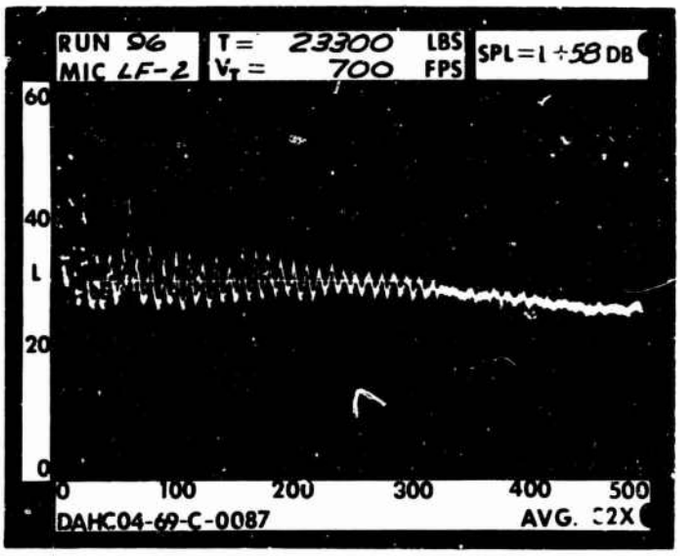

3 DIA.

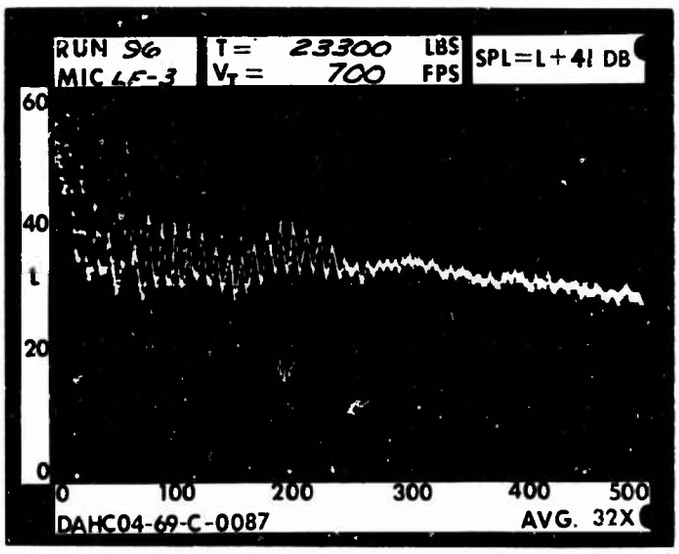

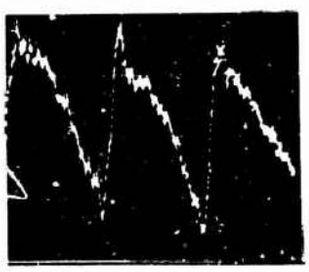

5 DIA.

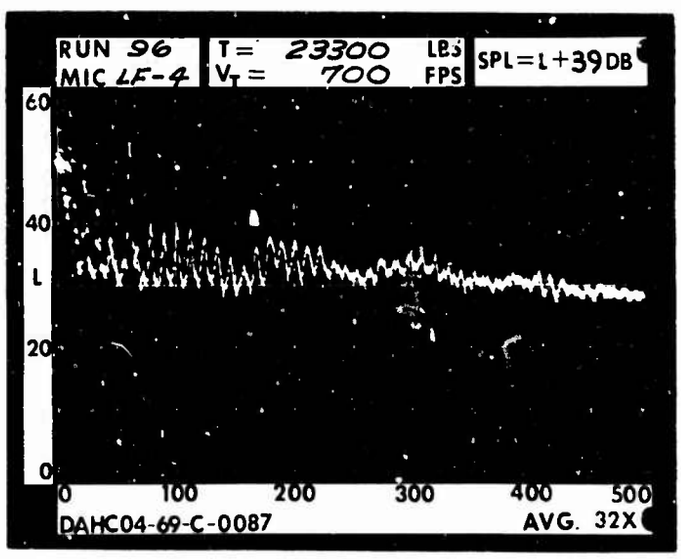

RUN 97

TIP SPEED 700 FT/SEC

THRUST 24300 LB

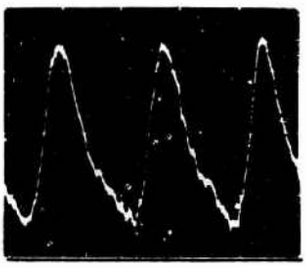

.2 RAD.

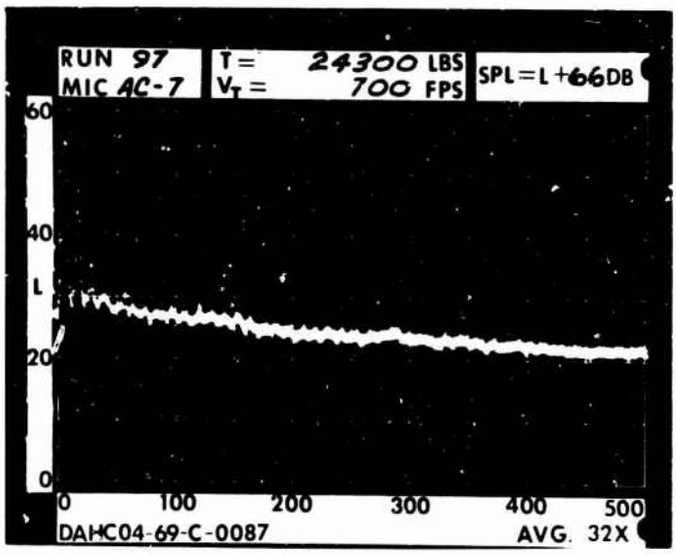

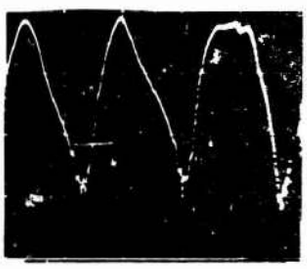

1 RAD.

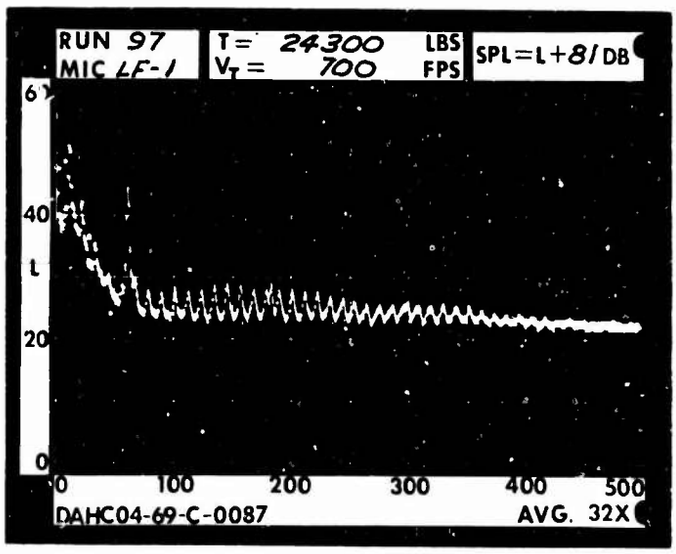

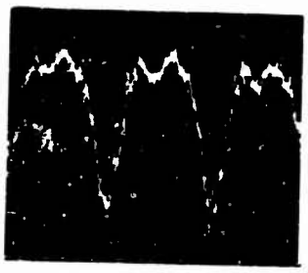

1 DIA.

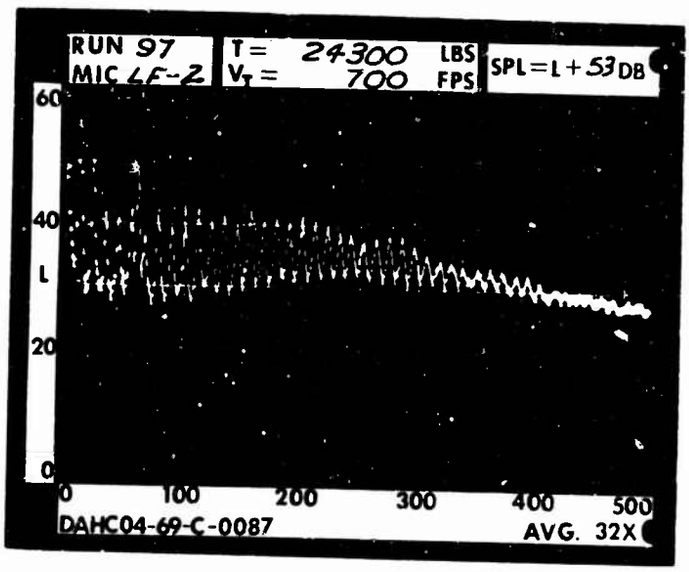

3 DIA.

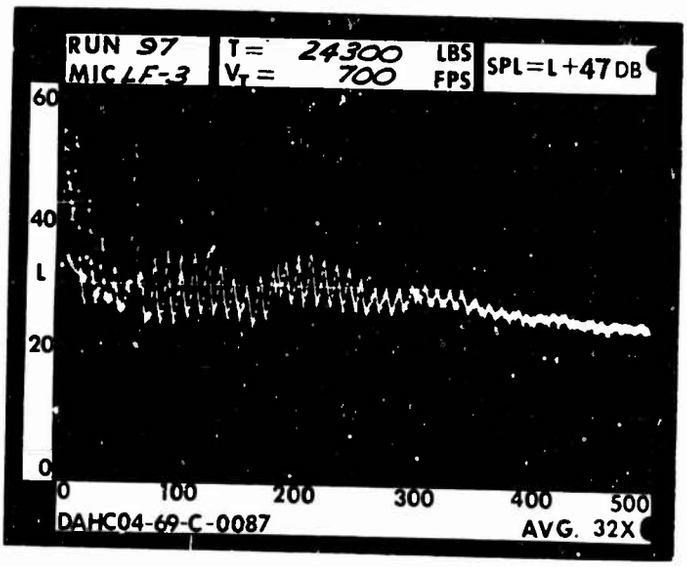

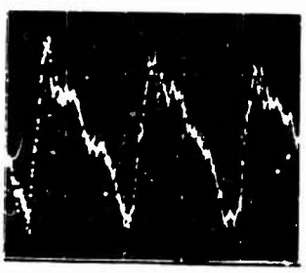

5 DIA.

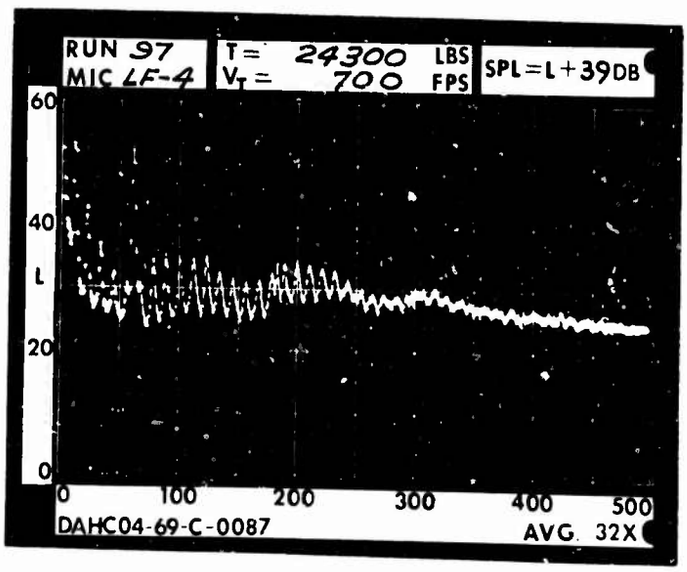

RUN 98

TIP SPEED 700 FT/SEC

THRUST 26100 LB

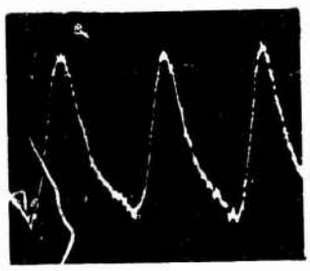

.2 RAD.

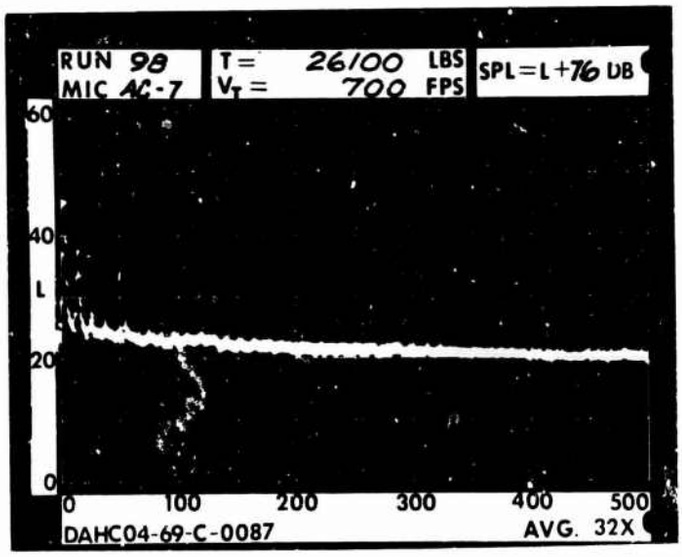

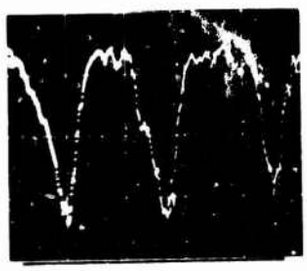

1 RAD.

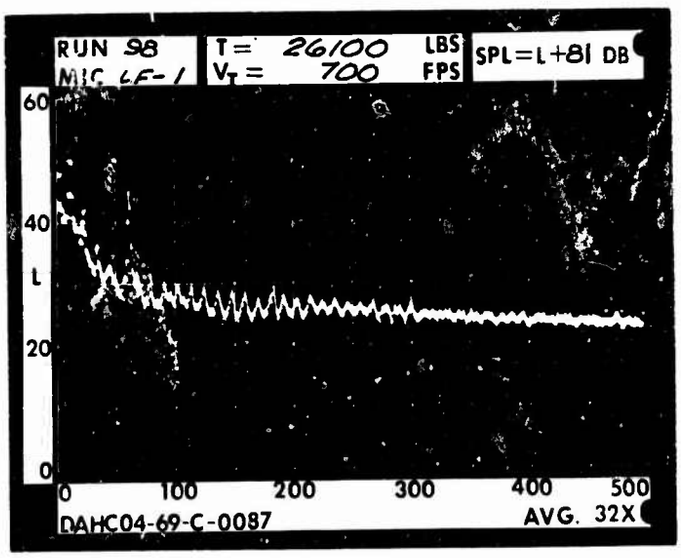

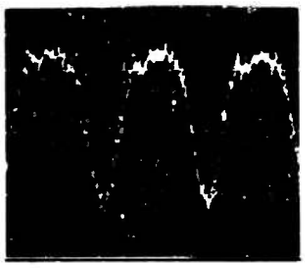

1 DIA.

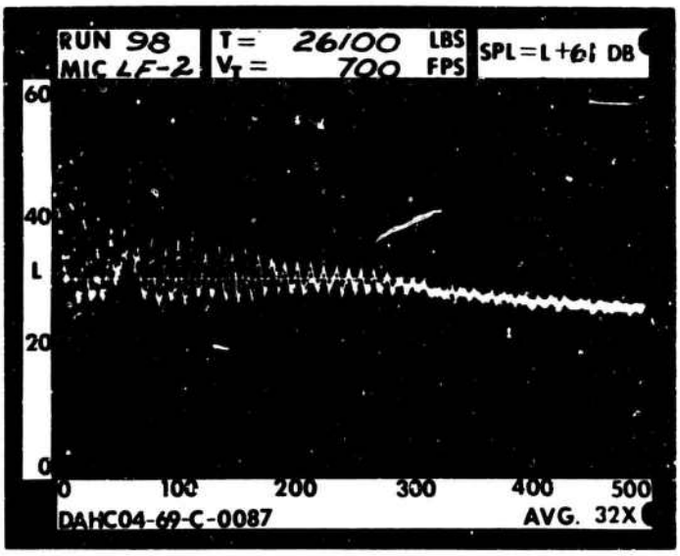

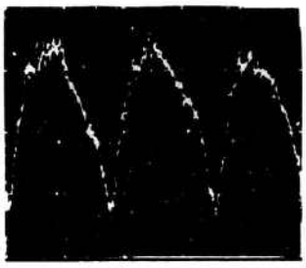

3 DIA.

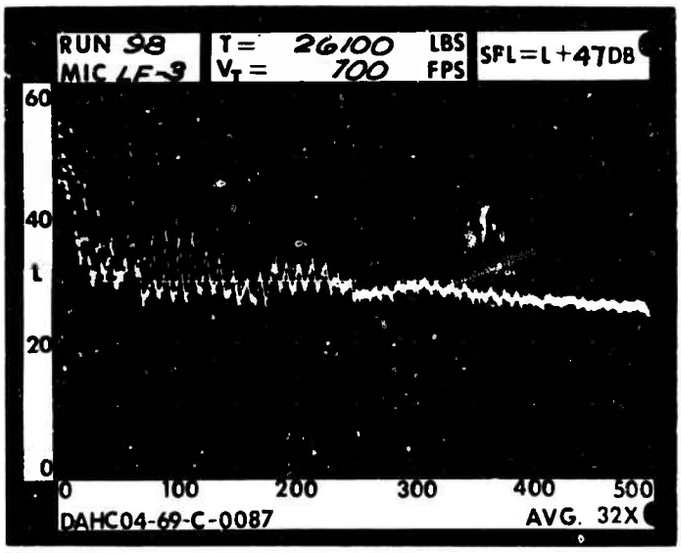

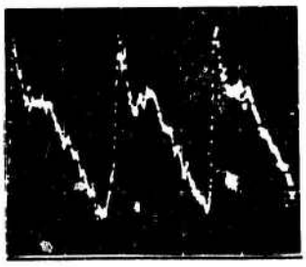

5 DIA.

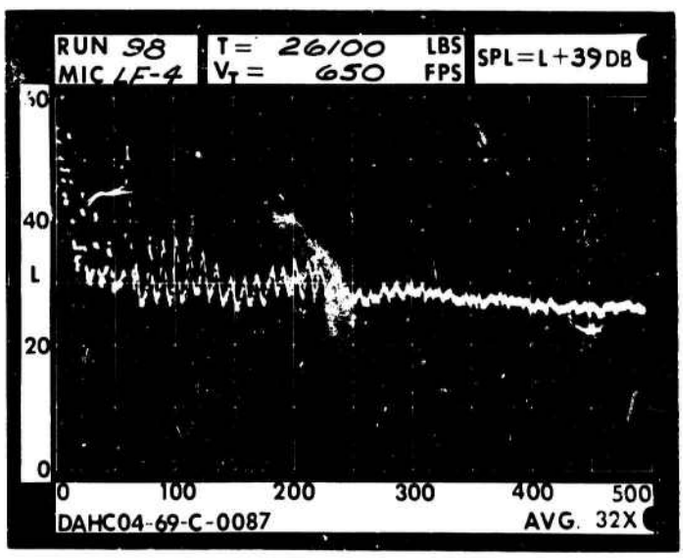

RUN 99

TIP SPEED 700 FT/SEC

THRUST 28100 LB

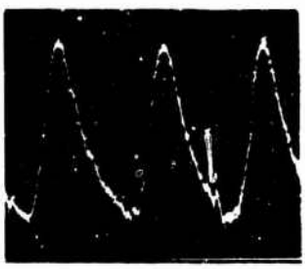

.2 RAD.

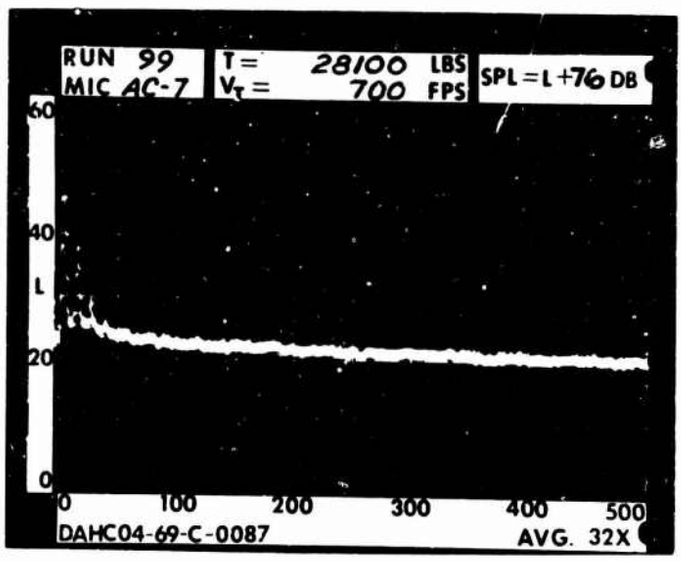

1 RAD.

1 DIA.

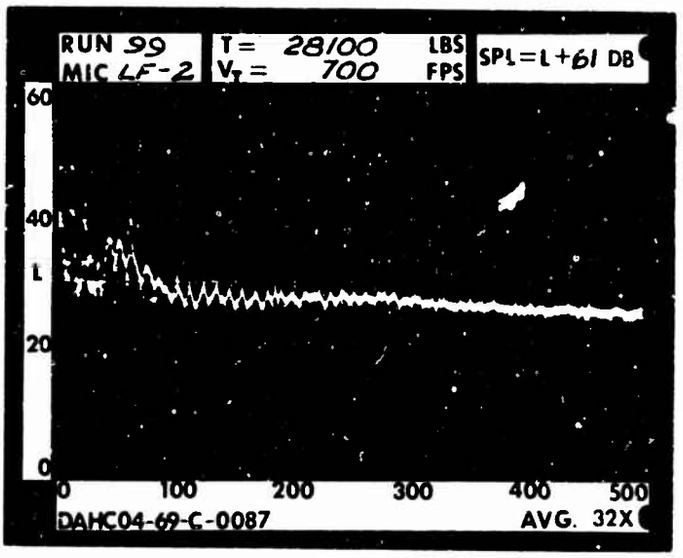

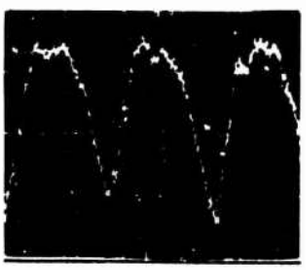

3 DIA.

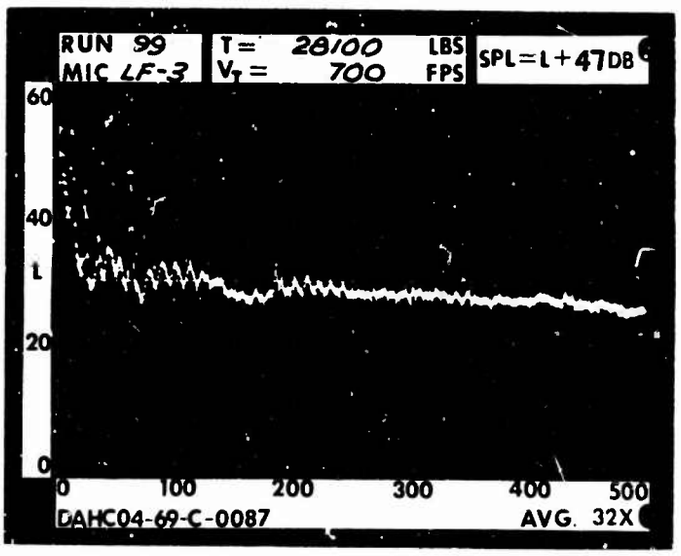

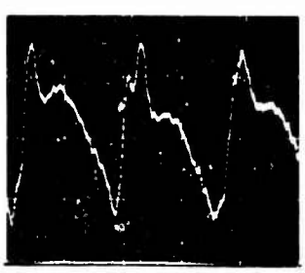

5 DIA.

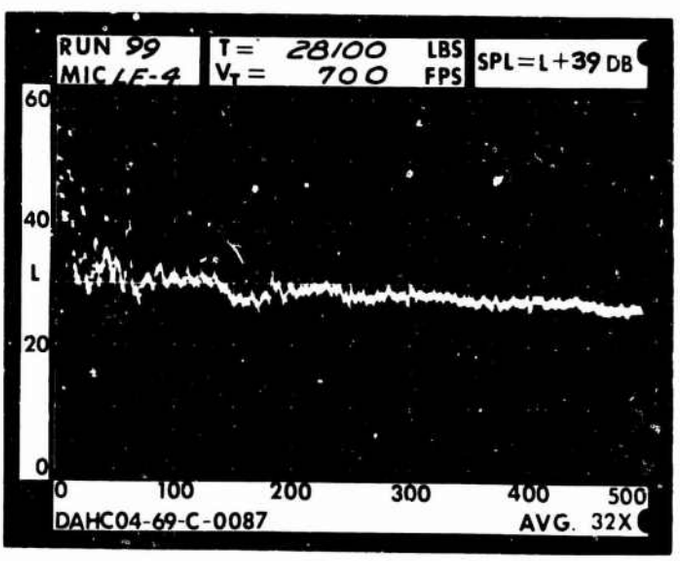

RUN 100

TIP SPEED 700 FT/SEC

THRUST 29200 LB

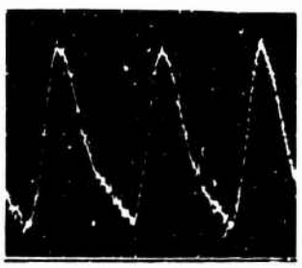

.2 RAD.

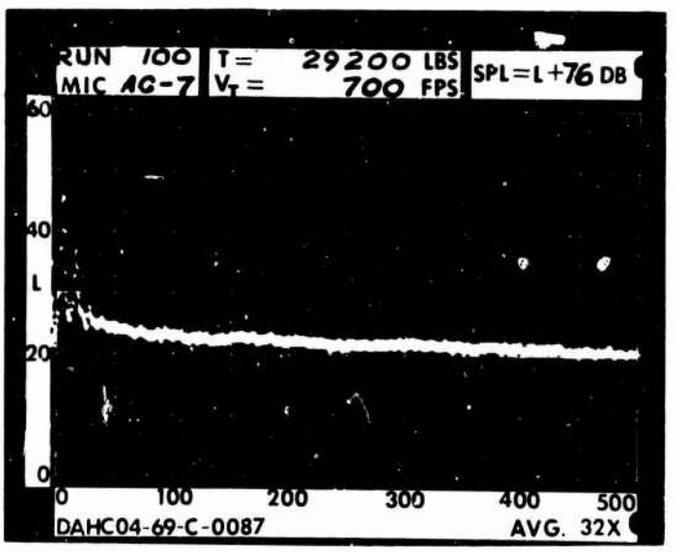

1 RAD.

1 DIA.

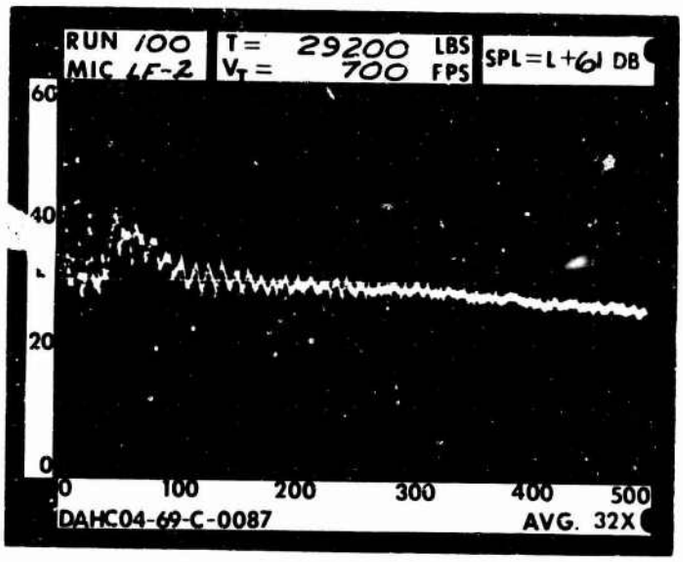

3 DIA.

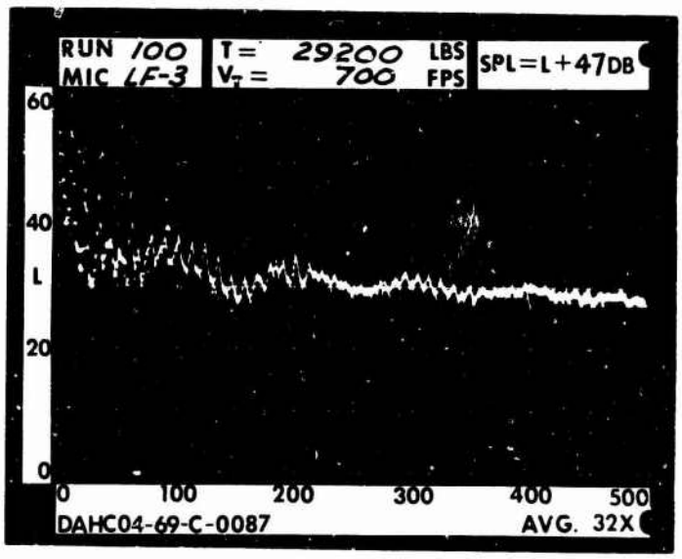

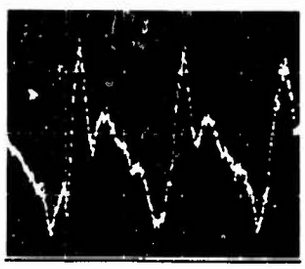

5 DIA.

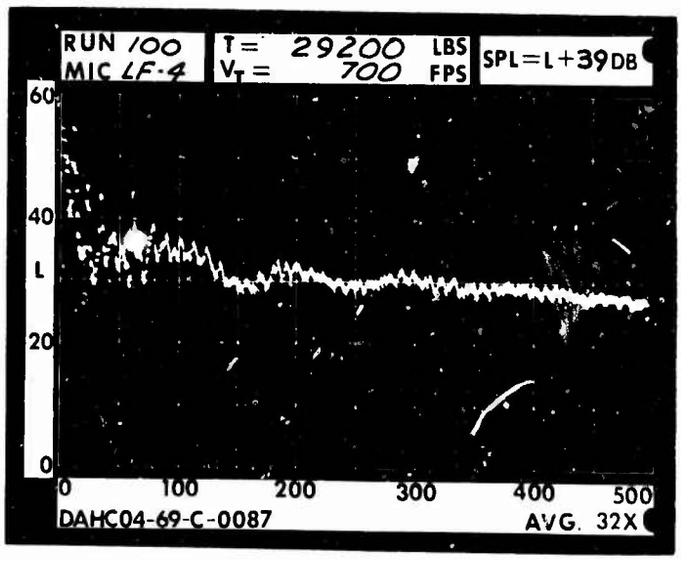

RUN 101

TIP SPEED 650 FT/SEC

THRUST 8600 LB

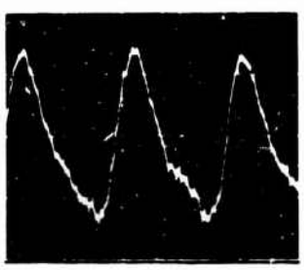

.2 RAD.

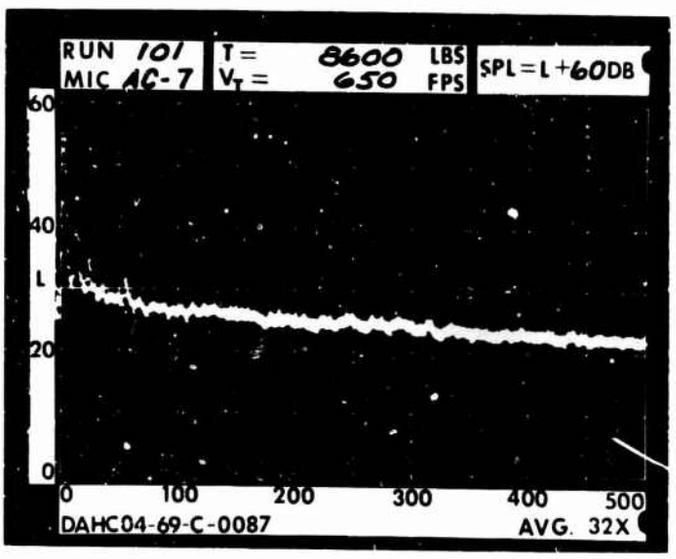

1 RAD.

1 DIA.

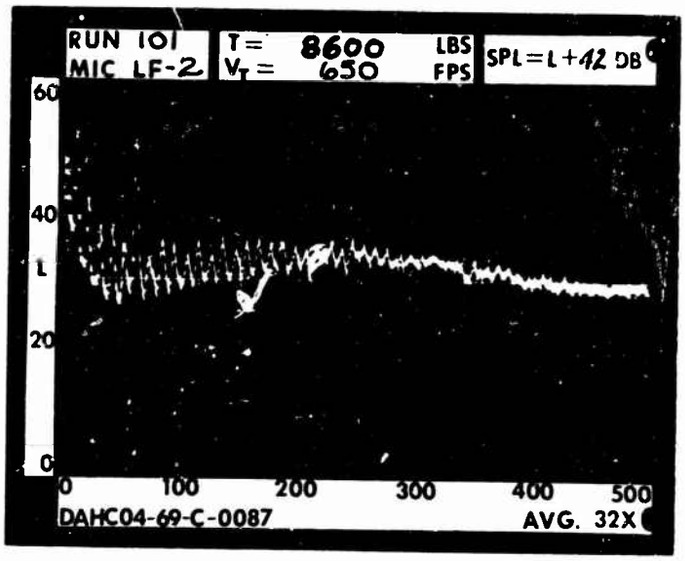

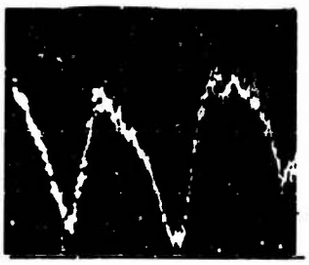

3 DIA.

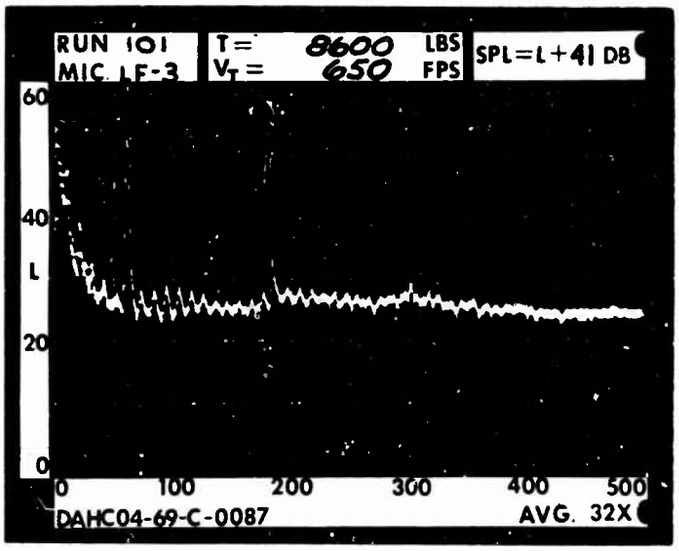

5 DIA.

RUN 102

TIP SPEED 650 FT/SEC

THRUST 12100 LB

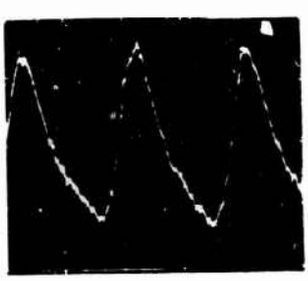

.2 RAD.

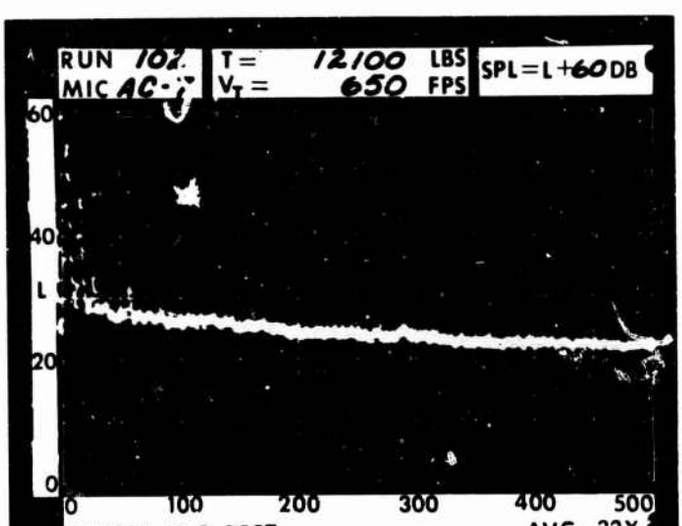

1 RAD.

1 DIA.

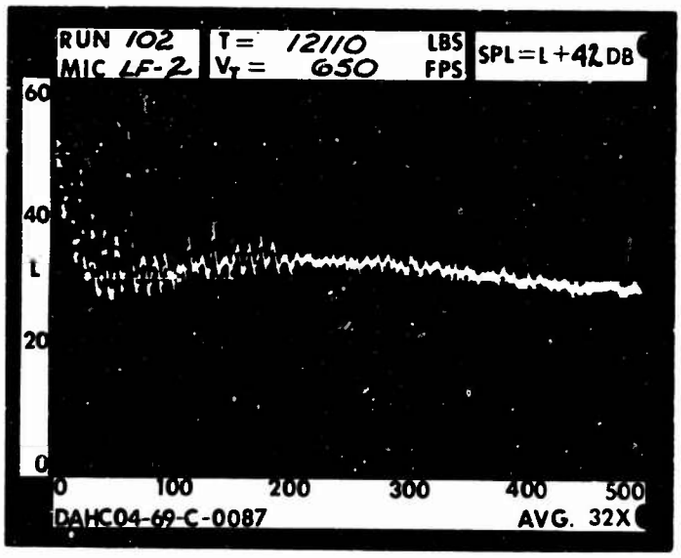

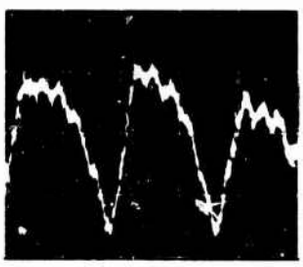

3 DIA.

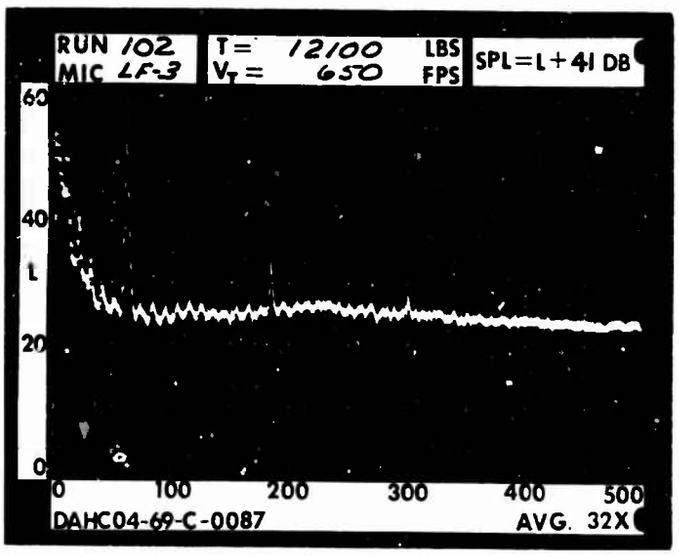

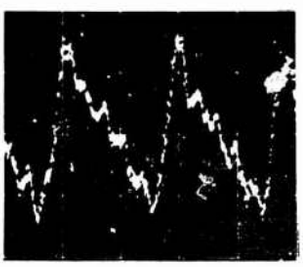

5 DIA.

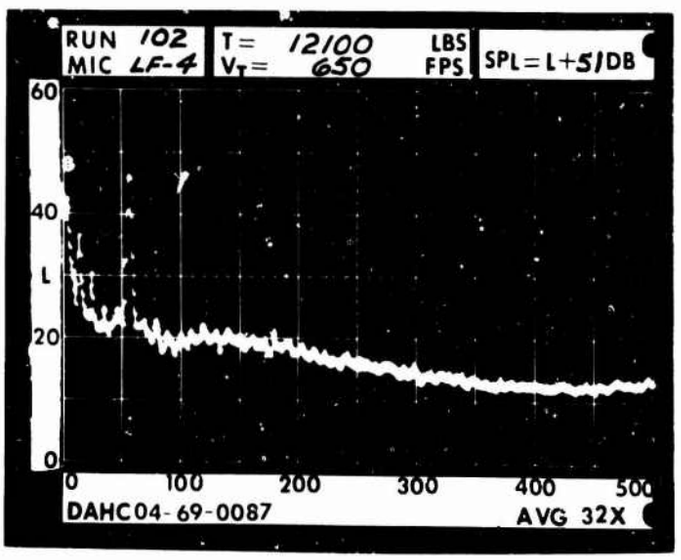

RUN 103

TIP SPEED 650 FT/SEC

THRUST 14800 LB

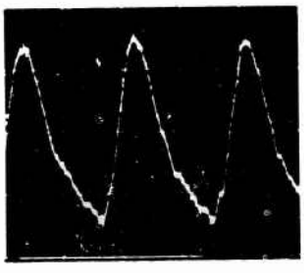

.2 RAD.

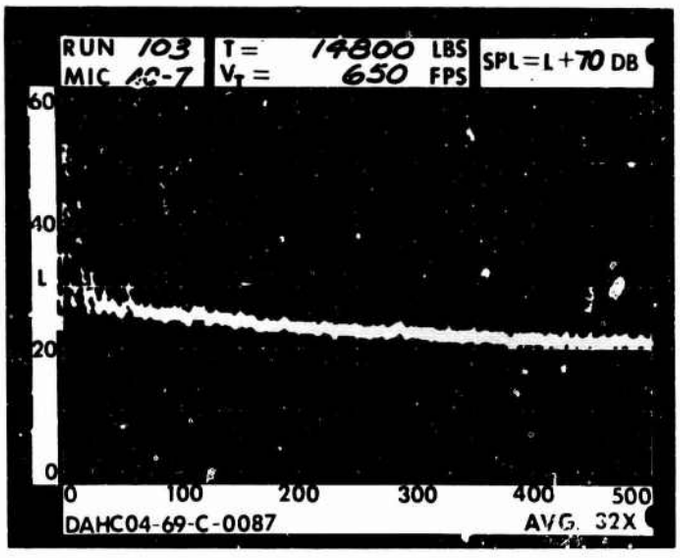

1 RAD.

1 DIA.

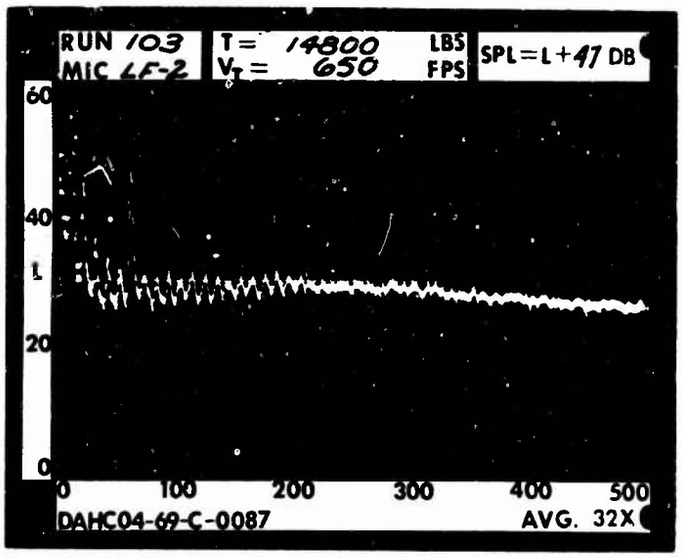

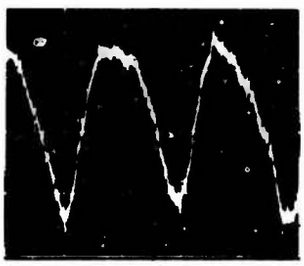

3 DIA.

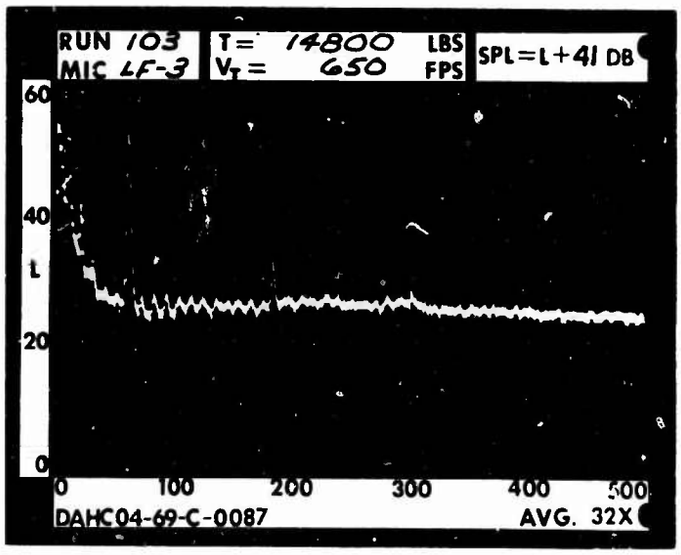

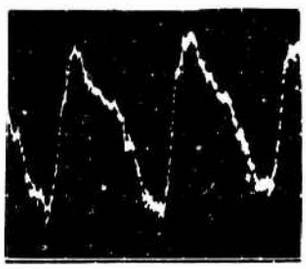

5 DIA.

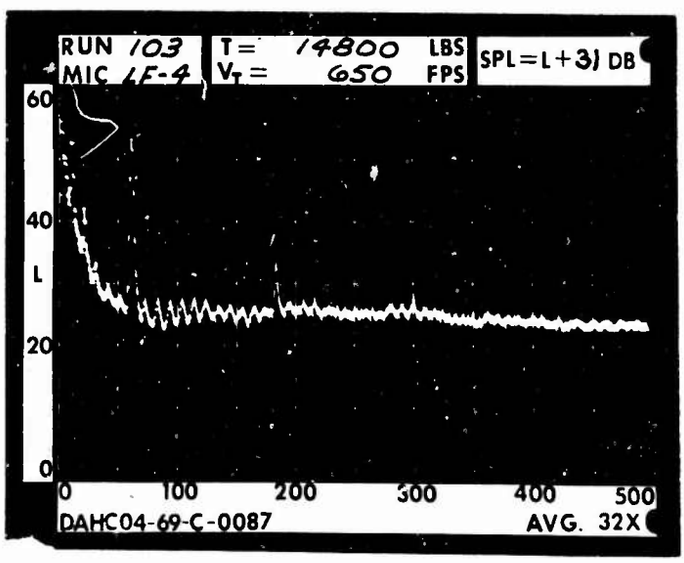

RUN 104

TIP SPEED 650 FT/SEC

THRUST 17400 LB

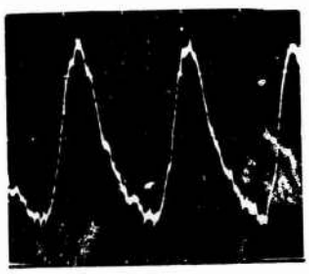

.2 RAD.

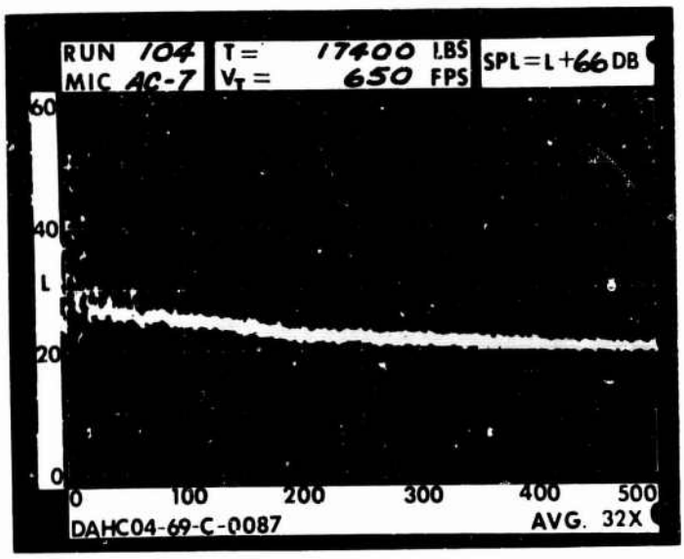

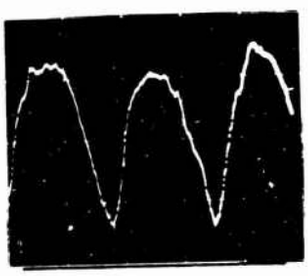

1 RAD.

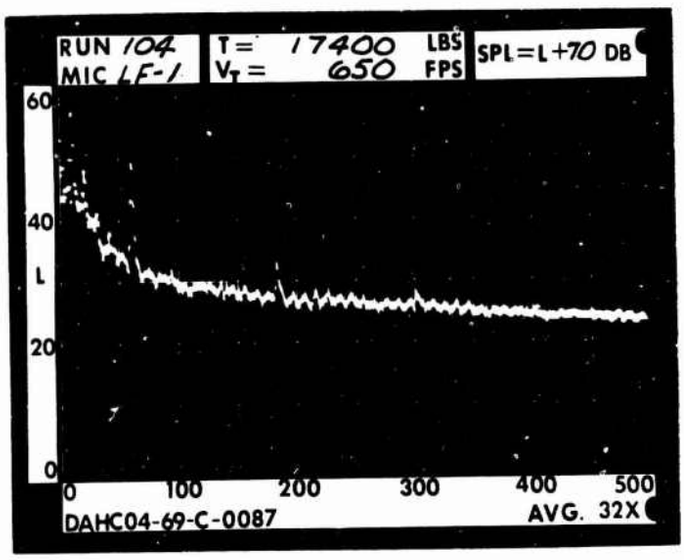

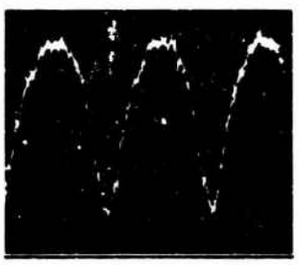

1 DIA.

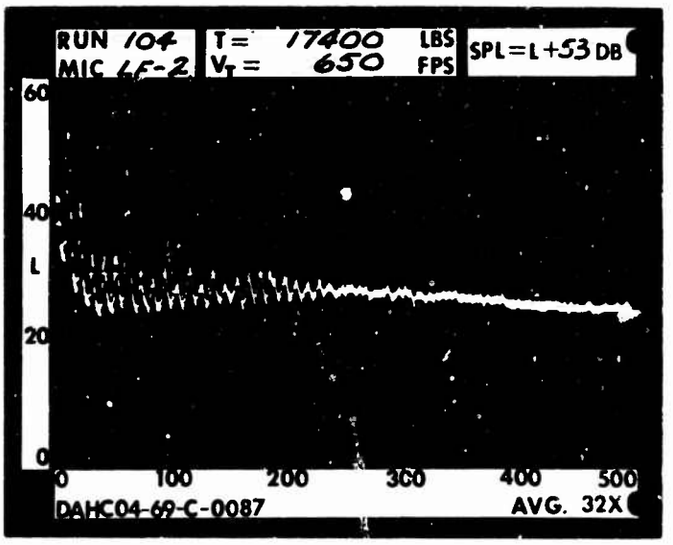

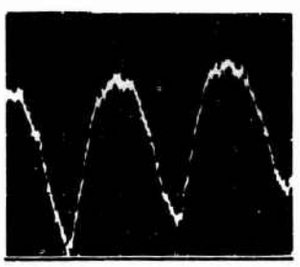

3 DIA.

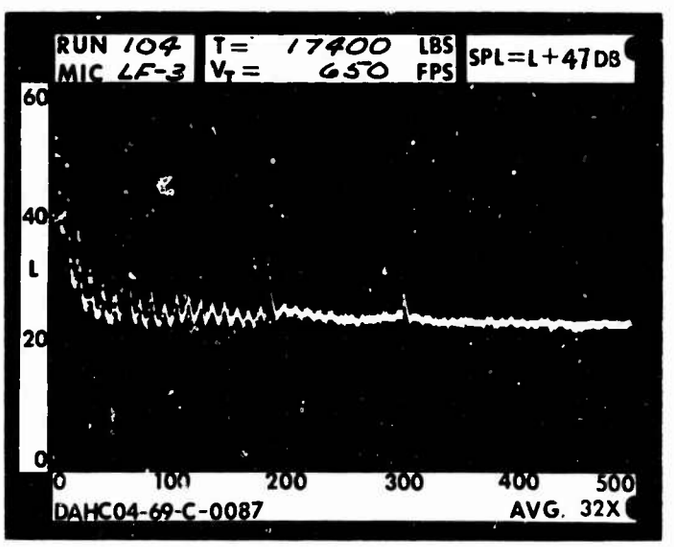

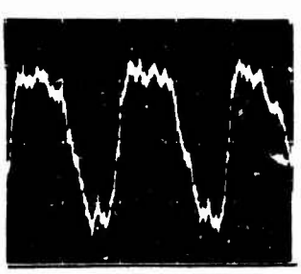

5 DIA.

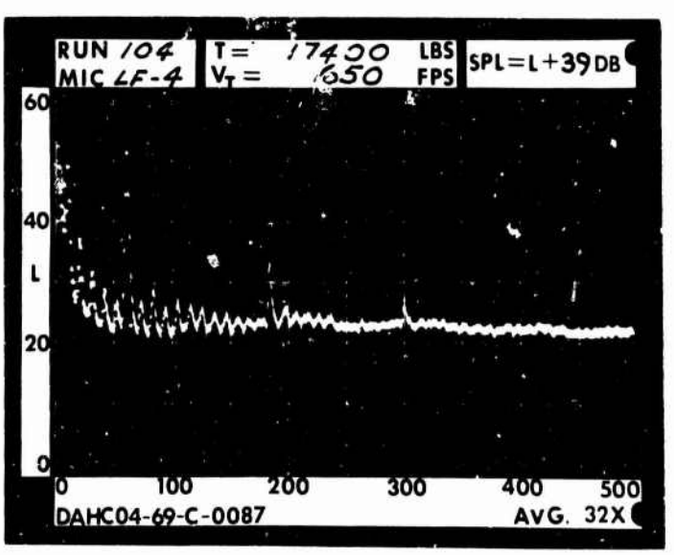

RUN 105

TIP SPEED 650 FT/SEC

THRUST 20500 LB

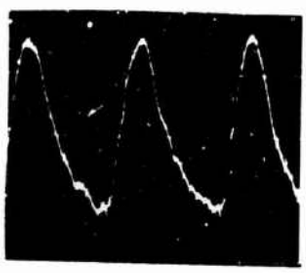

.2 RAD.

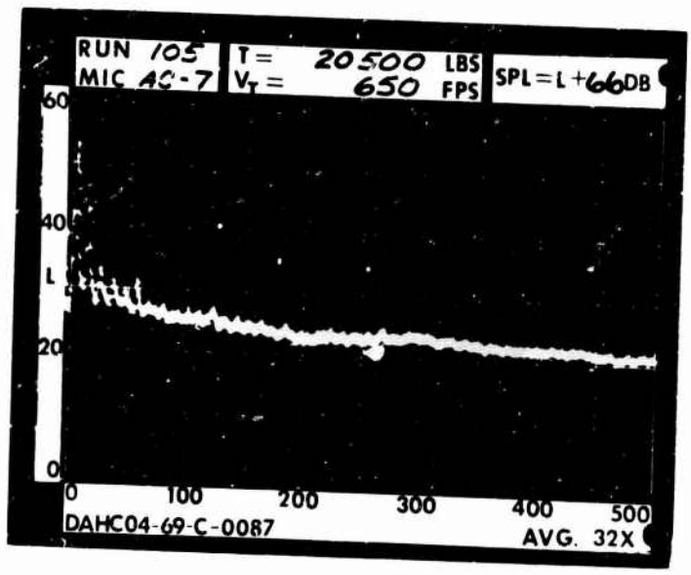

1 RAD.

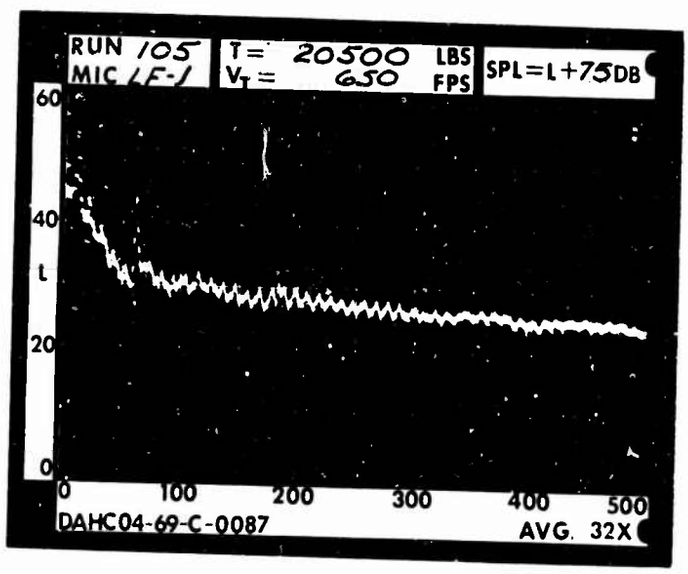

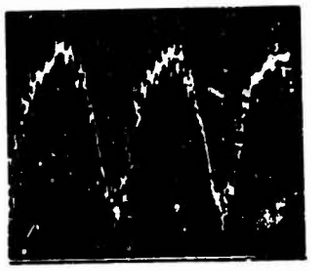

1 DIA.

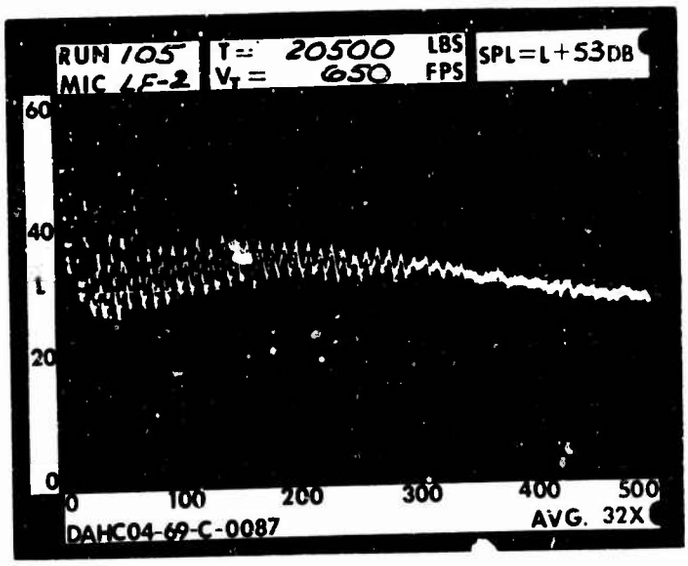

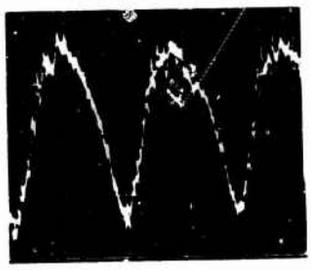

3 DIA.

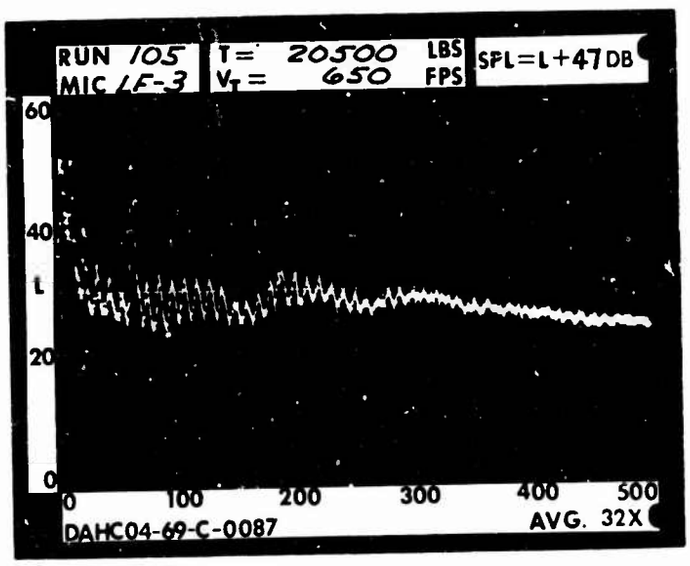

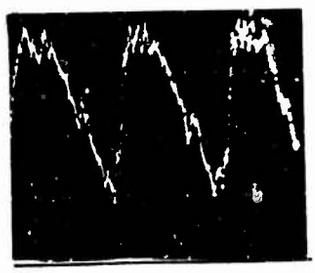

5 DIA.

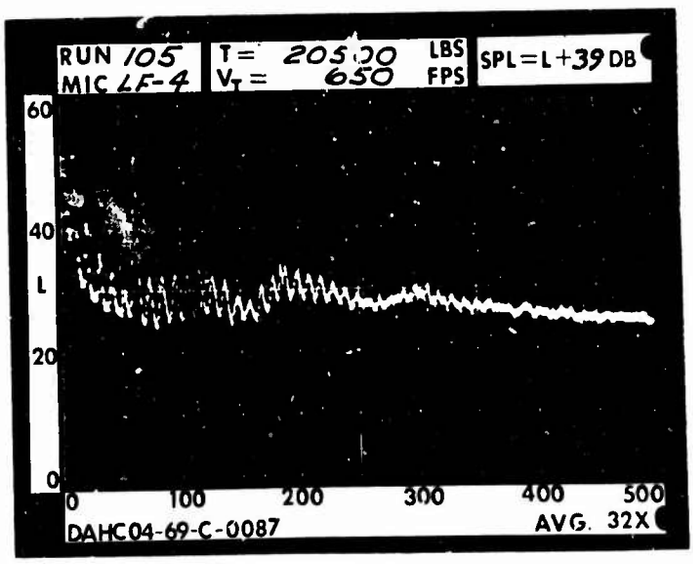

RUN 106

TIP SPEED 650 FT/SEC

THRUST 22900 LB

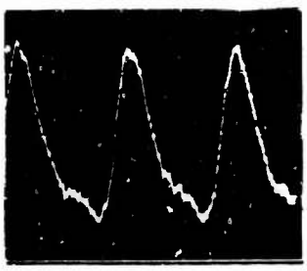

.2 RAD.

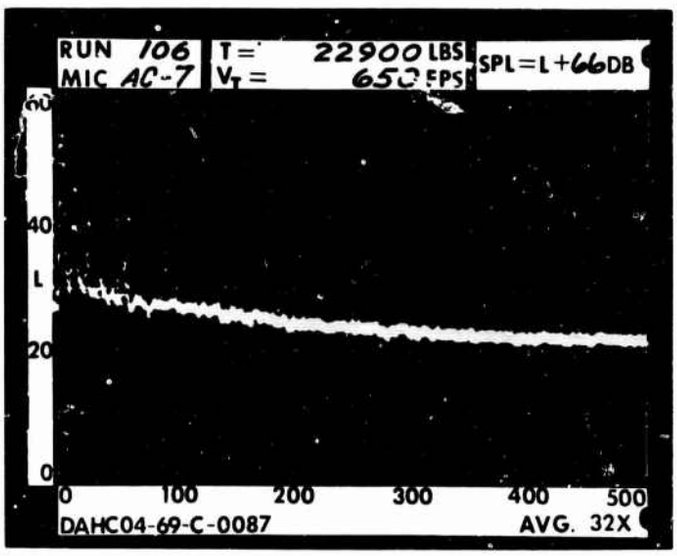

1 RAD.

1 DIA.

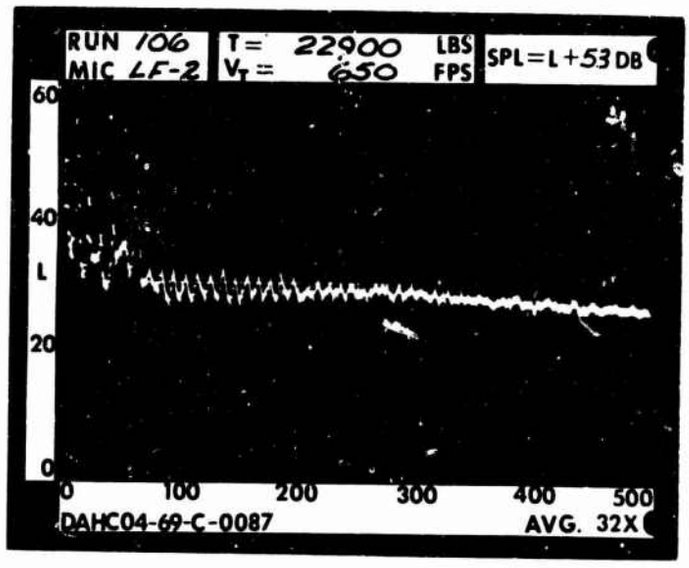

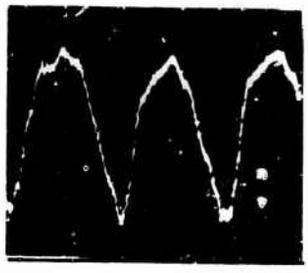

3 DIA.

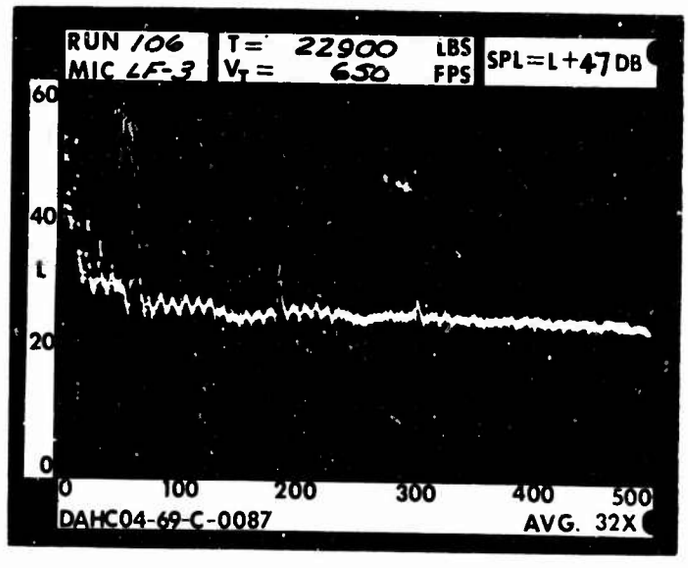

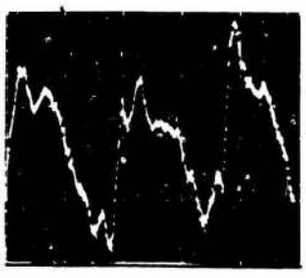

5 DIA.

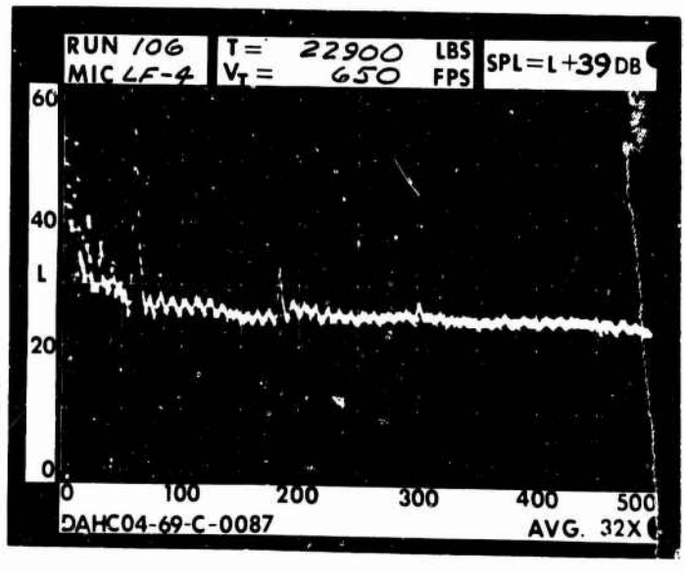

RUN 107

TIP SPEED 650 FT/SEC

THRUST 25300 LB

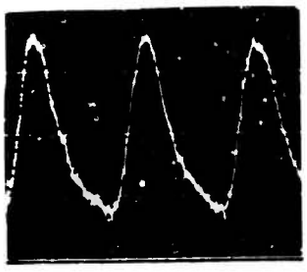

.2 RAD.

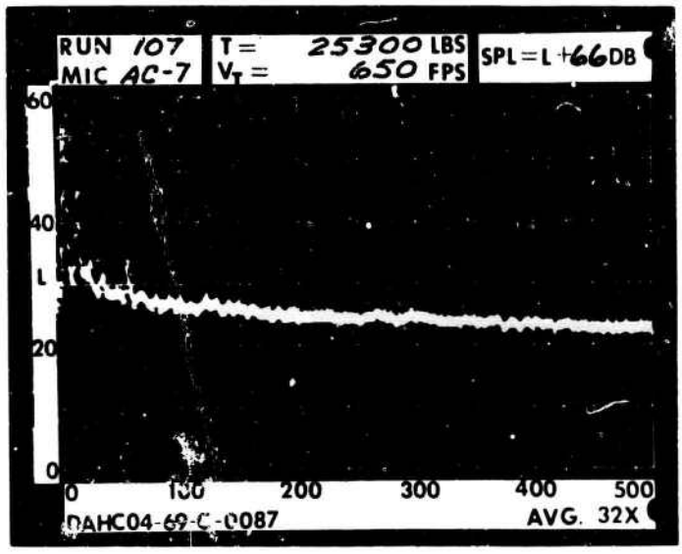

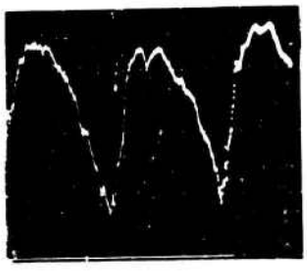

1 RAD.

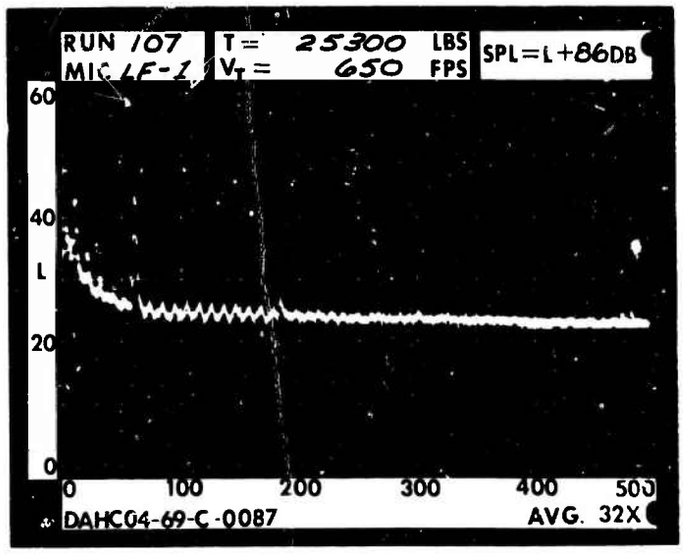

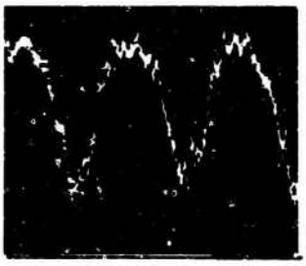

1 DIA.

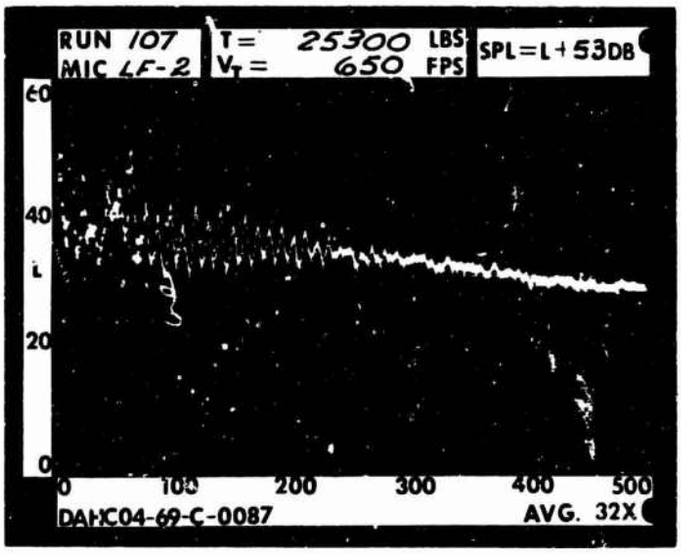

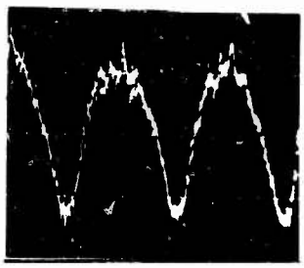

3 DIA.

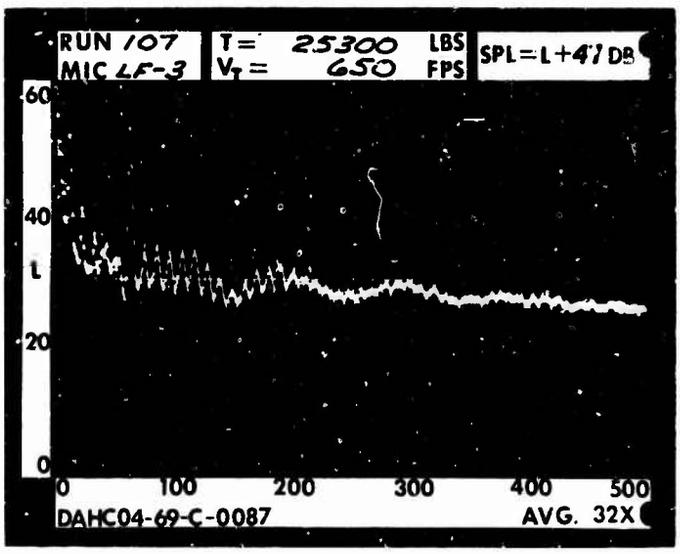

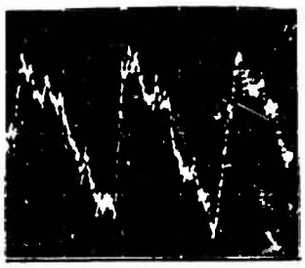

5 DIA.

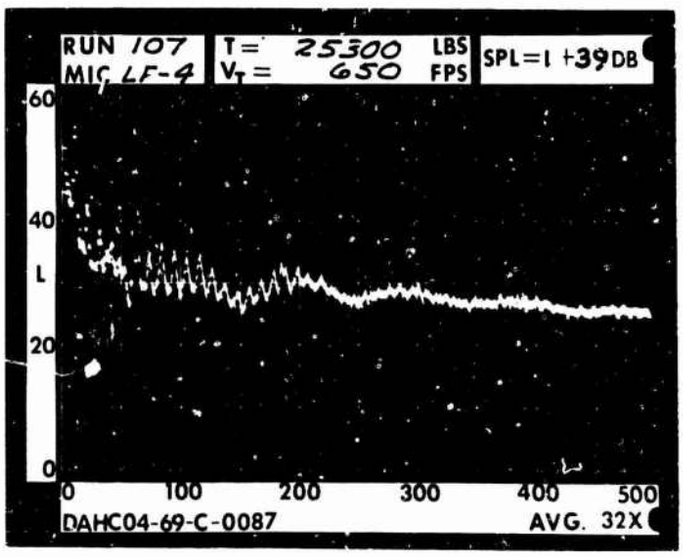

RUN 108

TIP SPEED 650 FT/SEC

THRUST 26700 LB

.2 RAD.

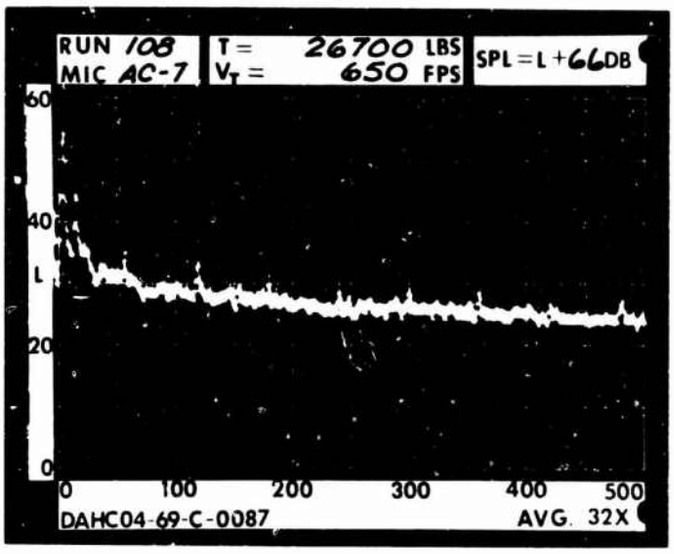

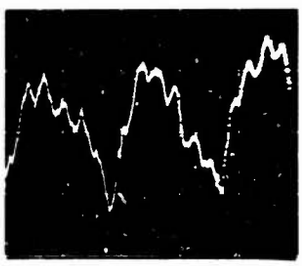

1 RAD.

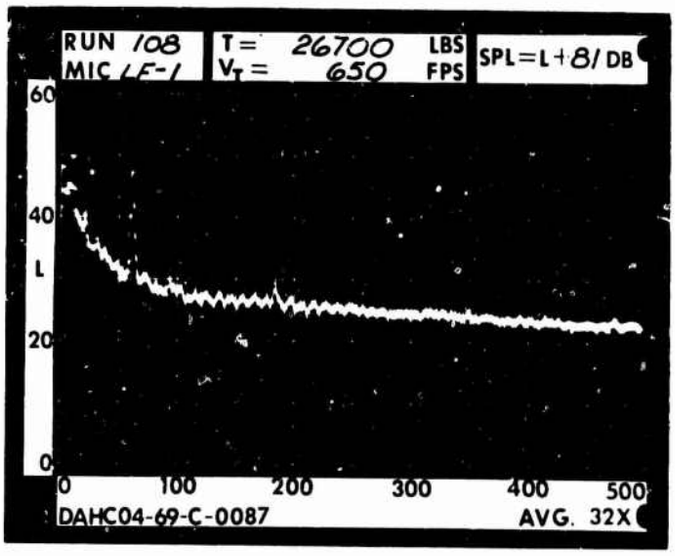

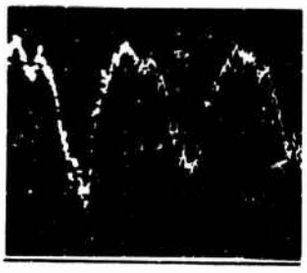

1 DIA.

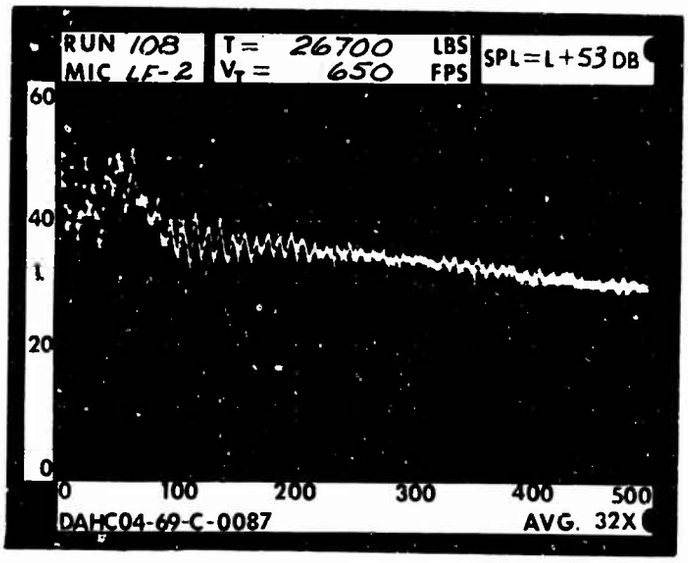

3 DIA.

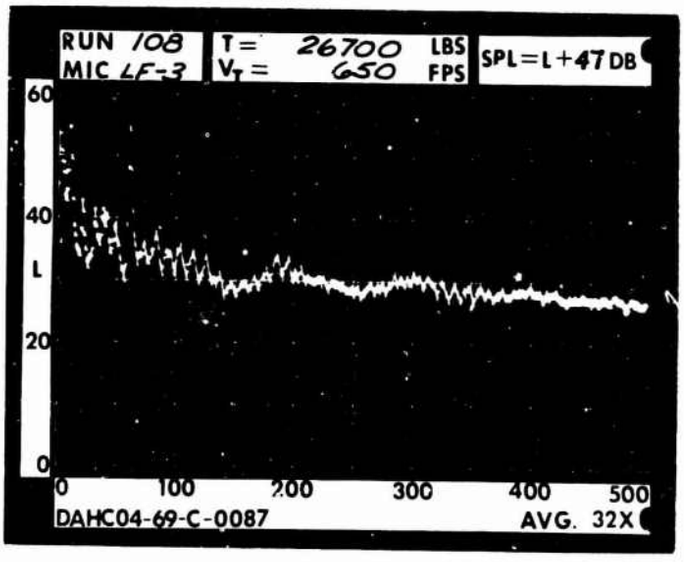

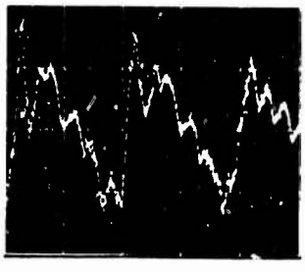

5 DIA.

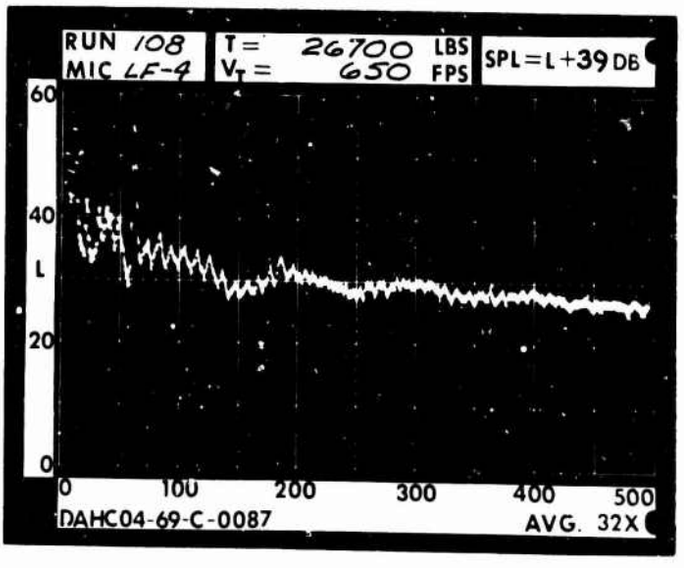

RUN 110

TIP SPEED 800 FT/SEC

THRUST 26700 LB

——————— .2 RAD.

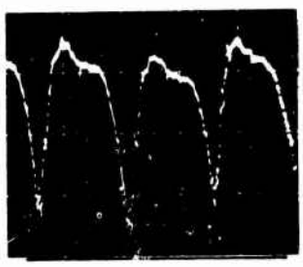

1 RAD.

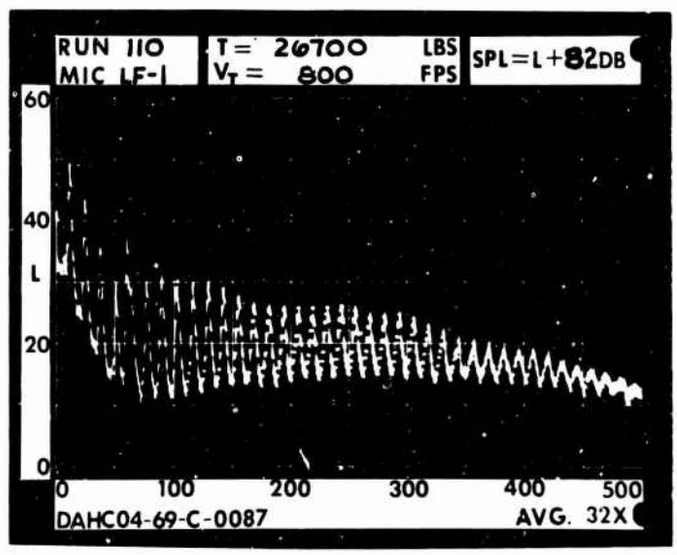

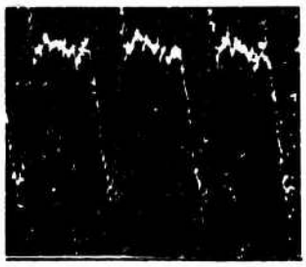

1 DIA.

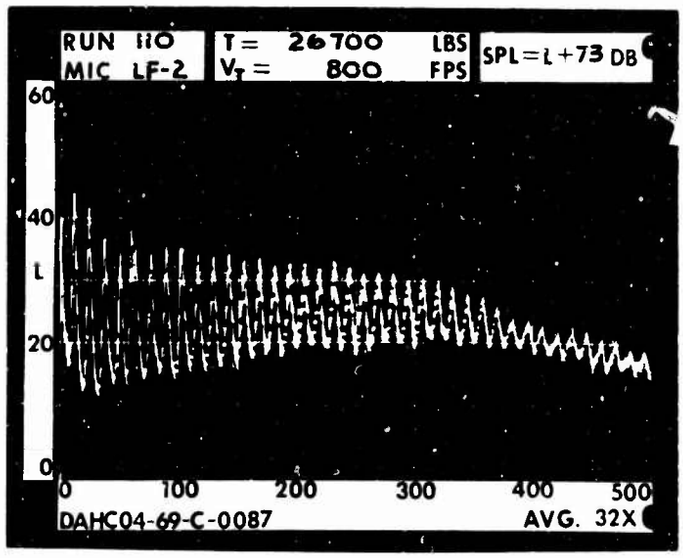

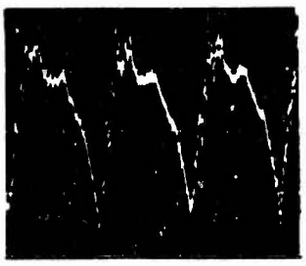

3 DIA.

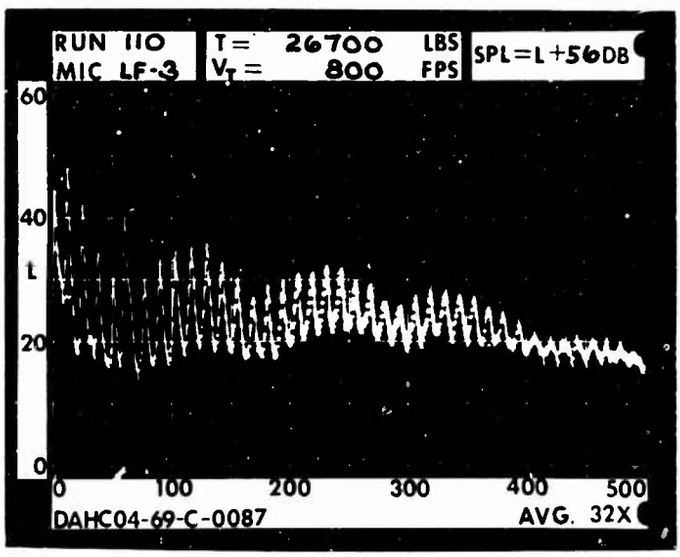

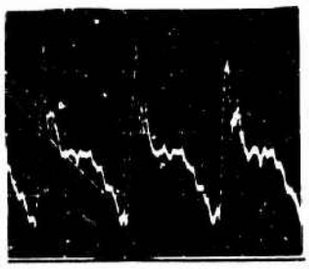

5 DIA.

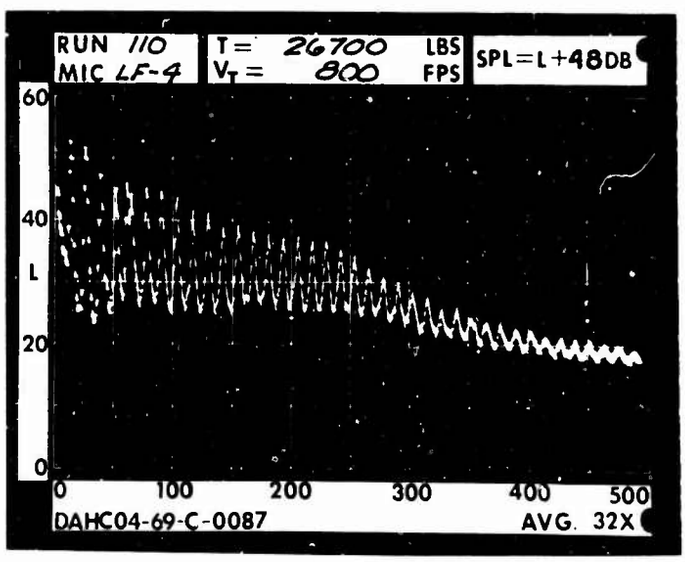

RUN 111

TIP SPEED 800 FT/SEC

THRUST 27400 LB

.2 RAD.

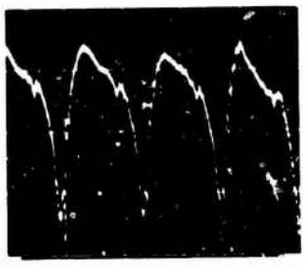

1 RAD.

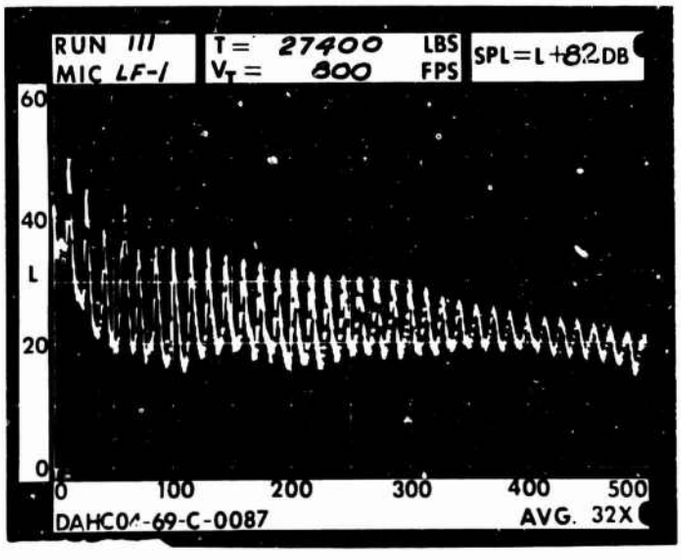

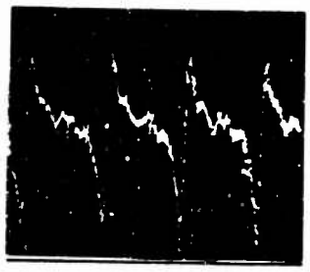

1 DIA.

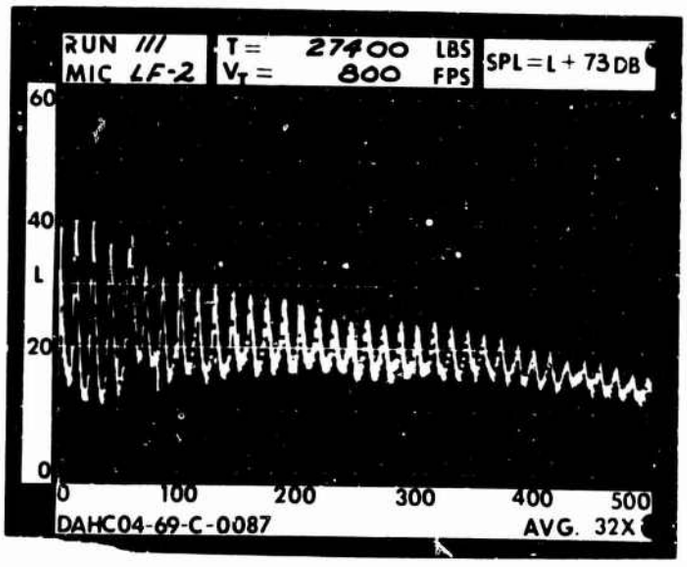

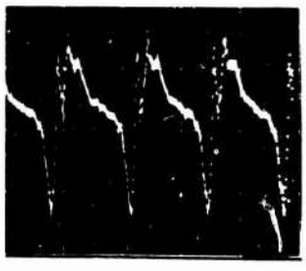

3 DIA.

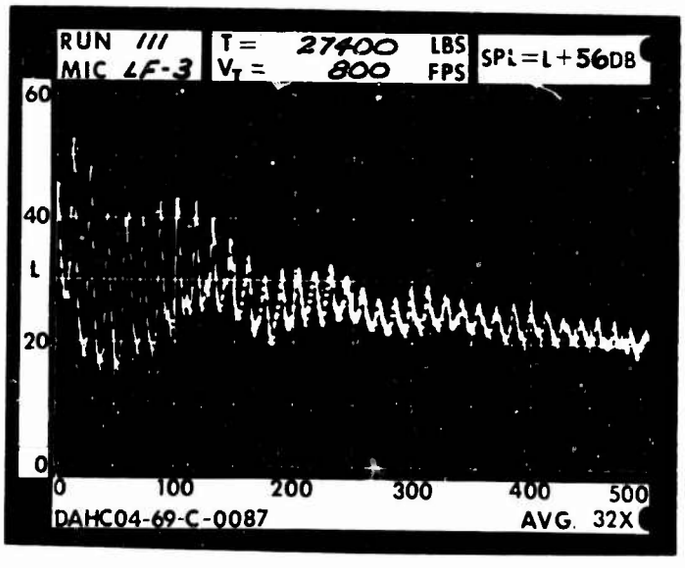

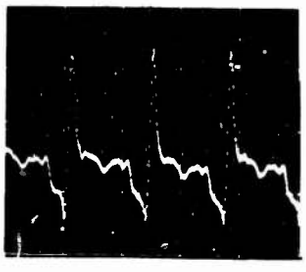

5 DIA.

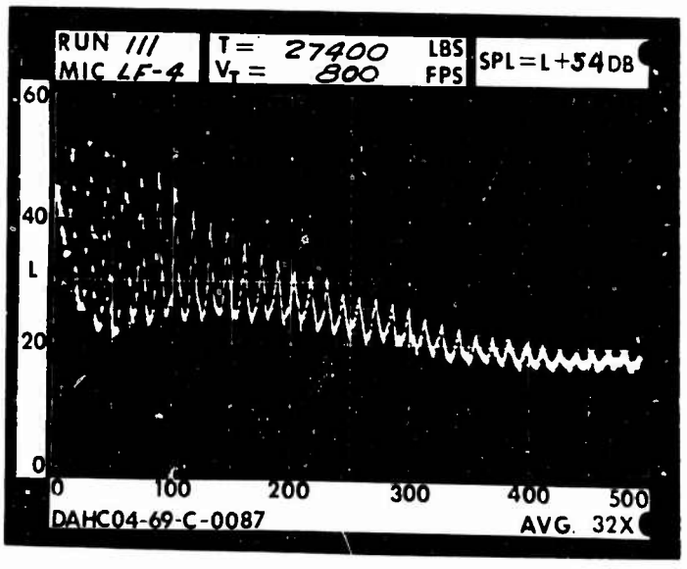

RUN 112

TIP SPEED 800 FT/SEC

THRUST 16800 LB

.2 RAD.

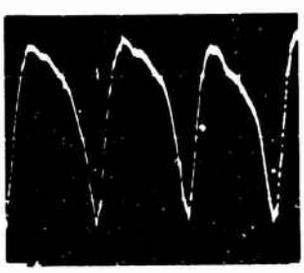

1 RAD.

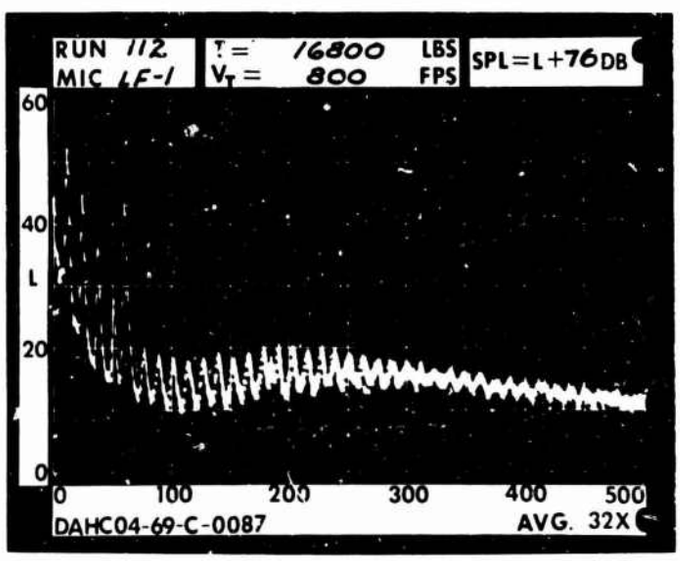

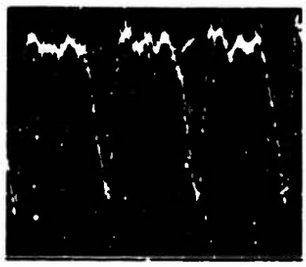

1 DIA.

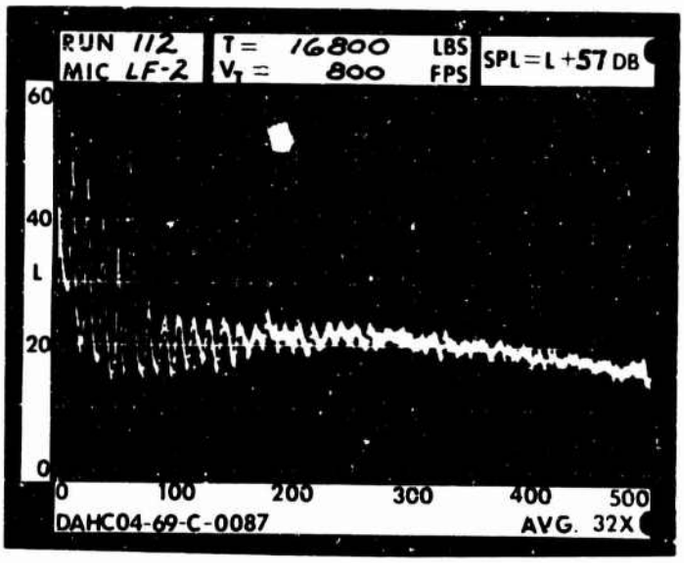

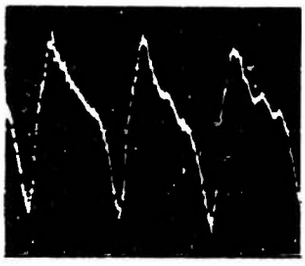

3 DIA.

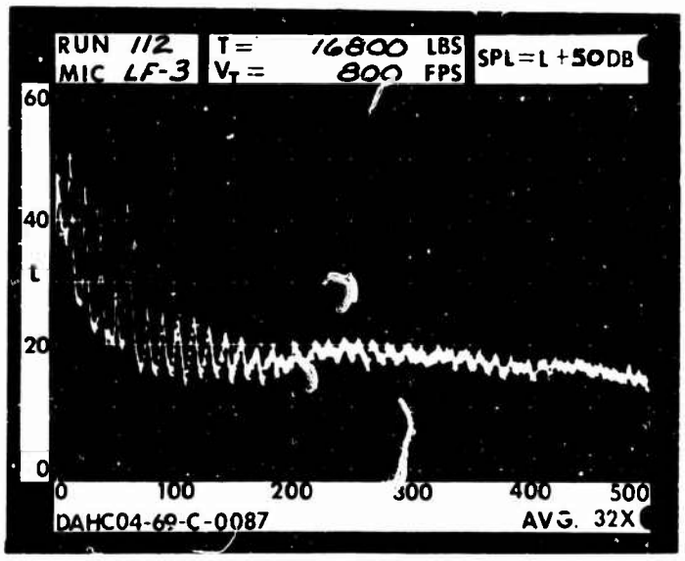

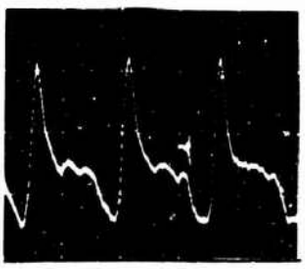

5 DIA.

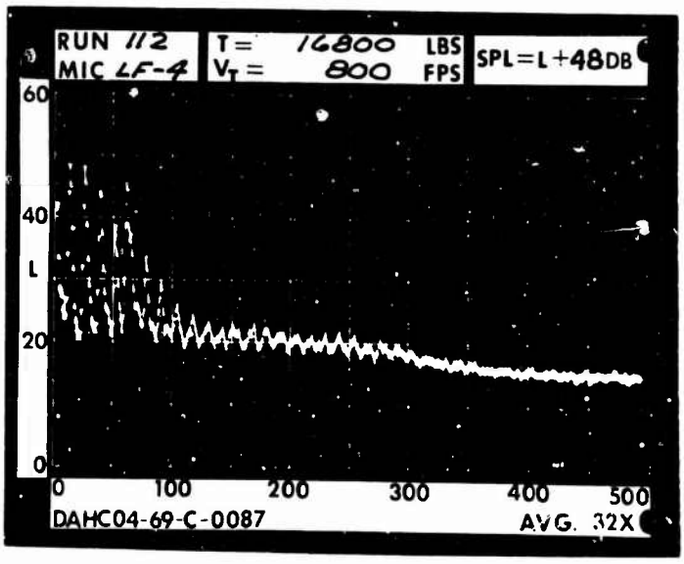

RUN 113

TIP SPEED 800 FT/SEC

THRUST 7700 LB

.2 RAD.

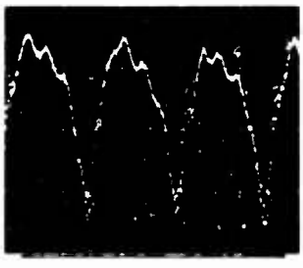

1 RAD.

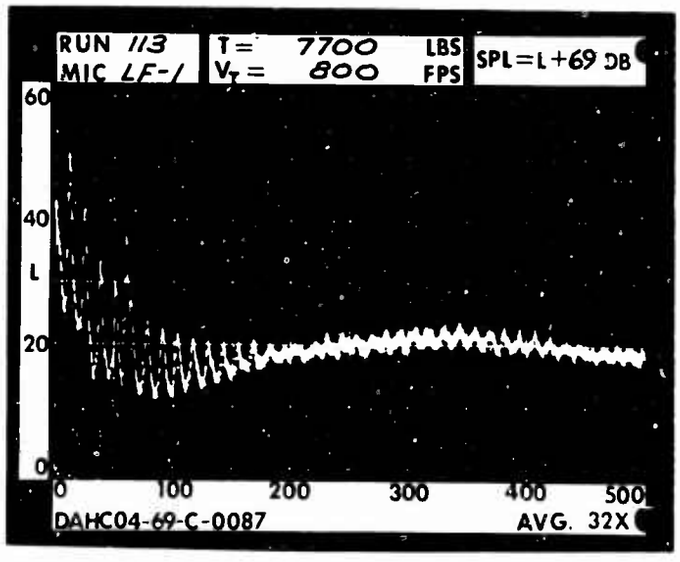

1 DIA.

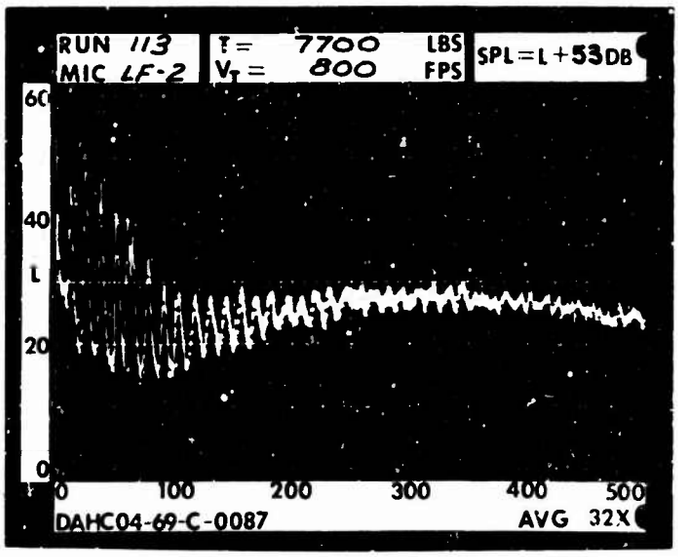

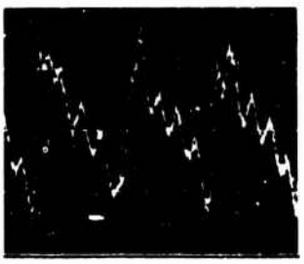

3 DIA.

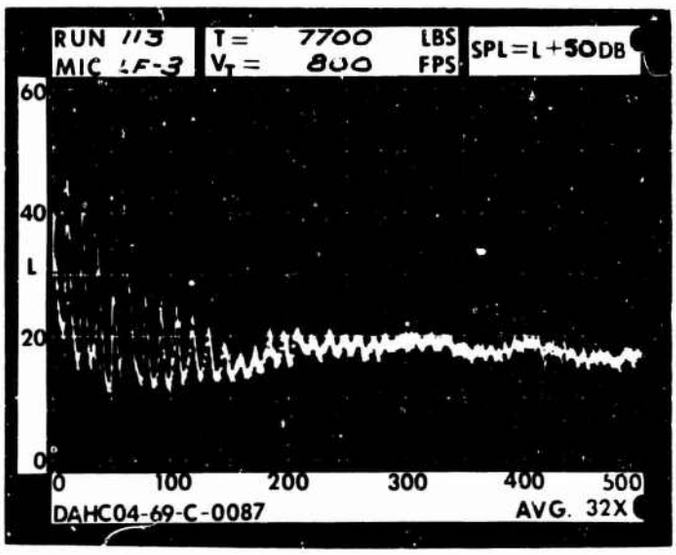

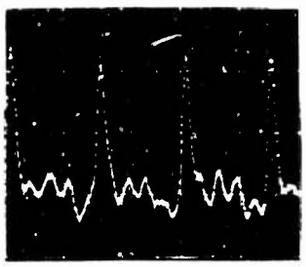

5 DIA.

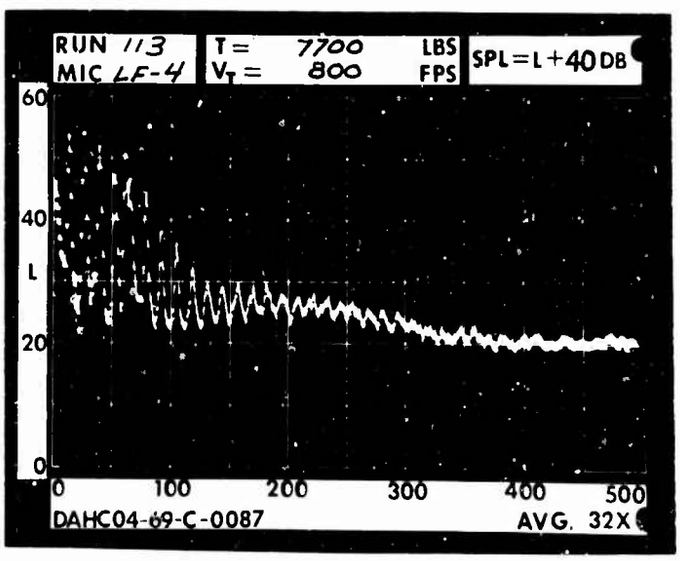

RUN 114

TIP SPEED 750 FT/SEC

THRUST 26800 LB

.2 RAD.

1 RAD.

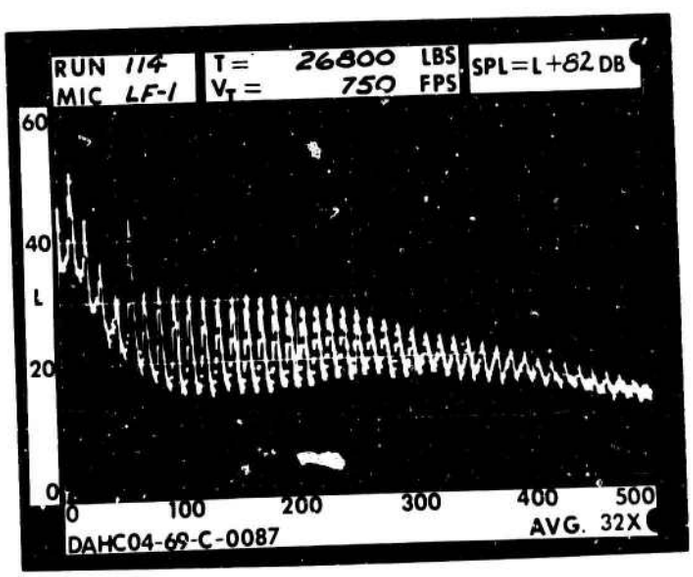

1 DIA.

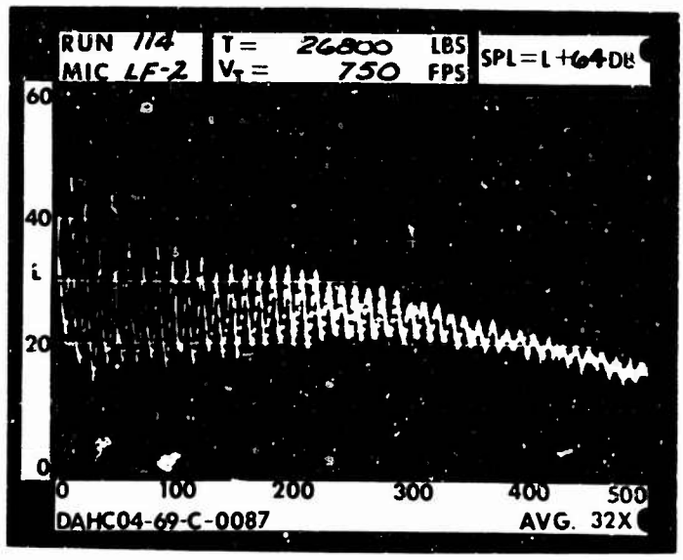

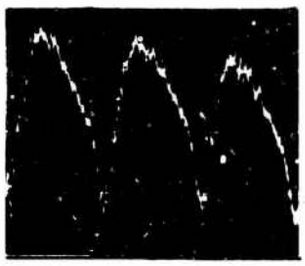

3 DIA.

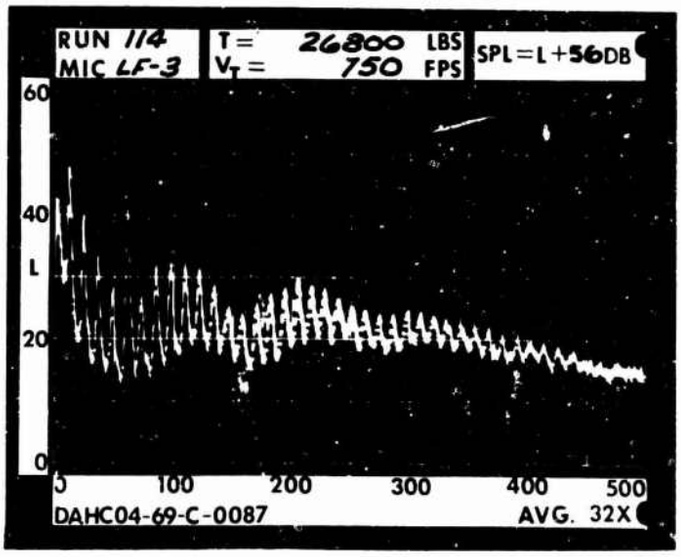

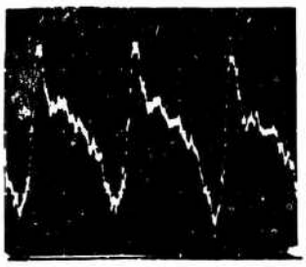

5 DIA.

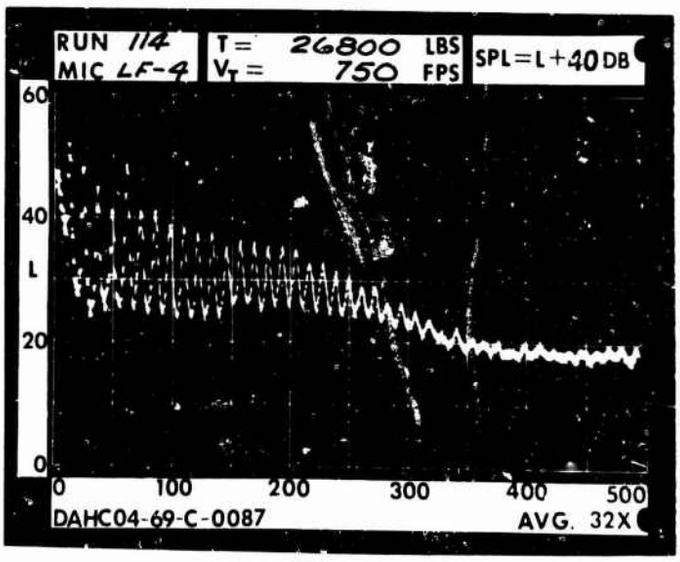

RUN 115

TIP SPEED 750 FT/SEC

THRUST 26900 LB

——————— .2 RAD.

——————— 1 RAD.

1 DIA.

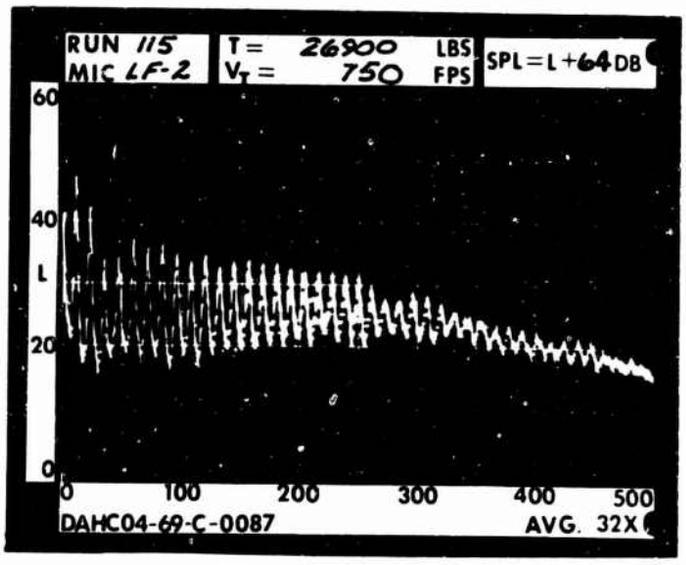

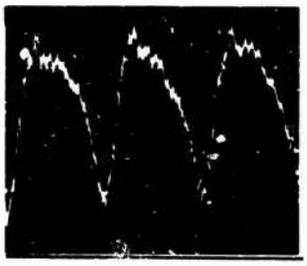

3 DIA.

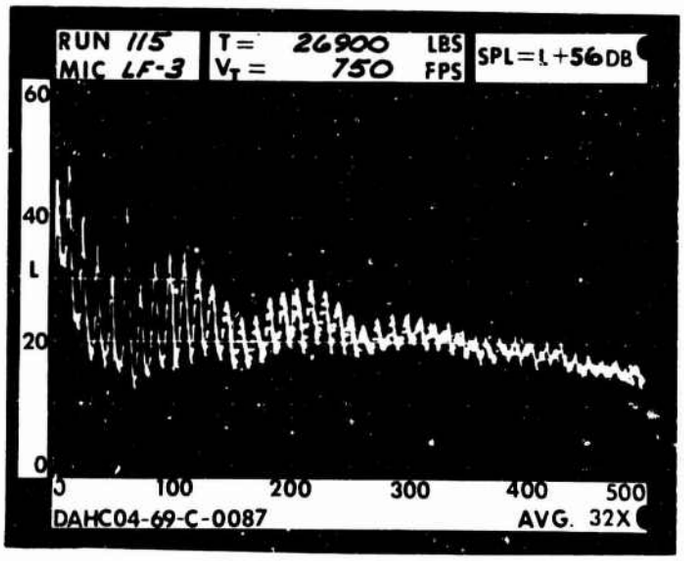

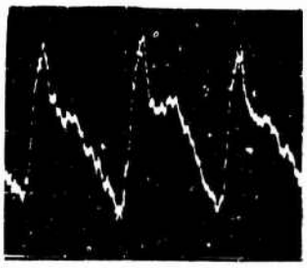

5 DIA.

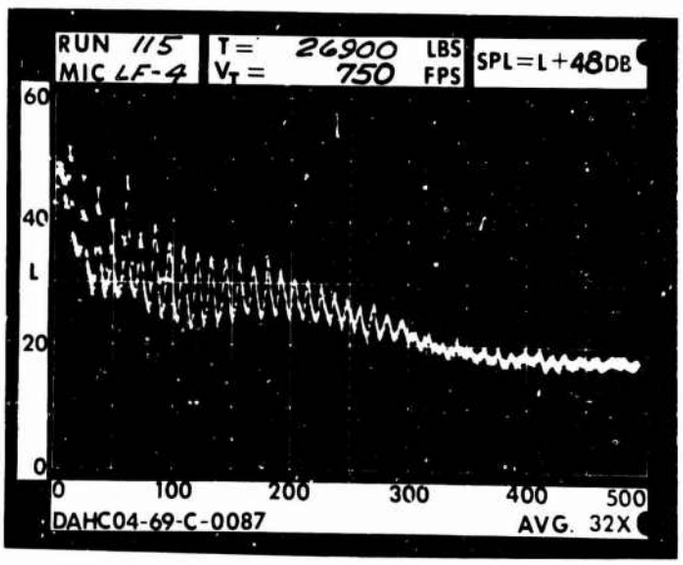

RUN 116

TIP SPEED 750 FT/SEC

THRUST 27100 LB

.2 RAD.

1 RAD.

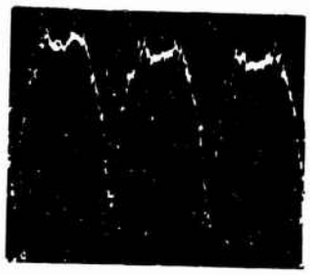

1 DIA.

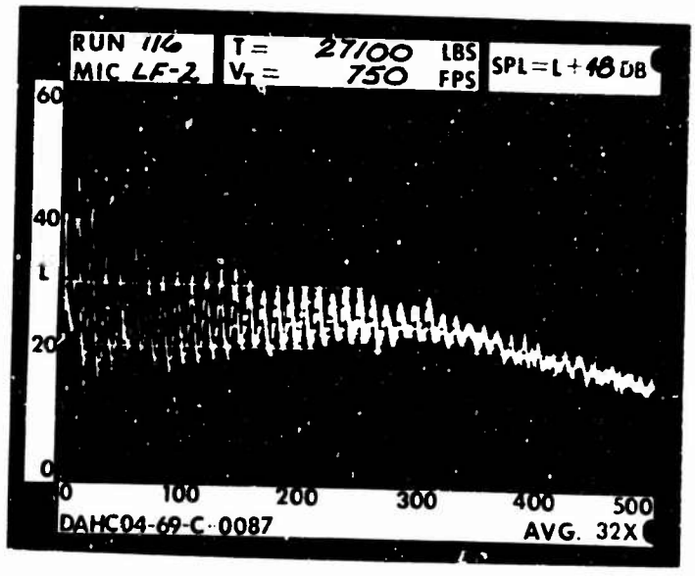

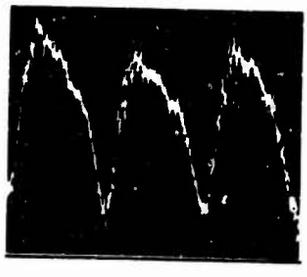

3 DIA.

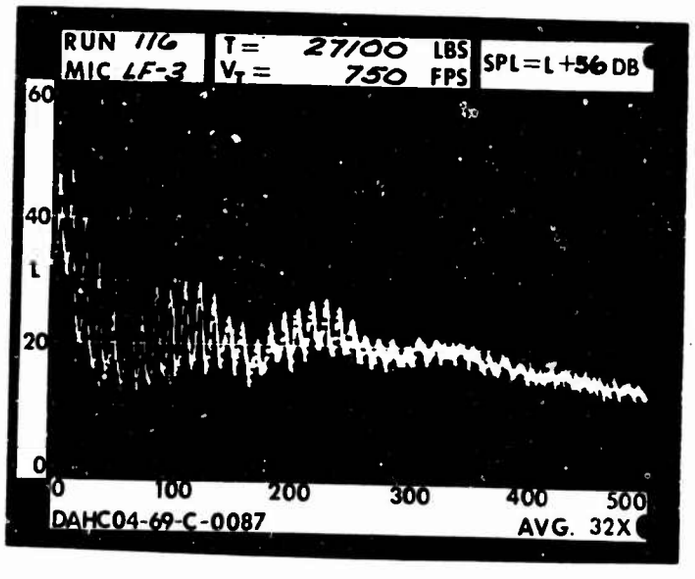

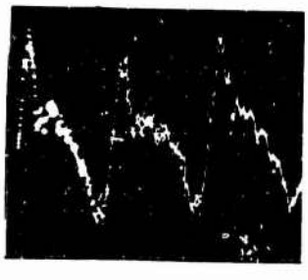

5 DIA.

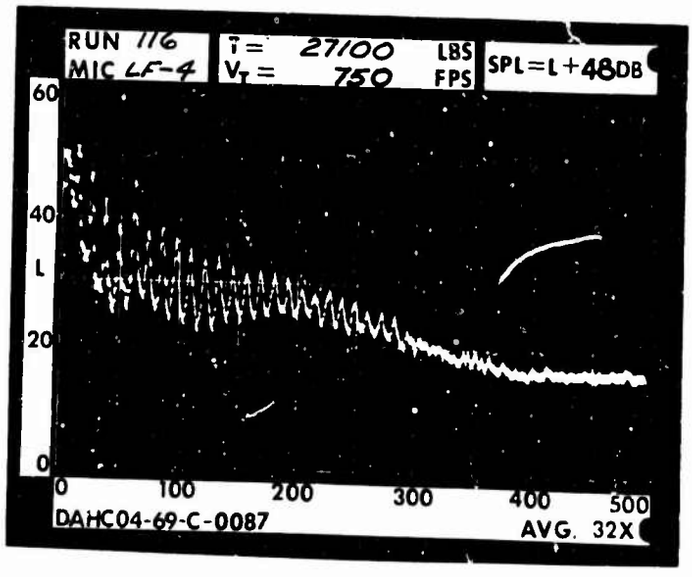

RUN 117

TIP SPEED 850 FT/SEC

THRUST 26800 LB

.2 RAD.

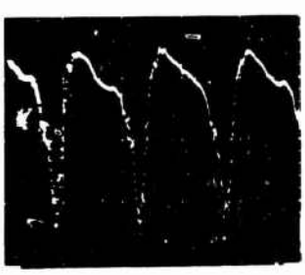

1 RAD.

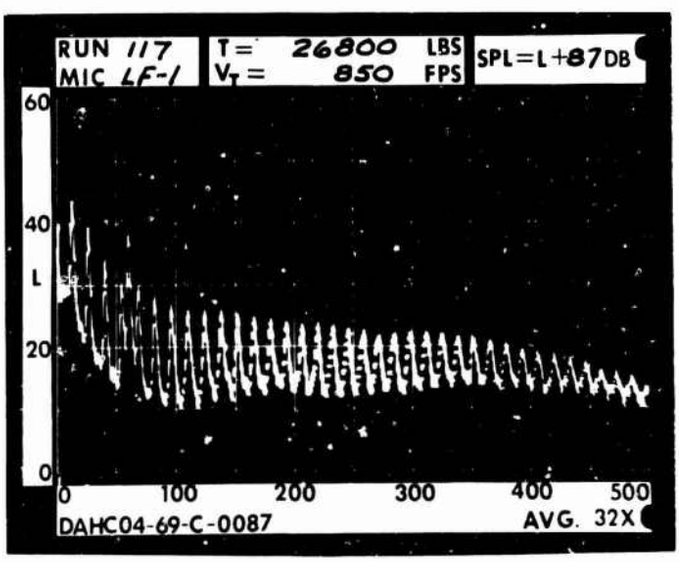

RUN 117

TIP SPEED 850 FT/SEC

THRUST 26800 LB

.2 RAD.

1 RAD.

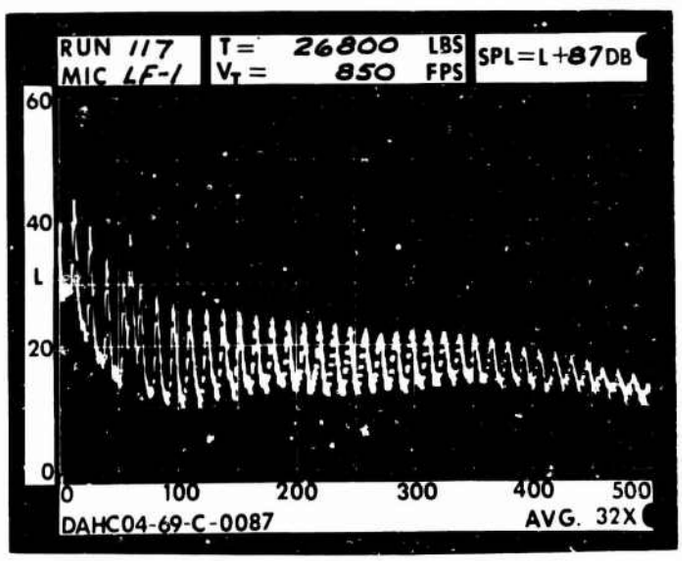

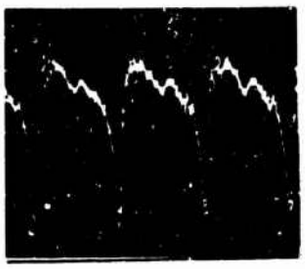

1 DIA.

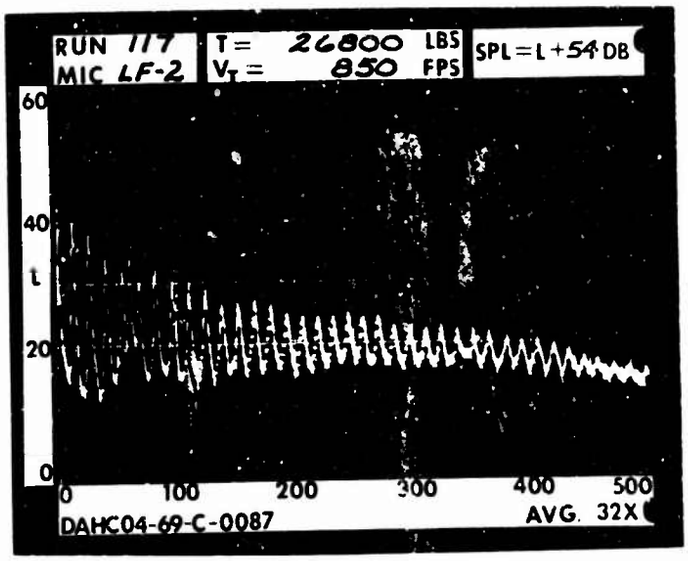

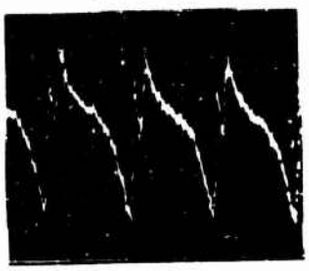

3 DIA.

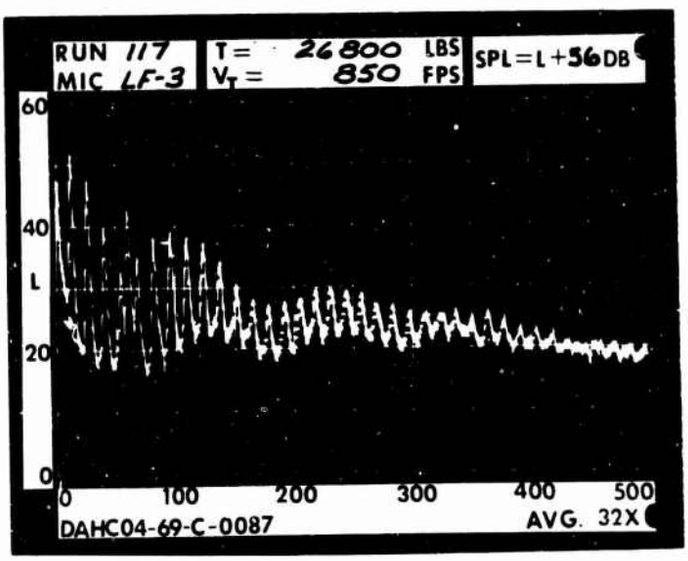

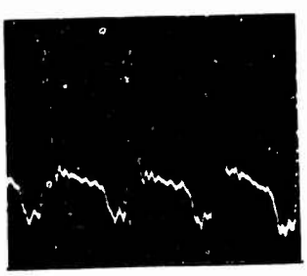

5 DIA.

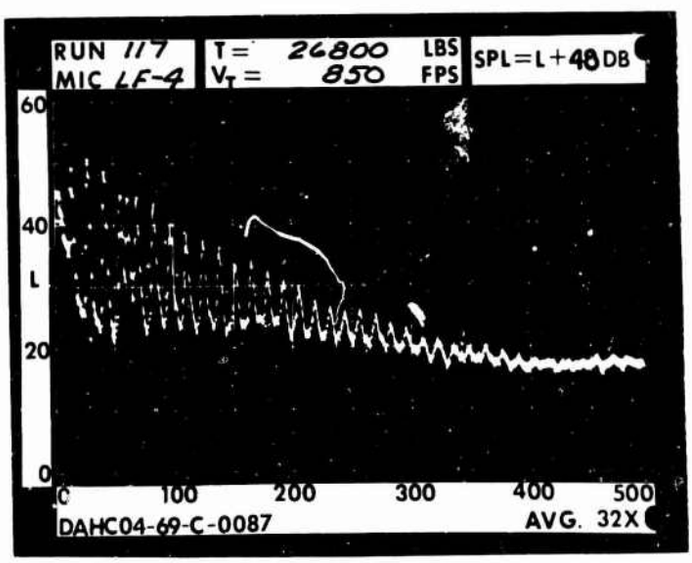

RUN 118

TIP SPEED 750 FT/SEC

THRUST 26100 LB

.2 RAD.

1 RAD.

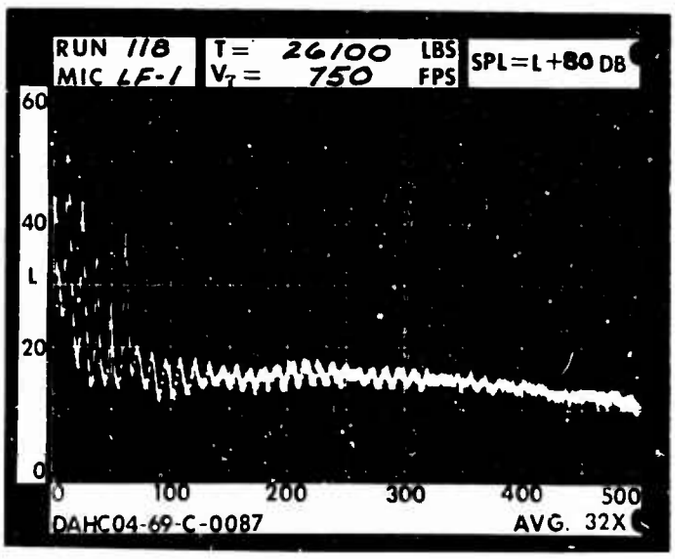

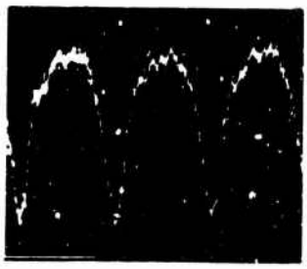

1 DIA.

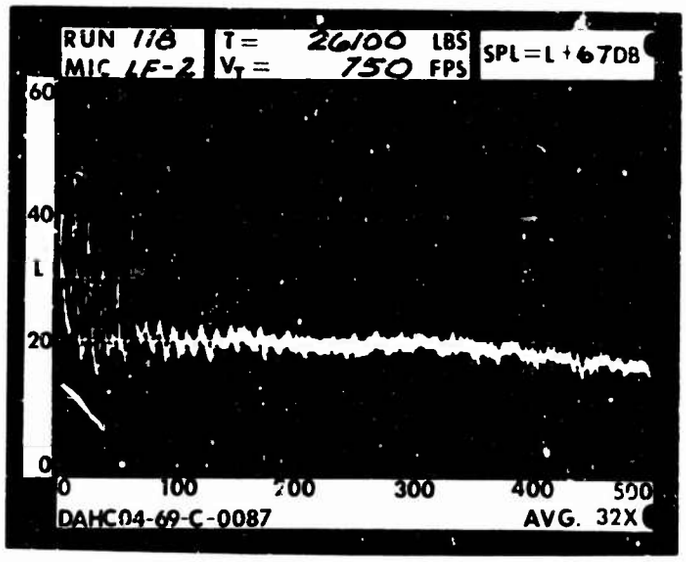

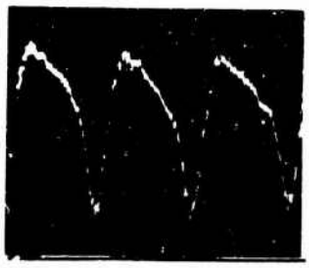

3 DIA.

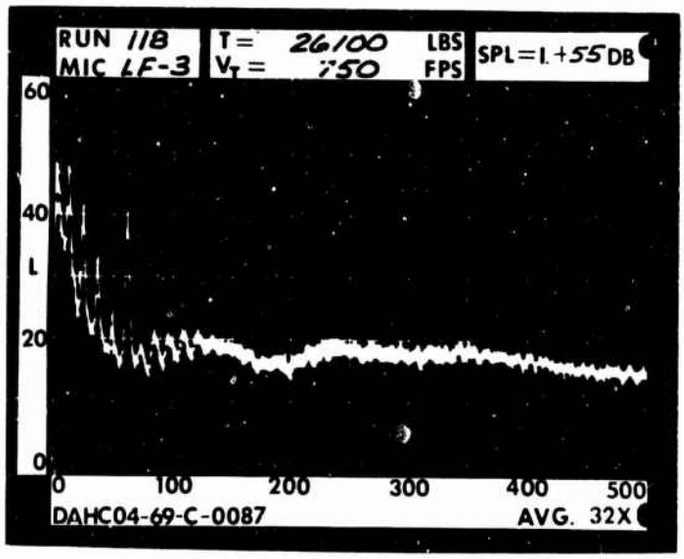

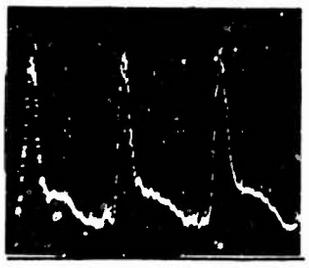

5 DIA.

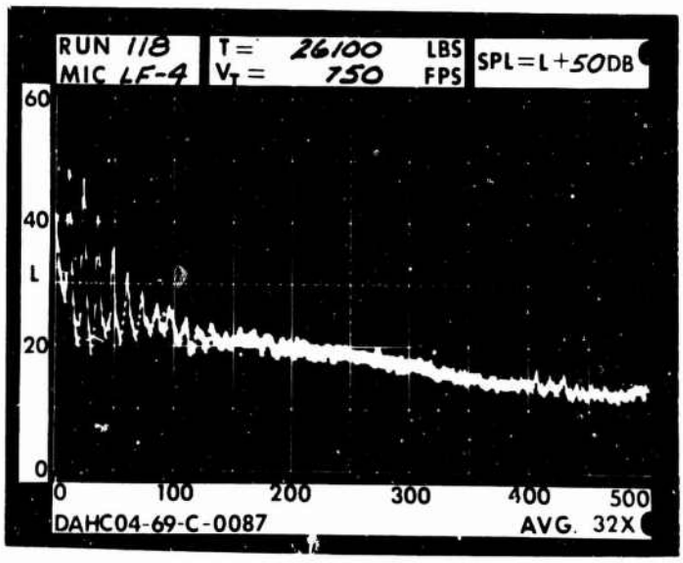

RUN 119

TIP SPEED 850 FT/SEC

THRUST 27600 LB

.2 RAD.

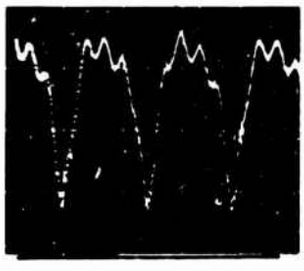

1 RAD.

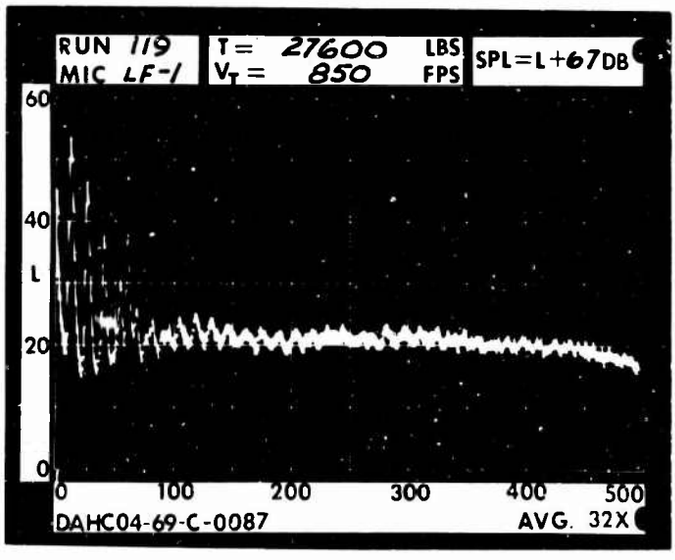

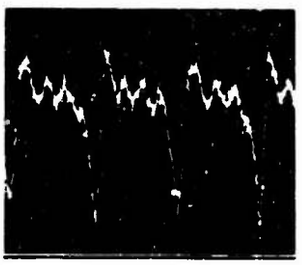

1 DIA.

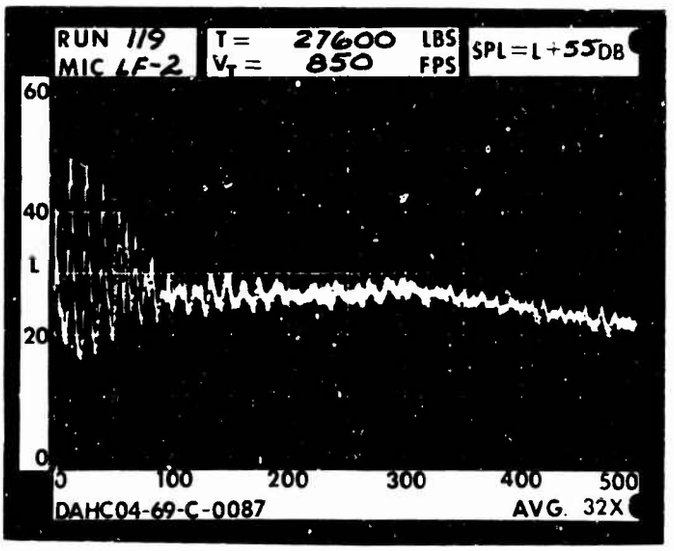

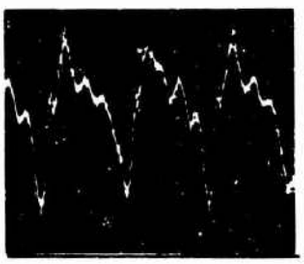

3 DIA.

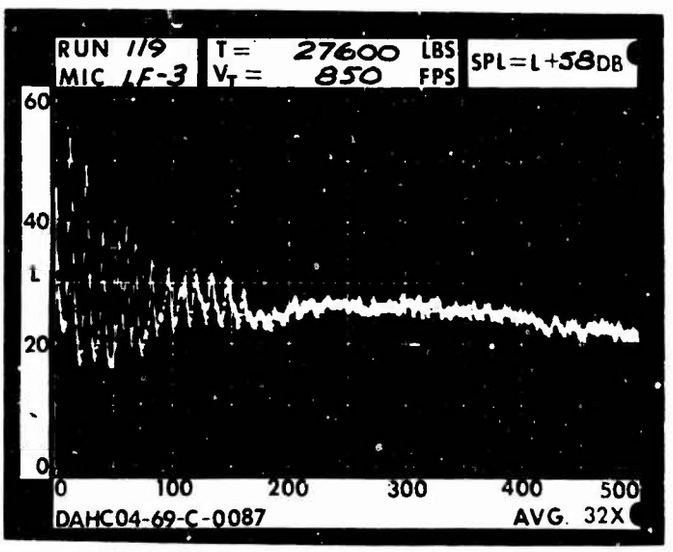

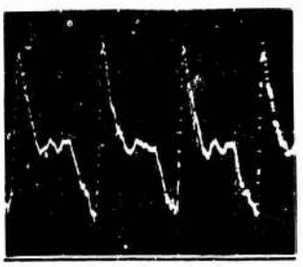

5 DIA.

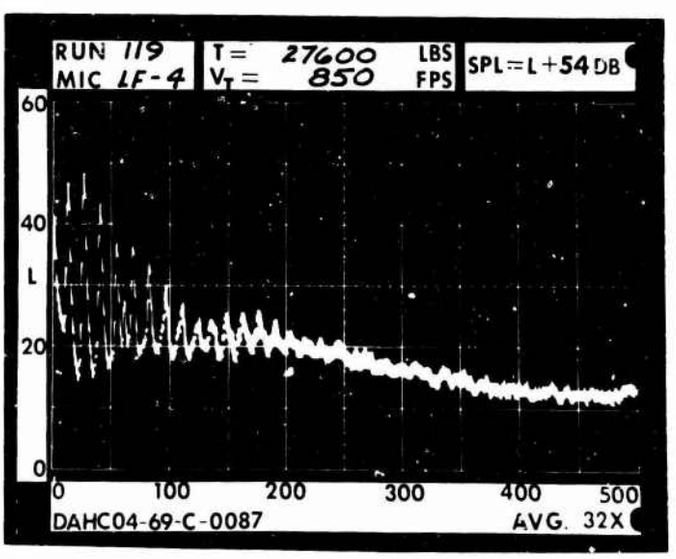

RUN 120

TIP SPEED 850 FT/SEC

THRUST 26900 LB

.2 RAD.

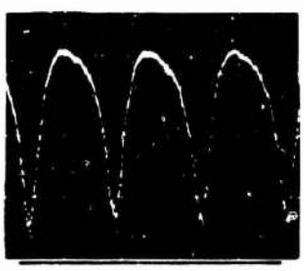

1 RAD.

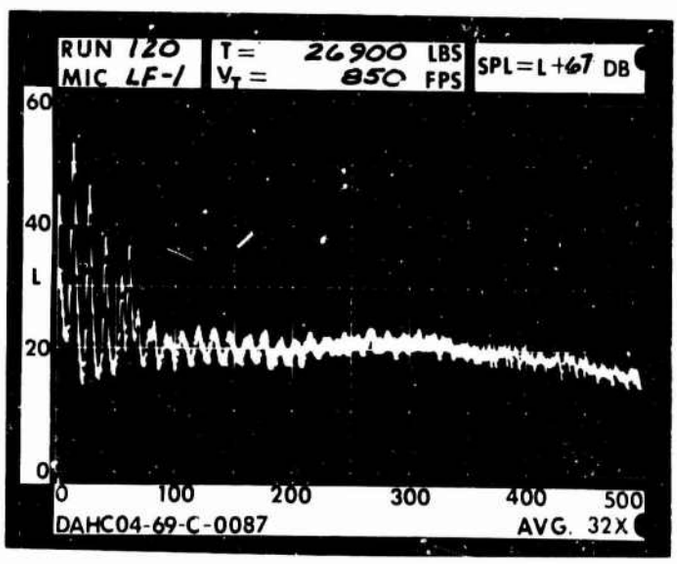

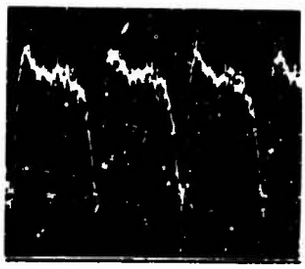

1 DIA.

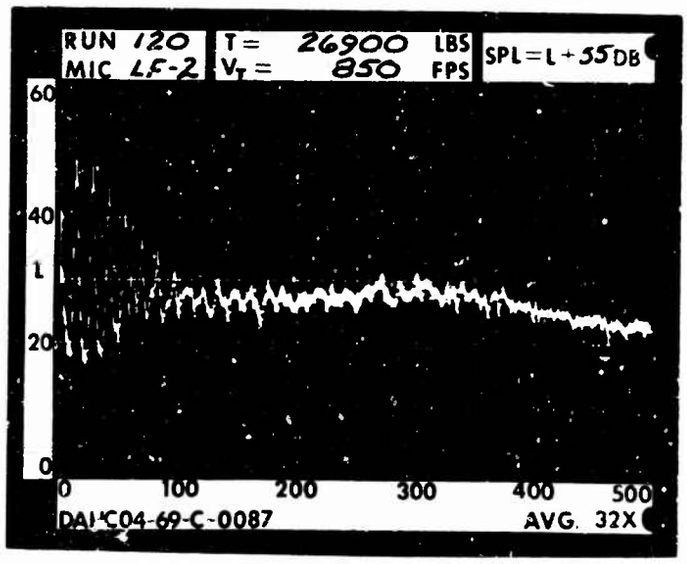

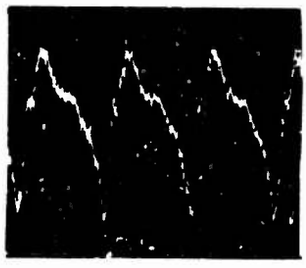

3 DIA.

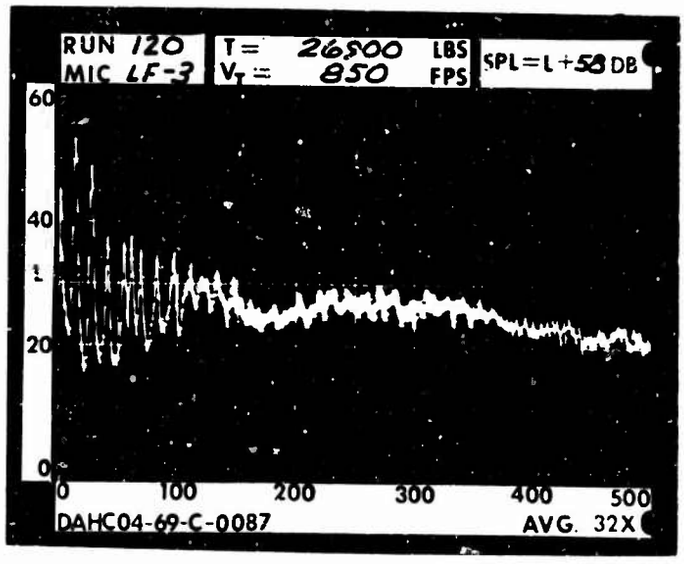

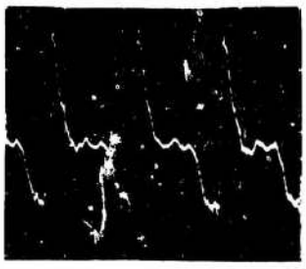

5 DIA.

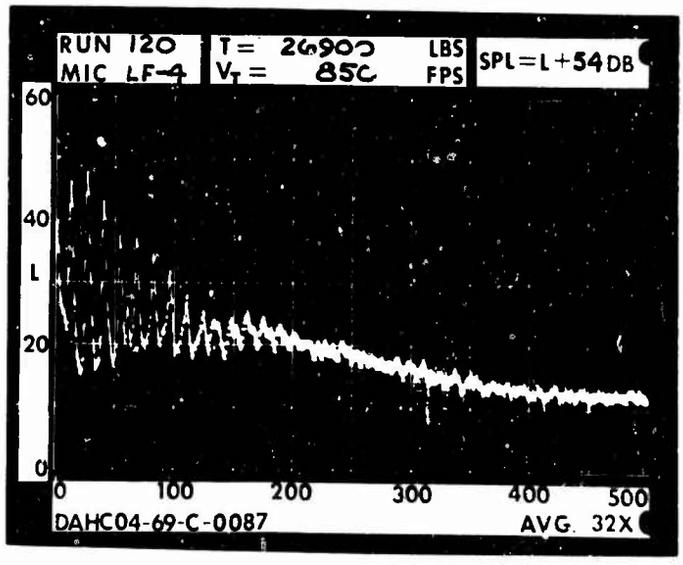

RUN 121

TIP SPEED 800 FT/SEC

THRUST 21300 LB

.2 RAD.

1 RAD.

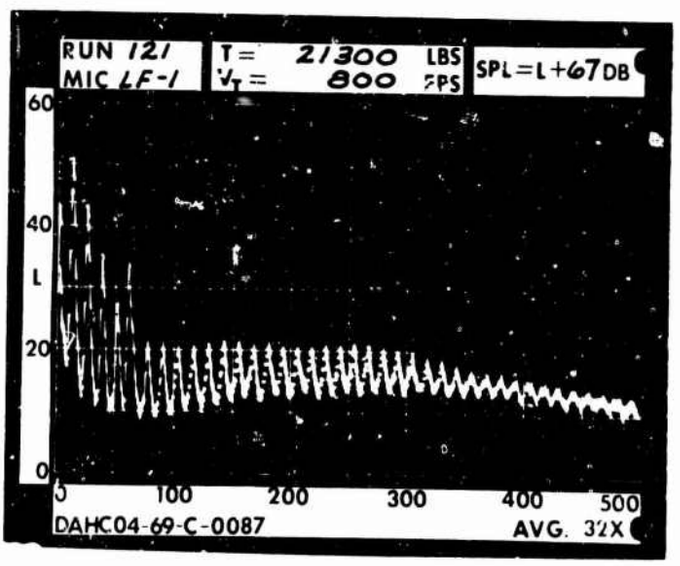

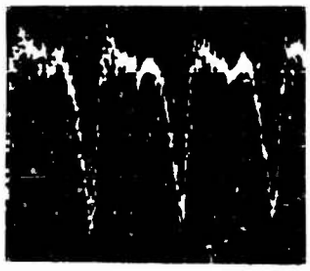

1 DIA.

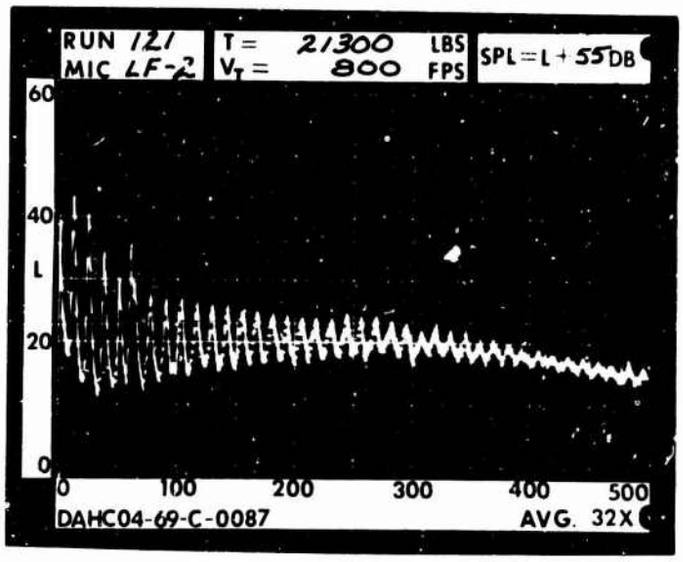

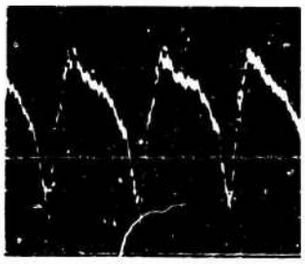

3 DIA.

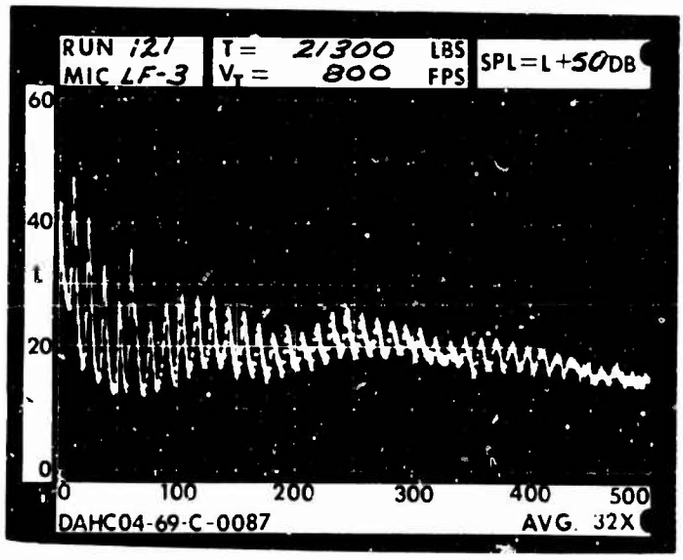

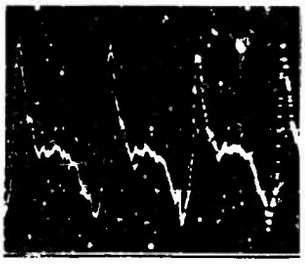

5 DIA.

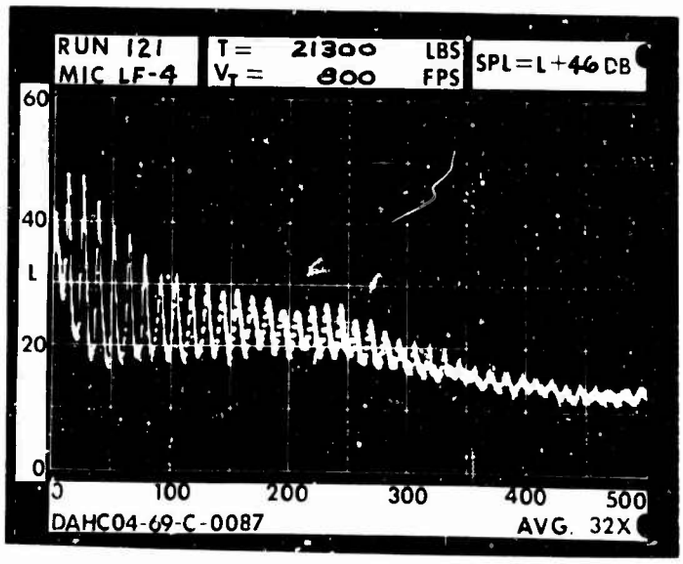

RUN 122

TIP SPEED 800 FT/SEC

THRUST 12100 LB

.2 RAD.

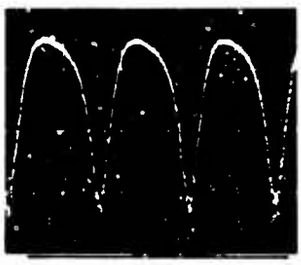

1 RAD.

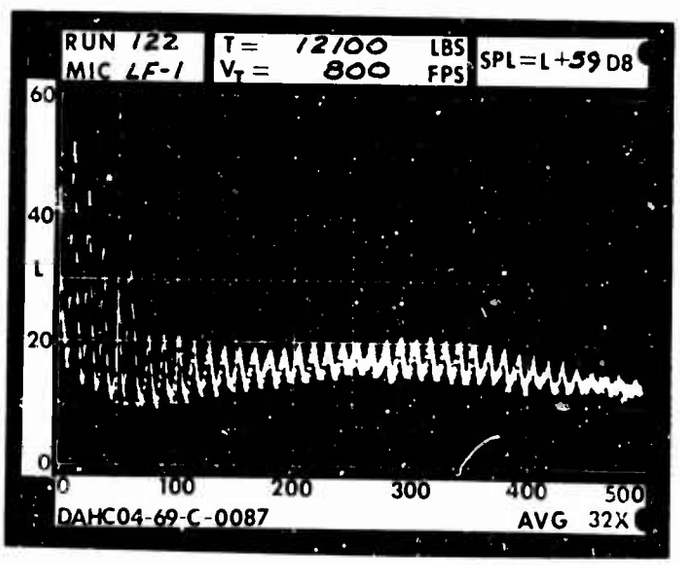

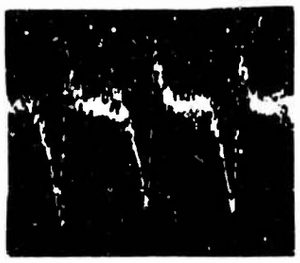

1 DIA.

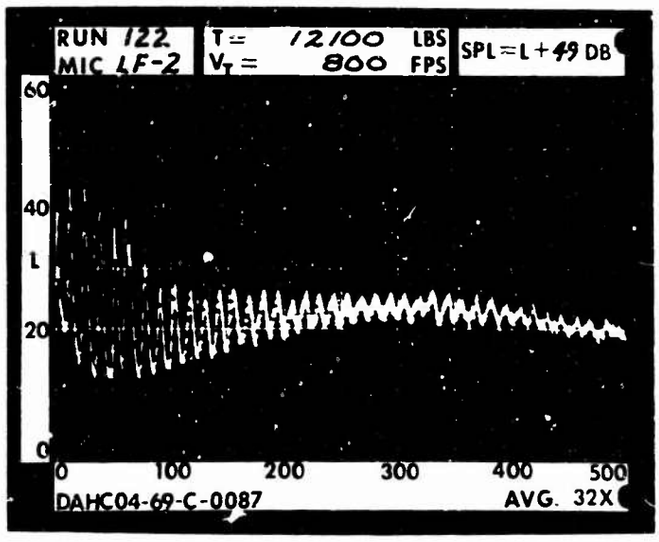

3 DIA.

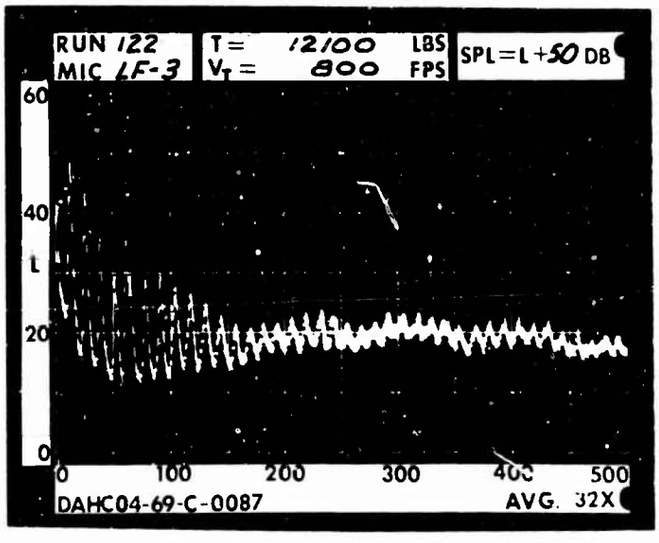

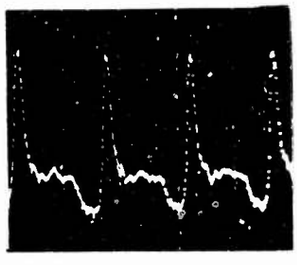

5 DIA.

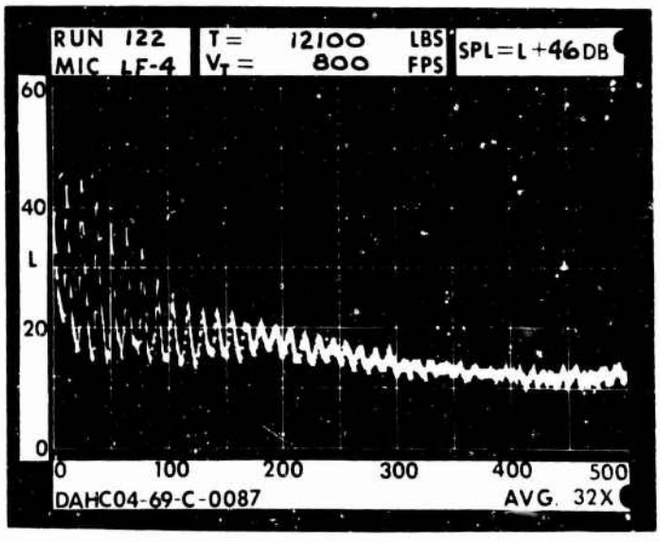

RUN 31

TIP SPEED 850 FT/SEC

THRUST 8300 LB

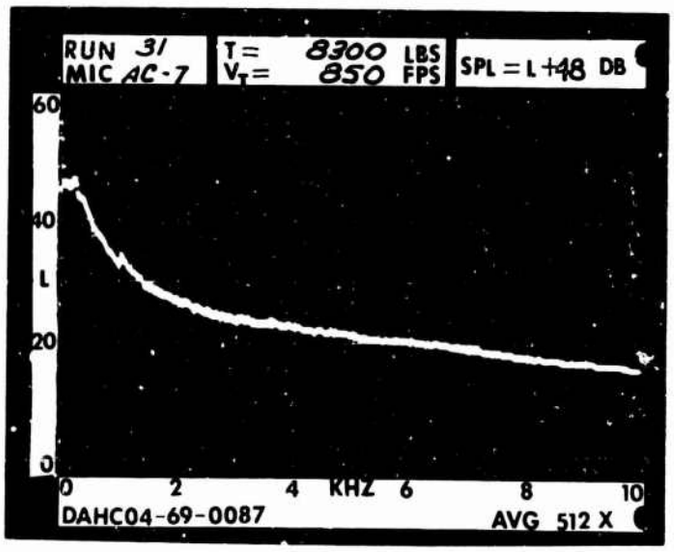

.2 RAD.

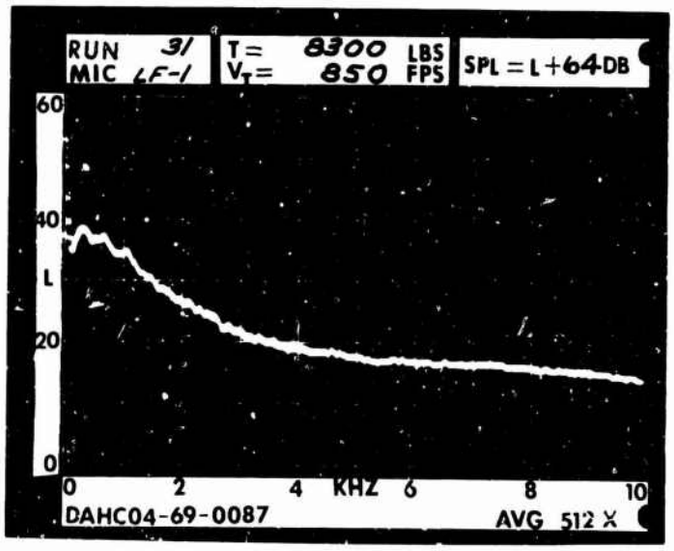

1 RAD.

1 DIA.

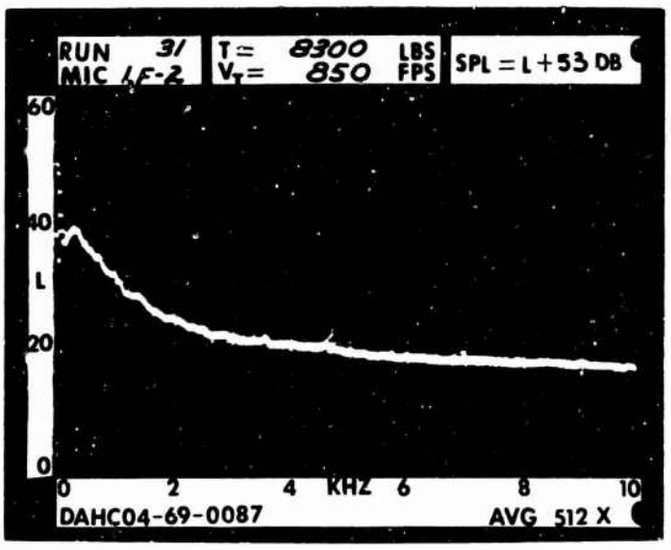

3 DIA.

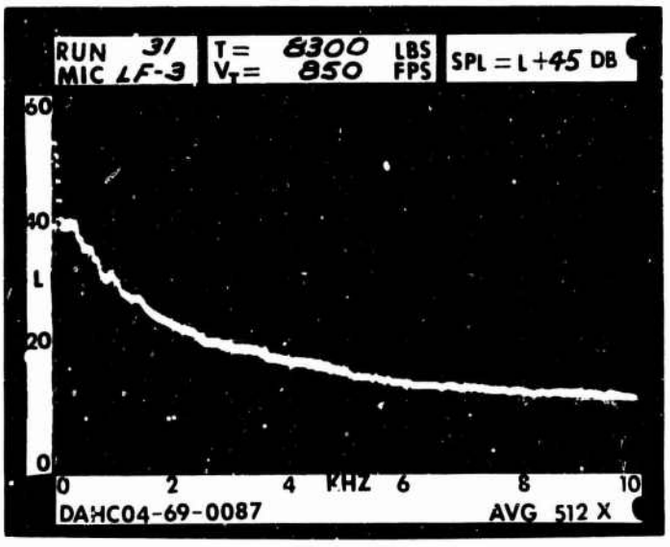

5 DIA.

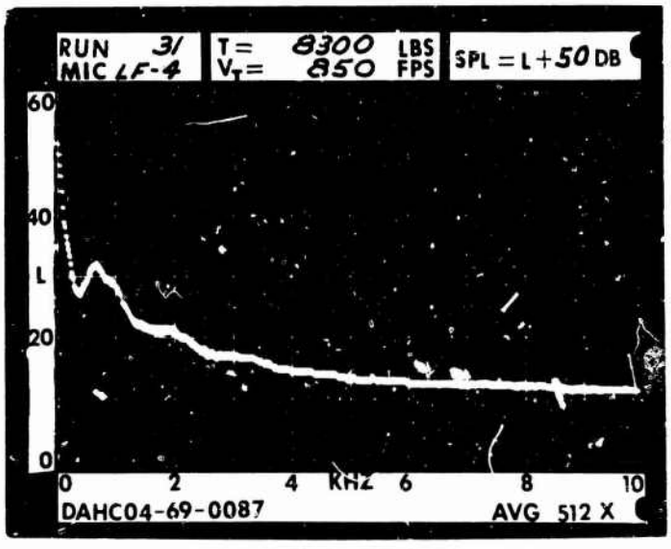

RUN 34

TIP SPEED 850 FT/SEC

THRUST 16900 LB

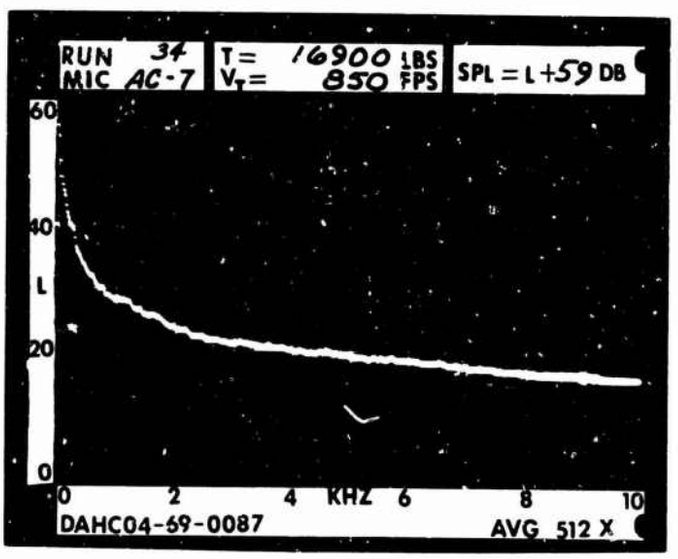

.2 RAD.

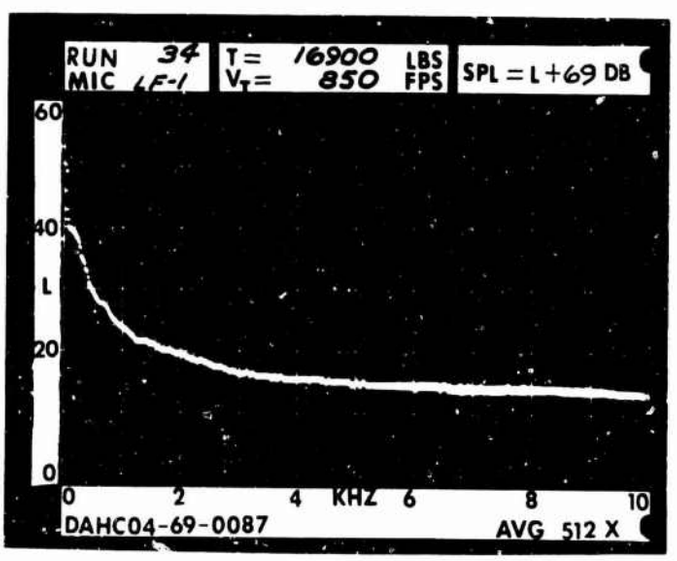

1 RAD.

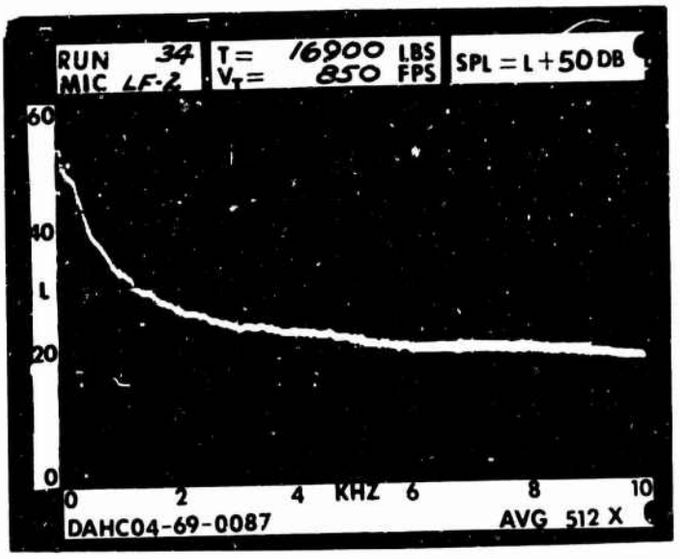

1 DIA.

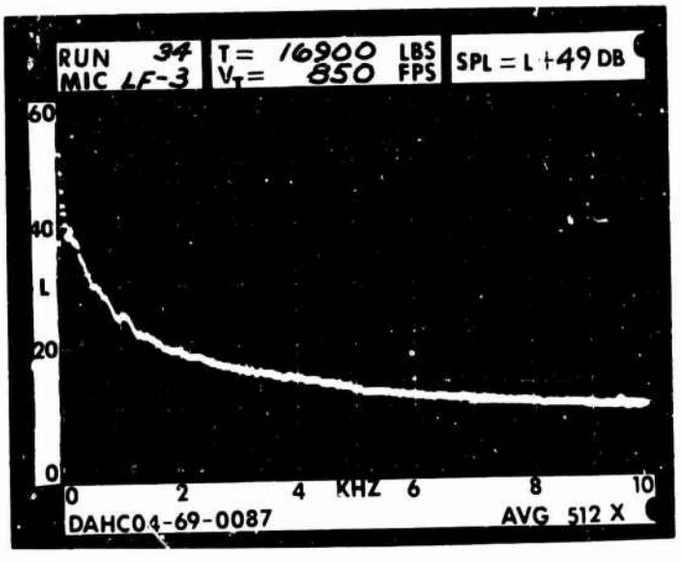

3 DIA.

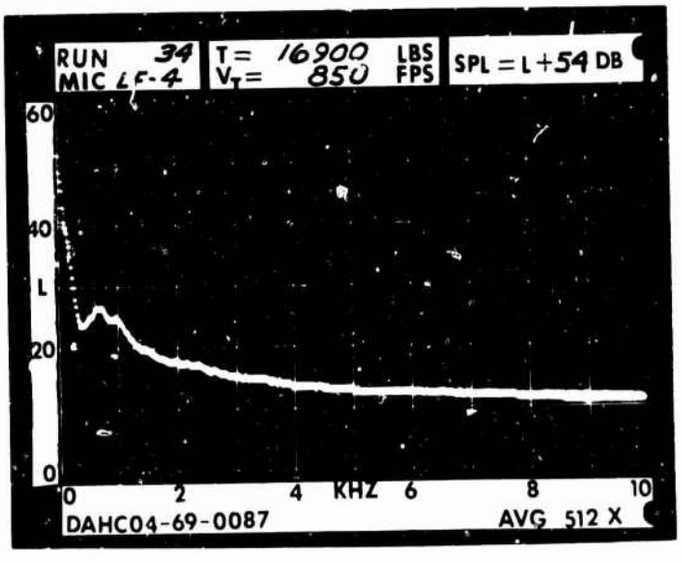

5 DIA.

RUN 36

TIP SPEED 850 FT/SEC

THRUST 26600 LB

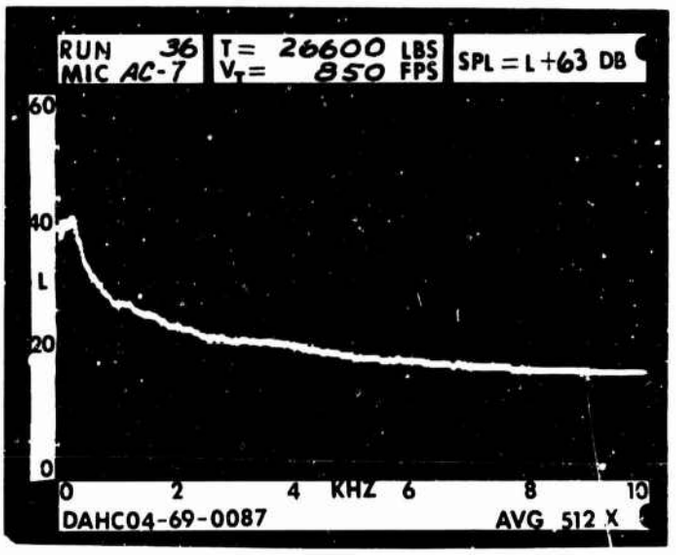

.2 RAD.

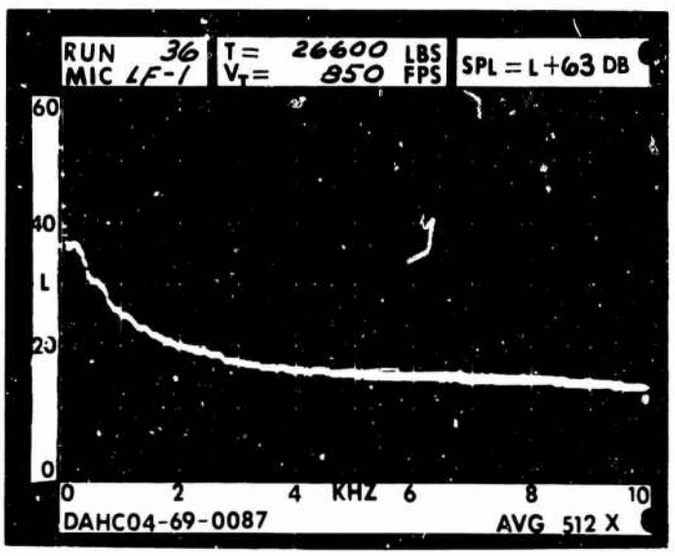

1 RAD.

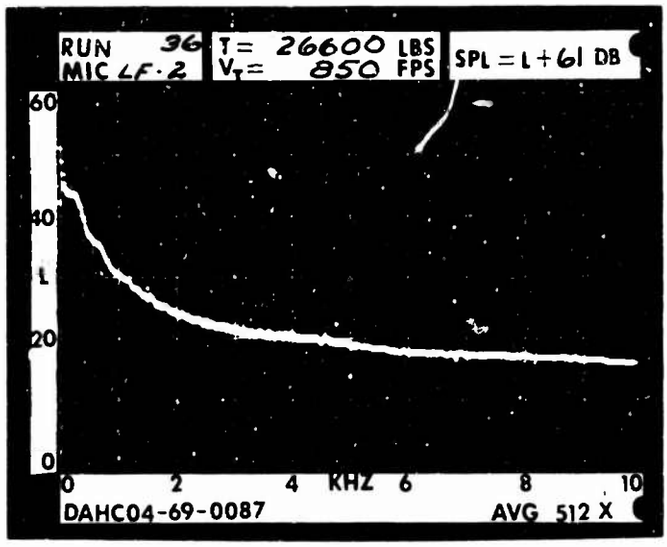

1 DIA.

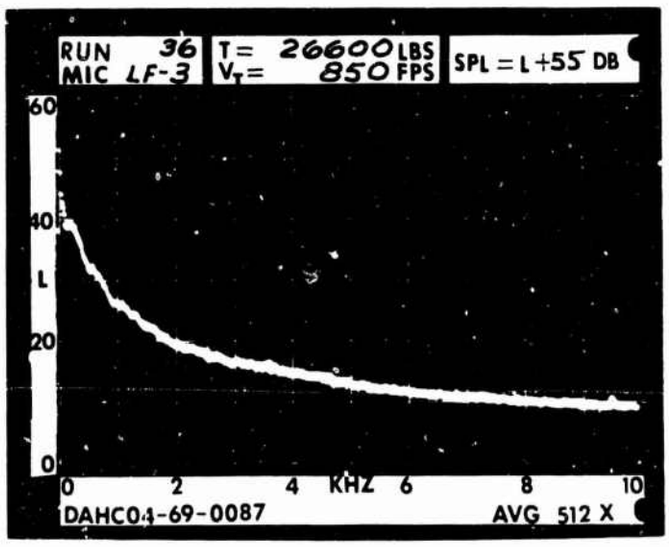

3 DIA.

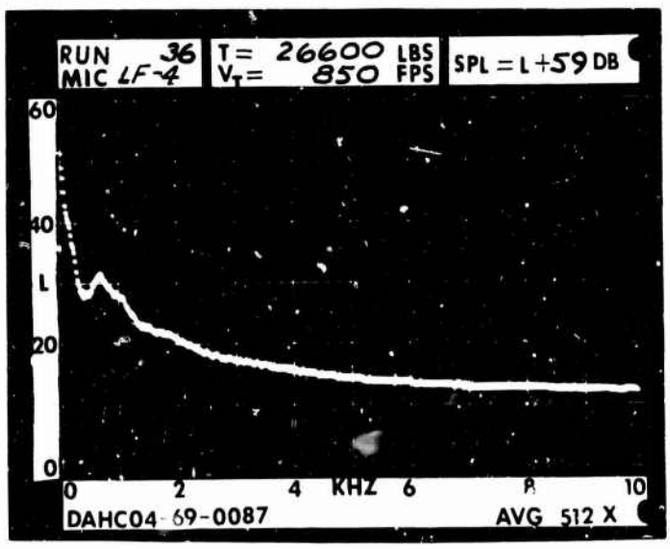

5 DIA.

RUN 51

TIP SPEED 750 FT/SEC

THRUST 9700 LB

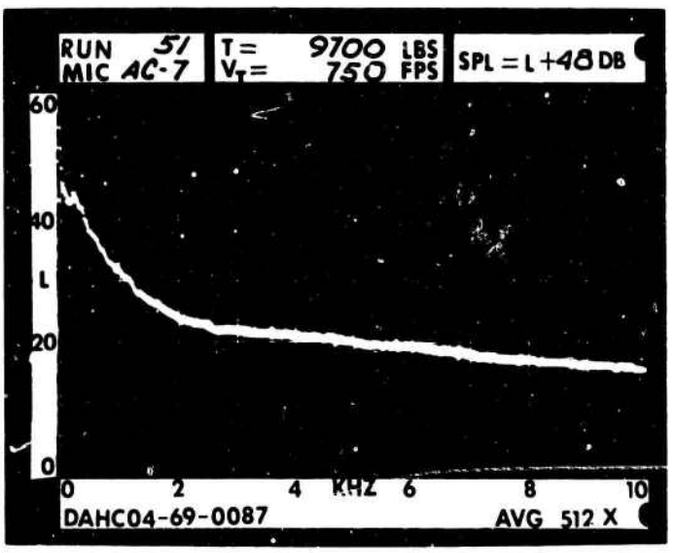

.2 RAD.

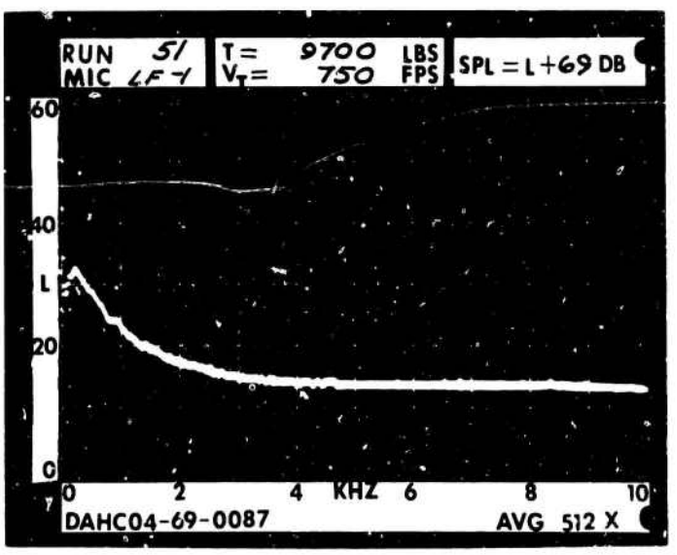

1 RAD.

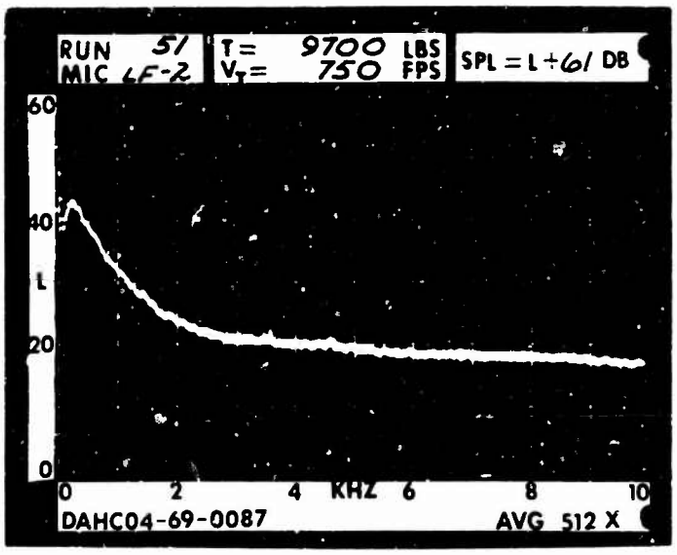

1 DIA.

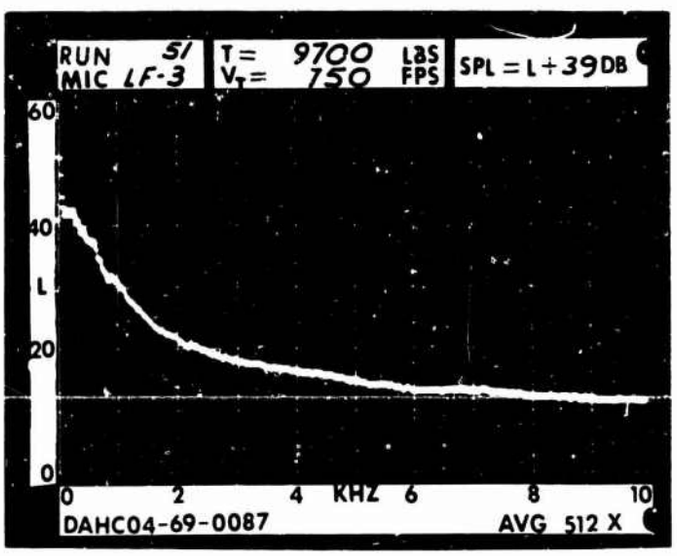

3 DIA.

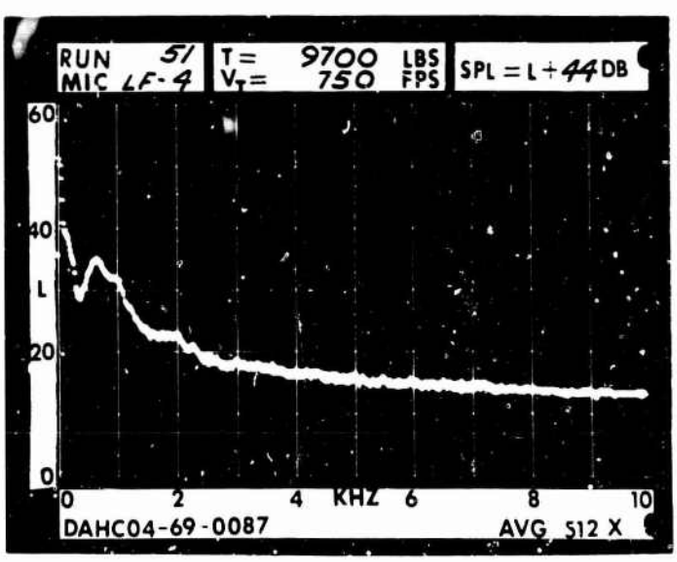

5 DIA.

RUN 54

TIP SPEED 750 FT/SEC

THRUST 19000 LB

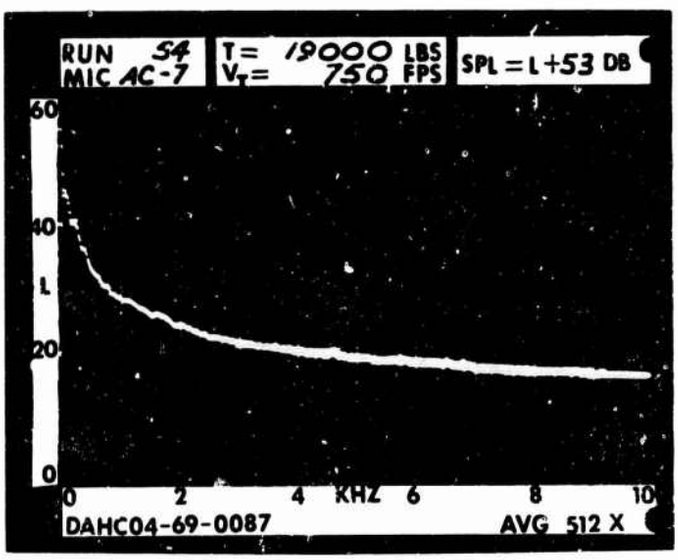

.2 RAD.

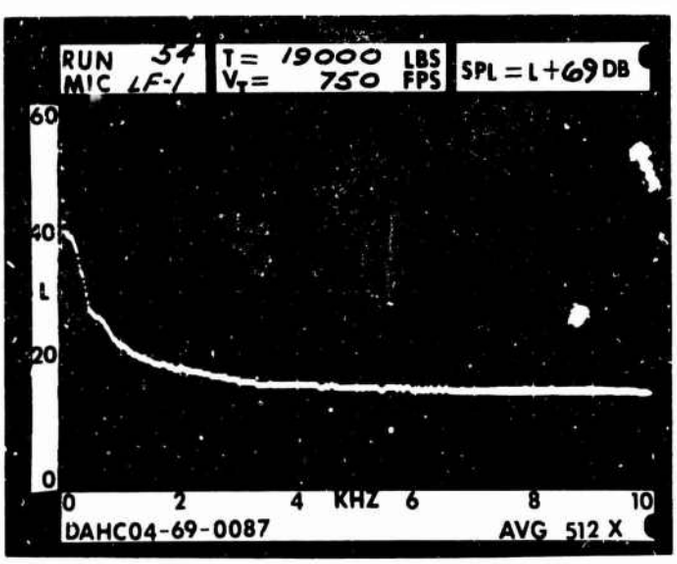

1 RAD.

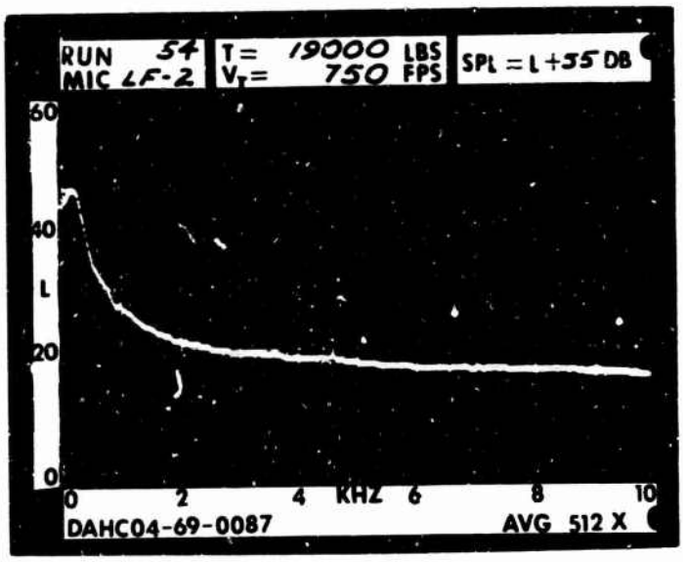

1 DIA.

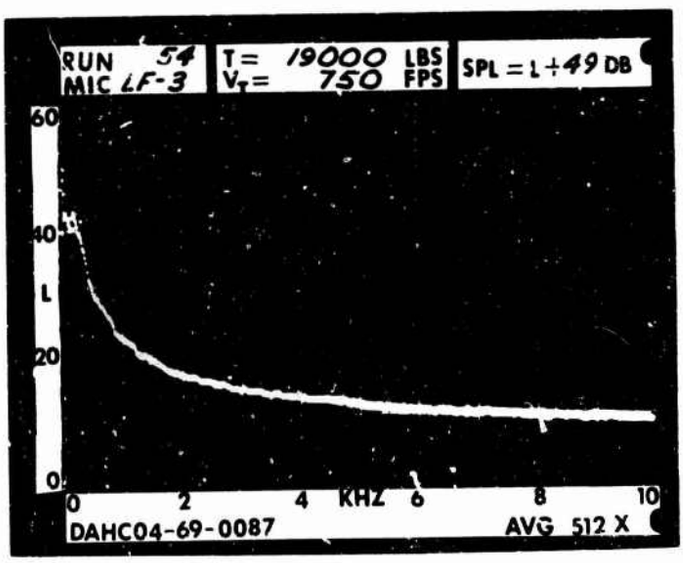

3 DIA.

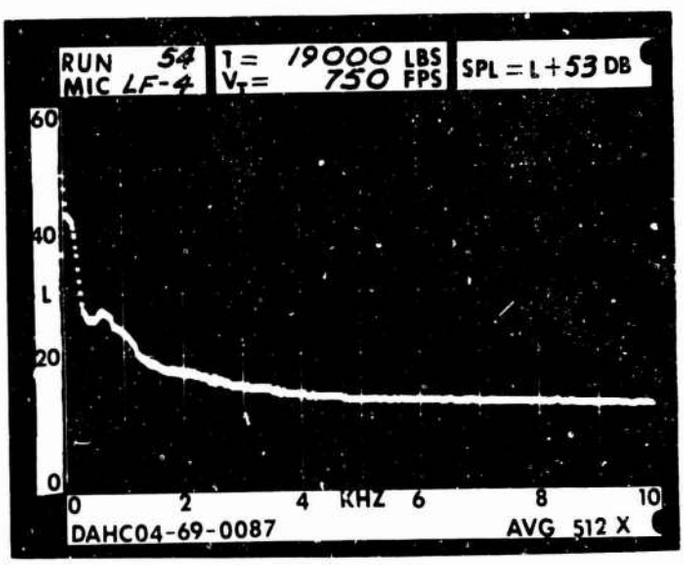

5 DIA.

RUN 57

TIP SPEED 750 FT/SEC

THRUST 27000 LB

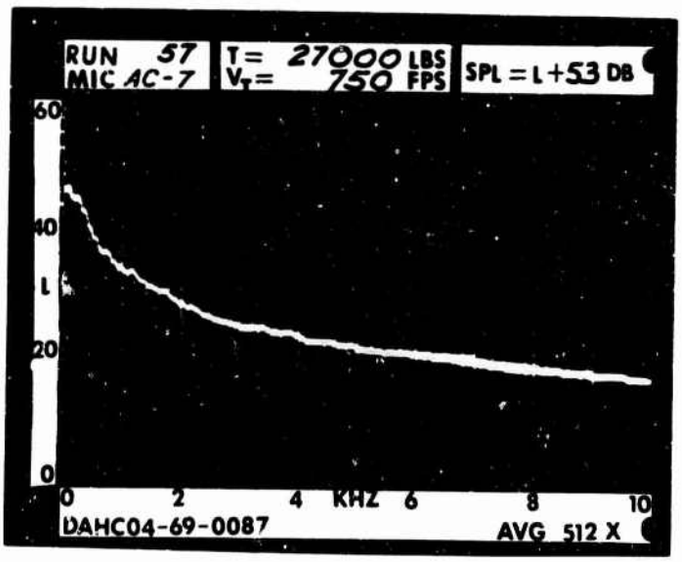

.2 RAD.

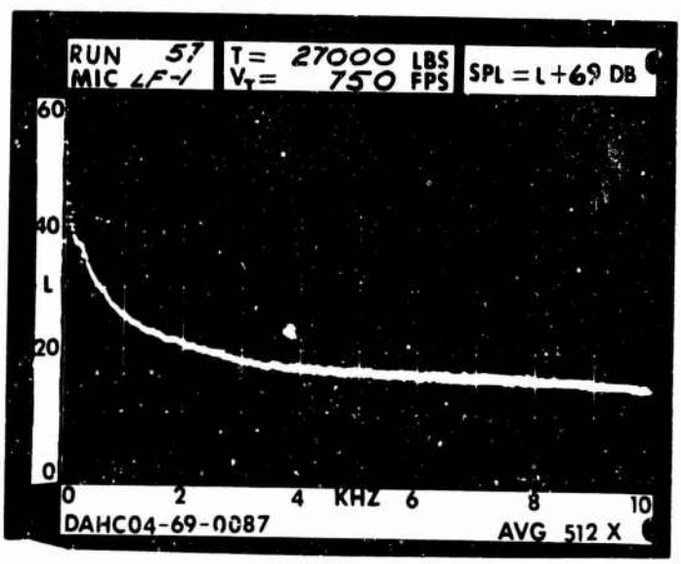

1 RAD.

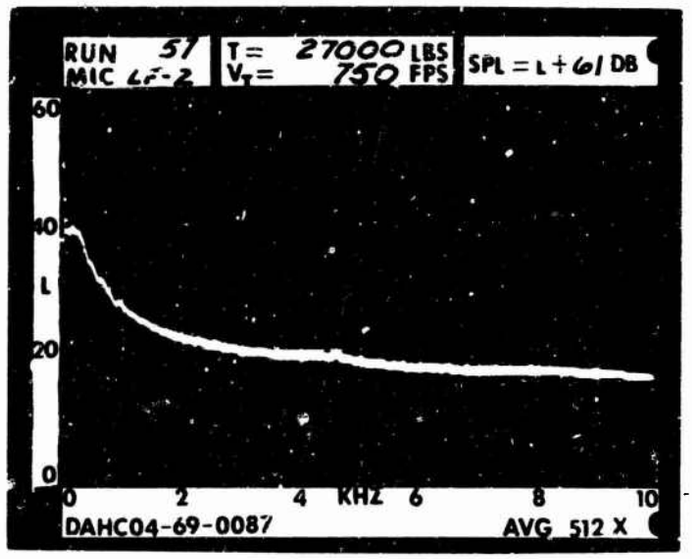

1 DIA.

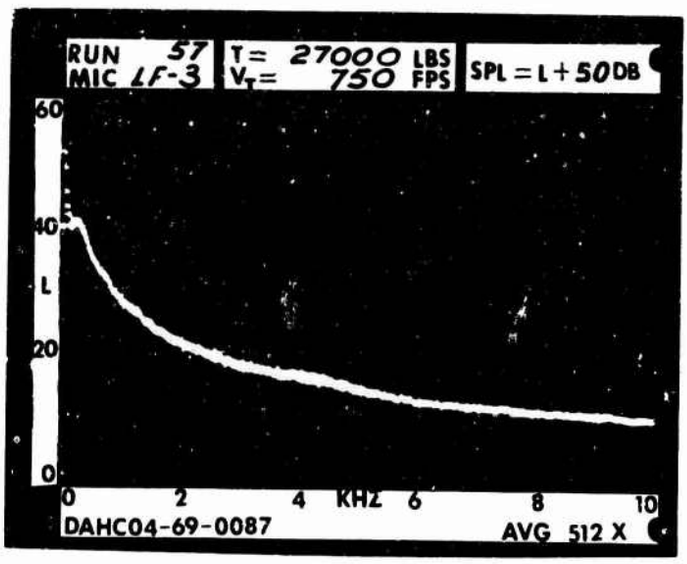

3 DIA.

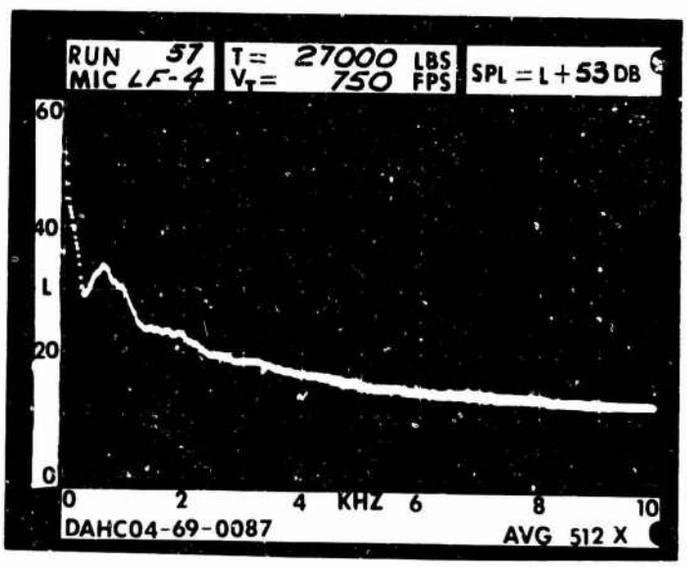

5 DIA.

RUN 101

TIP SPEED 650 FT/SEC

THRUST 8600 LB

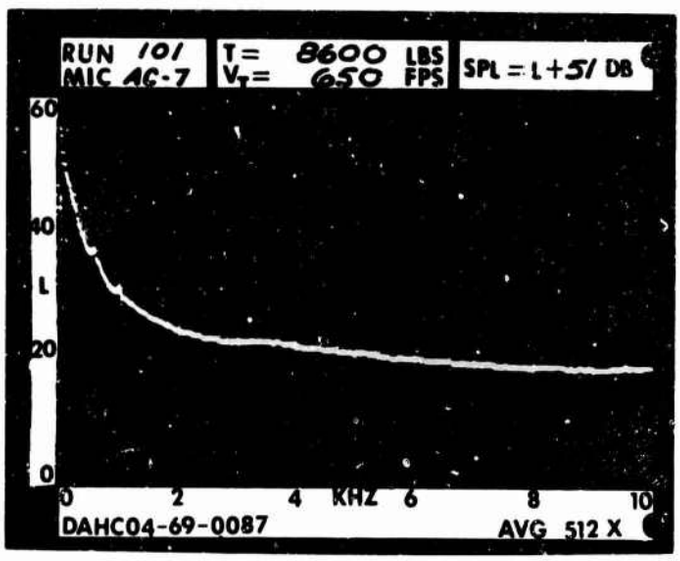

.2 RAD.

1 RAD.

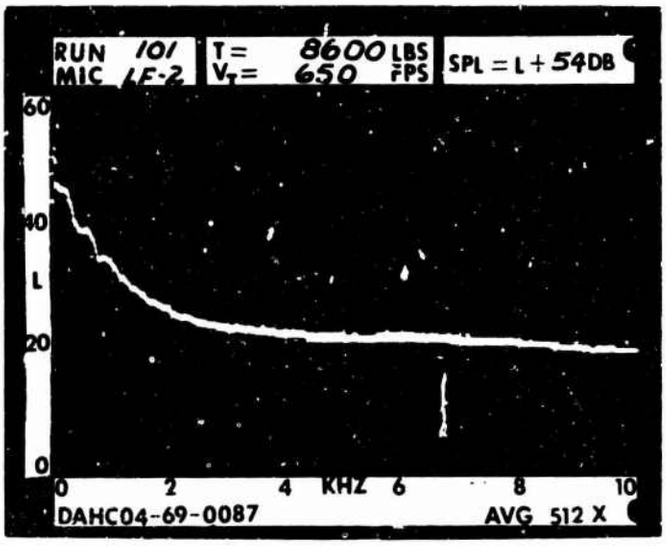

1 DIA.

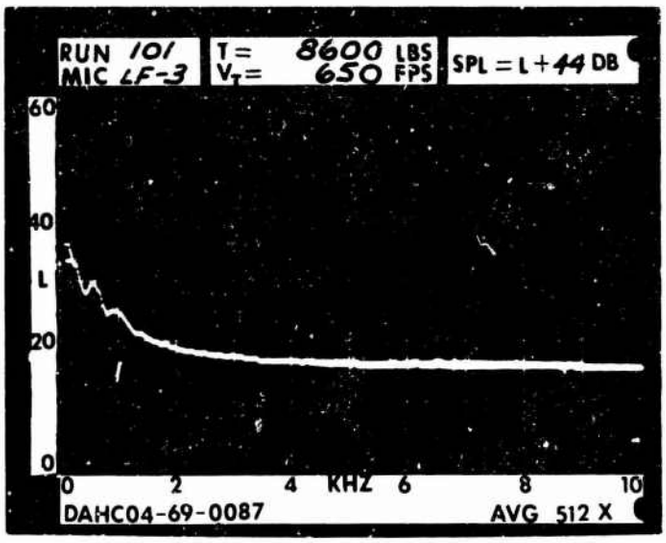

3 DIA.

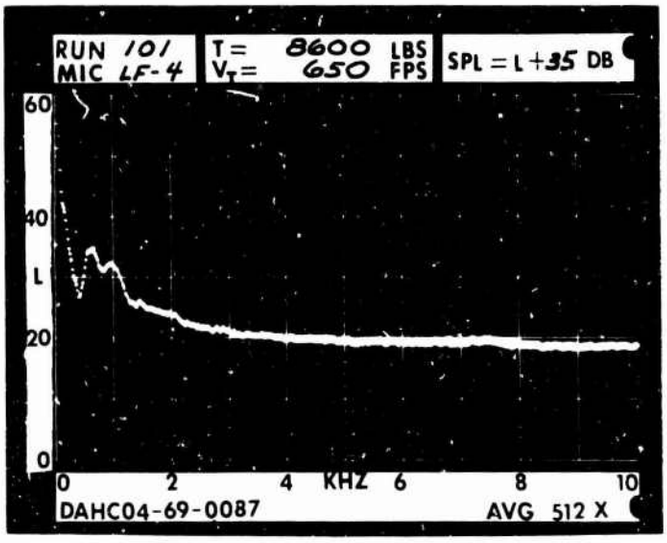

5 DIA.

RUN 108

TIP SPEED 650 FT/SEC

THRUST 17400 LB

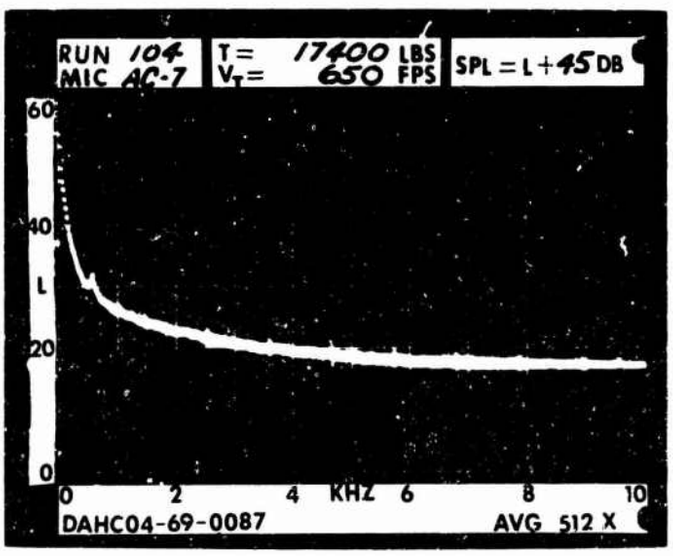

.2 RAD.

1 RAD.

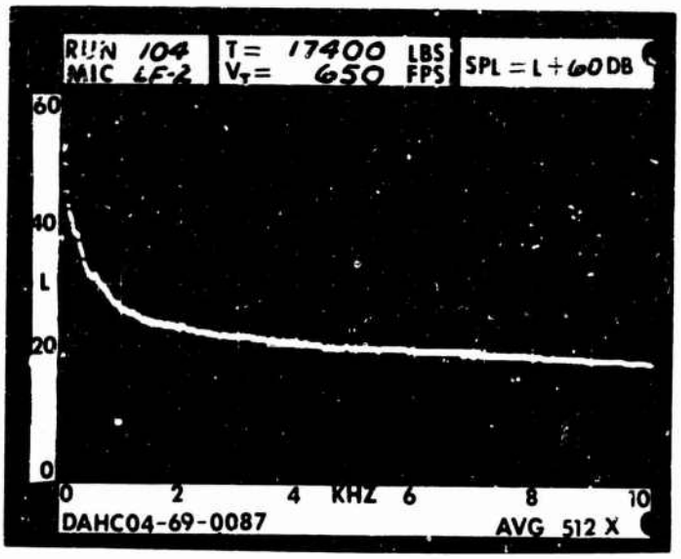

1 DIA.

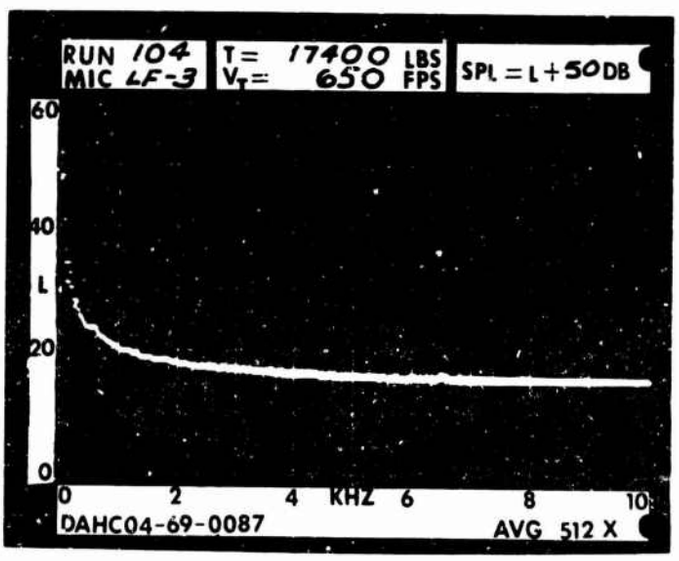

3 DIA.

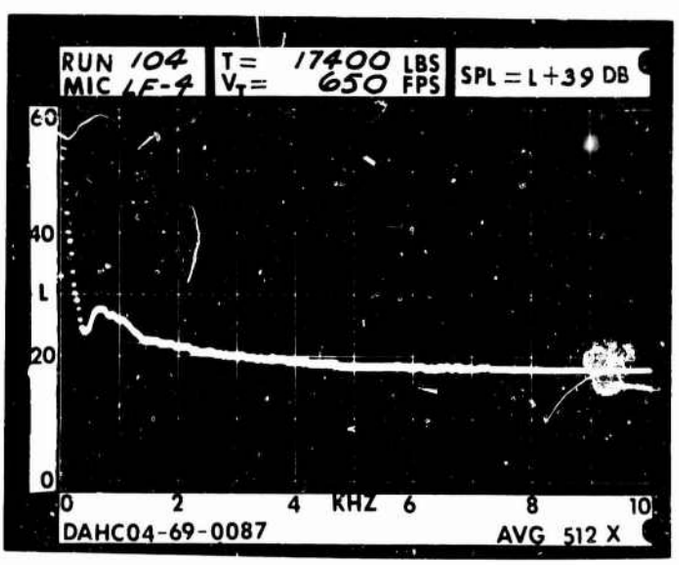

5 DIA.

RUN 103

TIP SPEED 650 FT/SEC

THRUST 26700 LB

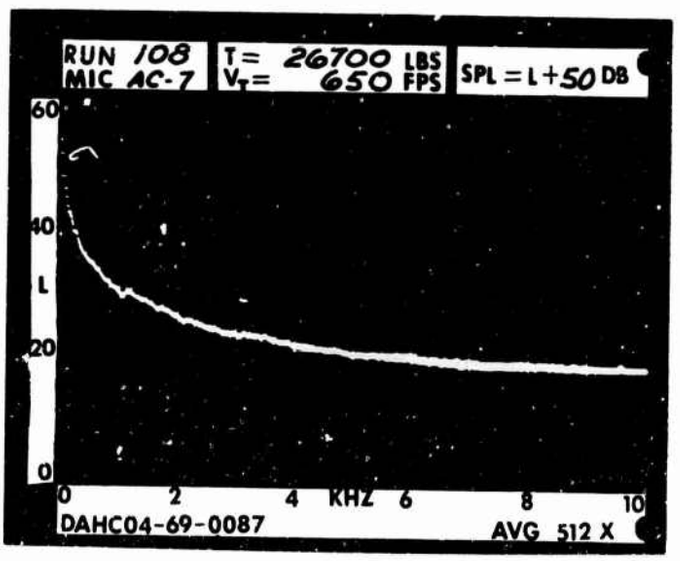

.2 RAD.

1 RAD.

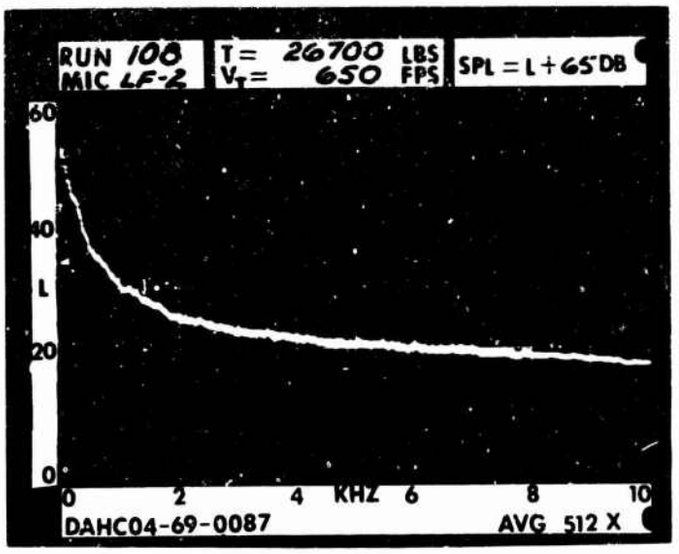

1 DIA.

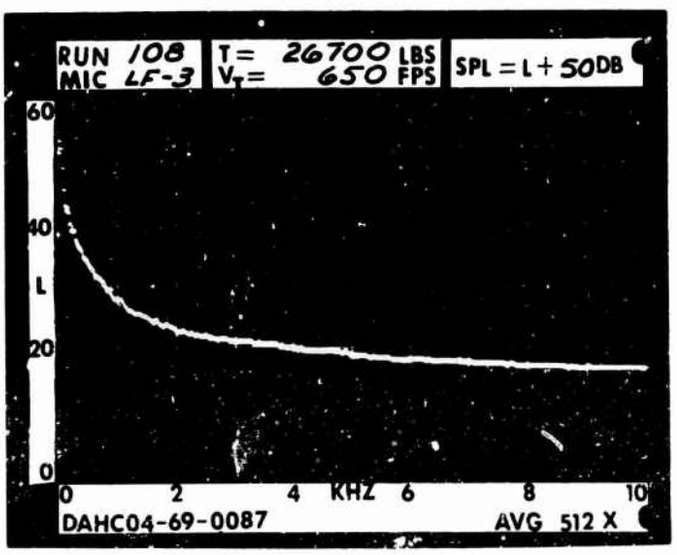

3 DIA.

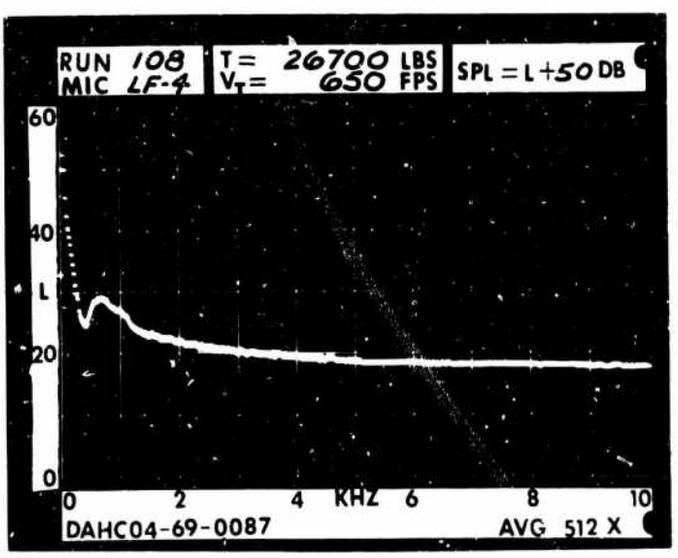

5 DIA.

GROUND MICROPHONES

RUN 31

TIP SPEED 850 FT/SEC

THRUST 8270 LB

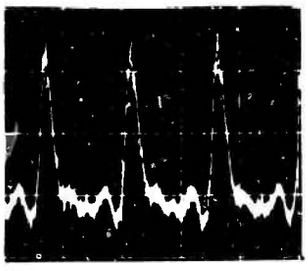

G1

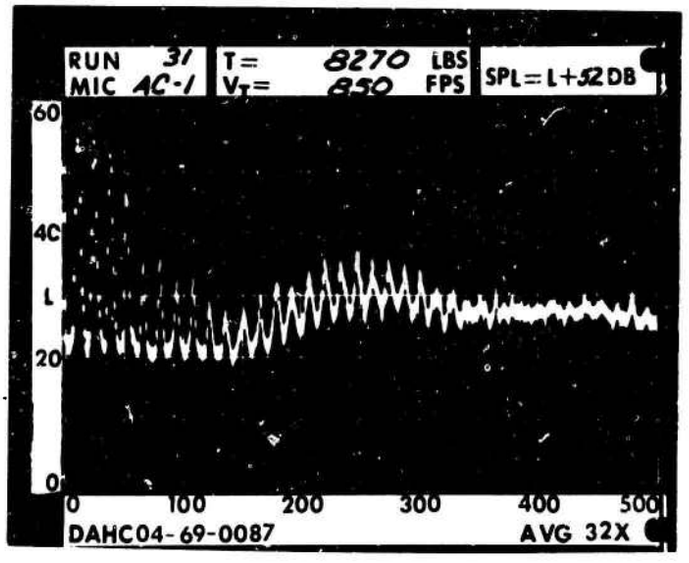

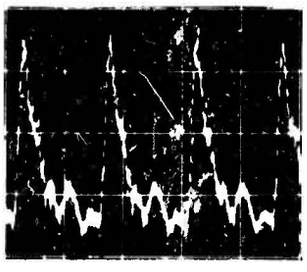

G2

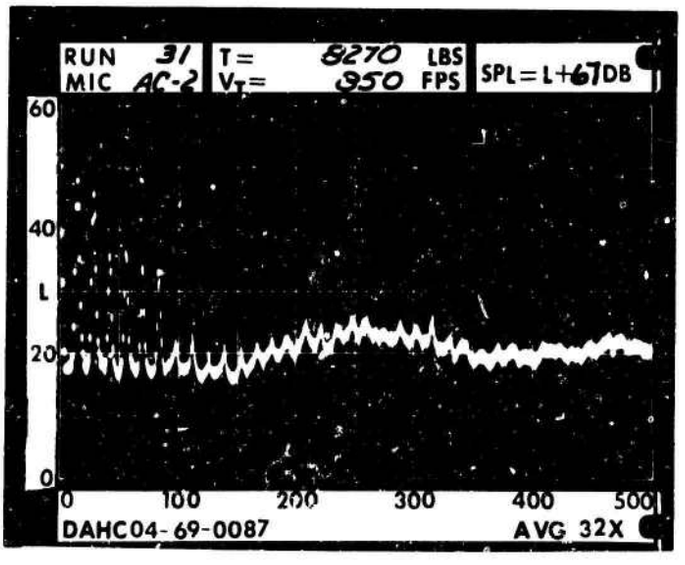

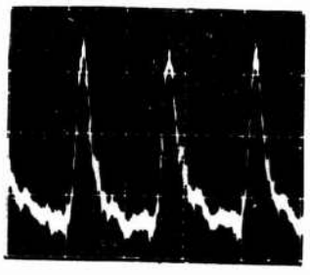

G3

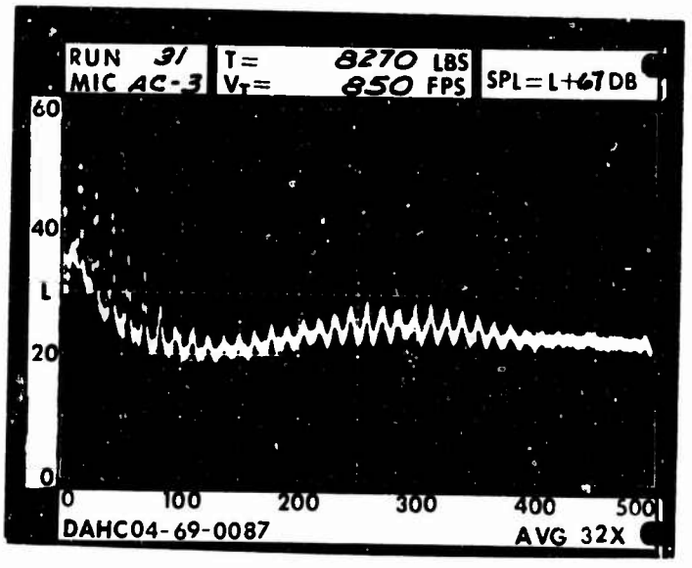
RUN 31
MIC AC-3
T= 8270 LBS
V_T= 850 FPS
SPL=L+67 DB
60
40
L
20
0
0
100
200
300
400
500
DAHC04-69-0087
AVG 32X

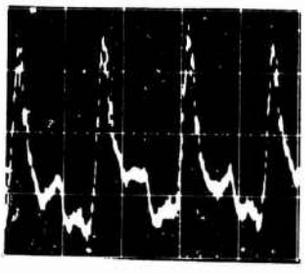

G4

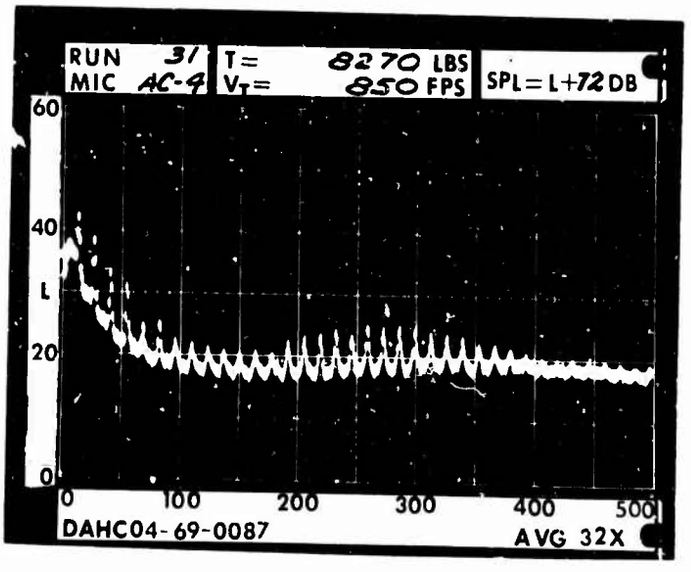
RUN 31
MIC AC-4
T= 8270 LBS
V_T= 850 FPS
SPL=L+72 DB
60
40
L
20
0
0
100
200
300
400
500
DAHC04-69-0087
AVG 32X

GROUND MICROPHONES

RUN 34

TIP SPEED 847 FT/SEC

THRUST 16860 LB

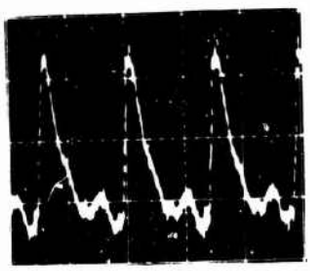

G1

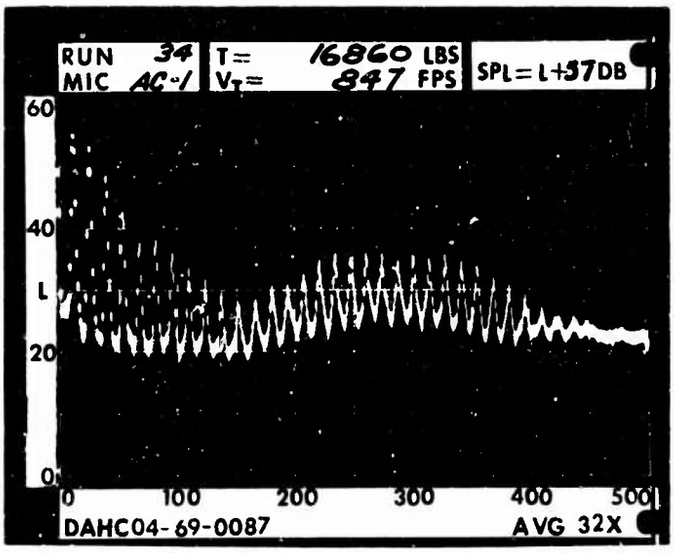

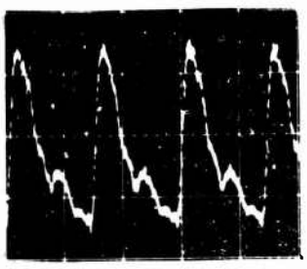

G2

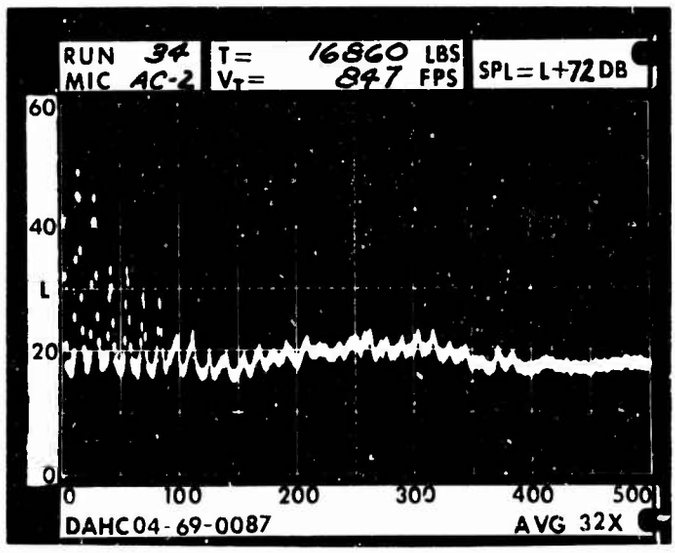

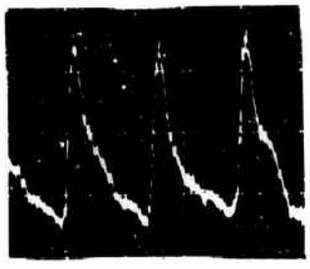

G3

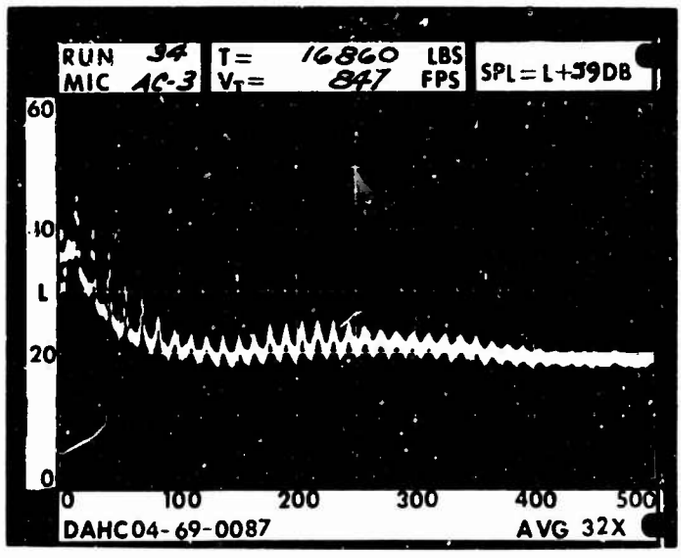
RUN 34
MIC AC-3
T= 16860 LBS
V_T= 847 FPS
SPL=L+79DB
60
40
L
20
0
0
100
200
300
400
500
DAHC04-69-0087
AVG 32X

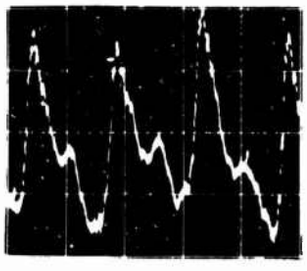

G4

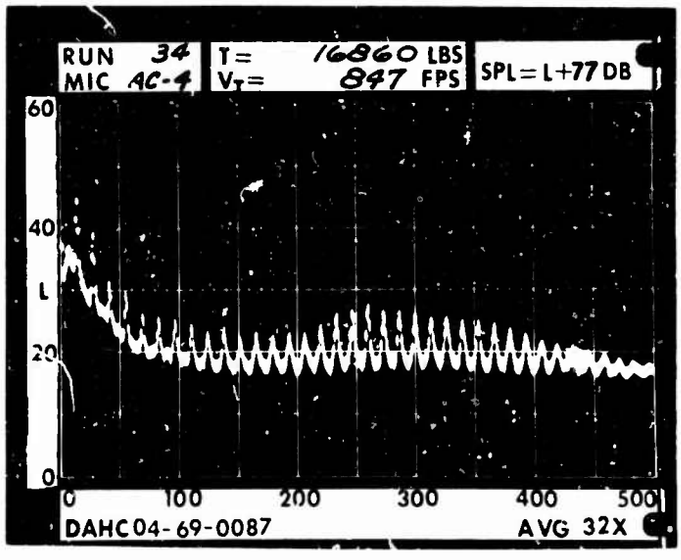
RUN 34
MIC AC-4
T= 16860 LBS
V_T= 847 FPS
SPL=L+77 DB
60
40
L
20
0
0
100
200
300
400
500
DAHC04-69-0087
AVG 32X

GROUND MICROPHONES

RUN 36

TIP SPEED 850 FT/SEC

THRUST 26630 LB

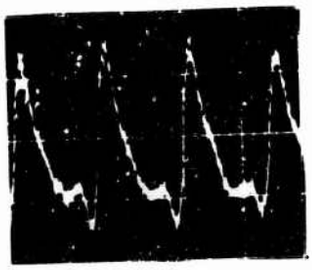

G1

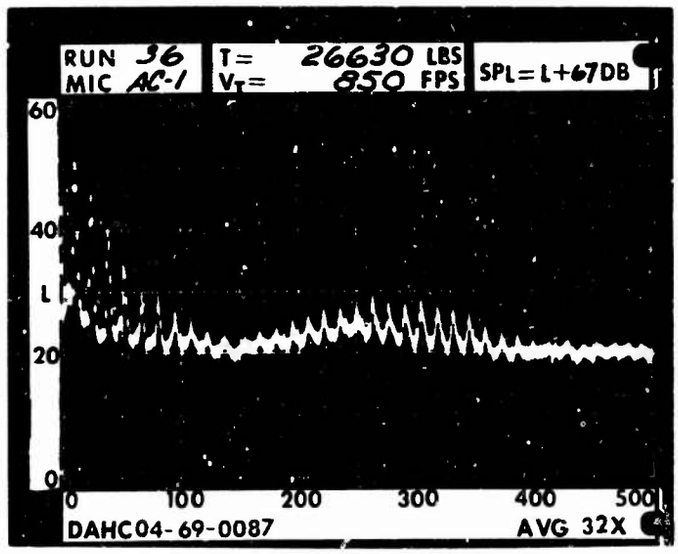

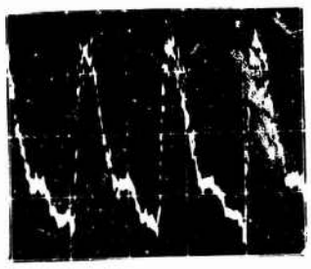

G2

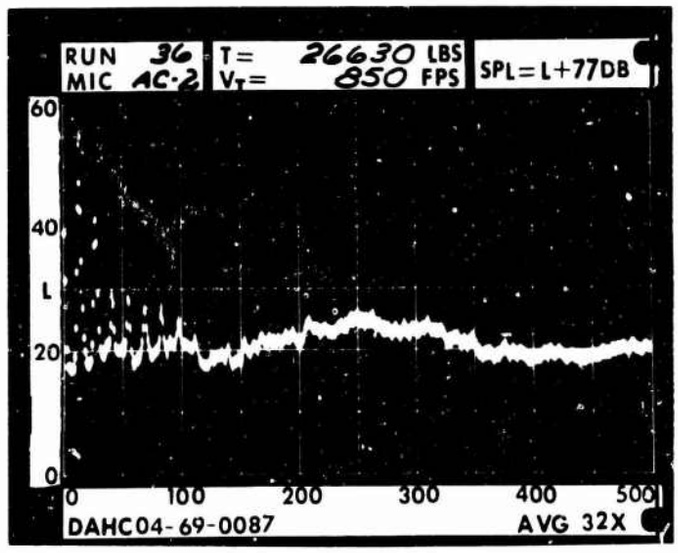

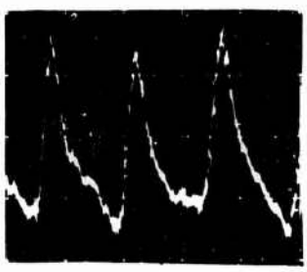

G3

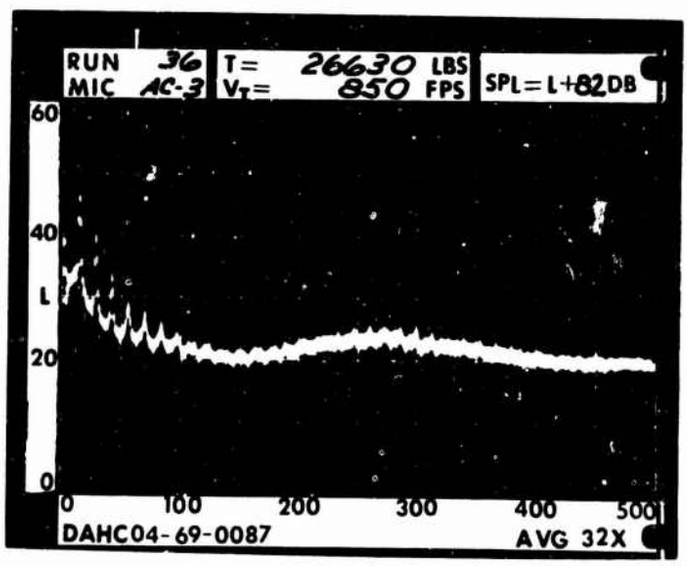
RUN 36
MIC AC-3
T= 26630 LBS
V_T= 850 FPS
SPL=L+82DB
60
40
L
20
0
0
100
200
300
400
500
DAHC04-69-0087
AVG 32X

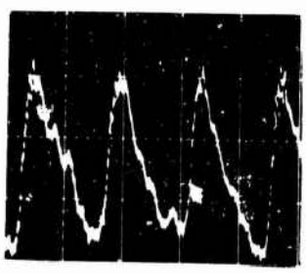

G4

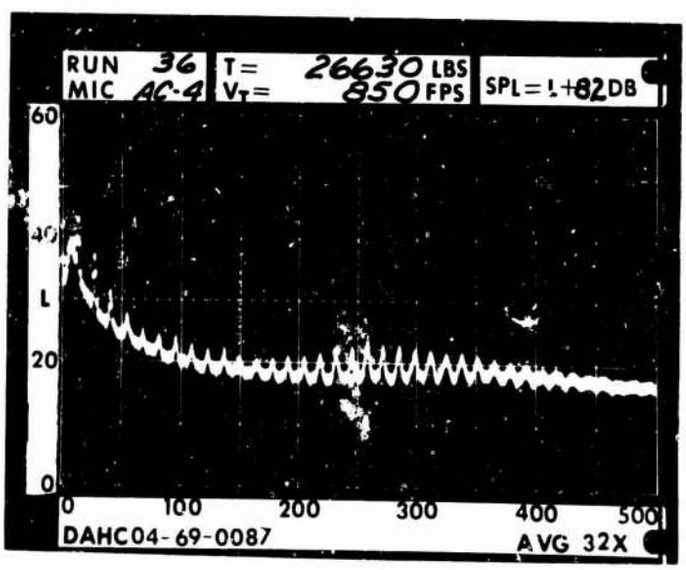
RUN 36
MIC AC-4
T= 26630 LBS
V_T= 850 FPS
SPL=L+82DB
60
40
L
20
0
0
100
200
300
400
500
DAHC04-69-0087
AVG 32X

GROUND MICROPHONES

RUN 51

TIP SPEED 753 FT/SEC

THRUST 9700 LB

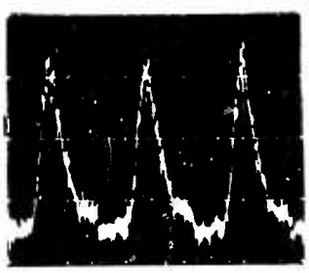

G1

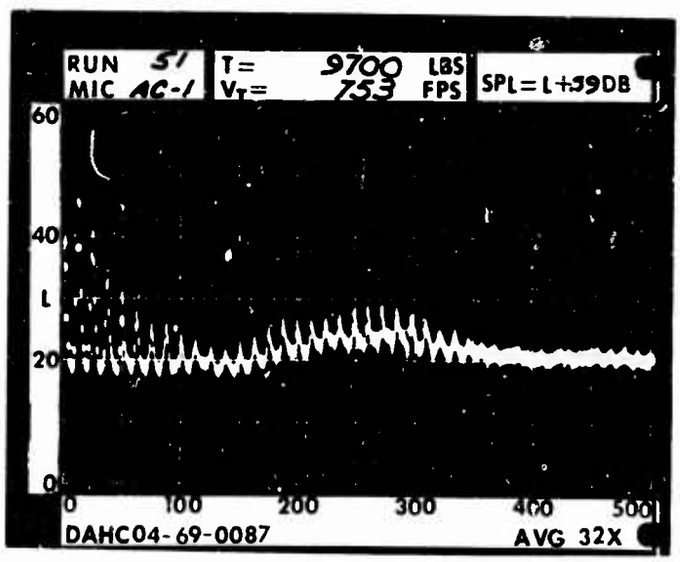

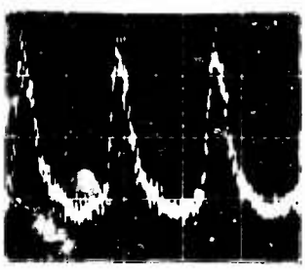

G2

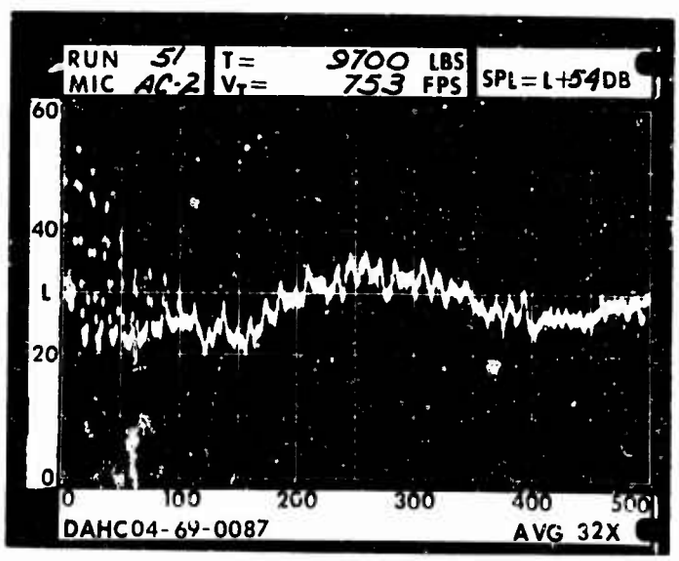

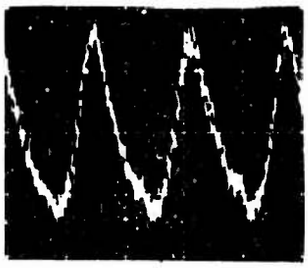

G3

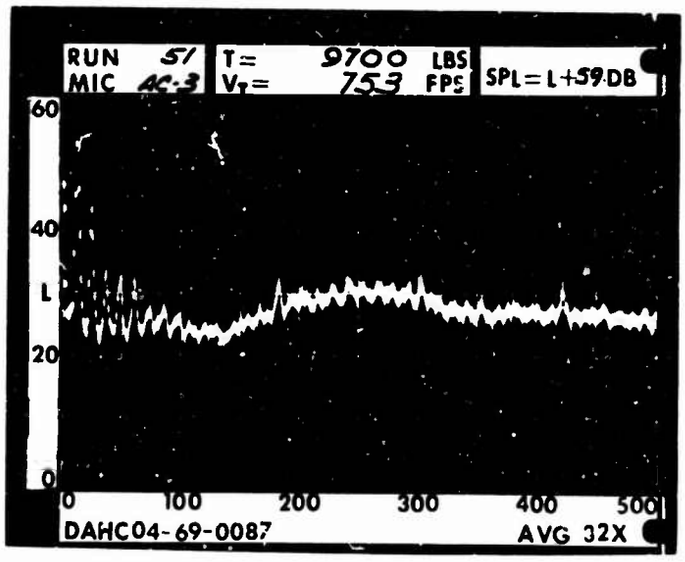
RUN 51
MIC AC-3
T= 9700 LBS
V_T= 753 FPS
SPL=L+59DB
60
40
L
20
0
0
100
200
300
400
500
DAHC04-69-0087
AVG 32X

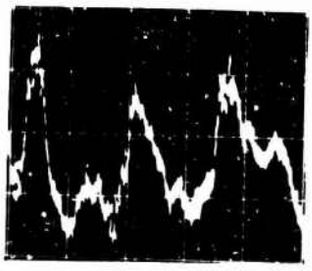

G4

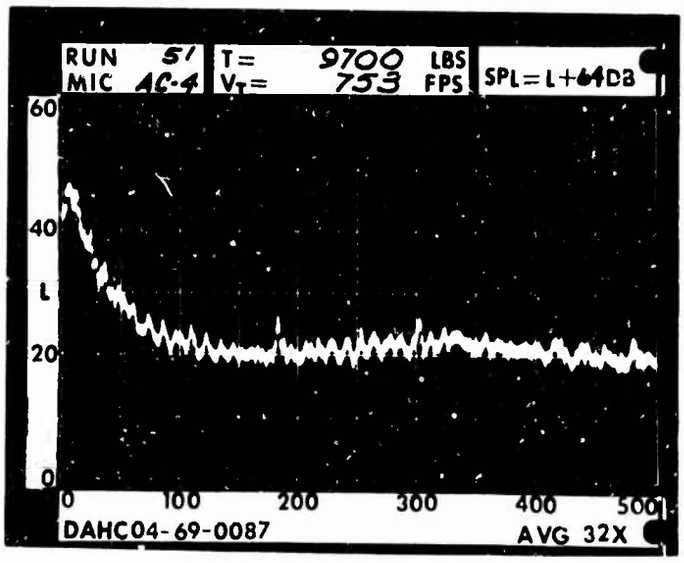
RUN 51
MIC AC-4
T= 9700 LBS
V_T= 753 FPS
SPL=L+64DB
60
40
L
20
0
0
100
200
300
400
500
DAHC04-69-0087
AVG 32X

GROUND MICROPHONES

RUN 54

TIP SPEED 750 FT/SEC

THRUST 18985 LB

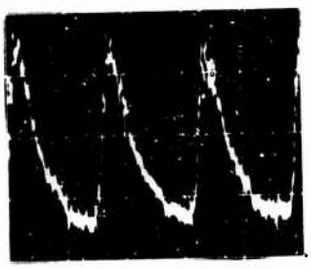

G1

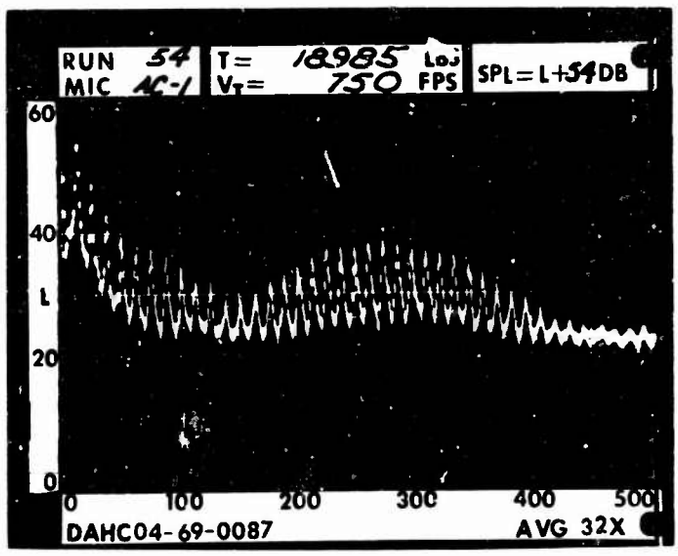

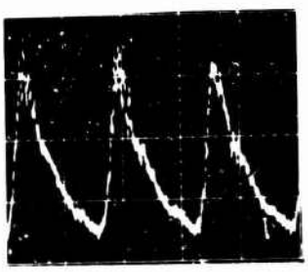

G2

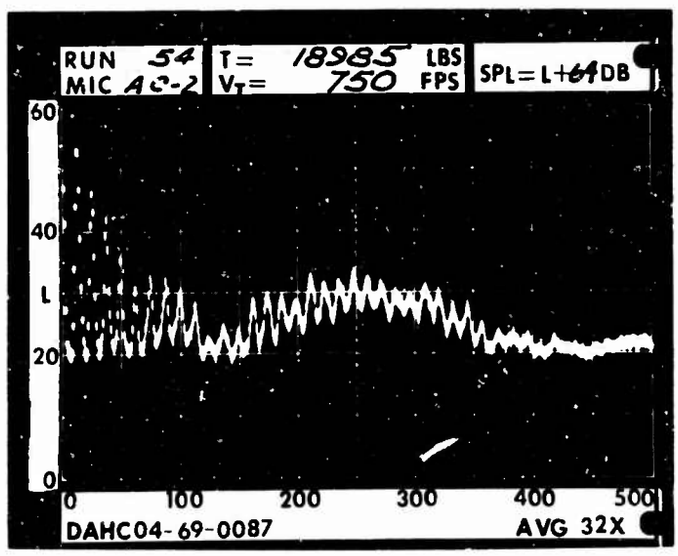

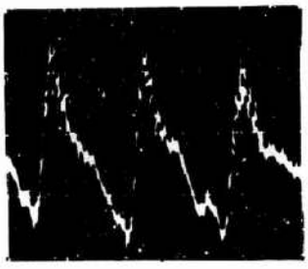

G3

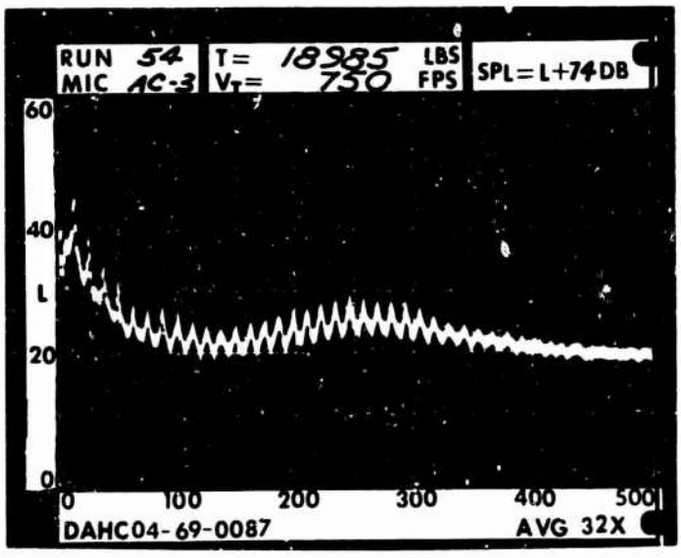
RUN 54
MIC AC-3
T= 18985 LBS
VT= 750 FPS
SPL=L+74DB
60
40
L
20
0
0
100
200
300
400
500
DAHC04-69-0087
AVG 32X

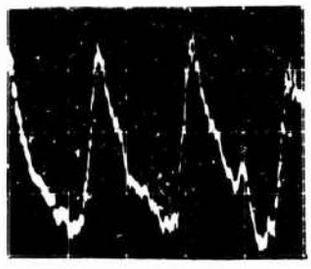

G4

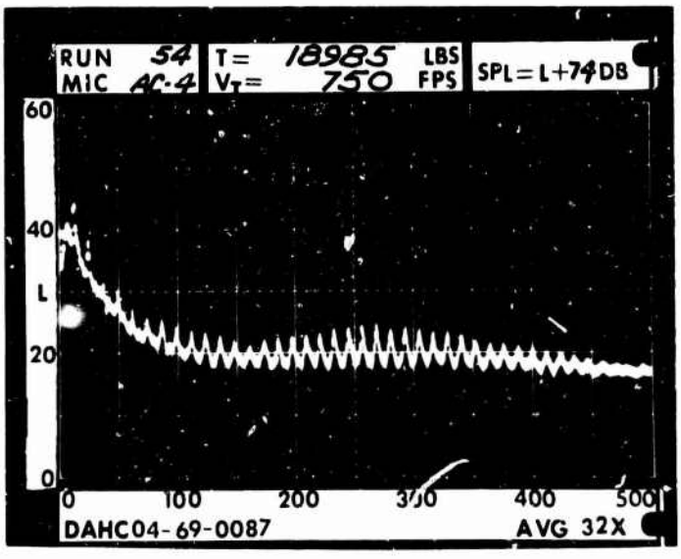
RUN 54
MIC AC-4
T= 18985 LBS
VT= 750 FPS
SPL=L+74DB
60
40
L
20
0
0
100
200
300
400
500
DAHC04-69-0087
AVG 32X

GROUND MICROPHONES

RUN 57

TIP SPEED 750 FT/SEC

THRUST 26960 LB

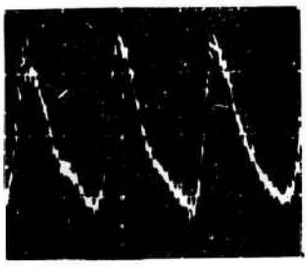

G1

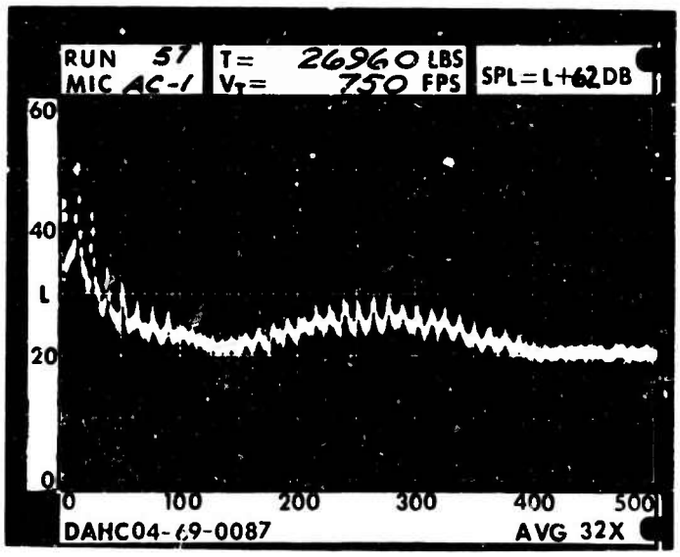

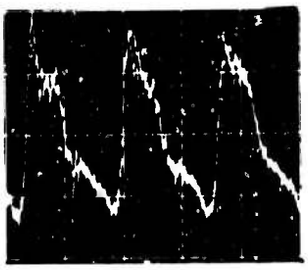

G2

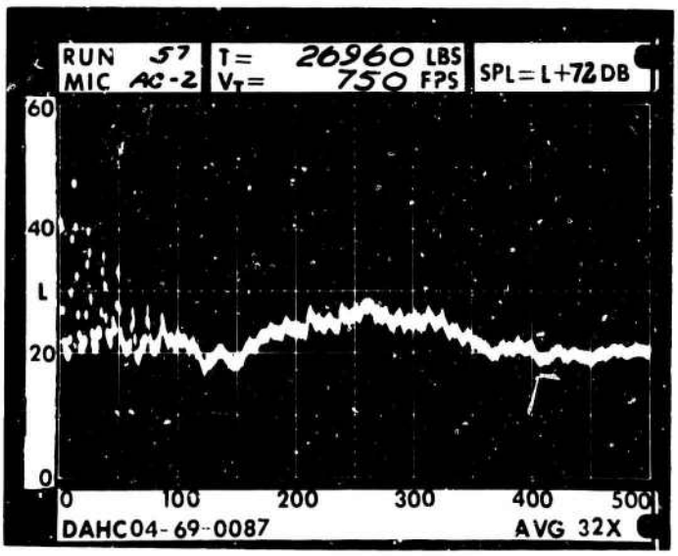

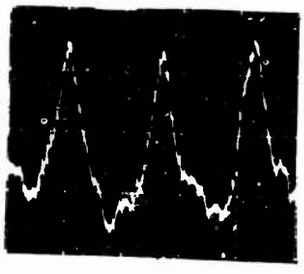

G3

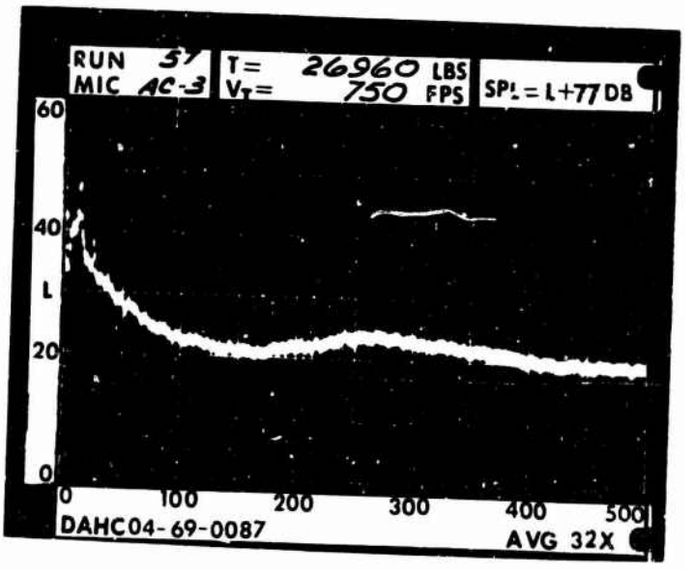
RUN 57
MIC AC-3
T= 26960 LBS
V_T= 750 FPS
SPL = L+77 DB
60
40
L
20
0
0
100
200
300
400
500
DAHC04-69-0087
AVG 32X

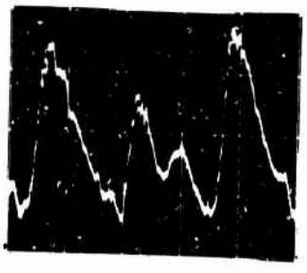

G4

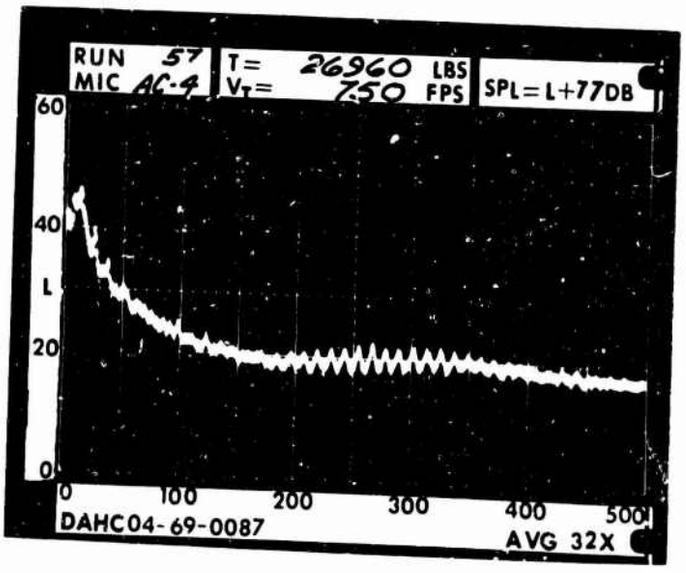
RUN 57
MIC AC-4
T= 26960 LBS
V_T= 750 FPS
SPL = L+77DB
60
40
L
20
0
0
100
200
300
400
500
DAHC04-69-0087
AVG 32X

RUN 57

GROUND MICROPHONES

RUN 101

TIP SPEED 650 FT/SEC

THRUST 8595 LB

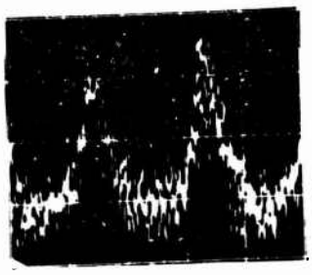

G1

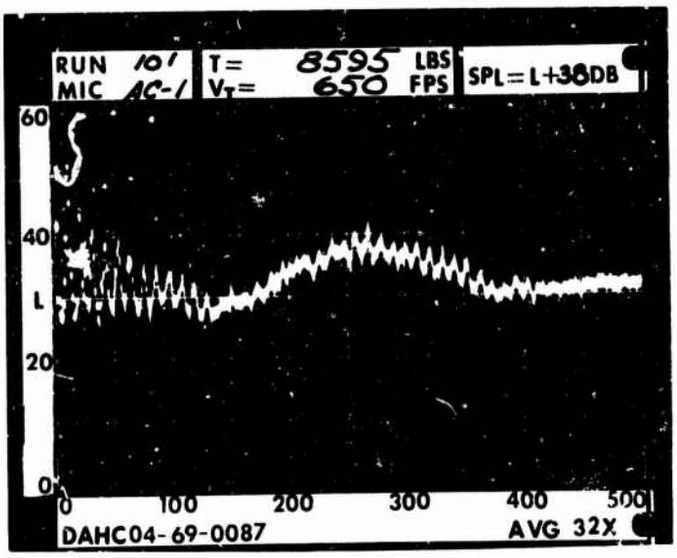

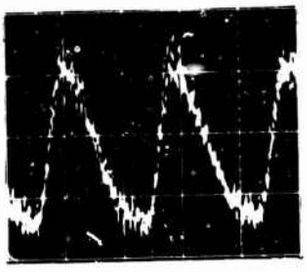

G2

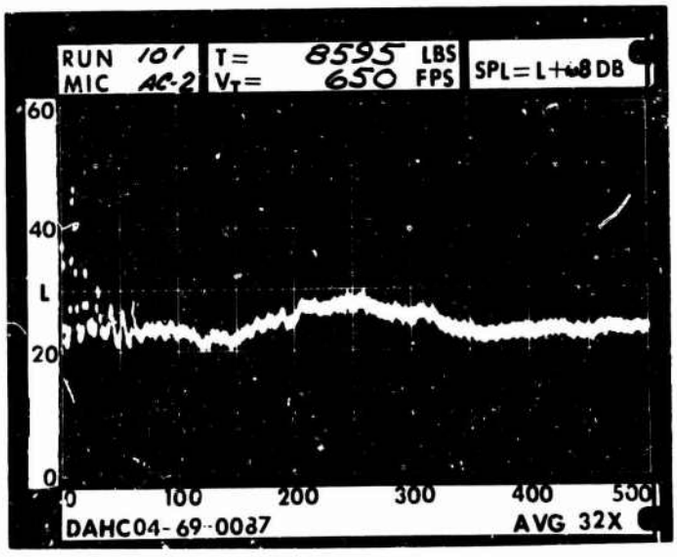

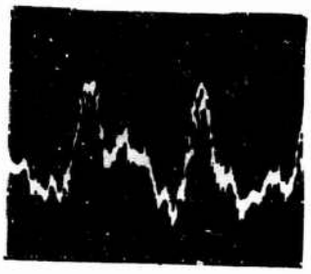

G3

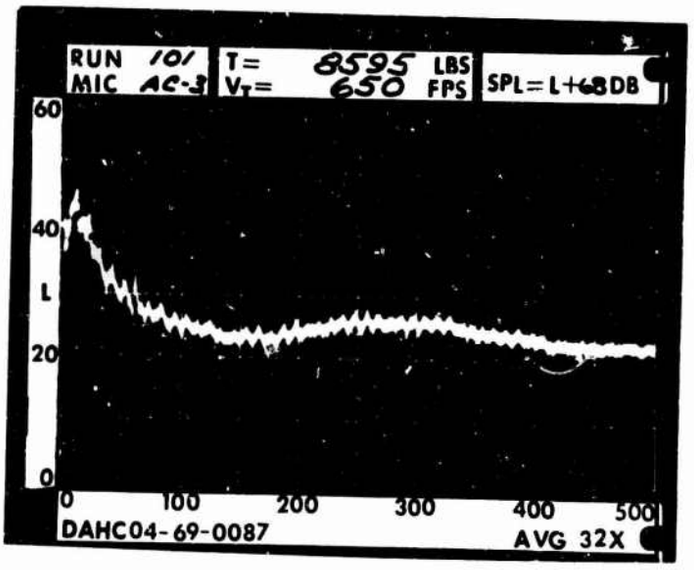
RUN 101
MIC AC-3
T= 8595 LBS
V_T= 650 FPS
SPL=L+68DB
60
40
L
20
0
0
100
200
300
400
500
DAHC04-69-0087
AVG 32X

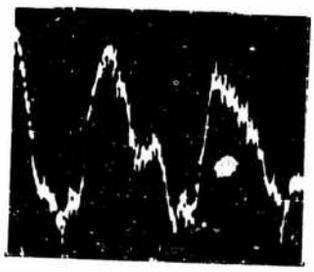

G4

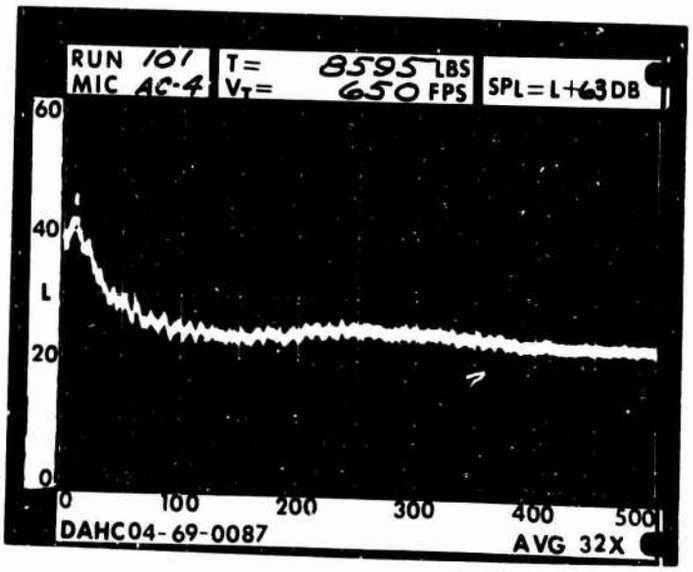
RUN 101
MIC AC-4
T= 8595 LBS
V_T= 650 FPS
SPL=L+63DB
60
40
L
20
0
0
100
200
300
400
500
DAHC04-69-0087
AVG 32X

GROUND MICROPHONES

RUN 104

TIP SPEED 650 FT/SEC

THRUST 17445 LB

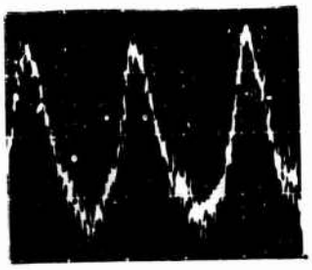

G1

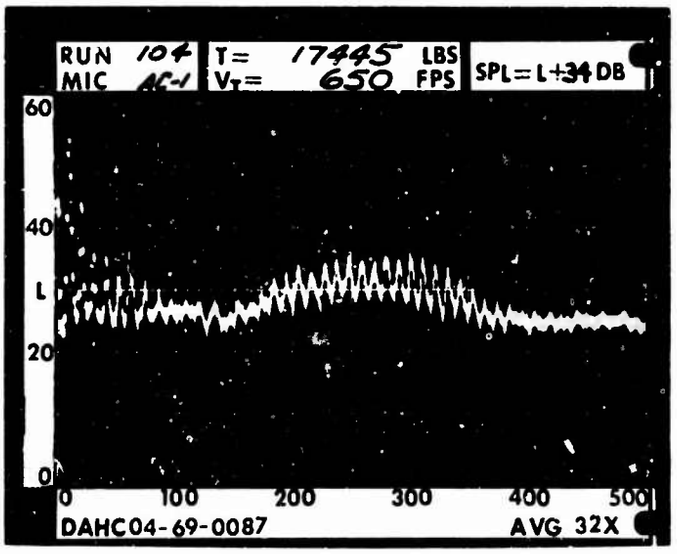

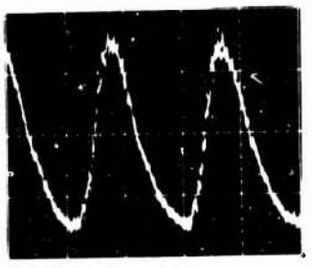

G2

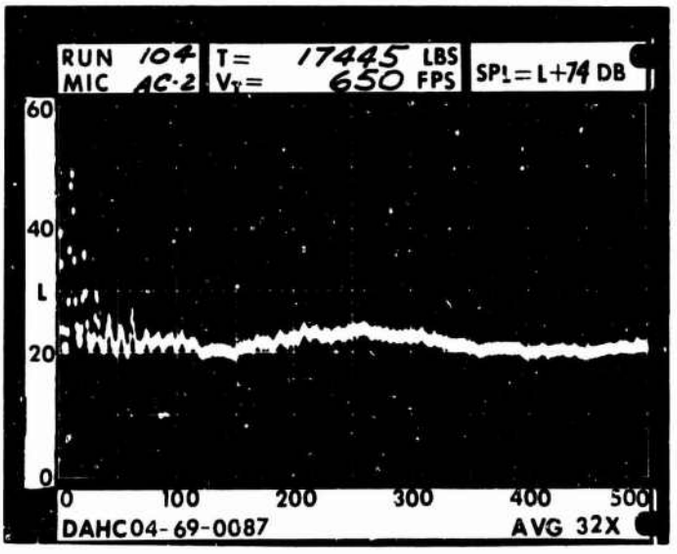

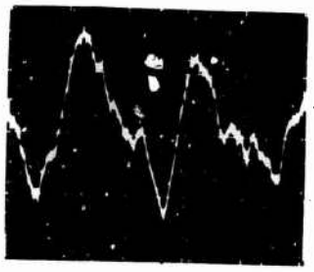

G3

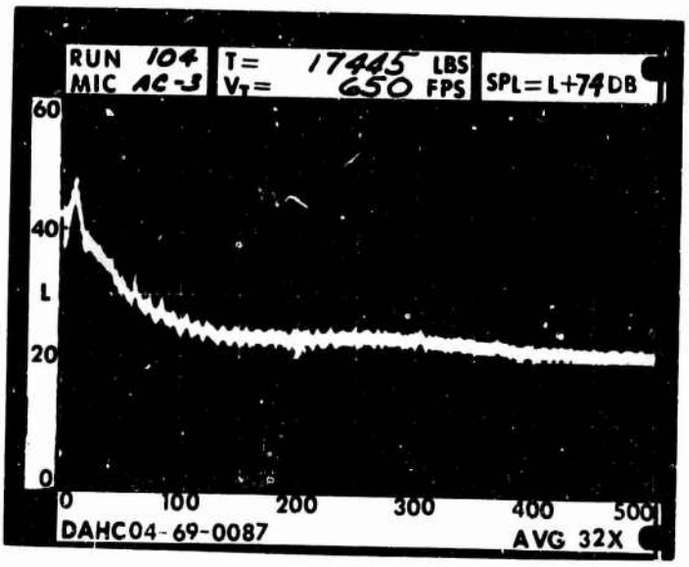
RUN 104
MIC AC-3
T= 17445 LBS
V_T= 650 FPS
SPL=L+74DB
60
40
L
20
0
0
100
200
300
400
500
DAHC04-69-0087
AVG 32X

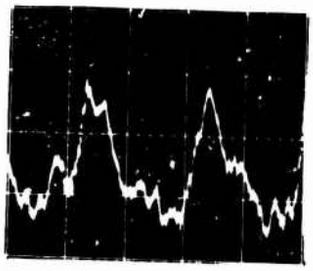

G4

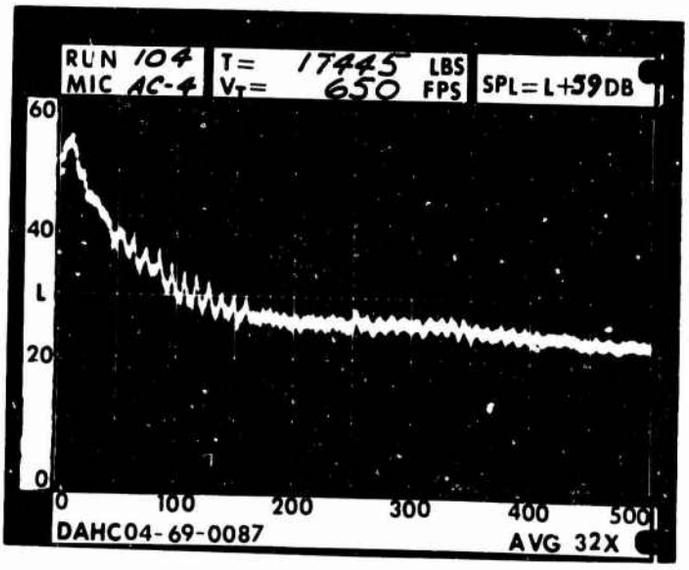
RUN 104
MIC AC-4
T= 17445 LBS
V_T= 650 FPS
SPL=L+59DB
60
40
L
20
0
0
100
200
300
400
500
DAHC04-69-0087
AVG 32X

GROUND MICROPHONES

RUN 108
TIP SPEED 650 FT/SEC
THRUST 26709 LB

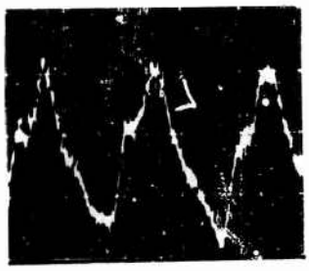

G1

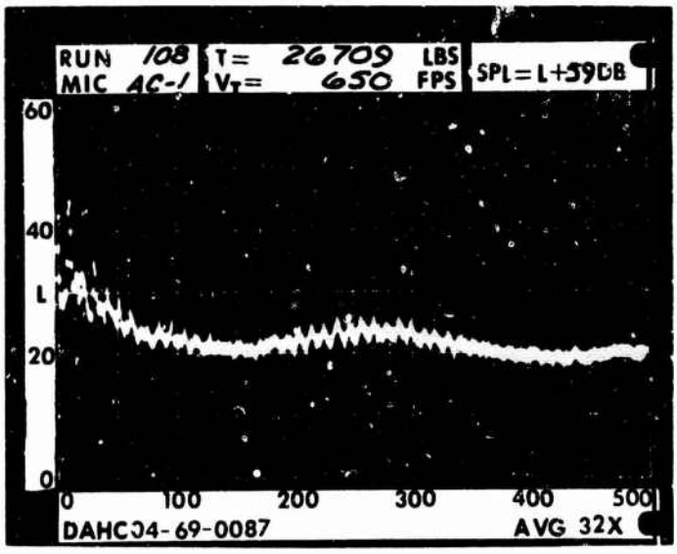

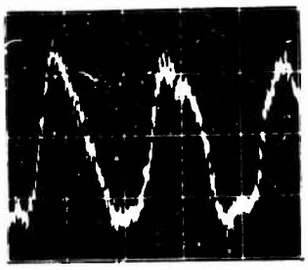

G2

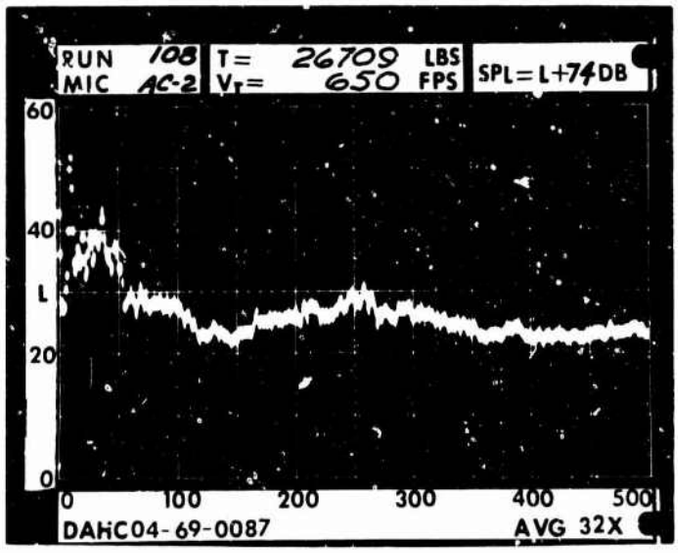

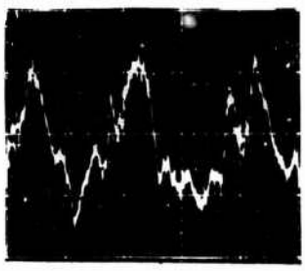

G3

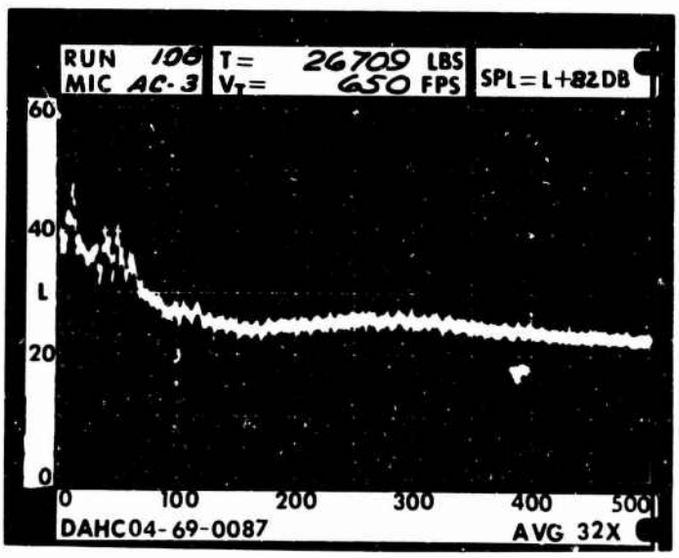
RUN 106
MIC AC-3
T= 26709 LBS
V_T= 650 FPS
SPL=L+82DB
60
40
L
20
0
0
100
200
300
400
500
DAHC04-69-0087
AVG 32X

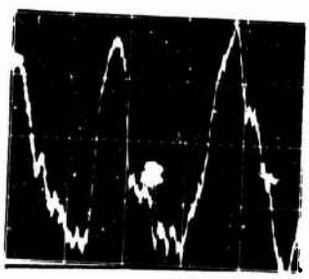

G4

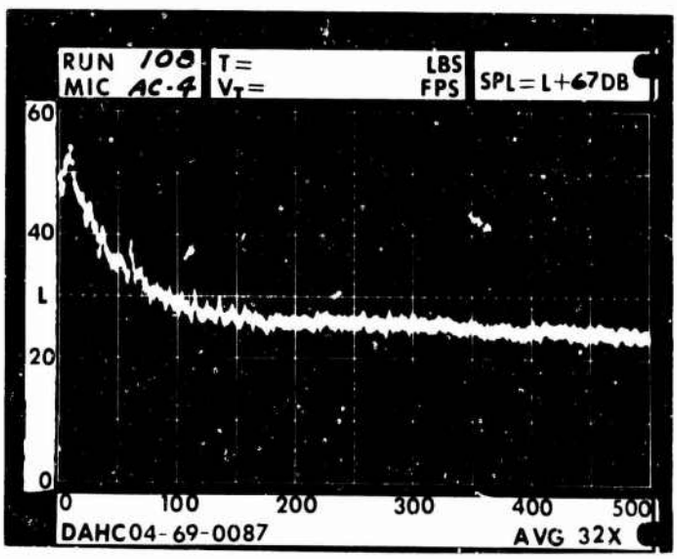
RUN 108
MIC AC-4
T=
LBS
V_T=
FPS
SPL=L+67DB
60
40
L
20
0
0
100
200
300
400
500
DAHC04-69-0087
AVG 32X

Unclassified

Security Classification

DOCUMENT CONTROL DATA - R & D

(Security classification of title, body of abstract and indexing annotation must be entered when the overall report is classified)

1. ORIGINATING ACTIVITY (Corporate author) The Boeing Company, Vertol Division	2a. REPORT SECURITY CLASSIFICATION Unclassified 2b. GROUP NA

3. REPORT TITLE

An Investigation of Noise Generation on a Hovering Rotor

4. DESCRIPTIVE NOTES (Type of report and inclusive dates)

Final Report: 30 June 69 - 30 January 71

5. AUTHOR(S) (First name, middle initial, last name)

H. Sternfeld
R. H. Spencer
J. O. Schairer

6. REPORT DATE	7a. TOTAL NO. OF PAGES	7b. NO. OF REFS
January 1971	353	

8a. CONTRACT OR GRANT NO.	9a. ORIGINATOR'S REPORT NUMBER(S)
DAHC04 69 C 0087	NA
b. PROJECT NO.	
c.	9b. OTHER REPORT NO(S) (Any other numbers that may be assigned this report)
d.	8704.2-E

10. DISTRIBUTION STATEMENT

Approved for public release; distribution unlimited.

11. SUPPLEMENTARY NOTES	12. SPONSORING MILITARY ACTIVITY
	U. S. Army Research Office-Durham Box CM, Duke Station Durham, North Carolina 27706

13. ABSTRACT

This report presents the results of a program of helicopter rotor noise measurement. The program was carried out using a 60-foot diameter CH-47B 3-bladed rotor on the Boeing-Vertol engineering rotor whirl tower. The primary objectives were: (1) To obtain acoustical data over a frequency range wide enough to define all elements of rotor noise under well-documented ambient conditions. (2) To measure the tip vortex position with respect to a trailing blade using high-speed cameras and smoke to visualize the tip vortex and to relate blade-vortex separation distance to noise level. (3) To determine the propagation characteristics of rotor noise. (4) To evaluate two current analytical procedures for predicting rotor noise against the measured data. Tipspeeds ranged from 600 to 900 fps and thrusts ranged from 6300 to 32,000 pounds (disk load 2.2 to 11.3 pounds per square foot).

14. KEY WORDS

Vortices
Rotors
Rotary wings
Aircraft noise
Helicopters

Unclassified